BACTERIAL SECRETION SYSTEMS, VOLUME II

EDITED BY: Ignacio Arechaga and Eric Cascales
PUBLISHED IN: Frontiers in Microbiology

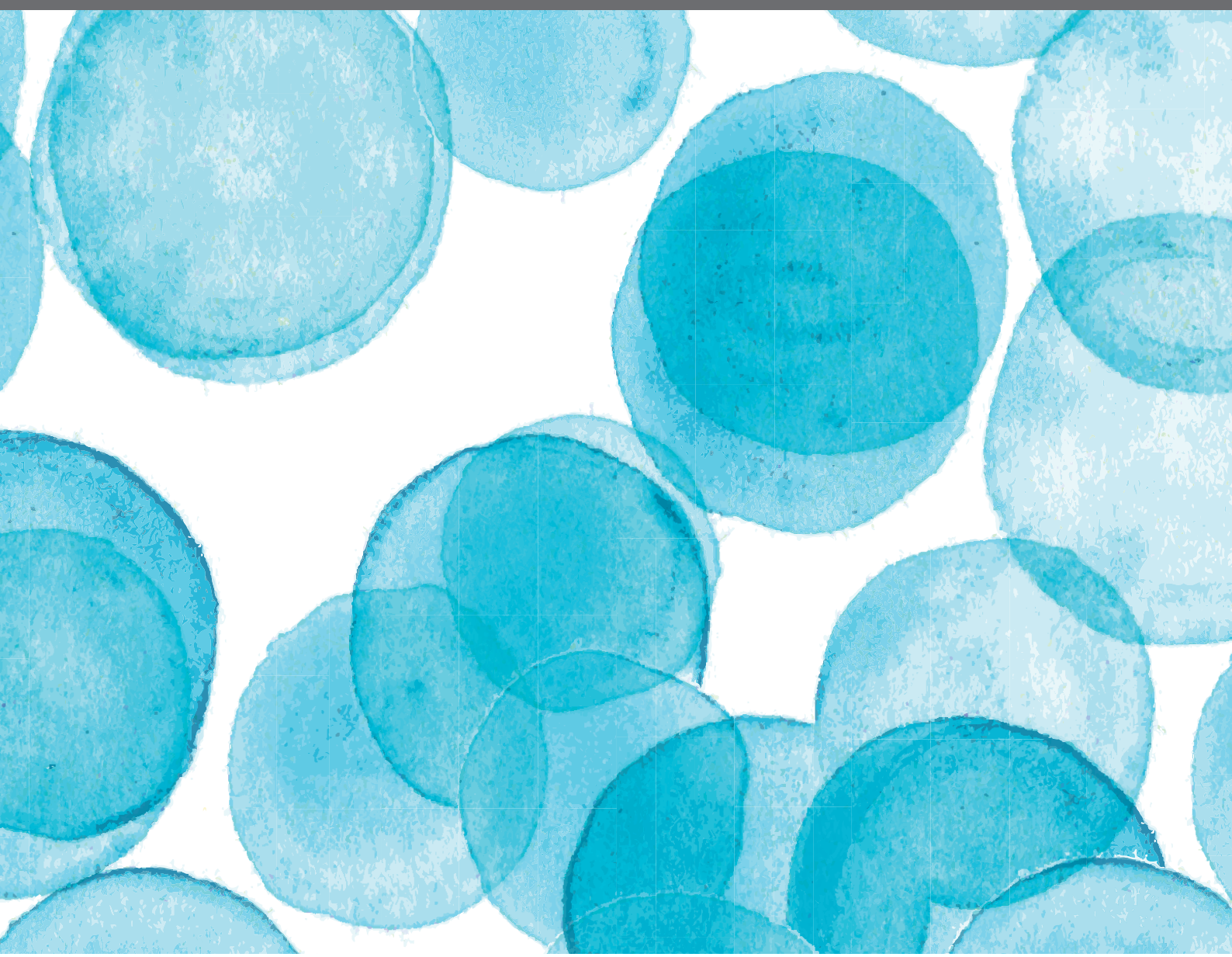

frontiers Research Topics

ISSN 1664-8714
ISBN 978-2-88976-375-7
DOI 10.3389/978-2-88976-375-7

About Frontiers

Frontiers is more than just an open-access publisher of scholarly articles: it is a pioneering approach to the world of academia, radically improving the way scholarly research is managed. The grand vision of Frontiers is a world where all people have an equal opportunity to seek, share and generate knowledge. Frontiers provides immediate and permanent online open access to all its publications, but this alone is not enough to realize our grand goals.

Frontiers Journal Series

The Frontiers Journal Series is a multi-tier and interdisciplinary set of open-access, online journals, promising a paradigm shift from the current review, selection and dissemination processes in academic publishing. All Frontiers journals are driven by researchers for researchers; therefore, they constitute a service to the scholarly community. At the same time, the Frontiers Journal Series operates on a revolutionary invention, the tiered publishing system, initially addressing specific communities of scholars, and gradually climbing up to broader public understanding, thus serving the interests of the lay society, too.

Dedication to Quality

Each Frontiers article is a landmark of the highest quality, thanks to genuinely collaborative interactions between authors and review editors, who include some of the world's best academicians. Research must be certified by peers before entering a stream of knowledge that may eventually reach the public - and shape society; therefore, Frontiers only applies the most rigorous and unbiased reviews.
Frontiers revolutionizes research publishing by freely delivering the most outstanding research, evaluated with no bias from both the academic and social point of view. By applying the most advanced information technologies, Frontiers is catapulting scholarly publishing into a new generation.

What are Frontiers Research Topics?

Frontiers Research Topics are very popular trademarks of the Frontiers Journals Series: they are collections of at least ten articles, all centered on a particular subject. With their unique mix of varied contributions from Original Research to Review Articles, Frontiers Research Topics unify the most influential researchers, the latest key findings and historical advances in a hot research area! Find out more on how to host your own Frontiers Research Topic or contribute to one as an author by contacting the Frontiers Editorial Office: frontiersin.org/about/contact

BACTERIAL SECRETION SYSTEMS, VOLUME II

Topic Editors:
Ignacio Arechaga, University of Cantabria, Spain
Eric Cascales, Aix-Marseille Université, France

Citation: Arechaga, I., Cascales, E., eds. (2022). Bacterial Secretion Systems, Volume II. Lausanne: Frontiers Media SA. doi: 10.3389/978-2-88976-375-7

Table of Contents

05 ***Editorial: Bacterial Secretion Systems, Volume II***
Ignacio Arechaga and Eric Cascales

08 ***Bioinformatic Analysis of the* Campylobacter jejuni *Type VI Secretion System and Effector Prediction***
Luca Robinson, Janie Liaw, Zahra Omole, Dong Xia, Arnoud H. M. van Vliet, Nicolae Corcionivoschi, Abderrahman Hachani and Ozan Gundogdu

28 ***Corrigendum: Bioinformatic Analysis of the* Campylobacter jejuni *Type VI Secretion System and Effector Prediction***
Luca Robinson, Janie Liaw, Zahra Omole, Dong Xia, Arnoud H. M. van Vliet, Nicolae Corcionivoschi, Abderrahman Hachani and Ozan Gundogdu

29 ***Compensating Complete Loss of Signal Recognition Particle During Co-translational Protein Targeting by the Translation Speed and Accuracy***
Liuqun Zhao, Gang Fu, Yanyan Cui, Zixiang Xu, Tao Cai and Dawei Zhang

42 ***Monitoring Bacterial Conjugation by Optical Microscopy***
Gerardo Carranza, Tamara Menguiano, Fernando Valenzuela-Gómez, Yolanda García-Cazorla, Elena Cabezón and Ignacio Arechaga

52 ***Multiple Roles of Flagellar Export Chaperones for Efficient and Robust Flagellar Filament Formation in* Salmonella**
Tohru Minamino, Yusuke V. Morimoto, Miki Kinoshita and Keiichi Namba

66 ***The Contribution of the Predicted Sorting Platform Component HrcQ to Type III Secretion in* Xanthomonas campestris pv. vesicatoria *Depends on an Internal Translation Start Site***
Christian Otten, Tanja Seifert, Jens Hausner and Daniela Büttner

83 ***The Cytoplasmic Domains of* Streptococcus mutans *Membrane Protein Insertases YidC1 and YidC2 Confer Unique Structural and Functional Attributes to Each Paralog***
Surabhi Mishra and L. Jeannine Brady

103 ***Roles of Type VI Secretion System in Transport of Metal Ions***
Xiaobing Yang, Hai Liu, Yanxiong Zhang and Xihui Shen

110 ***Pushing the Envelope: The Mysterious Journey Through the Bacterial Secretory Machinery, and Beyond***
Lucy Troman and Ian Collinson

122 ***Secretion Systems in Gram-Negative Bacterial Fish Pathogens***
Sophanit Mekasha and Dirk Linke

150 ***The Impact of* Bartonella *VirB/VirD4 Type IV Secretion System Effectors on Eukaryotic Host Cells***
Katja Fromm and Christoph Dehio

158 ***Expression, Localization, and Protein Interactions of the Partitioning Proteins in the Gonococcal Type IV Secretion System***
Melanie M. Callaghan, Birgit Koch, Kathleen T. Hackett, Amy K. Klimowicz, Ryan E. Schaub, Natalio Krasnogor and Joseph P. Dillard

174 ***Oligomerization of the FliF Domains Suggests a Coordinated Assembly of the Bacterial Flagellum MS Ring***
Giuseppina Mariano, Raquel Faba-Rodriguez, Soi Bui, Weilong Zhao, James Ross, Svetomir B. Tzokov and Julien R. C. Bergeron

186 *The Trimeric Autotransporter Adhesin YadA of* Yersinia enterocolitica *Serotype O:9 Binds Glycan Moieties*
Ina Meuskens, Juan Leva-Bueno, Paul Millner, Monika Schütz, Sally A. Peyman and Dirk Linke

198 *Identification of Type VI Secretion Systems Effector Proteins That Contribute to Interbacterial Competition in* Salmonella *Dublin*
Fernando A. Amaya, Carlos J. Blondel, María F. Barros-Infante, Dácil Rivera, Andrea I. Moreno-Switt, Carlos A. Santiviago and David Pezoa

211 *A Surface Exposed, Two-Domain Lipoprotein Cargo of a Type XI Secretion System Promotes Colonization of Host Intestinal Epithelia Expressing Glycans*
Alex S. Grossman, Cristian A. Escobar, Erin J. Mans, Nicholas C. Mucci, Terra J. Mauer, Katarina A. Jones, Cameron C. Moore, Paul E. Abraham, Robert L. Hettich, Liesel Schneider, Shawn R. Campagna, Katrina T. Forest and Heidi Goodrich-Blair

frontiers | Frontiers in Microbiology

EDITORIAL
published: 24 May 2022
doi: 10.3389/fmicb.2022.917591

Editorial: Bacterial Secretion Systems, Volume II

Ignacio Arechaga[1]* *and Eric Cascales*[2]*

[1] *Departamento de Biología Molecular, Instituto de Biomedicina y Biotecnología de Cantabria (IBBTEC), Universidad de Cantabria-CSIC, Santander, Spain,* [2] *Laboratoire d'Ingénierie des Systèmes Macromoléculaires, Institut de Microbiologie, Bioénergies et Biotechnologie, CNRS—Aix-Marseille Université, Marseille, France*

Keywords: secretion systems, bacteria, structural biology, microbiology, biochemistry

Editorial on the Research Topic

Bacterial Secretion Systems, Volume II

In 2019, a first volume of the Research Topic "*Bacterial Secretion Systems*" was published in Frontiers in Microbiology. This volume was comprised of 22 articles covering different aspects of bacterial secretion systems, offering a broad view on these multiprotein complexes responsible for the delivery of effectors in the environment or into target cells. In this second issue, which groups 15 articles, further insights on these fascinating nanomachines are uncovered.

Bacteria have developed sophisticated machineries to interact with the surrounding environment and with other cells. Some of these systems, like the Tat export pathway or the Sec machinery, broadly distributed in bacteria, are dedicated to protein translocation across or protein insertion into the cytoplasmic membrane. In addition, bacteria have evolved a vast repertoire of secretion pathways to transport effectors across the cell envelope. Up to date, 11 different secretion pathways (T1SS–T11SS), involved in substrate transport, protein exposition at the cell surface, pili assembly and motility, have been described. The T1SS, T3SS, T4SS and T6SS are large multiprotein complexes that span both the inner and outer membranes of Gram-negative bacteria and are thus capable to translocate effectors in a single step. Other systems, such as T2SS, T5SS, T9SS and T11SS require the assistance of the Sec or Tat export pathway to export first effectors in the periplasm before being selected by the secretion apparatus. Bacterial secretions systems can deliver a broad range of effectors, from small molecules to large macromolecules such as proteins and DNA. The understanding of the biogenesis and the mechanism of action of these secretion systems requires a combination of microbiology, genetics, biochemistry and biophysical approaches. This issue is constituted of four reviews and 11 research articles including two comprehensive bioinformatics studies.

Troman and Collinson provide an extensive review describing the journey of a protein across the cell envelope, emphasizing the molecular complexes responsible for protein export and insertion in the inner and outer membranes, the role of general or dedicated chaperones that assist protein folding and perform quality control and eventually degradation, and how the energy of the inner membrane is mobilized for outer membrane processes.

Two research articles provide novel information on protein export and inner membrane insertion pathways. Zhao et al. report the characterization of a suppressive mutation isolated when the signal recognition particle responsible for co-translational export is missing. They found that this mutation localizes in the Shine Dalgarno sequence of a gene encoding the S10 ribosomal protein, hence leading to a decrease in protein translation rate and accuracy. Mishra and Brady focus on the two YidC proteins encoded by *Streptococcus mutans*, YidC1 and YidC2. By targeting the less-conserved cytoplasmic domains of these proteins and engineering YidC1/YidC2 chimeras, they define specific contributions of these two paralogs in various growth conditions.

Edited and reviewed by:
Marc Strous,
University of Calgary, Canada

***Correspondence:**
Ignacio Arechaga
arechagai@unican.es
Eric Cascales
cascales@imm.cnrs.fr

Specialty section:
This article was submitted to Microbial Physiology and Metabolism, a section of the journal Frontiers in Microbiology

Received: *11 April 2022*
Accepted: *26 April 2022*
Published: *24 May 2022*

Citation:
Arechaga I and Cascales E (2022) Editorial: Bacterial Secretion Systems, Volume II. Front. Microbiol. 13:917591. doi: 10.3389/fmicb.2022.917591

Then, Mekasha and Linke provide a comprehensive review on secretion systems present in bacterial fish pathogens. They show that, such as their plant- or animal-pathogen counterparts, these pathogens use classical secretion systems, to deliver effectors that are key to the infection process. They note an overrepresentation of T6SS and T9SS in Bacteroidetes fish pathogens and of T1SS, T2SS, T3SS and autotransporter pathways in Proteobacterial fish pathogens.

Otten et al. provide novel information on the under characterized platform of plant pathogen T3SSs. They identified an internal translation start site in the *hrcQ* gene, leading to the synthesis of a shorter, C-terminal protein, $HrcQ_C$. This C-terminal domain interacts with and stabilizes the full-length HrcQ protein, and colocalizes with it at the T3SS. Finally, interactions between $HrcQ_C$ and the HrcD and HrpB4 T3SS components were found, suggesting that in addition to its chaperone role on HrcQ, $HrcQ_C$ likely participates as a structural component of the T3SS sorting platform.

It is now commonly admitted that T3SSs and flagellum have coevolved. Mariano et al. focus on the FliF subunit of the flagellum MS ring. They provide evidence on the oligomerization states of the FliF periplasmic Ring-Building Motifs (RBM) demonstrating that contrarily to RBM1, RBM2 and RBM3 form ring-like structures. They also report that RBM1 impacts RBM2 oligomerization and propose a role of the FliF RBMs for assembly of the MS ring and for the different symmetries adopted by these domains. Minamino et al. detail the role of chaperones required for formation of the flagellar filament. They show that three chaperones, FlgN, FliS and FliT are necessary for formation of robust filaments, as a triple mutant yields shorter filaments and releases unassembled filament subunit FliC in large amount in the medium. They then isolated suppressive mutations of the triple mutant, all located in FliC and destabilizing the FliC structure, suggesting that the role of the chaperones is to maintain FliC under an unfolded state for its efficient transport.

YadA is a trimeric autotransporter that serves as adhesin to facilitate adhesion of the bacterial cell onto the target host tissues. Using a battery of *in vivo* and *in vitro* assays, Meuskens et al. demonstrate that the *Yersinia enterocolitica* YadA adhesin does not only interact with host matrix protein such as fibronectin and collagen but also binds to glycan moieties, and notably with the N-linked glycans of the vitronectin and of heparin.

In the following review Yang et al. summarize the current knowledge and discuss the relationship between type VI secretion and metals. The T6SS, which is known as one of the key players in bacterial competition by directly injecting toxic effectors into the target bacterium, also participates to exploitative competition by collecting metals in the environment. They describe how T6SS secretes proteins that bind zinc, manganese, iron, copper or molybdenum, and what are the processes employed to take them back once loaded.

Robinson et al. performed a bioinformatic analyses of type VI secretion system (T6SS) gene clusters in *Campylobacter jejuni* strains to provide information on the prevalence of T6SS gene clusters and their genetic organization. Analyses of the *vgrG* genes and their neighborhoods allowed to list potential effectors with putative nuclease, lipase or peptidoglycan hydrolase activities. Amaya et al. provide evidence that the two T6SS associated to the SPI-6 and SPI-19 islands in the cattle-adapted *Salmonella enterica* Dublin pathogen participate to interbacterial competition. Comparative genomics allowed the authors to identify candidate effectors-immunity pairs, which were further shown to contribute to the antibacterial activity. These two works will be likely the bases for further studies aimed at better understanding the function of these T6SSs and the activities of the effectors delivered by these machines.

Fromm and Dehio review *Bartonella* T4SS effectors and their role on host cells. In addition to carrying a C-terminal bipartite Bep intracellular delivery (BID) domain responsible for selection and transport by the T4SS, most *Bartonella* effectors possess a FIC domain that mediate AMPylation of target proteins in the host. In addition, some T4SS effectors contains phosphorylation motifs that facilitate interaction with host proteins.

Further information on conjugative T4SSs is provided by the next two articles. Carranza et al. engineered functional fluorescent reporter fusions to the TrwB coupling protein and TrwK VirB4-like protein, which both associate to the inner membrane portion of the R388 conjugative T4SS, as well as to the TrwC relaxase. Fluorescence microscopy and super-resolution dSTORM revealed that while TrwC is diffuse in the cytoplasm, TrwB and TrwK localize as patches in the membrane. Interestingly they observed that TrwK segregated in a very few loci per cell, likely marking T4SSs, whereas the number of TrwB foci was much more important, suggesting that TrwB is more labile and can associate/dissociate from the T4SS. Interestingly, the three proteins significantly recoloalize to form polar foci during mating, at the sites of contact with the recipient cell. Callaghan et al. provide information on the ParA and ParB partitioning proteins associated to the T4SS in *Neisseria gonorrhoeae*. They present evidence that ParA and ParB translation is under the control of a riboswitch and that a stem loop in the 5′-UTR region participate in *parAB* regulation. Then then show that both ParA and ParB interact with the TraI relaxase, supporting the hypothesis that the ParAB complex facilitates TraI-mediated nicking at the site of secretion.

Finally, Grossman et al. present new information on the recently identified T11SS. The T11SS is comprised of an outer membrane β-barrel. In *Xenorhabdus nematophila*, the gene encoding the NilB T11SS barrel is coregulated with *nilC*, encoding a lipoprotein. Here, they show that NilC is surface-exposed in both *E. coli* and *X. nematophila* in a NilB-dependent manner, in agreement with the observation that NilC carries a T11SS-targeting C-terminal 8-stranded β-barrel.

Taken together, the reviews and articles published in this issue cover many aspects of macromolecule export and secretion in bacteria, from the prevalence and genetic organization of the gene clusters encoding these machines to mechanistic insights on how effectors are recruited and transported. It also highlights that this topic of research is very active and that many exciting discoveries are ahead of us.

AUTHOR CONTRIBUTIONS

IA and EC were the editors of the Research Topic "*Bacterial Secretion Systems, Volume II*." Both authors contributed to the article and approved the submitted version.

Conflict of Interest: The authors declare that the research was conducted in the absence of any commercial or financial relationships that could be construed as a potential conflict of interest.

Publisher's Note: All claims expressed in this article are solely those of the authors and do not necessarily represent those of their affiliated organizations, or those of the publisher, the editors and the reviewers. Any product that may be evaluated in this article, or claim that may be made by its manufacturer, is not guaranteed or endorsed by the publisher.

frontiers in Microbiology

ORIGINAL RESEARCH
published: 29 June 2021
doi: 10.3389/fmicb.2021.694824

Bioinformatic Analysis of the *Campylobacter jejuni* Type VI Secretion System and Effector Prediction

Luca Robinson[1], Janie Liaw[1], Zahra Omole[1], Dong Xia[2], Arnoud H. M. van Vliet[3], Nicolae Corcionivoschi[4,5], Abderrahman Hachani[6†] and Ozan Gundogdu[1†]*

[1] Faculty of Infectious and Tropical Diseases, London School of Hygiene & Tropical Medicine, London, United Kingdom, [2] Comparative Biomedical Sciences, Royal Veterinary College, London, United Kingdom, [3] School of Veterinary Medicine, Faculty of Health and Medical Sciences, University of Surrey, Guildford, United Kingdom, [4] Bacteriology Branch, Veterinary Sciences Division, Agri-Food and Biosciences Institute, Belfast, United Kingdom, [5] Bioengineering of Animal Science Resources, Banat University of Agricultural Sciences and Veterinary Medicine – King Michael the I of Romania, Timisoara, Romania, [6] The Peter Doherty Institute for Infection and Immunity, Department of Microbiology and Immunology, University of Melbourne, Melbourne, VIC, Australia

OPEN ACCESS

Edited by:
Eric Cascales, Aix-Marseille Université, France

Reviewed by:
Alessia Levante, University of Parma, Italy
Mohamed K. Fakhr, The University of Tulsa, United States

***Correspondence:**
Ozan Gundogdu
ozan.gundogdu@lshtm.ac.uk

† These authors share senior authorship

Specialty section:
This article was submitted to Microbial Physiology and Metabolism, a section of the journal Frontiers in Microbiology

Received: *13 April 2021*
Accepted: *07 June 2021*
Published: *29 June 2021*

Citation:
Robinson L, Liaw J, Omole Z, Xia D, van Vliet AHM, Corcionivoschi N, Hachani A and Gundogdu O (2021) Bioinformatic Analysis of the Campylobacter jejuni Type VI Secretion System and Effector Prediction. Front. Microbiol. 12:694824. doi: 10.3389/fmicb.2021.694824

The Type VI Secretion System (T6SS) has important roles relating to bacterial antagonism, subversion of host cells, and niche colonisation. *Campylobacter jejuni* is one of the leading bacterial causes of human gastroenteritis worldwide and is a commensal coloniser of birds. Although recently discovered, the T6SS biological functions and identities of its effectors are still poorly defined in *C. jejuni*. Here, we perform a comprehensive bioinformatic analysis of the *C. jejuni* T6SS by investigating the prevalence and genetic architecture of the T6SS in 513 publicly available genomes using *C. jejuni* 488 strain as reference. A unique and conserved T6SS cluster associated with the *Campylobacter jejuni* Integrated Element 3 (CJIE3) was identified in the genomes of 117 strains. Analyses of the T6SS-positive 488 strain against the T6SS-negative *C. jejuni* RM1221 strain and the T6SS-positive plasmid pCJDM202 carried by *C. jejuni* WP2-202 strain defined the "T6SS-containing CJIE3" as a pathogenicity island, thus renamed as *Campylobacter jejuni* Pathogenicity Island-1 (CJPI-1). Analysis of CJPI-1 revealed two canonical VgrG homologues, CJ488_0978 and CJ488_0998, harbouring distinct C-termini in a genetically variable region downstream of the T6SS operon. CJPI-1 was also found to carry a putative DinJ-YafQ Type II toxin-antitoxin (TA) module, conserved across pCJDM202 and the genomic island CJIE3, as well as several open reading frames functionally predicted to encode for nucleases, lipases, and peptidoglycan hydrolases. This comprehensive *in silico* study provides a framework for experimental characterisation of T6SS-related effectors and TA modules in *C. jejuni*.

Keywords: *Campylobacter jejuni*, Type VI Secretion System, T6SS effectors, T6SS immunity proteins, toxin-antitoxin, pathogenicity island

INTRODUCTION

Bacterial secretion systems, classified from Type I to X according to their genetic and structural organisation and composition, are protein transport machineries enabling niche colonisation, interaction with host cells, and bacterial antagonism (Costa et al., 2015; Palmer et al., 2021). Genes encoding for the Type VI Secretion System (T6SS) are present in more than 25% of *Proteobacteria* (Bingle et al., 2008; Barret et al., 2013). The injection of a panel of T6SS effectors into competing bacteria promotes the fitness of T6SS-positive strains in polymicrobial environments, including the gut ecosystem (Coulthurst, 2019; Wood et al., 2020). However, the T6SS is not restricted to bacterial antagonism and can mediate host-pathogen interactions. Some T6SS effectors bear anti-eukaryotic activities that subvert the host cell cytoskeleton, evade host defences by countering reactive oxygen species (ROS), and modulate the host inflammatory response (Hachani et al., 2016; Chen et al., 2019).

Despite the multiple roles of T6SSs in complex ecosystems, the genes encoding the T6SS core components are highly conserved into genomic clusters (Coulthurst, 2019). The structure of the T6SS shares features with the bacteriophage T4 contractile apparatus, with structural homology to the phage tail tube and spike proteins (Ho et al., 2014). A fully assembled T6SS apparatus requires a minimal set of 13 core components (Zoued et al., 2014). The machinery is characterised by a puncturing spike (VgrG) that structurally resembles the bacteriophage T4 gp27/gp5 proteins (typically sharpened by a Proline-Alanine-Alanine-Arginine (PAAR) protein), a contractile sheath (formed by the complex TssB and TssC) encasing a needle-like tube (Hcp/TssD) and capped by a core component (TssA) in the cytoplasm. A scaffold formed by a membrane-associated complex (TssJLM) and a cytoplasmic baseplate (TssEFGK) complete the system (**Figure 1**; Leiman et al., 2009; Zoued et al., 2014; Cianfanelli et al., 2016). Upon contraction, the TssBC sheath propels the VgrG-PAAR complex and associated effectors into target cells or the external milieu (Coulthurst, 2019). The contracted sheath can be depolymerised by the ATPase ClpV/TssH and released TssB and TssC subunits are recycled for assembly (Kapitein et al., 2013; Zoued et al., 2014).

Type VI Secretion System effectors exhibit a wide range of functions, mostly anti-bacterial, with some displaying transkingdom activities and few solely targetting eukaryotes (Alteri and Mobley, 2016). To date, T6SS effectors have been shown to harbour functions such as nucleases (Ma et al., 2014; Jana et al., 2019), lipases (Russell et al., 2013; Jiang et al., 2016), peptidoglycan hydrolases (Russell et al., 2011; Whitney et al., 2013), pore-forming activities (English et al., 2012; Fridman et al., 2020), actin cross-linking (Pukatzki et al., 2006), and anti-fungal activities (Trunk et al., 2018, 2019). Translocation of "cargo" effectors is mediated through their non-covalent interaction with Hcp, VgrG, or PAAR proteins, whilst "specialised" effectors consist of catalytic domains covalently fused to Hcp, VgrG, or PAAR proteins (Coulthurst, 2019). Anti-bacterial effector genes are often associated with cognate genes encoding for immunity proteins, producing effector-immunity pairs (Coulthurst, 2019). Immunity proteins are typically located in the cellular compartments targetted by their cognate effectors to prevent self-toxicity (Alcoforado Diniz et al., 2015).

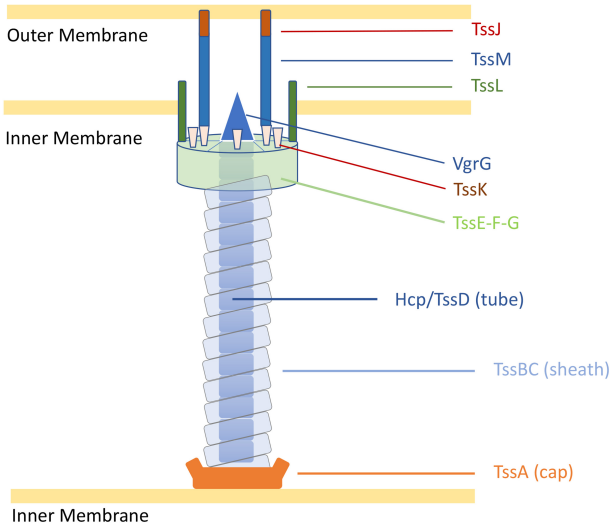

FIGURE 1 | Representation of the *C. jejuni* T6SS in extended state [adapted from Cherrak et al. (2019)]. Proteins are labelled according to the nomenclature used for *C. jejuni* T6SS components. Tss, Type six secretion.

Campylobacter jejuni is a gram-negative microaerophilic bacterium and one of the leading causes of human foodborne gastroenteritis worldwide (Burnham and Hendrixson, 2018). *C. jejuni* is abundant in the chicken gut, making handling and consumption of contaminated poultry products the primary foodborne transmission route to humans (Ijaz et al., 2018; McKenna et al., 2020). Although considered a commensal of the avian gut, *C. jejuni* can be an opportunistic pathogen in birds, depending on the genetics of host and bacterial strain (Humphrey et al., 2014; Wigley, 2015). *C. jejuni* infection in humans can cause bloody diarrhoea, fever, and abdominal pains. In low-resource regions, *C. jejuni* infections are common in young children and correlate with stunted growth and life-long physical and cognitive deficiencies (Amour et al., 2016). In high-resource regions, it is estimated that 1 in every 100 individuals develop a *C. jejuni*-related illness each year (Tam et al., 2012). It is still unclear how avian species can tolerate a high presence of *C. jejuni* without developing overt disease, yet a relatively low infectious dose leads to disease in humans (Gundogdu and Wren, 2020).

In *C. jejuni*, the T6SS biological functions have been associated with host colonisation, cell adhesion and invasion, survival in bile salts, contact-dependent lysis of erythrocytes, and contributing to oxidative stress (Lertpiriyapong et al., 2012; Bleumink-Pluym et al., 2013; Liaw et al., 2019). So far, Hcp has been suggested as a T6SS effector contributing to *C. jejuni* host cell adhesion and invasion (Lertpiriyapong et al., 2012; Bleumink-Pluym et al., 2013; Noreen et al., 2018); however, no evidence currently supports the direct contribution to these phenotypes by Hcp in isolation. Whilst few studies have indicated the prevalence of T6SS in *C. jejuni* (Harrison et al., 2014; Corcionivoschi et al., 2015; Ugarte-Ruiz et al., 2015), a larger

comprehensive bioinformatic analysis of T6SS within *C. jejuni* and the identification of associated effectors are still needed. In this study, we investigated the prevalence and genomic organisation of the T6SS in 513 publicly available *C. jejuni* genomes through screening of the major T6SS components, previously characterised T6SS effectors, and the integrative element *Campylobacter jejuni* Integrated Element 3 (CJIE3). Using *C. jejuni* 488 strain as reference we discovered a novel pathogenicity island (PAI) variant of CJIE3, reclassifying the "T6SS-containing CJIE3" as *Campylobacter jejuni* Pathogenicity Island-1 (CJPI-1). We also observed that two distinct VgrG proteins are present in the PAI of *C. jejuni* 488 strain, with a number of other *C. jejuni* strains also possessing both VgrG proteins. Using bioinformatic analysis, we identified a number of putative T6SS effectors and predicted toxin-antitoxin (TA) modules carried by the CJPI-1 PAI.

MATERIALS AND METHODS

Genome Sequencing, Assembly and Annotation of *C. jejuni* 488 Strain

Genome sequencing was performed as previously described by Ugarte-Ruiz et al. (2015) and adapted for this study. Briefly, paired-end Fastq data was generated on an Illumina MiSeq and assessed using FastQC (Andrews, 2010). Quality control of the sequencing reads was conducted using Trimmomatic (v0.39) ("leading" and "trailing" setting of 5, a "slidingwindow" setting of 4:20 and a "minlength" of 36 nucleotides) (Bolger et al., 2014). Assembly was performed with VelvetOptimiser (v2.2.6) using n50 optimisation and "kmer" length of 37 nucleotides (Zerbino and Birney, 2008; Gladman and Seemann, 2012). Contigs were ordered against T6SS-positive *C. jejuni* M129 strain (accession no. CP007749) (Konkel et al., 1992) using ABACAS (v1.3.1) (Assefa et al., 2009). Annotation of the genome was performed with prokka (v.1.14.6) (Seemann, 2014) using *C. jejuni* NCTC11168 strain (AL111168) (Parkhill et al., 2000). The genome was visualised and manually edited using Artemis and Artemis Comparison Tool (ACT) software (Carver et al., 2005, 2012).

In silico Identification of T6SS-Containing *C. jejuni* Genomes

Nucleotide and amino acid sequences of *C. jejuni* genomes were collected from the NCBI RefSeq genome database release 99 (May 2020) at assembly level "scaffold" or higher (NCBI, 1982b). Reference genomes 108 (JX436460) (Bleumink-Pluym et al., 2013), 43431 (genome sequence from Liaw et al., 2019), and the newly assembled 488 strain were also included into the genome dataset and a local nucleotide and protein database was constructed. Our local database was then filtered to remove genomes that possessed any of the following traits: a total genome size greater than 2 Mb, no assembly protein sequence data available to download from the RefSeq database, a total assembly possessing more than 200 contigs, or the genome possessed an Average Nucleotide Identity (ANI) of less than 95%. ANI was calculated using FastANI with a fragment length of 1000 bp against the reference *C. jejuni* NCTC11168 (AL111168) strain (Jain et al., 2018). A total of 41 genomes were removed from the dataset. Metadata, including host and sample location, was collected from the NCBI BioSample database (NCBI, 1982a). Genome visualisation was performed in Artemis (Carver et al., 2012).

BLASTP (Altschul et al., 1990) was employed to identify the 13 T6SS components amongst the *C. jejuni* genomes, using default parameters. The amino acid sequences of the 13 T6SS loci from reference strain 108 (JX36460), which carries a functional T6SS, was aligned against a local protein dataset created for the *C. jejuni* genomes (Bleumink-Pluym et al., 2013). A similarity percentage was calculated by dividing the bit-score value for each amino acid alignment by two times the specific lengths of the individual query amino acid sequence (Fridman et al., 2020). Protein presence was regarded positive when a minimum of 50% similarity was observed. *C. jejuni* genomes possessing at least 11 out of the 13 T6SS loci were considered to contain a T6SS (T6SS-positive), and those that possessed fewer than 11 were considered lacking a T6SS (T6SS-negative).

Identification of PAAR-Containing Proteins and Characterised T6SS Effectors

BLASTP (Altschul et al., 1990) was employed to identify the presence of PAAR-motif containing proteins and known T6SS effectors in the local *C. jejuni* genome database. Representative amino acid sequences from the NCBI-CDD were downloaded for the protein subclasses PAAR1, PAAR2, PAAR3, PAAR4, PAAR5, PAAR-Rhs, PAAR-CT1, and PAAR-CT2 (Marchler-Bauer et al., 2017; **Supplementary Data 1**). Amino acid sequences characterised as T6SS "cargo" effectors were downloaded from the NCBI Protein database (NCBI, 1982c; **Supplementary Table 1**). Proteins designated as "cargo" are independent effectors that do not exist as toxin domain-containing extensions of the major T6SS components Hcp, VgrG or PAAR. The amino acid sequences were aligned against a local protein dataset created for the *C. jejuni* genomes. A minimum threshold expected value of 1e-10 was implemented in the search where a value below this threshold was deemed a positive hit.

In silico Identification of CJIE3-Containing Genomes

To identify the presence of CJIE3 in the *C. jejuni* genome dataset, the gene *cje1094* (integrase) from reference strain RM1221 (CP000025) [denoted as a suitable candidate for PCR-identification of CJIE3 by Parker et al. (2006)], and genes *cje1105* and *cje1153*, were used in an *in silico* identification method. BLASTN (Altschul et al., 1990) was employed to align the nucleotide sequence of the genes against the local nucleotide dataset created for the *C. jejuni* genomes. A similarity percentage was calculated according to Fridman et al. (2020). To be regarded as positive for CJIE3, a minimum similarity of 50% was required to two of the three genes: *cje1094*, *cje1105*, and/or *cje1153*. To be regarded as possessing a T6SS-harbouing

plasmid, a minimum similarity of 50% was required to only gene *cje1094* and the presence of at least 11 T6SS loci (T6SS-positive). *C. jejuni* 108 strain was excluded from this analysis as it does not possess a whole genome sequence, thus reducing this analysis to 512 genomes.

Comparative Analysis and Alignment of *C. jejuni* Genomes and Plasmids

Artemis Comparison Tool and Clinker (Carver et al., 2005; Gilchrist and Chooi, 2021) were used to comparatively align the genome of the re-sequenced and assembled T6SS-positive *C. jejuni* 488 strain against strain RM1221 (CP000025) and annotated plasmid pCJDM202 (CP014743) (Fouts et al., 2005; Marasini and Fakhr, 2016). Amino acid identity was calculated with BLAST Global Alignment–Protein (Needleman-Wunsch Global Align), using default parameters (Altschul et al., 1990).

Functional Analysis of Predicted Proteins in CJPI-1

Webtools NCBI CDD-BLAST (Marchler-Bauer et al., 2017), SMART (Letunic and Bork, 2018), HmmScan (Potter et al., 2018), Pfam (El-Gebali et al., 2019), SCANPROSITE (de Castro et al., 2006), CDART (Geer et al., 2002), SUPERFAMILY (Gough et al., 2001), InterPro (Mitchell et al., 2019), and MOTIF (GenomeNet, 2015) were used to identify protein domains and characteristic motifs in the CJPI-1 predicted proteins. Signal peptides, transmembrane helices, and subcellular localisation were predicted using Psortb v3.0 (Yu et al., 2010), CELLO v2.5 (Yu et al., 2006), SignalP-5.0 (Armenteros et al., 2019), TMPred (Hofmann and Stoffel, 1993), and TMHMM (Sonnhammer et al., 1998) to assist in protein function prediction. Default parameters were used throughout, with an expected value (*E*-value) of 0.01 determined as a cut-off and organism group defined as Gram-negative where required. Protein functions were inferred following congruent predictions from at least 5 out of the 9 used webtools (**Supplementary Tables 2**, **3**). Structural homology modelling was performed using the Phyre2 and I-Tasser servers (Zhang, 2008; Kelley et al., 2015).

Characterisation of *vgrG* Genes in *C. jejuni* 488 Strain

To assess sequence identity, amino acid sequences for proteins encoded by *vgrG1* and *vgrG2* in *C. jejuni* 488 strain were analysed by BLASTP (Altschul et al., 1990) against the NCBI reference protein database, excluding *C. jejuni* to prevent self-hits. Multiple sequence alignment of *vgrG1* and *vgrG2* was conducted using Clustal Omega (Madeira et al., 2019).

BLASTN (Altschul et al., 1990) was employed to identify *vgrG* genes amongst the *C. jejuni* genomes. The nucleotide sequence of the *vgrG* gene from the T6SS-positive 108 strain (JX436460) was aligned against a local nucleotide dataset created for the T6SS-positive *C. jejuni* genomes of assembly level "complete" or higher (Bleumink-Pluym et al., 2013). A cut-off similarity percentage was calculated according to Fridman et al. (2020). To be regarded as positive for a *vgrG* gene, a minimum similarity of 50% was required. Full length VgrG protein sequences were then obtained from T6SS-positive assembly level genomes "complete" or higher and aligned using MUSCLE (Edgar, 2004) with default parameters. Genomes CJ017CC464, CJ018CCUA, and ZS007 were removed from the analysis due to disrupted open reading frames (ORFs). A phylogenetic tree was constructed from the alignment file using the Maximum-Likelihood method, with JTT modelling, partial deletion (95%), and bootstrapping (n = 500) parameters, conducted in the Molecular Evolutionary Genetics Analysis X (MEGAX) v. 10.1.8 software package (Kumar et al., 2018). The analysis contained 36 amino acid sequences.

Identification of Catalytic Residues in Putative T6SS Effectors

The amino acid sequences of the query proteins were searched against the NCBI-CDD (Marchler-Bauer et al., 2017), and the subsequent output alignments corresponding to identified domains were extracted and annotated to identify the conserved catalytic residues described (Zhang et al., 2012; Sun et al., 2015; Tak et al., 2019).

Prevalence of CJPI-1 Functionally Predicted Proteins Within the *C. jejuni* Protein Database

BLASTP (Altschul et al., 1990) was employed to identify the presence and genomic context of the CJPI-1 functionally predicted proteins amongst the *C. jejuni* genome database. The amino acid sequences were aligned against the local protein dataset created for the *C. jejuni* genomes. A similarity percentage was calculated according to Fridman et al. (2020). Protein presence regarded as positive required a minimum similarity of 50%. *C. jejuni* 108 strains was excluded from this analysis as it does not possess a whole genome sequence, therefore this analysis involved 512 genomes.

RESULTS AND DISCUSSION

Prevalence of the T6SS in *C. jejuni*

We have determined the prevalence of the T6SS in publicly available *C. jejuni* genomes (**Supplementary Table 4**) by compiling a local dataset of nucleotide and amino acid sequences from isolates with an assembly level "scaffold" or higher from the NCBI RefSeq genome database. This was further populated with *C. jejuni* 108 and 43431 reference strains and the newly assembled 488 strain, creating a total of 513 genomes. The prevalence study of 13 T6SS core components (TssA-TssM) against our local *C. jejuni* database classified 136 of the 513 (26.51%) *C. jejuni* genomes as T6SS-positive and 377 of the 513 (73.49%) as T6SS-negative (**Supplementary Tables 5**, **6**). Interestingly, two T6SS-negative *C. jejuni* strains, 255 and 10186, were found to possess 10 out of the 13 T6SS genes, with the genes *tagH*, *tssG*, and *vgrG* missing. Furthermore, the genome of *C. jejuni* OXC6589 strain was identified as the only one without a T6SS complete cluster to present the gene *hcp*. Our analysis of *C. jejuni* strains identified a single copy of the T6SS operon, with a conserved set of T6SS core genes sharing synteny with closely related species (**Table 1**). To

TABLE 1 | *C. jejuni* and *C. coli* strains studied to date with a T6SS.

Strain	Source	Country	References
C. jejuni 488	Human	Brazil	Liaw et al., 2019
C. jejuni 43431	Human	Canada	Penner et al., 1983
C. jejuni RC039	Chicken	United Kingdom	Corcionivoschi et al., 2015
C. jejuni 108	Human	United Kingdom	Bleumink-Pluym et al., 2013
C. jejuni 414	Bank vole	United Kingdom	Lertpiriyapong et al., 2012
C. coli RM2228	Chicken	United States	Bleumink-Pluym et al., 2013

date, all T6SS core structural components have been identified in *C. jejuni* with the exception of TssH (ClpV), the ATPase responsible for disassembly of the contracted sheath components, which is absent from all sequenced *C. jejuni* T6SS operons. This raises the possibility of an alternative mode of sheath disassembly, or the existence of a ClpV-like ATPase encoded distally from the T6SS cluster (Liaw et al., 2019).

Absence of Characterised T6SS Effectors in *C. jejuni* Genomes

Hitherto, no T6SS-associated effectors have been identified and/or characterised in T6SS-positive *C. jejuni* (Lertpiriyapong et al., 2012; Bleumink-Pluym et al., 2013; Liaw et al., 2019). Using 40 characterised 'cargo' effectors from a range of bacteria including *Pseudomonas aeruginosa*, *Serratia marcescens*, *Yersinia pseudotuberculosis*, and *Burkholderia thailandensis* (**Supplementary Table 1**), we performed BLASTP-homology searches for the presence of such effectors within *C. jejuni* strains. Searches returned no positive matches leading us to conclude that T6SS-containing *C. jejuni* may possess a subset of unique "cargo" effectors.

T6SS-Containing *Campylobacter jejuni* Integrated Element 3 Represents a Novel Pathogenicity Island Variant

The initial study of the T6SS in *C. jejuni* revealed its integration within the earlier acquired CJIE3; a genomic island displaying a mosaic gene arrangement and present in a number of *C. jejuni* strains, including RM1221 (a T6SS-negative *C. jejuni* strain) (Fouts et al., 2005; Bleumink-Pluym et al., 2013). Distribution analyses of CJIE3 in *C. jejuni* from human and avian isolates report varying prevalence of this integrated element, with only 10% of CJIE3 harbouring a T6SS (Bleumink-Pluym et al., 2013; Kovanen et al., 2019). In this study, we screened the CJIE3 integrase, *cje1094*, and genes *cje1105* and *cje1153*, using an *in silico* identification method against a local *C. jejuni* database as proxies for CJIE3 identification (**Supplementary Tables 8–10**). Integrase *cje1094* possesses strong homology to *A0W69_09480* harboured on the T6SS-positive megaplasmid pCJDM202 (**Table 2**), therefore, we included two further proxies to distinguish between T6SS-containing CJIE3 and T6SS-harbouring plasmids. We observed that 146 of the 512 (28.51%) genomes possessed the CJIE3, of which 117 (80.14%) were T6SS-positive (**Supplementary Table 4**). Therefore, 117 of the 135 (86.67%) T6SS-positive genomes were identified to possess the CJIE3 and 15 (2.93%) were found harbouring T6SS-positive plasmids (**Table 3**). Integration of the *C. jejuni* T6SS was described as occurring between homologues of the genes *cje1139* and *cje1141/cje1142* from the CJIE3 in RM1221 (Bleumink-Pluym et al., 2013). The genes *cje1141* and *cje1142* share homology to the major T6SS component *tssI/vgrG* and possess *rhs* (rearrangement hotspots) signatures, suggested to have mediated the integration of the T6SS into CJIE3 (Hill, 1999; Jackson et al., 2009; Bleumink-Pluym et al., 2013). Our data supports the findings that the T6SS has been integrated into the CJIE3, as a significant proportion of the T6SS-positive strains in this study also possess the CJIE3. Furthermore, we identified a number of CJIE3-positive genomes that do not possess a complete T6SS cluster, further supporting that integration of the T6SS has occurred subsequently to the acquisition of the integrated element (**Supplementary Table 4**; Bleumink-Pluym et al., 2013).

C. jejuni Integrated Element 3 belongs to a large family of mobile genetic elements (MGEs) and, as observed in integrative and conjugative elements, could potentially operate horizontal transfer of DNA regions between bacterial species during extended periods of close proximity (Dobrindt et al., 2004; Johnson and Grossman, 2015). MGEs can also exist as PAIs; a large subset of integrative elements (>10 kb) carrying virulence genes, such as secretion systems and their cognate effectors (Jarvis et al., 1995; da Cruz Campos et al., 2020). Members of the order *Bacteroidales* can display three different "genetic architectures," with two of these (GA1 and GA2) found on integrative conjugative elements (Coyne et al., 2016). CJIE3 shares sequence homology with proteins encoded on the *Campylobacter coli* RM2228 megaplasmid and 71-kb pathogenicity island HHGI1 of *Helicobacter hepaticus* ATCC51449, the latter possessing a T6SS (Fouts et al., 2005; Bartonickova et al., 2013). Interestingly, several *C. jejuni* megaplasmids also carry T6SS genes (Gunther et al., 2016; Marasini and Fakhr, 2016, 2017). Most recently, megaplasmids pCJDM202 and pCJDM67L from *C. jejuni* WP2-202 and OD2-67 strains, respectively, were found to harbour the T6SS cluster, along with the tetracycline resistance gene *tetO*, and T4SS conjugative DNA transfer systems (Marasini et al., 2020). The authors demonstrated that the presence of the T6SS on the megaplasmids contributed to enhanced haemolysis, suggested to support the survival of *C. jejuni* in retail meats (Marasini et al., 2020).

A newly re-sequenced and assembled genome of the T6SS-positive *C. jejuni* 488 strain was thus comparatively analysed against the genome of T6SS-negative *C. jejuni* RM1221 strain and T6SS-positive virulence megaplasmid pCJDM202 to investigate the genomic architecture and integration of the T6SS into the CJIE3 of *C. jejuni* (**Figure 2**). We propose to reclassify the T6SS-containing genomic island in the same chromosomal location as CJIE3 (between arginyl-tRNA-3 and *cje1156* in RM1221) as a new PAI-variant designated as CJPI-1. We observed that the ∼70 kb PAI is longer than the ∼50 kb CJIE3 of RM1221, containing an integrase/recombinase (*CJ488_0930*) gene (discussed below) and, like CJIE3, is located immediately adjacent to the chromosomal arginyl-tRNA (**Table 4**). The G + C% contents of both CJPI-1 and CJIE3 are lower than the average content of the 488 and RM1221

TABLE 2 | Predicted proteins in CJPI-1 of T6SS-positive *C. jejuni* 488 strain with the respective amino acid length and inferred function. Protein locus tags of homologous proteins found in the CJIE3 of RM1221 and pCJDM202 of WP2-202 are shown with the respective amino acid (aa) identity (%).

Locus (488)	Length (AA)	Putative function	Locus (RM1221)	AA identity (%) with RM1221	Locus (pCJDM202)	AA identity (%) with pCJDM202
CJ488_0928	35		CJE1092	97	–	–
CJ488_0929	116		CJE1093	100	A0W69_09485	63
CJ488_0930	312	*Integrase/Recombinase*	CJE1094	70	A0W69_09480	97
			CJE1095	26		
CJ488_0931	76		CJE1096	100	A0W69_09475	100
CJ488_0932	64	*WGR domain-like containing protein*	–	–	A0W69_09470	81
CJ488_0933	38		CJE1097	97	–	–
CJ488_0934	47		CJE1098	83	–	–
CJ488_0935	69	*Fic domain-containing protein*	CJE1100	68	–	–
CJ488_0936	46		CJE1101	57	–	–
CJ488_0937	75	*DinJ*	CJE1102	97	A0W69_09400	99
CJ488_0938	93	*YafQ endoribonuclease toxin*	CJE1103	92	A0W69_09395	99
CJ488_0939	40		–	–	–	–
CJ488_0940	52		CJE1105	28	–	–
CJ488_0941	99		CJE1105	51	–	–
CJ488_0942	58		CJE1106	43	–	–
CJ488_0943	70		CJE1106	52	–	–
CJ488_0944	572	*Conjugative transfer TraG-like protein*	CJE1107	92	A0W69_09385	58
CJ488_0945	267		CJE1109	97	A0W69_09380	98
CJ488_0946	433		CJE1110	67	A0W69_09375	67
			CJE1111	89	A0W69_09045	89
CJ488_0947	1140		CJE1112	20	A0W69_09050	98
			CJE1113	67		
CJ488_0948	359		CJE1114	74	A0W69_09055	94
					A0W69_09360	67
CJ488_0949	259		–	–	–	–
CJ488_0950	167		–	–	–	–
CJ488_0951	46		–	–	–	–
CJ488_0952	167		–	–	–	–
CJ488_0953	169		–	–	–	–
CJ488_0954	192		–	–	–	–
CJ488_0955	506		–	–	–	–
CJ488_0956	90		–	–	–	–
CJ488_0957	507	*Lipase (class 3) domain-containing protein*	CJE1115	64	A0W69_09355	62
CJ488_0958	130		–	–	–	–
CJ488_0959	178		–	–	–	–
CJ488_0960	41		–	–	–	–
CJ488_0961	225	*Lipase (class 3) domain-containing protein*	–	–	–	–
CJ488_0962	195	*Phage lysozyme-like containing protein*	–	–	–	–
CJ488_0963	119		–	–	–	–
CJ488_0964	1310		CJE1137	98	A0W69_09370	94
CJ488_0965	422		CJE1138	93	A0W69_09375	74
					A0W69_09045	54
CJ488_0966	299	*TagH*	CJE1139	100	A0W69_09040	100
CJ488_0967	1175	*TssM*	–	–	A0W69_09035	100
CJ488_0968	171	*Hcp*	–	–	A0W69_09030	99
CJ488_0969	257	*TssL*	–	–	A0W69_09025	100
CJ488_0970	465	*TssK*	–	–	A0W69_09020	100

(Continued)

TABLE 2 | Continued

Locus (488)	Length (AA)	Putative function	Locus (RM1221)	AA identity (%) with RM1221	Locus (pCJDM202)	AA identity (%) with pCJDM202
CJ488_0971	148	*TssJ*	–	–	A0W69_09015	99
CJ488_0972	415	*TssA*	–	–	A0W69_09010	99
CJ488_0973	161	*TssB*	–	–	A0W69_09005	100
CJ488_0974	484	*TssC*	–	–	A0W69_09000	100
CJ488_0975	130	*TssE*	–	–	A0W69_08995	99
CJ488_0976	573	*TssF*	–	–	A0W69_08990	100
CJ488_0977	302	*TssG*	–	–	A0W69_08985	99
CJ488_0978	883	*VgrG1*	CJE1141	53	A0W69_08980	76
CJ488_0979	317	*Ankyrin domain containing protein*	–	–	–	–
CJ488_0980	438	*Tox-REase-7 domain containing protein*	–	–	–	–
CJ488_0981	189		–	–	–	–
CJ488_0982	564	*Tox-REase-7 domain containing protein*	–	–	–	–
CJ488_0983	241	*Ankyrin-like protein*	–	–	–	–
CJ488_0984	53		–	–	–	–
CJ488_0985	154		–	–	–	–
CJ488_0986	416		–	–	–	–
CJ488_0987	116		–	–	–	–
CJ488_0988	121	*TNT domain-containing protein*	–	–	–	–
CJ488_0989	184		–	–	–	–
CJ488_0990	178		–	–	A0W69_08930	49
CJ488_0991	90		–	–	–	–
CJ488_0992	128		–	–	–	–
CJ488_0993	185		–	–	–	–
CJ488_0994	123	*AHH-nuclease domain-containing protein*	–	–	A0W69_08930	41
CJ488_0995	188		–	–	A0W69_08925	86
CJ488_0996	116	*DUF4299 family protein*	–	–	A0W69_08920	100
CJ488_0997	210		–	–	A0W69_08915	99
CJ488_0998	838	*VgrG2*	CJE1141	56	A0W69_08980	98
			CJE1142	35	A0W69_08910	35
CJ488_0999	245		CJE1150	60	–	–
CJ488_1000	57		–	–	–	–
CJ488_1001	286		–	–	–	–
CJ488_1002	650		CJE1151	43	A0W69_08945	51
CJ488_1003	424		CJE1152	55	–	–
CJ488_1004	415		CJE1153	96	–	–

genomes, respectively, confirming the hypothesis that both inserted genetic elements could be considered as independently acquired. Furthermore, a direct repeat sequence designated as the attachment (*att*) sites, "TCCTCTTGAGCGCACCAT," flanks both sides of the CJPI-1 and CJIE3 islands. Given the similarities between the integrated islands, CJPI-1 is most likely a derivative of CJIE3 that has undergone multiple recombination and/or genetic exchange events. We also discovered that only 30 proteins encoded in CJPI-1 share homology with those encoded in the CJIE3 of RM1221, highlighting differences in genetic composition (**Table 2**). Unlike CJIE3, CJPI-1 satisfies criteria commonly used to classify PAIs with the possession of the major T6SS components and putative effectors (discussed below). PAIs in other bacteria have also been found to carry T6SS clusters. Notably, HHGI-1 of *H. hepaticus* ATCC 51449 possesses a T6SS with a similar gene organisation to *C. jejuni* (Nano and Schmerk, 2007; Barker et al., 2009; Blondel et al., 2009; Bleumink-Pluym et al., 2013). In all, this data confirms that CJPI-1 can be considered as a *bona fide* PAI.

Comparative analysis of the CJPI-1 to the virulence plasmid pCJDM202 also revealed striking genetic similarities (**Figure 2**). 35 genes in CJPI-1 matched in pCJDM202, including the T6SS and several genes also found in the CJIE3 (**Table 2**). Interestingly, the T6SS of CJPI-1 and pCJDM202 share 96% nucleotide similarity across the entire gene cluster. Collectively, this data suggests that CJPI-1 may be resulting from a recombination event

TABLE 3 | *C. jejuni* strains containing CJIE3 by presence or absence of a T6SS.

Strain identity	No. of strains/total number of strains (%)		
	CJIE3+	CJIE3−	T6SS-harbouring plasmid
T6SS+	117/512 (22.85)	3/512 (0.59)	15/512 (2.93)
T6SS−	29/512 (5.66)	348/512 (67.97)	N/A
Total	146/512 (28.51)	351/512 (68.55)	15/512 (2.93)

of the CJIE3 and a T6SS-containing pCJMD202-like plasmid, leading to the acquisition and integration of the T6SS. However, further analyses are required to understand the genetic events leading to the acquisition of putative effectors (discussed below) which may have occurred through uptake events (mediated by prophages and plasmids conjugation).

Functionally Predicted Proteins Encoded in CJPI-1

Following the identification of this PAI-variant of CJIE3, we set out to bioinformatically investigate the genes encoded in CJPI-1 and assess their genomic context in relation to the PAI and/or T6SS operon. We identified several genes encoding for integrative elements, TA modules, and putative effectors (**Table 2** and **Figure 3**).

Integrase

A putative integrase/recombinase (*CJ488_0930*) was identified within CJPI-1, possessing homology to the CJE1094 integrase (70% aa identity) and CJE1095 (26% aa identity) of RM1221, and A0W69_09480 (97% aa identity) from pCJDM202. The CJPI-1 integrase exhibits a Phage_Integrase (PF00589) and a tyrosine recombinase XerD (TIGR02225) domain and is likely a combination of CJE1094 and CJE1095 proteins. Both domains belong to the C-terminal catalytic domains of the DNA breaking-rejoining enzymes superfamily (cl00213). Proteins of this family catalyse recombination of DNA, possessing site-specific integration functions identified in chromosomes, plasmids, and phage genomes (Nash, 1996; Grainge and Jayaram, 1999; Huber and Waldor, 2002). It is predicted that the CJPI-1 and CJIE3 homologous integrases may be responsible for the horizontal transfer and chromosomal integration of the genomic islands to naïve strains at *att* sites (Santoriello et al., 2020).

Toxin-Antitoxin Modules

CJ488_0935, encoded in CJPI-1, was predicted to belong to the globular Fic/Doc (PF02661) family, harbouring the conserved Fic-motif H-x-F-x-[DE]-[AG]-N-[GK]-R, including the catalytic histidine residue which contributes to AMPylation activity (Sprenger et al., 2017; Veyron et al., 2018). Within our local database, 61 out of the 512 (11.91%) genomes were found to possess the protein CJ488_0935, of which 37 were T6SS-positive (60.66%) and 24 were T6SS-negative (39.34%). Of the T6SS-negative genomes, 12 out of the 24 were found to contain the CJIE3 (**Supplementary Table 11**). The protein CJE1100 from RM1221 also shares homology to CJ488_0935 (68% aa identity). Identified in a number of bacterial virulence factors (including Type III and IV secreted effectors), the AMPylation activity of Fic proteins have been demonstrated to catalyse the post-translational modifications of host proteins. Such activity leads to cytotoxicity of targetted host cells, as demonstrated in VopS from *Vibrio parahaemolyticus* and IbpA from *Haemophilus somnus* (Schmid et al., 2006; Worby et al., 2009; Yarbrough et al., 2009; Engel et al., 2012).

Fic domains can also be found as part of Type II TA toxin modules, as recently discovered in *Campylobacter fetus* (Goepfert et al., 2013; Sprenger et al., 2017). TA modules consist of a pair of antagonistic genes that encode for a stable toxin and adjacent, unstable antitoxin (Page and Peti, 2016). Many bacterial and archaeal chromosomes bear TA modules, with roles ranging from plasmid inheritance, MGE stability, growth arrest, and control to stress responses (Leplae et al., 2011; Page and Peti, 2016; Fraikin et al., 2020). Type II TA modules are the most widely studied TA systems in bacteria and have been identified to maintain and stabilise integrative elements, as well as involved to increase colonisation and virulence in pathogenic bacteria (Wozniak and Waldor, 2009; Leplae et al., 2011; Norton and Mulvey, 2012). TA

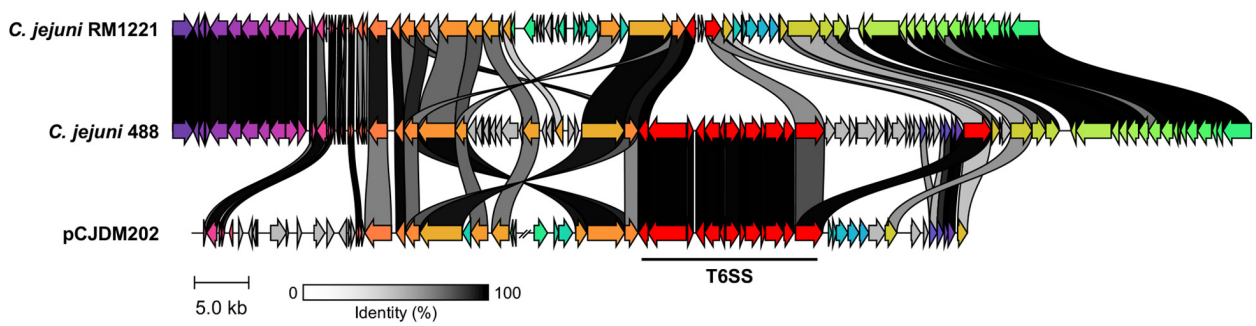

FIGURE 2 | Comparative analyses of CJPI-1 (middle) from T6SS-positive *C. jejuni* 488 strain to CJIE3 from T6SS-negative strain RM1221 (top) and T6SS-positive megaplasmid pCJDM202 (bottom) from *C. jejuni* WP2-202 strain. Homologous genes across the three strains share the same arrow colour and are connected by shaded bands corresponding to sequence identity (black = 100%, white = 0%). Red arrows represent major T6SS components. Sequences found in only one strain possess a grey arrow. Only regions of the megaplasmid associated with the T6SS and CJIE3/CJPI-1 regions have been included. The figure was constructed using Clinker.

TABLE 4 | Comparative overview of the sequence, gene content, and synteny characteristics of the CJPI-1 from *C. jejuni* 488 strain and CJIE3 from RM1221.

Characteristics	CJPI-1 (488)	CJIE3 (RM1221)
Length	∼70.3 kb	∼50.8 kb
CDS	77	62
Adjacent tRNA locus	Arginyl-tRNA	Arginyl-tRNA
Integrase locus tag	CJ488_0930c	CJE1094
G + C content	26.73%	26.62%
Genome G + C content	30.26%	30.31%
Flanking repeat sequence	TCCTCTTGAGCGCACCAT	TCCTCTTGAGCGCACCAT
Virulence factors	T6SS, putative effectors/toxins	N/A

modules have been characterised in *C. jejuni*, as observed in the pVir plasmids of 81-176 and IA3902 strains, and more recently in the YH002 strain isolated from retail beef liver (Shen et al., 2016; Ghatak et al., 2020).

Here, bioinformatic analysis inferred CJ488_0937 and CJ488_0938 as a putative Type II TA module, with the latter found to contain a predicted YafQ_toxin (PF15738) domain. YafQ toxins exhibit endoribonuclease activity and acts as the toxin component, with its activity inhibited by the cognate antitoxin DinJ (Motiejunaite et al., 2007; Prysak et al., 2009). Homologous proteins to CJ488_0938 were also found in RM1221 and pCJDM202, sharing 92 and 99% amino acid identity to CJE1103 and A0W69_09395, respectively. Within our local *C. jejuni* database, 95 out of the 512 (18.55%) genomes were found to possess the protein CJ488_0938, of which 64 were T6SS-positive (67.37%) and 31 were T6SS-negative (32.63%). Of the T6SS-negative genomes, 13 out of the 31 were found to contain the CJIE3 (**Supplementary Table 11**). The protein encoded by the upstream gene *CJ488_0937* (**Figure 3**) also shared an amino acid identity of 97% and 99% to proteins CJE1102 and A0W69_09400, respectively. CJ488_0937 does not possess any identifiable domains, therefore, we performed structural homology modelling of CJ488_0937 in the Phyre2 and I-Tasser servers using the amino acid sequence as a template (Zhang, 2008; Kelley et al., 2015). I-Tasser confidently identified the *Escherichia coli* DinJ-YafQ Type II TA complex (PDB: 4Q2U, Z-score: 1.60) as the most suitable candidate template for modelling, with an exclusive alignment to the DinJ antitoxin (PDB: 4Q2U_1) amino acid sequence. Further, both servers generated models with two predicted helix-turn-helix motifs suggesting, a DNA-binding function commonly identified in type II antitoxins (Aravind et al., 2005; Page and Peti, 2016). This is consistent with the DNA-binding ability and subsequent transcriptional autorepression activity of DinJ, the YafQ antitoxin (Ruangprasert et al., 2014). These elements suggest CJ488_0937 may be acting as the cognate DinJ antitoxin, with experimental confirmation warranted to validate these roles. To our knowledge, this is the first report of a DinJ-YafQ TA module in *Campylobacter* spp.

Conjugative Systems

The protein encoded by the gene *CJ488_0944* was predicted to contain a TraG N-terminal region (PF07916) domain and shares homology to proteins CJE1107 (92% aa identity) and A0W69_09385 (58% aa identity) from RM1221 and pCJDM202, respectively, with the latter annotated as a conjugation transfer protein TraG (Marasini and Fakhr, 2016). Within our local *C. jejuni* database, 93 out of the 512 (18.16%) genomes were found to possess the protein CJ488_0944 (average per genome = 1.04), of which 33 were T6SS-positive (35.48%) and 60 were T6SS-negative (64.52%). Of the T6SS-negative genomes, 5 out of the 60 were found to contain CJIE3 (**Supplementary Table 11**). The N-terminus of TraG is required for F pilus assembly; a long filament mediating the conjugative transfer of genetic material (Frost et al., 1994). Homologues of TraG and transfer coupling protein VirD4, a component of the *Agrobacterium tumefaciens* Type IVa secretion system (T4SSa), have been previously identified in the chromosomes of *C. jejuni* 81-176 and ATCC 43431, as well as in plasmids pCC31 and pTet (Batchelor et al., 2004; Poly et al., 2005; Chandran Darbari and Waksman, 2015). T4SS DNA conjugation systems were recently found harboured on megaplasmids in *C. jejuni* (Grohmann et al., 2018; Marasini et al., 2020). The T6SS-positive and TraG-containing megaplasmid pCJDM202 from *C. jejuni* WP2-202 strain was successfully transferred by conjugation to a T6SS-negative mutant NCTC11168 Nal^+ recipient cell, with the *hcp* gene observed in the transconjugants, thus demonstrating a role in the transfer of T6SS-containing megaplasmids to transconjugants (Marasini et al., 2020).

Putative Regulator

CJ488_0932 was predicted to contain the nucleic acid binding domain WGR (smart00773), belonging to the WGR superfamily (cl01581), and shares homology to the protein A0W69_09470 (81% aa identity) from pCJDM202. Within our local *C. jejuni* database, 63 out of the 512 (12.30%) genomes were found to possess the protein CJ488_0932, of which 51 were T6SS-positive (80.95%) and 12 were T6SS-negative (19.05%) (**Supplementary Table 11**). WGR domains have been identified in poly(ADP-ribose) polymerases of eukaryotes, as well as in a molybdate metabolism regulator in *E. coli* and a number of predicted proteins (Citarelli et al., 2010); however, the precise function of the domain remains unclear.

Putative Effectors

Lipases

A number of T6SS lipase effectors have been previously described to target bacterial and eukaryotic membranes (Miyata et al., 2011; Russell et al., 2013; Jiang et al., 2014). In CJPI-1, two predicted lipase (Lipase class 3) domain-containing proteins (PF01764), CJ488_0957 and CJ488_0961, were identified upstream of the T6SS operon (**Figure 3**), with the former sharing homology to the proteins CJE1115 (64% aa identity) and A0W69_09355 (62% aa identity) from RM1221 and pCJDM202, respectively. Within our local *C. jejuni* database, 108 out of the 512 (21.09%) genomes were found to possess the protein CJ488_0957 (average per genome = 1.06), of which 98 were T6SS-positive (90.74%) and 10 were T6SS-negative (9.26%). Furthermore, 49 out of the 512

(9.57%) genomes were found to possess the protein CJ488_0961 (average per genome = 1.00), of which 45 were T6SS-positive (91.84%) and four were T6SS-negative (8.16%) (**Supplementary Table 11**). Previous PF01764 domain-containing proteins have been predicted as T4SS effectors in several bacteria targetting prokaryotic membranes, suggesting these two lipase-domain containing proteins belong to a larger family of hydrolysing effectors that can be delivered by several effector delivery systems (Sgro et al., 2019).

Lysozyme

A phage lysozyme-like protein, CJ488_0962 was also inferred in CJPI-1 and predicted to contain a Phage_lysozyme (PF00959) and autolysin/endolysin family (cd00737) domain. Within our local *C. jejuni* database, 96 out of the 512 (18.75%) genomes were found to possess the protein CJ488_0962 (average per genome = 1.02), of which 91 were T6SS-positive (94.79%) and five were T6SS-negative (5.21%) (**Supplementary Table 11**). PF00959 is described as a glycoside hydrolase, associated with bacteriophage enzymes that degrade bacterial peptidoglycan in the cell wall (El-Gebali et al., 2019). Several characterised bacteriophage endolysins have been demonstrated to exhibit lytic antibacterial activity, containing both domains predicted in CJ488_0962 (Li et al., 2016; Ding et al., 2020). Interestingly, a prevalence study identifying endolysins in phage genomes identified PF00959 as the most frequently detected domain amongst analysed phage endolysins predicted to target *Proteobacteria* (Fernandez-Ruiz et al., 2018).

Diversity of Two VgrG Proteins Encoded in *C. jejuni* 488 Strain

The protein VgrG is an essential component of the T6SS with roles including the promotion of the T6SS machinery assembly, the puncturing of target cells, and the delivery of effectors via their C-terminal domains (Pukatzki et al., 2007). Orphan *vgrG* genes can be located distally from their cognate T6SS structural operons; however, to date only one VgrG protein has been described in T6SS-containing *C. jejuni* (De Maayer et al., 2011; Bleumink-Pluym et al., 2013; Lopez et al., 2020). Here, we have identified two *vgrG* genes in the CJPI-1 of *C. jejuni* 488 (**Figure 3**), hereafter referred to as, *vgrG1* (*CJ488_0978*) and *vgrG2* (*CJ488_0998*) (**Table 2** and **Supplementary Table 2**). Sequence alignment and identification of conserved and additional domains revealed a conserved N-terminal region possessing the VgrG domain (COG3501) and a region matching the superfamily VI_Rhs_Vgr (TIGR03361) (**Figure 4**). As observed in other bacteria, VgrG1 and VgrG2 differ in length, attributed to divergent C-terminal regions and associated domains (Hachani et al., 2011). The C-terminal region of VgrG1 (aa 564-883) shares an amino acid identity of 35% to the C-terminal region of VgrG2 (aa 564-838). Bioinformatic analysis revealed a Jag domain (COG1847, E-value: 0.008) in VgrG1, following the domain COG3501, which is potentially linked to RNA-binding. However, a structural homology search of the VgrG1 C-terminal region (aa 564-883) using Phyre2 matched to the C-terminal domain of the phage tail-lysozyme protein Gp5 (PDB: 1K28, Confidence: 100%). VgrG2 was found to contain a five superfamily/Gp5_C domain (PHA02596/PF06715) in its C-terminal region. The Gp5 C-terminal domain is commonly found in the bacteriophage T4 tail lysozyme protein Gp5 and VgrG proteins of bacteria, forming the membrane-puncturing β-helix structure of the spike proteins (Kanamaru et al., 2002; Pukatzki et al., 2007; El-Gebali et al., 2019). The C-termini Gp5 regions of some VgrG proteins may be also extended with catalytic domains (Hachani et al., 2011; Wettstadt et al., 2020). Furthermore, these extensions

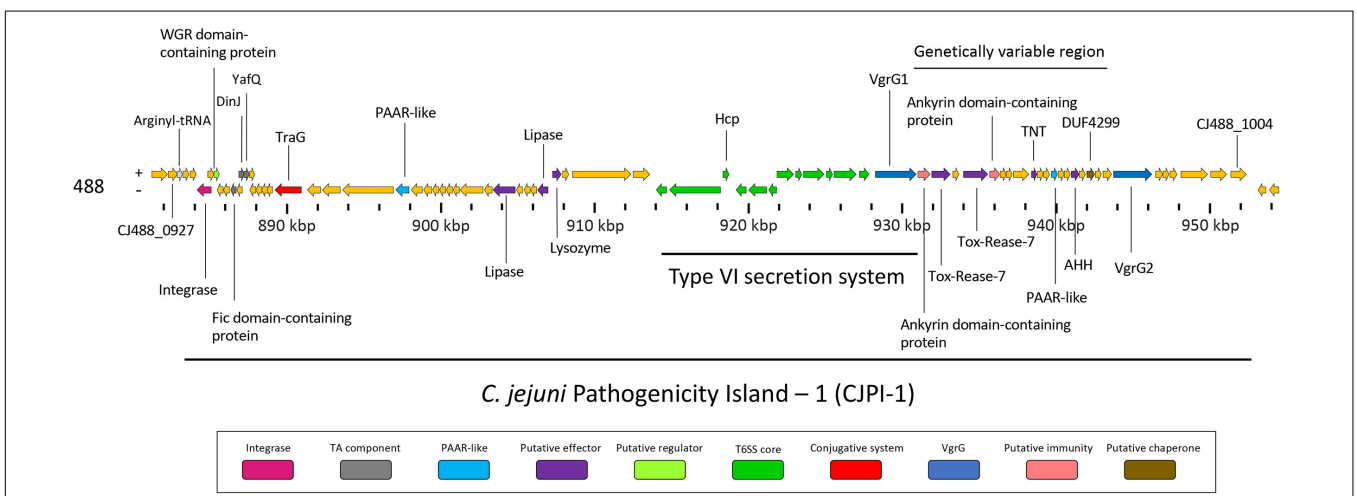

FIGURE 3 | Genomic architecture of the PAI CJPI-1 in T6SS-positive *C. jejuni* 488 strain. Coloured coding domain sequences (CDS) represent proteins with inferred functions and are labelled. The scale under the CDS represents the nucleotide position [kilobase pair (kbp)] of the pathogenicity island in the genome of *C. jejuni* 488 strain. The location of the T6SS and genetically variable region are also denoted. The positive (+) symbol on the left-hand side indicates the sense strand in the genome of *C. jejuni* 488 strain, whilst the negative (–) symbol indicates the antisense strand. Genes sizes are not to scale. Genes are coloured according to predicted function: integrases are shaded magenta, regulators are light green, TA components are grey, conjugative systems are red, putative effectors are purple, PAAR-like proteins are light blue, T6SS components are green, VgrGs are dark blue, putative immunity proteins are pink, and putative chaperone proteins are olive.

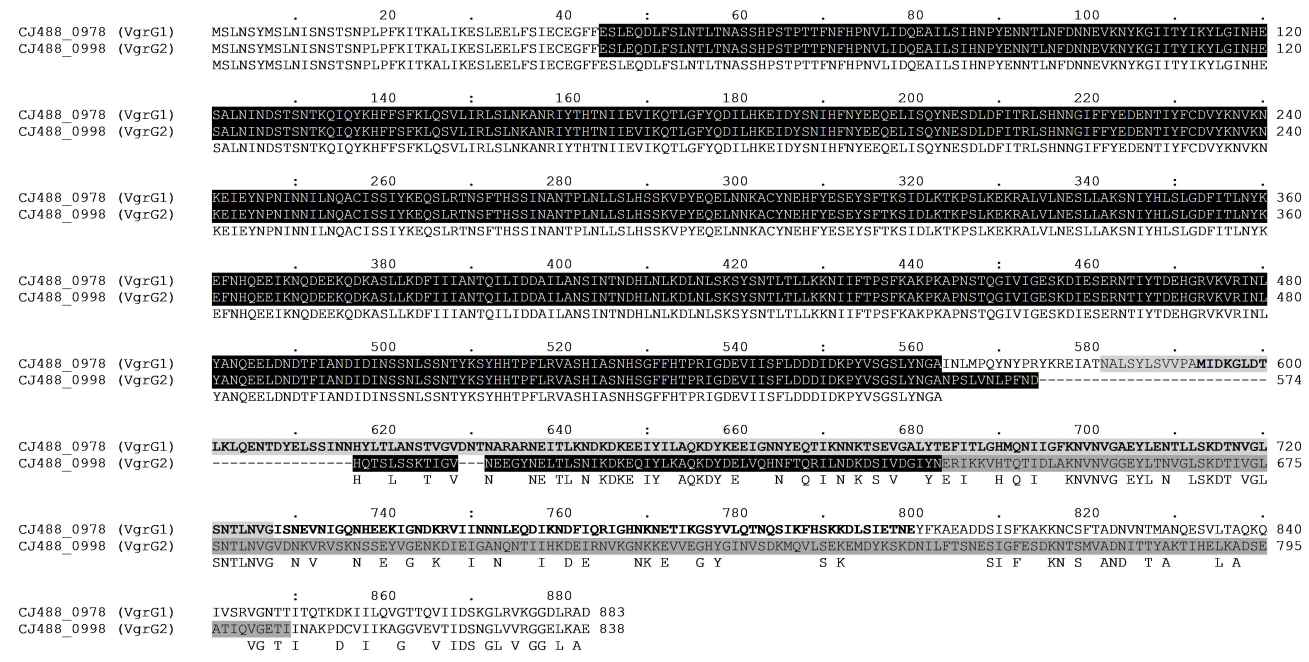

FIGURE 4 | Full amino acid sequence alignment of the two VgrG homologues present in T6SS-positive *C. jejuni* 488 strain using ClustalO. Conserved residues found in both sequences correspond to letters in *uppercase* below the aligned sequences. Protein locus tag and amino acid position are provided for each respective sequence. The N-terminal VgrG domain (COG3501) in both sequences is highlighted black. The Jag domain (COG1847) is highlighted light grey for VgrG1, while letters in bold represent the Phyre2 structural homology match to the C-terminal lysozyme domain of Gp5 (PDB: 1K28). The Gp5_C domain (PF06715) is highlighted dark grey for VgrG2.

may also contribute to the recruitment of additional effectors (Flaugnatti et al., 2020).

A BLASTP-homology search was then conducted to assess the sequence identity of VgrG1 and VgrG2 against the NCBI Reference Protein database. The amino acid sequence of VgrG1 shares homology with the VgrG proteins of *C. coli* (WP_070241948.1–98.87% aa identity) and to Epsilonproteobacteria *Helicobacter* sp. MIT 11-5569 (WP_138109445.1–69.88% aa identity). Similarly, the amino acid sequence of VgrG2 shares homology with the VgrG proteins of *C. coli* (WP_072231509.1–99.76% aa identity) and to *Helicobacter* sp. MIT 11-5569 (WP_181881862.1–79.01% aa identity). The highly homologous matches suggest that these species too possess more than one VgrG protein with similar, if not identical domain architectures to VgrG1 and VgrG2, respectively. Further exploration is needed to assess whether both VgrG proteins exist in T6SS-containing *C. coli* and/or *Helicobacter* spp. genomes.

Genomic analyses of T6SS-positive *C. jejuni* strains showed that a number of putative *vgrG* genes were located downstream of T6SS gene operons. A BLASTN search for *vgrG* detected 41 homologous genes in the T6SS-positive *C. jejuni* genomes (with assembly level "complete" or higher) (**Supplementary Table 12**). Interestingly, 1 of the 24 T6SS-positive "complete" *C. jejuni* genomes, IF1100, does not encode any *vgrG* gene, whereas 13 out of 24 encoded two or more. Phylogenetic analysis classified the VgrG proteins into two distinct clades, grouped with either VgrG1 or VgrG2 from *C. jejuni* 488 strain (**Figure 5**) (five VgrG amino acid sequences from genomes CJ017CC464, CJ018CCUA, and ZS007 were removed due to fragmented ORFs). A domain search using NCBI-CDD revealed that 28 of the 36 identified VgrG protein sequences contain an additional domain in the divergent C-terminus. Of which, 16 possessed the Jag (COG1847) domain, 12 possessed the five superfamily (PHA02596) domain, and eight possessed no identifiable domains (**Supplementary Table 13**). Collectively, this data suggests that two distinct VgrG proteins exist within the T6SS-positive *C. jejuni* isolates, with some strains bearing multiple VgrG proteins. It is predicted that isolates may exploit these different VgrG proteins in an interchangeable puncturing role in the spike complex, translocating specific effectors via interaction with the distinct C-terminal regions (Hachani et al., 2014; Jana and Salomon, 2019).

Investigation of PAAR-Motif in *C. jejuni* T6SS-Positive and T6SS-Negative Genomes

The T6SS puncturing structure is composed by a VgrG trimer further sharpened with a capping PAAR domain-containing protein tip (Wettstadt et al., 2020). To assess the prevalence of these "effector markers," the amino acid sequences of representative proteins belonging to all classes of PAAR subgroups found in the superfamily CL21497 were aligned against a local protein database of *C. jejuni* genomes (**Supplementary Data 1**). We identified only PAAR4 (representative protein AGP36489.1 of *Sorangium cellulosum*

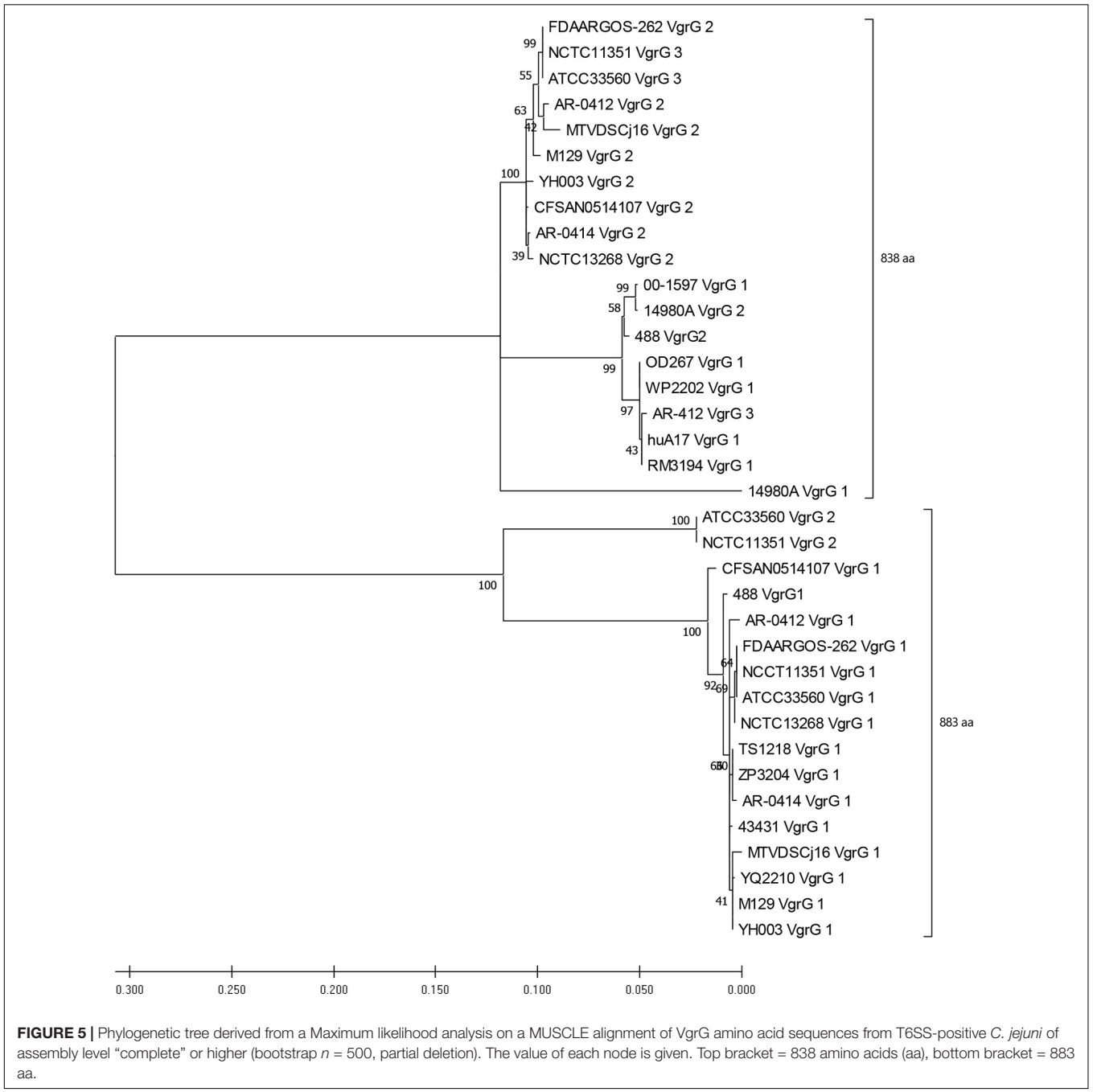

FIGURE 5 | Phylogenetic tree derived from a Maximum likelihood analysis on a MUSCLE alignment of VgrG amino acid sequences from T6SS-positive *C. jejuni* of assembly level "complete" or higher (bootstrap *n* = 500, partial deletion). The value of each node is given. Top bracket = 838 amino acids (aa), bottom bracket = 883 aa.

So0157-2) which matched positively to 500 genomes. However, the results were considered not significant as the alignment exclusively occurred at the C-terminal S41-peptidase domain (PF03572) of the representative protein and not the N-terminal PAAR-motif. We hypothesised that compared to other bacteria, significant sequence divergence in *C. jejuni* PAAR genes might exist and thus homology-based searches may not identify PAAR proteins. Further iterative based analysis (data not shown) was able to predict a novel PAAR-like domain (∼ 125 amino acids) present in two proteins within CJPI-1, CJ488_0948, and CJ488_0990, with the latter found in the genetically variable region downstream of the T6SS operon (**Figure 3**). Multiple sequence alignments uncovered the novel domain possesses a series of conserved cysteine and histidine residues similar to the PAAR-like domain DUF4280 (Rigard et al., 2016) and PAAR-containing proteins (Shneider et al., 2013) and is present in a wide range of bacterial families. A number of the PAAR-like domain-containing proteins possess N- or C-terminal extensions harbouring characterised toxin domains (**Figure 6**), conferring a toxin translocation function to PAAR in addition its sharpening role (Shneider et al., 2013). The predicted novel PAAR-like domain-containing proteins in strain 488 possessed no other

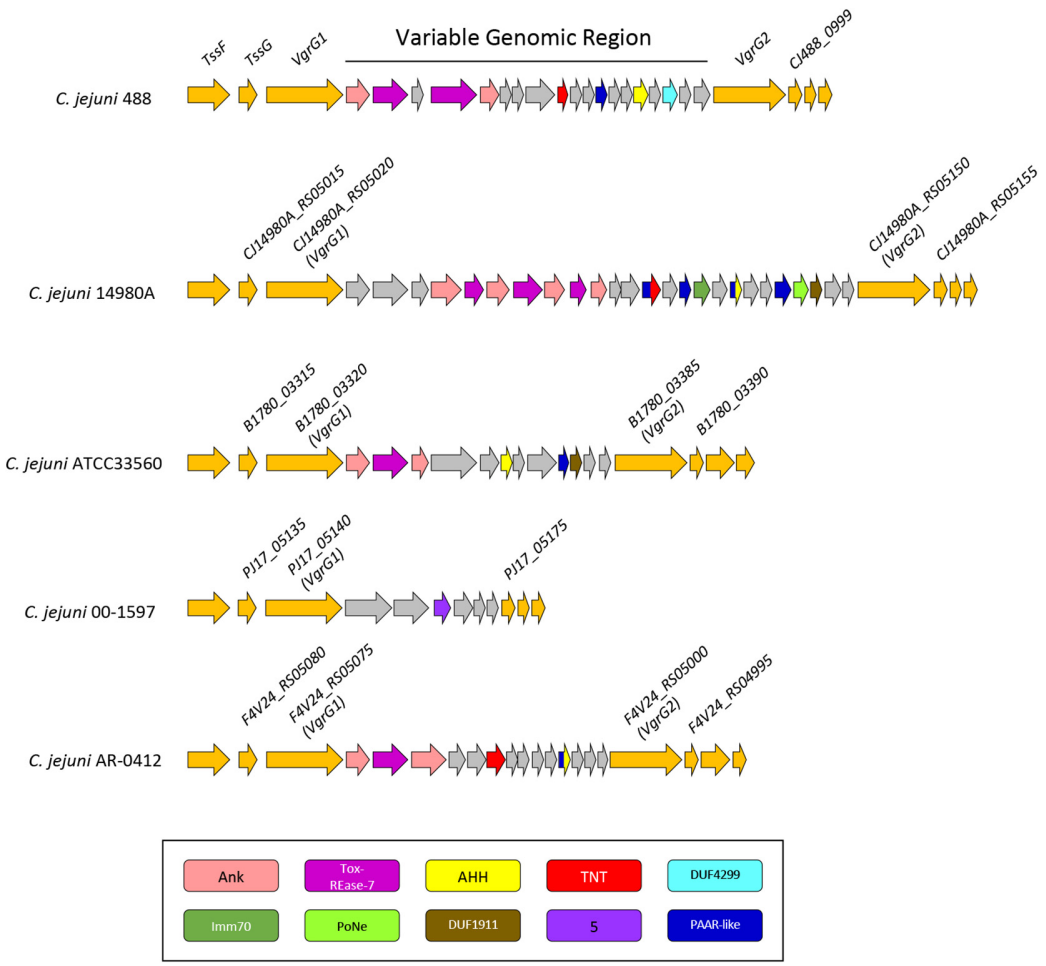

FIGURE 6 | Genomic architecture of the genetically variable region downstream of the T6SS operon in five T6SS-positive *C. jejuni* strains; 488, 14980A, ATCC33560, 00-1597, and AR-0412. Genes found within the variable region possessing a domain by NCBI CDD (Marchler-Bauer et al., 2017) are coloured according to the domains identified: Ankyrin domains are pink, Tox-REase-7 are purple, AHH are yellow, TNT are red, DUF4299 are sky blue, Imm70 are dark green, PoNe are light green, DUF1911 are brown, five superfamily domain are lavender, and PAAR-like are dark blue. Variable region genes with no predicted function or identifiable domains are shaded grey and genes neighbouring the variable region are orange. Gene sizes are not to scale. The corresponding locus tags for selected genes is labelled above accordingly.

identifiable domains, confining a sole sharpening role to these proteins in this strain (Shneider et al., 2013). An alignment using the amino acid sequences of representative proteins for MIX clans I–V was also conducted; however returned no positive matches (**Supplementary Table 7**; Salomon et al., 2014).

Putative T6SS-Associated Effectors Are Found in a Genetic Variable Region Downstream of the T6SS in CJPI-1

Genomic regions neighbouring *vgrG* genes often encode a number of hypothetical proteins, with many determined as T6SS effector and immunity proteins (De Maayer et al., 2011; Lopez et al., 2020). Analyses of T6SS-positive *C. jejuni* completely assembled genomes revealed a genetically variable region immediately downstream of the T6SS operon that did not share sequence identity to any ORFs found in the CJIE3 of strain RM1221. This region ranged from six genes in the 00-1597 strain, to 25 genes in the 14980A strain, located downstream of the main cluster gene *vgrG* and was commonly located upstream of the second orphan *vgrG* gene (**Figure 6**). Within this genetically variable region in 488, a number of ORFs between *vgrG1* and *vgrG2* were analysed using predictive programes (**Figure 3**). This resulted in the predicted identification of four putative effectors (CJ488_0980, CJ488_0982, CJ488_0988, and CJ488_0994), two ankyrin repeat domain-containing proteins (CJ488_0979 and CJ488_0983), and a DUF4299 family protein (CJ488_0996).

Among the putative effectors, proteins CJ488_0980 and CJ488_0982 contain predicted domains belonging to the restriction endonuclease family Tox-REase-7 (PF15649), whilst CJ488_0994 possesses a predicted domain belonging to the Tox-AHH HNH/ENDO VII superfamily nuclease (PF14412). Both domains belong to large toxin superfamilies with predicted functions as DNases/nucleases and are secreted by a wide range

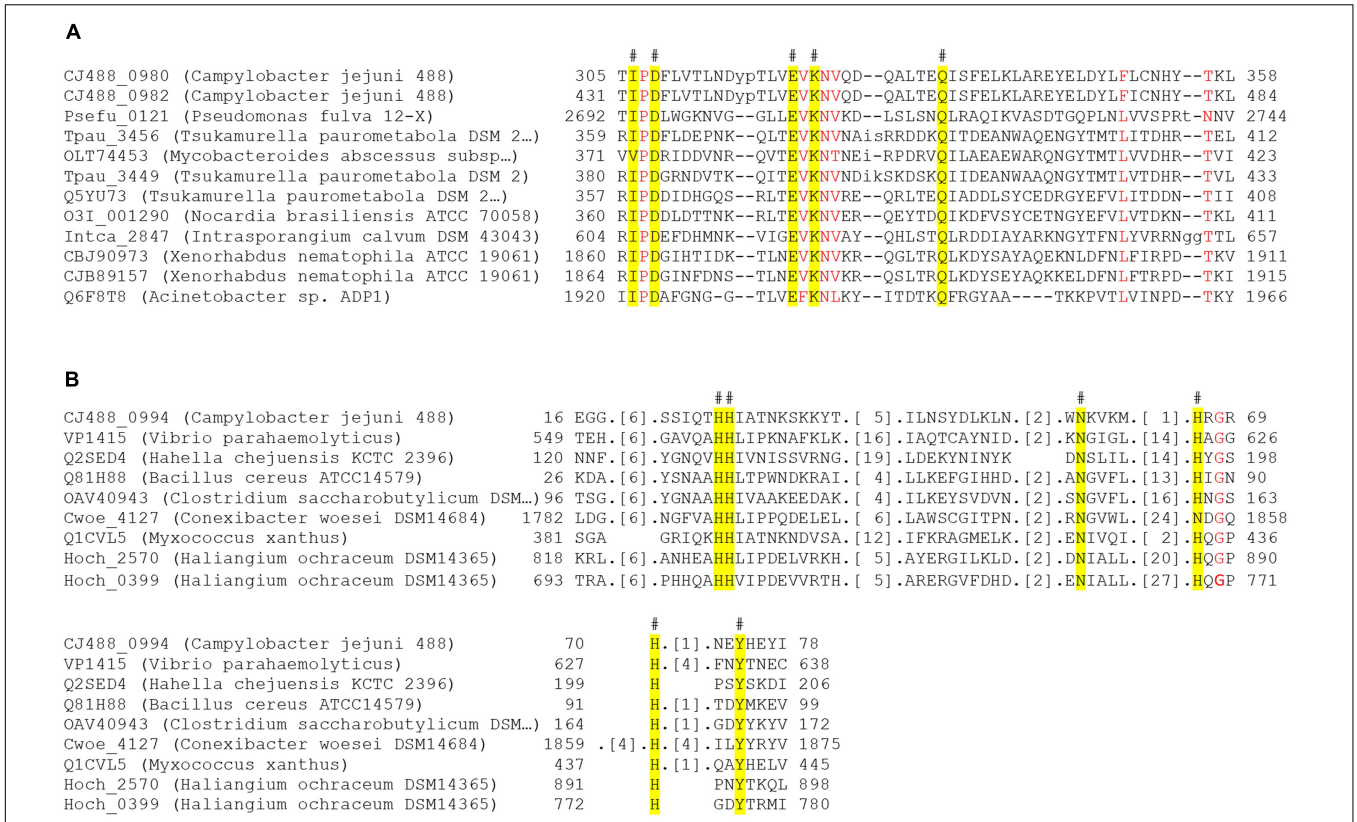

FIGURE 7 | Partial amino acid sequence alignment of Tox-REase-7 and AHH domain-containing representative amino acids against putative effectors downstream of the T6SS from *C. jejuni* 488 strain. **(A)** Alignment of CJ488_0980 and CJ488_0982 against Tox-REase-7 representative amino acids. **(B)** Alignment of CJ488_0994 against AHH representative amino acids. Catalytic residues for each domain are highlighted in yellow, and the hash (#) indicates the position of the residue in the *C. jejuni* 488 proteins. Red letters indicate amino acids with greater than 90% homology across all sequences for the alignment. Protein locus tag, organism name, and amino acid position are to the left and either side of the respective sequences.

of polymorphic effector delivery systems, including the T6SS (Zhang et al., 2011, 2012). CJ488_0994 shares weak homology to the protein A0W69_08930 (41% aa identity) from pCJDM202, also predicted to possess a Tox-AHH domain. Interestingly, none of the other inferred putative effectors were found on pCJDM202 or CJIE3, suggesting separate genetic transfer events have mediated the acquisition of these putative T6SS-associated effectors.

Both Tox-REase-7 domain-containing proteins, CJ488_0980 and CJ488_0982, contain the conserved catalytic residues IxD, ExK, and Q, and metal chelating site signature D-[EQ]xK, characteristic of REase-fold toxins, specifically Tox-REase-7 (**Figure 7A**). The AHH domain-containing protein CJ488_0994 also possesses the conserved catalytic residues HH, N, H, H, and Y, specific to the Tox-AHH fold/motif (**Figure 7B**; Zhang et al., 2012). Previous studies have successfully identified AHH domain-containing proteins as T6SS-associated effectors in both human and plant pathogenic bacterium, notably VP1415 from *V. parahaemolyticus*, therefore strengthening the prediction of CJ488_0994 as a T6SS effector (**Figure 7B**; Salomon et al., 2014; Santos et al., 2019). Within our local *C. jejuni* database, 88 out of the 512 (17.18%) genomes were identified to possess the protein CJ488_0980 (average per genome = 1.05), of which 87 were T6SS-positive (98.86%) and 1 was T6SS-negative (1.14%). The T6SS-negative genome was found to contain the CJIE3. Further, 100 out of 512 (19.53%) genomes were found to possess the protein CJ488_0994 (average per genome = 1.24), of which 95 were T6SS-positive (95%) and 5 were T6SS-negative (5%). Of the T6SS-negative genomes, 4 out of 5 were found to contain the CJIE3. Within the T6SS-positive population, 87 out of the 135 (64.44%) T6SS-positive genomes possessed the protein CJ488_0980 and 95 out of the 135 (70.37%) T6SS-positive genomes possessed the protein CJ488_0994 (**Supplementary Table 11**).

The final putative effector, CJ488_0988, was predicted to contain the C-terminal domain tuberculosis necrotising toxin (TNT) (PF14021) from the *Mycobacterium tuberculosis* protein CpnT (Sun et al., 2015). Within our local *C. jejuni* database, 83 out of the 512 (16.21%) genomes were found to possess the protein CJ488_0988 (average per genome = 1.12), of which 80 were T6SS-positive (96.39%) and three were T6SS-negative (3.61%). All of the T6SS-negative genomes were found to contain the CJIE3. Within the T6SS-positive population, 80 out of the 135 (59.26%) T6SS-positive genomes possessed the protein CJ488_0994 (**Supplementary Table 11**). TNT, characterised as a NAD^+- and $NAD(P)^+$-glycohydrolase, is transported to the cell

surface of *M. tuberculosis* by CpnT and released by proteolytic cleavage, where inside the eukaryotic target cell it depletes cellular NAD^+ inducing host-cell death (Danilchanka et al., 2014; Sun et al., 2015; Tak et al., 2019). The TNT domain of CJ488_0988 possesses the conserved residues Arg^5, Arg^{29}, and Gln^{101} (Arg^{757}, Arg^{780}, and Gln^{822} of TNT in *M. tuberculosis*), identified as the putative NAD^+ binding pocket essential for NAD^+ hydrolysis (Sun et al., 2015; Tak et al., 2019). The third tyrosine (Y) residue, Tyr^{765} in TNT of CpnT, was found to be replaced by a phenylalanine (F) residue, Phe^{13}, in the TNT domain of CJ488_0988. Mutations of the Tyr^{765} residue were demonstrated to significantly reduce the catalytic activity of TNT yet did not eradicate its cytotoxic activity (Sun et al., 2015; Tak et al., 2019). Structural homology of CJ488_0988 using the Phyre2 server confidently identified the domain TNT (PDB: 4QLP/c4qlpB, Confidence: 99.6%) as the most suitable template for modelling with a sequence coverage of 98%, indicating a high sequence and structural similarity (Kelley et al., 2015). Several interbacterial Type VI effectors have also been characterised to exhibit $NAD(P)^+$-glycohydrolase activity, inducing bacteriostasis in target cells (Whitney et al., 2015; Tang et al., 2018).

In bacteria, ankyrin repeat-containing proteins have been characterised to act as immunity proteins (ImmAnk) against decrosslinking enzymes and a wide range of T6SS-associated toxin domains, including Tox-AHH (Zhang et al., 2012; Lambert et al., 2015). Both predicted ankyrin repeat-containing proteins, CJ488_0979 and CJ488_0983, were found adjacent to the putative Tox-REase-7 effectors, CJ488_0980 and CJ488_0982, and are predicted to encode the cognate immunity proteins to the respective effectors, presenting two identical effector-immunity pairs. Immunity proteins for the remaining predicted effectors could not be determined using our *in silico* methods, suggesting they may play an anti-eukaryotic role and are not involved in interbacterial competition.

CJ488_0996 was predicted to contain the domain DUF4299 (PF14132) and shares homology to the protein A0W69_08920 (100%) from pCJDM2020. However, no further functional data was available. Within our local *C. jejuni* database, 127 out of the 512 (24.80%) genomes were found to possess the protein CJ488_0996 (average per genome = 1.06), of which 122 were T6SS-positive (96.06%) and five were T6SS-negative (3.94%) (**Supplementary Table 11**). The significantly high proportion of T6SS-positive genomes identified to possess CJ488_0996 suggests there is unknown link ensuring a strong conservation of both the T6SS and this DUF4299 domain-containing protein together. We speculate that the DUF4299 domain-containing protein may be playing an adaptor/chaperone protein role for the T6SS, as no identifiable toxin or effector domains could be determined (Liang et al., 2015; Bondage et al., 2016).

CONCLUSION

The roles of T6SSs have been associated with interbacterial competition, host colonisation and virulence, as well as environmental survival. We have conducted in this study a comprehensive bioinformatic analysis to understand the genotypic T6SS organisation and its functional roles in *C. jejuni*. Using more than 500 publicly available genomes, we have identified co-occurrence of the T6SS and the integrative element CJIE3, confirming their association. Interestingly, genetic recombination with a T6SS-harbouring pCJDM202-like plasmid gives the potential for chromosomal integration. The analysis of our newly re-sequenced and assembled T6SS-positive 488 strain shows poor homology between the "T6SS-containing genomic island" and CJIE3, thus endorsing the reclassification of the former as a PAI termed CJPI-1. To note, Clark et al. (2018) make a similar observation when comparing the genomes and proteomes of four *C. jejuni* strains; however, here we present a comprehensive bioinformatics overview of the dynamic *C. jejuni* genome, its respective T6SS, and prediction of associated effectors (Clark et al., 2018). Two canonical VgrG proteins were identified within T6SS-positive *C. jejuni* genomes, as well as a wide range of predicted T6SS effectors and toxins, with some found in a genetically variable region downstream of the T6SS. Furthermore, we uncovered a putative DinJ-YafQ Type II TA module with predicted links to the stability of MGEs within *C. jejuni*. However, we cannot exclude from our analyses the possibility of these toxins to be recognised by the T6SS and exploited as effectors (Yadav et al., 2021). Collectively, these observations emphasise the diversity of genetic elements within *C. jejuni* strains, highlighting their contributions to bacterial survival in a wide range of hosts (i.e., chickens and humans) and in mediating competition in polymicrobial environments via multiple virulence factors.

Our data predicts the first T6SS-associated effectors in *C. jejuni* and identifies their putative functions as nucleases and a NAD^+-glycohydrolase, based on their close proximity, high prevalence, and genomic context to the T6SS. Furthermore, the presence of putative anti-eukaryotic and anti-prokaryotic effectors suggests that *C. jejuni* encodes a multifunctional T6SS, as observed in other bacteria, that may have evolved during its evolutionary adaptation to host gastrointestinal tracts amongst polymicrobial communities (Miyata et al., 2013). Encoding a diverse repertoire of effectors, in close proximity to the T6SS operon, may allow for *C. jejuni* to secrete several effectors into prey cells and the surrounding milieu, overcoming bacterial competition and host defences to support its fitness.

This study also highlights that the acquisition of the T6SS and its related effectors into CJIE3 may have not occurred as a single event but rather upon multiple and independent genetic uptakes. Indeed, a small number of CJIE3-positive genomes were identified to possess some of the putative effectors in absence of a T6SS operon. This raises questions whether CJIE3-containing genomes once possessed a T6SS but was consequently lost through unknown events whilst retaining the putative effectors. Conversely, the effectors may have been associated to a number of pre-existing genes, some possibly as part of TA modules, subsequently repurposed as effectors upon successful acquisition of the T6SS into the genome via a plasmid, as previously mentioned. Interestingly, several T6SS-positive genomes were also identified to possess none of the putative effectors characterised in *C. jejuni* 488, suggesting they may instead harbour effector subsets that are yet to be discovered.

DATA AVAILABILITY STATEMENT

The original raw data used in this study are publicly available. This data can be found here: PRJEB41135. Publicly available datasets were analysed in this study. This data can be found here: https://www.ncbi.nlm.nih.gov.

AUTHOR CONTRIBUTIONS

OG and LR conceived the study. LR conducted the bioinformatic analysis and analysed the data. OG managed the study. LR, AH, and OG drafted the manuscript with contributions from JL, ZO, DX, AHMVV, and NC. All authors contributed to data interpretation.

ACKNOWLEDGMENTS

We thank Geunhye Hong and Cadi Davies for helpful discussions. We also thank Cadi Davies for her version of the 488 Fastq files. Data included in this study previously appeared in the online thesis of Robinson (2020).

SUPPLEMENTARY MATERIAL

The Supplementary Material for this article can be found online at: https://www.frontiersin.org/articles/10.3389/fmicb.2021.694824/full#supplementary-material

Supplementary Table 1 | List of characterised T6SS effectors screened against the local *C. jejuni* protein database.

Supplementary Table 2 | Domain and motif hits of predicted proteins in CJPI-1 using NCBI CDD-BLAST, Pfam, SMART, HmmScan, PROSITE, CDART, SUPERFAMILY, MOTIF, and InterPro.

Supplementary Table 3 | Results of subcellular localisation, signal prediction and transmembrane helices prediction of CJPI-1 predicted proteins with inferred functions using Psortb, CELLO, SignalP, TMPred, and TMHMM.

Supplementary Table 4 | Table of *C. jejuni* genomes "scaffold" level or higher under study with T6SS and CJIE3 analysis.

Supplementary Table 5 | BLASTP-homology search for T6SS proteins in the local *Campylobacter* protein database.

Supplementary Table 6 | Core T6SS proteins identified in the *C. jejuni* genomes under study.

Supplementary Table 7 | List of MIX proteins screened against the local *C. jejuni* protein database.

Supplementary Table 8 | BLASTN-homology search and analysis for *cje1094* in the local *Campylobacter* nucleotide database.

Supplementary Table 9 | BLASTN-homology search and analysis for *cje1105* in the local *Campylobacter* nucleotide database.

Supplementary Table 10 | BLASTN-homology search and analysis for *cje1153* in the local *Campylobacter* nucleotide database.

Supplementary Table 11 | Analysis of the BLASTP-homology searches for CJPI-1 functionally predicted proteins in the local *C. jejuni* protein database.

Supplementary Table 12 | BLASTN-homology search and analysis for *vgrG* genes in a local database of T6SS-positive *C. jejuni* genomes of assembly level "complete" or higher.

Supplementary Table 13 | NCBI-CDD webtool results for VgrG proteins from T6SS-positive *C. jejuni* genomes of assembly level "complete" or higher.

Supplementary Data 1 | PAAR amino acid sequences screened against the local *C. jejuni* protein database.

Supplementary Data 2 | *C. jejuni* 488 strain assembled GenBank (.gbk) file.

REFERENCES

Alcoforado Diniz, J., Liu, Y. C., and Coulthurst, S. J. (2015). Molecular weaponry: diverse effectors delivered by the Type VI secretion system. *Cell Microbiol.* 17, 1742–1751. doi: 10.1111/cmi.12532

Alteri, C. J., and Mobley, H. L. T. (2016). The versatile Type VI secretion system. *Microbiol. Spectr.* 4:10.1128/microbiolsec.VMBF-0026-2015. doi: 10.1128/microbiolspec.VMBF-0026-2015

Altschul, S. F., Gish, W., Miller, W., Myers, E. W., and Lipman, D. J. (1990). Basic local alignment search tool. *J. Mol. Biol.* 215, 403–410.

Amour, C., Gratz, J., Mduma, E., Svensen, E., Rogawski, E. T., Mcgrath, M., et al. (2016). Epidemiology and Impact of campylobacter infection in children in 8 low-resource settings: results from the MAL-ED study. *Clin. Infect. Dis.* 63, 1171–1179.

Andrews, S. (2010). *FastQC: A Quality Control Tool for High Throughput Sequence Data*. Available online at: http://www.bioinformatics.babraham.ac.uk/projects/fastqc/ (accessed October 5, 2020).

Aravind, L., Anantharaman, V., Balaji, S., Babu, M. M., and Iyer, L. M. (2005). The many faces of the helix-turn-helix domain: transcription regulation and beyond. *FEMS Microbiol. Rev.* 29, 231–262. doi: 10.1016/j.femsre.2004.12.008

Armenteros, J. J. A., Tsirigos, K. D., Sonderby, C. K., Petersen, T. N., Winther, O., Brunak, S., et al. (2019). SignalP 5.0 improves signal peptide predictions using deep neural networks. *Nat. Biotechnol.* 37, 420–423. doi: 10.1038/s41587-019-0036-z

Assefa, S., Keane, T. M., Otto, T. D., Newbold, C., and Berriman, M. (2009). ABACAS: algorithm-based automatic contiguation of assembled sequences. *Bioinformatics* 25, 1968–1969. doi: 10.1093/bioinformatics/btp347

Barker, J. R., Chong, A., Wehrly, T. D., Yu, J. J., Rodriguez, S. A., Liu, J., et al. (2009). The *Francisella tularensis* pathogenicity island encodes a secretion system that is required for phagosome escape and virulence. *Mol. Microbiol.* 74, 1459–1470. doi: 10.1111/j.1365-2958.2009.06947.x

Barret, M., Egan, F., and O'gara, F. (2013). Distribution and diversity of bacterial secretion systems across metagenomic datasets. *Environ. Microbiol. Rep.* 5, 117–126. doi: 10.1111/j.1758-2229.2012.00394.x

Bartonickova, L., Sterzenbach, T., Nell, S., Kops, F., Schulze, J., Venzke, A., et al. (2013). Hcp and VgrG 1 are secreted components of the H elicobacter hepaticus type VI secretion system and VgrG 1 increases the bacterial colitogenic potential. *Cell. Microbiol.* 15, 992–1011. doi: 10.1111/cmi.12094

Batchelor, R. A., Pearson, B. M., Friis, L. M., Guerry, P., and Wells, J. M. (2004). Nucleotide sequences and comparison of two large conjugative plasmids from different *Campylobacter* species. *Microbiology* 150, 3507–3517. doi: 10.1099/mic.0.27112-0

Bingle, L. E., Bailey, C. M., and Pallen, M. J. (2008). Type VI secretion: a beginner's guide. *Curr. Opin. Microbiol.* 11, 3–8.

Bleumink-Pluym, N. M., Van Alphen, L. B., Bouwman, L. I., Wosten, M. M., and Van Putten, J. P. (2013). Identification of a functional type VI secretion system in *Campylobacter jejuni* conferring capsule polysaccharide sensitive cytotoxicity. *PLoS Pathog.* 9:e1003393. doi: 10.1371/journal.ppat.1003393

Blondel, C. J., Jimenez, J. C., Contreras, I., and Santiviago, C. A. (2009). Comparative genomic analysis uncovers 3 novel loci encoding type six secretion systems differentially distributed in *Salmonella serotypes*. *BMC Genom.* 10:354. doi: 10.1186/1471-2164-10-354

Bolger, A. M., Lohse, M., and Usadel, B. (2014). Trimmomatic: a flexible trimmer for Illumina sequence data. *Bioinformatics* 30, 2114–2120. doi: 10.1093/bioinformatics/btu170

Bondage, D. D., Lin, J. S., Ma, L. S., Kuo, C. H., and Lai, E. M. (2016). VgrG C terminus confers the type VI effector transport specificity and is required for binding with PAAR and adaptor-effector complex. *Proc. Natl. Acad. Sci. U.S.A.* 113, E3931–E3940.

Burnham, P. M., and Hendrixson, D. R. (2018). *Campylobacter jejuni*: collective components promoting a successful enteric lifestyle. *Nat. Rev. Microbiol.* 16, 551–565. doi: 10.1038/s41579-018-0037-9

Carver, T., Harris, S. R., Berriman, M., Parkhill, J., and Mcquillan, J. A. (2012). Artemis: an integrated platform for visualization and analysis of high-throughput sequence-based experimental data. *Bioinformatics* 28, 464–469. doi: 10.1093/bioinformatics/btr703

Carver, T. J., Rutherford, K. M., Berriman, M., Rajandream, M. A., Barrell, B. G., and Parkhill, J. (2005). ACT: the artemis comparison tool. *Bioinformatics* 21, 3422–3423. doi: 10.1093/bioinformatics/bti553

Chandran Darbari, V., and Waksman, G. (2015). Structural biology of bacterial Type IV secretion systems. *Annu. Rev. Biochem.* 84, 603–629. doi: 10.1146/annurev-biochem-062911-102821

Chen, C., Yang, X., and Shen, X. (2019). Confirmed and potential roles of bacterial T6SSs in the intestinal ecosystem. *Front. Microbiol.* 10:1484. doi: 10.3389/fmicb.2019.01484

Cherrak, Y., Flaugnatti, N., Durand, E., Journet, L., and Cascales, E. (2019). Structure and activity of the Type VI secretion system. *Microbiol. Spectr.* 7, 329–342.

Cianfanelli, F. R., Monlezun, L., and Coulthurst, S. J. (2016). Aim, load, fire: the Type VI secretion system, a bacterial Nanoweapon. *Trends Microbiol.* 24, 51–62. doi: 10.1016/j.tim.2015.10.005

Citarelli, M., Teotia, S., and Lamb, R. S. (2010). Evolutionary history of the poly(ADP-ribose) polymerase gene family in eukaryotes. *BMC Evol. Biol.* 10:308. doi: 10.1186/1471-2148-10-308

Clark, C. G., Chen, C. Y., Berry, C., Walker, M., Mccorrister, S. J., Chong, P. M., et al. (2018). Comparison of genomes and proteomes of four whole genome-sequenced *Campylobacter jejuni* from different phylogenetic backgrounds. *PLoS One* 13:e0190836. doi: 10.1371/journal.pone.0190836

Corcionivoschi, N., Gundogdu, O., Moran, L., Kelly, C., Scates, P., Stef, L., et al. (2015). Virulence characteristics of hcp (+) *Campylobacter jejuni* and *Campylobacter coli* isolates from retail chicken. *Gut Pathog.* 7:20.

Costa, T. R., Felisberto-Rodrigues, C., Meir, A., Prevost, M. S., Redzej, A., Trokter, M., et al. (2015). Secretion systems in Gram-negative bacteria: structural and mechanistic insights. *Nat. Rev. Microbiol.* 13, 343–359. doi: 10.1038/nrmicro3456

Coulthurst, S. (2019). The Type VI secretion system: a versatile bacterial weapon. *Microbiology* 165, 503–515. doi: 10.1099/mic.0.000789

Coyne, M. J., Roelofs, K. G., and Comstock, L. E. (2016). Type VI secretion systems of human gut Bacteroidales segregate into three genetic architectures, two of which are contained on mobile genetic elements. *BMC Genom.* 17:58. doi: 10.1186/s12864-016-2377-z

da Cruz Campos, A. C., Couto, N., Lucas Da Silva Andrade, N., Friedrich, A. W., De Paula Rosa, A. C., Vieira Damasco, P., et al. (2020). Virulence and resistance properties of *E. coli* isolated from urine samples of hospitalized patients in Rio de Janeiro, Brazil - The role of mobile genetic elements. *Int. J. Med. Microbiol.* 310:151453. doi: 10.1016/j.ijmm.2020.151453

Danilchanka, O., Sun, J., Pavlenok, M., Maueroder, C., Speer, A., Siroy, A., et al. (2014). An outer membrane channel protein of *Mycobacterium tuberculosis* with exotoxin activity. *Proc. Natl. Acad. Sci. U.S.A.* 111, 6750–6755. doi: 10.1073/pnas.1400136111

de Castro, E., Sigrist, C. J., Gattiker, A., Bulliard, V., Langendijk-Genevaux, P. S., Gasteiger, E., et al. (2006). ScanProsite: detection of PROSITE signature matches and ProRule-associated functional and structural residues in proteins. *Nucleic Acids Res.* 34, W362–W365.

De Maayer, P., Venter, S. N., Kamber, T., Duffy, B., Coutinho, T. A., and Smits, T. H. (2011). Comparative genomics of the Type VI secretion systems of *Pantoea* and *Erwinia* species reveals the presence of putative effector islands that may be translocated by the VgrG and Hcp proteins. *BMC Genom.* 12:576. doi: 10.1186/1471-2164-12-576

Ding, Y., Zhang, Y., Huang, C., Wang, J., and Wang, X. (2020). An endolysin LysSE24 by bacteriophage LPSE1 confers specific bactericidal activity against multidrug-resistant *Salmonella* strains. *Microorganisms* 8:737. doi: 10.3390/microorganisms8050737

Dobrindt, U., Hochhut, B., Hentschel, U., and Hacker, J. (2004). Genomic islands in pathogenic and environmental microorganisms. *Nat. Rev. Microbiol.* 2, 414–424. doi: 10.1038/nrmicro884

Edgar, R. C. (2004). MUSCLE: multiple sequence alignment with high accuracy and high throughput. *Nucleic Acids Res.* 32, 1792–1797. doi: 10.1093/nar/gkh340

El-Gebali, S., Mistry, J., Bateman, A., Eddy, S. R., Luciani, A., Potter, S. C., et al. (2019). The Pfam protein families database in 2019. *Nucleic Acids Res.* 47, D427–D432.

Engel, P., Goepfert, A., Stanger, F. V., Harms, A., Schmidt, A., Schirmer, T., et al. (2012). Adenylylation control by intra- or intermolecular active-site obstruction in Fic proteins. *Nature* 482, 107–110. doi: 10.1038/nature10729

English, G., Trunk, K., Rao, V. A., Srikannathasan, V., Hunter, W. N., and Coulthurst, S. J. (2012). New secreted toxins and immunity proteins encoded within the Type VI secretion system gene cluster of *Serratia marcescens*. *Mol. Microbiol.* 86, 921–936. doi: 10.1111/mmi.12028

Fernandez-Ruiz, I., Coutinho, F. H., and Rodriguez-Valera, F. (2018). Thousands of novel endolysins discovered in uncultured phage genomes. *Front. Microbiol.* 9:1033. doi: 10.3389/fmicb.2018.01033

Flaugnatti, N., Rapisarda, C., Rey, M., Beauvois, S. G., Nguyen, V. A., Canaan, S., et al. (2020). Structural basis for loading and inhibition of a bacterial T6SS phospholipase effector by the VgrG spike. *EMBO J.* 39:e104129.

Fouts, D. E., Mongodin, E. F., Mandrell, R. E., Miller, W. G., Rasko, D. A., Ravel, J., et al. (2005). Major structural differences and novel potential virulence mechanisms from the genomes of multiple *Campylobacter* species. *PLoS Biol.* 3:e15. doi: 10.1371/journal.pbio.0030015

Fraikin, N., Goormaghtigh, F., and Van Melderen, L. (2020). Type II Toxin-antitoxin systems: evolution and revolutions. *J. Bacteriol.* 202:e00763-19.

Fridman, C. M., Keppel, K., Gerlic, M., Bosis, E., and Salomon, D. (2020). A comparative genomics methodology reveals a widespread family of membrane-disrupting T6SS effectors. *Nat. Commun.* 11:1085.

Frost, L. S., Ippen-Ihler, K., and Skurray, R. A. (1994). Analysis of the sequence and gene products of the transfer region of the F sex factor. *Microbiol. Rev.* 58, 162–210. doi: 10.1128/mr.58.2.162-210.1994

Geer, L. Y., Domrachev, M., Lipman, D. J., and Bryant, S. H. (2002). CDART: protein homology by domain architecture. *Genome Res.* 12, 1619–1623. doi: 10.1101/gr.278202

GenomeNet (2015). *MOTIF: Searching Protein Sequence Motifs*. Available online at: https://www.genome.jp/tools/motif/ (accessed July 1, 2020).

Ghatak, S., He, Y., Reed, S., and Irwin, P. (2020). Comparative genomic analysis of a multidrug-resistant *Campylobacter jejuni* strain YH002 isolated from Retail Beef Liver. *Foodborne Pathog. Dis.* 17, 576–584. doi: 10.1089/fpd.2019.2770

Gilchrist, C. L. M., and Chooi, Y. H. (2021). Clinker & clustermap.js: automatic generation of gene cluster comparison figures. *Bioinformatics* 2021:btab007.

Gladman, S., and Seemann, T. (2012). *"VelvetOptimiser". 2.2.5 ed.)*. Available online at: https://github.com/tseemann/VelvetOptimiser (accessed October 5, 2020).

Goepfert, A., Harms, A., Schirmer, T., and Dehio, C. (2013). "Type II toxin-antitoxin loci: The fic family," in *Prokaryotic Toxin-Antitoxins*, ed. G. Kenn (Heidelberg: Springer), 177–187. doi: 10.1007/978-3-642-33253-1_10

Gough, J., Karplus, K., Hughey, R., and Chothia, C. (2001). Assignment of homology to genome sequences using a library of hidden Markov models that represent all proteins of known structure. *J. Mol. Biol.* 313, 903–919. doi: 10.1006/jmbi.2001.5080

Grainge, I., and Jayaram, M. (1999). The integrase family of recombinase: organization and function of the active site. *Mol. Microbiol.* 33, 449–456. doi: 10.1046/j.1365-2958.1999.01493.x

Grohmann, E., Christie, P. J., Waksman, G., and Backert, S. (2018). Type IV secretion in Gram-negative and Gram-positive bacteria. *Mol. Microbiol.* 107, 455–471. doi: 10.1111/mmi.13896

Gundogdu, O., and Wren, B. W. (2020). Microbe profile: *Campylobacter jejuni*–survival instincts. *Microbiology* 166, 230–232. doi: 10.1099/mic.0.000906

Gunther, N. W., Reichenberger, E. R., and Bono, J. L. (2016). Complete genome sequence of UV-resistant *Campylobacter jejuni* RM3194, including an 81.08-kilobase plasmid. *Genome Announc.* 4:e0305-16.

Hachani, A., Allsopp, L. P., Oduko, Y., and Filloux, A. (2014). The VgrG proteins are "a la carte" delivery systems for bacterial type VI effectors. *J. Biol. Chem.* 289, 17872–17884. doi: 10.1074/jbc.m114.563429

Hachani, A., Lossi, N. S., Hamilton, A., Jones, C., Bleves, S., Albesa-Jove, D., et al. (2011). Type VI secretion system in *Pseudomonas aeruginosa*: secretion and multimerization of VgrG proteins. *J. Biol. Chem.* 286, 12317–12327.

Hachani, A., Wood, T. E., and Filloux, A. (2016). Type VI secretion and anti-host effectors. *Curr. Opin. Microbiol.* 29, 81–93. doi: 10.1016/j.mib.2015.11.006

Harrison, J. W., Dung, T. T., Siddiqui, F., Korbrisate, S., Bukhari, H., Tra, M. P., et al. (2014). Identification of possible virulence marker from *Campylobacter jejuni* isolates. *Emerg. Infect. Dis.* 20, 1026–1029.

Hill, C. W. (1999). Large genomic sequence repetitions in bacteria: lessons from rRNA operons and Rhs elements. *Res. Microbiol.* 150, 665–674. doi: 10.1016/s0923-2508(99)00125-4

Ho, B. T., Dong, T. G., and Mekalanos, J. J. (2014). A view to a kill: the bacterial type VI secretion system. *Cell Host Microb.* 15, 9–21. doi: 10.1016/j.chom.2013.11.008

Hofmann, K., and Stoffel, W. (1993). TMbase—a database of membrane spanning protein segments. *Biol. Chem. Hoppe Seyler* 374:166.

Huber, K. E., and Waldor, M. K. (2002). Filamentous phage integration requires the host recombinases XerC and XerD. *Nature* 417, 656–659. doi: 10.1038/nature00782

Humphrey, S., Chaloner, G., Kemmett, K., Davidson, N., Williams, N., Kipar, A., et al. (2014). *Campylobacter jejuni* is not merely a commensal in commercial broiler chickens and affects bird welfare. *mBio* 5:e01364-14.

Ijaz, U. Z., Sivaloganathan, L., Mckenna, A., Richmond, A., Kelly, C., Linton, M., et al. (2018). Comprehensive longitudinal microbiome analysis of the chicken cecum reveals a shift from competitive to environmental drivers and a window of opportunity for *Campylobacter*. *Front. Microbiol.* 9:2452. doi: 10.3389/fmicb.2018.02452

Jackson, A. P., Thomas, G. H., Parkhill, J., and Thomson, N. R. (2009). Evolutionary diversification of an ancient gene family (rhs) through C-terminal displacement. *BMC Genom.* 10:584. doi: 10.1186/1471-2164-10-584

Jain, C., Rodriguez, R. L., Phillippy, A. M., Konstantinidis, K. T., and Aluru, S. (2018). High throughput ANI analysis of 90K prokaryotic genomes reveals clear species boundaries. *Nat. Commun.* 9:5114.

Jana, B., Fridman, C. M., Bosis, E., and Salomon, D. (2019). A modular effector with a DNase domain and a marker for T6SS substrates. *Nat. Commun.* 10:3595.

Jana, B., and Salomon, D. (2019). Type VI secretion system: a modular toolkit for bacterial dominance. *Future Microbiol.* 14, 1451–1463. doi: 10.2217/fmb-2019-0194

Jarvis, K. G., Giron, J. A., Jerse, A. E., Mcdaniel, T. K., Donnenberg, M. S., and Kaper, J. B. (1995). Enteropathogenic *Escherichia coli* contains a putative type III secretion system necessary for the export of proteins involved in attaching and effacing lesion formation. *Proc. Natl. Acad. Sci. U.S.A.* 92, 7996–8000. doi: 10.1073/pnas.92.17.7996

Jiang, F., Wang, X., Wang, B., Chen, L., Zhao, Z., Waterfield, N. R., et al. (2016). The *Pseudomonas aeruginosa* Type VI secretion PGAP1-like effector induces host autophagy by activating endoplasmic reticulum stress. *Cell Rep.* 16, 1502–1509. doi: 10.1016/j.celrep.2016.07.012

Jiang, F., Waterfield, N. R., Yang, J., Yang, G., and Jin, Q. (2014). A *Pseudomonas aeruginosa* type VI secretion phospholipase D effector targets both prokaryotic and eukaryotic cells. *Cell Host Microb.* 15, 600–610. doi: 10.1016/j.chom.2014.04.010

Johnson, C. M., and Grossman, A. D. (2015). Integrative and Conjugative Elements (ICEs): what they do and how they work. *Annu. Rev. Genet.* 49, 577–601. doi: 10.1146/annurev-genet-112414-055018

Kanamaru, S., Leiman, P. G., Kostyuchenko, V. A., Chipman, P. R., Mesyanzhinov, V. V., Arisaka, F., et al. (2002). Structure of the cell-puncturing device of bacteriophage T4. *Nature* 415, 553–557. doi: 10.1038/415553a

Kapitein, N., Bonemann, G., Pietrosiuk, A., Seyffer, F., Hausser, I., Locker, J. K., et al. (2013). ClpV recycles VipA/VipB tubules and prevents non-productive tubule formation to ensure efficient type VI protein secretion. *Mol. Microbiol.* 87, 1013–1028. doi: 10.1111/mmi.12147

Kelley, L. A., Mezulis, S., Yates, C. M., Wass, M. N., and Sternberg, M. J. (2015). The Phyre2 web portal for protein modeling, prediction and analysis. *Nat. Protoc.* 10, 845–858. doi: 10.1038/nprot.2015.053

Konkel, M. E., Corwin, M. D., Joens, L. A., and Cieplak, W. (1992). Factors that influence the interaction of *Campylobacter jejuni* with cultured mammalian cells. *J. Med. Microbiol.* 37, 30–37. doi: 10.1099/00222615-37-1-30

Kovanen, S., Rossi, M., Pohja-Mykra, M., Nieminen, T., Raunio-Saarnisto, M., Sauvala, M., et al. (2019). Population genetics and characterization of *Campylobacter jejuni* isolates from Western Jackdaws and game birds in Finland. *Appl. Environ. Microbiol.* 85:e02365-18.

Kumar, S., Stecher, G., Li, M., Knyaz, C., and Tamura, K. (2018). MEGA X: molecular evolutionary genetics analysis across computing platforms. *Mol. Biol. Evol.* 35, 1547–1549. doi: 10.1093/molbev/msy096

Lambert, C., Cadby, I. T., Till, R., Bui, N. K., Lerner, T. R., Hughes, W. S., et al. (2015). Ankyrin-mediated self-protection during cell invasion by the bacterial predator *Bdellovibrio* bacteriovorus. *Nat. Commun.* 6:8884.

Leiman, P. G., Basler, M., Ramagopal, U. A., Bonanno, J. B., Sauder, J. M., Pukatzki, S., et al. (2009). Type VI secretion apparatus and phage tail-associated protein complexes share a common evolutionary origin. *Proc. Natl. Acad. Sci. U.S.A.* 106, 4154–4159. doi: 10.1073/pnas.0813360106

Leplae, R., Geeraerts, D., Hallez, R., Guglielmini, J., Dreze, P., and Van Melderen, L. (2011). Diversity of bacterial type II toxin-antitoxin systems: a comprehensive search and functional analysis of novel families. *Nucleic Acids Res.* 39, 5513–5525. doi: 10.1093/nar/gkr131

Lertpiriyapong, K., Gamazon, E. R., Feng, Y., Park, D. S., Pang, J., Botka, G., et al. (2012). *Campylobacter jejuni* type VI secretion system: roles in adaptation to deoxycholic acid, host cell adherence, invasion, and in vivo colonization. *PLoS One* 7:e42842. doi: 10.1371/journal.pone.0042842

Letunic, I., and Bork, P. (2018). 20 years of the SMART protein domain annotation resource. *Nucleic Acids Res.* 46, D493–D496.

Li, M., Li, M., Lin, H., Wang, J., Jin, Y., and Han, F. (2016). Characterization of the novel T4-like *Salmonella enterica* bacteriophage STP4-a and its endolysin. *Arch. Virol.* 161, 377–384. doi: 10.1007/s00705-015-2647-0

Liang, X., Moore, R., Wilton, M., Wong, M. J., Lam, L., and Dong, T. G. (2015). Identification of divergent type VI secretion effectors using a conserved chaperone domain. *Proc. Natl. Acad. Sci. U.S.A.* 112, 9106–9111. doi: 10.1073/pnas.1505317112

Liaw, J., Hong, G., Davies, C., Elmi, A., Sima, F., Stratakos, A., et al. (2019). The *Campylobacter jejuni* Type VI secretion system enhances the oxidative stress response and host colonization. *Front. Microbiol.* 10:2864. doi: 10.3389/fmicb.2019.02864

Lopez, J., Ly, P. M., and Feldman, M. F. (2020). The tip of the VgrG spike is essential to functional Type VI secretion system assembly in *Acinetobacter baumannii*. *mBio* 11:e02761-19.

Ma, L. S., Hachani, A., Lin, J. S., Filloux, A., and Lai, E. M. (2014). *Agrobacterium tumefaciens* deploys a superfamily of type VI secretion DNase effectors as weapons for interbacterial competition in planta. *Cell Host Microb.* 16, 94–104. doi: 10.1016/j.chom.2014.06.002

Madeira, F., Park, Y. M., Lee, J., Buso, N., Gur, T., Madhusoodanan, N., et al. (2019). The EMBL-EBI search and sequence analysis tools APIs in 2019. *Nucleic Acids Res.* 47, W636–W641.

Marasini, D., and Fakhr, M. K. (2016). Complete genome sequences of *Campylobacter jejuni* strains OD267 and WP2202 isolated from retail chicken livers and gizzards reveal the presence of novel 116-Kilobase and 119-kilobase megaplasmids with Type VI secretion systems. *Genome Announc.* 4:e01060-16.

Marasini, D., and Fakhr, M. K. (2017). Complete genome sequences of plasmid-bearing multidrug-resistant *Campylobacter jejuni* and *Campylobacter coli* strains with type VI secretion systems, isolated from retail turkey and pork. *Genome Announc.* 5:e01360-17.

Marasini, D., Karki, A. B., Bryant, J. M., Sheaff, R. J., and Fakhr, M. K. (2020). Molecular characterization of megaplasmids encoding the type VI secretion

system in *Campylobacter jejuni* isolated from chicken livers and gizzards. *Sci. Rep.* 10, 1–10.

Marchler-Bauer, A., Bo, Y., Han, L., He, J., Lanczycki, C. J., Lu, S., et al. (2017). CDD/SPARCLE: functional classification of proteins via subfamily domain architectures. *Nucleic Acids Res.* 45, D200–D203.

McKenna, A., Ijaz, U. Z., Kelly, C., Linton, M., Sloan, W. T., Green, B. D., et al. (2020). Impact of industrial production system parameters on chicken microbiomes: mechanisms to improve performance and reduce *Campylobacter*. *Microbiome* 8:128.

Mitchell, A. L., Attwood, T. K., Babbitt, P. C., Blum, M., Bork, P., Bridge, A., et al. (2019). InterPro in 2019: improving coverage, classification and access to protein sequence annotations. *Nucleic Acids Res.* 47, D351–D360.

Miyata, S. T., Bachmann, V., and Pukatzki, S. (2013). Type VI secretion system regulation as a consequence of evolutionary pressure. *J. Med. Microbiol.* 62, 663–676. doi: 10.1099/jmm.0.053983-0

Miyata, S. T., Kitaoka, M., Brooks, T. M., Mcauley, S. B., and Pukatzki, S. (2011). *Vibrio cholerae* requires the type VI secretion system virulence factor VasX to kill *Dictyostelium discoideum*. *Infect Immun.* 79, 2941–2949. doi: 10.1128/iai.01266-10

Motiejunaite, R., Armalyte, J., Markuckas, A., and Suziedeliene, E. (2007). *Escherichia coli* dinJ-yafQ genes act as a toxin-antitoxin module. *FEMS Microbiol. Lett.* 268, 112–119. doi: 10.1111/j.1574-6968.2006.00563.x

Nano, F. E., and Schmerk, C. (2007). The Francisella pathogenicity island. *Ann. N.Y. Acad. Sci.* 1105, 122–137. doi: 10.1196/annals.1409.000

Nash, H. A. (1996). "Site-specific recombination: integration, excision, resolution, and inversion of defined DNA segments," in *Escherichia coli and Salmonella: Cellular and Molecular Biology*, 2nd Edn, Vol. 2, ed. F. C. Neidhart (Washington, DC: American Society for Microbiology), 2363–2376.

NCBI (1982a). *BioSample*. Available online at: https://www.ncbi.nlm.nih.gov/biosample (accessed May 25, 2020).

NCBI (1982b). *Genome List - Genome*. Available online at: https://www.ncbi.nlm.nih.gov/genome/browse#!/overview/ (accessed May 25, 2020).

NCBI (1982c). *Protein*. Available online at: https://www.ncbi.nlm.nih.gov/protein/?term= (accessed May 25, 2020).

Noreen, Z., Jobichen, C., Abbasi, R., Seetharaman, J., Sivaraman, J., and Bokhari, H. (2018). Structural basis for the pathogenesis of *Campylobacter jejuni* Hcp1, a structural and effector protein of the Type VI secretion system. *FEBS J.* 285, 4060–4070. doi: 10.1111/febs.14650

Norton, J. P., and Mulvey, M. A. (2012). Toxin-antitoxin systems are important for niche-specific colonization and stress resistance of uropathogenic *Escherichia coli*. *PLoS Pathog.* 8:e1002954. doi: 10.1371/journal.ppat.1002954

Page, R., and Peti, W. (2016). Toxin-antitoxin systems in bacterial growth arrest and persistence. *Nat. Chem. Biol.* 12, 208–214. doi: 10.1038/nchembio.2044

Palmer, T., Finney, A. J., Saha, C. K., Atkinson, G. C., and Sargent, F. (2021). A holin/peptidoglycan hydrolase-dependent protein secretion system. *Mol. Microbiol.* 115, 345–355. doi: 10.1111/mmi.14599

Parker, C. T., Quinones, B., Miller, W. G., Horn, S. T., and Mandrell, R. E. (2006). Comparative genomic analysis of *Campylobacter jejuni* strains reveals diversity due to genomic elements similar to those present in C. jejuni strain RM1221. *J. Clin. Microbiol.* 44, 4125–4135. doi: 10.1128/jcm.01231-06

Parkhill, J., Wren, B. W., Mungall, K., Ketley, J. M., Churcher, C., Basham, D., et al. (2000). The genome sequence of the food-borne pathogen *Campylobacter jejuni* reveals hypervariable sequences. *Nature* 403, 665–668. doi: 10.1038/35001088

Penner, J. L., Hennessy, J. N., and Congi, R. V. (1983). Serotyping of*Campylobacter jejuni* and*Campylobacter coli* on the basis of thermostable antigens. *Eur. J. Clin. Microbiol.* 2, 378–383.

Poly, F., Threadgill, D., and Stintzi, A. (2005). Genomic diversity in *Campylobacter jejuni*: identification of C. jejuni 81-176-specific genes. *J. Clin. Microbiol.* 43, 2330–2338. doi: 10.1128/jcm.43.5.2330-2338.2005

Potter, S. C., Luciani, A., Eddy, S. R., Park, Y., Lopez, R., and Finn, R. D. (2018). HMMER web server: 2018 update. *Nucleic Acids Res.* 46, W200–W204. doi: 10.1093/nar/gky448

Prysak, M. H., Mozdzierz, C. J., Cook, A. M., Zhu, L., Zhang, Y., Inouye, M., et al. (2009). Bacterial toxin YafQ is an endoribonuclease that associates with the ribosome and blocks translation elongation through sequence-specific and frame-dependent mRNA cleavage. *Mol. Microbiol.* 71, 1071–1087. doi: 10.1111/j.1365-2958.2008.06572.x

Pukatzki, S., Ma, A. T., Revel, A. T., Sturtevant, D., and Mekalanos, J. J. (2007). Type VI secretion system translocates a phage tail spike-like protein into target cells where it cross-links actin. *Proc. Natl. Acad. Sci. U.S.A.* 104, 15508–15513. doi: 10.1073/pnas.0706532104

Pukatzki, S., Ma, A. T., Sturtevant, D., Krastins, B., Sarracino, D., Nelson, W. C., et al. (2006). Identification of a conserved bacterial protein secretion system in *Vibrio cholerae* using the Dictyostelium host model system. *Proc. Natl. Acad. Sci. U.S.A.* 103, 1528–1533. doi: 10.1073/pnas.0510322103

Rigard, M., Broms, J. E., Mosnier, A., Hologne, M., Martin, A., Lindgren, L., et al. (2016). *Francisella tularensis* IglG belongs to a novel family of PAAR-Like T6SS proteins and harbors a unique n-terminal extension required for virulence. *PLoS Pathog.* 12:e1005821. doi: 10.1371/journal.ppat.1005821

Robinson, L. (2020). *Bioinformatic Analysis of the Campylobacter jejuni Type VI Secretion System*, Masters Thesis. London: LSHTM.

Ruangprasert, A., Maehigashi, T., Miles, S. J., Giridharan, N., Liu, J. X., and Dunham, C. M. (2014). Mechanisms of toxin inhibition and transcriptional repression by *Escherichia coli* DinJ-YafQ. *J. Biol. Chem.* 289, 20559–20569. doi: 10.1074/jbc.m114.573006

Russell, A. B., Hood, R. D., Bui, N. K., Leroux, M., Vollmer, W., and Mougous, J. D. (2011). Type VI secretion delivers bacteriolytic effectors to target cells. *Nature* 475, 343–347.

Russell, A. B., Leroux, M., Hathazi, K., Agnello, D. M., Ishikawa, T., Wiggins, P. A., et al. (2013). Diverse type VI secretion phospholipases are functionally plastic antibacterial effectors. *Nature* 496, 508–512. doi: 10.1038/nature12074

Salomon, D., Kinch, L. N., Trudgian, D. C., Guo, X., Klimko, J. A., Grishin, N. V., et al. (2014). Marker for type VI secretion system effectors. *Proc. Natl. Acad. Sci. U.S.A.* 111, 9271–9276.

Santoriello, F. J., Michel, L., Unterweger, D., and Pukatzki, S. (2020). Pandemic *Vibrio cholerae* shuts down site-specific recombination to retain an interbacterial defence mechanism. *Nat. Commun.* 11:6246.

Santos, M. N. M., Cho, S. T., Wu, C. F., Chang, C. J., Kuo, C. H., and Lai, E. M. (2019). Redundancy and specificity of Type VI secretion vgrG loci in antibacterial activity of *Agrobacterium tumefaciens* 1D1609 strain. *Front. Microbiol.* 10:3004. doi: 10.3389/fmicb.2019.03004

Schmid, M. C., Scheidegger, F., Dehio, M., Balmelle-Devaux, N., Schulein, R., Guye, P., et al. (2006). A translocated bacterial protein protects vascular endothelial cells from apoptosis. *PLoS Pathog.* 2:e115. doi: 10.1371/journal.ppat.0020115

Seemann, T. (2014). Prokka: rapid prokaryotic genome annotation. *Bioinformatics* 30, 2068–2069. doi: 10.1093/bioinformatics/btu153

Sgro, G. G., Oka, G. U., Souza, D. P., Cenens, W., Bayer-Santos, E., Matsuyama, B. Y., et al. (2019). Bacteria-Killing Type IV secretion systems. *Front. Microbiol.* 10:1078. doi: 10.3389/fmicb.2019.01078

Shen, Z., Patil, R. D., Sahin, O., Wu, Z., Pu, X. Y., Dai, L., et al. (2016). Identification and functional analysis of two toxin–antitoxin systems in *Campylobacter jejuni*. *Mol. Microbiol.* 101, 909–923. doi: 10.1111/mmi.13431

Shneider, M. M., Buth, S. A., Ho, B. T., Basler, M., Mekalanos, J. J., and Leiman, P. G. (2013). PAAR-repeat proteins sharpen and diversify the type VI secretion system spike. *Nature* 500, 350–353. doi: 10.1038/nature12453

Sonnhammer, E. L., Von Heijne, G., and Krogh, A. (1998). A hidden Markov model for predicting transmembrane helices in protein sequences. *Proc. Int. Conf. Intell. Syst. Mol. Biol.* 6, 175–182.

Sprenger, H., Kienesberger, S., Pertschy, B., Poltl, L., Konrad, B., Bhutada, P., et al. (2017). Fic proteins of *Campylobacter fetus* subsp. venerealis form a network of functional toxin-antitoxin systems. *Front. Microbiol.* 8:1965. doi: 10.3389/fmicb.2017.01965

Sun, J., Siroy, A., Lokareddy, R. K., Speer, A., Doornbos, K. S., Cingolani, G., et al. (2015). The tuberculosis necrotizing toxin kills macrophages by hydrolyzing NAD. *Nat. Struct. Mol. Biol.* 22, 672–678. doi: 10.1038/nsmb.3064

Tak, U., Vlach, J., Garza-Garcia, A., William, D., Danilchanka, O., De Carvalho, L. P. S., et al. (2019). The tuberculosis necrotizing toxin is an NAD(+) and NADP(+) glycohydrolase with distinct enzymatic properties. *J. Biol. Chem.* 294, 3024–3036. doi: 10.1074/jbc.ra118.005832

Tam, C. C., Rodrigues, L. C., Viviani, L., Dodds, J. P., Evans, M. R., Hunter, P. R., et al. (2012). Longitudinal study of infectious intestinal disease in the UK (IID2 study): incidence in the community and presenting to general practice. *Gut* 61, 69–77. doi: 10.1136/gut.2011.238386

Tang, J. Y., Bullen, N. P., Ahmad, S., and Whitney, J. C. (2018). Diverse NADase effector families mediate interbacterial antagonism via the type VI secretion system. *J. Biol. Chem.* 293, 1504–1514. doi: 10.1074/jbc.ra117.000178

Trunk, K., Coulthurst, S. J., and Quinn, J. (2019). A New Front in Microbial Warfare-Delivery of Antifungal Effectors by the Type VI Secretion System. *J. Fungi* 5:50. doi: 10.3390/jof5020050

Trunk, K., Peltier, J., Liu, Y. C., Dill, B. D., Walker, L., Gow, N. A. R., et al. (2018). The type VI secretion system deploys antifungal effectors against microbial competitors. *Nat. Microbiol.* 3, 920–931. doi: 10.1038/s41564-018-0191-x

Ugarte-Ruiz, M., Stabler, R. A., Dominguez, L., Porrero, M. C., Wren, B. W., Dorrell, N., et al. (2015). Prevalence of Type VI Secretion System in Spanish *Campylobacter jejuni* Isolates. *Zoonoses Public Health* 62, 497–500. doi: 10.1111/zph.12176

Veyron, S., Peyroche, G., and Cherfils, J. (2018). FIC proteins: from bacteria to humans and back again. *Pathog. Dis.* 76:fty012.

Wettstadt, S., Lai, E. M., and Filloux, A. (2020). Solving the Puzzle: connecting a Heterologous *Agrobacterium tumefaciens* T6SS effector to a *Pseudomonas aeruginosa* spike complex. *Front. Cell Infect. Microbiol.* 10:291. doi: 10.3389/fcimb.2020.00291

Whitney, J. C., Chou, S., Russell, A. B., Biboy, J., Gardiner, T. E., Ferrin, M. A., et al. (2013). Identification, structure, and function of a novel type VI secretion peptidoglycan glycoside hydrolase effector-immunity pair. *J. Biol. Chem.* 288, 26616–26624. doi: 10.1074/jbc.m113.488320

Whitney, J. C., Quentin, D., Sawai, S., Leroux, M., Harding, B. N., Ledvina, H. E., et al. (2015). An interbacterial NAD(P)(+) glycohydrolase toxin requires elongation factor Tu for delivery to target cells. *Cell* 163, 607–619. doi: 10.1016/j.cell.2015.09.027

Wigley, P. (2015). Blurred lines: pathogens, commensals, and the healthy gut. *Front. Vet. Sci.* 2:40. doi: 10.3389/fvets.2015.00040

Wood, T. E., Aksoy, E., and Hachani, A. (2020). From welfare to warfare: the arbitration of host-microbiota interplay by the Type VI secretion system. *Front. Cell Infect. Microbiol.* 10:587948. doi: 10.3389/fcimb.2020.587948

Worby, C. A., Mattoo, S., Kruger, R. P., Corbeil, L. B., Koller, A., Mendez, J. C., et al. (2009). The fic domain: regulation of cell signaling by adenylylation. *Mol. Cell* 34, 93–103. doi: 10.1016/j.molcel.2009.03.008

Wozniak, R. A., and Waldor, M. K. (2009). A toxin-antitoxin system promotes the maintenance of an integrative conjugative element. *PLoS Genet.* 5:e1000439. doi: 10.1371/journal.pgen.1000439

Yadav, S. K., Magotra, A., Ghosh, S., Krishnan, A., Pradhan, A., Kumar, R., et al. (2021). Immunity proteins of dual nuclease T6SS effectors function as transcriptional repressors. *EMBO Rep.* 22:e51857.

Yarbrough, M. L., Li, Y., Kinch, L. N., Grishin, N. V., Ball, H. L., and Orth, K. (2009). AMPylation of Rho GTPases by Vibrio VopS disrupts effector binding and downstream signaling. *Science* 323, 269–272. doi: 10.1126/science.1166382

Yu, C. S., Chen, Y. C., Lu, C. H., and Hwang, J. K. (2006). Prediction of protein subcellular localization. *Proteins* 64, 643–651.

Yu, N. Y., Wagner, J. R., Laird, M. R., Melli, G., Rey, S., Lo, R., et al. (2010). PSORTb 3.0: improved protein subcellular localization prediction with refined localization subcategories and predictive capabilities for all prokaryotes. *Bioinformatics* 26, 1608–1615. doi: 10.1093/bioinformatics/btq249

Zerbino, D. R., and Birney, E. (2008). Velvet: algorithms for de novo short read assembly using de Bruijn graphs. *Genome Res.* 18, 821–829. doi: 10.1101/gr.074492.107

Zhang, D., De Souza, R. F., Anantharaman, V., Iyer, L. M., and Aravind, L. (2012). Polymorphic toxin systems: Comprehensive characterization of trafficking modes, processing, mechanisms of action, immunity and ecology using comparative genomics. *Biol. Direct.* 7:18. doi: 10.1186/1745-6150-7-18

Zhang, D., Iyer, L. M., and Aravind, L. (2011). A novel immunity system for bacterial nucleic acid degrading toxins and its recruitment in various eukaryotic and DNA viral systems. *Nucleic Acids Res.* 39, 4532–4552. doi: 10.1093/nar/gkr036

Zhang, Y. (2008). I-TASSER server for protein 3D structure prediction. *BMC Bioinform.* 9:40. doi: 10.1186/1471-2105-9-40

Zoued, A., Brunet, Y. R., Durand, E., Aschtgen, M. S., Logger, L., Douzi, B., et al. (2014). Architecture and assembly of the Type VI secretion system. *Biochim. Biophys. Acta* 1843, 1664–1673.

Conflict of Interest: The authors declare that the research was conducted in the absence of any commercial or financial relationships that could be construed as a potential conflict of interest.

frontiers in Microbiology

CORRECTION
published: 16 November 2021
doi: 10.3389/fmicb.2021.793252

Corrigendum: Bioinformatic Analysis of the *Campylobacter jejuni* Type VI Secretion System and Effector Prediction

Luca Robinson[1], *Janie Liaw*[1], *Zahra Omole*[1], *Dong Xia*[2], *Arnoud H. M. van Vliet*[3], *Nicolae Corcionivoschi*[4,5], *Abderrahman Hachani*[6†] *and Ozan Gundogdu*[1*†]

[1] Faculty of Infectious and Tropical Diseases, London School of Hygiene & Tropical Medicine, London, United Kingdom, [2] Comparative Biomedical Sciences, Royal Veterinary College, London, United Kingdom, [3] School of Veterinary Medicine, Faculty of Health and Medical Sciences, University of Surrey, Guildford, United Kingdom, [4] Bacteriology Branch, Veterinary Sciences Division, Agri-Food and Biosciences Institute, Belfast, United Kingdom, [5] Bioengineering of Animal Science Resources, Banat University of Agricultural Sciences and Veterinary Medicine – King Michael the I of Romania, Timisoara, Romania, [6] The Peter Doherty Institute for Infection and Immunity, Department of Microbiology and Immunology, University of Melbourne, Melbourne, VIC, Australia

OPEN ACCESS

Approved by:
Frontiers Editorial Office,
Frontiers Media SA, Switzerland

***Correspondence:**
Ozan Gundogdu
ozan.gundogdu@lshtm.ac.uk

[†]These authors share senior authorship

Specialty section:
This article was submitted to Microbial Physiology and Metabolism, a section of the journal Frontiers in Microbiology

Received: 11 October 2021
Accepted: 13 October 2021
Published: 16 November 2021

Citation:
Robinson L, Liaw J, Omole Z, Xia D, van Vliet AHM, Corcionivoschi N, Hachani A and Gundogdu O (2021) Corrigendum: Bioinformatic Analysis of the Campylobacter jejuni Type VI Secretion System and Effector Prediction. Front. Microbiol. 12:793252. doi: 10.3389/fmicb.2021.793252

Keywords: *Campylobacter jejuni*, Type VI Secretion System, T6SS effectors, T6SS immunity proteins, toxin-antitoxin, pathogenicity island

A Corrigendum on

Bioinformatic Analysis of the *Campylobacter jejuni* Type VI Secretion System and Effector Prediction

by Robinson, L., Liaw, J., Omole, Z., Xia, D., van Vliet, A. H. M., Corcionivoschi, N., Hachani, A., and Gundogdu, O. (2021). Front. Microbiol. 12:694824. doi: 10.3389/fmicb.2021.694824

In the original article, there was a mistake in Supplementary Data 2 (Data Sheet 2.ZIP) as published. The most up-to-date file was not used. The corrected file for Supplementary Data 2 has been updated in the original article.

The authors apologize for this error and state that this does not change the scientific conclusions of the article in any way. The original article has been updated.

frontiers in Microbiology

ORIGINAL RESEARCH
published: 09 July 2021
doi: 10.3389/fmicb.2021.690286

Compensating Complete Loss of Signal Recognition Particle During Co-translational Protein Targeting by the Translation Speed and Accuracy

*Liuqun Zhao[1,2], Gang Fu[1,3,4], Yanyan Cui[1], Zixiang Xu[1,4], Tao Cai[1] and Dawei Zhang[1,2,3,4]**

[1] Tianjin Institute of Industrial Biotechnology, Chinese Academy of Sciences, Tianjin, China, [2] Tianjin Institute of Industrial Biotechnology, University of Chinese Academy of Sciences, Beijing, China, [3] Key Laboratory of Systems Microbial Biotechnology, Chinese Academy of Sciences, Tianjin, China, [4] National Engineering Laboratory for Industrial Enzymes, Chinese Academy of Sciences, Tianjin, China

Signal recognition particle (SRP) is critical for delivering co-translational proteins to the bacterial inner membrane. Previously, we identified SRP suppressors in *Escherichia coli* that inhibit translation initiation and elongation, which provided insights into the mechanism of bypassing the requirement of SRP. Suppressor mutations tended to be located in regions that govern protein translation under evolutionary pressure. To test this hypothesis, we re-executed the suppressor screening of SRP. Here, we isolated a novel SRP suppressor mutation located in the Shine–Dalgarno sequence of the S10 operon, which partially offset the targeting defects of SRP-dependent proteins. We found that the suppressor mutation decreased the protein translation rate, which extended the time window of protein targeting. This increased the possibility of the correct localization of inner membrane proteins. Furthermore, the fidelity of translation was decreased in suppressor cells, suggesting that the quality control of translation was inactivated to provide an advantage in tolerating toxicity caused by the loss of SRP. Our results demonstrated that the inefficient protein targeting due to SRP deletion can be rescued through modulating translational speed and accuracy.

Keywords: signal recognition particle, suppressor screening, translational control, inner membrane protein, co-translational protein targeting

OPEN ACCESS

Edited by:
Ignacio Arechaga, University of Cantabria, Spain

Reviewed by:
Thomas Brüser, Leibniz University Hannover, Germany
Hui Li, Institute of Agricultural Quality Standards and Testing Technology for Agro Products, Chinese Academy of Agricultural Sciences, China

***Correspondence:**
Dawei Zhang
zhang_dw@tib.cas.cn

Specialty section:
This article was submitted to Microbial Physiology and Metabolism, a section of the journal Frontiers in Microbiology

Received: *02 April 2021*
Accepted: *09 June 2021*
Published: *09 July 2021*

Citation:
Zhao L, Fu G, Cui Y, Xu Z, Cai T and Zhang D (2021) Compensating Complete Loss of Signal Recognition Particle During Co-translational Protein Targeting by the Translation Speed and Accuracy. Front. Microbiol. 12:690286. doi: 10.3389/fmicb.2021.690286

INTRODUCTION

The signal recognition particle (SRP) is a highly conserved ribonucleoprotein complex that is involved in co-translational targeting of the ribosome-nascent chain complex to the endoplasmic reticulum of eukaryotes or the inner membrane of prokaryotes (Walter and Johnson, 1994; Pool, 2005). Although the size and composition of SRP are variable in different species, the key subunits of SRP are evolutionarily conserved (Saraogi and Shan, 2014). The *Escherichia coli* SRP is much simpler than that in eukaryotes, as it contains an essential and highly conserved subunit called the fifty-four homolog (Ffh), which is homologous to mammalian SRP54, and a small stable 4.5S RNA, which is homologous to domain IV in the mammalian 7S SRP RNA (Bernstein et al., 1993; Powers and Walter, 1997; Regalia et al., 2002). The *E. coli* SRP components can replace their mammalian homologs to mediate efficient co-translational protein targeting of mammalian proteins (Bernstein et al., 1993; Powers and Walter, 1997). This suggests that the subunit SRP54 and domain IV of

the 7S SRP RNA form the core elements of SRP, and SRP is remarkably conserved from bacteria to mammals. SRP is primarily responsible for delivering inner membrane proteins (Ulbrandt et al., 1997; Zhang and Shan, 2014). It recognizes hydrophobic transmembrane domains or signal sequences when they emerge from the ribosome exit tunnel (Ng et al., 1996). Furthermore, the nascent polypeptides must be targeted by SRP in a limited time window before they lose their competence due to aberrant aggregation (Siegel and Walter, 1998; Flanagan et al., 2003). Given the crowded cellular environment, it is challenging to correctly translocate newly synthesized proteins from the cytosol to the membrane.

SRP is generally essential in all three kingdoms of life (Egea et al., 2005; Akopian et al., 2013), except for the eukaryote *Saccharomyces cerevisiae* (Mutka and Walter, 2001) and prokaryotes *Streptococcus mutans* (Kremer et al., 2001) and *E. coli* (Zhao et al., 2021). In these cases, the global repression of protein synthesis is associated with the loss of SRP (Mutka and Walter, 2001; Hasona et al., 2007; Zhao et al., 2021). However, the precise mechanism of this tolerance remains poorly understood (Kremer et al., 2001; Mutka and Walter, 2001; Hasona et al., 2007; Zhao et al., 2021). One of the best-understood mechanisms is slowing the translation elongation rate that extends the time window for targeting translating ribosomes. Previous studies have demonstrated that slowing translation elongation speed contributes to improving protein folding and targeting (Siller et al., 2010; Zhang and Shan, 2012; Sherman and Qian, 2013). In co-translational translocation, protein folding and targeting are inherently coupled to translation elongation (du Plessis et al., 2011). The kinetic competition between protein translation elongation and targeting modulates the efficiency of the co-translational targeting pathway (Zhang and Shan, 2012; Chartron et al., 2016). In eukaryotes, the Alu domain of SRP arrests nascent chain translation elongation during its targeting, which is thought to pause translation elongation until the targeting is completed (Mason et al., 2000; Walter and Blobel, 1981). Furthermore, the Shine–Dalgarno (SD)-like sequence pauses translation before the second transmembrane domain exposed in *E. coli*, which facilitates the proper folding and targeting of membrane proteins (Fluman et al., 2014). Thus, the translation elongation is at the center of protein folding and targeting.

In our previous study, we identified SRP suppressors: two translation initiation factors IF2 and IF3, and a ribosomal protein RS3. The suppressor mutations decreased the translation initiation and elongation rate (Zhao et al., 2021). There are two possible explanations for the slowing translation elongation rate. First, it is possible that suppressor mutations directly inhibit the translation initiation and then decrease the translation elongation rate because the translation initiation rate is closely correlated with the elongation rate (Riba et al., 2019; Zhao et al., 2021). Alternatively, mutations that suppress the lack of SRP can directly affect the translation elongation rate, rather than indirectly decrease the rate of translation initiation. The ribosome is a hub in protein translation, which can directly modulate translation elongation (Pechmann et al., 2013; Sherman and Qian, 2013). Here, we isolated an SRP suppressor located at the SD sequence of ribosome S10 operon that could affect ribosome biogenesis. We addressed how the suppressor regulated the translation process and alleviated the fitness loss. Our results suggested that this mutation suppressed the loss of SRP, although the cell growth was severely inhibited and the targeting of SRP-dependent proteins was not completely compensated. This SRP suppressor reduced translation rate. Moreover, the translation initiation and elongation fidelity were decreased to improve cell viability. Overall, our results showed that mutations in the SD sequence of ribosome S10 operon contributed to protecting cells from lethal damages caused by the loss of SRP.

MATERIALS AND METHODS

Bacterial Strains, Plasmids, and Media

All bacterial strains, plasmids, and primers used in this study are listed in **Supplementary Table 1**. *E. coli* K-12 MG1655 derivative strains were grown either in LB medium or on LB agar at the indicated temperature. *E. coli* HDB51 strain, in which the expression of Ffh is under the control of an arabinose inducible promoter, was grown in LB medium containing 0.2% arabinose (Lee and Bernstein, 2001). The SRP suppressor strain MY1901 was isolated and validated as previously described (Zhao et al., 2021). The antibiotics kanamycin, gentamycin, ampicillin, and chloramphenicol were used at a concentration of 50, 10, 100, and 200 $\mu g\ ml^{-1}$, respectively. The *lac*, *trc*, and *tac* promoters were induced with 0.02 mM isopropyl-b-D-1-thiogalactopyranoside (IPTG). The *araBAD* promoter was induced with 0.2% arabinose.

Polysome Analysis, Cell Ultrastructure, and Proteomic Analysis

Strains were grown at 37°C at the early-exponential growth in LB medium and harvested by centrifugation (Zhao et al., 2021). Polysome analysis was performed as described (Zhao et al., 2021). The gradients were first extracted with a Piston Gradient Fractionator (Quan et al., 2005), and then their UV spectra were monitored by the ÄKTA equipment (Malecki et al., 2014). The scanning electron microscopy (SEM) and transmission electron microscopy (TEM) analyses were carried out as described previously (Zhao et al., 2021). The tested cells were randomly selected. The whole-cell lysates and inner membrane proteins of strains MY1901 and SRP^- were isolated and analyzed by liquid chromatography–tandem mass spectrometry (LC-MS/MS) as described (Wiśniewski et al., 2009; Wiśniewski and Mann, 2012; Tsolis and Economou, 2017; Zhao et al., 2021), with modifications. For seed culture, the strain MY1901 or HDB51 was inoculated in LB medium at 37°C overnight and the strain HDB51 was grown under the addition of 0.2% arabinose. The overnight culture of MY1901 was diluted into the fresh LB medium with an initial OD_{600} of 0.02–0.03. Strain MY1901 was harvested in the mid-exponential phase. The overnight culture of HDB51 was washed for three times with fresh LB medium and then incubated in LB with addition of 0.2% glucose with an initial OD_{600} of 0.03–0.04 for several hours, yielding the SRP^- strain. This strain was harvested when entering the stationary phase. Three sample replicates were prepared by performing collection of cells from independent cultures. We

used the Filter-Aided Sample Preparation (FASP) strategy for proteome analysis (Wiśniewski et al., 2009). The inner membrane fraction was separated by sucrose gradient (Tsolis and Economou, 2017). Then, the inner membrane was chemically treated by Na_2CO_3 and KCl to remove peripherally associated proteins (Zhao et al., 2021). The MS samples of inner membrane proteins were prepared by surface proteolysis (Tsolis and Economou, 2017). The sample was characterized by sequential window acquisition of all theoretical spectra (SWATH) analysis (Jylhä et al., 2018). The LC-MS/MS analysis was performed according to the previous study (Zhao et al., 2021). The obtained data were normalized by the median scale normalization (MedScale) method (Callister et al., 2006).

β-Galactosidase Assay

The b-galactosidase activity was assayed as previously described (Miller, 1972; O'Connor et al., 1997). Cells were grown in LB medium supplemented with 50 μg ml^{-1} kanamycin at 37°C. Protein induction was performed when MG1655Δ*lacZ* and MY1901Δ*lacZ* were grown to OD_{600} of 0.6–0.8 and 0.4–0.5, respectively. Two hours later, the cultures were harvested and assayed. β-Galactosidase activity from the plasmid encoding wild-type LacZ was used for normalization.

Measurements of Translation Efficiency and Initiation Fidelity

To determine the effects of mutated SD sequence on protein translation efficiency, we constructed plasmids carrying the *gfp* gene with the wild-type SD and suppressor mutation SD* under control of the promoter P_{S10} or P_{araBAD}. To analyze the translation initiation fidelity, a set of GFP variants was generated in which the start codon (AUG) and the initiator tRNA were replaced with different start codons and non-initiator tRNA codons, respectively. Several non-AUG start codons (GUG, UUG, AUA, and AUC) and non-initiator tRNA codons (UAG: CUA, CAC: GUG, and UAC: GUA) were used as potential start codons and initiator tRNA codons, respectively. *E. coli* cells were grown in 300 μl of LB medium with necessary antibiotics in a 96-well deep well culture plate at 37°C overnight in a stationary phase (MG1655Δ*lacZ*, OD_{600} > 3.0; MY1901Δ*lacZ*, OD_{600} > 1.0) followed by transferring and cellular fluorescence measurements (Hecht et al., 2017). For detecting the effects of SD sequence on translation efficiency and the fidelity of translation initiation, the strains containing empty vectors pJH30, pJH31, and pTrc99K lacking a reporter gene were used as controls. OD_{600} was measured to estimate culture density, followed by fluorescence (excitation = 488 nm, emission = 520 nm). Assays were carried out from at least three independent colonies. For the initiation fidelity assay, the fluorescence intensity of strains containing the plasmid encoding mutated GFP was normalized against the fluorescence intensity of wild-type or suppressor strains containing plasmid-encoded wild-type GFP.

Measurements of Translation Rates

Translation elongation rates were measured as described previously (Dai et al., 2016, 2018; Zhu et al., 2016). For seed culture, MG1655Δ*lacZ* and MY1901Δ*lacZ*Δ*cat* cells were cultured in LB medium at 37°C for several hours, then cultures were collected and washed with fresh MOPS medium. To improve the growth of the strains MG1655Δ*lacZ* and MY1901Δ*lacZ*Δ*cat*, they were grown in rich Glucose + cAA (0.2% glucose + 0.2% casamino acids) MOPS medium overnight as the pre-culture. The experiment culture was performed with an initial OD_{600} of 0.04–0.05. The subsequent collection and measurement methods were performed as previously described (Zhao et al., 2021). The translation elongation rate was measured based on the LacZα induction assay. The translation time of the first newly synthesized LacZα, T_α, was estimated by measuring the LacZα induction kinetics. The translation time of the first newly synthesized LacZα fused protein (FusA-LacZα or MsbA-LacZα), T_{total}, was obtained by the Schleif plot of the induction curve. The initiation time, T_{init}, equals $T_\alpha - \{90/[L/(T_{total}-T_\alpha)]\}$, where 90 is the 90 aa LacZα fragment and L is the length of the LacZα fusion protein (containing 10 aa linker). The translation elongation rate equals $(L + 90)/(T_{total}-T_{init})$. When MY1901Δ*lacZ*Δ*cat* grew in Glucose + cAA medium, the growth rate was about 0.6 h^{-1}. To eliminate the cell growth effect on translation elongation rate, the wild-type strain MG1655Δ*lacZ* was grown in Glycerol + NH_4Cl (0.2% glycerol + 10 mM NH_4Cl) MOPS medium and the growth rate was similar to 0.6 h^{-1}. The measurement of the elongation rate of MG1655Δ*lacZ* with the growth rate of 0.6 h^{-1} was performed similarly to that of MY1901Δ*lacZ*Δ*cat*. Translation initiation rate was estimated by a computational model homogeneous ribosome flow model (HRFM) (Margaliot and Tuller, 2012; Zarai et al., 2013, 2014). Based on the measured translation rate and elongation rate, the initiation rate can be calculated (Zhao et al., 2021).

Protein Targeting Assay *in vivo*

The biotinylation of proteins has been successfully applied to SRP-dependent protein targeting *in vivo* (Jander et al., 1996; Zhang and Shan, 2012). *E. coli* enzyme biotin ligase (BirA) can specially ligate biotin to a 15-amino acid peptide (GLNDIFEAQKIEWHE) termed the Avi-tag (Chen et al., 2005). The BirA and Avi-tagged proteins were co-expressed for biotinylation. Cells were co-transformed with recombinant vectors p15A-birA and pJH29-EspP/FtsQ/LacZ-Avi and grown overnight at 37°C. Then, overnight cultures were washed and diluted into 30 ml fresh LB medium at an initial OD_{600} of 0.02. For HDB51, the overnight culture grown in LB medium with 0.2% arabinose was washed and diluted into 30 ml fresh LB medium at an initial OD_{600} of 0.02 with or without arabinose to construct SRP^+ and SRP^- cells, respectively. When cultures reached an OD_{600} ~0.4–0.5 (SRP^- cells were cultured for 2–3 h), protein expression was induced by 0.5 mM IPTG, and 100 μM biotin was also added at this point. After 3 h of cultivation, cells were harvested by centrifugation. For Ffh depletion, 0.2% glucose was added 2 h before harvesting cells. Then, the samples were analyzed by SDS-PAGE and immunoblotting. Biotinylated proteins were detected by streptavidin-HRP and the total amount of protein was detected by anti-FLAG antibody. Detection was performed by the DAB substrate kit (Thermo Fisher Scientific, United States).

RESULTS

Characterization of an SRP Suppressor

A previous study in our laboratory demonstrated that SRP suppressors were all associated with protein translation (Zhao et al., 2021). To determine whether suppressor mutations of SRP are all mapped to chromosomal loci that influence protein translation and whether there is an alternative pathway to transport SRP substrates when the SRP pathway is blocked, we used the same suppressor approach as previously described to screen SRP suppressors (Zhao et al., 2021). We obtained another suppressor strain MY1901 that could survive when SRP was deleted (**Figure 1A**). The growth rate of MY1901 was significantly reduced compared with that of wild-type strain MG1655, demonstrating that the MY1901 strain had a severe growth defect. We also found a longer lag time during the growth course of MY1901 than that of MG1655 (**Figure 1A**), indicating that the lag time before regrowth bought time for cell adaptation in the absence of SRP. Whole-genome sequencing of the suppressor strain MY1901 and the original strain MG1655 allowed us to identify the suppressor mutation located in the SD sequence of ribosome S10 operon (**Figure 1B** and **Supplementary Table 2**). The S10 operon encodes 11 different ribosomal proteins (Zengel and Lindahl, 1994). To determine whether restoration of the wild-type alleles reverts the MY1901 strain to the wild-type growth phenotype, the Ffh expression and reverting suppressor mutation to the wild-type allele in the MY1901 strain were carried out (**Figure 1C**). The expression of Ffh markedly shortened the lag time and increased the growth rate (**Figure 1D**). Although reverting the suppressor mutation to the wild-type allele further increased the cell growth rate, the growth rate of strain MY1901FS was not equal to that of the wild-type strain MG1655 (**Figure 1D**). We also found that the growth rate of the MY1901 strain carrying the empty vector pTrc99K was a twofold decrease relative to that of the MY1901 strain without any plasmids (**Figures 1A,D**). Therefore, the plasmid pTrc99K caused a significant burden on cell growth of strain MY1901, which resulted in the growth rate of strain MY1901FS that did not fully recover to that of the wild-type strain. Thus, the deletion of Ffh and suppressor mutation indeed reduced cell growth. These results suggested that the mutation in the SD sequence of the S10 operon contributed to the cell growth without SRP and this mutation was a novel suppressor of SRP.

We hypothesized that the evolutionarily selective forces shaped the translation process during screening suppressors in SRP-deletion cells. Thus, we tried to improve cell growth through laboratory evolution. Strain MY1091 was evolved through 80 rounds of serial passage in the absence of any other selective pressure. The evolved strain showed an insignificant change in the growth rate but a shorter lag time before regrowth and increased biomass compared with the initial strains (**Supplementary Figure 1**). The laboratory evolved strains were sequenced and new changes in genes were identified (**Supplementary Table 2**). In the evolved strain MY1901, we found a mutation in the ribosomal protein S10 (RpsJ) belonging to the S10 operon, confirming that the S10 operon plays an important role in cell survival. Additionally, we obtained mutations in the DNA replication initiator protein DnaA (Hughes et al., 1988) and RNA polymerase RpoBC operon (Ishihama and Fukuda, 1980; **Supplementary Table 2**), which regulate gene expression. Taken together, protein synthesis plays a critical role in suppressing the loss of SRP.

Effects of SRP Suppressor on Ribosomal Protein Biogenesis

To examine the differences between wild-type and mutant SD sequence, the mfold web server (Zuker, 2003) was used to model mRNA structures of the S10 leader sequence containing the SD sequence. S10 leader is required for the regulation of S10 operon (Allen et al., 1999). We found a 2.4 kcal mol^{-1} difference in the minimum free energy of the thermodynamic ensemble of the predicted structure of mutant SD compared to the wild-type SD (**Supplementary Figure 2**), suggesting that the S10 leader with mutant SD was less stable. Because translation initiation is partially modulated by the SD sequence (Yang et al., 2016), the effects of the mutant SD sequence on protein translation were determined. The expression level of the green fluorescent protein (GFP) was used to characterize protein translation levels in cells. Regardless of whether under the original promoter P_{S10} or the arabinose inducible promoter P_{araBAD}, the expression level of GFP with the mutated SD (SD*) was significantly decreased (**Figure 2A**), confirming that the suppressor mutation weakened the binding of mRNA SD sequence to rRNA in ribosomes. This result suggested that the translation initiation rate of the S10 operon was reduced. To examine whether the suppressor mutation decreases the abundance of ribosomal proteins, the whole-cell lysates proteome of strain MY1901 was analyzed (**Supplementary Data Set 1A**). The expression level of each gene was normalized by that in wild-type strain MG1655 (Zhao et al., 2021). Unexpectedly, the levels of the S10 operon and even the overall ribosomal proteins were upregulated (**Figure 2B** and **Supplementary Data Set 1B**). Given that the growth rate is linearly correlated with the cell's active ribosome content (Scott et al., 2010) and the suppressor strain MY1901 showed a very low growth rate of 0.2 h^{-1} (**Figure 1A**), the active ribosomal protein content would be reduced. We speculated that the increased pool of ribosomal proteins may be caused by the accumulation of ribosomal proteins. There are two possibilities: one is that the ribosomes stalls at the translation initiation site (Zhao et al., 2021); the other is that cellular stress responses caused by the decreased active ribosome level induce the upregulation of ribosomal proteins, including the S10 operon. Thus, further studies are needed for a better understanding of the biogenesis of ribosomal proteins.

Translation Speed and Accuracy in Suppressor Cells

In order to test the potential relationship between the biogenesis of ribosomal proteins and protein translation, we first carried out polysome profiling, which could detect various defects of translation. The polysome profile of suppressor cells was changed

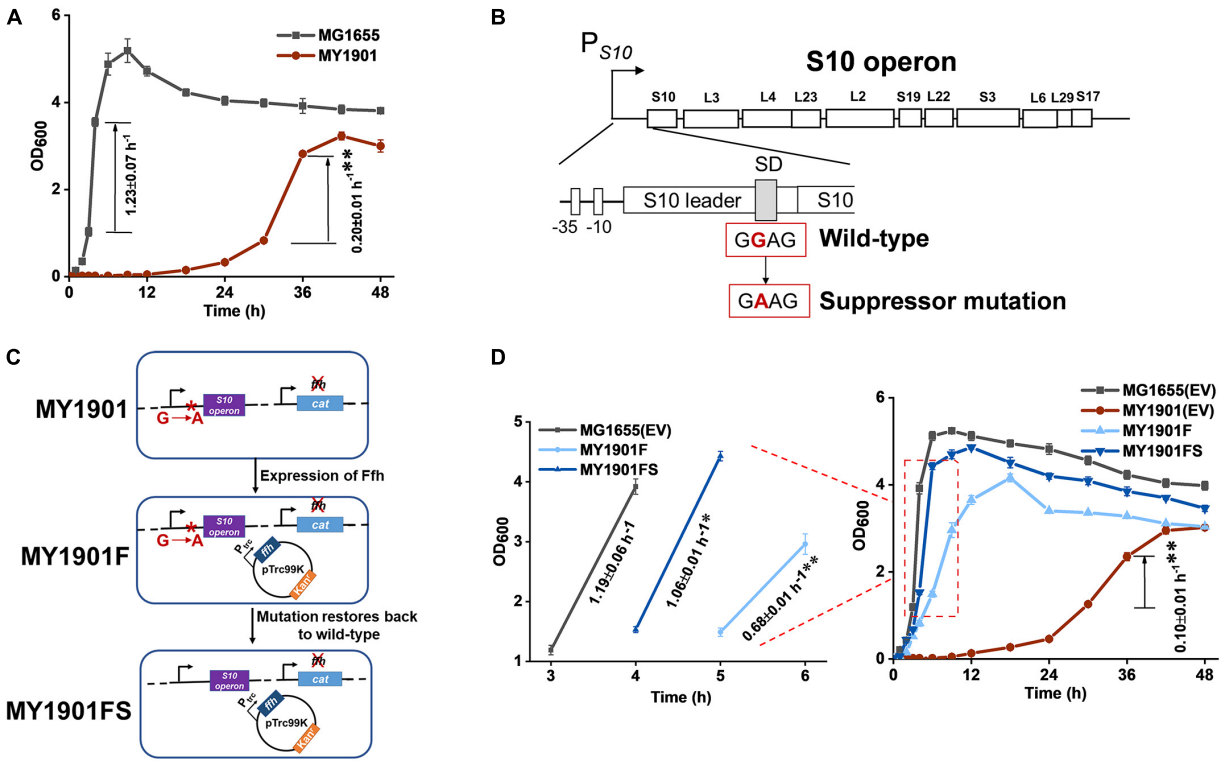

FIGURE 1 | Identification of SRP suppressor strain and its growth. **(A)** Growth curves and growth rates of the wild-type strain MG1655 and the suppressor strain MY1901. **(B)** The suppressor mutation sites in the SD sequence of S10 operon. The region and encoded ribosomal proteins of the S10 operon are shown. The wild-type SD sequence (GGAG) mutated into suppressor mutation (GAAG). **(C)** Restoration of the wild-type allele. Plasmid pTrc99K-Ffh was first transformed into strain MY1901, generating the strain MY1901F. Ffh protein was produced at low level in MY1901 to reduce the toxicity of overexpression of Ffh. Then, the suppressor mutation (GAAG) was restored to wild-type SD sequence (GGAG) by site-directed mutagenesis, generating the strain MY1901FS. **(D)** Growth curves and growth rates of four strains: MG1655 and MY1901carrying the empty vector (EV) pTrc99K, MY1901F, and MY1901FS. Strains MG1655 and MY1901 carrying the empty vector pTrc99K were used as control. Solid curves are the mean of three independent measurements, and error bars represent the standard deviation of the mean value. Growth rates were figured out from the logarithmic phase. All growth rates shown represent the mean ± standard deviation of three independent experiments. Statistical significance compared to wild-type strain using Student's *t*-test is indicated as follows: $^{*}P < 0.05$; $^{**}P < 0.01$.

relative to that of wild-type cells (**Figure 3A**). The 30S to 50S (30S/50S) ratio was not significantly altered in suppressor and wild-type strains, but 30S and 50S peaks of suppressor cells were higher than those of wild-type cells (**Figure 3A**), indicating an increase in the proportion of free subunits. The 70S peak of the wild-type cells was almost indistinguishable from that of suppressor cells (**Figure 3A**), suggesting that some 70S ribosomes paused at the translation initiation site, which can cause the ribosomal proteins accumulated in the cytoplasm (Zhao et al., 2021). We also observed that the polysome to 70S monosome (P/M) ratio was decreased in suppressor cells relative to that in wild-type cells (**Figure 3A**), suggesting that translation elongation was inhibited in suppressor cells. This result also demonstrates that the active ribosomal protein content in suppressor cells is reduced relative to that in wild-type cells. Thus, the protein translation efficiency is affected in suppressor cells.

Translation can be divided into four phases: initiation, elongation, termination, and ribosome recycling (Rodnina, 2018). We next compared the abundances of translation-associated factors *via* whole-cell lysate proteome analysis. Ribosome recycling factor (RRF) and elongation factor-G (EF-G) are involved in ribosome recycling (Prabhakar et al., 2017). The expression of RRF and EF-G was downregulated in the suppressor strain (**Figure 3B** and **Supplementary Data Set 1B**), indicating that the ribosome recycling was reduced, which may be caused by decreasing translation in suppressor cells. Although the expression of release factors mediating translation termination was upregulated, the efficiency of translation termination at three stop codons was only slightly increased (**Figures 3B,C**). This data showed that the translation termination rate was unaffected in suppressor cells. We observed that the protein abundance of elongation factors in suppressor cells was inconsistent and changed little in comparison with that in wild-type cells (**Figure 3B** and **Supplementary Data Set 1B**). To examine the efficiency of translation elongation, we measured its fidelity and speed through GFP fluorescence intensity measurement and LacZα induction assay, respectively. In strain MY1901, we observed a marked increase in translational frameshifting readthrough relative to that in the wild-type strain (**Figure 3D**), suggesting that the fidelity of translation elongation was decreased. Additionally, a LacZ induction assay was used to

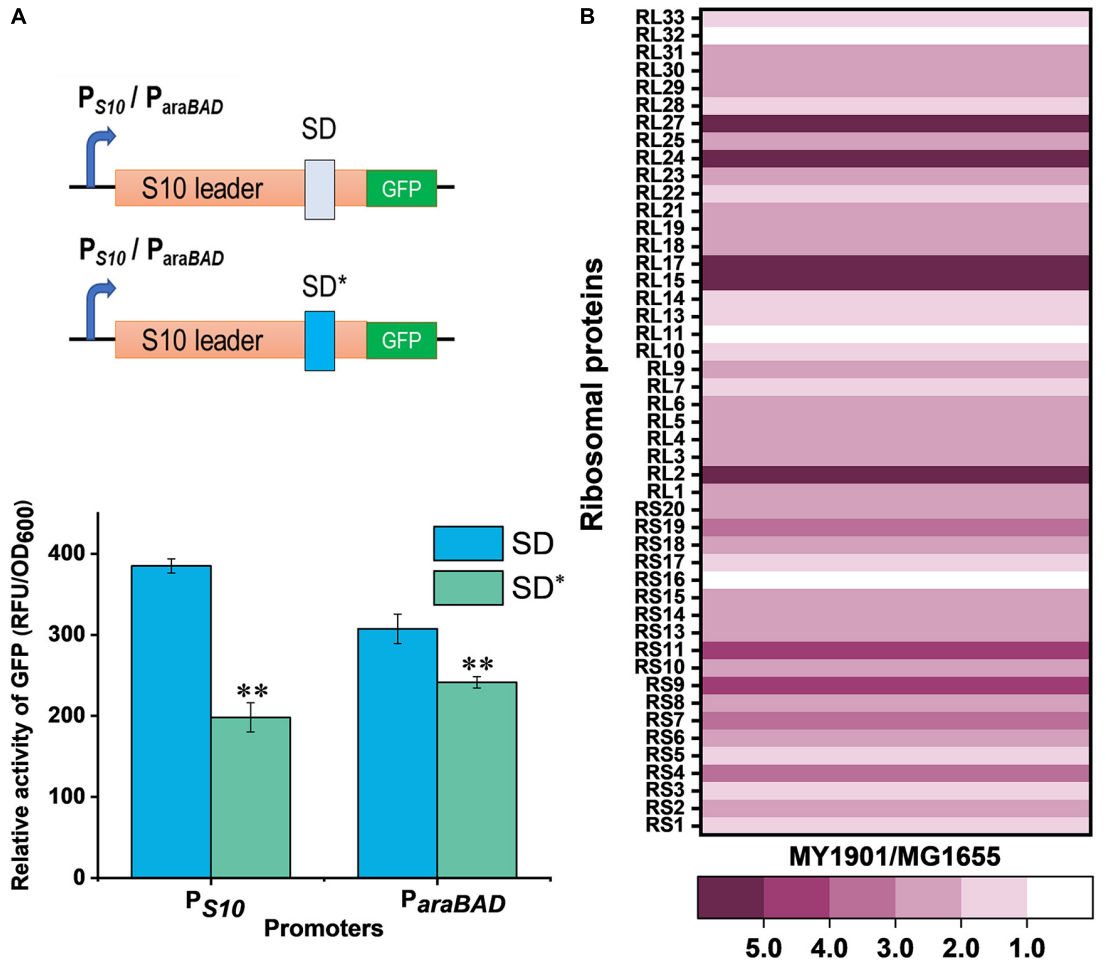

FIGURE 2 | Effects of SRP suppressor on ribosomal protein synthesis. **(A)** Effects of mutant SD sequence on protein translation. GFP was used as a reporter to measure gene expression. (Top) Graphical representation of GFP expression. P_{S10}/P_{araBAD}-GFP with wild-type SD and suppressor mutation SD* were introduced into cells. (Bottom) Fluorescence measurement of GFP. Data represent the mean of six independent experiments, and error bars represent the standard deviation of the mean value. Statistical significance compared to wild-type SD sequence using Student's *t*-test is indicated as follows: $^{*}P < 0.05$; $^{**}P < 0.01$. **(B)** Fold changes in the expression of ribosomal proteins in strain MY1901relative to that in strain MG1655 (**Supplementary Data Set 1B**).

measure the translation elongation speed (Zhu et al., 2016). We used a cytoplasmic protein FusA and an inner membrane protein MsbA to define the level of translation elongation rate (**Supplementary Figure 3**). When cells were grown at the same rich growth media (Glucose + cAA), the growth rates of wild-type and suppressor cells were approximately 1.0 h^{-1} (Zhao et al., 2021) and 0.6 h^{-1}, respectively (**Supplementary Figure 3A** and **Supplementary Table 3**). As expected, the translation elongation rate of suppressor cells was markedly decreased compared with that of wild-type cells (**Figure 3E** and **Supplementary Figures 3B–F**). As translation elongation rate closely depends on growth rate (Dai et al., 2016), we further reduced the growth rate of wild-type cells to 0.6 h^{-1} that was similar to that of suppressor cells (**Supplementary Figure 3A**). The elongation rate of the MsbA in suppressor cell was reduced by approximate 2.0 aa s^{-1} (amino acids per second) compared with that in wild-type cells, but the elongation rate of the FusA was similar in both wild-type and suppressor cells (**Figure 3E** and **Supplementary Figures 3B–F**). We also observed that the elongation rate of MsbA was slower than that of FusA (**Figure 3E** and **Supplementary Figures 3B–F**), which is consistent with the observation that the translation elongation speed of inner membrane proteins is slowed down during targeting, but not that of cytoplasmic proteins (Fluman et al., 2014).

For the expression of translation initiation factors in suppressor cells, IF1 and IF3 were downregulated, but IF2 was upregulated (**Figure 3B**). Given that IF2 accelerates ribosomal subunit joining, whereas IF1 and IF3 slowed down subunit association (Naaktgeboren et al., 1977; Ling and Ermolenko, 2015), the capacity of formation of 70S initiation complex may not be significantly impaired, although cells showed severe defects in growth. We next examined the translation initiation rate by a computational model called the homogeneous ribosome flow model (HRMF), in which the translation elongation rate

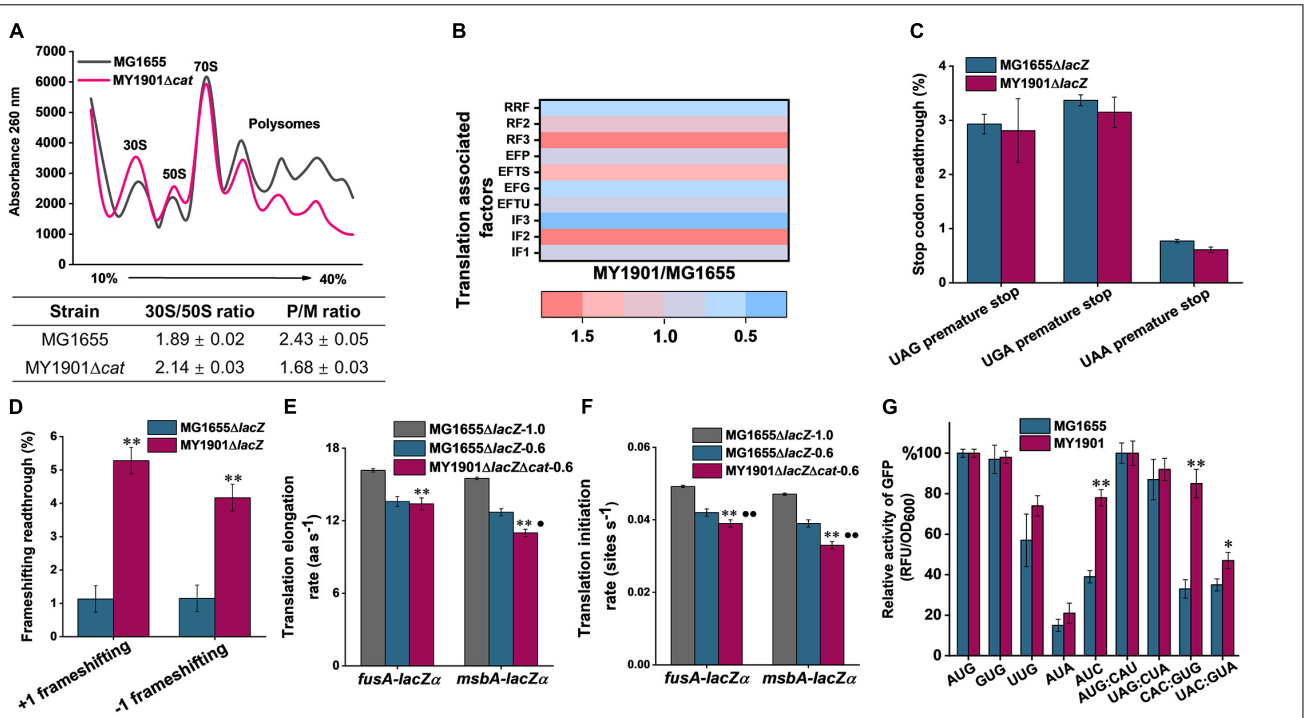

Strain	30S/50S ratio	P/M ratio
MG1655	1.89 ± 0.02	2.43 ± 0.05
MY1901Δ*cat*	2.14 ± 0.03	1.68 ± 0.03

FIGURE 3 | Effects of SRP suppressor on translation efficiency. **(A)** Polysome profiles of the wild-type strain MG1655 and the suppressor strain MY1901Δ*cat*. Data represent the mean ± standard deviation of three independent experiments. **(B)** Fold changes in the expression of translation associated factors in strain MY1901relative to that in MG1655 (**Supplementary Data Set 1B**). **(C,D)** Effect of suppressor mutation on stop-codon **(C)** and frameshifting **(D)** readthrough. All data are averages of at least three independent experiments, and error bars represent the standard deviation of the mean. b-Galactosidase activities of strains harboring the mutant LacZ reporters were calculated relative to those of the same strain harboring the wild-type LacZ. Statistical significance compared to the suppressor strain MY1901Δ*cat* using Student's *t*-test is indicated as follows: $^{*}P < 0.05$; $^{**}P < 0.01$. **(E)** The translation elongation rates of FusA-LacZα and MsbA-LacZα under different growth rates (MG1655Δ*lacZ*, 1.0 h^{-1}; MG1655Δ*lacZ*, 0.6 h^{-1}; MY1901Δ*lacZ*Δ*cat*, 0.6 h^{-1}). **(F)** The translation initiation rate of proteins was estimated based on their corresponding translation elongation rate. All data are averages of three independent experiments, and error bars represent the standard deviation of the mean value. Statistical significance compared to the strain MG1655Δ*lacZ* with growth rate 1.0 h^{-1} using Student's *t*-test is indicated as follows: $^{*}P < 0.05$; $^{**}P < 0.01$. Statistical significance compared to the strain MG1655Δ*lacZ* with growth rate 0.6 h^{-1} using Student's *t*-test is indicated as follows: $^{*}P < 0.05$; $^{**}P < 0.01$. **(G)** Initiation with various non-canonical start codons and non-initiator tRNA codons in the wild-type and suppressor strains. Relative activities of mutant GFP were calculated relative to that of the same strain harboring the wild-type GFP. The wild-type start codon was indicated as AUG, and the wild-type initiator tRNA was indicated as AUG: CAU. All data are averages of three independent experiments, and error bars represent the standard deviation of the mean value. Statistical significance compared to the strain MG1655 using Student's *t*-test is indicated as follows: $^{*}P < 0.05$; $^{**}P < 0.01$.

is assumed to be constant (Margaliot and Tuller, 2012). The translation initiation rate can be estimated by the measurable translation rate and translation elongation rate (**Supplementary Table 4**). The translation initiation rate in suppressor cells showed a similar trend to the translation elongation rate. The initiation rate of FusA was not markedly changed in the suppressor and wild-type cells when grown at the same growth rate (**Figure 3F**). However, the inner membrane protein MsbA had a slower translation initiation rate in suppressor cells than that in wild-type cells when grown at the same growth rate (**Figure 3F**). Thus, in suppressor cells, the translation initiation process was negatively affected, although the formation of the 70S initiation complex was not markedly influenced (**Figure 3A**). As translation initiation factors play a vital role in translation initiation fidelity (Ling and Ermolenko, 2015), we addressed whether the suppressor was detrimental to the fidelity of start codon selection and initiator tRNA binding. We changed the start codon of GFP from AUG to other two canonical start codons GUG and UUG, and two near cognates AUA and AUC (Hecht et al., 2017), and the initiator tRNA codon of GFP from AUG: CAU to non-initiator tRNAs UAG: CUA, CAC: GUG, and UAC: GUA. We measured the GFP fluorescence of these GFP variants in the wild-type and suppressor cells. We observed that the expression levels of GFP with three canonical start codons (AUG, GUG, UUG) and a near cognate (AUA) were similar in both wild-type and suppressor strains (**Figure 3G**). However, the expression level of GFP with the near cognate AUC as the start codon in the suppressor strain was significantly increased relative to that in the wild-type strain (**Figure 3G**). We also found that in the suppressor strain, the expression levels of GFP with non-initiator tRNAs CAC: GUG and UAC: GUA were significantly increased compared with those in the wild-type strain (**Figure 3G**). Additionally, the level of GFP with the initiator tRNA AUG: CAU in the suppressor strain was not changed relative to that in the wild-type strain (**Figure 3G**). Thus, the fidelity of translation initiation in the suppressor cells was decreased compared with that in wild-type cells. Taken together, the suppressor

cell trades translation speed and accuracy for cell survival in the absence of SRP.

SRP-Dependent Protein Targeting in Suppressor Cells

In *E. coli*, most inner membrane proteins are delivered by the co-translational SRP pathway (Elvekrog and Walter, 2015). In principle, SRP-dependent proteins are not properly targeted to the bacterial cytoplasmic membrane after Ffh depletion (Bernstein and Hyndman, 2001; Wickström et al., 2011). To test whether the suppressor mutation could suppress protein targeting defects, we first examined cell morphological changes by SEM and TEM. SEM images showed that the suppressor strain MY1901 still had typical rod morphology but had a rougher surface relative to the wild-type strain MG1655 (**Figure 4A** and **Supplementary Figure 4**). TEM images showed that the suppressor strain MY1901 retained cell wall integrity but had damaged inner membrane structure (**Figure 4A** and **Supplementary Figure 4**). MY1901 displayed a significant detachment of the inner membrane from the outer membrane (**Figure 4A** and **Supplementary Figure 4**). Thus, the suppressor mutation partially offsets the negative effects of the loss of the SRP pathway on the inner membrane protein translocation.

To gain an insight into the localization of inner membrane proteins, we performed proteomic analysis of inner membrane proteins in the wild-type strain MG1655 (Zhao et al., 2021) and the suppressor strain MY1901 (**Supplementary Data Set 1C**). The *E. coli* HDB51 was used as a control strain, in which the expression of Ffh was induced by arabinose (Lee and Bernstein, 2001). Depleted Ffh can be obtained after several hours of incubation in the presence of glucose, thus yielding the SRP$^-$ strain (Zhang et al., 2012). The inner membrane proteome analysis of SRP$^-$ was also conducted (**Supplementary Data Set 1C**). According to our previous study, we identified 262 SRP-dependent inner membrane proteins (Zhao et al., 2021). Our previous study has shown that the inner membrane proteins with a high abundance, such as proteins C_4-dicarboxylate sensor kinase DcuS and zinc transporter FieF, can be localized to the membrane (Zhao et al., 2021). This suggested that the high protein abundance can be used as an indicator of protein localization. We found that the abundance of many identified SRP-dependent inner membrane proteins in both MY1901 and SRP$^-$ cells was higher than their abundance in wild-type cells (**Figure 4B** and **Supplementary Data Set 1D**), indicating that these inner membrane proteins can target to the cytoplasmic membrane in the absence of SRP. This result is consistent with previous studies showing that inhibition of the SRP pathway only partially impedes inner membrane protein targeting (Ulbrandt et al., 1997; Newitt et al., 1999; Bernstein and Hyndman, 2001). We also found that more proteins were successfully targeted in the MY1901strain than in the SRP$^-$ strain (**Figure 4B**), suggesting that the suppressor mutation indeed plays a role in inner membrane protein targeting without SRP. FtsQ is an SRP-dependent protein, which is often used as a model protein for studying SRP-mediated protein targeting (Scotti et al., 1999; Zhang and Shan, 2012). However, the targeting of FtsQ was not significantly inhibited in strains SRP$^-$ and MY1901 (**Figure 4B** and **Supplementary Data Set 1D**). To examine the targeting level of FtsQ, we used a sensitive method based on protein biotinylation (Jander et al., 1996; Zhang and Shan, 2012). A small biotinylatable peptide Avi-tag was fused to the periplasmic domain of the targeted proteins. The biotinylated proteins would be the untargeted proteins in which the periplasmic domains are exposed in the cytosol. Thus, the protein biotinylation can be used for protein targeting assay. However, in contrast to the prediction of proteomic analysis, the FtsQ targeting showed a slight defect in both the SRP$^-$ and MY1901 strains (**Figure 4C**), suggesting that the suppressor mutation played little role in the targeting of FtsQ. We also found that the targeting levels of the SRP-independent protein EspP were similar in both wild-type and MY1901strains (**Figure 4C**), suggesting that the targeting of SRP-independent proteins was not affected by the loss of SRP. However, there was a slight defect in EspP targeting in SRP$^-$ strain. This may be caused by the secondary effect due to the defects of SRP-dependent transporters, such as SecY, SecG, and YajC (**Supplementary Figure 5A** and **Supplementary Data Set 1E**). We also found that the protein abundance of almost all identified membrane components of transporters in MY1901 was not lower than that in the SRP$^-$ strain (**Supplementary Figure 5A** and **Supplementary Data Set 1E**). These results indicated that the SRP suppressor partially contributed to inner membrane protein targeting and allowed for targeting of some SRP-dependent proteins without causing a failure of targeting of SRP-independent proteins.

Additionally, the expression of heat shock response related chaperones and proteases was not upregulated (**Supplementary Figure 5B** and **Supplementary Data Set 1B**), suggesting that the heat shock response played little role in compensating the loss of SRP, which is consistent with our previous study (Zhao et al., 2021). In strain MY1901, the protein abundance of SecA was not affected and other transport components such as SecYEG, YajC, SecD, YidC, SecF, and FtsY showed a decreased level relative to that in the wild-type strain (**Supplementary Figure 5A** and **Supplementary Data Set 1E**). Moreover, we found that the protein abundance of SecF in the MY1901 strain was significantly decreased relative to that in the SRP$^-$ strain (**Supplementary Figure 5A** and **Supplementary Data Set 1E**). This suggested that the component of the Sec translocon SecF may not be involved in the protein targeting process without SRP. In contrast, the protein abundance of SecY and FtsY in MY1901 was two times higher than that in the SRP$^-$ strain, which is likely caused by the effective targeting of inner membrane proteins with the assistance of translational control. Overall, protein transport components were unlikely to play a major role in mediating SRP-dependent protein targeting in the absence of SRP.

DISCUSSION

Co-translational protein targeting by SRP is an essential and conserved pathway that delivers most inner membrane proteins to their correct subcellular destinations (Saraogi and Shan, 2014). Our previous work revealed that SRP was not essential in

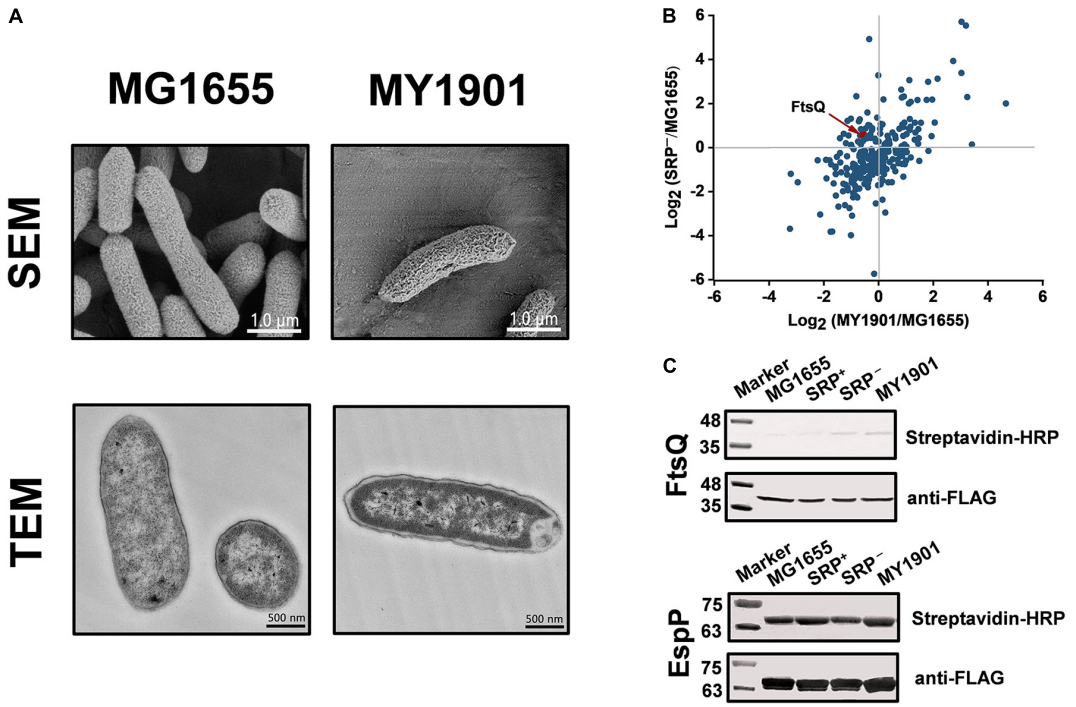

FIGURE 4 | Suppressor mutation suppresses targeting defects of partial inner membrane proteins. **(A)** Scanning electron microscopy (SEM) and transmission electron microscopy (TEM) analysis of the wild-type strain MG1655 and the suppressor strain MY1901. For SEM, the scale bar is 1.0 μm. For TEM, the scale bar is 500 nM. **(B)** Quantification of identified SRP-dependent inner membrane proteins in strains MY1901 and SRP$^-$ (**Supplementary Data Set 1D**). Protein abundance of MY1901 and SRP$^-$ is relative to that of wild-type MG1655. **(C)** FtsQ (left) and EspP (right) targeting assay by their biotinylation. SRP$^+$, Ffh expression in HDB51 strain; SRP$^-$, Ffh depletion in HDB51 strain.

E. coli when the translation initiation and elongation rate were decreased (Zhao et al., 2021). Isolation of suppressors is a useful strategy to provide insight into certain molecular mechanisms by suggesting which cellular component is involved in an inefficient process (Lee and Beckwith, 1986). The SRP suppressors involved in protein translation initiation have been identified before, and these suppressors affect the translation process (Zhao et al., 2021). In this study, we obtained an SRP suppressor associated with protein translation too. The regulation of translation may be a general way to mediate the translocation of SRP-dependent proteins in the absence of SRP.

We observed that in suppressor cells, the ribosomal protein expression was upregulated (**Figure 2B**) and the 30S and 50S ribosomal subunits accumulated (**Figure 3A**), but the content 70S ribosome complex was not markedly changed relative to those in the wild-type strain (**Figure 3A**). This led us to propose that the increased ribosomes are inactive and accumulate in the cytosol. Furthermore, in earlier works, deletion of SRP caused the downregulation of ribosomal proteins (Wickström et al., 2011; Zhang et al., 2012), which suggested that the absence of SRP alone cannot increase the level of ribosomal proteins. Thus, the SRP suppressor and cellular stress responses may play an important role in ribosomal protein synthesis.

In suppressor cells, the protein translation initiation was impeded (**Figure 3F**), but the initiation time of translation was constant in wild-type and suppressor cells under different growth rates (**Supplementary Table 3**), which suggested that the pausing at the start of the initiation can be negligible, and the process of 70S ribosome complex entry into the elongation cycle is slower in suppressor cells. Thus, the SRP suppressor may be associated with the transition from initiation to elongation. The closely related relationship between translation initiation and elongation (Riba et al., 2019) and the decreased translation initiation and elongation rates caused by the absence of SRP (**Figures 3E,F**) suggested the possibility that this SRP suppressor mutation can reduce either the translation initiation rate or the elongation rate.

Furthermore, we showed that the translation fidelity was decreased in suppressor cells (**Figures 3D,G**). Because the fidelity of translation initiation is modulated by the initiation factors (Ayyub et al., 2017; Caban et al., 2017) and the suppressor mutation was associated with the biogenesis of ribosomal proteins (**Figure 2B**), we speculated that the suppressor may indirectly regulate the fidelity of translation initiation by influencing the abundance of translation initiation factors (**Figure 3B**). We observed that the fidelity of translation elongation was also decreased, implying that suppressor mutation may inactivate the quality control system. Earlier works revealed that mistranslation could provide a growth advantage in response to stress (Gu et al., 2014; Mohler and Ibba, 2017). Hence, the decreased fidelity of translation initiation and elongation may result from the SRP deletion stress response.

Increasing evidence has supported the notion that the translation elongation of nascent polypeptide regulates the targeting of SRP-dependent proteins (du Plessis et al., 2011; Zhang and Shan, 2012), thus decreasing the elongation rate that contributes to the survival of SRP deletion cells. Decreasing the translation elongation rate extends the time window for protein targeting, which plays a critical role in suppressing the loss of SRP (Zhao et al., 2021). SRP binds to the ribosome-nascent chain complex when the N-terminus of the first TMD is exposed from the ribosome. The maximal SRP binding site is 55 amino acids from the ribosomal peptidyl transferase center in *E. coli* (Schibich et al., 2016). Assuming that ~30 amino acids can fit into the ribosome exit tunnel (Bornemann et al., 2008), 25 residues would be exposed outside the tunnel. At a translation elongation rate of ~15 aa s^{-1} in rapid growth conditions (Zhao et al., 2021), the maximum time required for protein localization is ~2 s (**Figure 5**). Thus, with the help of SRP, most translating ribosomes move to the membrane within this period in *E. coli*. Without SRP, suppressors slowed the translation elongation rate to ~11 aa s^{-1} (**Figure 3E** and **Supplementary Table 3**), which provides ~2 s for nascent chains of 55 amino acids to target to the inner membrane (**Figure 5**). However, it is not likely that nascent chains successfully target to the membrane within ~2 s without SRP. To get a longer time to find the membrane, the length of translating nascent chains is more likely longer than 55 amino acids. However, the nascent chain cannot exceed a specific length as aggregation would prevent protein from being targeted (Siegel and Walter, 1998; Flanagan et al., 2003), and this specific length is called the critical length (L) for targeting. Proteins with fewer transmembrane domains (TMDs) or longer first loop lengths have a longer critical length (Zhao et al., 2021). Furthermore, if the nascent chain exceeds a critical length of ~140 amino acids, it becomes translocation-incompetent (Siegel and Walter, 1998; Flanagan et al., 2003). In suppressor cells, the upper limit of the critical time for protein targeting would be ~10 s (**Figure 5**). If the targeting time of some SRP-dependent proteins exceeds 10 s, these proteins would not be targeted to the inner membrane in suppressor cells. Thus, the suppressor extends the time window to ~2–10 s (**Figure 5**). Taken together, this model shows that SRP greatly shortened the protein targeting time by 8 s, which minimizes the cost of targeting and maintains fast growth. Overall, our data suggest that in response to the deletion of SRP, suppressor cells attenuate translation elongation to give the translating ribosomes more time to find and target to the inner membrane.

As expected, the suppressor mutation can partially offset the defective targeting of inner membrane proteins (**Figure 4B**), which is consistent with the previous result (Zhao et al., 2021). Furthermore, we found that in the SRP depletion strain SRP^{-}, many proteins can successfully target to the inner membrane (**Figure 4B**). However, proper localization of these proteins cannot bypass the requirement of SRP (Phillips and Silhavy, 1992). We speculated that the proteins that could be correctly located in the suppressor strain MY1901 but not in SRP depletion strain SRP^{-} may be responsible for cell survival. We hypothesized that specific membrane protein targeting defects could block the essential cellular process, which would be responsible for the loss of cell viability. Among these localization defective proteins, only one protein PgsA is essential for *E. coli* (**Supplementary Data Set 1F**). PgsA catalyzes the step in the synthesis of the acidic phospholipids that are considered to be indispensable in multiple cellular processes (Gopalakrishnan et al., 1986; Kikuchi et al., 2000). We inferred that mislocalization of PgsA inhibited cell growth. Furthermore, in SRP^{-} strain, some transportation associated proteins (AsmA, Bcr, PheP, YbaL, and YidE) did not successfully target to the inner membrane (**Supplementary Data Set 1F**), which would impair membrane traffic and decrease energy production. More studies are needed to investigate the targeting of some proteins that determine whether cells can survive without SRP.

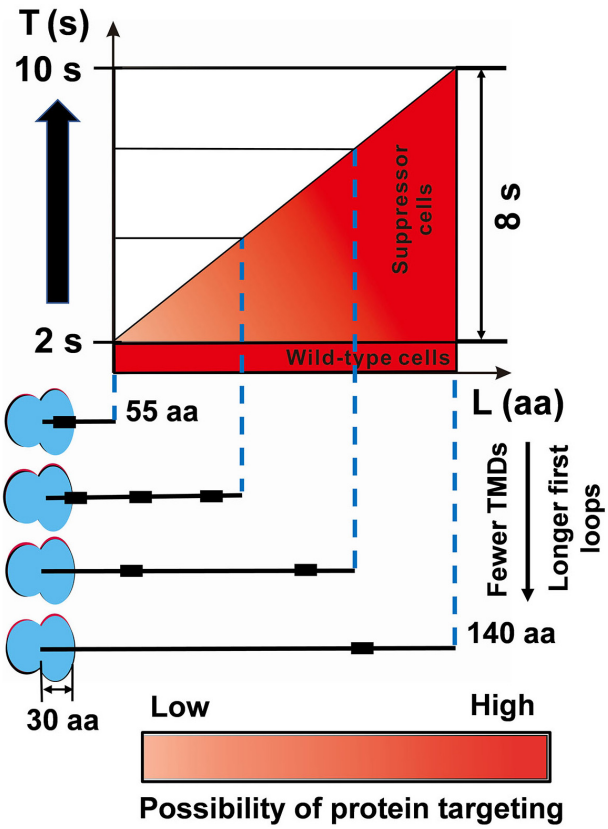

FIGURE 5 | The SRP suppressor extends the time window for protein targeting. In wild-type MG1655 cells, although the critical length (L) of inner membrane proteins is variable, the targeting time (T) is fast (~2 s). The suppressor cells with a slower elongation rate extended the time window for protein targeting to 2–10 s. For details and references, see section "Discussion."

SUMMARY

The SRP-dependent delivery pathway is essential for membrane protein biogenesis. Previously, we reported that SRP was non-essential in *Escherichia coli*, and slowing translation speed played a critical role in membrane protein targeting. Here, we identified

a novel SRP suppressor that is also involved in translation. We found that translation speed and accuracy regulate membrane protein targeting. A slowdown of translation speed extended the time window for protein targeting. Meanwhile, a moderate decrease in translation fidelity ensured a suitable translation speed for better cell growth. These results argued that translation control could be a practical way to compensate for the loss of SRP.

DATA AVAILABILITY STATEMENT

The raw data supporting the conclusions of this article will be made available by the authors, without undue reservation.

AUTHOR CONTRIBUTIONS

LZ, GF, and DZ designed the experiments. LZ and YC performed the experiments. LZ, YC, ZX, and TC analyzed the data. LZ and DZ wrote the manuscript. All authors contributed to the article and approved the submitted version.

FUNDING

This work was supported by the National Key R&D Program of China (2020YFA0907800) and Tianjin Synthetic Biotechnology Innovation Capacity Improvement Project (TSBICIP-KJGG-004-03 and TSBICIP-KJGG-006).

ACKNOWLEDGMENTS

We thank Dr. Manlu Zhu (Central China Normal University) for plasmid pKUT15-fusA-lacZα, Dr. Changhao Bi (TIB, CAS) for plasmid pRed_Cas9_ΔpoxB300, Dr. Harris D Bernstein (NIH) for strain HDB51 and plasmid pJH29, and Dr. Zhidan Zhang (TIB, CAS) for help with mass spectrometry.

SUPPLEMENTARY MATERIAL

The Supplementary Material for this article can be found online at: https://www.frontiersin.org/articles/10.3389/fmicb.2021.690286/full#supplementary-material

REFERENCES

Akopian, D., Shen, K., Zhang, X., and Shan, S. O. (2013). Signal recognition particle: an essential protein-targeting machine. *Annu. Rev. Biochem.* 82, 693–721. doi: 10.1146/annurev-biochem-072711-164732

Allen, T., Shen, P., Samsel, L., Liu, R., Lindahl, L., and Zengel, J. M. (1999). Phylogenetic analysis of L4-mediated autogenous control of the S10 ribosomal protein operon. *J. Bacteriol.* 181, 6124–6132. doi: 10.1128/jb.181.19.6124-6132.1999

Ayyub, S. A., Dobriyal, D., and Varshney, U. (2017). Contributions of the N- and C-Terminal domains of initiation Factor 3 to its functions in the fidelity of initiation and antiassociation of the ribosomal subunits. *J. Bacteriol.* 199:e00051-17.

Bernstein, H. D., and Hyndman, J. B. (2001). Physiological basis for conservation of the signal recognition particle targeting pathway in *Escherichia coli*. *J. Bacteriol.* 183, 2187–2197. doi: 10.1128/jb.183.7.2187-2197.2001

Bernstein, H. D., Zopf, D., Freymann, D. M., and Walter, P. (1993). Functional substitution of the signal recognition particle 54-kDa subunit by its *Escherichia coli* homolog. *Proc. Natl. Acad. Sci. U.S.A.* 90, 5229–5233. doi: 10.1073/pnas.90.11.5229

Bornemann, T., Jöckel, J., Rodnina, M. V., and Wintermeyer, W. (2008). Signal sequence-independent membrane targeting of ribosomes containing short nascent peptides within the exit tunnel. *Nat. Struct. Mol. Biol.* 15, 494–499. doi: 10.1038/nsmb.1402

Caban, K., Pavlov, M., Ehrenberg, M., and Gonzalez, R. L. Jr. (2017). A conformational switch in initiation factor 2 controls the fidelity of translation initiation in bacteria. *Nat. Commun.* 8:1475.

Callister, S. J., Barry, R. C., Adkins, J. N., Johnson, E. T., Qian, W. J., Webb-Robertson, B. J., et al. (2006). Normalization approaches for removing systematic biases associated with mass spectrometry and label-free proteomics. *J. Proteome Res.* 5, 277–286. doi: 10.1021/pr050300l

Chartron, J. W., Hunt, K. C., and Frydman, J. (2016). Cotranslational signal-independent SRP preloading during membrane targeting. *Nature* 536, 224–228. doi: 10.1038/nature19309

Chen, I., Howarth, M., Lin, W., and Ting, A. Y. (2005). Site-specific labeling of cell surface proteins with biophysical probes using biotin ligase. *Nat. Methods* 2, 99–104. doi: 10.1038/nmeth735

Dai, X., Zhu, M., Warren, M., Balakrishnan, R., Okano, H., Williamson, J. R., et al. (2018). Slowdown of translational elongation in *Escherichia coli* under hyperosmotic stress. *mBio* 9:e02375-17.

Dai, X., Zhu, M., Warren, M., Balakrishnan, R., Patsalo, V., Okano, H., et al. (2016). Reduction of translating ribosomes enables *Escherichia coli* to maintain elongation rates during slow growth. *Nat. Microbiol.* 2:16231.

du Plessis, D. J., Nouwen, N., and Driessen, A. J. (2011). The Sec translocase. *Biochim. Biophys. Acta.* 1808, 851–865. doi: 10.1016/j.bbamem.2010.08.016

Egea, P. F., Stroud, R. M., and Walter, P. (2005). Targeting proteins to membranes: structure of the signal recognition particle. *Curr. Opin. Struct. Biol.* 15, 213–220. doi: 10.1016/j.sbi.2005.03.007

Elvekrog, M. M., and Walter, P. (2015). Dynamics of co-translational protein targeting. *Curr. Opin. Chem. Biol.* 29, 79–86. doi: 10.1016/j.cbpa.2015.09.016

Flanagan, J. J., Chen, J. C., Miao, Y., Shao, Y., Lin, J., Bock, P. E., et al. (2003). Signal recognition particle binds to ribosome-bound signal sequences with fluorescence-detected subnanomolar affinity that does not diminish as the nascent chain lengthens. *J. Biol. Chem.* 278, 18628–18637. doi: 10.1074/jbc.m300173200

Fluman, N., Navon, S., Bibi, E., and Pilpel, Y. (2014). mRNA-programmed translation pauses in the targeting of *E. coli* membrane proteins. *eLife* 3:e03440.

Gopalakrishnan, A. S., Chen, Y. C., Temkin, M., and Dowhan, W. (1986). Structure and expression of the gene locus encoding the phosphatidylglycerophosphate synthase of *Escherichia coli*. *J. Biol. Chem.* 261, 1329–1338. doi: 10.1016/s0021-9258(17)36095-7

Gu, C., Begley, T. J., and Dedon, P. C. (2014). tRNA modifications regulate translation during cellular stress. *FEBS Lett.* 588, 4287–4296. doi: 10.1016/j.febslet.2014.09.038

Hasona, A., Zuobi-Hasona, K., Crowley, P. J., Abranches, J., Ruelf, M. A., Bleiweis, A. S., et al. (2007). Membrane composition changes and physiological adaptation by *Streptococcus mutans* signal recognition particle pathway mutants. *J. Bacteriol.* 189, 1219–1230. doi: 10.1128/jb.01146-06

Hecht, A., Glasgow, J., Jaschke, P. R., Bawazer, L. A., Munson, M. S., Cochran, J. R., et al. (2017). Measurements of translation initiation from all 64 codons in *E. coli*. *Nucleic Acids Res.* 45, 3615–3626. doi: 10.1093/nar/gkx070

Hughes, P., Landoulsi, A., and Kohiyama, M. (1988). A novel role for cAMP in the control of the activity of the *E. coli* chromosome replication initiator protein, DNAA. *Cell* 55, 343–350. doi: 10.1016/0092-8674(88)90057-8

Ishihama, A., and Fukuda, R. (1980). Autogenous and post-transcriptional regulation of RNA polymerase synthesis. *Mol. Cell. Biochem.* 31, 177–196.

Jander, G., Cronan, J., and Beckwith, J. (1996). Biotinylation in vivo as a sensitive indicator of protein secretion and membrane protein insertion. *J. Bacteriol.* 178, 3049–3058. doi: 10.1128/jb.178.11.3049-3058.1996

Jylhä, A., Nättinen, J., Aapola, U., Mikhailova, A., Nykter, M., Zhou, L., et al. (2018). Comparison of iTRAQ and SWATH in a clinical study with multiple time points. *Clin Proteomics* 15:24.

Kikuchi, S., Shibuya, I., and Matsumoto, K. (2000). Viability of an *Escherichia coli* pgsA null mutant lacking detectable phosphatidylglycerol and cardiolipin. *J. Bacteriol.* 182, 371–376. doi: 10.1128/jb.182.2.371-376.2000

Kremer, B. H., van der Kraan, M., Crowley, P. J., Hamilton, I. R., Brady, L. J., and Bleiweis, A. S. (2001). Characterization of the sat operon in *Streptococcus mutans*: evidence for a role of Ffh in acid tolerance. *J. Bacteriol.* 183, 2543–2552. doi: 10.1128/jb.183.8.2543-2552.2001

Lee, C. A., and Beckwith, J. (1986). Suppression of growth and protein secretion defects in *Escherichia coli* secA mutants by decreasing protein synthesis. *J. Bacteriol.* 166, 878–883. doi: 10.1128/jb.166.3.878-883.1986

Lee, H. C., and Bernstein, H. D. (2001). The targeting pathway of *Escherichia coli* presecretory and integral membrane proteins is specified by the hydrophobicity of the targeting signal. *Proc. Natl. Acad. Sci. U.S.A.* 98, 3471–3476. doi: 10.1073/pnas.051484198

Ling, C., and Ermolenko, D. N. (2015). Initiation factor 2 stabilizes the ribosome in a semirotated conformation. *Proc. Natl. Acad. Sci. U.S.A.* 112, 15874–15879. doi: 10.1073/pnas.1520337112

Malecki, M., Barria, C., and Arraiano, C. M. (2014). Characterization of the RNase R association with ribosomes. *BMC Microbiol.* 14:34. doi: 10.1186/1471-2180-14-34

Margaliot, M., and Tuller, T. (2012). On the steady-state distribution in the homogeneous ribosome flow model. *IEEE/ACM Trans. Comput. Biol. Bioinform.* 9, 1724–1736. doi: 10.1109/tcbb.2012.120

Mason, N., Ciufo, L. F., and Brown, J. D. (2000). Elongation arrest is a physiologically important function of signal recognition particle. *EMBO J.* 19, 4164–4174. doi: 10.1093/emboj/19.15.4164

Miller, J. H. (1972). *Experiments in Molecular Genetucs*. Cold Spring Harbor, NY: Cold Spring Harbor Laboratory Press.

Mohler, K., and Ibba, M. (2017). Translational fidelity and mistranslation in the cellular response to stress. *Nat. Microbiol.* 2:17117.

Mutka, S. C., and Walter, P. (2001). Multifaceted physiological response allows yeast to adapt to the loss of the signal recognition particle-dependent protein-targeting pathway. *Mol. Biol. Cell* 12, 577–588. doi: 10.1091/mbc.12.3.577

Naaktgeboren, N., Roobol, K., and Voorma, H. O. (1977). The effect of initiation factor IF-1 on the dissociation of 70-S ribosomes of *Escherichia coli*. *Eur. J. Biochem.* 72, 49–56. doi: 10.1111/j.1432-1033.1977.tb11223.x

Newitt, J. A., Ulbrandt, N. D., and Bernstein, H. D. (1999). The structure of multiple polypeptide domains determines the signal recognition particle targeting requirement of *Escherichia coli* inner membrane proteins. *J. Bacteriol.* 181, 4561–4567. doi: 10.1128/jb.181.15.4561-4567.1999

Ng, D. T., Brown, J. D., and Walter, P. (1996). Signal sequences specify the targeting route to the endoplasmic reticulum membrane. *J. Cell Biol.* 134, 269–278. doi: 10.1083/jcb.134.2.269

O'Connor, M., Thomas, C. L., Zimmermann, R. A., and Dahlberg, A. E. (1997). Decoding fidelity at the ribosomal A and P sites: influence of mutations in three different regions of the decoding domain in 16S rRNA. *Nucleic Acids Res.* 25, 1185–1193. doi: 10.1093/nar/25.6.1185

Pechmann, S., Willmund, F., and Frydman, J. (2013). The ribosome as a hub for protein quality control. *Mol. Cell* 49, 411–421. doi: 10.1016/j.molcel.2013.01.020

Phillips, G. J., and Silhavy, T. J. (1992). The *E. coli* ffh gene is necessary for viability and efficient protein export. *Nature* 359, 744–746. doi: 10.1038/359744a0

Pool, M. R. (2005). Signal recognition particles in chloroplasts, bacteria, yeast and mammals (review). *Mol. Membr. Biol.* 22, 3–15. doi: 10.1080/09687860400026348

Powers, T., and Walter, P. (1997). Co-translational protein targeting catalyzed by the *Escherichia coli* signal recognition particle and its receptor. *EMBO J.* 16, 4880–4886. doi: 10.1093/emboj/16.16.4880

Prabhakar, A., Capece, M. C., Petrov, A., Choi, J., and Puglisi, J. D. (2017). Post-termination ribosome intermediate acts as the gateway to ribosome recycling. *Cell Rep.* 20, 161–172. doi: 10.1016/j.celrep.2017.06.028

Quan, S., Zhang, N., French, S., and Squires, C. L. (2005). Transcriptional polarity in rRNA operons of *Escherichia coli* nusA and nusB mutant strains. *J. Bacteriol.* 187, 1632–1638. doi: 10.1128/jb.187.5.1632-1638.2005

Regalia, M., Rosenblad, M. A., and Samuelsson, T. (2002). Prediction of signal recognition particle RNA genes. *Nucleic Acids Res.* 30, 3368–3377. doi: 10.1093/nar/gkf468

Riba, A., Di Nanni, N., Mittal, N., Arhne, E., Schmidt, A., and Zavolan, M. (2019). Protein synthesis rates and ribosome occupancies reveal determinants of translation elongation rates. *Proc. Natl. Acad. Sci. U.S.A.* 116, 15023–15032. doi: 10.1073/pnas.1817299116

Rodnina, M. V. (2018). Translation in prokaryotes. *Cold Spring Harb. Perspect. Biol.* 10:a032664.

Saraogi, I., and Shan, S. O. (2014). Co-translational protein targeting to the bacterial membrane. *Biochim. Biophys. Acta* 1843, 1433–1441. doi: 10.1016/j.bbamcr.2013.10.013

Schibich, D., Gloge, F., Pohner, I., Björkholm, P., Wade, R., von Heijne, G., et al. (2016). Global profiling of SRP interaction with nascent polypeptides. *Nature* 536, 219–223. doi: 10.1038/nature19070

Scott, M., Gunderson, C. W., Mateescu, E. M., Zhang, Z., and Hwa, T. (2010). Interdependence of cell growth and gene expression: origins and consequences. *Science* 330, 1099–1102. doi: 10.1126/science.1192588

Scotti, P. A., Valent, Q. A., Manting, E. H., Urbanus, M. L., Driessen, A. J., Oudega, B., et al. (1999). SecA is not required for signal recognition particle-mediated targeting and initial membrane insertion of a nascent inner membrane protein. *J. Biol. Chem.* 274, 29883–29888. doi: 10.1074/jbc.274.42.29883

Sherman, M. Y., and Qian, S. B. (2013). Less is more: improving proteostasis by translation slow down. *Trends Biochem. Sci.* 38, 585–591. doi: 10.1016/j.tibs.2013.09.003

Siegel, V., and Walter, P. (1998). The affinity of signal recognition particle for presecretory proteins is dependent on nascent chain length. *EMBO J.* 7, 1769–1775. doi: 10.1002/j.1460-2075.1988.tb03007.x

Siller, E., DeZwaan, D. C., Anderson, J. F., Freeman, B. C., and Barral, J. M. (2010). Slowing bacterial translation speed enhances eukaryotic protein folding efficiency. *J. Mol. Biol.* 396, 1310–1318. doi: 10.1016/j.jmb.2009.12.042

Tsolis, K. C., and Economou, A. (2017). Quantitative proteomics of the *E. coli* membranome. *Methods Enzymol.* 586, 15–36. doi: 10.1016/bs.mie.2016.09.026

Ulbrandt, N. D., Newitt, J. A., and Bernstein, H. D. (1997). The *E. coli* signal recognition particle is required for the insertion of a subset of inner membrane proteins. *Cell* 88, 187–196. doi: 10.1016/s0092-8674(00)81839-5

Walter, P., and Blobel, G. (1981). Translocation of proteins across the endoplasmic reticulum III. Signal recognition protein (SRP) causes signal sequence-dependent and site-specific arrest of chain elongation that is released by microsomal membranes. *J. Cell Biol.* 91, 557–561. doi: 10.1083/jcb.91.2.557

Walter, P., and Johnson, A. E. (1994). Signal sequence recognition and protein targeting to the endoplasmic reticulum membrane. *Annu. Rev. Cell Biol.* 10, 87–119. doi: 10.1146/annurev.cb.10.110194.000511

Wickström, D., Wagner, S., Baars, L., Ytterberg, A. J., Klepsch, M., van Wijk, K. J., et al. (2011). Consequences of depletion of the signal recognition particle in *Escherichia coli*. *J. Biol. Chem.* 286, 4598–4609. doi: 10.1074/jbc.m109.081935

Wiśniewski, J. R., and Mann, M. (2012). Consecutive proteolytic digestion in an enzyme reactor increases depth of proteomic and phosphoproteomic analysis. *Anal. Chem.* 84, 2631–2637. doi: 10.1021/ac300006b

Wiśniewski, J. R., Zougman, A., Nagaraj, N., and Mann, M. (2009). Universal sample preparation method for proteome analysis. *Nat. Methods* 6, 359–362. doi: 10.1038/nmeth.1322

Yang, C., Hockenberry, A. J., Jewett, M. C., and Amaral, L. A. N. (2016). Depletion of Shine-Dalgarno sequences within bacterial coding regions is expression dependent. *G3 (Bethesda)* 6, 3467–3474. doi: 10.1534/g3.116.032227

Zarai, Y., Margaliot, M., and Tuller, T. (2013). Explicit expression for the steady-state translation rate in the infinite-dimensional homogeneous ribosome flow model. *IEEE/ACM Trans. Comput. Biol. Bioinform.* 10, 1322–1328. doi: 10.1109/tcbb.2013.120

Zarai, Y., Margaliot, M., and Tuller, T. (2014). Maximizing protein translation rate in the ribosome flow model: the homogeneous case. *IEEE/ACM Trans. Comput. Biol. Bioinform.* 11, 1184–1195. doi: 10.1109/tcbb.2014.2330621

Zengel, J. M., and Lindahl, L. (1994). Diverse mechanisms for regulating ribosomal protein synthesis in *Escherichia coli*. *Prog. Nucleic Acid Res. Mol. Biol.* 47, 331–370. doi: 10.1016/s0079-6603(08)60256-1

Zhang, D., and Shan, S. O. (2012). Translation elongation regulates substrate selection by the signal recognition particle. *J. Biol. Chem.* 287, 7652–7660. doi: 10.1074/jbc.m111.325001

Zhang, D., Sweredoski, M. J., Graham, R. L., Hess, S., and Shan, S. O. (2012). Novel proteomic tools reveal essential roles of SRP and importance of proper membrane protein biogenesis. *Mol. Cell. Proteomics* 11:M111.011585.

Zhang, X., and Shan, S. O. (2014). Fidelity of cotranslational protein targeting by the signal recognition particle. *Annu. Rev. Biophys.* 43, 381–408.

Zhao, L., Cui, Y., Fu, G., Xu, Z., Liao, X., and Zhang, D. (2021). Signal recognition particle suppressor screening reveals the regulation of membrane protein targeting by the translation rate. *mBio* 12:e02373-20.

Zhu, M., Dai, X., and Wang, Y. P. (2016). Real time determination of bacterial in vivo ribosome translation elongation speed based on LacZαlpha complementation system. *Nucleic Acids Res.* 44:e155.

Zuker, M. (2003). Mfold web server for nucleic acid folding and hybridization prediction. *Nucleic Acids Res.* 31, 3406–3415. doi: 10.1093/nar/gkg595

Conflict of Interest: The authors declare that the research was conducted in the absence of any commercial or financial relationships that could be construed as a potential conflict of interest.

frontiers in Microbiology

ORIGINAL RESEARCH
published: 04 October 2021
doi: 10.3389/fmicb.2021.750200

Monitoring Bacterial Conjugation by Optical Microscopy

Gerardo Carranza†, Tamara Menguiano, Fernando Valenzuela-Gómez, Yolanda García-Cazorla†, Elena Cabezón and Ignacio Arechaga**

Departamento de Biología Molecular, Instituto de Biomedicina y Biotecnología de Cantabria (IBBTEC), Universidad de Cantabria–CSIC, Santander, Spain

Bacterial conjugation is the main mechanism for horizontal gene transfer, conferring plasticity to the genome repertoire. This process is also the major instrument for the dissemination of antibiotic resistance genes. Hence, gathering primary information of the mechanism underlying this genetic transaction is of a capital interest. By using fluorescent protein fusions to the ATPases that power conjugation, we have been able to track the localization of these proteins in the presence and absence of recipient cells. Moreover, we have found that more than one copy of the conjugative plasmid is transferred during mating. Altogether, these findings provide new insights into the mechanism of such an important gene transfer device.

Keywords: antibiotic resistance, bacterial conjugation, fluorescence microscopy, conjugative ATPases, T4SS

OPEN ACCESS

Edited by:
Peter Graumann, University of Marburg, Germany

Reviewed by:
Praveen Kumar Singh, Max Planck Institute for Terrestrial Microbiology, Germany
Xavier Bellanger, Université de Lorraine, France

****Correspondence:***
Elena Cabezón
cabezone@unican.es
Ignacio Arechaga
arechagai@unican.es

†Present address:
Gerardo Carranza, Spanish Institute of Oceanography, Santander, Spain
Yolanda García-Cazorla, European Food Safety Authority, Parma, Italy

Specialty section:
This article was submitted to Microbial Physiology and Metabolism, a section of the journal Frontiers in Microbiology

Received: *30 July 2021*
Accepted: *14 September 2021*
Published: *04 October 2021*

Citation:
Carranza G, Menguiano T, Valenzuela-Gómez F, García-Cazorla Y, Cabezón E and Arechaga I (2021) Monitoring Bacterial Conjugation by Optical Microscopy. Front. Microbiol. 12:750200. doi: 10.3389/fmicb.2021.750200

INTRODUCTION

Horizontal gene transfer is the main pathway for the widespread dissemination of antibiotic resistance genes (Mazel and Davies, 1999; de la Cruz and Davies, 2000; Rice, 2009; von Wintersdorff et al., 2016; Koraimann, 2018). The three main mechanisms involved in horizontal gene transfer are transformation, phage transduction and conjugation (Popa and Dagan, 2011; Daubin and Szollosi, 2016). Conjugation is particularly relevant, as it is responsible of the transmission of large plasmid DNA molecules (Waters, 1999; Smillie et al., 2010). The transfer of conjugative DNA requires a sophisticated machinery to carry out DNA mobilization and mating pair formation (de la Cruz et al., 2010; Cabezon et al., 2015; Zechner et al., 2017).

In Gram negative bacteria, conjugation is initiated by a specific protein that recognizes a DNA sequence in the plasmid (origin of transfer) and, upon a nucleophilic cleavage, remains covalently bound to the DNA (Byrd and Matson, 1997; Chandler et al., 2013). This multi-domain protein, named relaxase, is a large protein that is transported across the membranes of donor and recipient cells bound to the DNA (Draper et al., 2005; Garcillan-Barcia et al., 2007). This is a particular challenging process considering the size of the protein substrate, which ranges from 900 to 1,800 kDa, as in the case of TraI, the relaxase of the conjugative plasmid F (Frost et al., 1994), which is a member of the IncF family. In the IncW plasmid R388, the cleavage reaction occurs via a nucleophilic attack by relaxase TrwC on the 5′-side of the DNA phosphate. This transesterification reaction results in a covalent linkage between protein and DNA (Guasch et al., 2003; Gonzalez-Perez et al., 2007). After the cleavage reaction, donor DNA synthesis begins from the 3′end of the cleaved strand, so the single stranded DNA copy (ssDNA) that is transferred to the recipient cell is replaced by the new synthesized DNA strand.

In this way, conjugative DNA is transferred across the membrane channel covalently bound to the relaxase protein. The process is carried out with the help of another ATPase known as coupling

protein (Cabezon et al., 1997). This hexameric ATPase, named TrwB in plasmid R388, couples the energy released from ATP hydrolysis to ssDNA pumping through the secretion channel (Tato et al., 2005; Cabezon and de la Cruz, 2006). The nucleoprotein complex formed by the conjugative DNA and the relaxase are meant to cross the membranes of donor and recipient cell through a secretion channel known as Type IV Secretion System (T4SS). This is a large macromolecular complex formed by 11 different subunits that spans the inner and outer membranes of donor cells (Alvarez-Martinez and Christie, 2009; Christie et al., 2014; Cabezon et al., 2015). At the base of the channel there are two hexameric ATPases that participate both in the biogenesis of T4SS and in the transport of the nucleoprotein complex (Cascales and Christie, 2003; Atmakuri et al., 2004; Arechaga et al., 2008; Peña et al., 2012). These ATPases are VirB4 and VirB11, named TrwK and TrwD, respectively, in the R388 plasmid system. VirB4 protein is the largest and most conserved constituent of T4SS (Fernandez-Lopez et al., 2006; Guglielmini et al., 2013). This protein is essential for the assembly of the T4S pilus, playing a fundamental role in powering the system. VirB11 also plays an essential role in the first steps of the DNA translocation pathway (Atmakuri et al., 2004). It has been suggested that VirB11 acts as a molecular switch between pilus biogenesis and substrate transport (Ripoll-Rozada et al., 2013), but it is worth noting that is not found in all T4SS. F plasmids, for instance, do not code for a VirB11 homolog (Frost et al., 1994; Lawley et al., 2003).

In the last few years, much progress has been done in the understanding of the genetic contribution and molecular architecture of the different components of the conjugative system. However, there are still important open questions on how this process is actually occurring. Here, by using optical microscope methods, we provide direct evidence on the localization of the most important proteins that drive the conjugation process in *Escherichia coli*. We have labeled with fluorescent constructs the relaxase, the coupling protein and the largest ATPase of the T4SS in R388 plasmid, and we have found that the pattern of localization of these proteins change upon contact with recipient cells. Furthermore, we have been able to visualize the result of the conjugation process and we have gathered evidence that indicates that more than one copy of the conjugative plasmid ends up in the recipient cell.

MATERIALS AND METHODS

Cloning of Fluorescent Fusion Proteins

Combinations of different fluorescent markers fusioned to *trwB*, *trwC*, and *trwK* genes were created using plasmid pIM09 as a template (I. Matilla, doctoral thesis). pIM09 contains a fusion of trwB, GFP, and kanamicine resistance genes cloned in a pBR322 derivative vector (**Supplementary Figure 6**). The FRT Kanamycin resistance cassette was obtained from pKD4 plasmid (Datsenko and Wanner, 2000). For TrwC fluorescent constructs, *trwC* gene was obtained from R388 plasmid by PCR, adding *Hin*dIII and *Xho*I restriction sites at both ends (oligonucleotides 1 and 2 from **Supplementary Table 2**). For TrwK constructs, oligonucleotides 3 and 4 with the same restriction sites were used (**Supplementary Table 2**).

In order to create different fluorescent variants, *mCherry*, *mKate2*, and *mEOS* genes were obtained from pROD25 plasmid (Reyes-Lamothe et al., 2008) (oligonucleotides 5 and 6), pBAD33_*mKate2* plasmid (Addgene) (Shcherbo et al., 2007) (oligonucleotides 7 and 8), and from a pRSETa_*mEos4b* vector (Paez-Segala et al., 2015) (Addgene) (oligonucleotides 9 and 10). In all cases, the fluorescent variants were inserted into *Xho*I and *BamH1* restriction sites from pIM09 plasmid. TrwBmCherry was also cloned in a pHis vector to estimate membrane co-location with the fluorescent dye Nonyl-Acridine Orange (NAO), which is a membrane specific stain.

Fluorescent fusion constructs in plasmid pIM09 were then amplified by PCR, by using oligonucleotides containing 50 bases that perfectly matched the flanking R388 sequence where the constructs had to be inserted. Oligonucleotides 11 and 12 were used for *trwB* constructs, oligonucleotides 13 and 14 for *trwC* constructs and oligonucleotides 15 and 16 for *trwK* constructs (**Supplementary Table 2**). The amplified fragments were purified in an agarose gel and transformed into a *E. coli* TB10 strain containing R388 plasmid for homologous recombination. Recombination was activated by growing cells at 42°C, as previously reported. Cells were plated on LB agar containing kanamycin (50 μg/ml) and trimethoprim (20 μg/ml) to select the recombinant R388 plasmids. The selected plasmids were subsequently analysed by sequencing.

Bacterial Conjugation Assays

Conjugation donor strains were derivatives of *E. coli* K12 strain MG1655 carrying either a kanamycin-resistance derivative of plasmid R388 (plasmid pSU2007) or a R388 plasmid expressing the conjugative proteins TrwB, TrwC, and TrwK fused with different fluorescent tags under its natural promotor in plasmid R388. Overnight cultures of MG1655 cells carrying each of these constructs grown in LB medium were mated (1:1) with recipient strain UB1637 as described previously (Peña et al., 2011), with the exception of SeqA-GFP experiments, in which a MG1655 Dam methylase deficient strain (*Dam*$^-$) (Palmer and Marinus, 1994) was used as a recipient. Cells were collected by centrifugation and resuspended in fresh LB medium. Samples were placed on Millipore filters (0.2 μm) for 1 h at 37°C. Then, the filter was washed in LB and resuspended. Dilutions (1:10 to 1:10^3) were plated, selecting for transconjugant and donor cells with appropriate antibiotics. Transconjugants were selected on L-agar plates containing streptomycin (300 μg/ml) and kanamycin (50 μg/ml). Conjugation frequencies were calculated as a ratio between the number transconjugants versus donor cells.

Standard Fluorescence Microscopy

For standard microscopy, microscope slides covered with melted agarose and framed with a Frame-Seal Incubation Chamber (Biorad) were used. M9 minimal media (200 μl) was mixed with low melting point agarose (1.5%, w/v) and added into the cavity formed by the adhesive frame. This chamber was protected with another microscope slide. Pads were cooled down for 30 min at room temperature. Seeding cultures of MG1655 cells, previously

grown in M9 minimal media with glucose as carbon source (2 μl, 0.1 $OD600_{nm}$), were spread onto circular agarose pads (6 mm) and, after drying, were covered with a coverslip. For conjugation experiments, MG1655 donor cells and UB1637 recipient cells were grown overnight in M9 minimal media. Next day, a 1:1,000 dilution was prepared and cells were grown until the optical density ($OD600_{nm}$) reached a value of 0.6. Then, donor and recipient cells were mixed at a 1: 2 ratio in a final volume of 400 μl. Cells were then centrifuged and resuspended in 40 μl of M9 medium. Aliquots (2 μl) were spread onto a slice of agarose dissolved in minimal medium as indicated above, and the sample was incubated during 15 min at 37°C for mating.

Standard fluorescence microscopy was carried out using a Zeiss Axio Imager M1 upright fluorescence microscope (Zeiss Plan-Neofluar _100/1.30 NAOil Ph3 objective), equipped with a 12 bits B&W camera (AxioCam MRm), using a standard rhodamine filter unit (Ex. 546/12 – Em. 608/65). Green fluorescence of mGFP and mCitrine was detected by using a standard GFP filter unit (Ex. 470/40 – Em. 525/50). Membranes were visualized with Acridine Orange 10-nonyl bromide (NAO, Sigma-Aldrich). NAO fluorescence was also detected using the same GFP filter unit.

Time Lapse and TIRF Microscopy

Bacterial cells were grown as indicated previously. Samples were placed onto a cover glass–bottom imaging dish, with the bacteria sandwiched between the agarose pads and the cover glass. The dish was placed into a custom stage insert, which holds the dish tightly. After sealing with Parafilm^R or grease, bacteria cells were seeded onto individual agarose pads and incubated for 10 min at 37°C.

Live conjugation was monitored in a Nikon Eclipse Ti2 microscope equipped with a Hamamatsu ORCA-Flash 4.0 camera using a CFI Apochromat TIRF100xc Oil objective. For TIRF imaging, a Nikon A1 confocal laser microscope equipped with Hamamatsu 9100-C2 camera and a Plan Apochromat TIRF 100x Oil DIC HN2 objective was used. Super-resolution imaging (d-STORM) was performed in an Olympus IX-73 microscope equipped with 100xoTIRF Olympus UAPON objective and an iXon ULTRA897 EMCCD camera (Andor). Image analysis was carried out using Fiji/ImageJ software (National Institutes of Health, United States).

Membrane Fractionation and Immunodetection of the Fluorescent Conjugative ATPases

Cells were harvested by centrifugation at 4,000 × *g* and re-suspended in a buffer containing 50 mM Tris, pH 7.5, 0.5 mM EDTA, 0.1% PMSF. Cells were lysed in a TS cell disruptor (Constant Systems, United Kingdom) at 25 kpsi. Lysates were centrifuged at 800 × *g* (15 min), followed by another centrifugation at 10,000 × *g* (15 min) to remove unbroken debris. Membranes were collected by ultracentrifugation at 100,000 × *g* (30 min). The pellet (membrane fraction) was re-suspended in 50 mM Tris, pH 7.5, 0.5 mM EDTA, 0.1% PMSF, and 2% SDS. Protein samples were run in a SDS-PAGE, transferred to a nitrocellulose filter and incubated with rabbit antiserum (anti-TrwC, anti-TrwB, and anti-TrwK, respectively). Images were obtained after incubation with an IRDye anti-rabbit IgG (goat) antibody conjugate, using an Odyssey scanner (Li-Cor Biosciences).

RESULTS

Localization of the Main Conjugative ATPases in Donor Cells in the Absence of the Host

Conjugative ATPases are key players in plasmid transfer. They assist in the processing and transport of conjugative DNA from donor to recipient cells. In order to assess the subcellular location of these proteins, different fluorescent tags were attached to the main three ATPases involved in the conjugative process of plasmid R388, our model system.

The first step in conjugation is the formation of the relaxase/DNA complex that will be transferred to the recipient cell. The relaxase is a large protein with two functional domains: a N-terminal domain, that produces the nick on the DNA, and a C-terminal helicase domain involved in the processing of the DNA (Grandoso et al., 1994). In R388 plasmid, the relaxase protein is TrwC. Based on biochemical and structural information, we have generated a repertoire of fusion proteins at the C-terminus of TrwC with several fluorescent tags (mGFP, mCherry, mEos4, and mKate2), cloned directly in the conjugative R388 plasmid, under its natural promotor. We followed a similar strategy with the two other main ATPases of the system: TrwB, also known as the coupling protein, which is involved in the transport of the DNA (Cabezon and de la Cruz, 2006), and TrwK, a large ATPase (Arechaga et al., 2008) localized at the base of the T4SS channel (Atmakuri et al., 2004; Hu et al., 2019). These ATPases are the VirD4- and VirB4-homologs in the *Agrobacterium tumefaciens* system, respectively (Atmakuri et al., 2004; Cabezon et al., 2015). In both cases, the fluorescent tag was also inserted at the C-terminus. TrwB (VirD4) is a membrane protein with two transmembrane α-helices at the N-terminal end, and TrwK (VirB4) is bound to the transmembrane protein TrwM (VirB3) also by the N-terminus (in some VirB4 homologs both proteins are fused as only one protein) (Arechaga et al., 2008). Therefore, the best location for the fluorescent tags was, in all cases, the C-terminal ends.

We checked that the fluorescent tags did not hamper the *in vivo* function of these proteins in mating assays, which allowed us to conclude that fusion proteins of TrwC, TrwB, and TrwK with various fluorescent labels (GFP, mCherry, mKate2, or mEos4) were functional for R388 plasmid transfer, although with lower conjugation frequencies than the wild type plasmid (**Supplementary Table 1**). Moreover, expression of the three fluorescent ATPases was also checked by immunodetection assays (**Figure 1**). The subcellular location of the three fluorescent variants in donor cells was similar to that expected in the wild type version. Thus, we were able to determine that TrwCmKate2,

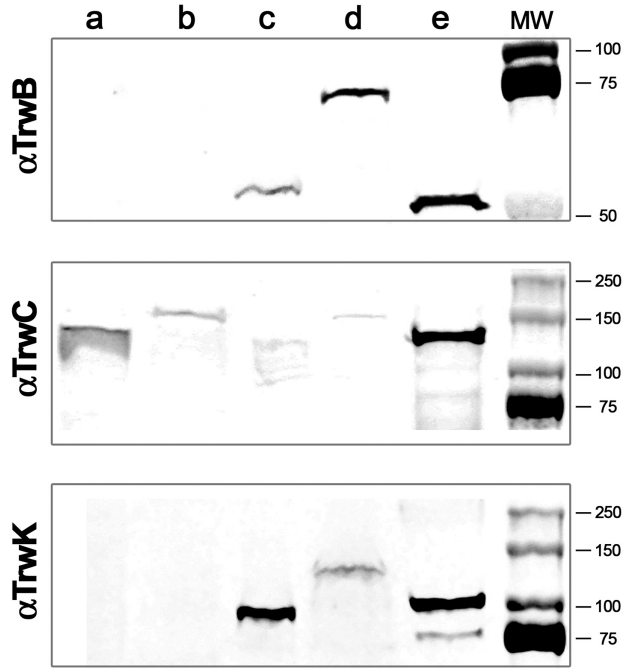

FIGURE 1 | Immunodetection and subcellular localization of conjugative ATPases. MG1655 *Escherichia coli* cells were transformed with R388 wild type plasmid or with R388 encoding for TrwBmKate2, TrwCmKate2, or TrwKmKate2. Cells were grown to stationary phase and harvested by centrifugation. Cell pellets were re-suspended and lysed by mechanical methods. Soluble and membrane fractions were separated by ultra-centrifugation. Aliquots of each fraction were run in a SDS-PAGE. Gels were transferred to a nitrocellulose membrane and incubated with antibodies anti-TrwB (*upper panel*), anti-TrwC (*middle panel*), or anti-TrwK (*bottom panel*) and then revealed with IRDye. *Upper panel*: (a) wild type R388 soluble fraction, (b) R388_TrwBmKate2 soluble fraction, (c) wild type R388 membrane fraction, (d) R388_TrwBmKate2 membrane fraction, and (e) purified TrwBΔN70 protein. *Middle panel*: (a) wild type R388 soluble fraction, (b) R388_TrwCmKate2 soluble fraction, (c) wild type R388 membrane fraction, (d) R388_TrwCmKate2 membrane fraction, and (e) purified TrwC protein. *Bottom panel*: (a) wild type R388 soluble fraction, (b) R388_TrwKmKate2 soluble fraction, (c) wild type R388 membrane fraction, (d) R388_TrwKmKate2 membrane fraction, and (e) purified TrwK protein. Estimated MW values for TrwB, TrwBmKate2, and TrwBΔN70 proteins are 56.3, 82.4, and 48.6 kDa, respectively. Estimated MW values for TrwC and TrwCmKate2 proteins are 107.4 and 133.5 kDa, respectively. Estimated MW values for TrwK and TrwKmKate2 proteins are 93.8 and 119.9 kDa, respectively.

TrwBmKate2, and TrwKmKate3 were expressed and targeted in a way similar to wild type TrwC, TrwB, and TrwK, respectively. TrwB and TrwK were associated to the membrane fraction and TrwC was found mainly in the cytoplasm, as expected.

Next step was to determine by optical microscopy the localization of these proteins before and during conjugation. TrwB, which is a membrane protein, when fused to mKate2, was forming fluorescent foci randomly localized at the periphery of the donor cells (**Figure 2A**, **Supplementary Movie 1**, and **Supplementary Figure 1**). This membrane localization of TrwB was also confirmed with a TrwBmCherry fluorescent variant by using the fluorescent dye Nonyl-Acridine Orange (NAO), which is a membrane specific stain (**Supplementary Figure 2**). A similar membrane localization pattern was observed by super-resolution d-STORM microscopy in cells in which TrwB was fused to mGFP (**Supplementary Figure 3**). In contrast, TrwC, which is a soluble protein, was widely distributed along the cytoplasm (**Figure 2B**), regardless of the different fluorescent constructs.

In the absence of recipient cells, the high number of TrwB foci observed indicated that the system is unconstrained (**Supplementary Figure 1** and **Supplementary Movie 1**). Likewise, the number of TrwC foci in the absence of recipient cells and their localization, widely disseminated across the cell, enforced this idea. In contrast to TrwB and TrwC, the number of TrwK foci was limited to ∼6 foci/cell (**Figure 2C**). TrwK is an essential part of the T4SS, which ensembles as a hexamer or as double hexamer at the base of the channel (Arechaga et al., 2008; Low et al., 2014). Therefore, it might be a good indicative to evaluate the number of Type IV transport systems per cell. The membrane localization of TrwKmKate2 was also confirmed by TIRF microscopy (**Supplementary Figure 4**), since foci localized in the membrane can be visualized by this technique. These results indicate that TrwB and TrwC proteins remain widely distributed across the bacterial cell in the absence of receptors, whereas the assembly of T4SS is limited to a few copies (around six per bacterial cell).

Pattern Distribution Upon Contact With the Recipient Cell

Next, we studied the localization of these ATPases upon contact with the recipient cells to determine if the distribution of these proteins changed during the conjugative process. In these experiments, TrwB, TrwC, and TrwK proteins fused to mKate2 and placed in R388 plasmid under the natural promoters (*PtrwA* for *trwB* and *trwC* and *PkorA* for *trwK*) were expressed in donor cells, whereas green fluorescent proteins (mGFP or mCitrine) were expressed in the recipient cell. After incubating both donor and recipient cells during 1 h, images were acquired. Inspection of the distribution pattern of TrwBmKate2 and TrwCmKate2 showed a dramatic change in the localization of these proteins (**Figure 3**), as compared with that observed in the absence of recipient cells (**Figure 2**) (see also fluorescent intensity profiles in **Supplementary Figure 5**). In the presence of recipient cells, TrwBmKate2 localized close to the poles, in contrast to the random distribution on the membranes in its absence. Even more dramatic was the change in the localization pattern of TrwCmKate2. In the presence of recipient cells, TrwCmKate2 formed defined foci, mainly localized at the poles (**Figure 3B**), whereas in its absence, TrwCmKate2 was widely distributed in the cytoplasm (**Figure 2B**). These changes in the localization pattern were also identified in the case of TrwKmKate2 (**Figure 3C**), with a tendency to migrate to the pole cells upon contact with recipients.

Monitoring Bacterial Conjugation

Once the localization of the different proteins was determined both in the presence and absence of recipient cells, the next step was trying to obtain live images of bacterial conjugation. Donor and recipient cells with different fluorescence markers

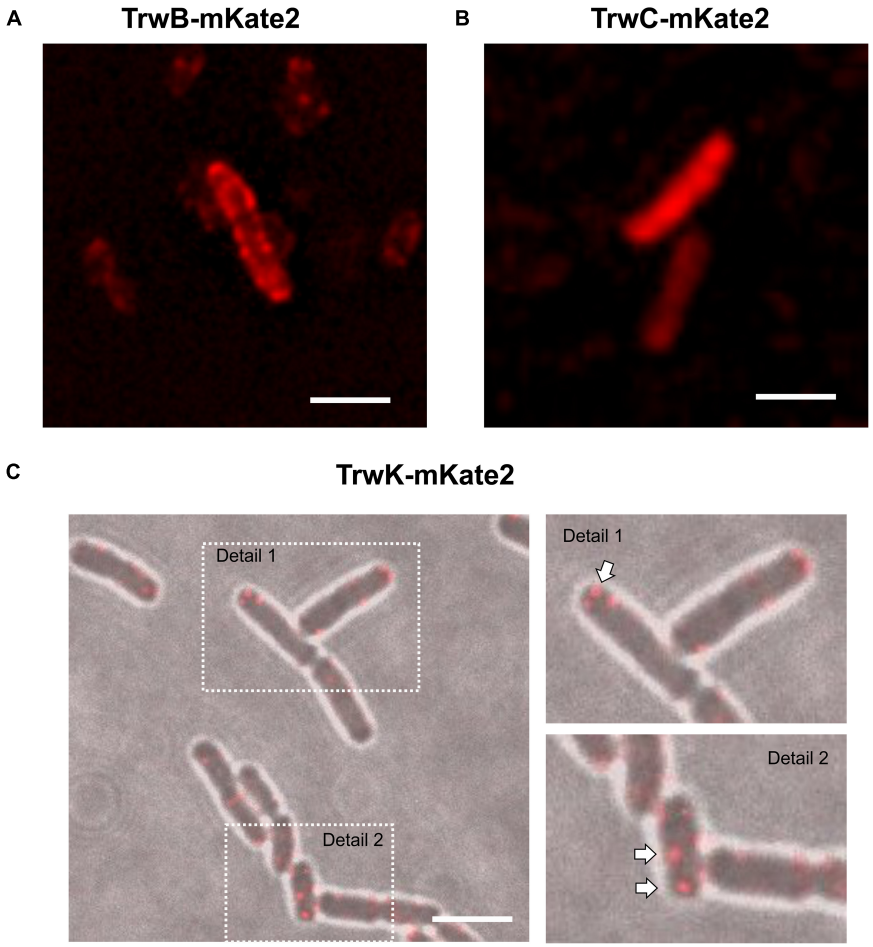

FIGURE 2 | Localization of conjugative proteins in donor cells in the absence of recipients. MG1655 cells expressing TrwBmKate2 **(A)**, TrwCmKate2 **(B)**, and TrwKmKate2 **(C)** were grown in M9 minimal media and examined by fluorescent microscopy. In all cases, fusion proteins are expressed under its respective natural promoter in plasmid R388. TrwBmKate2 was widely distributed in the membrane **(A)** (see also **Supplementary Movie 1**), TrwCmKate2 was dispersed in the cytoplasm **(B)** and TrwKmKate2 was found forming discrete foci (around six per cell) **(C)**, which might indicate the number of secretion systems assembled. In this last case, phase contrast/color bright field images are shown to better visualize both the foci, and the bacterial cells. (Scale bar: 2 μM).

were incubated together and plated on the microscope slides. However, although many different strategies were followed, we were unable to monitor *in situ* nucleoprotein transfer by placing donor and recipient cells directly under the microscope. As previously mentioned, fluorescent variants were found to be functional in mating assays. The insertion of the fluorescent tags into the R388 plasmid only decreased transfer efficiency by 1–2 logs in plates (**Supplementary Table 1**). In fact, when cells expressing TrwBmkate2 or TrwCmkate2 were mated and transferred immediately to the pad, transconjugants were observed, regardless of the fluorescent tag (**Figure 4**). As discussed later, conjugation on the pad seems to be inhibited by unknown reasons, despite temperature and atmospheric CO_2 conditions were kept constant.

In order to circumvent this problem, we decided to study R388 conjugation by monitoring the fluorescence of the protein SeqA fused to GFP in the recipient cell (SeqA-GFP), following a strategy similar to that used with plasmid F (Babic et al., 2008). SeqA is a protein that binds to hemi-methylated DNA (Lu et al., 1994; Brendler and Austin, 1999), preferentially to newly replicated DNA, with high affinity in cells producing Dam methylase. In Dam methylase deficient cells (*Dam*$^-$) (Palmer and Marinus, 1994) this binding is prevented, and fluorescence of SeqA is undetectable. Following this strategy, we mated *Dam*$^+$ donor cells harboring R388:*trwBmKate2* with *Dam*$^-$ recipient cells in which the seqA-GFP fusion construct was inserted in the chromosome under the control of the native seqA promoter, replacing the seqA gene. Once a R388 plasmid single DNA strand is transferred from a donor cell (with methylase activity) to a recipient cell, a copy of complementary non-methylated DNA will be synthesized to generate a hybrid hemi-methylated DNA, promoting SeqA-GFP binding. Therefore, conjugation events would be directly related to the number of green fluorescent foci observed in transconjugant cells. As expected, when *Dam*$^-$ donor cells were used for conjugation, no fluorescent foci were observed in the recipient cells (data not shown). Upon complementation,

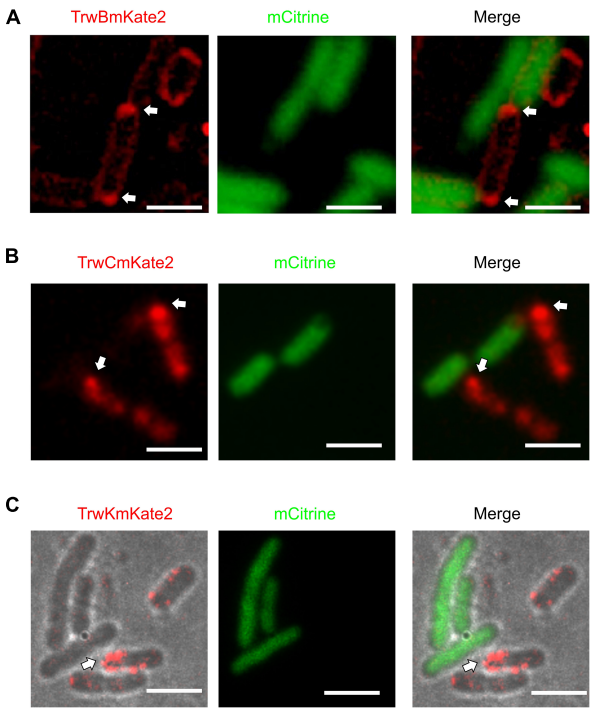

FIGURE 3 | Localization of conjugative proteins in the presence of recipient cells. MG1655 donor cells expressing TrwBmKate2 **(A)**, TrwCmKate2 **(B)**, and TrwKmKate2 **(C)** under their respective natural promotors in R388 plasmid were mixed with UB1637 recipient cells expressing the fluorescent protein mCitrine. Fluorescence of mKate2 protein derivatives in donors (red) and mCitrine (green) in recipients is shown on the left and central panels, recorded at 630 and 540 nm, respectively. The right panel shows the merged images. Upon contact between both donor and recipient cells, the conjugative fluorescent proteins localize at the poles, on those specific areas that are in close contact with a recipient cell. In panel C, phase contrast/color bright field images are shown to better visualize both, the foci and the bacterial cells. The arrow shows the areas in the donor cell where the conjugative ATPases are compiled upon contact with the recipient cell. [Scale bars: 2 μM **(A)** and 3 μM **(B,C)**].

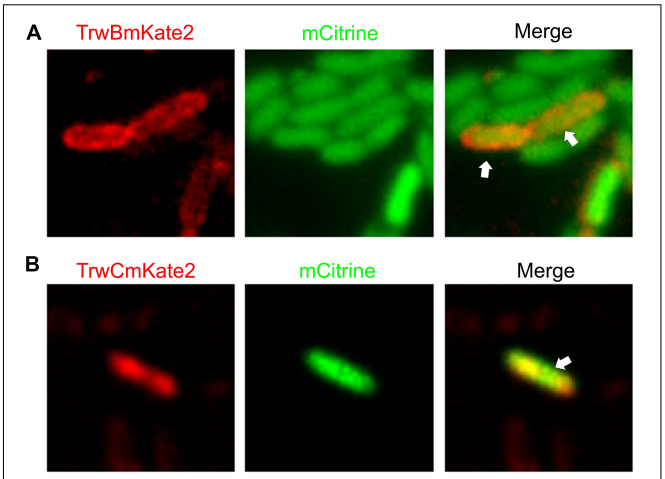

FIGURE 4 | Visualization of transconjugant cells. MG1655 donor cells hosting R388:*trwBmKate2* **(A)** or R388:*trwCmKate2* **(B)** were mixed with UB1637 recipient cells expressing mCitrine. Conjugation was performed in enriched M9 minimal media plates and then, cells were transferred to the microscope for image-recording. Images were recorded at different emission wavelengths (540 and 630 nm, for mCitrine and mKate2, respectively) at the same location, in order to discriminate donor, recipient and transconjugant cells. Merged images show the transconjugant cells in orange (*right panel*). These transconjugants are UB1637 cells expressing mCitrine that, after receiving the R388 plasmid, have started to express TrwBmKate2 **(A)** or TrwCmKate2 **(B)**, encoded by the plasmid.

transconjugants start to express TrwBmKate2 protein, which could be identified as cells expressing TrwBmKate2 plus the SeqA-GFP foci (**Figure 5**). Surprisingly, in some transconjugant cells (∼16%), we were able to observe more than one green foci (**Figures 5B,C**), which implies that more than one copy of the R388 plasmid has been transferred. The implications of this finding will be discussed lately.

DISCUSSION

Since the discovery of bacterial conjugation as the main mechanism of horizontal gene transfer (Lederberg and Tatum, 1946), great advances have been done in the understanding of the genetic mechanisms driving this process (Frost and Koraimann, 2010; Cabezon et al., 2015; Hu et al., 2019). Direct observation of horizontal gene transfer has been previously reported for F plasmid (Babic et al., 2008), which uses a long pilus to mate in liquid media (Paranchych and Frost, 1988; Clarke et al., 2008). However, many questions about how this process is really happening remain open. For instance, it is not clear yet how DNA is transferred, which is the signal that triggers the process, or even how the bacterial cells respond to that elusive signal. Here, trying to shed light to some of these questions, we have cloned the relaxase, the coupling protein, and the biggest and most conserved T4SS component (TrwK/VirB4) fused with a repertoire of fluorescent probes to visualize the different stages associated to the conjugative process. Although several experiments with fluorescent conjugative proteins have been previously reported (Clarke et al., 2008; Bauer et al., 2011; Arends et al., 2012; Segura et al., 2014; Nolivos et al., 2019), there is not a description of the localization of the proteins involved in each stage of the conjugative process. Furthermore, previous reports were mainly carried out with the fluorescent fusion proteins cloned in artificial expression vectors. It is known that the over-expression of fluorescent proteins under those circumstances may produce experimental artifacts, including protein aggregation or saturation of protein targeting machinery, leading to inappropriate localization (Day and Davidson, 2009). In order to prevent these problems, in this work, functional fluorescent proteins were expressed from its native promoter in plasmid R388.

After checking that the fluorescent fusions were functional, the next step was to localize these proteins in bacterial donor cells in the absence of recipients. We observed that, under these conditions, the number of copies of the coupling protein and the relaxase was much higher than the number of copies (around 6) of the conjugative R388 plasmid (Guynet et al., 2011).

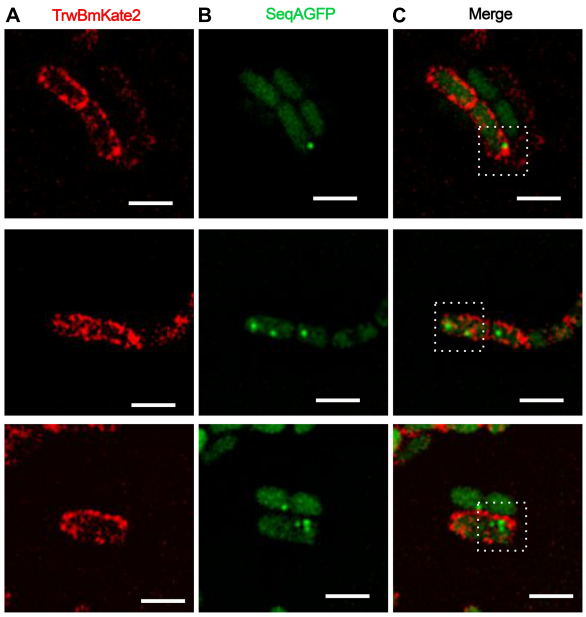

FIGURE 5 | Conjugative R388 transfer visualized as fluorescent SeqA-GFP foci in recipient cells. MG1655 *dam*$^{+}$ donor cells hosting R388:*trwBmKate2* were mated with *dam*$^{-}$ recipient cells expressing SeqA-GFP from the chromosome. Conjugation was performed in enriched M9 minimal media plates and then, cells were transferred to the microscope for image-recording. Transconjugants were monitored by the presence of fluorescent foci, indicating the binding of SeqA-GFP to hemy-methylated DNA. In some transconjugant cells, up to three independent foci were detected. Images show the same pad of transconjugant cells recorded at different emission wavelengths: 630 nm for mKate2 (**A**, red) and 540 nm for SeqA-GFP (**B**, green). The merged images in panel **(C)** show the fluorescent foci of SeqA-GFP plus TrwBmKate2 in the membrane, which is expressed from the recently transferred R388 plasmid. (Scale bar: 2 μM).

This result indicates that, even in the absence of receptor cells, *dtr* (DNA processing and transfer) genes are being expressed. However, *trwk* gene, which is part of the *mpf* (mating pore formation) operon, is more strictly downregulated, as judged by the low number of foci observed (around 6). As previously shown (Fernandez-Lopez et al., 2014), when the full regulatory network of the R388 is present, all plasmid promoters are repressed. However, it is important to note that *dtr* and *mpf* genes have distinctive transcriptional regulators (Fernandez-Lopez et al., 2014) and, therefore, a differential transcription of these genes could result in different expression levels, as observed in this work.

There are also differences in the localization pattern of these proteins (**Supplementary Figure 5**). In the absence of recipient cells, the coupling protein TrwB is uniformly dispersed along the membrane, whereas the relaxase is widely spread in the cytoplasm (**Figure 2**). TrwK, the main ATPase of the T4SS is always located bound to the membrane (**Figure 2C**), thanks to its interaction with TrwM, an integral membrane protein (Arechaga et al., 2008). TrwK is essential for the assembly of the T4S pilus. It docks onto the base of the secretion channel (Low et al., 2014) and plays a fundamental role in powering the assembly and function of the T4SS. Therefore, TrwK foci would be a good indicator of the number of secretion systems assembled in the donor cell. This is in agreement with data published previously (Gilmour et al., 2001), in which an average of five to six fluorescent foci were observed in the membrane of cells expressing TrhC protein (the VirB4-homolog from R27 plasmid), fused to GFP at the C-terminus (Gilmour et al., 2001; Gunton et al., 2005). Interestingly, these authors showed that most of the R27 transfer proteins were required for focus formation (Gilmour and Taylor, 2004).

In this work we have also observed that the localization of conjugative ATPases changed dramatically upon contact with the recipient cells. Under these conditions, these proteins tend to migrate to the poles of the cell (**Figure 3**), specifically to those areas in close contact with a recipient cell. This result indicates that such a contact triggers some sort of signal that dictates the reorganization of the conjugative ATPases. This is particularly evident in the case of the coupling protein TrwB and in TrwC.

In a next step, we focused on trying to observe bacterial conjugation directly on the pad, under the microscope light. However, under our experimental conditions, we were unable to observe cells mating on the microscope pad. Bacterial cells that in normal circumstances are able to conjugate, seem to stop mating as soon as they are placed on the microscope pad. Several hypotheses could explain this observation, based on a physical perturbation of the bacterial cells. The light of the microscope might be inhibiting the conjugation process. Alternatively, it might be possible that the pad of agar in which the cells are embedded is not ideal for bacterial conjugation. To circumvent this problem, we opted for mating donor and recipient cells in enriched solid M9 minimal media and, then, transfer the cells to the microscope pad for image recording. By using this approach, we were able to obtain images of transconjugants (**Figure 4**). These transconjugants can be identified as receptors expressing m-Citrine that have also received an R388 plasmid that expresses either TrwBmKate2 (4A) or TrwCmKate2 (4B) fusion proteins.

Additionally, we opted for monitoring the onset of transconjugants by using as receptors *dam*$^{-}$ cells harboring the *seqA* gene fused to GFP. SeqA is a protein that only binds to hemi-methylated DNA (Brendler and Austin, 1999; Waldminghaus and Skarstad, 2009). When a methylated copy of the R388 plasmid enters the recipient cell, a complementary non-methylated strand will be generated by the host. Under these conditions, SeqA-GFP is able to bind to the DNA and fluorescence can be recorded. Similar experiments were previously described to monitor horizontal gene transfer in *E. coli* mediated by the F pili (Babic et al., 2008) or in the gram positive *Bacillus subtilis* (Babic et al., 2011). In the case of F pili, conjugation events were visualized between cells separated as far as 12 μM, although in some cases cell-to-cell contacts were also observed. This is due to the dynamics of the thin, flexible F pili (Clarke et al., 2008), which can undergo cycles of retraction and extension forced by the addition or separation of subunits at the cell proximal end. Here, however, we deal with a very short, rigid pilus prepared for conjugation within solid media, which is characteristic of IncW plasmids. Therefore, cell-to-cell contact is the most likely scenario.

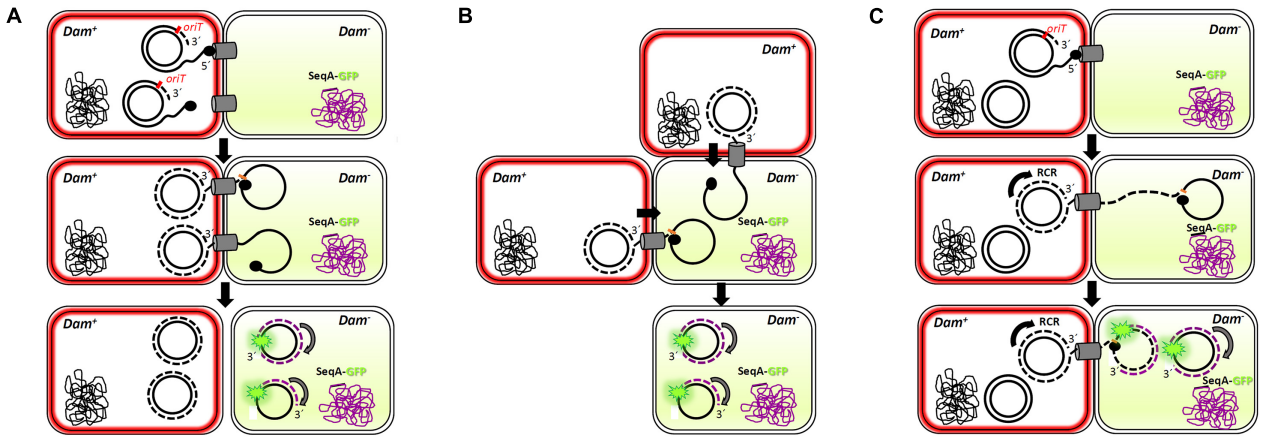

FIGURE 6 | Multi-transfer of conjugative R388 plasmid. The passage of more than one copy of the conjugative plasmid from donor to recipient cells, as shown by the presence of more than one foci in the recipient cell (**Figure 5**), is compatible with three models. Dam$^+$ donor cells contain R388 plasmid copies that express TrwB-mKate2 protein, coloring the membrane in red. Dam$^-$ recipient cells express SeqA-GFP protein from the chromosome, under the control of the native SeqA promoter. Methylated DNA is represented in black, whereas no methylated DNA is in purple. SeqA-GFP expression in the recipient cell is diffuse in the absence of hemi-methylated DNA. Only when a methylated copy of the plasmid is transferred and DNA replication starts in the recipient cell, SeqA-GFP is able to form compact foci. In model 1 **(A)**, conjugation might occur simultaneously from two or more secretion systems in contact with the same recipient cell, giving rise to at least two fluorescent foci. In model 2 **(B)**, two donor cells would transfer the plasmid simultaneously to the same recipient cell. In model 3 **(C)**, only one secretion system is functional but, since the transfer of plasmid ssDNA is accomplished of rolling circle replication (RCR) in the donor cell, multiple single-stranded linear copies of the plasmid (a concatemer) would be transferred bound to the relaxase TrwC. Once in the recipient cell, a new cleavage by TrwC on the *nic* site would re-circularize the plasmid DNA, resolving as many plasmid copies as those present in the concatemer. The synthesis of the complementary non-methylated strand would be associated to SeqA-GFP binding, observed as fluorescent foci.

Interestingly, and similarly to what was observed for the F-plasmid in previous reports (Babic et al., 2008), more than one foci could be imaged in some transconjugant cells (**Figure 5**). This result implies that more than one copy of the conjugative plasmid has been transferred to the recipient cell, which, *a priori*, is in contradiction with the incompatibility exclusion principle. A plausible explanation might be that there is a lag between the entrance of the conjugative plasmid and the expression of the entry exclusion factor (Garcillan-Barcia and de la Cruz, 2008). On this basis, although a splitting of the hemi-methylated DNA segments during plasmid replication cannot be entirely ruled out, three different scenarios could be foreseen (**Figure 6**). In a first scenario, conjugation might occur simultaneously through two or even three secretion systems in contact with the same recipient cell. Consistent with this idea is the observation of several T4SS assembled in donor cells. Alternatively, two different donor cells might contact simultaneously the same receptor cell. In a third scenario, only one secretion system from a single donor cell would be involved. In this case, upon DNA cleavage by TrwC, DNA synthesis by rolling circle replication (RCR) would produce multiple single-stranded linear copies of the plasmid (a concatemer). While DNA synthesis still goes on in the donor cell, the relaxase would be transferred covalently bound to the resultant concatemer. Once in the recipient cell, a new cleavage by TrwC on the *nic* site would re-circularize the plasmid DNA, resolving as many plasmid copies as those present in the concatemer (**Figure 6**). Once the plasmid DNA copies have been processed in the recipient cell, the transferred lagging strands will be replicated as complementary non- methylated DNA, which would explain the existence of more than one focus in the host. This scenario is supported by previous work (Gonzalez-Perez et al., 2007), in which it has been proposed that tyrosine 18 in TrwC is responsible for the initiation of replication at *oriT* in the donor cell, while tyrosine 26 promotes termination of leading strand replication in the recipient cell.

CONCLUSION

In this work, bacterial conjugation has been characterized by fluorescence microscopy. By labeling the main ATPases that drive conjugative DNA processing and substrate transport across Type IV secretion systems, we have been able to follow dynamic changes in its localization pattern upon contact with recipient cells. These results provide a better understanding of bacterial conjugation.

DATA AVAILABILITY STATEMENT

The original contributions presented in the study are included in the article/**Supplementary Material**, further inquiries can be directed to the corresponding authors.

AUTHOR CONTRIBUTIONS

GC, TM, FV-G, and YG-C performed the experiments. IA designed the work. EC and IA supervised the work and wrote the manuscript. All authors contributed to the article and approved the submitted version.

FUNDING

This work was supported by the Spanish Ministerio de Ciencia e Innovación (MINECO) Grants BFU2016-78521-R and PID2019-104251GB-I00.

ACKNOWLEDGMENTS

We appreciate the help of Scherer and Kaminski (University of Cambridge, United Kingdom) for d-STORM image acquisition and Madrazo (Microscopy Unit, IDIVAL, Santander, Spain) for the technical support with TIRF microscopy. We are also grateful to Fernández-López (IBBTEC, Santander, Spain) for helpful discussions and the supply of cells expressing SeqA-GFP protein.

SUPPLEMENTARY MATERIAL

The Supplementary Material for this article can be found online at: https://www.frontiersin.org/articles/10.3389/fmicb.2021.750200/full#supplementary-material

REFERENCES

Alvarez-Martinez, C. E., and Christie, P. J. (2009). Biological diversity of prokaryotic type IV secretion systems. *Microbiol. Mol. Biol. Rev.* 73, 775–808. doi: 10.1128/MMBR.00023-09

Arechaga, I., Pena, A., Zunzunegui, S., del Carmen Fernandez Alonso, M., Rivas, G., and de la Cruz, F. (2008). ATPase activity and oligomeric state of TrwK, the VirB4 homologue of the plasmid R388 type IV secretion system. *J. Bacteriol.* 190, 5472–5479. doi: 10.1128/JB.00321-08

Arends, K., Schiwon, K., Sakinc, T., Hubner, J., and Grohmann, E. (2012). Green fluorescent protein-labeled monitoring tool to quantify conjugative plasmid transfer between Gram-positive and Gram-negative bacteria. *Appl. Environ. Microbiol.* 78, 895–899. doi: 10.1128/AEM.05578-11

Atmakuri, K., Cascales, E., and Christie, P. J. (2004). Energetic components VirD4, VirB11 and VirB4 mediate early DNA transfer reactions required for bacterial type IV secretion. *Mol. Microbiol.* 54, 1199–1211. doi: 10.1111/j.1365-2958.2004.04345.x

Babic, A., Berkmen, M. B., Lee, C. A., and Grossman, A. D. (2011). Efficient gene transfer in bacterial cell chains. *MBio* 2:11. doi: 10.1128/mBio.00027-11

Babic, A., Lindner, A. B., Vulic, M., Stewart, E. J., and Radman, M. (2008). Direct visualization of horizontal gene transfer. *Science* 319, 1533–1536. doi: 10.1126/science.1153498

Bauer, T., Rosch, T., Itaya, M., and Graumann, P. L. (2011). Localization pattern of conjugation machinery in a Gram-positive bacterium. *J. Bacteriol.* 193, 6244–6256. doi: 10.1128/JB.00175-11

Brendler, T., and Austin, S. (1999). Binding of SeqA protein to DNA requires interaction between two or more complexes bound to separate hemimethylated GATC sequences. *EMBO J.* 18, 2304–2310. doi: 10.1093/emboj/18.8.2304

Byrd, D. R., and Matson, S. W. (1997). Nicking by transesterification: the reaction catalysed by a relaxase. *Mol. Microbiol.* 25, 1011–1022. doi: 10.1046/j.1365-2958.1997.5241885.x

Cabezon, E., and de la Cruz, F. (2006). TrwB: an F(1)-ATPase-like molecular motor involved in DNA transport during bacterial conjugation. *Res. Microbiol.* 157, 299–305. doi: 10.1016/j.resmic.2005.12.002

Cabezon, E., Ripoll-Rozada, J., Pena, A., de la Cruz, F., and Arechaga, I. (2015). Towards an integrated model of bacterial conjugation. *FEMS Microbiol. Rev.* 39, 81–95. doi: 10.1111/1574-6976.12085

Cabezon, E., Sastre, J. I, and de la Cruz, F. (1997). Genetic evidence of a coupling role for the TraG protein family in bacterial conjugation. *Mol. Gen. Genet.* 254, 400–406. doi: 10.1007/s004380050432

Cascales, E., and Christie, P. J. (2003). The versatile bacterial type IV secretion systems. *Nat. Rev. Microbiol.* 1, 137–149. doi: 10.1038/nrmicro753

Chandler, M., de la Cruz, F., Dyda, F., Hickman, A. B., Moncalian, G., and Ton-Hoang, B. (2013). Breaking and joining single-stranded DNA: the HUH endonuclease superfamily. *Nat. Rev. Microbiol.* 11, 525–538. doi: 10.1038/nrmicro3067

Christie, P. J., Whitaker, N., and Gonzalez-Rivera, C. (2014). Mechanism and structure of the bacterial type IV secretion systems. *Biochim. Biophys. Acta.* 2014:19. doi: 10.1016/j.bbamcr.2013.12.019

Clarke, M., Maddera, L., Harris, R. L., and Silverman, P. M. (2008). F-pili dynamics by live-cell imaging. *Proc. Natl. Acad. Sci. USA* 105, 17978–17981. doi: 10.1073/pnas.0806786105

Datsenko, K. A., and Wanner, B. L. (2000). One-step inactivation of chromosomal genes in *Escherichia coli* K-12 using PCR products. *Proc. Natl. Acad. Sci. USA* 97, 6640–6645. doi: 10.1073/pnas.120163297

Daubin, V., and Szollosi, G. J. (2016). Horizontal gene transfer and the history of life. *Cold Spring Harb. Perspect. Biol.* 8:a018036. doi: 10.1101/cshperspect.a018036

Day, R. N., and Davidson, M. W. (2009). The fluorescent protein palette: tools for cellular imaging. *Chem. Soc. Rev.* 38, 2887–2921. doi: 10.1039/b901966a

de la Cruz, F., and Davies, J. (2000). Horizontal gene transfer and the origin of species: lessons from bacteria. *Trends Microbiol.* 8, 128–133.

de la Cruz, F., Frost, L. S., Meyer, R. J., and Zechner, E. L. (2010). Conjugative DNA metabolism in Gram-negative bacteria. *FEMS Microbiol. Rev.* 34, 18–40. doi: 10.1111/j.1574-6976.2009.00195.x

Draper, O., Cesar, C. E., Machon, C., delaCruz, F., and Llosa, M. (2005). Site-specific recombinase and integrase activities of a conjugative relaxase in recipient cells. *Proc. Natl. Acad. Sci. USA* 102, 16385–16390. doi: 10.1073/pnas.0506081102

Fernandez-Lopez, R., DelCampo, I., Revilla, C., Cuevas, A., and delaCruz, F. (2014). Negative feedback and transcriptional overshooting in a regulatory network for horizontal gene transfer. *PLoS Genet.* 10:e1004171. doi: 10.1371/journal.pgen.1004171

Fernandez-Lopez, R., Garcillan-Barcia, M. P., Revilla, C., Lazaro, M., Vielva, L., and delaCruz, F. (2006). Dynamics of the IncW genetic backbone imply general trends in conjugative plasmid evolution. *FEMS Microbiol. Rev.* 30, 942–966. doi: 10.1111/j.1574-6976.2006.00042.x

Frost, L. S., Ippen-Ihler, K., and Skurray, R. A. (1994). Analysis of the sequence and gene products of the transfer region of the F sex factor. *Microbiol. Rev.* 58, 162–210.

Frost, L. S., and Koraimann, G. (2010). Regulation of bacterial conjugation: balancing opportunity with adversity. *Future Microbiol.* 5, 1057–1071. doi: 10.2217/fmb.10.70

Garcillan-Barcia, M. P., and de la Cruz, F. (2008). Why is entry exclusion an essential feature of conjugative plasmids? *Plasmid* 60, 1–18. doi: 10.1016/j.plasmid.2008.03.002

Garcillan-Barcia, M. P., Jurado, P., Gonzalez-Perez, B., Moncalian, G., Fernandez, L. A., and delaCruz, F. (2007). Conjugative transfer can be inhibited by blocking relaxase activity within recipient cells with intrabodies. *Mol. Microbiol.* 63, 404–416. doi: 10.1111/j.1365-2958.2006.05523.x

Gilmour, M. W., Lawley, T. D., Rooker, M. M., Newnham, P. J., and Taylor, D. E. (2001). Cellular location and temperature-dependent assembly of IncHI1 plasmid R27-encoded TrhC-associated conjugative transfer protein complexes. *Mol. Microbiol.* 42, 705–715. doi: 10.1046/j.1365-2958.2001.02682.x

Gilmour, M. W., and Taylor, D. E. (2004). A subassembly of R27-encoded transfer proteins is dependent on TrhC nucleoside triphosphate-binding motifs for function but not formation. *J. Bacteriol.* 186, 1606–1613. doi: 10.1128/jb.186.6.1606-1613.2004

Gonzalez-Perez, B., Lucas, M., Cooke, L. A., Vyle, J. S., de la Cruz, F., and Moncalian, G. (2007). Analysis of DNA processing reactions in bacterial conjugation by using suicide oligonucleotides. *EMBO J.* 26, 3847–3857. doi: 10.1038/sj.emboj.7601806

Grandoso, G., Llosa, M., Zabala, J. C., and de la Cruz, F. (1994). Purification and biochemical characterization of TrwC, the helicase involved in plasmid R388 conjugal DNA transfer. *Eur. J. Biochem.* 226, 403–412.

Guasch, A., Lucas, M., Moncalian, G., Cabezas, M., Perez-Luque, R., Gomis-Ruth, F. X., et al. (2003). Recognition and processing of the origin of transfer DNA by conjugative relaxase TrwC. *Nat. Struct. Biol.* 10, 1002–1010. doi: 10.1038/nsb1017

Guglielmini, J., de la Cruz, F., and Rocha, E. P. (2013). Evolution of conjugation and type IV secretion systems. *Mol. Biol. Evol.* 30, 315–331. doi: 10.1093/molbev/mss221

Gunton, J. E., Gilmour, M. W., Alonso, G., and Taylor, D. E. (2005). Subcellular localization and functional domains of the coupling protein, TraG, from IncHI1 plasmid R27. *Microbiology* 151, 3549–3561. doi: 10.1099/mic.0.28255-0

Guynet, C., Cuevas, A., Moncalian, G., and de la Cruz, F. (2011). The stb operon balances the requirements for vegetative stability and conjugative transfer of plasmid R388. *PLoS Genet.* 7:e1002073. doi: 10.1371/journal.pgen.1002073

Hu, B., Khara, P., and Christie, P. J. (2019). Structural bases for F plasmid conjugation and F pilus biogenesis in *Escherichia coli*. *Proc. Natl. Acad. Sci. USA* 116, 14222–14227. doi: 10.1073/pnas.1904428116

Koraimann, G. (2018). Spread and persistence of virulence and antibiotic resistance genes: a ride on the f plasmid conjugation module. *EcoSal. Plus* 8:18. doi: 10.1128/ecosalplus.ESP-0003-2018

Lawley, T. D., Klimke, W. A., Gubbins, M. J., and Frost, L. S. (2003). F factor conjugation is a true type IV secretion system. *FEMS Microbiol. Lett.* 224, 1–15. doi: 10.1016/S0378-1097(03)00430-0

Lederberg, J., and Tatum, E. L. (1946). Gene recombination in *Escherichia coli*. *Nature* 158:558. doi: 10.1038/158558a0

Low, H. H., Gubellini, F., Rivera-Calzada, A., Braun, N., Connery, S., Dujeancourt, A., et al. (2014). Structure of a type IV secretion system. *Nature* 508, 550–553. doi: 10.1038/nature13081

Lu, M., Campbell, J. L., Boye, E., and Kleckner, N. (1994). SeqA: a negative modulator of replication initiation in E. coli. *Cell* 77, 413–426. doi: 10.1016/0092-8674(94)90156-2

Mazel, D., and Davies, J. (1999). Antibiotic resistance in microbes. *Cell Mol. Life Sci.* 56, 742–754.

Nolivos, S., Cayron, J., Dedieu, A., Page, A., Delolme, F., and Lesterlin, C. (2019). Role of AcrAB-TolC multidrug efflux pump in drug-resistance acquisition by plasmid transfer. *Science* 364, 778–782. doi: 10.1126/science.aav6390

Paez-Segala, M. G., Sun, M. G., Shtengel, G., Viswanathan, S., Baird, M. A., Macklin, J. J., et al. (2015). Fixation-resistant photoactivatable fluorescent proteins for CLEM. *Nat. Methods* 12, 215–218. doi: 10.1038/nmeth.3225

Palmer, B. R., and Marinus, M. G. (1994). The dam and dcm strains of *Escherichia coli*–a review. *Gene* 143, 1–12. doi: 10.1016/0378-1119(94)90597-5

Paranchych, W., and Frost, L. S. (1988). The physiology and biochemistry of pili. *Adv. Microb. Physiol.* 29, 53–114. doi: 10.1016/s0065-2911(08)60346-x

Peña, A., Matilla, I., Martin-Benito, J., Valpuesta, J. M., Carrascosa, J. L., de la Cruz, F., et al. (2012). The hexameric structure of a conjugative VirB4 protein ATPase provides new insights for a functional and phylogenetic relationship with DNA translocases. *J. Biol. Chem.* 287, 39925–39932. doi: 10.1074/jbc.M112.413849

Peña, A., Ripoll-Rozada, J., Zunzunegui, S., Cabezon, E., delaCruz, F., and Arechaga, I. (2011). Autoinhibitory regulation of TrwK, an essential VirB4 ATPase in type IV secretion systems. *J. Biol. Chem.* 286, 17376–17382. doi: 10.1074/jbc.M110.208942

Popa, O., and Dagan, T. (2011). Trends and barriers to lateral gene transfer in prokaryotes. *Curr. Opin. Microbiol.* 14, 615–623. doi: 10.1016/j.mib.2011.07.027

Reyes-Lamothe, R., Possoz, C., Danilova, O., and Sherratt, D. J. (2008). Independent positioning and action of *Escherichia coli* replisomes in live cells. *Cell* 133, 90–102. doi: 10.1016/j.cell.2008.01.044

Rice, L. B. (2009). The clinical consequences of antimicrobial resistance. *Curr. Opin. Microbiol.* 12, 476–481. doi: 10.1016/j.mib.2009.08.001

Ripoll-Rozada, J., Zunzunegui, S., delaCruz, F., Arechaga, I., and Cabezon, E. (2013). Functional interactions of VirB11 traffic ATPases with VirB4 and VirD4 molecular motors in type IV secretion systems. *J. Bacteriol.* 195, 4195–4201. doi: 10.1128/JB.00437-13

Segura, R. L., Aguila-Arcos, S., Ugarte-Uribe, B., Vecino, A. J., de la Cruz, F., Goni, F. M., et al. (2014). Subcellular location of the coupling protein TrwB and the role of its transmembrane domain. *Biochim. Biophys. Acta* 1838, 223–230. doi: 10.1016/j.bbamem.2013.08.016

Shcherbo, D., Merzlyak, E. M., Chepurnykh, T. V., Fradkov, A. F., Ermakova, G. V., Solovieva, E. A., et al. (2007). Bright far-red fluorescent protein for whole-body imaging. *Nat. Methods* 4, 741–746. doi: 10.1038/nmeth1083

Smillie, C., Garcillan-Barcia, M. P., Francia, M. V., Rocha, E. P., and de la Cruz, F. (2010). Mobility of plasmids. *Microbiol. Mol. Biol. Rev.* 74, 434–452. doi: 10.1128/MMBR.00020-10

Tato, I., Zunzunegui, S., delaCruz, F., and Cabezon, E. (2005). TrwB, the coupling protein involved in DNA transport during bacterial conjugation, is a DNA-dependent ATPase. *Proc. Natl. Acad. Sci. USA* 102, 8156–8161. doi: 10.1073/pnas.0503402102

von Wintersdorff, C. J., Penders, J., van Niekerk, J. M., Mills, N. D., Majumder, S., van Alphen, L. B., et al. (2016). Dissemination of Antimicrobial Resistance in Microbial Ecosystems through Horizontal Gene Transfer. *Front. Microbiol.* 7:173. doi: 10.3389/fmicb.2016.00173

Waldminghaus, T., and Skarstad, K. (2009). The *Escherichia coli* SeqA protein. *Plasmid* 61, 141–150. doi: 10.1016/j.plasmid.2009.02.004

Waters, V. L. (1999). Conjugative transfer in the dissemination of beta-lactam and aminoglycoside resistance. *Front. Biosci.* 4:D433–D456.

Zechner, E. L., Moncalian, G., and delaCruz, F. (2017). Relaxases and Plasmid Transfer in Gram-Negative Bacteria. *Curr. Top Microbiol. Immunol.* 413, 93–113. doi: 10.1007/978-3-319-75241-9_4

Conflict of Interest: The authors declare that the research was conducted in the absence of any commercial or financial relationships that could be construed as a potential conflict of interest.

Publisher's Note: All claims expressed in this article are solely those of the authors and do not necessarily represent those of their affiliated organizations, or those of the publisher, the editors and the reviewers. Any product that may be evaluated in this article, or claim that may be made by its manufacturer, is not guaranteed or endorsed by the publisher.

frontiers in Microbiology

ORIGINAL RESEARCH
published: 06 October 2021
doi: 10.3389/fmicb.2021.756044

Multiple Roles of Flagellar Export Chaperones for Efficient and Robust Flagellar Filament Formation in *Salmonella*

Tohru Minamino[1], Yusuke V. Morimoto[2,3], Miki Kinoshita[1] and Keiichi Namba[1,4,5]*

[1]*Graduate School of Frontier Biosciences, Osaka University, Suita, Japan,* [2]*Department of Physics and Information Technology, Faculty of Computer Science and Systems Engineering, Kyushu Institute of Technology, Iizuka, Japan,* [3]*Japan Science and Technology Agency, PRESTO, Kawaguchi, Japan,* [4]*RIKEN SPring-8 Center and Center for Biosystems Dynamics Research, Suita, Japan,* [5]*JEOL YOKOGUSHI Research Alliance Laboratories, Osaka University, Suita, Japan*

FlgN, FliS, and FliT are flagellar export chaperones specific for FlgK/FlgL, FliC, and FliD, respectively, which are essential component proteins for filament formation. These chaperones facilitate the docking of their cognate substrates to a transmembrane export gate protein, FlhA, to facilitate their subsequent unfolding and export by the flagellar type III secretion system (fT3SS). Dynamic interactions of the chaperones with FlhA are thought to determine the substrate export order. To clarify the role of flagellar chaperones in filament assembly, we constructed cells lacking FlgN, FliS, and/or FliT. Removal of either FlgN, FliS, or FliT resulted in leakage of a large amount of unassembled FliC monomers into the culture media, indicating that these chaperones contribute to robust and efficient filament formation. The Δ*flgN* Δ*fliS* Δ*fliT* (ΔNST) cells produced short filaments similarly to the Δ*fliS* mutant. Suppressor mutations of the ΔNST cells, which lengthened the filament, were all found in FliC and destabilized the folded structure of FliC monomer. Deletion of FliS inhibited FliC export and filament elongation only after FliC synthesis was complete. We propose that FliS is not involved in the transport of FliC upon onset of filament formation, but FliS-assisted unfolding of FliC by the fT3SS becomes essential for its rapid and efficient export to form a long filament when FliC becomes fully expressed in the cytoplasm.

Keywords: bacterial flagella, chaperone, flagellar assembly, flagellar filament, protein secretion

OPEN ACCESS

Edited by:
Eric Cascales,
Aix-Marseille Université, France

Reviewed by:
Ben Spiller,
Vanderbilt University,
United States
Anastassios Economou,
KU Leuven, Belgium

****Correspondence:***
Tohru Minamino
tohru@fbs.osaka-u.ac.jp

Specialty section:
This article was submitted to Microbial Physiology and Metabolism, a section of the journal Frontiers in Microbiology

Received: *09 August 2021*
Accepted: *08 September 2021*
Published: *06 October 2021*

Citation:
Minamino T, Morimoto YV, Kinoshita M and Namba K (2021) Multiple Roles of Flagellar Export Chaperones for Efficient and Robust Flagellar Filament Formation in Salmonella. Front. Microbiol. 12:756044. doi: 10.3389/fmicb.2021.756044

INTRODUCTION

Many pathogenic bacteria utilize flagella to swim in viscous fluids to reach and attach to host cells for effective infection and colonization. The flagellum of *Salmonella enterica* serovar Typhimurium (thereafter referred to as *Salmonella*) is composed of the basal body, which acts as a rotary motor fueled by proton motive force (PMF) across the cell membrane, the filament, which functions as a helical propeller to produce the thrust that drives swimming motility and the hook connecting the basal body and filament to act as a universal joint. Flagellar assembly begins with the basal body, followed by the hook (FlgE) with the help of the hook

cap (FlgD). After completion of hook assembly, the hook cap is replaced by FlgK, and 11 FlgK and FlgL subunits are assembled to form the hook-filament junction structure at the hook tip to start filament assembly. Five FliD molecules self-assemble into the filament cap at the tip of the junction structure, and finally, tens of thousands of flagellin molecules (FliC or FljB) polymerize into the long helical filament with the help of the filament cap (**Figure 1**; Minamino and Namba, 2004; Nakamura and Minamino, 2019).

To build the flagella beyond the inner and outer membranes, flagellar building blocks are translocated across the cell membrane *via* the flagellar type III secretion system (fT3SS), diffuse down the central channel of the growing flagellar structure, and assemble at the distal end. The fT3SS consists of a PMF-driven transmembrane export gate complex made of FlhA, FlhB, FliP, FliQ, and FliR and a cytoplasmic ATPase complex composed of FliH, FliI, and FliJ (Minamino, 2014; Minamino et al., 2020b). Because the cytoplasmic ATPase ring complex is dispensable for flagellar protein export, the export gate complex works not only as a PMF-driven protein transporter but also as a PMF-driven unfoldase (Minamino and Namba, 2008; Paul et al., 2008; Terashima et al., 2018, 2020). In addition, FlgN, FliA, FliS, and FliT act as cytoplasmic export chaperones specific for FlgK/FlgL, FlgM, FliC, and FliD, respectively (Fraser et al., 1999; Auvray et al., 2001; Aldridge et al., 2006).

In *Salmonella*, flagellar genes are divided into three classes according to their transcriptional hierarchy (**Figure 1**; Kutsukake et al., 1990). Class 1 genes, *flhD* and *flhC*, encode a positive regulator required for the transcription of class 2 genes. The class 2 genes encode proteins required for the structure and assembly of hook-basal body (HBB). FliA is a class 2 gene product and acts as the flagellum-specific sigma factor (σ^{28}) that transcribes class 3 genes encoding proteins required for filament formation, motility, and chemotaxis (Ohnishi et al., 1990). Such transcriptional coordination ensures that flagellar building blocks, motor proteins, and proteins involved in chemotactic signaling are expressed in different stages during flagellar assembly (Chevance and Hughes, 2008). First, the fT3SS transports six rod-type (FliE, FlgB, FlgC, FlgF, FlgG, and FlgJ) and

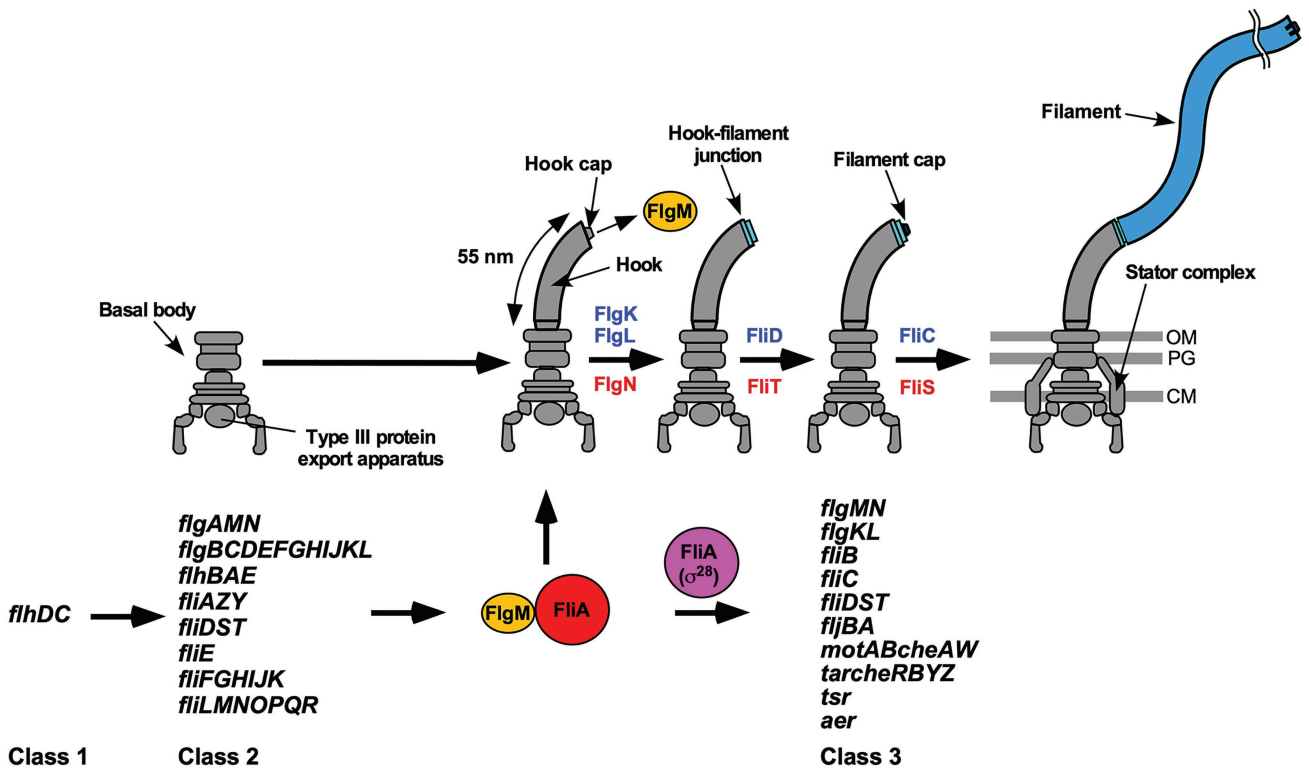

FIGURE 1 | Flagellar assembly and hierarchical flagellar gene expression. Flagellar assembly begins with the basal body, followed by the hook (FlgE) with the help of the hook cap (FlgD). Upon completion of hook assembly, the hook cap is replaced by FlgK. FlgK and FlgL self-assemble at the hook tip in this order to form the hook-filament junction structure. Then, FliD forms the filament cap at the tip of the junction and promotes the assembly of FliC into the long helical filament. During hook-basal body (HBB) assembly, FlhD and FlhC, which are class 1 gene products, act as a transcriptional activator to induce the transcription of class 2 genes required for HBB formation. When the hook length reaches its mature length of 55 nm in *Salmonella*, the flagellar type III secretion system (fT3SS) switches its substrate specificity from rod- and hook-type proteins to filament-type ones, thereby terminating hook assembly and filament assembly at the hook tip. As a result, FlgM is secreted *via* the fT3SS into the culture media, and so FliA acts as a flagellum-specific sigma factor (σ^{28}) to transcribe class 3 genes encoding proteins required for filament formation, motility, and chemotaxis. FlgN, FliT, and FliS act as flagellar export chaperones specific for FlgK/FlgL, FliD, and FliC, respectively. These chaperones facilitate the docking of their substrates to the fT3SS for efficient and rapid protein unfolding and export. Except for the *fliC* gene, the *flgKL*, *flgMN*, and *fliDST* genes are transcribed from both class 2 and class 3 promoters. OM, outer membrane; PG, peptidoglycan layer; CM, cytoplasmic membrane.

three hook-type (FlgD, FlgE, and FliK) proteins to produce the HBB (Minamino, 2018). At this stage, four filament-type proteins (FlgK, FlgL, FlgM, FliD) and four export chaperones (FlgN, FliA, FliS, FliT) are also expressed along with other class 2 gene products (**Figure 1**). However, the fT3SS does not transport these filament-type proteins until HBB assembly is complete (Minamino et al., 1999). FlgM functions as an anti-sigma factor to suppress the σ^{28} activity of FliA during HBB assembly (Ohnishi et al., 1992). When the hook reaches its mature length of about 55 nm, the fT3SS switches its substrate specificity from rod- and hook-type proteins to filament-type ones, thereby terminating HBB assembly and initiating filament formation (Kutsukake et al., 1994a). As a result, FlgM is secreted *via* the fT3SS into the culture media, allowing FliA to act as σ^{28} to transcribe the *fliC* gene to start forming the filament at the hook tip (**Figure 1**; Hughes et al., 1993; Kutsukake, 1994). Thus, the fT3SS appears to coordinate gene expression with assembly. In addition, the FlgN, FliS, and FliT chaperones also regulate the expression levels of class 2 and 3 genes to control the number of flagella per cell (Yokoseki et al., 1996; Karlinsey et al., 2000a; Aldridge et al., 2010; Xu et al., 2014).

FlgN, FliS, and FliT adopt highly α-helical structures (Evdokimov et al., 2003; Imada et al., 2010; Kinoshita et al., 2016). They bind to the intrinsically disordered C-terminal region of their cognate substrates not only to suppress their premature aggregation and proteolysis in the cytoplasm (Fraser et al., 1999; Bennett et al., 2001; Aldridge et al., 2003; Ozin et al., 2003) but also to efficiently transfer their substrates to the fT3SS export gate (Thomas et al., 2004; Bange et al., 2010; Imada et al., 2010; Minamino et al., 2012a,b; Kinoshita et al., 2013). Interactions between the flagellar chaperones and their cognate substrates induce rearrangements of helices in the chaperone structures to regulate the affinities for their binding partners during the protein export process (Thomas et al., 2004; Evans et al., 2006; Bange et al., 2010; Imada et al., 2010; Kinoshita et al., 2013, 2016; Khanra et al., 2016).

The C-terminal cytoplasmic domain of FlhA ($FlhA_C$) forms a ring-like structure in the fT3SS as the docking platform for the export substrates and ensures the strict order of flagellar protein export (Abrusci et al., 2013; Terahara et al., 2018; Inoue et al., 2019, 2021; Minamino et al., 2012a). The FlgN, FliS, and FliT chaperones in complex with their cognate substrates bind to $FlhA_C$ with nanomolar affinity (Bange et al., 2010; Minamino et al., 2012a; Kinoshita et al., 2013; Xing et al., 2018). Highly conserved tyrosine residues of chaperones, Tyr-122 of FlgN, Tyr-10 of FliS, and Tyr-106 of FliT, are critical for the interaction with $FlhA_C$ at its specific binding pocket (Minamino et al., 2012a; Kinoshita et al., 2013; Altegoer et al., 2018; Xing et al., 2018). The FlgN(Y122A) and FliS(Y10S) substitutions reduce the secretion levels of FlgK/FlgL and FliC, respectively, suggesting that the flagellar chaperones promote the docking of their cognate substrates to the $FlhA_C$ ring and that the interaction of these chaperones with $FlhA_C$ assists efficient protein unfolding and transport by the transmembrane export gate complex (Minamino et al., 2012a; Kinoshita et al., 2013; Furukawa et al., 2016).

FlgN and FliT bind to FliI and FliJ, whereas FliS does not (Thomas et al., 2004; Evans et al., 2006; Bange et al., 2010; Imada et al., 2010; Minamino et al., 2012b; Sajó et al., 2014). This distinct characteristic of FliS would be related to the fact that the number of FliC subunits per filament is three orders of magnitude higher than that of FlgK, FlgL, and FliD subunits (Minamino and Namba, 2004). Because FliI and FliJ bind to $FlhA_C$, it has been proposed that interactions of FlgN and FliT with FliI and FliJ provide an advantage for efficient docking of FlgK, FlgL, and FliD to the $FlhA_C$ ring prior to the export of a largely excessive amount of FliC molecules (Evans et al., 2006; Bange et al., 2010; Minamino et al., 2016; Inoue et al., 2018). However, it remains unclear how these chaperones determine the substrate export order for efficient flagellar filament assembly.

Salmonella cells lacking FliS (thereafter referred to as ΔS, **Table 1**) produce very short filaments with their lengths shorter than 3 μm (Yokoseki et al., 1995). Extragenic suppressor mutations in FliC allow the ΔS cells to produce longer flagellar filaments (Furukawa et al., 2016). These suppressor mutations significantly destabilize the folded structure of FliC monomer. Furthermore, they do not affect the binding affinity of FliC for $FlhA_C$ at all (Furukawa et al., 2016). These observations suggest that the PMF-driven unfolding step of FliC monomer by the transmembrane export gate complex limits the export rate of FliC in the ΔS mutant (Furukawa et al., 2016). However, it remains unknown why the filament growth of the ΔS mutant stops at short lengths and how FliS supports the export gate

TABLE 1 | Strains and plasmids used in this study.

Salmonella strains	Abbreviated name	Relevant characteristics	Source or reference
SJW1103	WT	Wild type for motility and chemotaxis	Yamaguchi et al., 1984
SJW2177	ΔK	*flgK*	Homma et al., 1984
MM9001	ΔN	Δ*flgN*::*tetRA*	Minamino et al., 2012a
MM9101	ΔS	Δ*fliS*::*km*	This study
MM9102	ΔS/P*araBAD-fliS*	Δ*fliS*::*km* Δ*araBAD*::*fliS*	This study
MM9103	ΔS/P*araBAD-fliS* T-POP	Δ*fliS*::*km* Δ*araBAD*::*fliS* P*flhDC*::T-POP (DEL-25)	This study
MM9104	ΔT	Δ*fliT*::*km*	This study
MM9105	ΔNS	Δ*flgN*::*tetRA* Δ*fliS*::*km*	This study
MM9106	ΔNT	Δ*flgN*::*tetRA* Δ*fliT*::*km*	This study
MM9107	ΔST	Δ*fliS-fliT*::*km*	This study
MM9108	ΔNST	Δ*flgN*::*tetRA* Δ*fliS-fliT*::*Km*	This study
MMC9108-1	ΔNST *fliC*(Δ195–274)	Δ*flgN*::*tetRA* Δ*fliS-fliT*::*km fliC*(Δ195–274)	This study
MMC9108-2	ΔNST *fliC*(R92S)	Δ*flgN*::*tetRA* Δ*fliS-fliT*::*km fliC*(R92S)	This study
MMC9108-3	ΔNST *fliC*(Δ245–289)	Δ*flgN*::*tetRA* Δ*fliS-fliT*::*km fliC*(Δ245–289)	This study
MMC9108-4	ΔNST *fliC*(E153A)	Δ*flgN*::*tetRA* Δ*fliS-fliT*::*km fliC*(E153A)	This study
MMC9108-5	ΔNST *fliC*(Q128R)	Δ*flgN*::*tetRA* Δ*fliS-fliT*::*km fliC*(Q128R)	This study
MM9109	ΔM	Δ*flgM*::*km*	This study

complex to facilitate FliC unfolding for its efficient transport to form a long filament.

To clarify the role of the flagellar export chaperones in filament assembly, we constructed flagellar chaperone-deficient mutants and analyzed their efficiency of filament formation. We show that removal of either FlgN, FliS, or FliT causes leakage of a significantly larger amount of unassembled FliC monomers into the culture media compared to the *Salmonella* wild-type strain (hereafter referred to as WT), suggesting that these chaperones not only assist the export of their cognate substrates but also contribute to efficient and robust filament formation. We also show that FliS-assisted unfolding of FliC by the export gate complex becomes essential for rapid and efficient export of FliC to form a long filament after FliC synthesis is complete.

MATERIALS AND METHODS

Salmonella Strains, Transductional Crosses, and DNA Sequencing

Salmonella strains used in this study are listed in **Table 1**. To isolate spontaneous pseudorevertants from the *Salmonella* Δ*flgN* Δ*fliS* Δ*fliT* cells, 50-μl overnight cultures were streaked out on soft agar plates [1% (w/v) tryptone, 0.5% (w/v) NaCl, 0.35% (w/v) Bacto agar], and the plates were incubated at 30°C for 2 days to look for swarms emerging from each streak. Six motile colonies were isolated from such swarms. P22-mediated transductional crosses were carried out with p22HT*int* (Schmiger, 1972). DNA sequencing reactions were carried out using BigDye v3.1 (Applied Biosystems), and the reaction mixtures were analyzed by a 3,130 Genetic Analyzer (Applied Biosystems).

Motility Assay

Fresh colonies were inoculated onto soft agar plates and incubated at 30°C. At least seven independent colonies of each mutant strain were analyzed.

Secretion Assay

Salmonella cells were grown in L-broth [1% (w/v) tryptone, 0.5% (w/v) yeast extract, 0.5% (w/v) NaCl] at 30°C with shaking until the cell density had reached an OD_{600} of ca. 1.2–1.4, and then, each culture was heated at 65°C for 5 min to depolymerize the filaments into flagellin monomers, followed by centrifugation (8,000 × *g*, 5 min, 4°C) to obtain the cell pellet and supernatant separately. Proteins in whole cellular and culture supernatant fractions were normalized to the OD_{600} unit of each culture to give a constant number of *Salmonella* cells. Each cell pellet was resuspended in SDS-loading buffer [62.5 mM Tris-HCl, pH 6.8, 2% sodium dodecyl sulfate (SDS), 10% glycerol, 0.001% bromophenol blue] containing 1 μl of 2-mercaptoethanol. Proteins in the culture supernatants were precipitated by 10% trichloroacetic acid (TCA), suspended in a Tris-SDS loading buffer (one volume of 1 M Tris, nine volumes of SDS-loading buffer) containing 1 μl of 2-mercaptoethanol and heated at 95°C for 3 min. After SDS-polyacrylamide gel electrophoresis (SDS-PAGE), immunoblotting with polyclonal anti-FlgK, anti-FlgL or anti-FliD antibody was carried out as described previously (Minamino and Macnab, 1999). Detection was performed with Amersham ECL Prime western blotting detection reagent (Cytiva). Chemiluminescence signals were captured by a Luminoimage analyzer LAS-3000 (GE Healthcare). At least three independent experiments were performed.

Observation of Negatively Stained *Salmonella* Cells by Electron Microscopy

Salmonella cells were exponentially grown in 5 ml of L-broth at 30°C. A 5 μl of each cell culture was applied to a carbon-coated copper grid and negatively stained with 0.5% (w/v) phosphotungstic acid, pH 6.5. Micrographs were recorded at a magnification of ×1,200 with a JEM-1011 transmission electron microscope (JEOL) operating at 100 kV.

FliC Leakage Measurements During Flagellar Filament Assembly

Salmonella cells were grown in 5 ml of L-broth at 30°C with very gentle shaking to avoid mechanical shearing of flagellar filaments until the cell density had reached an OD_{600} of ca. 1.2–1.4.

To prepare total extracellular FliC subunits (filaments attached to *Salmonella* cell bodies and unassembled FliC monomers secreted into the culture media), a 1.5 ml of culture was heated at 65°C for 5 min to depolymerize the filaments into FliC monomers, followed by centrifugation (8,000 × *g*, 5 min, 4°C) to obtain the cell pellet and culture supernatant separately. Proteins in the culture supernatant were precipitated by 10% TCA, suspended in a Tris-SDS loading buffer, and heated at 95°C for 3 min.

To prepare polymerized FliC subunits (filaments attached to the cell bodies), a 1.5 ml of culture was centrifuged (8,000 × *g*, 5 min, 4°C), and the cell pellet and culture supernatant were collected separately. The cell pellet was suspended in a 1.5 ml of PBS (8 g of NaCl, 0.2 g of KCl, 3.63 g of Na_2HPO_4 $12H_2O$, 0.24 g of KH_2PO_4, pH 7.4 per liter) and heated at 65°C for 5 min, followed by centrifugation (8,000 × *g*, 5 min, 4°C) to obtain the cell pellet and supernatant, which contained cytoplasmic FliC molecules and depolymerized FliC monomers, respectively. Depolymerized FliC monomers in the supernatant were precipitated by 10% TCA, suspended in a Tris-SDS loading buffer, and heated at 95°C for 3 min.

To prepare FliC monomers leaked out into the culture media during filament assembly, the culture supernatant was ultracentrifuged at 85,000 × *g* for 1 h at 4°C, and the pellet and supernatant, which contained flagellar filaments detached from the cell bodies during shaking culture and FliC monomers leaked out into the culture media, respectively, were collected separately. FliC monomers in the supernatant were precipitated by 10% TCA, suspended in the Tris/SDS loading buffer and heated at 95°C for 3 min.

Samples were analyzed by SDS-PAGE with Coomassie Brilliant Blue (CBB) staining. Gel images were captured by a Luminoimage analyzer LAS-3000 (GE Healthcare). The band intensity was

analyzed using an image analysis software, CS Analyzer 4 (ATTO, Tokyo, Japan). Three independent measurements were performed.

Tetracycline-Induced Secretion Assay

Salmonella Δ*fliS* Δ*araBAD*::*fliS* cells with a T-POP insertion, which is located between the *flhDC* promoter and the transcription start site (Karlinsey et al., 2000b), were grown overnight in L-broth at 30°C and diluted 100-fold into 25 ml of fresh L-broth. When the cell density reached an OD_{600} of 0.5, tetracycline and arabinose was added to a final concentration of 15 μg/ml and 0.2% (w/v), respectively. Samples were taken at 0, 15, 30, 45, 60, 90, 120, and 180 min after tetracycline addition and heated at 65°C for 5 min. After centrifugation (8,000 × *g*, 5 min, 4°C), proteins in the culture supernatant fraction were prepared by TCA. After SDS-PAGE, immunoblotting with polyclonal anti-FliC or anti-FlgM antibody was carried out. The band intensity of each blot was analyzed using an image analysis software, CS Analyzer 4 (ATTO, Tokyo, Japan). Four independent measurements were carried out.

Observation of Flagellar Filaments

A 50 μl of overnight culture of *Salmonella* wild-type and Δ*fliS* Δ*araBAD*::*fliS* cells were inoculated into fresh 5 ml of L-broth and grown at 30°C with shaking until the cell density had reached an OD_{600} of *ca.* 0.5. After addition of arabinose at a final concentration of 0.2%, 100 μl of the culture was collected at 1, 3, 6, 10, and 14 h and washed with motility buffer (10 mM potassium phosphate, 0.1 mM EDTA, pH 7.0). In the experiment using a T-POP insertion, *Salmonella* Δ*fliS* Δ*araBAD*::*fliS* cells with the T-POP insertion were grown in L-broth at 30°C for 3 h, and then, tetracycline and arabinose were added at a final concentration of 15 μg/ml and 0.2% (w/v), respectively. The cells were collected at the indicated time intervals and washed with the motility buffer. The cells were attached to a cover slip (Matsunami glass, Japan), and unattached cells were washed away with motility buffer. Then, flagellar filaments were labelled with Alexa Fluor 594 (Invitrogen) as described before (Minamino et al., 2014). Epifluorescence of Alexa Fluor 594 was observed by an inverted fluorescence microscope (IX-83, Olympus) with a 100× oil immersion objective lens (UPLSAPO100XO, NA 1.4, Olympus) and a sCMOS camera (Prime 95B, Photometrics). Fluorescence images were analyzed using ImageJ software version 1.53 (National Institutes of Health). Statistical analyses were done using Prism 9 software (GraphPad). Comparisons were performed using a two-tailed Student's *t*-test. A value of $p < 0.05$ was considered to be statistically significant difference.

RESULTS

Effect of FliS Deletion on Motility of the Δ*flgN* Mutant

A *Salmonella* Δ*flgN* mutant (thereafter referred to as ΔN, **Table 1**) cannot efficiently transport FlgK and FlgL to the hook tip to form the hook-filament junction structure (Bennett et al., 2001; Kutsukake et al., 1994b), and so only about 35% of the ΔN cells produce a single flagellar filament and generate a small motility ring on soft agar plates (**Supplementary Figure 1A**; Minamino et al., 2021). Loss-of-function mutations of either ClpXP, FlgM, or FliT increase the expression levels of FlgK and FlgL, thereby significantly increasing the probability of hook-filament junction formation even in the absence of FlgN (Aldridge et al., 2003). Removal of FliS increases the secretion level of FlgM, which in turn increases the expression level of class 3 genes (Yokoseki et al., 1996), raising the possibility that FliS deletion also increases the probability of filament assembly in the absence of FlgN. To investigate this possibility, we constructed the ΔN mutant containing the Δ*fliS*::*km* allele (thereafter referred to as ΔNS, **Table 1**) or the Δ*fliT*::*km* allele (thereafter referred to as ΔNT, **Table 1**). In agreement with a previous result, removal of FliT restored motility of the ΔN mutant to a considerable degree (**Supplementary Figure 1A**). As expected, the cytoplasmic levels of FlgK and FlgL were higher in the ΔNS and ΔNT mutants than the ΔN mutant (**Supplementary Figure 1B**, left panels, second and third rows). Deletion of FliS increased the secretion levels of FlgK and FlgL by the ΔN mutant in a way similar to FliT deletion (**Supplementary Figure 1B**, right panels, second and third rows). These observations suggest that the over-expression of FlgK and FlgL caused by removal of either FliS or FliT compensates for the lack of FlgN chaperone activity.

To investigate how deletion of FliS or FliT affects the probability of filament formation by the ΔN mutant, we isolated polymerized FliC subunits in the filament form and unassembled FliC monomers leaked into the culture media separately and analyzed them by SDS-PAGE with CBB staining. In the wild-type cells, about 85% of FliC subunits assembled into the filaments, and the remaining 15% existed as monomer in the culture supernatant (**Figure 2A**). In the ΔN mutant, more than 80% of FliC subunits existed as monomer in the culture supernatant (**Figure 2C**), indicating that the ΔN mutant cannot efficiently form the hook-filament junction at the hook tip. Additional deletion of FliS or FliT partially suppressed FliC leakage by the ΔN mutant (**Figures 2D,E**). Because the lack of the hook-filament junction structure causes complete leakage of unassembled FliC monomers into the culture media without filament formation (**Figure 2B**; Homma et al., 1984), this suggests that the ΔNS and ΔNT cells form the junction structure even in the absence of FlgN. However, a much larger amount of FliC still existed as monomer in the culture supernatant (**Figures 2D,E**), indicating that the ΔNS and ΔNT mutants are not able to form the hook-filament junction so efficiently. Interestingly, deletion of either FliS or FliT alone or both also increased the amount of unassembled FliC monomers leaking out into the culture supernatant even in the presence of FlgN (**Figures 2F–H**). Because FliC leakage by the WT cells into the culture media was minimal during filament assembly (**Figure 2A**), the flagellar export chaperones are required for efficient and robust filament formation.

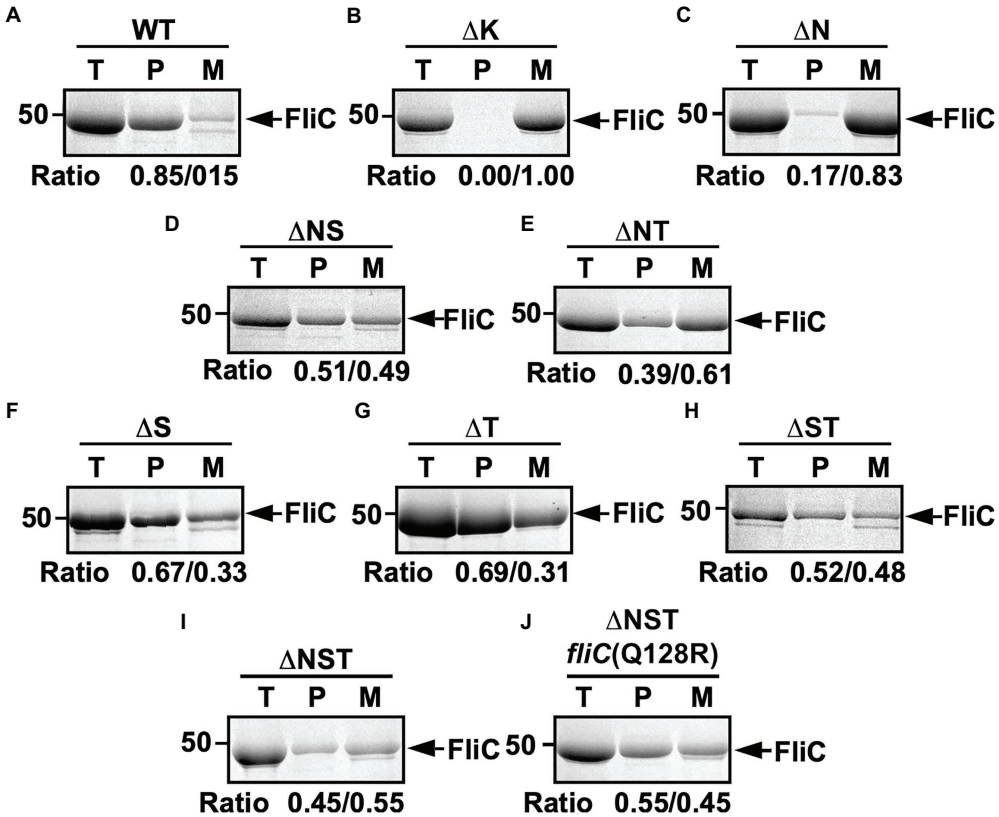

FIGURE 2 | Effect of removal of flagellar export chaperones on FliC leakage during filament assembly. Measurements of FliC monomers leaked out into the culture media. CBB-staining SDS gels of total extracellular FliC proteins (indicated as T), polymerized FliC subunits in the filament (indicated as P), and FliC monomers leaked into the culture media (indicated as M) of **(A)** wild-type (WT), **(B)** *flgK* (ΔK), **(C)** Δ*flgN* (ΔN), **(D)** Δ*flgN* Δ*fliS* (ΔNS), **(E)** Δ*flgN* Δ*fliT* (ΔNT), **(F)** Δ*fliS* (ΔS), **(G)** Δ*fliT* (ΔT), **(H)** Δ*fliS* Δ*fliT* (ΔST), **(I)** Δ*flgN* Δ*fliS* Δ*fliT* (ΔNST), and **(J)** Δ*flgN* Δ*fliS* Δ*fliT fliC*(Q128R) [ΔNST *fliC*(Q128R)]. The position of 50 kDa molecular mass marker is indicated on the left. The band densities of polymerized FliC subunits and FliC monomers leaked into the culture media were normalized by the total extracellular FliC level in each strain, and then, the relative ratio of the polymerized and secreted FliC subunits was calculated. We performed three independent measurements.

Effect of Flit Deletion on FliD Export

FliT is required for efficient FliD export for its assembly as the filament cap to promote FliC assembly to form a long filament as the helical propeller. However, motility of the Δ*fliT* mutant (thereafter referred to as ΔT, **Table 1**) was worse than the WT only slightly and almost the same as the Δ*flgM* mutant (thereafter referred to as ΔM; **Supplementary Figure 2A**). To clarify why FliT deletion does not inhibit motility so significantly, we compared the cytoplasmic and secretion levels of FliD between the ΔS, ΔT, and ΔM mutants (**Supplementary Figure 2B**). Deletion of either FliS, FliT, or FlgM increased the cytoplasmic level of FliD considerably compared to the WT (**Supplementary Figure 2B**, second row, left panel). This is consistent with the fact that FliT also acts as a negative regulator in the flagellar regulon so that removal of FliT results in a considerable increase in the expression level of class 3 genes, similar to the ΔM mutant (Yokoseki et al., 1996). However, the secretion level of FliD by the ΔT mutant was lower than that by the ΔS and ΔM mutants (**Supplementary Figure 2B**, second row, right panel), confirming that FliT is required for efficient FliD transport. Thus, the over-expression of FliD caused by removal of FliT compensates for the lack of FliT chaperone activity to some level, thereby allowing the ΔT mutant to produce long helical filaments.

Effect of Removal of all Three Flagellar Export Chaperones on Flagellar Filament Formation

It has been reported that the ΔS and Δ*fliS* Δ*fliT* mutants (thereafter referred to as ΔST, **Table 1**) produce shorter flagellar filaments than WT (**Supplementary Figure 1C**; Yokoseki et al., 1995). To investigate whether the ΔNS mutant also produces short flagellar filaments, we negatively stained the ΔNS cells and observed their filaments by electron microscopy (**Supplementary Figure 1C**). As expected, the ΔNS cells produced short filaments. Interestingly, the ΔNT mutant, of which motility was better than the ΔNS mutant but worse than the ΔT mutant (**Supplementary Figure 1A**), produced long filaments in a way similar to the WT and ΔT cells (**Supplementary Figure 1C**). Therefore, we conclude that FliS is directly involved in efficient elongation of the flagellar filament.

To address why the over-expression of FliC caused by removal of FliS cannot compensate for the lack of FliS chaperone activity, we constructed the Δ*flgN* Δ*fliS* Δ*fliT* mutant (**Supplementary Figures 1A,B**; thereafter referred to as ΔNST, **Table 1**) and analyzed the filament length of the ΔNST cells (**Figure 3** and **Supplementary Table 1**). All the WT cells produced long filaments with an average length of 8.9 ± 1.9 μm ($n = 50$). In contrast, 90.0 and 85.1% of the ΔS and ΔNST cells produced the filaments of shorter lengths, with an average length of 3.0 ± 0.7 μm ($n = 50$) and 2.8 ± 0.8 μm ($n = 50$), respectively, which are almost three times shorter than the wild-type length. This suggests that removal of FliS alone not only reduces the probability of filament formation slightly but also markedly inhibits the elongation of the filament structure. Because the ΔNST mutant displayed a short filament phenotype in a way similar to the ΔS mutant, we conclude that FliS is the most important chaperone for efficient FliC export and assembly to form a long filament.

Isolation of Pseudorevertants From the ΔNST Mutant

We found that the ΔS, ΔST, and ΔNST mutants leaked more unassembled FliC monomers into the culture media than the WT cells (**Figure 2**). Furthermore, we also found that about 10 and 15% of the ΔS and ΔNST cells produced no visible filaments (**Supplementary Table 1**). These observations raised the possibility that the short filament phenotype of these mutants may be a consequence of inefficient FliC polymerization rather than inefficient FliC export. To investigate this possibility, we isolated six bypass mutants from the ΔNST mutant (**Figure 4**). Motility of these pseudorevertants, as illustrated by MMC9108-3 [ΔNST *fliC*(Δ245–289)] and MMC9108-5 [ΔNST *fliC*(Q128R)], was better than that of the ΔNST mutant although not at the level of the WT strain (**Figure 4A**). The filaments produced by these bypass mutants were longer than those of the parental ΔNST mutant (**Figure 4B**). Consistently, the fraction of FliC assembled into the filament was larger in the bypass mutants than the ΔNST mutant (**Figures 2I,J**), indicating that the filament elongation process became more efficient by these bypass mutations even in the absence of FliS.

P22-mediated transduction experiments showed that all the bypass mutations were located within the *fliC* gene. Therefore, we sequenced the *fliC* gene of these bypass mutants. They can be divided into two categories (**Figure 4C**). The first category consists of missense mutations: R92S, Q128R, and E153A. The other category consists of two in-frame deletions: residues 195–275 (isolated twice) and residues 245–289. We mapped the point mutations on the atomic model of FliC core fragment consisting of three domains, D1, D2, and D3 (Samatey et al., 2001). It has been reported that the FliC(R92S) and FliC(Q128R) mutations induce a conformational change of domain D1, thereby destabilizing the entire fold of FliC (Furukawa et al., 2016). Because Glu-153 interacts with Asn-150 to stabilize the β-hairpin in domain D1, we assume that the FliC(E153A) substitution may affect this β-hairpin structure, thereby destabilizing domain D1. Domain D3 of FliC largely determines the thermal stability of FliC monomer (Muskotál et al., 2010). Consistently, deletion of either residues 195–233 or residues

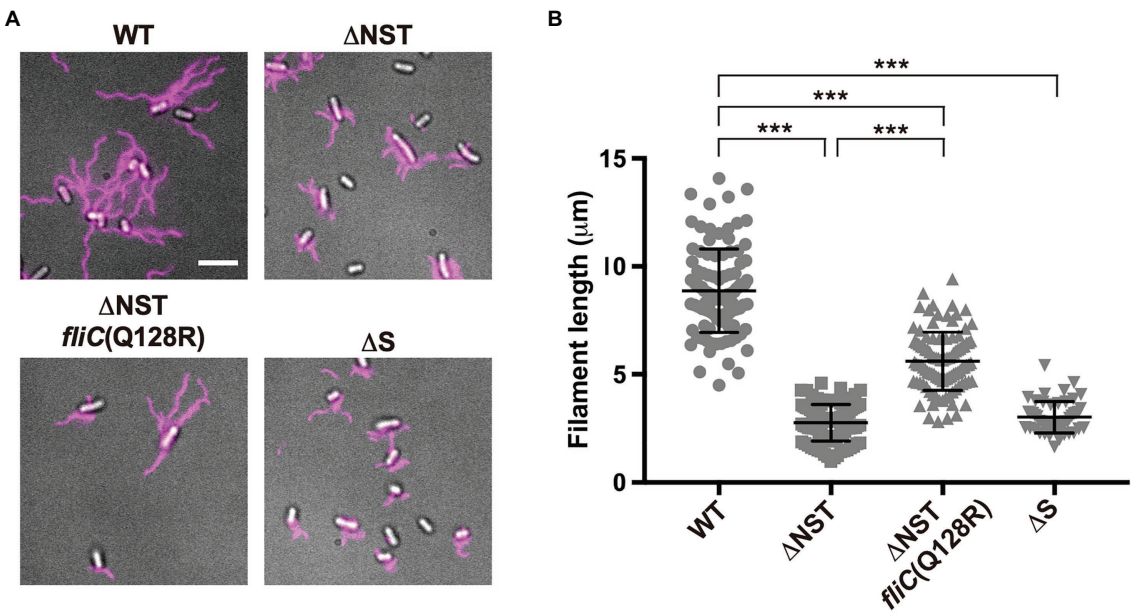

FIGURE 3 | Effect of deletion of FliS on filament length. **(A)** Fluorescent images of the WT, ΔNST, ΔNST *fliC*(Q128R), and ΔS cells. The cells were grown in L-broth until the cells reached the stationary phase, and then, flagellar filaments were labelled with a fluorescent dye, Alexa Fluor 594. The fluorescence images of the filaments labelled with Alexa Fluor 594 (magenta) were merged with the DIC images of the cell bodies. Scale bar, 5.0 μm. **(B)** Scatter plots of flagellar filament length. Filament length is the average of 50 filaments, and vertical lines are standard deviations. Comparisons between datasets were performed using a two-tailed Student's *t*-test. A value of $p < 0.05$ was considered to be statistically significant difference. ***, $p < 0.001$ (also see **Supplementary Table 1**).

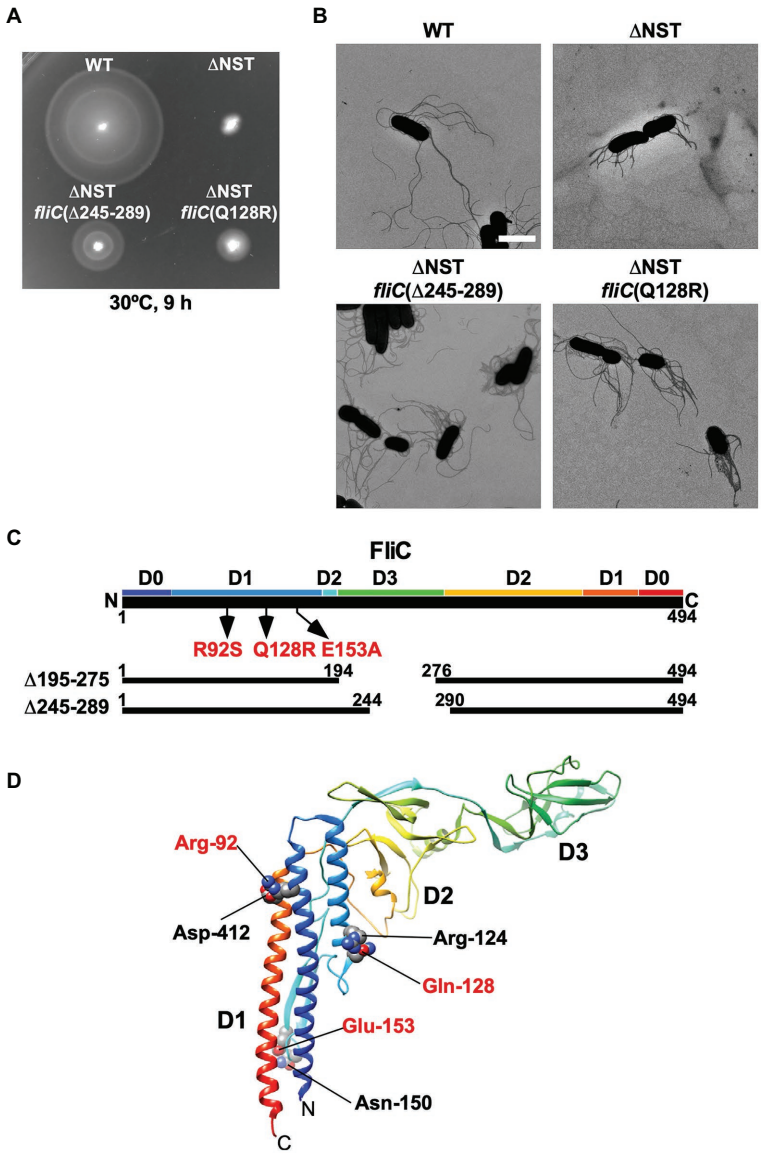

FIGURE 4 | Isolation of pseudorevertants from the ΔNST mutant. **(A)** Motility of WT, ΔNST and its bypass mutants, ΔNST *fliC*(Δ245–289) and ΔNST *fliC*(Q128R). Plates were incubated at 30°C for 9 h. **(B)** Electron micrographs of WT, ΔNST, ΔNST *fliC*(Δ245–289), and ΔNST *fliC*(Q128R) cells. Cells were negatively stained with 0.5% (w/v) phosphotungstic acid (pH 6.5). Micrographs were taken at a magnification of ×1,200. Scale bar, 2 μm. **(C)** Locations of bypass mutations in FliC. FliC consists of four domains, D0, D1, D2, and D3. The point mutations in FliC are indicated by arrows. In-frame deletion variants of FliC lacking residues 195–274 and residues 245–289 are shown by solid lines. **(D)** Location of mutated residues in the atomic structure of the F41 fragment of *Salmonella* FliC (PDB ID: 1IO1). The F41 fragment of FliC, which lacks N-terminal 52 and C-terminal 44 residues, consists of domains D1, D2, and D3. The Cα backbone is color-coded from blue to red, going through the rainbow colors from the N- to the C-terminus. Arg-92, Gln-128, and Glu-153 interact with Asp-412, Arg-124, and Asn-150, respectively, to stabilize domain D1 of FliC.

219–243 in domain D3, which can overcome the loss of FliS chaperone activity, destabilizes the entire structure of FliC monomer (Furukawa et al., 2016). FliS binds to the extreme C-terminal region of FliC (Ozin et al., 2003), indicating that FliC synthesis is complete prior to export. Because an interaction between FliS and $FlhA_C$ is required for efficient FliC export (Bange et al., 2010; Kinoshita et al., 2013), we conclude that the strong FliS-$FlhA_C$ interaction allows the PMF-driven export gate complex to efficiently unfold FliC monomer for its export as suggested before (Furukawa et al., 2016).

Effect of FliS Depletion on the Elongation of Flagellar Filament

To investigate when the PMF-driven export gate complex requires FliS for efficient unfolding process of FliC monomer during filament assembly, we constructed a *Salmonella* ΔS Δ*araBAD*::*fliS* strain (thereafter referred to as ΔS/P_{araBAD}-*fliS*), in which FliS is expressed from an arabinose-inducible P_{araBAD} promoter at the *araBAD* locus on the chromosome. The ΔS/P_{araBAD}-*fliS* cells were exponentially grown at 30°C to express and accumulate FliC subunits in the cytoplasm, and then,

arabinose was added at a final concentration of 0.2% (w/v) to express FliS. We collected cell samples at regular time intervals, labelled their flagellar filaments with a fluorescent dye (**Figure 5A**), and measured the filament length (**Figure 5B** and **Supplementary Table 2**). When FliS was expressed by adding arabinose, the average flagellar filament length gradually increased with the culture time and reached almost the wild-type length. In contrast, when FliS was not expressed, the filament length remained at about 2.5 μm even after a prolonged incubation time. These results suggest that the export gate complex can transport FliC molecules into the cell exterior in a FliS-independent manner in the early stage of filament assembly and that FliS assists efficient unfolding and transport of FliC molecules by the export gate complex to produce long flagellar filaments.

Effect of FliS Depletion on the Secretion of FlgM and FliC in the Early Stage of Filament Assembly

During HBB assembly, FlgM binds to FliA to inhibit its σ^{28} activity (Ohnishi et al., 1992). Upon completion of hook assembly, the fT3SS switches the rod- and hook-type mode to the filament-type mode and starts secreting FlgM into the culture media (**Figure 1**). As a result, FliA becomes σ^{28} to induce the transcription of the *fliC* gene (Hughes et al., 1993; Kutsukake, 1994). FliS also binds to FlgM to suppress FlgM secretion during filament assembly to avoid undesirable over-expression of class 3 genes (Yokoseki et al., 1996; Galeva et al., 2014; Xu et al., 2014). Because FliS is expressed from the class 2 promoter of the *fliDST* operon during HBB assembly (**Figure 1**; Chevance and Hughes, 2008), we hypothesized that FliS may function as a negative regulator to inhibit FlgM secretion upon onset of filament formation and then may become an export chaperone somewhat later to escort FliC to the $FlhA_C$ ring. Because precise measurement of the export rate of flagellar building blocks requires the external onset control of flagellar gene expression, we constructed the ΔS/P_{araBAD}-*fliS* strain containing T-POP, in which FlhD and FlhC are expressed from a tetracycline-inducible promoter only in the presence of tetracycline (Karlinsey et al., 2000b). The ΔS/P_{araBAD}-*fliS* T-POP cells were grown at 30°C in L-broth until OD_{600} reached *ca.* 0.4–0.6. After adding tetracycline with or without arabinose, the cells were collected at regular time intervals and heated at 65°C for 5 min to prepare total extracellular FliC molecules (FliC polymerized into the filaments attached to *Salmonella* cell bodies and FliC monomers secreted into the culture media) as well as extracellular FlgM molecules, followed by immunoblotting with polyclonal anti-FlgM or FliC antibody to measure the amounts of FlgM and FliC (**Figure 6A**). When FliS was expressed by adding arabinose, the level of FlgM secretion was lower than that in the absence of FliS (**Figure 6A**, upper panels and **Figure 6B**, left panel). In contrast, the secretion level of FliC was higher when FliS was expressed (**Figure 6A**, lower panels and **Figure 6B**, right panel). Consistently, the filament growth, which started at around 60 min after tetracycline induction, showed a steady elongation rate to form long filaments in the presence of FliS but was much slower and retarded at markedly shorter lengths in the absence of FliS (**Figures 6C,D** and **Supplementary Table 3**). These results suggest that the PMF-driven export gate complex requires FliS to facilitate

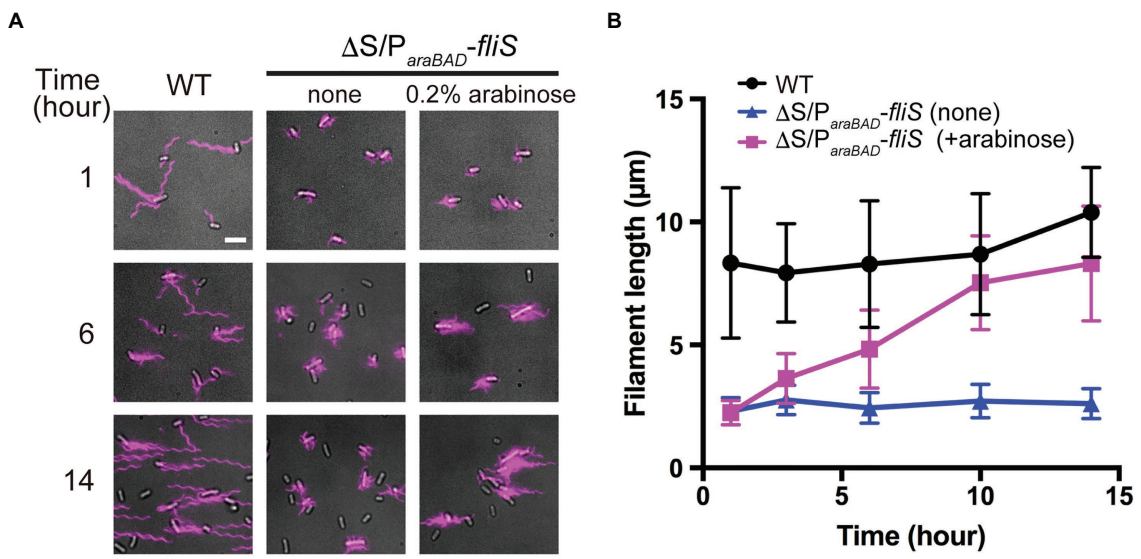

FIGURE 5 | Effect of FliS expression on filament growth. **(A)** Fluorescent images of Δ*fliS* Δ*araBAD*::*fliS* (ΔS/P*araBAD-fliS*) cells. The ΔS/P*araBAD-fliS* cells were exponentially grown at 30°C to express and accumulate FliC subunits in the cytoplasm, and then, arabinose was added at a final concentration of 0.2%(w/v) to induce the expression of FliS from the *araBAD* promoter on the chromosome. Cells were collected at the indicated time intervals, followed by labelling their flagellar filaments with a fluorescent dye. Wild-type cell (WT) was used as the positive control. Scale bar, 5.0 μm. **(B)** Average length of flagellar filaments. Filament length is the average of 50 filaments, and vertical lines are standard deviations (also see **Supplementary Table 2**).

unfolding and transport of FliC for rapid growth of the filament to form long ones for high level motility.

DISCUSSION

Flagellar filament assembly begins with the assembly of the hook-filament junction at the hook tip, followed by the filament cap and finally the filament with the help of the filament cap (**Figure 1**). The flagellar export chaperones facilitate the docking of their cognate filament-type substrates to the $FlhA_C$ ring, thereby allowing the fT3SS to efficiently transport the substrates into the central channel of the growing flagellar structure (Bange et al., 2010; Minamino et al., 2012a; Kinoshita et al., 2013; Furukawa et al., 2016). FlgN and FliT require the cytoplasmic ATPase complex consisting of FliH, FliI, and FliJ to efficiently bind to the $FlhA_C$ ring, whereas FliS does not (Thomas et al., 2004; Evans et al., 2006; Bange et al., 2010; Sajó et al., 2014; Minamino et al., 2016; Inoue et al., 2018). These observations lead to a plausible hypothesis that such differences in the binding affinity of flagellar chaperones for the cytoplasmic ATPase complex contribute to the ordered export of their cognate substrates for efficient formation and growth of the flagellar filament after hook assembly. Because FliS does not bind to the cytoplasmic ATPase complex (Sajó et al., 2014), it raises an interesting question of how FliC subunit is unfolded?

To clarify how the flagellar export chaperones facilitate the docking of their cognate substrates to $FlhA_C$, which is followed by subsequent unfolding and transport of the export substrates by the fT3SS, we constructed the ΔNS, ΔNT, and ΔNST mutants and found that deletion of either FliS, FliT, or both

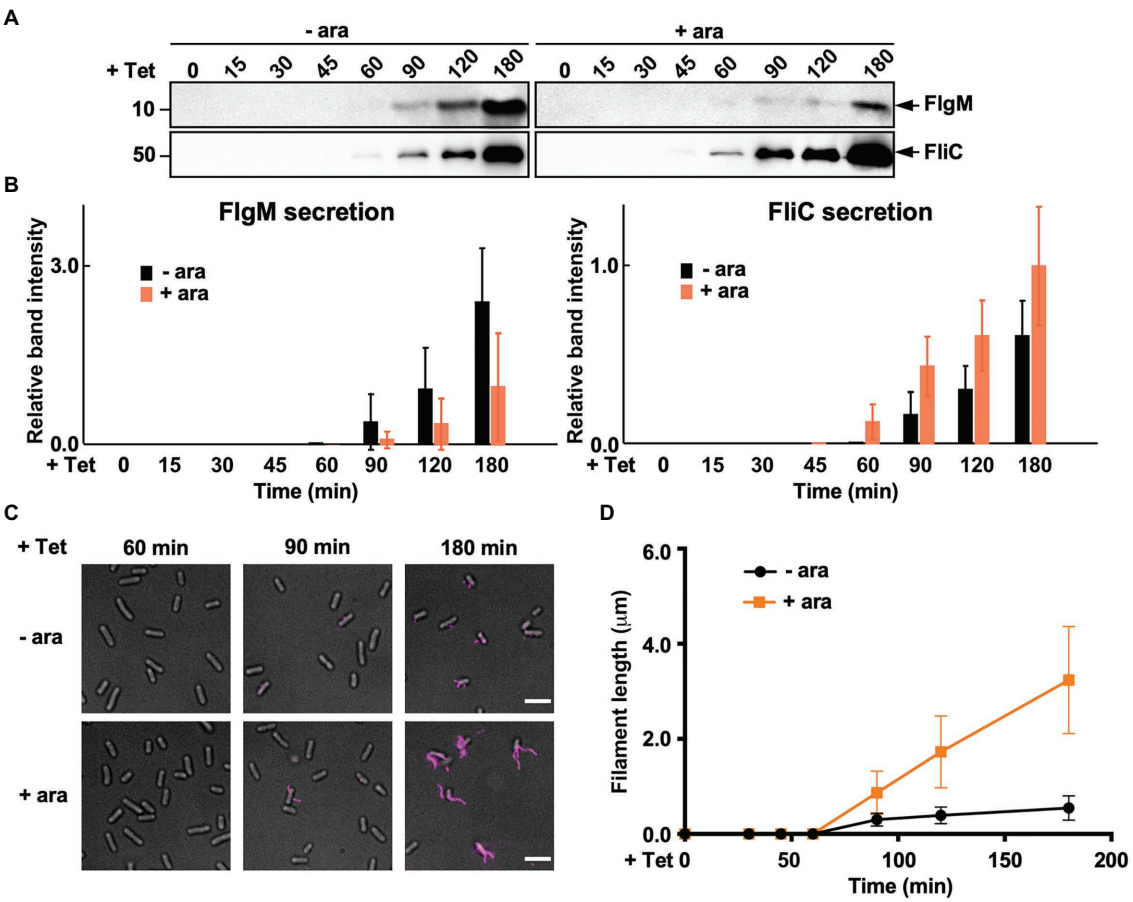

FIGURE 6 | Measurements of the secretion rates of FlgM and FliC using ΔS/P*araBAD-fliS* cells containing a T-pop insertion. **(A)** Immunoblotting, using polyclonal anti-FlgM (upper panel) or anti-FliC (lower panel) antibody, of heat-treated cultures of ΔS/P*araBAD-fliS* T-pop cells. The ΔS/P*araBAD-fliS* T-pop cells were grown at 30°C in L-broth until the cell density reached an OD_{600} of 0.5. After adding tetracycline with (+ara) or without (–ara) arabinose, cell cultures were collected at 0, 15, 30, 45, 60, 90, 120, and 180 min and heated at 65°C for 5 min to depolymerize flagellar filaments into FliC monomers. Molecular mass markers are indicated on the left. **(B)** Relative extracellular levels of FlgM (left panel) and FliC (right panel). The density of each FlgM or FliC band on immunoblots was normalized for the level of FlgM and FliC in $FliS^+$ cells at 180 min. These data were the average of four independent experiments. Vertical bars indicate standard deviations. **(C)** Fluorescent images of the ΔS/P*araBAD-fliS* T-pop cells. The cells were exponentially grown in L-broth. After adding tetracycline with or without arabinose, the cells were collected at the indicated time intervals, followed by labelling their flagellar filaments with a fluorescent dye. **(D)** Average length of flagellar filaments. Filament length was the average of 50 filaments. Vertical lines indicate standard deviations (also see **Supplementary Table 3**).

increased the expression levels of FlgK and FlgL, thereby significantly increasing the probability of assembling the hook-filament junction at the hook tip even in the absence of FlgN (**Figure 2**). The ΔNS, ΔNT, and ΔNST mutants still leaked a large amount of unassembled FliC monomers into the culture media (**Figures 2D,E,I**). Furthermore, the ΔS and ΔT mutants also leaked more FliC monomers into the culture media than the WT (**Figures 2F,G**). These results indicate that FlgN, FliT, and FliS all prevent unassembled FliC monomers from leaking out into the culture media during filament assembly. Therefore, we conclude that the binding of these flagellar chaperones to $FlhA_C$ is required for efficient and robust filament formation at the hook tip.

The transmembrane export gate complex utilizes PMF across the cytoplasmic membrane to facilitate protein unfolding and injection into the central channel of the growing structure with a diameter of about 1.3 nm (Minamino and Namba, 2008; Paul et al., 2008; Fujii et al., 2017). This has been verified by *in vitro* reconstitution experiments using inverted membrane vesicles (Terashima et al., 2018, 2020). To investigate why the ΔNST mutant produces short flagellar filaments (**Figure 3**), we isolated pseudorevertants from the ΔNST mutant and found that all suppressor mutations are located in the *fliC* gene (**Figure 4**). FliS binds not only to the extreme C-terminal region of FliC but also to domain D1 of FliC (Altegoer et al., 2018). It has been shown that the R92S and Q128R substitutions in domain D1 of FliC and deletion of domain D3 destabilize the folded structure of FliC monomer (Furukawa et al., 2016). We also confirmed that FliS is required for efficient FliC export for elongation of the filament beyond a certain length around 2.5 μm (**Figure 5**). Because FliS itself does not have the unfoldase activity (Furukawa et al., 2016), we suggest that FliS must be assisting the unfolding process of FliC by the PMF-driven export gate complex and, in the absence of FliS, the rate of FliC export is significantly limited by a lower rate of FliC unfolding by the export gate complex alone. Because the export of flagellar building blocks is not obligatorily coupled to protein translation (Hirano et al., 2003; Terashima et al., 2018, 2020), we suggest that an interaction between FliS and $FlhA_C$ becomes essential for efficient unfolding and transport of FliC by the export gate complex to form long filaments after FliC synthesis is complete (**Figure 7**).

Why can *Salmonella* cells lacking FliS produce short filaments? FliS binds to FlgM to prevent its secretion *via* the fT3SS into

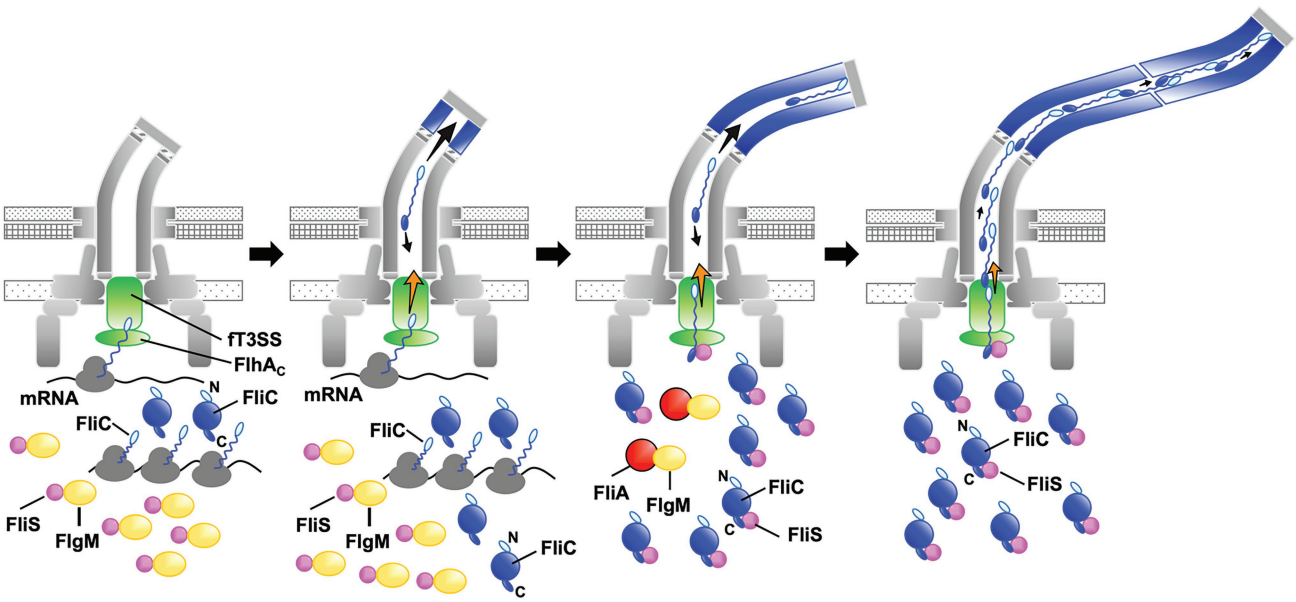

FIGURE 7 | Model for processive filament assembly at the hook tip. Flagellar filament assembly is composed of two distinct, FliS-independent and FliS-dependent processes. Upon completion of the hook structure, FlgM is secreted *via* the flagellar type III secretion system (fT3SS) into the culture media, thereby allowing FliA to act as a flagellum-specific sigma factor to drive the transcription of the *fliC* gene. As a result, a large amount of FliC is accumulated in the cytoplasm. FliC monomers are then unfolded and injected into the central channel of the flagellum by fT3SS one after another and transported to the distal end by diffusion to start forming the filament. Upon onset of this filament assembly, FliS binds to FlgM to inhibit FlgM secretion, and so FliC secretion and flagellar filament formation occur in a FliS-independent manner (left and left middle panels, steps 1 and 2). Then, FliS transfers FlgM to FliA to avoid the over-expression of FliC during filament assembly and becomes an export chaperone to assist FliC unfolding and export by fT3SS. FliS binds to the extreme C-terminal region of FliC with high affinity and facilitates FliC docking to the $FlhA_C$ ring. FliS also supports the fT3SS to efficiently unfold and inject FliC subunits into the central channel of the flagellum, which is followed by their diffusion down to the distal end of the growing structure where they assemble to form the filament (middle right, step 3). At the beginning of filament assembly, the distance from the fT3SS export gate to the assembly point is short, and the time for unfolded FliC monomers to reach the distal end is relatively short. The central channel may not be so crowded by FliC monomers, and therefore, the fT3SS export gate may not require such strong force to unfold and inject FliC into the central channel as it requires later when the filament becomes longer. FliS-assisted FliC unfolding would not be necessary in this stage when the filament is short (middle right, step 3). As the filament elongates, however, the diffusion time progressively increases, making the central channel very crowded (right, step 4). The fT3SS export gate now requires much stronger force for FliC unfolding and injection to continue filament growth, and FliS-assisted unfolding of FliC becomes essential in this later stage of filament assembly. That is why FliS deletion stops filament growth at relatively short lengths.

the culture media during filament assembly. As a result, FlgM becomes the anti-sigma factor again to suppress the σ^{28} activity of FliA to control the number of flagella per cell (Yokoseki et al., 1996; Galeva et al., 2014; Xu et al., 2014). In this study, we analyzed the secretion rates of FlgM and FliC in the early stage of filament assembly and found that FliS suppressed FlgM secretion and facilitated FliC secretion, thereby allowing cells expressing FliS to produce long flagellar filaments (**Figure 6**). The filament length of cells lacking FliS remained about 2.5 μm even after a prolonged incubation time (**Figure 5**). Thus, it seems likely that the fT3SS can transport FliC molecules in a FliS-independent manner for a short period after onset of filament formation, and that is why the cells lacking FliS can produce short flagellar filaments. Because it has been reported that the untranslated region of mRNA around the start codon of the *fliC* gene is involved in the targeting of FliC molecules to the fT3SS (Singer et al., 2014), we propose that FliS-independent FliC export may occur in a co-translational manner when FliS is busy inhibiting FlgM secretion (**Figure 7**).

Why does the filament growth stop in the absence of FliS although a large amount of FliC is expressed in the cytoplasm? The filament elongation rate is determined as the sum of the PMF-driven injection rate of FliC monomer by the fT3SS at the flagellar base and the diffusion rate of FliC subunit inside the long and narrow channel along the length of the flagellum (Chen et al., 2017; Renault et al., 2017). In the early stage of filament assembly, the distance from the export gate to the assembly point is short, and so the diffusion time is short. As a result, the PMF-driven unfolding and injection steps of FliC by the fT3SS are the rate-limiting in the filament growth, and each FliC subunit reaches its assembly point without encountering any other subunits (**Figure 7**). As the filament elongates, the diffusion time progressively increases, and it eventually becomes comparable to or longer than the unfolding and injection time. At this stage, the central channel of the growing filament would be crowded with FliC subunits, thereby decreasing the diffusion rate (**Figure 7**). The export gate would then need a stronger force to unfold and inject FliC monomers or some assistance in the unfolding process to keep the effective injection rate for continued filament growth. Because FliC mutations that destabilized the folded structure of FliC monomer allowed the cells lacking FliS to produce long filaments (**Figure 4**), we propose that the PMF-driven export gate complex requires the interaction of FliS with $FlhA_C$ to facilitate efficient and rapid unfolding and injection of FliC at the flagellar base so that the newly injected FliC subunit can push many unfolded FliC subunits crowded in the long central channel to the distal growing end for continued elongation of the long filament (**Figure 7**). This indicates that the efficient growth of the long flagellar filament is achieved by a delicate balance between the PMF-driven FliC unfolding and injection force at the export gate and the diffusion rate of unfolded FliC monomers crowded in the narrow and long central channel of the filament.

The assembly of FliC subunits into the filament occurs by a template-structure-driven mechanism. Both intrinsically disordered N- and C-terminal segments of FliC form domain D0 in the innermost core of the filament when FliC monomers polymerize into the filament structure with the help of the FliD cap. Intermolecular interactions between the D0 domains of FliC subunits and those between domain D0 of FliC and domain D0 of FliD are required for filament assembly (Yonekura et al., 2003; Al-Otaibi et al., 2020). Even though FlgN and FliT are present, the ΔS mutant leaked more FliC monomers out into the culture media than the WT cells (**Figure 2F**). This raises the possibility that FliS may affect the local conformation of the N- and/or C-terminal segments of FliC, which in turn affects the proper folding of other domains to make it easier for the PMF-driven export gate complex to unfold the entire FliC molecule for its efficient export for filament assembly.

DATA AVAILABILITY STATEMENT

The original contributions presented in the study are included in the article/**Supplementary Material**, further inquiries can be directed to the corresponding author.

AUTHOR CONTRIBUTIONS

TM and KN conceived and designed the research and wrote the paper based on discussion with YM and MK. TM, MK, and YM performed the experiments and analyzed the data. All authors contributed to the article and approved the submitted version.

FUNDING

This work was supported in part by JSPS KAKENHI Grant Numbers JP26293097 and JP19H03182 (to TM), JP18K14638 and JP20K15749 (to MK), JP18K06159 and JP21K06099 (to YM) and JP25000013 (to KN), and MEXT KAKENHI Grant Numbers JP15H01640 and JP20H05532 (to TM), and JST PRESTO Grant Number JPMJPR204B (to YM). This work has also been partially supported by JEOL YOKOGUSHI Research Alliance Laboratories of Osaka University to KN.

ACKNOWLEDGMENTS

We acknowledge Kelly T. Hughes for his kind gift of *Salmonella* P_{flhDC}::T-POP (DEL-25), Δ*flgN*::*tetRA*, Δ*fliS*::*km*, Δ*fliT*::*km*, Δ*fliST*::*km* and Δ*araBAD*::*fliS* alleles, Kouhei Ohnishi for his kind gift of polyclonal anti-FlgM antibody and Tomoko Miyata, Yumi Inoue, and Yasuyo Abe for technical assistance.

SUPPLEMENTARY MATERIAL

The Supplementary Material for this article can be found online at: https://www.frontiersin.org/articles/10.3389/fmicb.2021.756044/full#supplementary-material

REFERENCES

Abrusci, P., Vergara-Irigaray, M., Johnson, S., Beeby, M. D., Hendrixson, D. R., Roversi, P., et al. (2013). Architecture of the major component of the type III secretion system export apparatus. *Nat. Struct. Mol. Biol.* 20, 99–104. doi: 10.1038/nsmb.2452

Aldridge, P., Karlinsey, J. E., and Hughes, K. T. (2003). The type III secretion chaperone FlgN regulates flagellar assembly via a negative feedback loop containing its chaperone substrates FlgK and FlgL. *Mol. Microbiol.* 49, 1333–1345. doi: 10.1046/j.1365-2958.2003.03637.x

Aldridge, P. D., Karlinsey, J. E., Aldridge, C., Birchall, C., Thompson, D., Yagasaki, J., et al. (2006). The flagellar-specific transcription factor, sigma28, is the Type III secretion chaperone for the flagellar-specific anti-sigma28 factor FlgM. *Genes Dev.* 20, 2315–2326. doi: 10.1101/gad.380406

Aldridge, C., Poonchareon, K., Saini, S., Ewen, T., Soloyva, A., Rao, C. V., et al. (2010). The interaction dynamics of a negative feedback loop regulates flagellar number in *Salmonella enterica* serovar Typhimurium. *Mol. Microbiol.* 78, 1416–1430. doi: 10.1111/j.1365-2958.2010.07415.x

Al-Otaibi, N. S., Taylor, A. J., Farrell, D. P., Tzokov, S. B., DiMaio, F., Kelly, D. J., et al. (2020). The cryo-EM structure of the bacterial flagellum cap complex suggests a molecular mechanism for filament elongation. *Nat. Commun.* 11:3210. doi: 10.1038/s41467-020-16981-4

Altegoer, F., Mukherjee, S., Steinchen, W., Bedrunka, P., Linne, U., Kearns, D. B., et al. (2018). FliS/flagellin/FliW heterotrimer couples type III secretion and flagellin homeostasis. *Sci. Rep.* 8:11552. doi: 10.1038/s41598-018-29884-8

Auvray, F., Thomas, J., Fraser, G. M., and Hughes, C. (2001). Flagellin polymerisation control by a cytosolic export chaperone. *J. Mol. Biol.* 308, 221–229. doi: 10.1006/jmbi.2001.4597

Bange, G., Kümmerer, N., Engel, C., Bozkurt, G., Wild, K., and Sinning, I. (2010). FlhA provides the adaptor for coordinated delivery of late flagella building blocks to the type III secretion system. *Proc. Natl. Acad. Sci. U. S. A.* 107, 11295–11300. doi: 10.1073/pnas.1001383107

Bennett, J. C., Thomas, J., Fraser, G. M., and Hughes, C. (2001). Substrate complexes and domain organization of the *Salmonella* flagellar export chaperones FlgN and FliT. *Mol. Microbiol.* 39, 781–791. doi: 10.1046/j.1365-2958.2001.02268.x

Chen, M., Zhao, Z., Yang, J., Peng, K., Baker, M. A., Bai, F., et al. (2017). Length-dependent flagellar growth of *Vibrio alginolyticus* revealed by real time fluorescent imaging. *elife* 6:e22140. doi: 10.7554/eLife.22140

Chevance, F. F., and Hughes, K. T. (2008). Coordinating assembly of a bacterial macromolecular machine. *Nat. Rev. Microbiol.* 6, 455–465. doi: 10.1038/nrmicro1887

Evans, L. D. B., Stafford, G. P., Ahmed, S., Fraser, G. M., and Hughes, C. (2006). An escort mechanism for cycling of export chaperones during flagellum assembly. *Proc. Natl. Acad. Sci. U. S. A.* 103, 17474–17479. doi: 10.1073/pnas.0605197103

Evdokimov, A. G., Phan, J., Tropea, J. E., Routzahn, K. M., Peters, H. K., Pokross, M., et al. (2003). Similar modes of polypeptide recognition by export chaperones in flagellar biosynthesis and type III secretion. *Nat. Struct. Biol.* 10, 789–793. doi: 10.1038/nsb982

Fraser, G. M., Bennett, J. C. Q., and Hughes, C. (1999). Substrate-specific binding of hook-associated proteins by FlgN and FliT, putative chaperones for flagellum assembly. *Mol. Microbiol.* 32, 569–580. doi: 10.1046/j.1365-2958.1999.01372.x

Fujii, T., Kato, T., Hiraoka, K. D., Miyata, T., Minamino, T., Chevance, F., et al. (2017). Identical folds used for distinct mechanical functions of the bacterial flagellar rod and hook. *Nat. Commun.* 8:14276. doi: 10.1038/ncomms14276

Furukawa, Y., Inoue, Y., Sakaguchi, A., Mori, Y., Fukumura, T., Miyata, T., et al. (2016). Structural stability of flagellin subunit affects the rate of flagellin export in the absence of FliS chaperone. *Mol. Microbiol.* 102, 405–416. doi: 10.1111/mmi.13469

Galeva, A., Moroz, N., Yoon, Y. H., Hughes, K. T., Samatey, F. A., and Kostyukova, A. S. (2014). Bacterial flagellin-specific chaperone FliS interacts with anti-sigma factor FlgM. *J. Bacteriol.* 196, 1215–1221. doi: 10.1128/JB.01278-13

Hirano, T., Minamino, T., Namba, K., and Macnab, R. M. (2003). Substrate specificity classes and the recognition signal for *Salmonella* type III flagellar export. *J. Bacteriol.* 185, 2485–2492. doi: 10.1128/JB.185.8.2485-2492.2003

Homma, M., Fujita, H., Yamaguchi, S., and Iino, T. (1984). Excretion of unassembled flagellin by *Salmonella typhimurium* mutants deficient in hook-associated proteins. *J. Bacteriol.* 159, 1056–1059. doi: 10.1128/jb.159.3.1056-1059.1984

Hughes, K. T., Gillen, K. L., Semon, M. J., and Karlinsey, J. E. (1993). Sensing structural intermediates in bacterial flagellar assembly by export of a negative regulator. *Science* 262, 1277–1280. doi: 10.1126/science.8235660

Imada, K., Minamino, T., Kinoshita, M., Furukawa, Y., and Namba, K. (2010). Structural insight into the regulatory mechanisms of interactions of the flagellar type III chaperone FliT with its binding partners. *Proc. Natl. Acad. Sci. U. S. A.* 107, 8812–8817. doi: 10.1073/pnas.1001866107

Inoue, Y., Kinoshita, M., Kida, M., Takekawa, N., Namba, K., Imada, K., et al. (2021). The FlhA linker mediates flagellar protein export switching during flagellar assembly. *Commun. Biol.* 4:646. doi: 10.1038/s42003-021-02177-z

Inoue, Y., Morimoto, Y. V., Namba, K., and Minamino, T. (2018). Novel insights into the mechanism of well-ordered assembly of bacterial flagellar proteins in *Salmonella*. *Sci. Rep.* 8:1787. doi: 10.1038/s41598-018-20209-3

Inoue, Y., Ogawa, Y., Kinoshita, M., Terahara, N., Shimada, M., Kodera, N., et al. (2019). Structural insight into the substrate specificity switching mechanism of the type III protein export apparatus. *Structure* 27, 965–976. doi: 10.1016/j.str.2019.03.017

Karlinsey, J. E., Lonner, J., Brown, K. L., and Hughes, K. T. (2000a). Translation/secretion coupling by type III secretion systems. *Cell* 102, 487–497. doi: 10.1016/s0092-8674(00)00053-2

Karlinsey, J. E., Tanaka, S., Bettenworth, V., Yamaguchi, S., Boos, W., Aizawa, S. I., et al. (2000b). Completion of the hook-basal body complex of the *Salmonella typhimurium* flagellum is coupled to FlgM secretion and *fliC* transcription. *Mol. Microbiol.* 37, 1220–1231. doi: 10.1046/j.1365-2958.2000.02081.x

Khanra, N., Rossi, P., Economou, A., and Kalodimos, C. G. (2016). Recognition and targeting mechanisms by chaperones in flagellum assembly and operation. *Proc. Natl. Acad. Sci. U. S. A.* 113, 9798–9803. doi: 10.1073/pnas.1607845113

Kinoshita, M., Hara, N., Imada, K., Namba, K., and Minamino, T. (2013). Interactions of bacterial chaperone-substrate complexes with FlhA contribute to coordinating assembly of the flagellar filament. *Mol. Microbiol.* 90, 1249–1261. doi: 10.1111/mmi.12430

Kinoshita, M., Nakanishi, Y., Furukawa, Y., Namba, K., Imada, K., and Minamino, T. (2016). Rearrangements of α-helical structures of FlgN chaperone control the binding affinity for its cognate substrates during flagellar type III export. *Mol. Microbiol.* 101, 656–670. doi: 10.1111/mmi.13415

Kutsukake, K. (1994). Excretion of the anti-sigma factor through a flagellar substructure couples flagellar gene expression with flagellar assembly in *Salmonella typhimurium*. *Mol. Gen. Genet.* 243, 605–612. doi: 10.1007/BF00279569

Kutsukake, K., Minamino, T., and Yokoseki, T. (1994a). Isolation and characterization of FliK-independent flagellation mutants from *Salmonella typhimurium*. *J. Bacteriol.* 176, 7625–7629. doi: 10.1128/jb.176.24.7625-7629.1994

Kutsukake, K., Ohya, Y., and Iino, T. (1990). Transcriptional analysis of the flagellar regulon of *Salmonella typhimurium*. *J. Bacteriol.* 172, 741–747. doi: 10.1128/jb.172.2.741-747.1990

Kutsukake, K., Okada, T., Yokoseki, T., and Iino, T. (1994b). Sequence analysis of the *flgA* gene and its adjacent region in *Salmonella typhimurium*, and identification of another flagellar gene, *flgN*. *Gene* 143, 49–54. doi: 10.1016/0378-1119(94)90603-3

Minamino, T. (2014). Protein export through the bacterial flagellar type III export pathway. *Biochim. Biophys. Acta* 1843, 1642–1648. doi: 10.1016/j.bbamcr.2013.09.005

Minamino, T. (2018). Hierarchical protein export mechanism of the bacterial flagellar type III protein export apparatus. *FEMS Microbiol. Lett.* 365:fny117. doi: 10.1093/femsle/fny117

Minamino, T., Doi, H., and Kutsukake, K. (1999). Substrate specificity switching of the flagellum-specific export apparatus during flagellar morphogenesis in *Salmonella typhimurium*. *Biosci. Biotechnol. Biochem.* 63, 1301–1303. doi: 10.1271/bbb.63.1301

Minamino, T., Inoue, Y., Kinoshita, M., and Namba, K. (2020a). FliK-driven conformational rearrangements of FlhA and FlhB are required for export

switching of the flagellar protein export apparatus. *J. Bacteriol.* 202, e00637–e00619. doi: 10.1128/JB.00637-19

Minamino, T., Kinoshita, M., Inoue, Y., Morimoto, Y. V, Ihara, K., Koya, S., et al. (2016). FliH and FliI ensure efficient energy coupling of flagellar type III protein export in *Salmonella*. *Microbiology Open.* 5, 424–435. doi: 10.1002/mbo3.340

Minamino, T., Kawamoto, A., Kinoshita, M., and Namba, K. (2020b). Molecular organization and assembly of the export apparatus of flagellar type III secretion systems. *Curr. Top. Microbiol. Immunol.* 427, 91–107. doi: 10.1007/82_2019_170

Minamino, T., Kinoshita, M., Hara, N., Takeuchi, S., Hida, A., Koya, S., et al. (2012a). Interaction of a bacterial flagellar chaperone FlgN with FlhA is required for efficient export of its cognate substrates. *Mol. Microbiol.* 83, 1775–1788. doi: 10.1111/j.1365-2958.2011.07964.x

Minamino, T., Kinoshira, M., Imada, K., and Namba, K. (2012b). Interaction between FliI ATPase and a flagellar chaperone FliT during bacterial flagellar export. *Mol. Microbiol.* 83, 168–178. doi: 10.1111/j.1365-2958.2011.07924.x

Minamino, T., Kinoshira, M., Morimoto, Y. V., and Namba, K. (2021). The FlgN chaperone activates the Na^+-driven engine of the *Salmonella* flagellar protein export apparatus. *Commun. Biol.* 4:335. doi: 10.1038/s42003-021-01865-0

Minamino, T., and Macnab, R. M. (1999). Components of the *Salmonella* flagellar export apparatus and classification of export substrates. *J. Bacteriol.* 181, 1388–1394. doi: 10.1128/JB.181.5.1388-1394.1999

Minamino, T., Morimoto, Y. V., Kinoshita, M., Aldridge, P. D., and Namba, K. (2014). The bacterial flagellar protein export apparatus processively transports flagellar proteins even with extremely infrequent ATP hydrolysis. *Sci. Rep.* 4:7579. doi: 10.1038/srep07579

Minamino, T., and Namba, K. (2004). Self-assembly and type III protein export of the bacterial flagellum. *J. Mol. Microbiol. Biotechnol.* 7, 5–17. doi: 10.1159/000077865

Minamino, T., and Namba, K. (2008). Distinct roles of the FliI ATPase and proton motive force in bacterial flagellar protein export. *Nature* 451, 485–488. doi: 10.1038/nature06449

Muskotál, A., Seregélyes, C., Sebestyén, A., and Vonderviszt, F. (2010). Structural basis for stabilization of the hypervariable D3 domain of *Salmonella flagellin* upon filament formation. *J. Mol. Biol.* 403, 607–615. doi: 10.1016/j.jmb.2010.09.024

Nakamura, S., and Minamino, T. (2019). Flagella-driven motility of bacteria. *Biomol. Ther.* 9:279. doi: 10.3390/biom9070279

Ohnishi, K., Kutsukake, K., Suzuki, H., and Iino, T. (1990). Gene *fliA* encodes an alternative sigma factor for flagellar operons in *Salmonella typhimurium*. *Mol. Gen. Genet.* 6, 139–147. doi: 10.1007/BF00261713

Ohnishi, K., Kutsukake, K., Suzuki, H., and Iino, T. (1992). A novel transcriptional regulation in the flagellar regulon of *Salmonella typhimurium*: an anti-sigma factor inhibits the activity of the flagellum-specific sigma factor, sigma F. *Mol. Microbiol.* 6, 3149–3157. doi: 10.1111/j.1365-2958.1992.tb01771.x

Ozin, A.J., Claret, L., and Auvray, F., and, Hughes, C. (2003). The FliS chaperone selectively binds the disordered flagellin C-terminal D0 domain central to polymerisation. *FEMS Microbiol. Lett.* 219, 219–224. doi: 10.1016/S0378-1097(02)01208-9

Paul, K., Erhardt, M., Hirano, T., Blair, D. F., and Hughes, K. T. (2008). Energy source of flagellar type III secretion. *Nature* 451, 489–492. doi: 10.1038/nature06497

Renault, T. T., Abraham, A. O., Bergmiller, T., Paradis, G., Rainville, S., Charpentier, E., et al. (2017). Bacterial flagella grow through an injection-diffusion mechanism. *elife* 6:e23136. doi: 10.7554/eLife.23136

Sajó, R., Liliom, K., Muskotál, A., Klein, A., Závodszky, P., Vonderviszt, F., et al. (2014). Soluble components of the flagellar export apparatus, FliI, FliJ, and FliH, do not deliver flagellin, the major filament protein, from the cytosol to the export gate. *Biochim. Biophys. Acta* 1843, 2414–2423. doi: 10.1016/j.bbamcr.2014.07.004

Samatey, F. A., Imada, K., Nagashima, S., Vonderviszt, F., Kumasaka, T., Yamamoto, M., et al. (2001). Structure of the bacterial flagellar protofilament and implications for a switch for supercoiling. *Nature* 410, 331–337. doi: 10.1038/35066504

Schmiger, H. (1972). Phage P22 mutants with increased or decreased transduction abilities. *Mol. Gen. Genet.* 119, 75–88. doi: 10.1007/BF00270447

Singer, H. M., Erhardt, M., and Hughes, K. T. (2014). Comparative analysis of the secretion capability of early and late flagellar type III secretion substrates. *Mol. Microbiol.* 93, 505–520. doi: 10.1111/mmi.12675

Terahara, N., Inoue, Y., Kodera, N., Morimoto, Y. V., Uchihashi, T., Imada, K., et al. (2018). Insight to structural remodeling of the FlhA ring responsible for bacterial flagellar type III protein export. *Sci. Adv.* 4:eaao7054. doi: 10.1126/sciadv.aao7054

Terashima, H., Kawamoto, A., Tastumi, C., Namba, K., Minamino, T., and Imada, K. (2018). In vitro reconstitution of functional type III protein export and insights into flagellar assembly. *MBio* 9, e00988–e00981. doi: 10.1128/mBio.00988-18

Terashima, H., Tastumi, C., Kawamoto, A., Namba, K., Minamino, T., and Imada, K. (2020). In vitro autonomous construction of the flagellar axial structure in the inverted membrane vesicles. *Biomol. Ther.* 10:126. doi: 10.3390/biom10010126

Thomas, J., Stafford, G. P., and Hughes, C. (2004). Docking of cytosolic chaperone-substrate complexes at the membrane ATPase during flagellar type III protein export. *Proc. Natl. Acad. Sci. U. S. A.* 101, 3945–3950. doi: 10.1073/pnas.0307223101

Xing, Q., Shi, K., Portaliou, A., Rossi, P., Economou, A., and Kalodimos, C. G. (2018). Structure of chaperone-substrate complexes docked onto the export gate in a type III secretion system. *Nat. Commun.* 9:1773. doi: 10.1038/s41467-018-04137-4

Xu, S., Peng, Z., Cui, B., Wang, T., Song, Y., Zhang, L., et al. (2014). FliS modulates FlgM activity by acting as a non-canonical chaperone to control late flagellar gene expression, motility and biofilm formation in *Yersinia pseudotuberculosis*. *Environ. Microbiol.* 16, 1090–1104. doi: 10.1111/1462-2920.12222

Yamaguchi, S., Fujita, H., Sugata, K., Taira, T., and Iino, T. (1984). Genetic analysis of H2, the structural gene for phase-2 flagellin in *Salmonella*. *J. Gen. Microbiol.* 130, 255–265. doi: 10.1099/00221287-130-2-255

Yokoseki, T., Iino, T., and Kutsukake, K. (1996). Negative regulation by *fliD*, *fliS*, and *fliT* of the export of the flagellum-specific anti-sigma factor, FlgM, in *Salmonella typhimurium*. *J. Bacteriol.* 178, 899–901. doi: 10.1128/jb.178.3.899-901.1996

Yokoseki, T., Kutsukake, K., Ohnishi, K., and Iino, T. (1995). Functional analysis of the flagellar genes in the *fliD* operon of *Salmonella typhimurium*. *Microbiology* 141, 1715–1722. doi: 10.1099/13500872-141-7-1715

Yonekura, K., Maki-Yonekura, S., and Namba, K. (2003). Complete atomic model of the bacterial flagellar filament by electron cryomicroscopy. *Nature* 424, 643–650. doi: 10.1038/nature01830

Conflict of Interest: The authors declare that the research was conducted in the absence of any commercial or financial relationships that could be construed as a potential conflict of interest.

Publisher's Note: All claims expressed in this article are solely those of the authors and do not necessarily represent those of their affiliated organizations, or those of the publisher, the editors and the reviewers. Any product that may be evaluated in this article, or claim that may be made by its manufacturer, is not guaranteed or endorsed by the publisher.

frontiers in Microbiology

ORIGINAL RESEARCH
published: 14 October 2021
doi: 10.3389/fmicb.2021.752733

The Contribution of the Predicted Sorting Platform Component HrcQ to Type III Secretion in *Xanthomonas campestris* pv. *vesicatoria* Depends on an Internal Translation Start Site

*Christian Otten, Tanja Seifert, Jens Hausner† and Daniela Büttner**

Department of Genetics, Institute for Biology, Martin Luther University Halle-Wittenberg, Halle, Germany,

OPEN ACCESS

Edited by:
Eric Cascales,
Aix-Marseille Université, France

Reviewed by:
Chuck Shaker Farah,
University of São Paulo, Brazil
Anirban Chakraborty,
University of Texas Medical Branch at Galveston, United States

***Correspondence:**
Daniela Büttner
daniela.buettner@genetik.uni-halle.de

†Present address:
Jens Hausner,
Icon Genetics GmbH, Halle, Germany

Specialty section:
This article was submitted to Microbial Physiology and Metabolism, a section of the journal Frontiers in Microbiology

Received: *03 August 2021*
Accepted: *22 September 2021*
Published: *14 October 2021*

Citation:
Otten C, Seifert T, Hausner J and Büttner D (2021) The Contribution of the Predicted Sorting Platform Component HrcQ to Type III Secretion in Xanthomonas campestris pv. vesicatoria Depends on an Internal Translation Start Site. Front. Microbiol. 12:752733. doi: 10.3389/fmicb.2021.752733

Pathogenicity of the Gram-negative bacterium *Xanthomonas campestris* pv. *vesicatoria* depends on a type III secretion (T3S) system which translocates effector proteins into plant cells. T3S systems are conserved in plant- and animal-pathogenic bacteria and consist of at least nine structural core components, which are designated Sct (secretion and cellular translocation) in animal-pathogenic bacteria. Sct proteins are involved in the assembly of the membrane-spanning secretion apparatus which is associated with an extracellular needle structure and a cytoplasmic sorting platform. Components of the sorting platform include the ATPase SctN, its regulator SctL, and pod-like structures at the periphery of the sorting platform consisting of SctQ proteins. Members of the SctQ family form a complex with the C-terminal protein domain, $SctQ_C$, which is translated as separate protein and likely acts either as a structural component of the sorting platform or as a chaperone for SctQ. The sorting platform has been intensively studied in animal-pathogenic bacteria but has not yet been visualized in plant pathogens. We previously showed that the SctQ homolog HrcQ from *X. campestris* pv. *vesicatoria* assembles into complexes which associate with the T3S system and interact with components of the ATPase complex. Here, we report the presence of an internal alternative translation start site in *hrcQ* leading to the separate synthesis of the C-terminal protein region ($HrcQ_C$). The analysis of genomic *hrcQ* mutants showed that $HrcQ_C$ is essential for pathogenicity and T3S. Increased expression levels of *hrcQ* or the T3S genes, however, compensated the lack of $HrcQ_C$. Interaction studies and protein analyses suggest that $HrcQ_C$ forms a complex with HrcQ and promotes HrcQ stability. Furthermore, $HrcQ_C$ colocalizes with HrcQ as was shown by fluorescence microscopy, suggesting that it is part of the predicted cytoplasmic sorting platform. In agreement with this finding, $HrcQ_C$ interacts with the inner membrane ring protein HrcD and the SctK-like linker protein HrpB4 which contributes to the docking of the HrcQ complex to the membrane-spanning T3S apparatus. Taken together, our data suggest that $HrcQ_C$ acts as a chaperone for HrcQ and as a structural component of the predicted sorting platform.

Keywords: type III secretion, plant-pathogenic bacterium, *Xanthomonas*, sorting platform, internal translation initiation, C ring, chaperone, SctK proteins

INTRODUCTION

Pathogenicity of many Gram-negative animal- and plant-pathogenic bacteria depends on the translocation of bacterial effector proteins into eukaryotic cells where they interfere with cellular processes to the benefit of the pathogen. Translocation of effector proteins is often mediated by a type III secretion (T3S) system which is a highly complex protein delivery system and structurally related to the bacterial flagellum (Büttner and Bonas, 2010; Dean, 2011; Büttner, 2016; Wagner et al., 2018). Both systems are, therefore, referred to as translocation-associated and flagellar T3S systems (Abby and Rocha, 2012). The conservation of T3S system components of flagellar and translocation-associated T3S systems from different bacterial species suggests a similar core architecture of the secretion apparatus. Conserved core components of translocation-associated T3S systems from animal-pathogenic bacteria are designated Sct (secretion and cellular translocation) followed by a letter which refers to the nomenclature of T3S system components from *Yersinia* spp. (Hueck, 1998; Deng et al., 2017; Wagner and Diepold, 2020). Structural studies revealed that several Sct proteins are involved in the assembly of the ring structures of the T3S system in the outer membrane (OM) and inner membrane (IM; Deng et al., 2017; Lara-Tejero and Galan, 2019). The OM ring of T3S systems is assembled by members of the SctC secretin family and is associated with an extracellular appendage which is referred to as T3S needle in animal- or pilus in plant-pathogenic bacteria and serves as a transport channel for secreted proteins to the host-pathogen interface (Büttner, 2012; Deng et al., 2017; Habenstein et al., 2020). The translocation of effector proteins into eukaryotic target cells is mediated by the T3S translocon, which inserts as a homo- or heterooligomeric protein channel into the eukaryotic plasma membrane (Mattei et al., 2011; Dey et al., 2019).

The IM rings of the T3S system are assembled by SctD proteins on the outer and SctJ proteins on the inner side and surround the export apparatus, which consists of an $SctR_5$-$SctS_4$-$SctT_1$ complex situated above the IM in the periplasm as was shown for the T3S systems from *Salmonella* spp. and *Shigella flexneri* (Dietsche et al., 2016; Zilkenat et al., 2016; Kuhlen et al., 2018; Johnson et al., 2019; Miletic et al., 2021). The $SctR_5$-$SctS_4$-$SctT_1$ complex is associated with the additional export apparatus components SctU and SctV, which insert into the IM and contain large cytoplasmic domains presumably involved in substrate binding (Büttner, 2012; Wagner et al., 2018). SctV forms a nonameric ring structure and is linked *via* members of the SctO family of coiled-coil proteins to the cytoplasmic ATPase complex of the T3S system (Gazi et al., 2008; Wagner et al., 2018; Singh and Wagner, 2019). The ATPase SctN forms a hexameric complex and is connected *via* six spoke-like structures formed by SctL dimers to six pods consisting of members of the SctQ protein family as was shown in *Salmonella* spp. and *S. flexneri* (Lara-Tejero, 2019; Lara-Tejero and Galan, 2019; Tachiyama et al., 2019). The wheel-like SctN-SctL-SctQ complex is a part of the cytoplasmic sorting platform, a dynamic structure that can assemble in the bacterial cytoplasm independently of the membrane-spanning portion of the T3S system (Diepold et al., 2015, 2017; Zhang et al., 2017; Rocha et al., 2018; Lara-Tejero, 2019; Milne-Davies et al., 2021; Wimmi et al., 2021). Recruitment of the cytoplasmic components to the IM ring of the T3S system is mediated by SctK proteins acting as linkers between the cytoplasmic domain of SctD and the SctQ pods (Diepold et al., 2010; Hu et al., 2017; Zhang et al., 2017; Tachiyama et al., 2019; Otten and Büttner, 2021).

SctQ proteins are also termed C ring proteins because their flagellar homologs FliM and FliN form a ring-like structure at the cytoplasmic side of the flagellum (Minamino et al., 2019). FliN corresponds to the C-terminal region of SctQ proteins ($SctQ_C$), which are often translated as separate proteins following translation initiation at an internal start codon as shown, for example, for *Yersinia* spp., *Salmonella* spp., and *S. flexneri* (Yu et al., 2011; Bzymek et al., 2012; McDowell et al., 2016; Lara-Tejero et al., 2019). In some pathogens, however, for example, the plant pathogen *Pseudomonas syringae*, $SctQ_C$ is encoded by a separate gene (Fadouloglou et al., 2004). $SctQ_C$ proteins were shown to interact with SctQ and were identified as essential structural components of the T3S systems in *Yersinia* spp. and *S. flexneri* (Bzymek et al., 2012; Diepold et al., 2015; McDowell et al., 2016; Rocha et al., 2018). In *Salmonella* spp., however, $SctQ_C$ was proposed to act as a chaperone which promotes the stability of SctQ (Yu et al., 2011; Lara-Tejero et al., 2019). The contribution of SctQ and $SctQ_C$ to the assembly of the sorting platform and to T3S has been intensively analyzed in animal-pathogenic bacteria, whereas the exact role of corresponding HrcQ proteins from plant pathogens is still largely unknown.

In our laboratory, we study T3S in the plant-pathogenic bacterium *Xanthomonas campestris* pv. *vesicatoria* (also designated *Xanthomonas euvesicatoria*) which is the causal agent of bacterial spot disease in pepper and tomato plants (Jones et al., 2004; Timilsina et al., 2020). Pathogenicity of *X. campestris* pv. *vesicatoria* depends on the T3S system which is encoded by the chromosomal *hrp* (hypersensitive response and pathogenicity) gene cluster (Büttner and Bonas, 2010; Timilsina et al., 2020). The term *hrp* refers to the essential contribution of the gene cluster to bacterial pathogenicity in susceptible plants and the elicitation of the HR in resistant plants (Büttner and He, 2009; Deng et al., 2017). The HR is a rapid local cell death at the infection site and depends on the recognition of single type III effectors in plants with matching resistance genes (Jones and Dangl, 2006; Gill et al., 2015). *hrp* gene expression is activated when the bacteria enter the plant tissue or are cultivated in special minimal media (Schulte and Bonas, 1992). *hrp* genes are regulated by HrpG and HrpX, which are encoded outside the *hrp* gene cluster (Wengelnik et al., 1996; Wengelnik and Bonas, 1996). Eleven Hrp proteins, designated Hrc (Hrp conserved), are conserved in animal and/or plant pathogens and presumably constitute the core structural elements of the T3S system (Büttner, 2012). Among the functionally characterized Hrc proteins is the predicted C ring protein HrcQ which is encoded by the first gene of the *hrpD* operon and essential for pathogenicity and T3S (Rossier et al., 2000). We previously reported that HrcQ localizes to the bacterial cytoplasm and

to the membranes under T3S-permissive conditions and that it interacts with components of the ATPase complex and the export apparatus (Lorenz et al., 2012). Fluorescence microscopy studies in *X. campestris* pv. *vesicatoria* showed that a HrcQ-sfGFP (superfolder green fluorescent protein) fusion protein forms foci in the presence of a functional T3S system, thus indicating the assembly of the predicted sorting platform (Hausner et al., 2019). Foci formation was reduced in strains lacking the non-conserved HrpB4 protein which links HrcQ to the cytoplasmic domain of the IM ring component HrcD and thus likely acts similarly to SctK proteins from animal-pathogenic bacteria (Otten and Büttner, 2021).

In the present study, we identified and analyzed a C-terminal HrcQ derivative ($HrcQ_C$) which results from internal translation initiation in *hrcQ*. Complementation studies revealed that the internal translation start site is essential for pathogenicity when *hrcQ* is expressed *in cis*. Expression of *hrcQ* with mutated internal translation start site *in trans*, however, restored pathogenicity in a *hrcQ* deletion mutant overexpressing the T3S system. This suggests that the loss of $HrcQ_C$ can be compensated by increased expression levels of T3S genes. Protein studies revealed that $HrcQ_C$ contributes to HrcQ stability and thus likely acts as a chaperone for HrcQ. Furthermore, the results of interaction and localization studies suggest that $HrcQ_C$ interacts and colocalizes with HrcQ and also binds to known HrcQ interaction partners. When analyzed by fluorescence microscopy, $HrcQ_C$ colocalized with HrcQ and contributed to the assembly of HrcQ complexes. Our data, therefore, suggest that $HrcQ_C$ might act as both chaperone and structural component of the predicted sorting platform.

MATERIALS AND METHODS

Bacterial Strains and Growth Conditions

Bacterial strains and plasmids used in this study are listed in **Supplementary Table S1**. *Escherichia coli* strains were cultivated at 37°C in lysogeny broth (LB) medium, *X. campestris* pv. *vesicatoria* strains at 30°C in nutrient-yeast extract-glycerol (NYG) medium or minimal medium A (MA, pH 7.0) supplemented with sucrose (10 mM) and casamino acids (0.3%; Daniels et al., 1984; Ausubel et al., 1996). Plasmids were introduced into *E. coli* by electroporation and into *X. campestris* pv. *vesicatoria* by electroporation or conjugation. Antibiotics were added to the media at the following final concentrations: ampicillin, 100 µg/ml; kanamycin, 25 µg/ml; rifampicin, 100 µg/ml; spectinomycin, 100 µg/ml, gentamycin, 15 µg/ml; streptomycin, 25 µg/ml; and nalidixic acid, 15 µg/ml.

Plant Material and Plant Infections

For infection studies, *X. campestris* pv. *vesicatoria* bacteria were resuspended in 1 mM $MgCl_2$ and infiltrated at densities of 1×10^8 colony-forming units (CFU) ml^{-1} into leaves of the near-isogenic pepper cultivars Early Cal Wonder (ECW), ECW-10R and ECW-30R using a needle-less syringe (Minsavage et al., 1990; Kousik and Ritchie, 1998). Infected plants were incubated in growth chambers for 16 h of light at 28°C and 8 h of darkness at 22°C. The HR was documented 1–2 dpi (days post inoculation) after destaining of the leaves in 70% ethanol. Disease symptoms were photographed 1–9 dpi. The results of infection experiments were reproduced at least two times with different transformants.

Generation of *hrcQ* Expression Constructs

For the generation of *hrcQ* expression constructs with mutations in possible start codons, construct pB-PStophrcQ containing *hrcQ* downstream of the native promoter was used as a template for PCR reactions with primers amplifying the whole plasmid and annealing to each other. Mutations of putative start codons from GTG (V1) or TTG to GCG encoding alanine were introduced by the primer sequences. The PCR amplicons were transferred into *E. coli* after a *Dpn*I digest, and constructs with single mutations were used as templates to introduce additional mutations.

To generate an expression construct encoding HrcQ-sfGFP under control of the native promoter, the annotated *hrcQ* coding sequence and 299 bp upstream region were amplified from *X. campestris* pv. *vesicatoria* strain 85–10 by PCR and subcloned into pICH41021 as blunt-end fragment using *Sma*I and ligase. Subsequent ligation with *sfgfp* (construct pEX-A-sfgfp) into the *Bsa*I sites of pBRM-P by Golden Gate cloning (Engler et al., 2008) resulted in construct pB-PhrcQ-sfGFP. The mutation in codon 203 was introduced by PCR using primers which annealed back-to-back to pB-PhrcQ-sfGFP and contained *Bpi*I sites for Golden Gate-based religation of the PCR product. The M211A mutation was inserted using complementary primers annealing to pB-PhrcQ-sfGFP, and the PCR amplicon was transferred into *E. coli* after *Dpn*I digest. Using a similar strategy, mutations leading to the M203A and M211A amino acid exchanges were introduced into pB-PhrcQ which encodes HrcQ-c-Myc under control of the native promoter.

For the generation of expression constructs containing $hrcQ_{M211A}$-*c-myc* downstream of the *lac* promoter, $hrcQ_{M211A}$ was amplified by PCR using pB-$PhrcQ_{M211A}$ as a template. The PCR product was subcloned into pICH41021 as blunt-end fragment after *Sma*I digest and ligation. $hrcQ_{M211A}$ was ligated into the Golden Gate-compatible pBRM and into the *Bsa*I sites of the bacterial adenylate cyclase-based two-hybrid (BACTH) vectors $pUT18_{GG}$, $pUT18C_{GG}$, $pKT25_{GG}$, and $pKNT25_{GG}$.

For *in cis* expression of $hrcQ_{M211A}$ in *X. campestris* pv. *vesicatoria*, the gene was amplified by PCR using pB-$PhrcQ_{M211A}$ as template and assembled with a module containing the native *hrcQ* promoter in pLAND-P, in frame with a C-terminal 3 × c-Myc epitope-encoding sequence. To insert $hrcQ_{M211A}$-*c-myc* into the genome of *X. campestris* pv. *vesicatoria*, pLAND-$PhrcQ_{M211A}$ was conjugated into strains 85–10Δ*hrcQ* and 85*Δ*hrcQ*. Double homologous recombination events led to the insertion of $hrcQ_{M211A}$-*c-myc* into the *hpaFG* region and were selected as described previously (Huguet et al., 1998).

To generate $hrcQ_C$ expression constructs, the corresponding region of *hrcQ* without stop codon was amplified by PCR, subcloned as blunt-end fragment into pICH41021, and ligated into the *Bsa*I sites of pBRM and the Golden Gate-compatible BACTH vectors. Additionally, $hrcQ_C$ was ligated with a PCR

amplicon corresponding to the native *hrcQ* promoter into the *Bsa*I sites of pBRM-P. To generate a glutathione S-transferase (GST)-HrcQ$_C$ expression construct, two modules corresponding to *hrcQ*$_C$ and *ptac-gst* (encodes GST under control of the *ptac* promoter) were inserted into the *Bsa*I sites of pBRM-P-stop, resulting in pB-P-ptacGST-hrcQ$_C$.

Generation of Modular T3S Gene Cluster Constructs

Modular T3S gene cluster constructs were generated as described in the **Supplementary Material** and are summarized in **Supplementary Figure S6** and **Supplementary Table S1** (Hausner et al., 2019).

Immunodetection of Proteins

Proteins were analyzed by SDS-PAGE and immunoblotting, using antibodies directed against the c-Myc and FLAG epitope, GST, HrcJ, HrcQ, AvrBs3, and HrpB1, respectively (Knoop et al., 1991; Rossier et al., 2000). Horseradish peroxidase-labeled anti-mouse, anti-rabbit, or anti-goat antibodies were used as secondary antibodies. Binding of antibodies was visualized by enhanced chemiluminescence.

Analysis of *in vitro* T3S

In vitro T3S assays were performed as described (Rossier et al., 2000). Briefly, bacteria were grown overnight in MA medium (pH 7.0) supplemented with sucrose (10 mM) and casamino acids (0.3%) and resuspended in MA medium (pH 5.3) containing 50 μg/ml BSA (bovine serum albumin) and 10 μM thiamine at an $OD_{600\,nm}$ of 0.15. The cultures were incubated on a rotary shaker overnight at 30°C, and the bacterial cells and secreted proteins were separated by filtration using low protein binding filters. Proteins in the culture supernatant were precipitated by the addition of trichloroacetic acid and resuspended in 20 μl of Laemmli buffer. Total cell extracts and culture supernatants were analyzed by SDS-PAGE and immunoblotting.

Interaction Studies Using the BACTH System

BACTH assays were performed using the EUROMEDEX BACTH system kit. Expression constructs were transformed into JM109 *E. coli* cells to analyze protein synthesis. For this, bacterial cultures were induced with IPTG (isopropyl-*β*-D-thiogalactopyranoside; 2 mM final concentration) at an OD_{600} of 0.6–0.8 and incubated on a rotary shaker for 2 h at 37°C. Bacterial cells were collected by centrifugation, resuspended in Laemmli buffer, and analyzed by immunoblotting, using a FLAG epitope-specific antibody.

For protein-protein interaction studies, expression constructs encoding T18 and T25 fusion proteins were cotransformed into chemically competent DHM1 or BTH101 *E. coli* strains, and transformants were plated on LB plates containing kanamycin and gentamicin. Four colonies per transformation were used to inoculate LB overnight cultures with appropriate antibiotics, which were incubated overnight at 30°C on a rotary shaker. Two μl of the overnight cultures was spotted on selective LB plates containing X-gal (5-bromo-4-chloro-3-indolyl-β-D-galactopyranoside; 40 μg/ml) and 2 mM IPTG. The plates were incubated at 22°C, and the color of the colonies was monitored over a period of three to 5 days. The experiments were performed at least three times with four different transformants from independent cotransformations.

GST Pull-Down Assays

For GST pull-down assays, expression constructs encoding GST, GST-HrcQ$_C$, HrcQ-c-Myc, and HrcQ$_{M211A}$-c-Myc interaction partners were introduced into *E. coli* BL21(DE3) cells and grown in LB medium until OD_{600} 0.6–0.8. Gene expression was induced by 2 mM IPTG (final concentration). After 2 h of incubation at 37°C, bacterial cells were harvested by centrifugation, resuspended in PBS (phosphate-buffered saline), and lysed using a French press. The lysates were centrifuged to remove cell debris, and soluble GST and GST-HrcQ$_C$ proteins were immobilized on a glutathione sepharose matrix according to the manufacturer's instructions (GE Healthcare). The matrix with immobilized GST and GST-HrcQ$_C$ proteins was washed and incubated with bacterial lysates containing HrcQ-c-Myc or HrcQ$_{M211A}$-c-Myc for 2 h at 4°C on an overhead shaker. After washing of the matrix, bound proteins were eluted with Laemmli buffer. Cell lysates and eluted proteins were analyzed by SDS-PAGE and immunoblotting, using c-Myc epitope- and GST-specific antibodies.

Fluorescence Microscopy

For fluorescence microscopy studies, *X. campestris* pv. *vesicatoria* strains were grown overnight in MA medium (pH 7.0) supplemented with sucrose (10 mM) and casamino acids (0.3%). Cells were resuspended in MA medium (pH 5.3) supplemented with BSA and thiamine as described above at an $OD_{600\,nm}$ of 0.15 and incubated on a tube rotator at 30°C for 1 h. Bacteria were transferred onto a microscopy slide on top of a pad of 1% agarose dissolved in MA medium (pH 5.3) as described (Hausner et al., 2019). Fluorescence was inspected with a confocal laser scanning microscope (Leica STELLARIS 8) with a 60× magnification objective and 5× digital magnification. Specific filter sets were used for sfGFP (excitation at 485 nm; emission at 510 nm) and mKOκ (excitation at 551 nm; emission at 563 nm). Fluorescent foci were counted in approximately 300 cells of three transconjugants for each strain.

RESULTS

A Putative Internal Translation Start Site in *hrcQ* Contributes to Protein Function and Synthesis of HrcQ$_C$

The predicted C ring component HrcQ is encoded by the first gene of the *hrpD* operon in the *hrp* gene cluster from *X. campestris* pv. *vesicatoria* and is conserved in *Xanthomonas* spp. (73–93% amino acid identity; **Figure 1**; **Supplementary Figures S1, S2**). The C-terminal region of HrcQ also shares 27–34% amino acid identity with corresponding regions of HrcQ proteins from

plant pathogens and SctQ proteins from the animal pathogens *Yersinia* spp. and *Salmonella* spp. In contrast, no significant homology was detected between HrcQ and the SctQ proteins EscQ from *E. coli* and Spa33 from *S. flexneri*, suggesting that these proteins are not conserved in every species (**Figure 1**; **Table 1**).

Several *sctQ* genes from animal-pathogenic bacteria contain internal translation initiation sites which lead to the separate synthesis of the C-terminal protein regions ($SctQ_C$; Yu et al., 2011; Bzymek et al., 2012; McDowell et al., 2016; Lara-Tejero et al., 2019). In *hrcQ* from *X. campestris* pv. *vesicatoria*, there are two ATG codons at positions 203 and 211 which could serve as additional internal translation start sites for the separate synthesis of the C-terminal region of HrcQ ($HrcQ_C$) and are conserved in *hrcQ* genes from *Xanthomonas* spp. (**Supplementary Figure S1**). A potential Shine Dalgarno sequence (GAGG) is present 11 nucleotides upstream of codon 211 (**Figure 1**). To investigate a possible internal translation initiation in *hrcQ* transcripts, we generated expression constructs encoding HrcQ derivatives with M203A or M211A mutations (mutation of the ATG to GCG) under control of the native promoter and in fusion with a C-terminal 3 × c-Myc epitope. For complementation studies, expression constructs were transferred to *X. campestris* pv. *vesicatoria hrcQ* deletion mutants, and transformants were infiltrated into leaves of susceptible and resistant pepper plants. When analyzed in *X. campestris* pv. *vesicatoria* strain 85–10Δ*hrcQ*, $HrcQ_{M203A}$-c-Myc but not $HrcQ_{M211A}$-c-Myc restored the wild-type phenotype with respect to disease symptoms in susceptible and the HR induction in resistant plants (**Figure 2A**). Both HrcQ derivatives complemented the mutant phenotype of strain 85–10*hrpG**Δ*hrcQ* (85*Δ*hrcQ*), which contains HrpG*, a constitutively active version of the key regulator HrpG (**Figure 2A**). HrpG* leads to constitutive expression of T3S genes and accelerated plant reactions (Wengelnik et al., 1999). We, therefore, assume that the negative effect of the M211A mutation was compensated by overexpression of the T3S genes in the presence of HrpG*.

Immunoblot analysis of bacterial cell extracts containing HrcQ-c-Myc or $HrcQ_{M203A}$-c-Myc led to the detection of HrcQ and a derivative thereof at a size of approximately 20 kDa corresponding to the size of the predicted internal translation product (**Figure 2A**). In contrast, significantly reduced amounts of the full-length protein and no internal translation product were detectable in bacterial cell extracts containing $HrcQ_{M211A}$-c-Myc (**Figure 2A**), suggesting that the ATG codon at position 211 serves as additional internal translation start site and also contributes to the stability of HrcQ.

Given the low levels of $HrcQ_{M211A}$-c-Myc, we also analyzed HrcQ-sfGFP fusions containing M203A or M211A mutations. We previously showed that HrcQ-sfGFP complements the *hrcQ* mutant phenotype and forms fluorescent foci in bacterial cells in the presence of a functional T3S system (Hausner et al., 2019). Plant infection studies showed that HrcQ-sfGFP and $HrcQ_{M203A}$-sfGFP complemented the mutant phenotypes of strain 85–10Δ*hrcQ* with respect to HR induction and disease symptoms, whereas no complementation was observed for $HrcQ_{M211A}$-sfGFP (**Figure 2B**). When analyzed in strain 85*Δ*hrcQ*, however, $HrcQ_{M211A}$-sfGFP restored pathogenicity and HR induction in susceptible and resistant plants, respectively, suggesting that the negative effect of the M211A mutation was compensated by the overexpression of the T3S genes as was observed for HrcQ-c-Myc derivatives (see above; **Figures 2A,B**). Immunoblot analyses led to the detection of HrcQ-sfGFP and truncated derivatives thereof at sizes of approximately 30 and 40 kDa, which likely correspond to cleaved sfGFP and the predicted additional translation product of HrcQ-sfGFP, respectively (**Figure 2B**). The M211A but not the M203A mutation abolished the detection of the truncated 40 kDa HrcQ-sfGFP derivative (**Figure 2B**). Notably, the M211A mutation did not significantly affect the levels of full-length HrcQ-sfGFP, suggesting that the sfGFP fusion partner stabilizes HrcQ in the presence of the M211A mutation when expressed *in trans* (**Figure 2B**). Taken together, we conclude that the ATG codon at position 211 of *hrcQ* contributes to protein function and serves as an additional translation start site of *hrcQ*. This is supported by the presence of a potential Shine Dalgarno sequence upstream of codon 211 which is conserved in *hrcQ* genes from *Xanthomonas* spp. (**Figure 1**; **Supplementary Figure S1**).

In cis Expression of *hrcQM211A* Abolishes Pathogenicity

Next, we investigated a possible effect of the copy number on $HrcQ_{M211A}$ function. For this, we inserted *hrc*Q_{M211A}-*c-myc* including the native *hrcQ* promoter into the *hpaFG* region of strains 85–10Δ*hrcQ* and 85*Δ*hrcQ*. The *hpaFG* region is located adjacent to the *hrp* gene cluster and serves as a landing platform for gene insertion (Tamir-Ariel et al., 2007; Lorenz et al., 2012). We previously showed that the genomic insertion of *hrcQ-c-myc* under control of the native promoter restores pathogenicity in *hrcQ* deletion mutants (Lorenz et al., 2012; **Figure 3A**). In contrast, expression of *hrc*Q_{M211A}*-c-myc in cis* did not complement the phenotypes of strains 85–10Δ*hrcQ* and 85*Δ*hrcQ*, suggesting that the ATG codon at position 211 is essential for pathogenicity when *hrcQ* is present as a single copy in the chromosome (**Figure 3A**).

To analyze whether pathogenicity of genomic *hrc*Q_{M211A} mutants could be restored by ectopic expression of *hrc*Q_c *in trans*, we introduced expression constructs containing *hrc*Q_c-*c-myc* under control of the native or the *lac* promoter into strains 85–10*hrcQ::hrc*Q_{M211A} and 85*Δ*hrcQ::hrc*Q_{M211A}. Immunoblot analysis of bacterial cell extracts showed that $HrcQ_C$-c-Myc was stably synthesized (**Figure 3B**; **Supplementary Figure S3**; see also below). When bacteria were infiltrated into leaves of susceptible and AvrBs1-responsive resistant pepper plants, ectopic expression of *hrc*Q_C-*c-myc* under control of the native promoter restored pathogenicity, whereas expression of *hrc*Q_C-*c-myc* under control of the *lac* promoter only partially complemented the mutant phenotype of strain 85*Δ*hrcQ::hrc*Q_{M211A} but not of strain 85–10Δ*hrcQ::hrc*Q_{M211A} (**Figure 3B**; **Supplementary Figure S3**). Ectopic expression of *hrc*Q_C under control of the *lac* or the native promoter in strain 85*Δ*hrcQ::hrc*Q_{M211A}, however, restored HR induction in ECW-30R pepper plants which recognize the effector protein

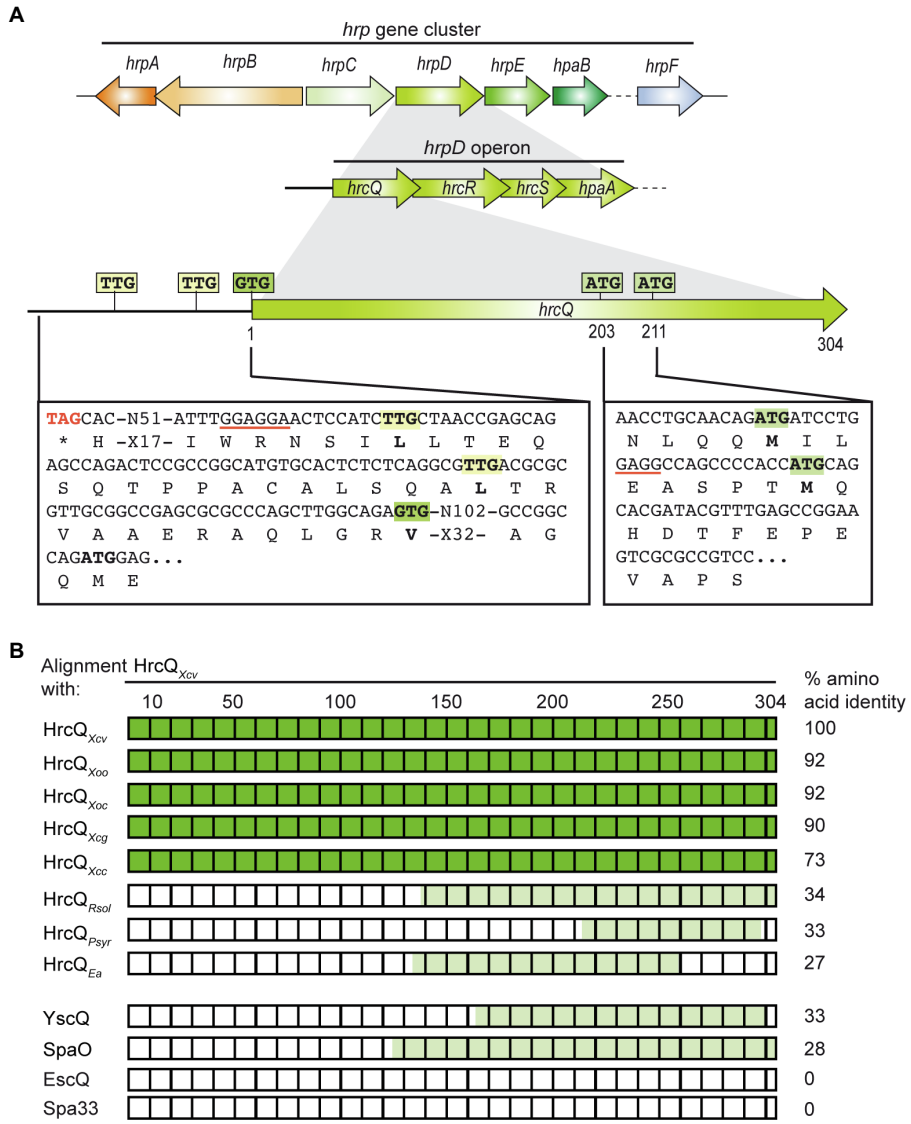

FIGURE 1 | Genetic localization of *hrcQ* in the *hrp* gene cluster from *Xanthomonas campestris* pv. *vesicatoria* and alignments of HrcQ and SctQ protein sequences. **(A)** HrcQ is encoded by the first gene of the *hrpD* operon of the *hrp* gene cluster. The promoter region upstream of the annotated GTG start codon of *hrcQ* contains two TTG codons which could serve as alternative translation start sites and are located 13 and 30 codons upstream of the GTG codon. *hrcQ* also contains two potential internal translation start sites at codon positions 203 and 211. Potential Shine Dalgarno sequences are underlined. Letters refer to amino acids. Operons and genes are represented by arrows. **(B)** Comparison of HrcQ protein sequences from plant-pathogenic bacteria and SctQ proteins from animal-pathogenic bacteria. HrcQ from *X. campestris* pv. *vesicatoria* is represented by rectangles, numbers on top refer to amino acids. The percentage of amino acid identities is indicated on the right side. Protein regions of HrcQ from *X. campestris* pv. *vesicatoria* with more than 70% amino acid identities are shown in dark green and regions with lower sequence identities in light green. The following sequences were compared by pairwise sequence alignments: HrcQ from *X. campestris* pv. *vesicatoria* (*Xcv*, GenBank accession number CAJ22054), HrcQ from *X. oryzae* pv. *oryzae* (*Xoo*, GenBank accession number AAK08059), HrcQ from *X. oryzae* pv. *oryzicola* (GenBank accession number ABH07401), HrcQ from *X. citri* pv. *glycines* (*Xcg*, GenBank accession number AAP34348), HrcQ from *X. campestris* pv. *campestris* (*Xcc*, GenBank accession number CAP52441), HrcQ from *Ralstonia solanacearum* GMI1000 (*Rsol*, GenBank accession number CAD18012), HrcQ from *Pseudomonas syringae* pv. *syringae* (*Psyr*, GenBank accession number ACU65038), HrcQ from *E. amylovora* (*Ea*, GenBank accession number AAB06004), YscQ from *Yersinia enterocolitica* (GenBank accession number AAK69226), SpaO from *Salmonella enterica* subsp. *enterica* serovar *Typhimurium* (GenBank accession number AAC43863), EscQ from *Escherichia coli* O157:H7 (GenBank accession number QkQ88880), and Spa33 from *Shigella flexneri* (GenBank accession number AAP79015).

AvrBs3 (Römer et al., 2009; **Figure 3B**). For these experiments, an *avrBs3* expression construct was additionally introduced into strain 85*Δ*hrcQ*::*hrcQ*$_{M211A}$ and derivatives thereof. When analyzed in the wild-type strain 85–10, ectopic expression of *hrcQ*$_C$-*c-myc* under control of the *lac* promoter interfered with pathogenicity, suggesting that it exerts a dominant-negative effect (**Figure 3C**). No complementation by HrcQ$_C$ was observed in the *hrcQ* deletion mutant 85*Δ*hrcQ*, suggesting that the N-terminal region of HrcQ is required for protein function (**Supplementary Figure S3**).

TABLE 1 | Amino acid similarities between HrcQ from *Xanthomonas campestris* pv. *vesicatoria* and HrcQ/SctQ proteins from other bacterial species.

	Percentage of amino acid identities/similarities[1]								
	$HrcQ_{Rsol}$	**$HrcQ_{Pss}$**	**$HrcQ_{aPst}$**	**$HrcQ_{bPst}$**	**$HrcQ_{Ea}$**	**$YscQ_{Yent}$**	**$Spa33_{Sflex}$**	**$SpaO_{Sent}$**	**$EscQ_{EPEC}$**
Length	354	393	238	137	338	307	293	303	305
$HrcQ_{Xcv}$	34/48	33/50	41/56	None	27/38[2]	33/50	None	28/46	None
	54%	28%	11%		41%	46%		59%	
$HrcQ_{C/Xcv}$	40/60	36/53	None	30/46[2]	36/47	36/61	None	30/59	None
	84%	73%		77%	41%	88%		71%	
$HrcQ_{Rsol}$	100	31/44	29/41	44/66	None	33/56	26/52	26/45	None
	100%	61%	20%	7%		20%	19%	48%	
$HrcQ_{Pss}$	31/44	100	30/47	60/75	30/43	27/48	22/39	26/42	None
	26%	100%	30%	17%	96%	45%	22%	21%	
$HrcQ_{aPst}$	29/41	30/47	100	53/63	33/46	44/64	None	None	None
	26%	88%	100%	7%	83%	14%			
$HrcQ_{bPst}$	44/66	45/59	50/59	100	53/70	29/51	None	25/44	None
	19%	94%	16%	100%	43%	51%		59%	
$HrcQ_{Ea}$	25/40	31/44	33/46	55/72	100	26/42	18/40	28/45	None
	45%	96%	58%	20%	100%	45%	42%	23%	
$YscQ_{Yent}$	33/56	27/48	44/64	29/51	25/40	100	26/44	75%	None
	23%	40%	12%	22%	47%	100%	22%	28/40	
$Spa33_{Sflex}$	26/52	22/39	None	20/46	None	26/44	100	24/42	None
	22%	31%		18%		23%	100%	98%	
$SpaO_{Sent}$	26/45	26/42	None	27/46	28/43	28/40	24/47	100	58/75
	47%	27%		22%	21%	77%	97%	100%	3%
$EscQ_{EPEC}$	None	None	None	None	None	None	None	58/75	100
								3%	100%

[1]*The following protein sequences were used for the alignments: HrcQ from X. campestris pv. vesicatoria (Xcv; GenBank accession number CAJ22054), HrcQ from R. solanacearum (Rsol; GenBank accession number CAD18012.1), HrcQ from Pseudomonas syringae pv. syringae (Pss; GenBank accession number ACU65038.1), HrcQ from E. amylovora (Ea; GenBank accession number AAB06004.2), YscQ from Yersinia enterocolitica (Yent; GenBank accession number AAK69226.1), Spa33 from S. flexneri (Sflex; GenBank accession number AAP79015.1), SpaO from Salmonella enterica subsp. enterica serovar Typhimurium (Sent; GenBank accession number AAC43863.1), EscQ from enteropathogenic E. coli (EPEC; GenBank accession number QKQ88880.1). The percentage of query cover, that is, the percentage of the sequence which was aligned to the input sequence given on top of each column, is indicated below the percentage of amino acid identities or similarities.*

[2]*A word size of 2 instead of 3 was used.*

To investigate the effect of the internal translation start site in *hrcQ* on *in vitro* T3S, bacteria were grown in secretion medium. Total cell extracts and culture supernatants were analyzed by immunoblotting using antibodies specific for the effector protein AvrBs3 and the IM ring component HrcJ. As reported previously, deletion of *hrcQ* abolished the detectable secretion of AvrBs3 (**Figure 3B**; Rossier et al., 2000). T3S was restored by expression of *hrcQ-c-myc in cis*, albeit not to wild-type levels (**Figure 3B**). No complementation was observed upon *in cis* expression of $hrcQ_{M211A}$-*c-myc*, whereas expression of $hrcQ_C$ *in trans* under control of the *lac* or the native promoter partially restored T3S in strain 85*Δ*hrcQ::*$hrcQ_{M211A}$ (**Figure 3B**). Taken together, these results suggest that $HrcQ_C$ can act *in trans* and that the loss of pathogenicity of genomic $hrcQ_{M211A}$ mutants is, therefore, likely caused by the lack of $hrcQ_C$ expression and not by a negative effect of the M211A mutation *per se* on HrcQ stability or folding.

Identification of Putative Translation Start Sites in the Promoter Region of *hrcQ*

Analysis of the additional HrcQ translation product revealed that $HrcQ_C$-c-Myc migrated at a slightly higher molecular weight when encoded under control of the native instead of the *lac* promoter (**Figure 3B**; **Supplementary Figure S3**). This suggests the presence of a translation start site upstream of the annotated start codon of *hrcQ*. Inspection of the *hrcQ* promoter sequence revealed two TTG codons, 13 and 30 codons, respectively, upstream of the annotated GTG start codon, which are also present in the upstream regions of annotated *hrcQ* genes from other *Xanthomonas* spp. (**Figure 1**; **Supplementary Figure S1**). TTG codons can serve as alternative translation start sites and presumably lead to reduced gene expression (Belinky et al., 2017). Given that the translation start site of *hrcQ* has not yet been experimentally confirmed, we investigated the importance of the annotated start codon and, therefore, mutated the GTG codon to GCG in an expression construct encoding HrcQ under control of the native promoter. Complementation studies showed that the resulting $HrcQ_{V1A}$ protein complemented the phenotype of strain 85*Δ*hrcQ* with respect to disease symptoms and the HR in susceptible and resistant pepper plants (**Figure 4**).

To investigate a possible translation initiation upstream of the annotated start codon, we generated additional expression constructs with mutations in the TTG codons upstream of the annotated start of *hrcQ* (hereafter referred to as codon positions +13 and +30; **Figure 1**) leading to L-to-A (mutation of TTG to GCG) amino acid exchanges. All HrcQ derivatives containing single, double, or triple mutations complemented the mutant phenotype of strain 85*Δ*hrcQ* (**Figure 4**). Complementation of the *hrcQ* mutant phenotype by

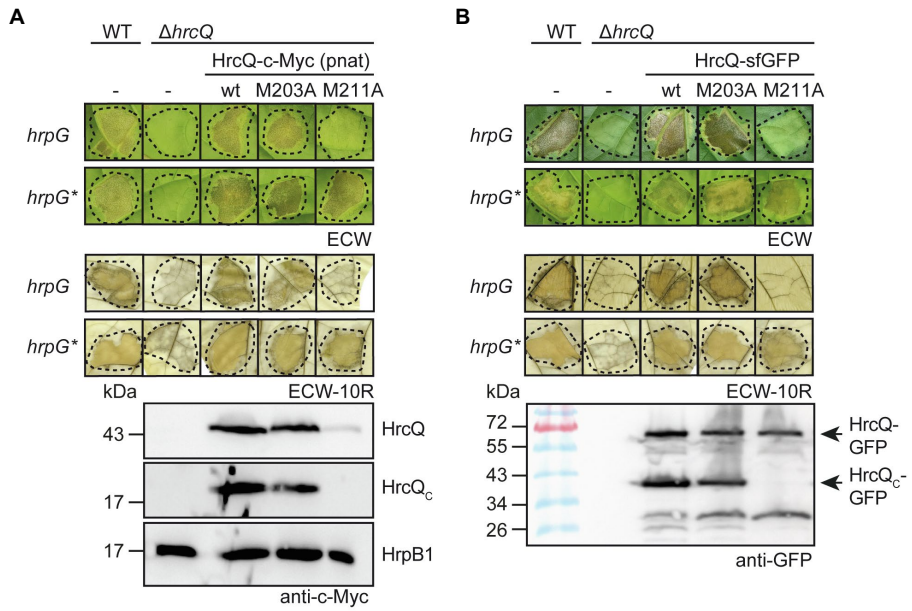

FIGURE 2 | The predicted internal translation start site at codon position 211 of *hrcQ* contributes to pathogenicity of *X. campestris* pv. *vesicatoria*. **(A)** A HrcQ derivative with an M211A mutation does not restore pathogenicity in strain 85–10Δ*hrcQ*. *Xanthomonas campestris* pv. *vesicatoria* strains 85–10 (WT, *hrpG*), 85* (WT, *hrpG**) and *hrcQ* deletion mutant derivatives (Δ*hrcQ*) thereof without plasmid (–) or with expression constructs encoding HrcQ-c-Myc (wt), $HrcQ_{M203A}$-c-Myc (M203A) or $HrcQ_{M211A}$-c-Myc (M211A) under control of the native promoter as indicated were infiltrated into leaves of susceptible Early Cal Wonder (ECW) and resistant ECW-10R pepper plants. Disease symptoms were photographed 8 dpi. For the better visualization of the HR, leaves were bleached in ethanol 2 dpi. Dashed lines indicate the infiltrated areas. For the analysis of HrcQ proteins, bacteria were grown in minimal medium and equal amounts of cell extracts were analyzed by immunoblotting using a c-Myc epitope-specific antibody. The blot shows the extracts of *hrpG** strains and was reprobed with an antibody specific for the predicted inner rod protein HrpB1 to demonstrate equal loading. **(B)** The M211A mutation in a HrcQ-sfGFP fusion protein interferes with protein function. Strains 85–10, 85*, and *hrcQ* deletion mutant derivatives thereof without plasmid (–) or containing expression constructs encoding HrcQ-sfGFP fusions with or without M203A or M211A mutations were infiltrated into leaves of susceptible and resistant pepper plants. Disease symptoms and the HR were monitored as described in **(A)**. For protein detection, equal amounts of cell extracts were analyzed by immunoblotting using a GFP-specific antibody. Arrows indicate the size of HrcQ-GFP and $HrcQ_C$-GFP. Experiments were performed three times with similar results.

$HrcQ_{V1A/L+13A/L+30A}$ was confirmed in strain 85–10Δ*hrcQ* (**Supplementary Figure S4**). Immunoblot analysis of bacterial protein extracts revealed that L + 13A mutations led to reduced HrcQ levels irrespective of the presence of the annotated start codon (**Figure 4**). L + 30A mutations further decreased HrcQ levels, whereas mutation of all three putative start codons abolished the detection of the corresponding HrcQ derivative (**Figure 4**). The presence of a putative Shine Dalgarno sequence eight nucleotides upstream the TTG codon at position +30, which is also conserved in the upstream regions of annotated *hrcQ* genes from other *Xanthomonas* spp. (**Supplementary Figure S1**) and the fact that the L + 30A mutation had the most severe effect on HrcQ protein levels strongly suggests the contribution of this codon to translation initiation of *hrcQ*. Given the presence of a stop codon 72 nucleotides upstream (see **Figure 1**), mutation of all three potential start codons in a *hrcQ* expression construct presumably led to translation initiation downstream of the GTG codon, thus resulting in a low-level synthesis of an N-terminally truncated but functional HrcQ derivative which is not detectable by immunoblot analysis (**Figure 4**). An ATG codon 105 nucleotides downstream of the annotated GTG codon might serve as translation start in the construct encoding $HrcQ_{V1A/L+13A/L+30A}$ (**Figure 1**). Taken together, we conclude that translation of the native *hrcQ* gene is initiated at the TTG codon located 30 codons upstream of the annotated GTG start site. Notably, the annotated start site of *hrcQ* from *X. campestris* pv. *campestris* is located immediately upstream of the TTG codon which is conserved in *hrcQ* and upstream sequences of *Xanthomonas* spp. (**Supplementary Figure S1**).

Interaction Studies With $HrcQ_C$

To investigate whether HrcQ and $HrcQ_C$ interact with each other as reported for SctQ and $SctQ_C$ proteins from animal-pathogenic bacteria (Diepold, 2020), we used a BACTH assay, which depends on the reconstitution of the catalytic domain of the adenylate cyclase (Cya) from two subdomains (T18 and T25). The interaction of T18 and T25 fusion proteins leads to the assembly of functional Cya and thus to the synthesis of cAMP, which activates the expression of the *lac* operon in *E. coli* reporter strains lacking the native *cya* gene (Karimova et al., 1998; Battesti and Bouveret, 2012).

For BACTH assays, we generated expression constructs encoding HrcQ, $HrcQ_C$, and $HrcQ_{M211A}$ as N- or C-terminal fusion partners of the T18 and T25 domains. Immunoblot analysis of bacterial cell extracts revealed that all HrcQ fusion proteins were stably synthesized (**Supplementary Figure S5**). Protein-protein interactions were analyzed in the *E. coli* reporter

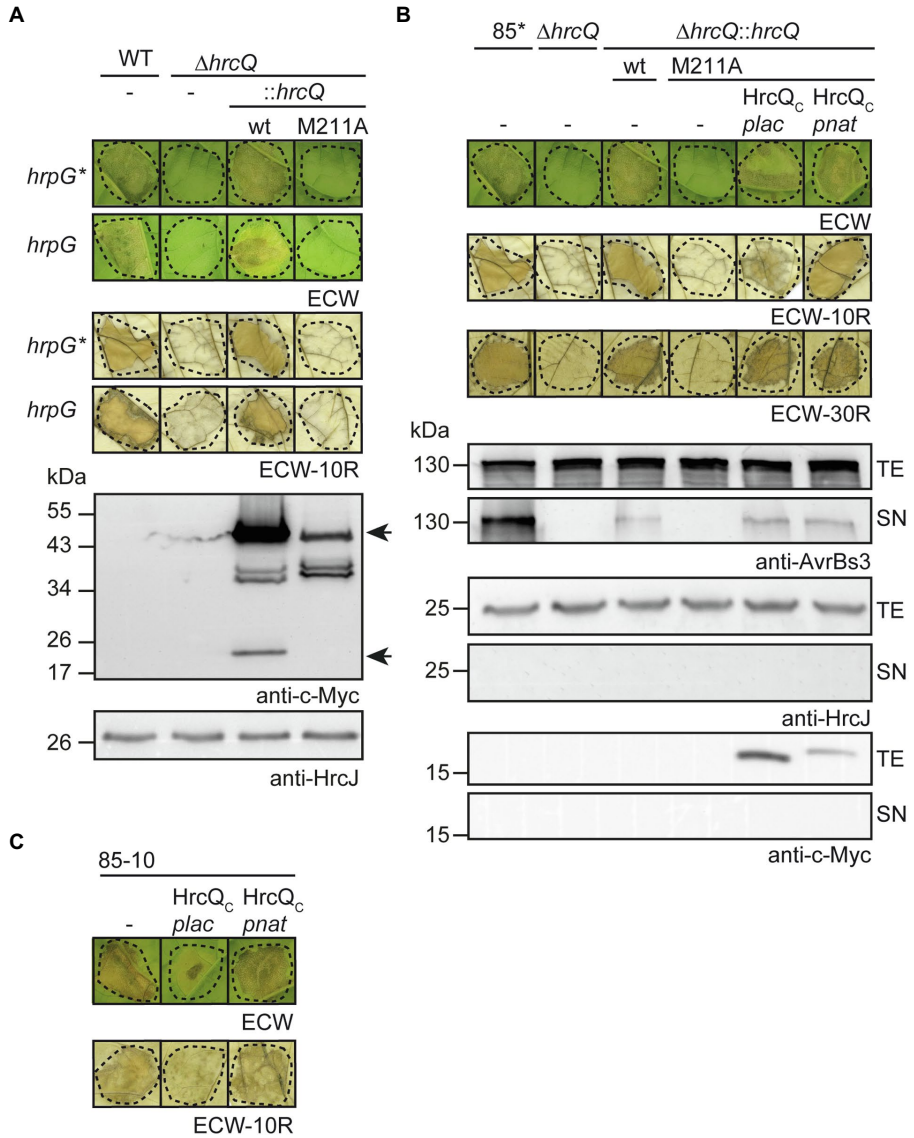

FIGURE 3 | Contribution of the internal translation start codon to pathogenicity of *X. campestris* pv. *vesicatoria*. **(A)** *In cis* expression of $hrcQ_{M211A}$ abolishes pathogenicity. *Xanthomonas campestris* pv. *vesicatoria* strains 85–10 (WT, *hrpG*), 85* (WT, *hrpG**), and *hrcQ* deletion mutant derivatives thereof containing *hrcQ-c-myc* (wt) or $hrcQ_{M211A}$-*c-myc* (M211A) inserted into the genomic *hpaFG* region under control of the native promoter were infiltrated into leaves of susceptible ECW and resistant ECW-10R pepper plants. Disease symptoms were photographed 8 dpi. For the better visualization of the HR, leaves were bleached in ethanol 2 dpi. Dashed lines indicate the infiltrated areas. For protein analysis, bacteria were grown in minimal medium and equal amounts of cell extracts were analyzed by immunoblotting using a c-Myc epitope-specific antibody. The blot shows the extracts of *hrpG** strains and was reprobed with an antibody specific for the inner membrane (IM) ring protein HrcJ to demonstrate equal loading. Arrows indicate signals corresponding to the size of HrcQ-c-Myc and the predicted internal translation product $HrcQ_C$-c-Myc. **(B)** *In trans* expression of $HrcQ_C$ restores pathogenicity of genomic $hrcQ_{M211A}$ mutants and *in vitro* type III secretion (T3S). Strains 85* and 85*Δ*hrcQ* (Δ*hrcQ*) with or without genomic insertion of *hrcQ-c-myc* (wt) or $hrcQ_{M211A}$-*c-myc* (M211A) and containing either no plasmid (–) or expression constructs encoding $HrcQ_C$-c-Myc under control of the native (*pnat*) or the *lac* (*plac*) promoter as indicated were infiltrated into leaves of susceptible ECW, AvrBs1-responsive ECW-10R, and AvrBs3-responsive ECW-30R pepper plants. Dashed lines indicate the infiltrated areas. Disease symptoms were photographed 8 dpi. For the better visualization of the HR, leaves were bleached in ethanol 2 dpi. For *in vitro* T3S assays, bacteria were incubated in secretion medium, and equal amounts of total cell extracts (TE) and culture supernatants (SN) were analyzed by immunoblotting using antibodies specific for AvrBs3, the IM ring component HrcJ and the c-Myc epitope. For the analysis of *in vitro* T3S of AvrBs3, *X. campestris* pv. *vesicatoria* strains contained an expression construct encoding AvrBs3 under control of the *lac* promoter. **(C)** Ectopic expression of $hrcQ_C$ under control of the *lac* promoter exerts a negative effect on pathogenicity. Strain 85–10 without plasmid (–) or containing expression constructs encoding $HrcQ_C$ under control of the *lac* (*plac*) or the native (*pnat*) promoter as indicated was infiltrated into leaves of susceptible and resistant plants and plant reactions were documented as described in **(A)**. Experiments in **(A–C)** were performed three times with similar results.

strain DHM1, and bacteria were grown on indicator plates containing X-Gal and IPTG. We detected an interaction of HrcQ with itself and with $HrcQ_C$ in all possible combinations (**Figure 5A**). Given that the self-interaction of the full-length protein was detected with N-terminal T18 and T25 fusion partners, it likely did not result from the interaction

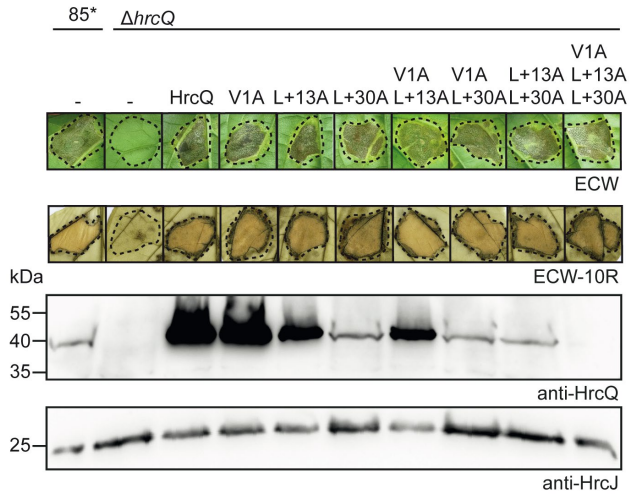

FIGURE 4 | *hrcQ* derivatives with mutations in predicted start codons restore pathogenicity in a *hrcQ* deletion mutant. Strains 85* and 85*Δ*hrcQ* without plasmid (–) or containing expression constructs encoding HrcQ and mutant derivatives thereof with mutations in predicted start sites as indicated under control of the native promoter were infiltrated into leaves of susceptible ECW and resistant ECW-10R pepper plants. Dashed lines indicate the infiltrated areas. Disease symptoms were photographed 8 dpi. For the better visualization of the HR, leaves were bleached in ethanol 2 dpi. For protein analysis, equal amounts of cell extracts were analyzed by immunoblotting using HrcQ- and HrcJ-specific antibodies. Experiments were performed three times with similar results.

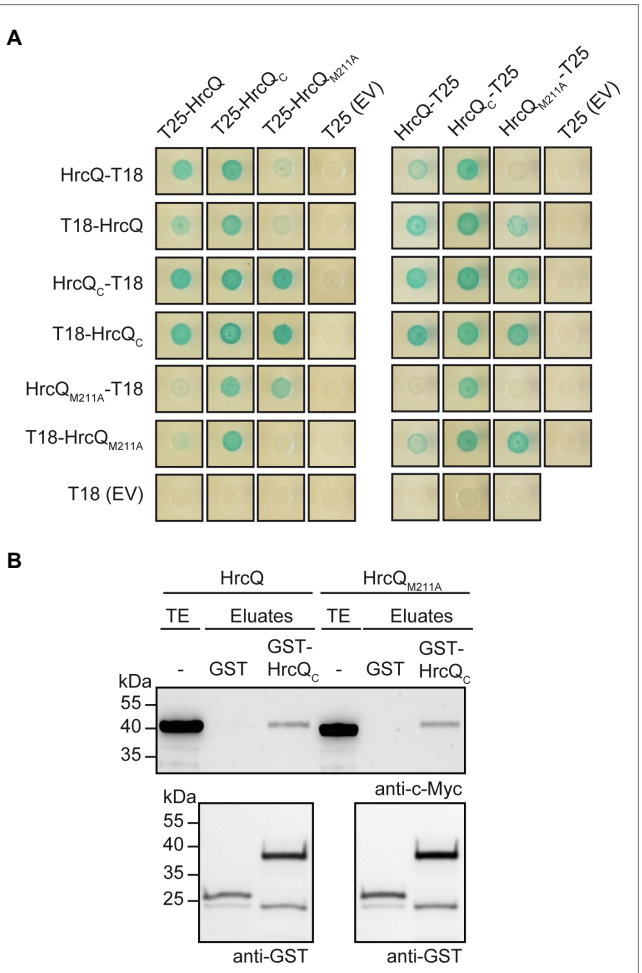

FIGURE 5 | Interaction studies with HrcQ and $HrcQ_C$. **(A)** *In vivo* interaction studies with HrcQ derivatives using the BACTH system. Expression constructs encoding T18 and T25 fusions of HrcQ, $HrcQ_{M211A}$ and $HrcQ_C$ were cotransformed into *E. coli* DHM1 cells as indicated. As controls, T18 and T25 fusions were cotransformed with the corresponding empty vectors (EV) encoding T18 or T25. Bacterial cultures were grown on indicator plates and photographs were taken after 3 days. Spots of one representative culture per interaction are shown. Cotransformations were performed three times. Four different transformants for every combination were analyzed in every experiment with similar results. All proteins were stably synthesized as is shown in **Supplementary Figure S5**. **(B)** *In vitro* interaction studies with HrcQ and $HrcQ_C$. GST and GST-$HrcQ_C$ were immobilized on glutathione sepharose and incubated with bacterial lysates containing HrcQ-c-Myc (HrcQ) or $HrcQ_{M211A}$-c-Myc ($HrcQ_{M211A}$) as indicated. Total cell extracts (TE) and eluted proteins (eluates) were analyzed by immunoblotting using c-Myc epitope- and GST-specific antibodies. Experiments were performed three times with similar results.

of two $HrcQ_C$ derivatives. When compared with the HrcQ self-interaction, the interaction of HrcQ with $HrcQ_{M211A}$ and the self-interaction of $HrcQ_{M211A}$ appeared to be reduced for several combinations (**Figure 5A**). To confirm the results of the BACTH studies, we performed *in vitro* GST pull-down assays. For this, GST and GST-$HrcQ_C$ were immobilized on a glutathione sepharose matrix and incubated with bacterial lysates containing C-terminally 3 × c-Myc epitope-tagged HrcQ and $HrcQ_{M211A}$, respectively. HrcQ-c-Myc and $HrcQ_{M211A}$-c-Myc coeluted with GST-$HrcQ_C$ but not with GST, which confirms the interaction between the full-length HrcQ protein and $HrcQ_C$ (**Figure 5B**).

We also investigated whether $HrcQ_C$ interacts with the IM ring component HrcD and the cytoplasmic HrpB4 protein. We previously identified HrcD and HrpB4 as interaction partners of HrcQ and reported that HrpB4 likely acts similarly to SctK proteins from animal pathogens as a linker between HrcQ and the cytoplasmic domain of HrcD (Otten and Büttner, 2021). In the present study, the results of BACTH assays showed that $HrcQ_C$ interacts with both HrcD and HrpB4 when analyzed as T18 or T25 fusion, suggesting a possible contribution of $HrcQ_C$ to the docking of HrcQ complexes to the IM ring (**Figures 6A,B**).

Localization Studies With Fluorescent HrcQ and $HrcQ_C$ Fusion Proteins

Next, we analyzed the contribution of the internal translation start site on complex formation by a HrcQ-sfGFP fusion protein. Previous fluorescence microscopy studies showed that a HrcQ-sfGFP reporter fusion assembles into complexes (Hausner et al., 2019). For these experiments, we used a modular expression construct containing the *hrp* gene cluster, regulatory (*hrpG** and *hrpX*) and accessory (*hpaH* and *xopA*) genes (Hausner et al., 2019). The accessory genes encoding HpaH and XopA contribute to the assembly of the T3S system in the periplasm and to efficient effector translocation, respectively (Noël et al., 2002; Hausner et al., 2017). The modular design of the construct,

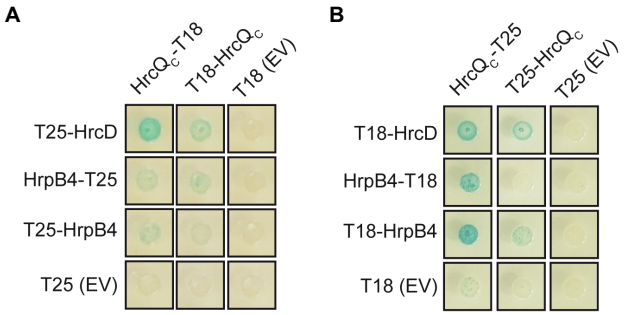

FIGURE 6 | $HrcQ_C$ interacts with HrcD and HrpB4. **(A,B)** $HrcQ_C$ interacts with HrcD and HrpB4. T25 and T18 fusions of $HrcQ_C$, HrpB4, and HrcD were cotransformed into DHM1 cells as indicated. As controls, T18 and T25 fusions were cotransformed with the corresponding empty vectors (EV) encoding T18 or T25. Bacterial cultures were grown on indicator plates and photographs were taken after 3 days. Spots of one representative culture per interaction are shown. All fusion proteins were stably synthesized as shown previously (Otten and Büttner, 2021). Cotransformations were performed three times. Four different transformants for every combination were analyzed in every experiment with similar results.

which is referred to as *hrp_HAGX* and was assembled by Golden Gate cloning from single gene and promoter modules, allows the insertion of reporter genes and the deletion of single or multiple genes of the T3S gene cluster (Hausner et al., 2019). *hrcQ-sfgfp* was inserted at position 6 of a modular T3S gene cluster lacking the native *hrcQ* gene (**Figure 7A**; **Supplementary Figure S6**). The resulting construct was analyzed in the *hrp*-deficient *X. campestris* pv. *vesicatoria* strain 85*Δ*hrp*_fs*HAGX*, which lacks the T3S gene cluster and functional *hrpG*, *hrpX*, *xopA*, and *hpaH* genes. As reported previously, the modular construct restored pathogenicity in strain 85*Δ*hrp*_fs*HAGX*, suggesting that it was functional and that HrcQ-sfGFP complemented the *hrcQ* mutant phenotype (Hausner et al., 2019; **Figure 7B**).

To analyze the influence of the internal translation start site in *hrcQ-sfgfp*, we generated modular T3S gene cluster constructs lacking the native *hrcQ* gene and containing $hrcQ_{M211A}$*-sfgfp*, $hrcQ_C$*-sfgfp* or a combination of $hrcQ_{M211A}$*-sfgfp* and $hrcQ_C$*-mKOκ* (mKusabira Orange kappa; Tsutsui et al., 2008). mKOκ is an orange fluorescent protein, used here for colocalization of HrcQ and $HrcQ_C$. *sfgfp* and *mKOκ* fusions were inserted adjacent to the *hrp* gene clusters at positions 6 and 2′ of the modular constructs (**Figure 7A**). Plant infection experiments revealed that the *hrcQ* mutant phenotype was complemented by HrcQ-sfGFP but not by $HrcQ_{M211A}$-sfGFP with respect to disease symptoms and the HR (**Figure 7B**). This is in line with the results obtained for the genomic $hrcQ_{M211A}$ mutation and confirms the finding that the M211A mutation interferes with HrcQ function (see above). Coexpression of $HrcQ_{M211A}$-sfGFP with $HrcQ_C$-mKOκ restored pathogenicity in the absence of the native *hrcQ* gene, suggesting that $HrcQ_C$ can act *in trans* as described above (**Figure 7B**). Immunoblot analysis revealed that all proteins were stably synthesized (**Figure 7C**). The M211A mutation abolished the detection of the $HrcQ_C$-sfGFP derivative and led to reduced levels of the full-length HrcQ-sfGFP protein (**Figure 7C**). Notably, wild-type protein levels of $HrcQ_{M211A}$-sfGFP were restored in the presence of $HrcQ_C$-mKOκ, suggesting that reduced stability was not caused by the M211A mutation *per se* (**Figure 7C**).

For localization studies, *X. campestris* pv. *vesicatoria* bacteria were grown under T3S-permissive conditions in minimal medium (pH 5.3) and inspected with a confocal laser scanning microscope. As observed previously, HrcQ-sfGFP formed one to four fluorescent foci per cell (**Figure 8A**; Hausner et al., 2019; Otten and Büttner, 2021). No foci were detected when the *hrpA-hpaB* operons had been replaced by dummy modules, confirming that the assembly of HrcQ-sfGFP depends on the T3S system (Hausner et al., 2019). The presence of the M211A mutation reduced foci formation by HrcQ-sfGFP (**Figure 8A**). $HrcQ_C$-sfGFP itself did not form foci in the absence of the full-length HrcQ protein (**Figure 8A**). The analysis of sfGFP and mKOκ fluorescence revealed that $HrcQ_{M211A}$-sfGFP and $HrcQ_C$-mKOκ colocalize, suggesting that HrcQ and $HrcQ_C$ are part of the same protein complex (**Figure 8A**). We, therefore, assume that $HrcQ_C$ is a component of the predicted sorting platform and promotes complex formation by HrcQ.

$HrcQ_C$ Is Part of the Predicted Sorting Platform Which Associates With the Cytoplasmic Domain of the IM Ring Component HrcD

We previously showed that efficient foci formation by HrcQ-sfGFP in *X. campestris* pv. *vesicatoria* depends on the IM ring component HrcD. Thus, in the absence of HrcD, HrcQ-sfGFP forms one bright fluorescent spot which presumably corresponds to a cytoplasmic HrcQ-containing protein complex (Otten and Büttner, 2021). HrcQ is likely attached *via* the SctK-like protein HrpB4 to the cytoplasmic N-terminal domain of the IM ring component HrcD (Otten and Büttner, 2021). To confirm this hypothesis, we deleted codons 2–92 of *hrcD* in the modular T3S gene cluster construct and analyzed the effect of this mutation on bacterial pathogenicity and on the localization of HrcQ-sfGFP, $HrcQ_{M211A}$-sfGFP and $HrcQ_C$-mKOκ.

As expected, deletion of the N-terminal domain of HrcD led to a loss of pathogenicity of strain 85*Δ*hrp*_fs*HAGX* containing corresponding modular T3S gene cluster expression constructs but did not affect the stability of HrcQ derivatives (**Supplementary Figure S7**). Fluorescence microscopy studies showed that HrcQ-sfGFP forms one bright fluorescent spot in *hrcD* deletion and $hrcD_{\Delta 2-92}$ mutant strains, suggesting that the cytoplasmic domain of HrcD is required for efficient foci formation by HrcQ-sfGFP (**Figure 8B**). To investigate whether $HrcQ_C$ is part of the cytoplasmic protein complex, we performed colocalization studies as described above with $HrcQ_{M211A}$-sfGFP and $HrcQ_C$-mKOκ. Both proteins were stably synthesized and colocalized in the absence of the cytoplasmic domain of HrcD in one fluorescent spot per cell (**Figure 8B**; **Supplementary Figure S7**). This is in agreement with the hypothesis that $HrcQ_C$ associates with HrcQ-containing protein

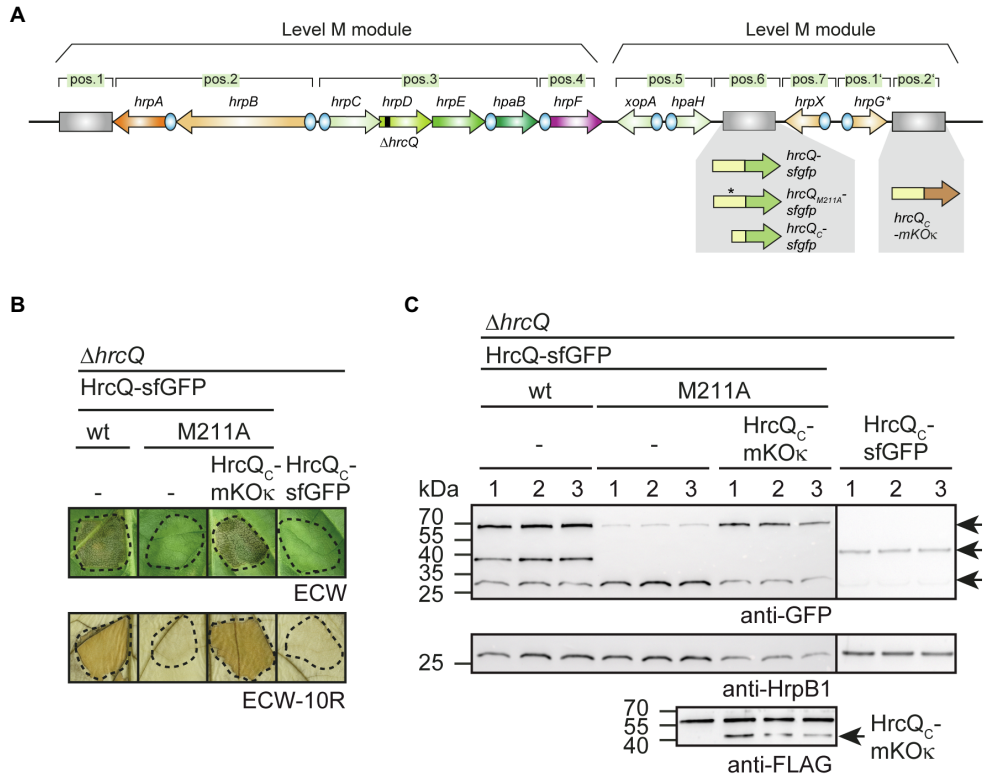

FIGURE 7 | Analysis of fluorescent HrcQ and $HrcQ_C$ fusions. **(A)** Schematic representation of the modular T3S gene cluster construct. Genes are represented by arrows, promoters by blue circles. Grey rectangles represent dummy modules that were replaced by reporter fusions such as *hrcQ-sfgfp*, $hrcQ_{M211A}$*-sfgfp*, and $hrcQ_C$*-mKO*κ as indicated. The deletion in *hrcQ* is represented by a black rectangle. The names of single operons and genes are given above the arrows. The constructs were assembled in different steps using the Golden Gate-based modular cloning technique as described previously (Hausner et al., 2019). Specific overhangs of gene or operon modules determined their positions (pos.) in the final level P constructs which were assembled from two level M modules as indicated. **(B)** Complementation studies with fluorescent HrcQ fusions. Strain 85*Δ*hrp_fs*HAGX with plasmids containing the modular T3S gene cluster with a deletion in the native *hrcQ* gene (Δ*hrcQ*) and including accessory and regulatory genes as depicted in **(A)** was used for the experiments. The modular T3S gene cluster constructs encoded HrcQ-sfGFP (wt), $HrcQ_{M211A}$-sfGFP (M211A) or $HrcQ_C$-sfGFP at position 6 and $HrcQ_C$-mKOκ at position 2' of the modular construct (depicted in **A**) as indicated and bacteria were infiltrated into leaves of susceptible ECW and resistant ECW-10R pepper plants. Dashed lines indicate the infiltrated areas. Disease symptoms were photographed 8 dpi. For the better visualization of the HR, leaves were bleached in ethanol 2 dpi. **(C)** Immunological detection of fluorescent HrcQ fusions. Three transconjugants (labeled 1, 2, and 3) of each strain described in **(B)** were cultivated in minimal medium (T3S-permissive conditions), and cell extracts were analyzed by immunoblotting using antibodies specific for GFP and HrpB1. $HrcQ_C$-mKOκ contains a C-terminal FLAG epitope and was detected using a FLAG-specific antibody. The signals corresponding to the size of HrcQ-sfGFP, $HrcQ_C$-sfGFP, and a GFP cleavage product are indicated by arrows in the upper blot. The arrow in the lower blot indicates the signal corresponding to the size of $HrcQ_C$-mKOκ. The additional signal at the size of approximately 60 kDa presumably results from unspecific binding of the antibody and is also detected in protein extracts which do not contain FLAG epitope-tagged proteins. Experiments were performed three times with similar results.

complexes and shows that the colocalization of HrcQ and $HrcQ_C$ does not depend on the docking of the HrcQ complex to the cytoplasmic domain of HrcD.

DISCUSSION

HrcQ from *X. campestris* pv. *vesicatoria* is a conserved Hrc component of the T3S system and likely involved in the assembly of the predicted cytoplasmic sorting platform. Comparative sequence analyses revealed that HrcQ shares limited sequence similarities with other HrcQ proteins and with SctQ proteins from animal-pathogenic bacteria. Notably, no similarity was detected between HrcQ and the SctQ proteins EscQ and Spa33 from EPEC and *S. flexneri*, respectively, suggesting that HrcQ and SctQ proteins are not conserved in all species (**Figure 1**). We also noticed that the N-terminal regions of HrcQ proteins from plant pathogens are highly sequence variable and differ in length. This is presumably due to different positions of the annotated translation start codons, which have not been experimentally validated in most cases (**Supplementary Figure S2**). Our findings suggest that translation of *hrcQ* from *X. campestris* pv. *vesicatoria* is initiated upstream of the annotated GTG start codon, thus resulting in a protein with 30 additional amino acids. Unexpectedly, the analysis of HrcQ derivatives with mutations in all three potential start codons revealed that the N-terminal region is dispensable for the contribution of HrcQ to pathogenicity. The finding that the N-terminal HrcQ deletion derivative was not detectable by

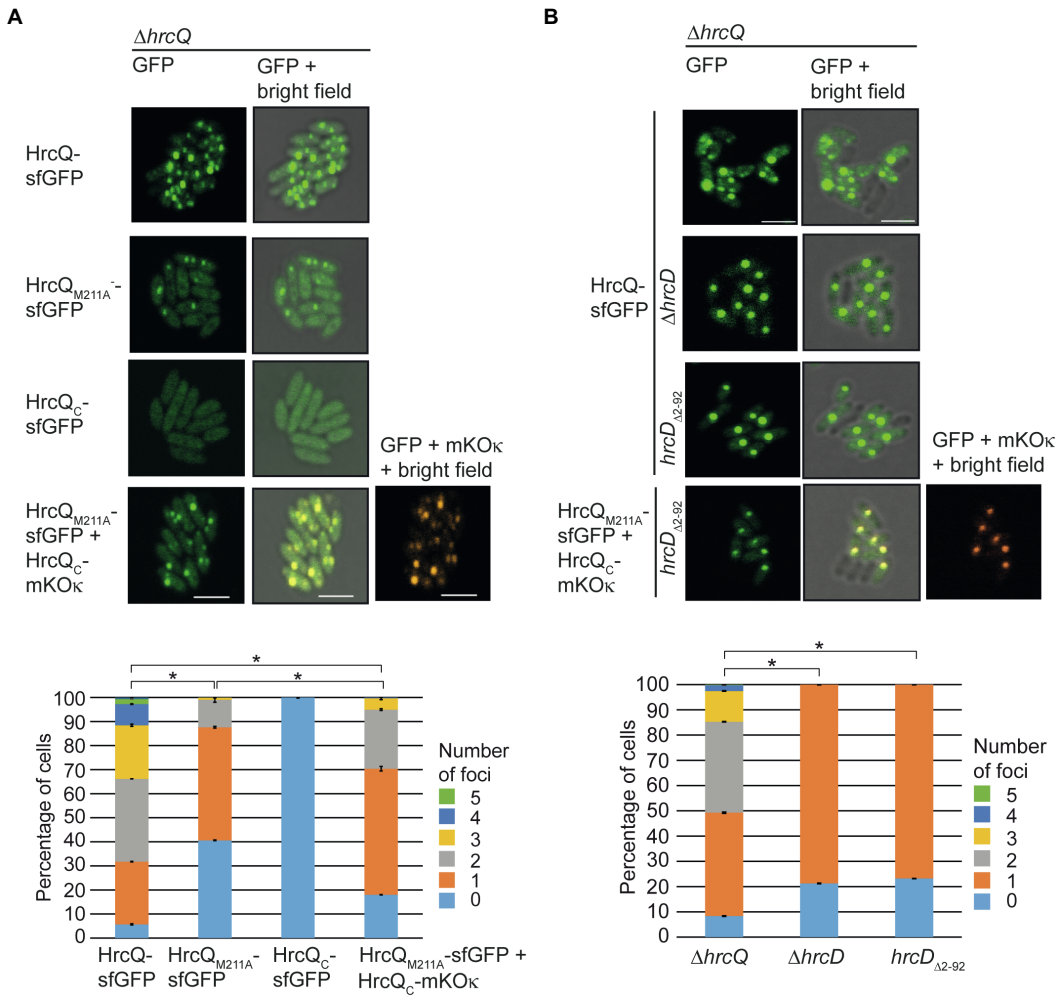

FIGURE 8 | Fluorescent fusions of HrcQ and $HrcQ_C$ colocalize independently of their association with the T3S system. **(A)** Colocalization of sfGFP fusions of $HrcQ_{M211A}$ and $HrcQ_C$. *Xanthomonas campestris* pv. *vesicatoria* strain 85*Δ*hrp*_fs*HAGX* with plasmids containing the modular T3S gene cluster, accessory, and regulatory genes with a deletion in the native *hrcQ* gene (Δ*hrcQ*) and encoding HrcQ-sfGFP, $HrcQ_{M211A}$-sfGFP, $HrcQ_C$-sfGFP, or a combination of $HrcQ_C$-sfGFP and $HrcQ_C$-mKOκ as indicated were incubated under T3S-permissive conditions and analyzed by fluorescent microscopy. One representative image for every strain is shown. The size bar corresponds to 2 μm. The pictures in the right panels result from an overlay of the signals from the fluorescent channel for GFP and/or mKOκ with the bright field images. Fluorescent foci were counted in approximately 300 cells per strain in three transconjugants. Asterisks indicate a significant difference between the number of foci in strains with a $p < 0.05$ based on the results of a chi-squared test. Experiments were performed three times with similar results with different transconjugants for each strain. The results from one representative experiment are shown. **(B)** Fluorescent fusions of $HrcQ_{M211A}$ and $HrcQ_C$ colocalize in the bacterial cytoplasm. Strain 85*Δ*hrp*_fs*HAGX* with plasmids containing the modular T3S gene cluster, accessory, and regulatory genes with a deletion in the native *hrcQ* gene (Δ*hrcQ*), additional deletions in *hrcD* (Δ*hrcD*), or codons 2–92 of *hrcD* ($hrcD_{\Delta 2\text{-}92}$) and encoding HrcQ fusion proteins as indicated was grown in secretion medium. The formation of fluorescent foci was analyzed as described in **(A)**. Experiments were performed three times with similar results.

immunoblot analysis suggests that low levels of HrcQ are sufficient to promote T3S.

We also investigated the presence of an additional internal translation start codon which was reported for the *sctQ* genes *spaO* and *ssaQ* in the SPI-1 and SPI-2 T3S gene clusters from *Salmonella* spp. (Yu et al., 2011; Bernal et al., 2019; Lara-Tejero et al., 2019) as well as for *yscQ* from *Yersinia* spp. (Bzymek et al., 2012; Diepold et al., 2015) and *spa33* from *S. flexneri* (McDowell et al., 2016; Kadari et al., 2019). The analysis of mutant HrcQ derivatives showed that the ATG codon at position 211 is required for the detection of the additional *hrcQ* translation product, suggesting that this codon serves as internal translation start site leading to the synthesis of $HrcQ_C$ (**Figure 2**). Notably, complementation studies revealed that expression of $hrcQ_{M211A}$ *in trans* restored pathogenicity in *hrcQ* deletion mutants when analyzed in strains which constitutively expressed the T3S genes in the presence of HrpG*, a mutant derivative of the key regulator HrpG. In contrast, no complementation was observed in *hrpG* wild-type strains and when $hrcQ_{M211A}$ was expressed either *in cis* as a single copy gene or coexpressed with the T3S genes on the same plasmid (**Figures 2, 3, 7**). This suggests that the loss of internal translation initiation can be compensated by increased expression levels of $HrcQ_{M211A}$ and T3S system components

and points to a role of $HrcQ_C$ as accessory rather than essential structural component of the T3S system.

In animal-pathogenic bacteria, truncated translation products of *sctQ* genes likely act as accessory proteins or essential structural components of the T3S system. Mutations of the internal translation start sites in *spaO* and *ssaQ* encoded in the SPI-1 and SPI-2 clusters from *Salmonella* spp., respectively, did not abolish T3S, suggesting that $SpaO_C$ and $SsaQ_C$ are not essential for the activity of the T3S system (Yu et al., 2011; Bernal et al., 2019). Notably, however, low levels of $SpaO_C$, which presumably resulted from proteolysis, were still produced when the internal start codon was mutated and could be sufficient to restore T3S (Bernal et al., 2019; Lara-Tejero et al., 2019). In contrast to the findings reported for SpaO and SsaQ, mutations of the internal translation start sites in *yscQ* from *Yersinia* spp. and *spa33* from *S. flexneri* abrogated T3S (Bzymek et al., 2012; McDowell et al., 2016). This points to an essential role of $YscQ_C$ and $Spa33_C$ in T3S. It should, however, be noted that mutations in the internal start codons of *sctQ* genes from *Salmonella* spp., *Yersinia* spp., and *S. flexneri* were introduced into the genome by allelic exchange (Bzymek et al., 2012; Diepold et al., 2015; McDowell et al., 2016; Lara-Tejero et al., 2019). It would be interesting to investigate whether enhanced expression of T3S genes in combination with expression of *sctQ* mutant derivatives *in trans* could restore T3S in *Yersinia* spp. and *S. flexneri* $sctQ_C$ mutant strains as observed in *X. campestris* pv. *vesicatoria hrpG** strains upon expression of $hrcQ_{M211A}$ *in trans*.

In the present study, immunoblot analysis of protein extracts revealed that the M211A mutation led to decreased HrcQ levels, suggesting that $HrcQ_C$ stabilizes the full-length HrcQ protein (**Figures 2, 3**). The effect of the M211A mutation on protein function and HrcQ stability was likely due to the absence of internal translation initiation and not caused by an effect of the mutation *per se* on protein folding or stability because pathogenicity in $hrcQ_{M211A}$ mutant strains was restored upon expression of $hrcQ_C$ *in trans* (**Figure 3**). Furthermore, wild-type levels of $HrcQ_{M211A}$ derivatives were restored upon separate expression of $hrcQ_C$, suggesting that $HrcQ_C$ stabilizes the full-length HrcQ protein (**Figure 7**). These findings demonstrate that $HrcQ_C$ is functional when encoded by a separate gene and might act as a chaperone for the full-length HrcQ protein as was proposed for $SpaO_C$ and $SsaQ_C$ from *Salmonella* which stabilize the respective full-length proteins (Yu et al., 2011; Bernal et al., 2019; Lara-Tejero et al., 2019). A predicted role of $HrcQ_C$ as a chaperone for HrcQ is in line with the finding that $HrcQ_C$ interacts with the full-length HrcQ protein and with itself (**Figure 5**). It remains to be investigated whether HrcQ and $HrcQ_C$ form a heterotrimeric complex as was reported for the full-length and C-terminal translation products of *spaO* (Bernal et al., 2019), *yscQ* (Bzymek et al., 2012) and *spa33* (McDowell et al., 2016). $HrcQ_C$ contains a SPOA (surface presentation of antigen) domain which was also identified in SctQ proteins from animal-pathogenic bacteria and is likely involved in protein–protein interactions including homo-dimerization (Bzymek et al., 2012; Notti et al., 2015; McDowell et al., 2016; Bernal et al., 2019; Lara-Tejero et al., 2019).

To localize $HrcQ_C$ and to analyze whether it is required for the assembly of HrcQ complexes, we performed fluorescence microscopy studies with HrcQ, $HrcQ_{M211A,}$ and $HrcQ_C$ as fusion partners of sfGFP or mKOk. Our studies showed that HrcQ and $HrcQ_C$ colocalize and that a $HrcQ_C$-sfGFP fusion did not form fluorescent foci in the absence of the full-length HrcQ protein (**Figure 8**). This suggests that the integration of $HrcQ_C$ into the predicted sorting platform depends on HrcQ. Given that mutation of the internal translation start site reduced but did not abolish foci formation by a fluorescent HrcQ fusion, $HrcQ_C$ likely promotes the assembly or association of HrcQ complexes with the T3S system but is not an essential component of the predicted sorting platform. Thus, the contribution of $HrcQ_C$ to T3S differs from that of $YscQ_C$ from *Yersinia* spp. which is likely an essential structural component of the sorting platform (Diepold et al., 2015). Similarly to $YscQ_C$, $SpaO_C$ from *Salmonella* spp. is essential for the efficient assembly of the sorting platform of the T3S system (Lara-Tejero et al., 2019). Notably, however, $SpaO_C$ associates with soluble sorting platform subcomplexes but does not colocalize with the assembled final complex, suggesting that it stabilizes SpaO prior to its integration into the sorting platform (Bernal et al., 2019; Lara-Tejero et al., 2019). We predict a similar chaperone-like function for $HrcQ_C$; however, in contrast to $SpaO_C$, $HrcQ_C$ remains associated with the predicted sorting platform and might facilitate its assembly or docking to the membrane-spanning secretion apparatus.

Previous analysis of HrcQ-sfGFP in different *X. campestris* pv. *vesicatoria* mutant strains revealed that the HrcQ complex likely associates with the IM ring component HrcD *via* the linker protein HrpB4, which acts similarly to SctK proteins from animal pathogens. HrpB4 interacts with both HrcQ and HrcD and contributes to foci formation by HrcQ-sfGFP (Otten and Büttner, 2021). The interaction of HrpB4 with HrcD depends on the cytoplasmic N-terminal domain of HrcD which presumably provides the docking site for HrpB4 (Otten and Büttner, 2021). In contrast to the essential role of SctK proteins from animal-pathogenic bacteria, however, HrpB4 only contributes to the docking of HrcQ complexes to the T3S system, suggesting that HrcQ can directly associate with HrcD in the absence of HrpB4 (Otten and Büttner, 2021). In agreement with this hypothesis, we previously detected an interaction between HrcQ and HrcD which likely depends on the cytoplasmic domain of HrcD (Otten and Büttner, 2021). In the present study, we observed that both HrcD and HrpB4 also interact with $HrcQ_C$, suggesting that $HrcQ_C$ contributes to the association of the predicted sorting platform with the T3S system (**Figure 6**).

The docking of HrcQ complexes to the T3S system depends on HrcD because HrcQ-sfGFP accumulates in the cytoplasm resulting in one bright fluorescent spot in the absence of HrcD or the cytoplasmic domain of HrcD (Otten and Büttner, 2021; **Figure 8**). Given that HrcQ and $HrcQ_C$ still colocalize in *hrcD* mutant strains, the assembly of the predicted HrcQ-$HrcQ_C$-containing complex does not depend on the association of HrcQ with the IM ring. We, therefore, assume that $HrcQ_C$ is an integral component of the predicted cytoplasmic sorting platform, even when it is detached from the T3S system. Taken together, we conclude from our findings that $HrcQ_C$

stabilizes HrcQ and integrates together with HrcQ into the predicted cytoplasmic sorting platform.

DATA AVAILABILITY STATEMENT

The original contributions presented in the study are included in the article/**Supplementary Material**, further inquiries can be directed to the corresponding author.

AUTHOR CONTRIBUTIONS

CO, TS, JH, and DB designed and performed the research and analyzed the data. CO wrote the manuscript and reviewed the text. DB wrote the manuscript and obtained the funding. All authors contributed to the article and approved the submitted version.

FUNDING

This study was supported by grants from the Deutsche Forschungsgemeinschaft (BU2145/9-1 and BU2145/10-1) to DB.

ACKNOWLEDGMENTS

We thank Ulla Bonas for helpful comments on the manuscript, Matthias Jordan for technical assistance, and the DFG for funding.

SUPPLEMENTARY MATERIAL

The Supplementary Material for this article can be found online at: https://www.frontiersin.org/articles/10.3389/fmicb.2021.752733/full#supplementary-material

REFERENCES

Abby, S. S., and Rocha, E. P. (2012). The non-flagellar type III secretion system evolved from the bacterial flagellum and diversified into host-cell adapted systems. *PLoS Genet.* 8:e1002983. doi: 10.1371/journal.pgen.1002983

Ausubel, F. M., Brent, R., Kingston, R. E., Moore, D. D., Seidman, J. G., Smith, J. A., et al. (eds.) (1996). *Current Protocols in Molecular Biology*. New York, NY: Wiley.

Battesti, A., and Bouveret, E. (2012). The bacterial two-hybrid system based on adenylate cyclase reconstitution in *Escherichia coli*. *Methods* 58, 325–334. doi: 10.1016/j.ymeth.2012.07.018

Belinky, F., Rogozin, I. B., and Koonin, E. V. (2017). Selection on start codons in prokaryotes and potential compensatory nucleotide substitutions. *Sci. Rep.* 7:12422. doi: 10.1038/s41598-017-12619-6

Bernal, I., Bornicke, J., Heidemann, J., Svergun, D., Horstmann, J. A., Erhardt, M., et al. (2019). Molecular organization of soluble type III secretion system sorting platform complexes. *J. Mol. Biol.* 431, 3787–3803. doi: 10.1016/j.jmb.2019.07.004

Büttner, D. (2012). Protein export according to schedule – architecture, assembly and regulation of type III secretion systems from plant and animal pathogenic bacteria. *Microbiol. Mol. Biol. Rev.* 76, 262–310. doi: 10.1128/MMBR.05017-11

Büttner, D. (2016). Behind the lines - actions of bacterial type III effector proteins in plant cells. *FEMS Microbiol. Rev.* 40, 894–937. doi: 10.1093/femsre/fuw026

Büttner, D., and Bonas, U. (2010). Regulation and secretion of *Xanthomonas* virulence factors. *FEMS Microbiol. Rev.* 34, 107–133. doi: 10.1111/j.1574-6976.2009.00192.x

Büttner, D., and He, S. Y. (2009). Type III protein secretion in plant pathogenic bacteria. *Plant Physiol.* 150, 1656–1664. doi: 10.1104/pp.109.139089

Bzymek, K. P., Hamaoka, B. Y., and Ghosh, P. (2012). Two translation products of *Yersinia yscQ* assemble to form a complex essential to type III secretion. *Biochemistry* 51, 1669–1677. doi: 10.1021/bi201792p

Daniels, M. J., Barber, C. E., Turner, P. C., Cleary, W. G., and Sawczyc, M. K. (1984). Isolation of mutants of *Xanthomonas campestris* pathovar *campestris* showing altered pathogenicity. *J. Gen. Microbiol.* 130, 2447–2455.

Dean, P. (2011). Functional domains and motifs of bacterial type III effector proteins and their roles in infection. *FEMS Microbiol. Rev.* 35, 1100–1125. doi: 10.1111/j.1574-6976.2011.00271.x

Deng, W., Marshall, N. C., Rowland, J. L., McCoy, J. M., Worrall, L. J., Santos, A. S., et al. (2017). Assembly, structure, function and regulation of type III secretion systems. *Nat. Rev. Microbiol.* 15, 323–337. doi: 10.1038/nrmicro.2017.20

Dey, S., Chakravarty, A., Guha Biswas, P., and De Guzman, R. N. (2019). The type III secretion system needle, tip, and translocon. *Protein Sci.* 28, 1582–1593. doi: 10.1002/pro.3682

Diepold, A. (2020). Assembly and post-assembly turnover and dynamics in the type III secretion system. *Curr. Top. Microbiol. Immunol.* 427, 35–66. doi: 10.1007/82_2019_164

Diepold, A., Amstutz, M., Abel, S., Sorg, I., Jenal, U., and Cornelis, G. R. (2010). Deciphering the assembly of the *Yersinia* type III secretion injectisome. *EMBO J.* 29, 1928–1940. doi: 10.1038/emboj.2010.84

Diepold, A., Kudryashev, M., Delalez, N. J., Berry, R. M., and Armitage, J. P. (2015). Composition, formation, and regulation of the cytosolic c-ring, a dynamic component of the type III secretion injectisome. *PLoS Biol.* 13:e1002039. doi: 10.1371/journal.pbio.1002039

Diepold, A., Sezgin, E., Huseyin, M., Mortimer, T., Eggeling, C., and Armitage, J. P. (2017). A dynamic and adaptive network of cytosolic interactions governs protein export by the T3SS injectisome. *Nat. Commun.* 8:15940. doi: 10.1038/ncomms15940

Dietsche, T., Tesfazgi Mebrhatu, M., Brunner, M. J., Abrusci, P., Yan, J., Franz-Wachtel, M., et al. (2016). Structural and functional characterization of the bacterial type III secretion export apparatus. *PLoS Pathog.* 12:e1006071. doi: 10.1371/journal.ppat.1006071

Engler, C., Kandzia, R., and Marillonnet, S. (2008). A one pot, one step, precision cloning method with high throughput capability. *PLoS One* 3:e3647. doi: 10.1371/journal.pone.0003647

Fadouloglou, V. E., Tampakaki, A. P., Glykos, N. M., Bastaki, M. N., Hadden, J. M., Phillips, S. E., et al. (2004). Structure of HrcQB-C, a conserved component of the bacterial type III secretion systems. *Proc. Natl. Acad. Sci. U. S. A.* 101, 70–75. doi: 10.1073/pnas.0304579101

Gazi, A. D., Bastaki, M., Charova, S. N., Gkougkoulia, E. A., Kapellios, E. A., Panopoulos, N. J., et al. (2008). Evidence for a coiled-coil interaction mode of disordered proteins from bacterial type III secretion systems. *J. Biol. Chem.* 283, 34062–34068. doi: 10.1074/jbc.M803408200

Gill, U. S., Lee, S., and Mysore, K. S. (2015). Host versus nonhost resistance: distinct wars with similar arsenals. *Phytopathology* 105, 580–587. doi: 10.1094/PHYTO-11-14-0298-RVW

Habenstein, B., El Mammeri, N., Tolchard, J., Lamon, G., Tawani, A., Berbon, M., et al. (2020). Structures of type III secretion system needle filaments. *Curr. Top. Microbiol. Immunol.* 427, 109–131. doi: 10.1007/82_2019_192

Hausner, J., Hartmann, N., Jordan, M., and Büttner, D. (2017). The predicted lytic transglycosylase HpaH from *Xanthomonas campestris* pv. *vesicatoria* associates with the type III secretion system and promotes effector protein translocation. *Infect. Immun.* 85:e00788-16. doi: 10.1128/IAI.00788-16

Hausner, J., Jordan, M., Otten, C., Marillonnet, S., and Büttner, D. (2019). Modular cloning of the type III secretion gene cluster from the plant-pathogenic bacterium *Xanthomonas euvesicatoria*. *ACS Synth. Biol.* 8, 532–547. doi: 10.1021/acssynbio.8b00434

Hu, B., Lara-Tejero, M., Kong, Q., Galan, J. E., and Liu, J. (2017). In situ molecular architecture of the *Salmonella* type III secretion machine. *Cell* 168, 1065.e1010–1074.e1010. doi: 10.1016/j.cell.2017.02.022

Hueck, C. J. (1998). Type III protein secretion systems in bacterial pathogens of animals and plants. *Microbiol. Mol. Biol. Rev.* 62, 379–433. doi: 10.1128/MMBR.62.2.379-433.1998

Huguet, E., Hahn, K., Wengelnik, K., and Bonas, U. (1998). *hpaA* mutants of *Xanthomonas campestris* pv. *vesicatoria* are affected in pathogenicity but retain the ability to induce host-specific hypersensitive reaction. *Mol. Microbiol.* 29, 1379–1390.

Johnson, S., Kuhlen, L., Deme, J. C., Abrusci, P., and Lea, S. M. (2019). The structure of an injectisome export gate demonstrates conservation of architecture in the core export gate between flagellar and virulence type III secretion systems. *mBio* 10:e00818-19. doi: 10.1128/mBio.00818-19

Jones, J. D., and Dangl, J. L. (2006). The plant immune system. *Nature* 444, 323–329. doi: 10.1038/nature05286

Jones, J. B., Lacy, G. H., Bouzar, H., Stall, R. E., and Schaad, N. W. (2004). Reclassification of the xanthomonads associated with bacterial spot disease of tomato and pepper. *Syst. Appl. Microbiol.* 27, 755–762. doi: 10.1078/0723202042369884

Kadari, M., Lakhloufi, D., Delforge, V., Imbault, V., Communi, D., Smeesters, P., et al. (2019). Multiple proteins arising from a single gene: the role of the Spa33 variants in *Shigella* T3SS regulation. *Microbiology* 8:e932. doi: 10.1002/mbo3.932

Karimova, G., Pidoux, J., Ullmann, A., and Ladant, D. (1998). A bacterial two-hybrid system based on a reconstituted signal transduction pathway. *Proc. Natl. Acad. Sci. U. S. A.* 95, 5752–5756.

Knoop, V., Staskawicz, B., and Bonas, U. (1991). Expression of the avirulence gene *avrBs3* from *Xanthomonas campestris* pv. *vesicatoria* is not under the control of *hrp* genes and is independent of plant factors. *J. Bacteriol.* 173, 7142–7150. doi: 10.1128/jb.173.22.7142-7150.1991

Kousik, C. S., and Ritchie, D. F. (1998). Response of bell pepper cultivars to bacterial spot pathogen races that individually overcome major resistance genes. *Plant Dis.* 82, 181–186. doi: 10.1094/PDIS.1998.82.2.181

Kuhlen, L., Abrusci, P., Johnson, S., Gault, J., Deme, J., Caesar, J., et al. (2018). Structure of the core of the type III secretion system export apparatus. *Nat. Struct. Mol. Biol.* 25, 583–590. doi: 10.1038/s41594-018-0086-9

Lara-Tejero, M. (2019). The type III secretion system sorting platform. *Curr. Top. Microbiol. Immunol.* 427, 133–142. doi: 10.1007/82_2019_167

Lara-Tejero, M., and Galan, J. E. (2019). The injectisome, a complex nanomachine for protein injection into mammalian cells. *EcoSal Plus* 8, 245–259. doi: 10.1128/ecosalplus.ESP-0039-2018

Lara-Tejero, M., Qin, Z., Hu, B., Butan, C., Liu, J., and Galan, J. E. (2019). Role of SpaO in the assembly of the sorting platform of a *Salmonella* type III secretion system. *PLoS Pathog.* 15:e1007565. doi: 10.1371/journal.ppat.1007565

Lorenz, C., Hausner, J., and Büttner, D. (2012). HrcQ provides a docking site for early and late type III secretion substrates from *Xanthomonas*. *PLoS One* 7:e51063. doi: 10.1371/journal.pone.0051063

Mattei, P. J., Faudry, E., Job, V., Izore, T., Attree, I., and Dessen, A. (2011). Membrane targeting and pore formation by the type III secretion system translocon. *FEBS J.* 278, 414–426. doi: 10.1111/j.1742-4658.2010.07974.x

McDowell, M. A., Marcoux, J., McVicker, G., Johnson, S., Fong, Y. H., Stevens, R., et al. (2016). Characterisation of *Shigella* Spa33 and *Thermotoga* FliM/N reveals a new model for C-ring assembly in T3SS. *Mol. Microbiol.* 99, 749–766. doi: 10.1111/mmi.13267

Miletic, S., Fahrenkamp, D., Goessweiner-Mohr, N., Wald, J., Pantel, M., Vesper, O., et al. (2021). Substrate-engaged type III secretion system structures reveal gating mechanism for unfolded protein translocation. *Nat. Commun.* 12:1546. doi: 10.1038/s41467-021-21143-1

Milne-Davies, B., Wimmi, S., and Diepold, A. (2021). Adaptivity and dynamics in type III secretion systems. *Mol. Microbiol.* 115, 395–411. doi: 10.1111/mmi.14658

Minamino, T., Kinoshita, M., and Namba, K. (2019). Directional switching mechanism of the bacterial flagellar motor. *Comput. Struct. Biotechnol. J.* 17, 1075–1081. doi: 10.1016/j.csbj.2019.07.020

Minsavage, G. V., Dahlbeck, D., Whalen, M. C., Kearny, B., Bonas, U., Staskawicz, B. J., et al. (1990). Gene-for-gene relationships specifying disease resistance in *Xanthomonas campestris* pv. *vesicatoria* – pepper interactions. *Mol. Plant-Microbe Interact.* 3, 41–47. doi: 10.1094/MPMI-3-041

Noël, L., Thieme, F., Nennstiel, D., and Bonas, U. (2002). Two novel type III system-secreted proteins of *Xanthomonas campestris* pv. *vesicatoria* are encoded within the *hrp* pathogenicity island. *J. Bacteriol.* 184, 1340–1348. doi: 10.1128/JB.184.5.1340-1348.2002

Notti, R. Q., Bhattacharya, S., Lilic, M., and Stebbins, C. E. (2015). A common assembly module in injectisome and flagellar type III secretion sorting platforms. *Nat. Commun.* 6:7125. doi: 10.1038/ncomms8125

Otten, C., and Büttner, D. (2021). HrpB4 from *Xanthomonas campestris* pv. *vesicatoria* acts similarly to SctK proteins and promotes the docking of the predicted sorting platform to the type III secretion system. *Cell. Microbiol.* 23:e13327. doi: 10.1111/cmi.13327

Rocha, J. M., Richardson, C. J., Zhang, M., Darch, C. M., Cai, E., Diepold, A., et al. (2018). Single-molecule tracking in live *Yersinia enterocolitica* reveals distinct cytosolic complexes of injectisome subunits. *Integr. Biol.* 10, 502–515. doi: 10.1039/C8IB00075A

Römer, P., Strauss, T., Hahn, S., Scholze, H., Morbitzer, R., Grau, J., et al. (2009). Recognition of AvrBs3-like proteins is mediated by specific binding to promoters of matching pepper *Bs3* alleles. *Plant Physiol.* 150, 1697–1712. doi: 10.1104/pp.109.139931

Rossier, O., Van den Ackerveken, G., and Bonas, U. (2000). HrpB2 and HrpF from *Xanthomonas* are type III-secreted proteins and essential for pathogenicity and recognition by the host plant. *Mol. Microbiol.* 38, 828–838. doi: 10.1046/j.1365-2958.2000.02173.x

Schulte, R., and Bonas, U. (1992). Expression of the *Xanthomonas campestris* pv. *vesicatoria hrp* gene cluster, which determines pathogenicity and hypersensitivity on pepper and tomato, is plant inducible. *J. Bacteriol.* 174, 815–823. doi: 10.1128/jb.174.3.815-823.1992

Singh, N., and Wagner, S. (2019). Investigating the assembly of the bacterial type III secretion system injectisome by *in vivo* photocrosslinking. *Int. J. Med. Microbiol.* 309:151331. doi: 10.1016/j.ijmm.2019.151331

Tachiyama, S., Chang, Y., Muthuramalingam, M., Hu, B., Barta, M. L., Picking, W. L., et al. (2019). The cytoplasmic domain of MxiG interacts with MxiK and directs assembly of the sorting platform in the *Shigella* type III secretion system. *J. Biol. Chem.* 294, 19184–19196. doi: 10.1074/jbc.RA119.009125

Tamir-Ariel, D., Navon, N., and Burdman, S. (2007). Identification of genes in *Xanthomonas campestris* pv. *vesicatoria* induced during its interaction with tomato. *J. Bacteriol.* 189, 6359–6371. doi: 10.1128/JB.00320-07

Timilsina, S., Potnis, N., Newberry, E. A., Liyanapathiranage, P., Iruegas-Bocardo, F., White, F. F., et al. (2020). *Xanthomonas* diversity, virulence and plant-pathogen interactions. *Nat. Rev. Microbiol.* 18, 415–427. doi: 10.1038/s41579-020-0361-8

Tsutsui, H., Karasawa, S., Okamura, Y., and Miyawaki, A. (2008). Improving membrane voltage measurements using FRET with new fluorescent proteins. *Nat. Methods* 5, 683–685. doi: 10.1038/nmeth.1235

Wagner, S., and Diepold, A. (2020). A unified nomenclature for injectisome-type type III secretion systems. *Curr. Top. Microbiol. Immunol.* 427, 1–10. doi: 10.1007/82_2020_210

Wagner, S., Grin, I., Malmsheimer, S., Singh, N., Torres-Vargas, C. E., and Westerhausen, S. (2018). Bacterial type III secretion systems: a complex device for the delivery of bacterial effector proteins into eukaryotic host cells. *FEMS Microbiol. Lett.* 365:fny201. doi: 10.1093/femsle/fny201

Wengelnik, K., and Bonas, U. (1996). HrpXv, an AraC-type regulator, activates expression of five of the six loci in the *hrp* cluster of *Xanthomonas campestris* pv. *vesicatoria*. *J. Bacteriol.* 178, 3462–3469. doi: 10.1128/jb.178.12.3462-3469.1996

Wengelnik, K., Rossier, O., and Bonas, U. (1999). Mutations in the regulatory gene *hrpG* of *Xanthomonas campestris* pv. *vesicatoria* result in constitutive expression of all *hrp* genes. *J. Bacteriol.* 181, 6828–6831. doi: 10.1128/JB.181.21.6828-6831.1999

Wengelnik, K., Van den Ackerveken, G., and Bonas, U. (1996). HrpG, a key *hrp* regulatory protein of *Xanthomonas campestris* pv. *vesicatoria* is homologous to two-component response regulators. *Mol. Plant-Microbe Interact.* 9, 704–712. doi: 10.1094/MPMI-9-0704

Wimmi, S., Balinovic, A., Jeckel, H., Selinger, L., Lampaki, D., Eisemann, E., et al. (2021). Dynamic relocalization of cytosolic type III secretion system components prevents premature protein secretion at low external pH. *Nat. Commun.* 12:1625. doi: 10.1038/s41467-021-23080-5

Yu, X. J., Liu, M., Matthews, S., and Holden, D. W. (2011). Tandem translation generates a chaperone for the *Salmonella* type III secretion system protein SsaQ. *J. Biol. Chem.* 286, 36098–36107. doi: 10.1074/jbc.M111.278663

Zhang, Y., Lara-Tejero, M., Bewersdorf, J., and Galan, J. E. (2017). Visualization and characterization of individual type III protein secretion machines in live bacteria. *Proc. Natl. Acad. Sci. U. S. A.* 114, 6098–6103. doi: 10.1073/pnas.1705823114

Zilkenat, S., Franz-Wachtel, M., Stierhof, Y. D., Galan, J. E., Macek, B., and Wagner, S. (2016). Determination of the stoichiometry of the complete bacterial type III secretion needle complex using a combined quantitative proteomic approach. *Mol. Cell. Proteomics* 15, 1598–1609. doi: 10.1074/mcp.M115.056598

Conflict of Interest: The authors declare that the research was conducted in the absence of any commercial or financial relationships that could be construed as a potential conflict of interest.

Publisher's Note: All claims expressed in this article are solely those of the authors and do not necessarily represent those of their affiliated organizations, or those of the publisher, the editors and the reviewers. Any product that may be evaluated in this article, or claim that may be made by its manufacturer, is not guaranteed or endorsed by the publisher.

frontiers in Microbiology

ORIGINAL RESEARCH
published: 02 November 2021
doi: 10.3389/fmicb.2021.760873

The Cytoplasmic Domains of *Streptococcus mutans* Membrane Protein Insertases YidC1 and YidC2 Confer Unique Structural and Functional Attributes to Each Paralog

*Surabhi Mishra and L. Jeannine Brady**

Department of Oral Biology, University of Florida, Gainesville, FL, United States

Integral and membrane-anchored proteins are pivotal to survival and virulence of the dental pathogen, *Streptococcus mutans*. The bacterial chaperone/insertase, YidC, contributes to membrane protein translocation. Unlike *Escherichia coli,* most Gram-positive bacteria contain two YidC paralogs. Herein, we evaluated structural features that functionally delineate *S. mutans* YidC1 and YidC2. Bacterial YidCs contain five transmembrane domains (TMD), two cytoplasmic loops, and a cytoplasmic tail. Because *S. mutans* YidC1 (SmYidC1) and YidC2 (SmYidC2) cytoplasmic domains (CD) are less well conserved than are TMD, we engineered ectopic expression of the 14 possible YidC1-YidC2 CD domain swap combinations. Growth and stress tolerance of each was compared to control strains ectopically expressing unmodified *yidC1* or *yidC2*. Acid and osmotic stress sensitivity are associated with *yidC2* deletion. Sensitivity to excess zinc was further identified as a Δ*yidC1* phenotype. Overall, YidC1 tolerated CD substitutions better than YidC2. Preferences toward particular CD combinations suggested potential intramolecular interactions. *In silico* analysis predicted salt-bridges between C1 and C2 loops of YidC1, and C1 loop and C-terminal tail of YidC2, respectively. Mutation of contributing residues recapitulated Δ*yidC1*- and Δ*yidC2*-associated phenotypes. Taken together, this work revealed the importance of cytoplasmic domains in distinct functional attributes of YidC1 and YidC2, and identified key residues involved in interdomain interactions.

Keywords: structure-function, *YidC*, *Streptococcus mutans*, insertase, paralogs, bacterial stress tolerance

OPEN ACCESS

Edited by:
Ignacio Arechaga, University of Cantabria, Spain

Reviewed by:
Yoshihiro Yamaguchi, Osaka City University, Japan
Etana Padan, Hebrew College, United States

****Correspondence:***
L. Jeannine Brady
jbrady@dental.ufl.edu

Specialty section:
This article was submitted to Microbial Physiology and Metabolism, a section of the journal Frontiers in Microbiology

Received: *18 August 2021*
Accepted: *30 September 2021*
Published: *02 November 2021*

Citation:
Mishra S and Brady LJ (2021) The Cytoplasmic Domains of Streptococcus mutans Membrane Protein Insertases YidC1 and YidC2 Confer Unique Structural and Functional Attributes to Each Paralog. Front. Microbiol. 12:760873. doi: 10.3389/fmicb.2021.760873

INTRODUCTION

The Gram-positive oral pathogen *Streptococcus mutans* is a leading cause of dental caries (Hamada and Slade, 1980), with certain strains also associated with bacterial endocarditis (Lockwood et al., 1974; McGhie et al., 1977; Moore et al., 1977; Smith et al., 1977; Vose et al., 1987; Nomura et al., 2006). This species' ability to rapidly utilize available dietary sugars and produce large amounts of acids, coupled with high tolerance to numerous environmental stressors, gives it a competitive advantage among its co-colonizers in the oral cavity. In addition, an ability to form robust biofilms, a high level of genetic competence enabling robust adaptability, and production of anti-microbial compounds such as mutacins contribute to its pathogenic potential [reviewed in

Lemos et al. (2019)]. Most known virulence attributes of *S. mutans* stem from secreted or integral membrane proteins. Thus, a more complete understanding of the components of *S. mutans* protein translocation and integral membrane insertion pathways is of significant interest.

Membrane biogenesis in bacteria is largely a co-translational process that involves the signal recognition particle (SRP) pathway working in conjunction with the SecYEG translocon and/or a membrane protein insertase called YidC [reviewed in Koch et al. (2003) and Steinberg et al. (2018)]. YidC is ubiquitously present in all three domains of life and belongs to the Oxa/Alb/YidC family of insertases found in mitochondria, chloroplasts, and bacteria, respectively. Most details related to membrane biogenesis in bacteria, including contributions by YidC, have come from research in the model Gram-negative bacterium *Escherichia coli* (Samuelson et al., 2000; Scotti et al., 2000; Urbanus et al., 2001; van Bloois et al., 2004; van der Laan et al., 2004; Yi et al., 2004; Price et al., 2010; Kumazaki et al., 2014b). However, Gram-positive bacteria differ from their Gram-negative counterparts both in terms of the composition of the translocation machinery and the essentiality of individual components for survival [reviewed in Lewis and Brady (2015)]. Three key distinctions that differentiate the protein translocation machinery of Gram-positive bacteria from Gram-negative bacteria include: 1) the non-essentiality of the SRP components, Ffh, scRNA, and/or the SRP receptor FtsY, 2) the presence of two or sometimes more paralogs of YidC in Gram-positive bacteria that can be eliminated individually without lethality, and 3) the presence of an accessory SRP protein, YlxM (Hasona et al., 2005; Williams et al., 2014). Phenotypic characterization of *S. mutans* mutants has revealed overlapping features of SRP- and YidC2-deficient strains, with both being growth impaired under environmental stress (acid/osmotic/oxidative) as well as non-stress conditions. In contrast, a Δ*yidC1* mutant has previously shown no obvious growth or stress-sensitivity phenotype (Hasona et al., 2005; Palmer et al., 2012). Combinatorial deletion of *ffh* and *yidC2*, or *yidC1* and *yidC2,* is lethal in *S. mutans,* while a Δ*ffh*/Δ*yidC1* double deletion strain survives suggesting that the presence of YidC2 alone can confer viability in this organism (Mishra et al., 2019). Membrane proteomic analyses of Δ*ffh*, Δ*yidC1*, Δ*yidC2,* and Δ*ffh*/*yidC1* strains suggested a high degree of functional redundancy between YidC1 and YidC2, with gain of function mutations within *yidC1* in a Δ*yidC2* background also identified (Mishra et al., 2019). A gain of function mutation has also been identified in *Bacillus subtilis* YidC1 (SpoIIIJ) enabling it to survive lethality caused by high σ^M levels that interfere with intrinsic resistance to cell wall targeting antibiotics (Zhao et al., 2019). Work to characterize *S. mutans* YidC1 and YidC2 (SmYidC1 and SmYidC2) interactomes *via* immunocapture and chemical crosslinking experiments revealed several differences between apparent YidC1 and YidC2 interaction partners, and suggested both overlapping and individual substrate preferences (Lara Vasquez et al., 2021). Taken together results of phenotypic, proteomic, and protein-protein interaction analyses of WT, Δ*yidC1,* and Δ*yidC2* mutants have suggested significant unique features of SmYidC1 and SmYidC2 despite a high degree of functional overlap. Phenotypic distinctions between *B. subtilis* Δ*yidC1*(*spoIIIJ)* and Δ*yidC2(yqjG)* mutants have also been reported (Errington et al., 1992; Saller et al., 2011; Zhao et al., 2019). Therefore, it is of broad general interest to understand why Gram-positive bacteria generally contain two distinct paralogs of YidC, and to identify specific structural features that confer individual activities of YidC1 compared to YidC2.

Primary sequence comparison demonstrates ∼27% identity and ∼47% homology (Emboss-Needleman tool) between *S. mutans* YidC1 and YidC2. A key feature delineating YidC1 and YidC2 is the longer and more basic C-terminal tail of YidC2. Indeed, acid stress tolerance was partially restored in a Δ*yidC2* background when the YidC1 tail was replaced with that of YidC2 (Palmer et al., 2012). Later, crystal structure characterization combined with site-directed mutagenesis of *B. halodurans* YidC2 showed that its C1 cytoplasmic loop is flexible, and that its deletion impairs membrane insertase activity (Kumazaki et al., 2014a). Primary sequence analyses and crystal structures illustrate that all mature YidCs consist of five transmembrane domains (TM2-TM6) that are interspersed with cytoplasmic loop 1 (C1), cytoplasmic loop 2 (C2), and a cytoplasmic C-terminal tail (T). In consideration of the fact that protein synthesis occurs in the cytoplasm, YidC cytoplasmic domains would be expected to participate not only in specific interactions with other co-translational translocation machinery components but also with substrates destined for insertion. In *E.* coli, incoming substrates have been hypothesized to interact initially with the YidC C1 loop followed by interaction with a conserved arginine residue within transmembrane domain TM2 for insertion (Kol et al., 2008; Kumazaki et al., 2014a,c). More recently, molecular dynamics simulation showed that the crystallographically unresolved cytoplasmic C2 loop of BhYidC2 plays an important role in stabilizing this insertase's structure (Harkey et al., 2019).

In the current work, we engineered a panel of chimeric *yidC1/2* constructs in which one or more YidC1 cytoplasmic domains were substituted for those of YidC2, and vice versa. The chimeric variants were integrated into the bacterial chromosome and ectopically expressed from the *gtfA* locus in a genetic background in which endogenous *yidC1* and *yidC2* had both been eliminated. Each strain was characterized in terms of growth and survival under non-stress and stress conditions including acid, osmotic, and metal excess. This revealed a novel phenotype for the Δ*yidC1* mutant, that was not shared by the Δ*yidC2* strain, namely sensitivity to excess Zn(II). Three dimensional (3D)-structure prediction tools were also utilized to evaluate structural constraints within each of the various YidC1/2 chimeric proteins compared to unmodified YidC1 and YidC2. Our experimental results suggest considerable plasticity of YidC1 function in that this paralog could accommodate any combination of cytoplasmic domain substitutions without significant impact on the phenotypes tested. In contrast, YidC2 structure appeared less malleable with a preference for specific combinations of cytoplasmic domains in order to support growth under non-stress as well as environmental stress conditions. Lastly, prediction tools identified putative interactions between cytoplasmic loops 1 and 2 of YidC1, and between cytoplasmic

loop 1 and the C-terminal tail of YidC2, which appeared to stem from stabilizing salt-bridges within YidC1 and YidC2, respectively. Amino acids involved in these putative salt-bridges, K91 and E190 in YidC1, and E92 and K253 in YidC2, were substituted with alanine by site-directed mutagenesis and confirmed to contribute to paralog-specific functions.

MATERIALS AND METHODS

Bacterial Strains, Plasmids and Growth Conditions

Bacterial strains and plasmids used in this study are listed in **Supplementary Table 1**. All of the *S. mutans* mutants used in this study were derived from *S. mutans* strain UA159 (Ajdic et al., 2002). *S. mutans* strains were routinely grown in Todd-Hewitt broth (BBL, Becton Dickinson) supplemented with 0.3% yeast extract (THYE) at 37°C in 5% CO_2/95% air atmosphere (v/v). Spectinomycin (1 mg ml^{-1}), kanamycin (1 mg ml^{-1}), or erythromycin (10 mg ml^{-1}) were added, where appropriate, for the growth and selection of *S. mutans* strains. *E. coli* strain C2987 (NEB) was used for standard cloning procedures and routinely grown in Luria–Bertani medium (10 g l^{-1} tryptone, 5 g l^{-1} yeast extract and 5 g l^{-1} NaCl) at 37°C with vigorous shaking or on LB agar (1.5%) with appropriate selection. Ampicillin (100 μg ml^{-1}), kanamycin (50 μg ml^{-1}), or erythromycin (250 μg ml^{-1}) were used for the growth and selection of *E. coli* transformants.

Construction of Chimeric *yidC1* and *yidC2* Genes

The Gibson assembly method was used to construct 14 different chimeric genes of *yidC1* and *yidC2* with DNA encoding one, two, or three cytoplasmic domains swapped with the corresponding regions from the other paralog. Details of the chimeric YidC1/2 proteins are provided in **Supplementary Table 2**. DNA fragments corresponding to the specific regions of the *yidC1* and *yidC2* within each chimera were PCR-amplified using primers listed in **Supplementary Table 3**. PCR products were assembled between *Nde*I/*Bam*HI sites of pET15b using NEBuilder HiFi DNA Assembly kit (NEB) following the manufacturer's instructions and transformed into C2987 competent *E. coli* (NEB) by heat shock. Chimeric *yidC1/2* fragments subcloned in pET15b were PCR-amplified using end primers and subcloned between *Xba*I/*Bsr*GI sites of the *S. mutans* integration vector, pBGE. These constructs were subsequently used for integration at the non-essential *gtfA* locus.

Site-Directed Mutagenesis of *yidC1* and *yidC2*

A standard PCR-based technique involving partially overlapping primers (**Supplementary Table 3**) was used for site-directed mutagenesis. pSM15 and pSM20 were used as templates for the mutagenesis of *yidC1* and *yidC2* genes, respectively (Zheng et al., 2004). For subsequent integration into *S. mutans*, genes containing the engineered point mutations were first subcloned into the integration vector, pBGE, and transformants were selected for resistance to erythromycin.

Construction of *Streptococcus mutans* Strains Expressing Chimeric *yidC1/2*

Construction of *S. mutans* strains expressing a single chimeric CD-substituted *yidC1* or *yidC2* backbone gene was done in three steps. First *yidC1* or *yidC2* was deleted from the UA159 genome. *yidC1* was eliminated by allelic exchange with a spectinomycin resistant marker (*aad9*) using the pCR2.1-DyidC1Sp plasmid (Palmer et al., 2012). The resultant Δ*yidC1* strain (SM2001) was next transformed with pBGE plasmids containing either the wild-type (WT) or a chimeric *yidC1* gene and selected for resistance to spectinomycin (1 mg ml^{-1}) or erythromycin (10 mg ml^{-1}). Lastly *yidC2* was deleted from the WT- or chimeric *yidC1*-expressing strain by allelic replacement with *aphA-3* encoding kanamycin resistance. The Δ*yidC2:aphA-3* cassette for *yidC2* deletion was generated by allelic exchange with a kanamycin resistant marker using pAH342 plasmid (Hasona et al., 2005). Similarly, chimeric *yidC2* expressing strains were constructed by initial deletion of *yidC2* using the Δ*yidC2:aphA-3* cassette followed by integration of chimeric *yidC2* at the *gtfA* locus and subsequent deletion of *yidC1* by allelic replacement with *aad9*. Expression of site-directed point mutants of *yidC1* and *yidC2* genes was carried out as described above for chimeric *yidC1* and *yidC2*. Deletion of *yidC1* and *yidC2,* and integration of point mutated or chimeric *yidC1/2*, were confirmed by PCR and sequencing of the relevant genomic loci. Production of the WT or chimeric YidC1/YidC2 polypeptide was confirmed in each genetically engineered strain by Western blot using monospecific anti-YidC1 and anti-YidC2 antibodies (Palmer et al., 2012; **Supplementary Figure 1**).

Bacterial Growth Under Non-stress and Stress Conditions

Growth of each *S. mutans* strain was monitored using a Bioscreen C instrument (Growth Curves United States, Piscataway, NJ, United States). Overnight (O/N) cultures were grown in THYE with appropriate antibiotic selection at 37°C in air with 5% CO_2. For precultures, O/N cultures were diluted 1:50 (or 1:20 for very slow growing strains) into 2 ml THYE without selection and grown to OD_{600} of 0.2–0.4. Precultures were then diluted to OD_{600} = 0.005 in 1 mL of prewarmed THYE and 300 ml of each dilution was transferred in triplicate to wells of a Bioscreen micro-well plate. A sterile mineral oil overlay (50 μL) was added on top of cultures in each well to measure growth under anaerobic conditions. Cell density was measured spectrophotometrically (OD_{600}) every 30 min for up to 48 h of growth at 37°C. To assess the effect of oxygen stress, the overlay of sterile mineral oil was omitted. To assess the effect of acid stress, cells were grown in THYE adjusted to pH 5.0. To assess osmotic stress, THYE was supplemented with 3% NaCl. Metal intoxication experiments involved addition of 5 mM $FeSO_4$ (added from a stock of 1 M $FeSO_4$ prepared in 0.1 N HCl), 5 mM $MnCl_2$, or 2.5 mM $ZnCl_2$ to THYE. Bioscreen plate wells were not overlayed with mineral oil when bacteria were grown under metal-excess conditions.

Measurement of Plating Efficiency by Spot Dilution

Strains were grown to mid-exponential phase (OD_{600} = 0.2–0.4) in THYE from an O/N culture in THYE with appropriate antibiotic selection. Cultures were then adjusted to OD_{600} = 0.2, and serial 10-fold dilutions were made in THYE. Four microliter aliquots of each dilution were spotted on THYE agar (pH 7.0, pH 5.0, 3% NaCl, 5 mM $FeSO_4$, 5 mM $MnCl_2$, or 2.5 mM $ZnCl_2$). Plates were incubated at 37°C in air with 5% CO_2 for 2 days before visual inspection and documentation.

Bioinformatic Analyses and 3D Structure Prediction and Comparison

YidC sequence logo was created by alignment of YidC1 and YidC2 sequences of ten Gram-positive bacterial species using the weblogo tool[1] (Schneider and Stephens, 1990). The clustal omega alignment of YidC1 and YidC2 sequences was entered into the webtool to generate the sequence logo image. Physico-chemical properties of various chimeric YidC1 and YidC2 proteins were evaluated with the Protparam web tool[2] using their primary amino acid sequences (Gasteiger et al., 2005). Three-dimensional structures of the wild-type proteins and chimeric YidC1 and YidC2 variants were predicted using I-TASSER (*Roy et al., 2010*). Protein structures were analyzed with Pymol (PyMOL Molecular Graphics System, Version 1.2r3pre, Schrödinger, LLC). Structure comparisons were done to determine the best alignment (lowest root mean square deviation over the largest number of amino acids) of two proteins using the cealign plugin in Pymol (Shindyalov and Bourne, 1998).

RESULTS

Cytoplasmic Domains of YidC1 and YidC2 Are Less Conserved Than Their *Trans*-Membrane Domains

Functional differences in paralogous proteins often arise as a result of sequence-structure differences acquired through mutations (Conrad and Antonarakis, 2007), with other contributing factors including distinct gene neighborhood, operon organization, and genetic regulation (Zallot et al., 2016). A high resolution crystal structure of BhYidC2 lacking the N-terminal domain and C-terminal tail region is available (Kumazaki et al., 2014a); however, this information alone is not sufficient to explain distinct functional attributes of multiple YidC paralogs of Gram-positive bacteria.

To begin to explore the structural features that likely contribute to characteristic functional activities of SmYidC1 vs. SmYidC2, we first carried out *in silico* analysis and comparison of their structures. Pairwise comparison showed ∼27% identity and ∼47% similarity between SmYidC1 and SmYidC2 (EMBOSS Needle tool). Both paralogs are predicted to be lipoproteins with cleavable signal peptide sequences (PRED-LIPO and Signal P 4.0), and hydropathy analysis by various webtools indicates a post-cleavage structure containing five transmembrane domains (TMDs) connected by two cytoplasmic loops: C1 and C2, and a hydrophilic C-terminal tail for both proteins (Stoffel, 1993; Krogh et al., 2001; Bagos et al., 2008; Petersen et al., 2011; **Figure 1A**). Despite low sequence similarity, SmYidC1 and SmYidC2 are predicted to have similar topological architectures except that the cytoplasmic C-terminal tail region of YidC2 is significantly longer and more basic than that of YidC1 (63 compared to 38 amino acids). Overlaying topology predictions onto the aligned amino acid sequences illustrates that a greater degree of identity/homology (red boxes/texts in **Figure 1B**, respectively) is observed between the TMDs of SmYidC1 and SmYidC2 compared to their cytoplasmic loops and C-terminal tails (**Figure 1B**).

We also extended our pairwise comparison of SmYidC1 and SmYidC2 to the respective YidC orthologs from other Gram-positive bacteria to determine if the sequence diversity observed within the cytoplasmic regions is limited to *S. mutans* or extends to other species. The results of multiple YidC1/YidC2 sequence alignments from various Gram-positive bacteria are shown in **Supplementary Figure 2**. Conservation of residues was plotted using Weblogo (**Supplementary Figure 3**). Interestingly, in all cases of dual YidC paralogs, higher sequence conservation was observed within regions that align with the SmYidC1 and SmYidC2 TMDs, especially TM3. The highest degree of variation was observed among the YidC C-terminal tails, which did not align significantly enough to be included in the Weblogo representation (**Supplementary Figures 2, 3**).

Since crystallographic data is not available for SmYidC1/2, we used I-TASSER (Iterative Threading ASSEmbly Refinement) to generate their 3D-models (Roy et al., 2010; **Figure 1C**). Three dimensional models of SmYidC1 and SmYidC2 resemble the crystal structure of the BhYidC (PDB nos. 3WO6 and 3WO7) core region, which also contains TMDs (TM2-TM5) and three cytoplasmic domains: C1 loop, C2 loop, and C-terminal tail. When predicted 3D-models of SmYidC1 and SmYidC2 were compared to one another, the Cα atoms superimposed with a root mean square deviation (RMSD) of 4.11 Å over 232 residues (**Figure 1C**). The 3D structure comparison further showed that the C1 and C2 cytoplasmic loops of YidC1 and YidC2, as well as their C-terminal tails, did not superimpose as well as their TMDs. Taken together, sequence and structural analyses clearly indicate that the TMDs are more highly conserved than are the cytoplasmic domains of YidC1 and YidC2. We therefore hypothesized that cytoplasmic regions likely confer paralog-specific functional activities to the two *S. mutans* insertases.

Design and *in silico* Characterization of Chimeric *yidC1/2*

Previous work from our laboratory revealed the significance of the C-terminal tails in conferring functional differences

[1]https://weblogo.berkeley.edu/logo.cgi

[2]https://web.expasy.org/protparam/

between SmYidC1 and SmYidC2. When a Δ*yidC2* deletion strain was engineered to harbor tail-swapped versions of YidC1 or YidC2, stress-sensitivity of the mutant strain was partially restored by ectopic expression of chimeric YidC1 harboring the YidC2 tail, while the mutant phenotype was worsened by expression of chimeric YidC2 harboring the YidC1 tail (Palmer et al., 2012). Notably, these experiments were conducted in a Δ*yidC2* mutant background, in which a functionally active native YidC1 remained in addition to the chimeric ectopic YidCs. In the current work, we extended our analysis by swapping all three cytoplasmic domains including loops C1, C2, and the C-terminal tails singly and in combination, and constitutively expressing each chimeric gene as the sole paralog from the ectopic *gtfA* locus in the genome so that the contribution of each individual domain toward the particular phenotype of interest could be specifically addressed. Combinatorial exchange of two and three different cytoplasmic domains were included in these experiments so that potential interactions among the YidC1 or YidC2 cytoplasmic domains could also be assessed. Schematic representations of YidC1, YidC2, and the 14 different domain swapped chimeric constructs are illustrated in **Figure 2**. Throughout the paper, the YidC1 backbone and cytoplasmic domains are indicated in regular type, while the YidC2 backbone and cytoplasmic domains are indicated in bold.

In silico characterization of YidC1, YidC2, and their chimeric variants included determination of pI, number of positively and negatively charged amino acids, instability index (II), grand average hydropathy (GRAVY) using Exapsy ProtParam tools and structural comparison using predicted 3D models (**Table 1** and **Supplementary Figure 4**). Theoretical pI calculations showed that both YidC1 and YidC2 are basic proteins (pI = 10 and 10.25, respectively), with the pI values of chimeric YidC1 and YidC2 proteins remaining close to those of the WT versions. Next, we determined the hydrophobicity of the proteins by calculating their GRAVY scores such that positive values represent hydrophobic proteins while negative values indicate hydrophilic proteins (Kyte and Doolittle, 1982). As expected for membrane proteins, GRAVY scores of YidC1 and YidC2 were both above 0; however, the C1 loop of YidC1 and C-terminal tail of YidC2 were more hydrophilic compared to their respective counterparts. Swapping these domains indeed lowered the predicted hydrophobicity of the chimeric proteins.

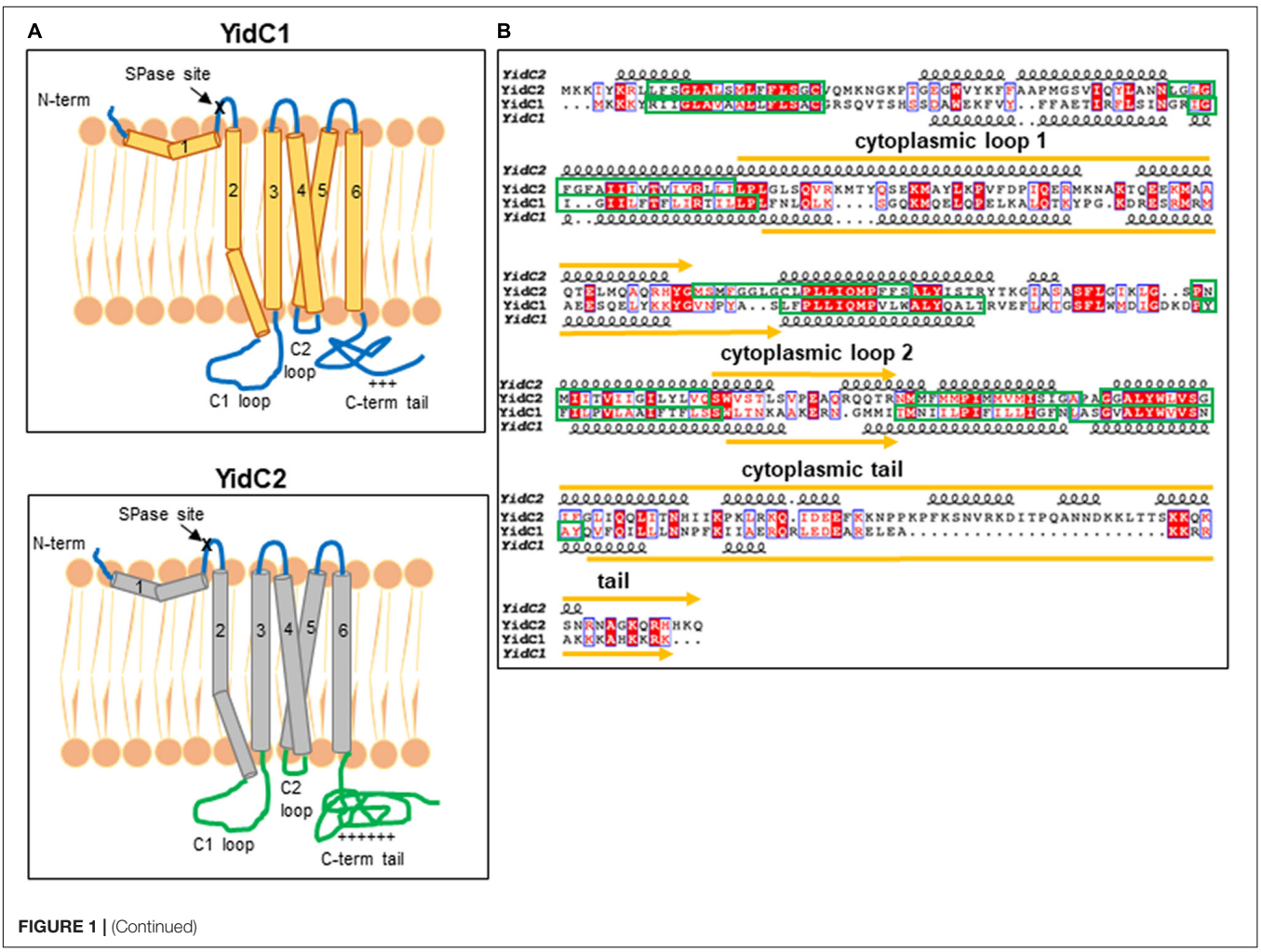

FIGURE 1 | (Continued)

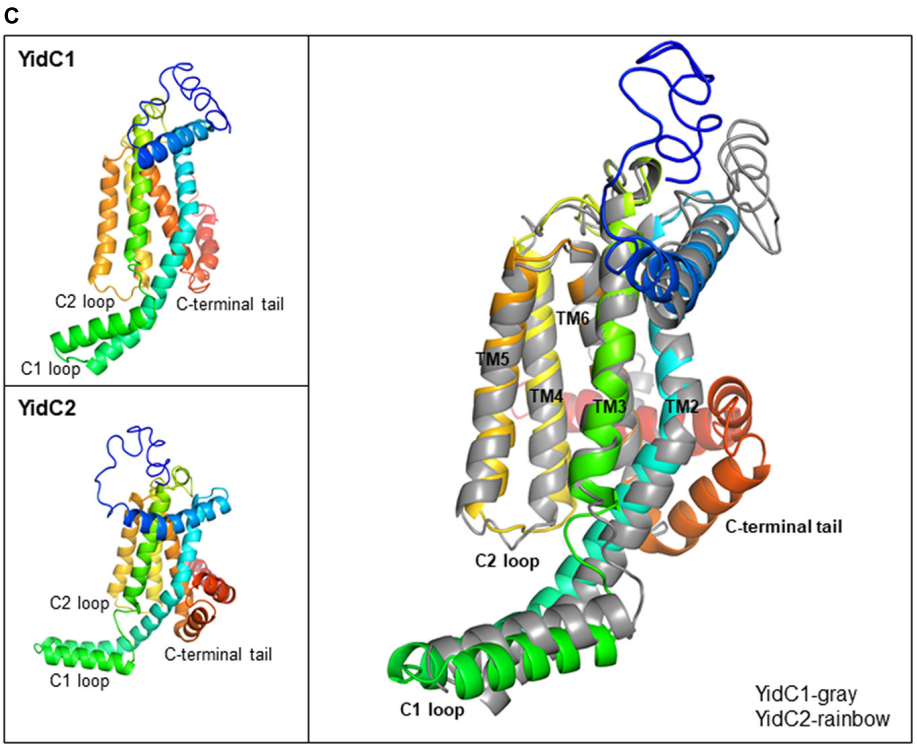

FIGURE 1 | *In silico* comparison of *S. mutans* YidC1 and YidC2. **(A)** Predicted membrane topologies of YidC1 and YidC2 using TM-Pred [TMpred Server (vital-it.ch)]. The mature YidC1 and YidC2 proteins each contain five TM domains and three cytoplasmic regions: C1 loop, C2 loop, and C-terminal tail. " + + + " or " + + + + + " refers to the relative positivity of the charged C-terminal tails of Sm YidC1 and YidC2. **(B)** Alignment of primary and secondary structures of SmYidC1 and SmYidC2 predicted by I-TASSER [I-TASSER server for protein structure and function prediction (umich.edu)]. Amino acid sequences were aligned using the Clustal Omega Program (EMBOSS-Needle) and presented using the ESPript2.2 program (Gouet et al., 1999). Identical residues are highlighted by red boxes, while similar residues are highlighted by red text. Indicated secondary structural helices are based on iTasser-predicted 3D structures. Green boxes correspond to transmembrane domains and yellow lines represent cytoplasmic domains. **(C)** Cartoon representations of the superimposed I-TASSER-predicted 3D structures of YidC1 and YidC2 with YidC1 shown in gray and YidC2 shown as rainbow colored from N- to C-terminus. The YidC2 structure superimposes on YidC1 with a root-mean-square deviation of 4.11 Å for all the Cα atoms (for over 232 residues).

We were also interested to know the effect of individual and combinatorial domain substitutions on chimeric YidC1/2 structures (**Supplementary Figure 4**). We used I-TASSER to predict the 3D structures of each variant and compared them with the 3D structures of the WT proteins, evaluating similarity with each WT protein based on lowest RMSD values over the largest number of amino acids using the cealign plugin in Pymol (Shindyalov and Bourne, 1998; **Table 1**). Alignment data showed higher RMSD values for most of the YidC1 chimeras, which suggests that YidC1 structure is less rigid compared to that of YidC2. That is, most of the domain swaps impacted the 3D structure of YidC1. On the other hand, most of the chimeric YidC2 proteins, except **YidC2**-C1 and **YidC2**-C1,C2, aligned better with unmodified YidC2 than with unmodified YidC1. Therefore, the core domain structure of YidC2 appears more rigid with most of the domain swaps not substantially deviating from that predicted for unmodified YidC2. In agreement with physicochemical characterization of the chimeric YidC proteins, C1 loop substitutions in both YidC1 and YidC2 notably altered alignment with their respective unmodified proteins. Substitution of all three domains within YidC1 (YidC1-**C1,C2,T**) made this chimera dissimilar to both YidC1 and YidC2, while **YidC2**-C1,C2,T was similar to YidC2 but did not align well with YidC1.

Construction and Characterization of *yidC1* and *yidC2* Ectopic Expression Strains

We next evaluated *S. mutans* strains expressing the 14 different chimeric versions of *yidC1* or *yidC2*. The chimeric *yidC* genes, or unmodified controls, were introduced into the non-essential *gtfA* locus for expression in a *S. mutans* genetic background in which native *yidC1* and *yidC2* had been both eliminated. Strain constructions were carried out in a step-wise manner to overcome the lethality caused by simultaneous elimination of genes encoding both YidCs. Thus, native *yidC1* or *yidC2* was deleted before integrating a chimeric or unmodified gene at the *gtfA* locus. This was followed by deletion of the residual native *yidC2* or *yidC1*, and resulted in each engineered *S. mutans* strain ectopically expressing a single *yidC* variant under control of the *gtfA* promoter. Production of each WT or chimeric YidC1/2 polypeptide was confirmed by Western blot with appropriate

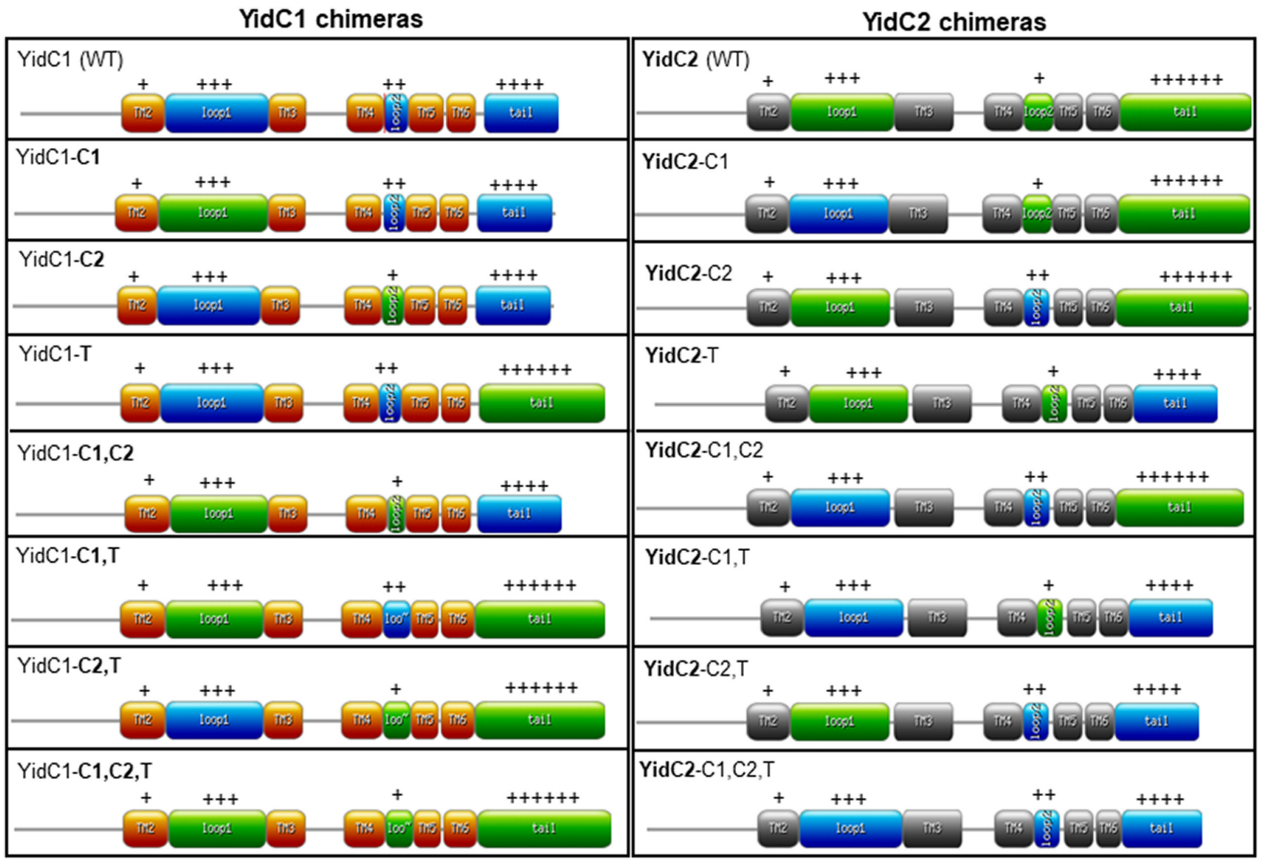

FIGURE 2 | Schematic representation of unmodified and chimeric YidC1 and YidC2 polypeptides. YidC1 transmembrane (TM) domains are illustrated in orange and cytoplasmic domains (CD) in blue. YidC2 TM domains are illustrated in gray and CD in green. Chimeric constructs were designed using the web-based https://prosite.expasy.org/mydomains/tool. Regular text indicates YidC1-derived backbone or CD. Bold text indicates YidC2-derived backbone or CD. " + + + " or " + + + + + " refers to the relative positivity of the charged C-terminal tails of Sm YidC1 and YidC2.

monospecific anti-YidC1 or YidC2 rabbit antisera generated against synthetic peptides corresponding to the cytoplasmic tail domains (**Supplementary Figure 1**).

After their construction, we first evaluated the growth of the *S. mutans* strains that ectopically expressed *yidC1* or *yidC2* in both single deletion and double Δ*yidC1*/Δ*yidC2* deletion backgrounds compared to the UA159 parental strain under non-stress and environmental stress conditions (acid and osmotic) (**Figure 3**). As expected, growth under all three conditions was notably diminished only in the *yidC2* single mutant. When growth was evaluated under aerated conditions in both broth culture and on agar plates, results were similar to those under non-stress conditions (**Supplementary Figure 5**). Under non-stress and osmotic stress conditions, the Δ*yidC1*/Δ*yidC2-yidC1** ectopic expression strain grew at a rate comparable to that of the UA159 parent, while the Δ*yidC1*/Δ*yidC2-yidC2** ectopic expression strain grew more slowly (**Figures 3A,B,E,F** and **Supplementary Table 4**). Neither ectopic expression of *yidC1,* nor *yidC2,* restored the WT level of growth under acid stress conditions (**Figures 3C,D**). Incomplete rescue when *yidC1* or *yidC2* were expressed ectopically rather than from their endogenous locations likely reflects the lack of native gene regulation when non-native promoters and loci are employed. Indeed, our prior membrane proteome characterization of WT, Δ*yidC1,* and Δ*yidC2* strains showed that YidC2 levels were increased in a Δ*yidC1* background, although a similar increase in YidC1 was not observed in the Δ*yidC2* mutant (Mishra et al., 2019). Because the focus of the current work is a structure-function analysis of the YidC1 and YidC2 polypeptides themselves, and not an evaluation of gene regulation or expression, all subsequent functional assays were performed using the ectopically-expressed unmodified *yidC1* or *yidC2* genes in a Δ*yidC1*/Δ*yidC2* background, rather than the UA159 parent strain, as the basis for of comparison of the chimeric *yidC1/2* variants.

YidC1, but Not YidC2, Successfully Tolerates Individual or Combinatorial Substitution of Its Cytoplasmic Domains

None of the individual or combinatorial substitutions of YidC2 cytoplasmic domains into YidC1 resulted in diminished growth of *S. mutans* compared to ectopic expression of unmodified *yidC1* under non-stress conditions (**Figure 4A** and

TABLE 1 | Physico-chemical evaluation of YidC1 and YidC2 chimeric polypeptides.

Proteins	No. of amino acids	Theoretical pI	Total no. of charged residues	Molecular weight (kD)	GRAVY	Instability Index	RMSD (YidC1, αC-αC)	RMSD (YidC2, αC-αC)
YidC1	271	10	+ 40 and −21	31.327	0.093	43.53	NA	4.12 Å
YidC2	310	10.25	+ 41 and −13	34.923	0.023	38.36	4.12 Å	NA
Chimeric YidCs								
YidC1-**C1**	273	10.05	+ 39 and −20	31.588	0.178	46.32	3.73 Å	3.16 Å
YidC1-**C2**	273	10	+ 39 and −21	31.596	0.052	45.82	3.65 Å	3.23 Å
YidC1-**T**	297	10.08	+ 44 and −20	34.241	−0.094	41.57	3.29 Å	3.2 Å
YidC1-**C1, C2**	275	10.05	+ 38 and −20	31.857	0.136	48.57	3.97 Å	3.65 Å
YidC1-**C1, T**	299	10.13	+ 43 and −19	34.503	−0.016	44.13	3.19 Å	3.63 Å
YidC1-**C2, T**	299	10.09	+ 43 and −20	34.510	−0.131	43.67	4.13 Å	2.76 Å
YidC1-**C1, C2, T**	301	10.14	+ 42 and −19	34.772	−0.053	46.21	4.2 Å	4.43 Å
YidC2-C1	308	10.19	+ 42 and −14	34.662	−0.053	36.13	3.89 Å	3.34 Å
YidC2-C2	308	10.24	+ 42 and −13	34.654	0.059	25.9	2.93 Å	2.85 Å
YidC2-T	284	10.18	+ 37 and −14	32.009	0.212	39.94	4.02 Å	2.80 Å
YidC2-C1, C2	306	10.18	+ 43 and −14	34.393	−0.017	33.64	3.94 Å	3.4 Å
YidC2-C1, T	282	10.12	+ 38 and −15	31.748	0.131	37.51	3.6 Å	2.46 Å
YidC2-C2, T	282	10.17	+ 38 and −14	31.740	0.254	37.26	3.95 Å	2.13 Å
YidC2-C1, C2, T	280	10.12	+ 39 and −15	31.478	0.172	34.79	4.4 Å	2.82 Å
Point mutations								
YidC1^{K91A}	271	9.97	+ 39 and −21	31.27	0.114	43.53	3.50 Å	2.68 Å
YidC1^{E190A}	271	10.05	+ 40 and −20	31.27	0.113	42.82	3.50 Å	3.53 Å
YidC2^{E92A}	310	10.29	+ 41 and −12	34.86	0.04	38.33	3.02 Å	2.82 Å
YidC2^{K253A}	310	10.23	+ 40 and −13	34.86	0.041	36.41	3.61 Å	2.88 Å

YidC1 backbone and cytoplasmic domains are indicated in plain text while YidC2 backbone and cytoplasmic domains are indicated in bold.

Supplementary Table 4). Similar results were obtained when each of the strains was grown on solid media (**Supplementary Figure 6**). These results suggest that any of the three cytoplasmic domains of YidC2 can successfully replace those of YidC1, individually or in combination, to support growth and survival of *S. mutans* in the absence of external environmental stressors. Next, we tested strains harboring chimeric YidC2 variants compared to the unmodified YidC2 polypeptide (**Figure 4B**). Most of the chimeric YidC2 variants, except for **YidC2**-C1,T, exhibited decreased growth compared to the unmodified YidC2 control strain. Similar results were observed when the strains were grown under aerated rather than anaerobic conditions except that the **YidC2**-C1,T variant more closely resembled that of the unmodified YidC2 control (**Supplementary Figure 6** and **Supplementary Table 4**). Growth on solid media also followed a similar pattern to that observed in liquid media (**Supplementary Figure 6**). The strain harboring the **YidC2**-C2 chimera was noteworthy in that after an extended lag phase it achieved a substantially higher yield compared to the unmodified YidC2 control strain (**Figure 4B**). Subsequent subculture in THYE did not alter this strain's growth kinetics suggesting that delayed growth and increased yield was not the result of a suppressor mutation, but rather physiological adaptation in broth culture. The negative impact of expression of most of the chimeric *yidC2* variants on *S. mutans* growth illustrates that individual YidC1 and YidC2 cytoplasmic domains are not functionally equivalent. YidC2 structure appears less malleable and tolerant of substitutions than that of YidC1. YidC2 function was perturbed by all domain substitutions except for **YidC2**-C1,T. These results are consistent with the notion that putative interactions occur between cytoplasmic domains such that specific combinatorial substitutions are preferred. The C1 loops of YidC1 and YidC2 are of similar size suggesting that primary sequence rather than overall length plays an important role in C1 functional attributes. In contrast, the C2 loops and C-terminal tails of YidC1 and YidC2 vary in both size and sequence.

Domain Substitutions Within YidC1 Impact *S. mutans* Tolerance to Acid and Osmotic Stress Less So Than Domain Substitutions Within YidC2

Growth in acidified medium (pH 5.0) of the strain with chimeric YidC1-**T** was negatively affected, whereas the strain harboring YidC1-**C2** demonstrated improved growth, and that with YidC1-**C1** appeared unaffected (**Figure 4C** and **Supplementary Table 4**). This suggests specific influences of the cytoplasmic tail and C2 loop on the structure and function of YidC1 compared to YidC2. Combinatorial replacement of YidC2 C1 and C2, or the YidC2 C1 and tail domains, into YidC1 revealed notably enhanced growth of the chimeric strains in acid conditions (**Figure 4C** and **Supplementary Table 4**). This suggests potential interactions

between certain pairs of cytoplasmic domains that may not be replicated with heterologous partners. Surprisingly, growth yield under acid conditions was notably diminished in the YidC1-**C1,C2,T** triple chimeric strain. This pronounced negative affect implies a collective behavior of the YidC2 cytoplasmic domains in the context of the YidC1 backbone that cannot be attributed to a single domain substitution, or pairs of substitutions. Growth of the YidC1 chimeric strains on pH 5.0 agar plates was consistent with that in liquid media (**Supplementary Figure 7**), although differences among strains were not as pronounced, possibly because plates were grown in 5% v/v CO_2 saturated air rather than anaerobically.

The impact of domain swapping on acid tolerance was even more apparent when YidC1 cytoplasmic domains were introduced into YidC2 (**Figure 4D**). With the exceptions of the simultaneous exchange of the YidC1 C1 loop and tail into YidC2 (**YidC2**-C1,T) or the YidC1 C2 loop and tail into YidC2 (**YidC2**-C2,T), all other combinations of domain substitutions resulted in worsened growth of the YidC2 chimeric strains. The negative impact of the YidC1 C1 loop was ameliorated, and growth of the chimeric YidC2 strain was notably enhanced, when the YidC1 tail was exchanged as well (**YidC2**-C1,T). Simultaneous substitution of YidC1's C2 loop and tail with those of YidC2 (**YidC2**-C2,T) also alleviated the negative impact of single substitution of the C2 loop (**YidC2**-C2). However, simultaneous transfer of all three of YidC1 cytoplasmic domains into YidC2 (**YidC2**-C1,C2,T) again resulted in a seriously impaired chimeric insertase unable to contend with acid stress. Taken together, these results indicate specific functional attributes of YidC2 compared to YidC1 cytoplasmic domains that must be expressed in the proper combination and context to achieve optimal functional activity.

Exchange of any combination of YidC2 cytoplasmic domains into YidC1 had little to no effect on the ability of the YidC1 chimeric strains to grow in the presence of high salt in liquid culture (**Figure 4E**), or on agar plates (**Supplementary Figure 7**). In stark contrast, introducing YidC1 cytoplasmic domains into YidC2 had substantial negative effects on the ability of the YidC2 chimeric strains to grow during osmotic stress (**Figure 4F** and **Supplementary Figure 7**), the only exception being co-substitution of the YidC1 C1 loop and tail-domains into YidC2 (**YidC2**-C1,T) which modestly enhanced growth. The most detrimental impact on growth in high salt was observed when only the C2 loop of YidC1 was introduced into YidC2 (**YidC2**-C2). This effect was partially alleviated when the C2 loop was exchanged in combination with the YidC2 C1 loop or C-terminal tail (**YidC2**-C1,C2 or **YidC2**-C2,T). The chimeric strain harboring YidC2 with all three cytoplasmic domains exchanged for those of YidC1 (**YidC2**-C1,C2,T) was only minimally impacted during growth in the presence of high salt when compared to ectopic expression of unmodified *yidC2*. Thus, the results of domain swapping experiments vary considerably depending on the phenotype being evaluated, as well as on the backbone of the insertase under study. This information is expected to become even more enlightening as YidC1- compared to YidC2-specfic substrates responsible for predominant Δ*yidC1* and Δ*yidC2* mutant phenotypes are identified in future studies. Collectively, the results shown in **Figure 4** suggest optimal function when the C1 loop and C-terminal tail are paired from the same paralog; however, that beneficial pairing can be obfuscated when all three domains are co-transferred.

YidC1 Is Specifically Required During *Streptococcus mutans* Growth in Excess Zinc

Our recent membrane proteomic analysis of Δ*yidC1* and Δ*yidC2* deletion mutants, as well as characterization of YidC1 and YidC2 interactomes, suggested a potential involvement of the YidC insertases in metal homeostasis (**Supplementary Table 5**; Mishra et al., 2019; Lara Vasquez et al., 2021). This is a logical supposition given the membrane localization of integral components of metal ion import and efflux systems. We therefore evaluated growth and survival of Δ*yidC1* and Δ*yidC2* mutants, and ectopic expression strains, in media supplemented with salts of transition metals including zinc, iron, and manganese (**Figure 5** and **Supplementary Table 4**). These growth experiments were carried out under aerated conditions since transition metals are redox-active and their toxicity is therefore linked to oxygen (Storz and Imlay, 1999; Moore and Helmann, 2005). The most striking result of these experiments was a complete inability of the Δ*yidC1* deletion strain to grow in the presence of excess Zn(II) (**Figure 5A**). Zn(II) is a highly abundant and tightly regulated transition metal that acts as a cofactor for multiple bacterial proteins [reviewed in Chandrangsu et al. (2017)]. Results were similar on agar plates containing 2.5 mM $ZnCl_2$ (**Supplementary Figure 8**). Ectopic expression of *yidC1* in the Δ*yidC1* and Δ*yidC1*/Δ*yidC2* backgrounds was largely able to complement the Zn toxicity phenotype. In contrast, deletion of *yidC2* had far less impact on the ability of *S. mutans* to grow in the presence of excess Zn(II) (**Figure 5B**). Deletion of *yidC1* had no obvious impact on *S. mutans* growth under conditions of Fe(II) or Mn(II) excess (**Figures 5C,E**), while growth of the Δ*yidC2* was modestly diminished under these conditions (**Figures 5D,F**). Growth of the Δ*yidC1*/Δ*yidC2-yidC1* ectopic expression strain was somewhat diminished compared to the UA159 parent strain in the presence of excess Fe(II). In contrast, the strain engineered to express ectopic *yidC2,* while viable in the presence of excess Zn(II), Fe(II), or Mn(II), was severely growth-impaired under these conditions (**Figures 5B,D,F**). The ability of this strain, which lacks endogenous or ectopic *yidC1,* to grow at all in the presence of excess Zn(II) was initially surprising, but can be explained if the YidC1 and YidC2 paralogs have differential effects on import of particular metals as opposed to efflux. For example, if YidC1 is responsible for insertion of a critical zinc exporter, then inefficient insertion of a metal importer by ectopic expression of *yidC2* would render the cells less susceptible to normally toxic levels of Zn(II) in the extracellular environment. While identification of specific membrane-localized importer vs. exporter substrates is beyond the scope of the current study, evaluation of metal toxicity provides another useful phenotypic property to assess the impact of cytoplasmic domain swaps on YidC1 and YidC2 behavior compared to the unmodified insertases.

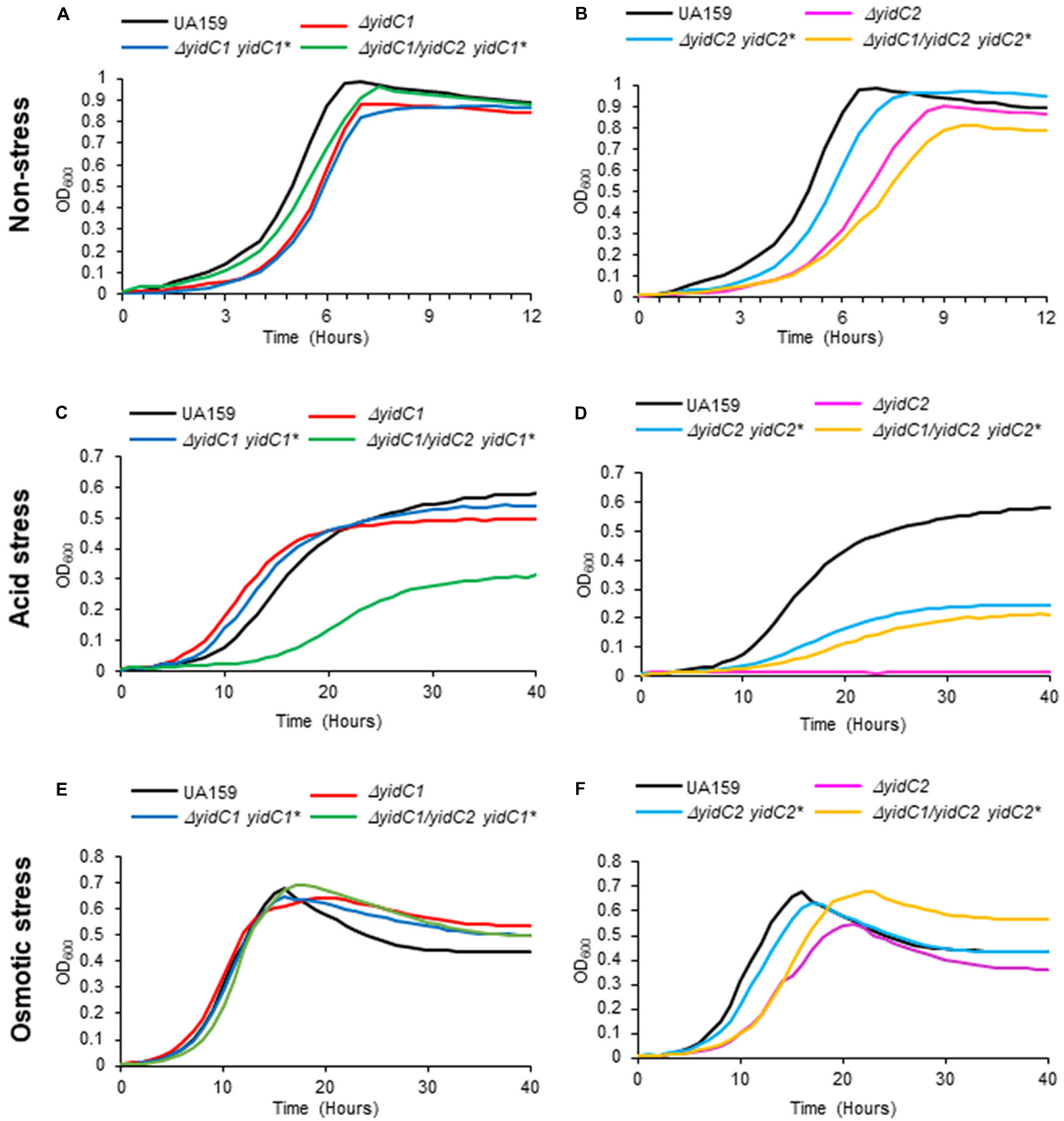

FIGURE 3 | Evaluation of growth of *S. mutans* wild-type, D*yidC1/2* mutants, and ectopic expression strains under non-stress, acid-stress, and salt-stress conditions. Growth of the wild-type UA159 parent strain compared to Δ*yidC1* **(A,C,E)** or Δ*yidC2* **(B,D,F)** deletion mutants, and strains complemented by ectopic expression (*) from the *gtfA* locus of *yidC1* or *yidC2* in single Δ*yidC1/2* or double Δ*yidC1/*Δ*yidC2* backgrounds. **(A,B)** Growth in THYE, pH 7). **(C,D)** Growth in THYE acidified to pH 5.0. **(E,F)** Growth in THYE supplemented with 3% NaCl. Growth measurements were carried out at least three times with each sample assayed in triplicate. Data shown are mean replicates of an independent experiment.

Substitution of the cytoplasmic domains of YidC2 into YidC1 had little impact on growth of the chimeric strains in Fe(II), Mn(II), or Zn(II) compared to the unmodified YidC1 control, except that the YidC1-**C1,T** variant grew slightly less well in the presence of excess Zn(II) and slightly better in the presence of excess Fe(II) than the other strains (**Figures 6A,E**). This strain also achieved a notably lower cell yield during growth in excess Mn(II), and is the first example thus far whereby a homologous pairing of C1 and C-terminal tail domains was apparently detrimental. Overall, these results demonstrate that

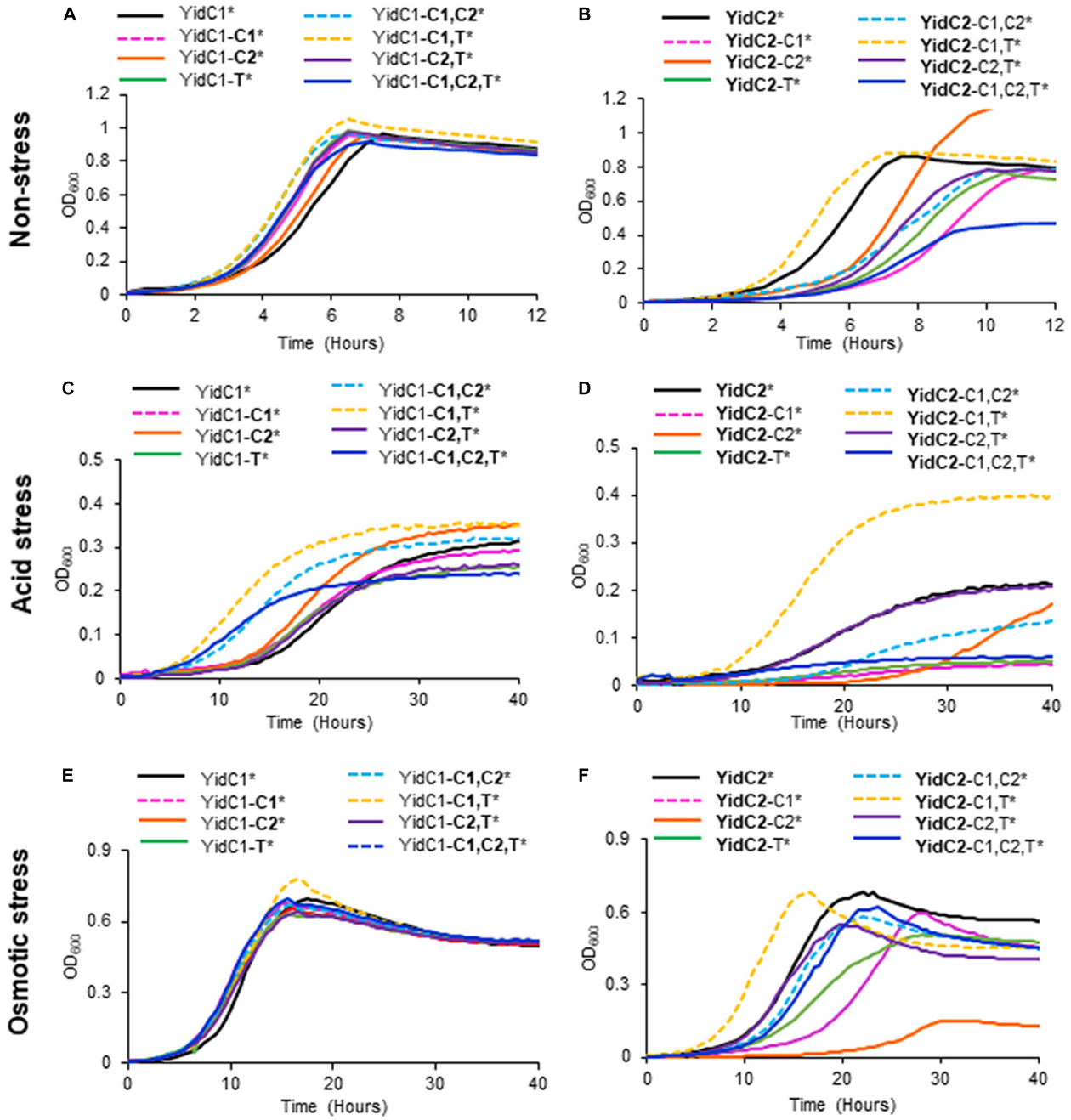

FIGURE 4 | Effect of YidC1/2 cytoplasmic domain substitutions on *S. mutans* growth under non-stress, acid-stress, or salt-stress conditions. Growth of strains complemented by ectopic expression (*) from the *gtfA* locus of unmodified *yidC1* **(A,C,E)** or *yidC2* **(B,D,F)** compared to corresponding cytoplasmic domain (CD) swap variants in a double Δ*yidC1*/Δ*yidC2* background. **(A,B)** Growth in THYE, pH 7). **(C,D)** Growth in THYE acidified to pH 5.0. **(E,F)** Growth in THYE supplemented with 3% NaCl. Growth measurements were carried out at least three times with each sample assayed in triplicate. Data shown are mean replicates of an independent experiment. Regular text indicates YidC1 backbone or CD. Bold text indicates YidC2 backbone or CD.

YidC1 supports the growth of *S. mutans* in the presence of high levels of the metals tested, and that this paralog's function in this regard is not severely impacted by exchange of its cytoplasmic domains with those of YidC2. The lower cell yield of the YidC1-**C1,T** variant during growth in Mn(II) could stem from increased import or decreased export, or both, of this particular metal. In the case of strains harboring chimeric YidC2 variants, all combinations of single, double, and triple domain swaps of YidC1 cytoplasmic domains into YidC2 improved growth in the presence of Mn(II), with the chimeric **YidC2**-C2 strain achieving a notably higher cell yield (**Figure 6F**). Results were similar in the presence of excess Fe(II) (**Figure 6D**), suggesting that

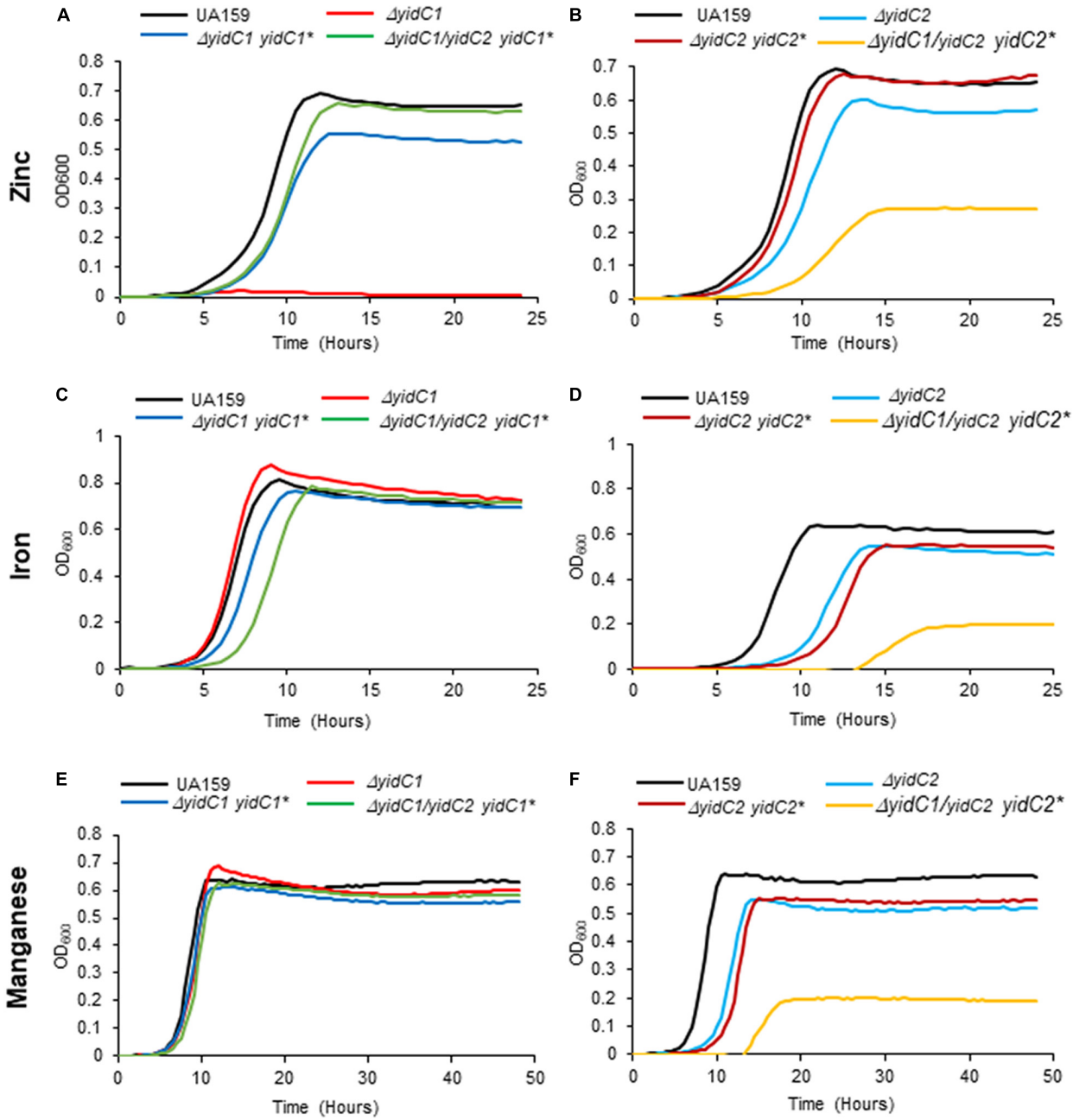

FIGURE 5 | Evaluation of growth of *S. mutans* wild-type, Δ*yidC1/2* mutants, and ectopic expression strains under excess transition metal conditions. Growth of the wild-type UA159 parent strain compared to Δ*yidC1* **(A,C,E)** or Δ*yidC2* **(B,D,F)** deletion mutants, and strains complemented by ectopic expression (*) from the *gtfA* locus of *yidC1* or *yidC2* in single Δ*yidC1/2* or double Δ*yidC1/DyidC2* backgrounds. **(A,B)** Growth in THYE, pH 7, supplemented with 2.5 mM $ZnCl_2$ under aerating conditions. **(C,D)** Growth in THYE, pH 7, supplemented with 5 mM $MnCl_2$ under aerating conditions. **(E,F)** Growth in THYE, pH 7, supplemented with 5 mM $MnCl_2$ under aerating conditions. Growth measurements were carried out at least three times with each sample assayed in triplicate. Data shown are mean replicates of an independent experiment.

overlapping import/efflux systems may contribute to Mn(II) and Fe(II) homeostasis, and that YidC1 cytoplasmic domains, particularly the C2 loop, are more effective than those of YidC2 in the insertion of relevant substrates that limit toxicity by these two metals. The impact of the chimeric YidC2 variants in the presence of excess Zn(II) was strikingly different than in the presence of excess Fe(II) or Mn(II) (**Figure 6B**). This suggests that *S. mutans* contends with Zn(II) in a different way than it does the other two metals. In this case, incorporation of either the YidC1 C1 loop (**YidC2**-C1), or C2 loop (**YidC2**-C2), into YidC2 severely diminished the ability of the variant insertases to contend with toxic levels of Zn(II). In contrast, all other combinations

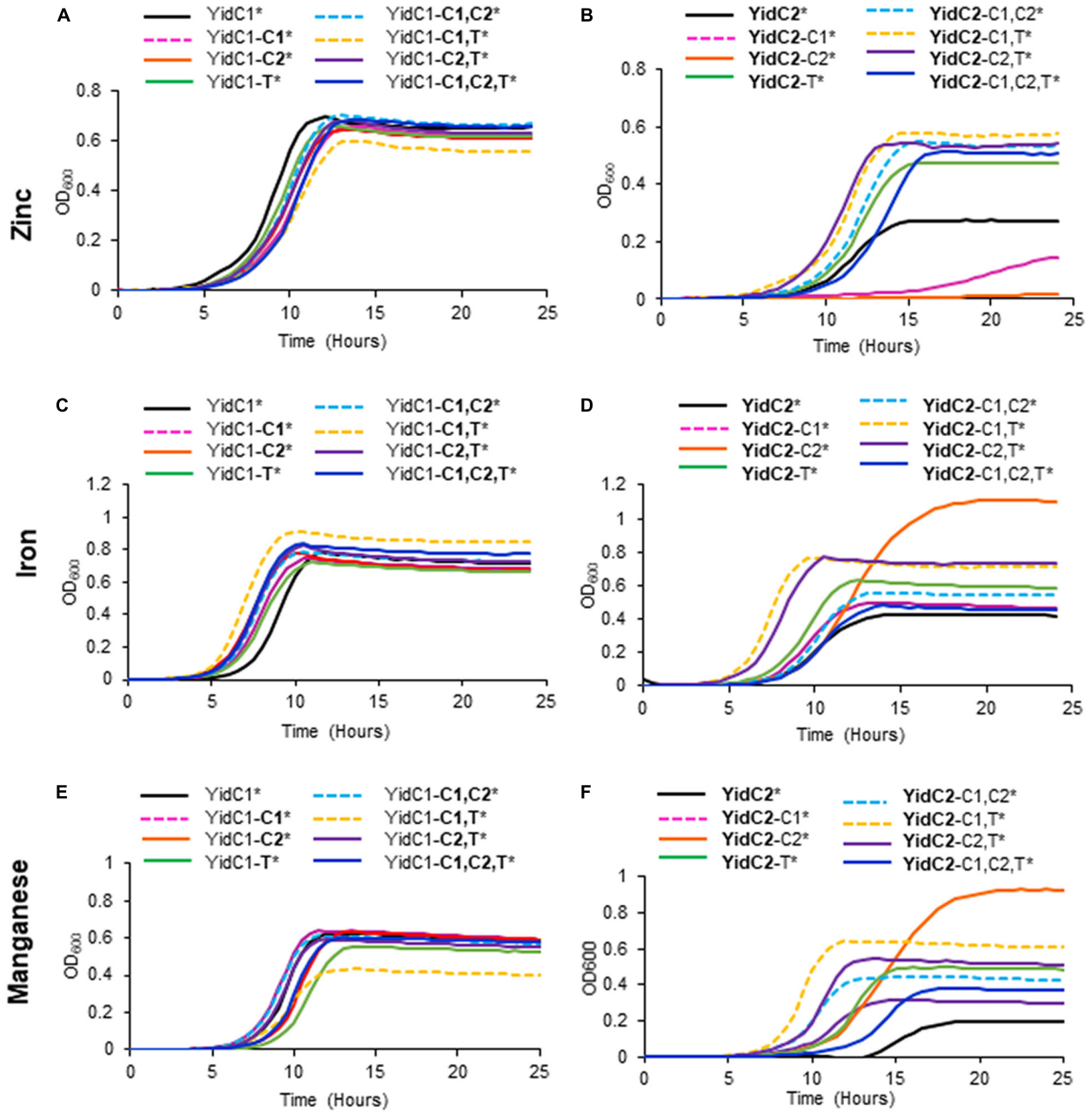

FIGURE 6 | Effect of YidC1/2 cytoplasmic domain substitutions on *S. mutans* growth under excess transition metal conditions. Growth of strains complemented by ectopic expression (*) from the *gtfA* locus of unmodified *yidC1* **(A,C,E)** or *yidC2* **(B,D,F)** compared to corresponding cytoplasmic domain (CD) swap variants in a double Δ*yidC1*/Δ*yidC2* background. **(A,B)** Growth in THYE, pH 7, supplemented with 2.5 mM $ZnCl_2$ under aerating conditions. **(C,D)** Growth in THYE, pH 7, supplemented with 5 mM $MnCl_2$ under aerating conditions. **(E,F)** Growth in THYE, pH 7, supplemented with 5 mM $MnCl_2$ under aerating conditions. Growth measurements were carried out at least three times with each sample assayed in triplicate. Data shown are mean replicates of an independent experiment. Regular text indicates YidC1 backbone or CD. Bold text indicates YidC2 backbone or CD.

of domain exchanges substantially improved growth in excess Zn(II). Thus, when the YidC1 C1 and C2 loops were exchanged together, or in combination with the YidC1 C-terminal tail, the net effect on the YidC2 chimeric polypeptides was to enable the cells to better contend with a high level of environmental Zn(II)- again either due to diminished uptake or increased export of this particular metal. The amelioration of the detrimental impact of single substitution of the YidC1 C1 or C2 into YidC2 by co-exchange with other potentially interactive cytoplasmic domains highlights the likely importance of cooperative effects of the cytoplasmic domains of each insertase to accomplish appropriate membrane protein insertion to support specific cellular activities.

YidC1 and YidC2 Possess Distinct Interdomain Salt Bridges Whose Disruption Diminishes YidC1- and YidC2-Associated Activities

As detailed above, phenotypic characterization of strains producing chimeric YidC1 and YidC2 variants demonstrated preferences for combinatorial replacement of certain cytoplasmic domains over individual substitutions suggesting specific functional inter-domain interactions. Salt bridges (electrostatic interaction between charged residues) often play an important role in the conformational stability of proteins (Ban et al., 2019). All three cytoplasmic domains of YidC1, as well as those of YidC2, contain multiple charged residues that could potentially be involved in formation of salt bridges. We used an *in silico* approach to identify those amino acid residues within the YidC1 and YidC2 cytoplasmic domains most likely to form salt bridges, and measured the distance between the putative donor and acceptor atoms of the residues involved (**Supplementary Table 6**). Potential intra-domain interactions were identified within the C1 loop and C-terminal tail of YidC1, and within the C1 loop, C2 loop, and C-terminal tail of YidC2. In addition, putative inter-domain interactions between YidC1 amino acid residues K91 (C1 loop) and E190 (C2 loop) (**Figure 7A**), and YidC2 residues E92 (C1 loop) and K253 (C-terminal tail) (**Figure 7B**), were identified. The predicted distances between the side chains of both of these pairs of charged residues were <3Å, supporting the likelihood of their interaction. Multiple sequence alignment of YidC1s from various oral streptococci showed that both the K91 and E190 residues are highly conserved (**Supplementary Figure 2**). Alignment of YidC2 sequences from various oral streptococci showed YidC2 E92 and K253 also to be highly conserved (**Supplementary Figure 2**). Therefore, we hypothesized that these residues in particular are decisive contributors to the respective functions of YidC1 and YidC2.

To examine the functional relevance of key residues predicted by *in silico* analysis to form stabilizing interactions within the YidC1 or YidC2 structures, we used site-directed mutagenesis to change each of these charged residues to an alanine. The modified *yidC1* or *yidC2* genes were expressed similarly to the chimeric genes under control of the *gtfA* promoter in a Δ*yidC1*/Δ*yidC2* background for phenotypic characterization. Measurement of growth kinetics under non-stress conditions showed that the strains engineered to produce YidC2E92A or YidC2K253A were clearly affected compared to the unmodified YidC2 control strain. The negative impact of the YidC2 E92 and K253 mutations on growth of the *yidC2* ectopic expression strain was also observed by dilution plating of log-phase cultures. In contrast, strains producing YidC1K91A or YidC1E190A did not show any obvious difference in growth compared to ectopic expression of unmodified *yidC1* (**Figure 8A**). Thus, the YidC1 point mutations did not appear to impact its general housekeeping functions. However, when the ability of the point mutant strains to tolerate environmental stress conditions reflective of previously identified YidC1- and YidC2-associated functions was assessed, the apparent importance of the putative salt bridges was striking. The ability of ectopically expressed *yidC1* to support *S. mutans* growth in the presence of excess zinc was clearly abolished by the K91A and E190A point mutations (**Figure 8B**). Next, we measured the impact of point mutations within YidC2 on growth of *S. mutans* in THYE acidified to pH 5.0 (**Figure 8C**). Both the E92A and K253A point mutations destroyed the ability of YidC2 to contend with acid stress. Taken together, these results confirm that the residues predicted to form salt bridges within YidC1 and YidC2, respectively, do in fact contribute to the respective functional activities of each paralog under specific environmental conditions.

DISCUSSION

YidC belongs to the Oxa1/Alb3/YidC family of proteins present in all three domains of the life, and plays a pivotal role in the proper folding and insertion of membrane proteins in bacteria (Dalbey and Kuhn, 2015; Chen et al., 2019). When discovered in *E. coli*, YidC was demonstrated to be essential for viability (Samuelson et al., 2000). Later, discovery of two different paralogs in Gram-positive bacteria, including *B. subtilis* and *S. mutans,* showed that at least one YidC is required for growth and survival under various environmental conditions, although they are not equally effective (Errington et al., 1992; Tjalsma et al., 2003; Hasona et al., 2005; Saller et al., 2011; Palmer et al., 2012; Mishra et al., 2019; Zhao et al., 2019). Subsequent proteomic analysis of *S. mutans* membrane preparations from mutants lacking either *yidC1* or *yidC2,* coupled with characterization of the YidC1 compared to YidC2 interactomes, further revealed paralog-specific activities as well as overlap in their functional capabilities (Mishra et al., 2019; Lara Vasquez et al., 2021). Thus, when one paralog is eliminated, the residual paralog must accomplish many of the basic housekeeping needs of the cell. However, each paralog cannot fully accomplish the specific functions mediated by the other, thereby manifesting in characteristic phenotypic consequences. As expected for paralogous bacterial proteins, divergent SmYidC1 and SmYidC2 amino acid sequences have retained low sequence identity (∼30%). Nevertheless, their similar membrane topologies and largely superimposable predicted 3D structures are consistent with their high degree of functional overlap. Other than disparate roles for the C-terminal tails (Palmer et al., 2012), specific structural features responsible for distinct YidC1- and YidC2-associated functional attributes have not been characterized. The absence of SmYidC1 and SmYidC2 crystallographic data, the numerous yet unidentified paralog-specific membrane-localized substrates, and the current lack of experimental methods to carry out membrane protein insertion assays using exclusively components of Gram-positive translation and translocation machineries have hindered our understanding of YidC1- vs. YidC2-specific structure-function features. In this study, we utilized insights obtained from *in silico* sequence-structure analyses to engineer all possible cytoplasmic domain-swapped versions of YidC1/2 and tested growth of the chimeric variants under those environmental conditions known (acid, high salt), or predicted (excess metal), to contribute to paralog-specific phenotypes.

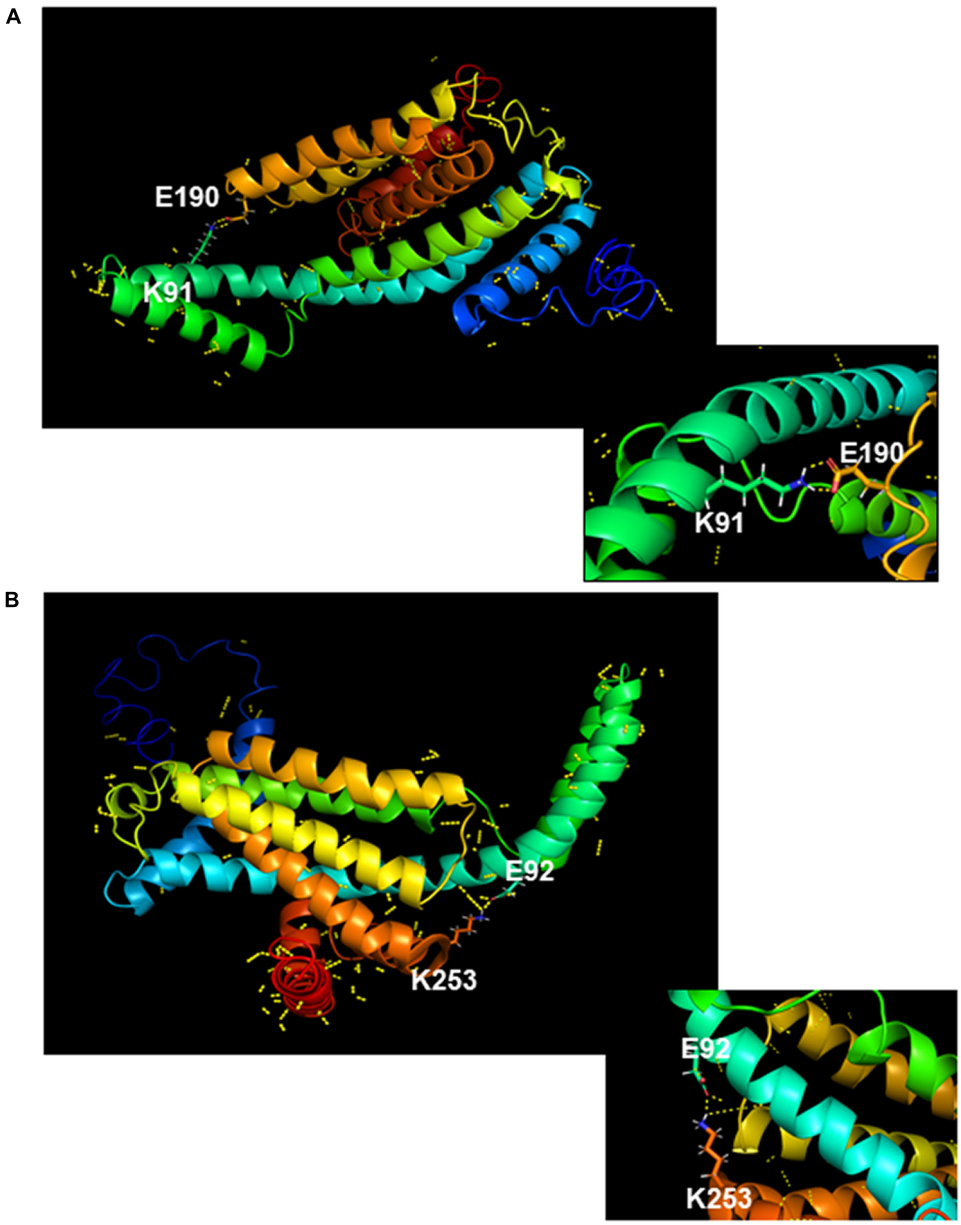

FIGURE 7 | *In silico* modeling of salt bridge formation between cytoplasmic domains of YidC1 or YidC2. **(A)** Putative polar contacts on the side chains of YidC1 (yellow) were mapped and displayed using the Pymol Plugin. The salt bridge between residues K91 and E190 is shown enlarged in the box. **(B)** Putative polar contacts on the side chains of YidC2 (yellow) were mapped and displayed using the Pymol Plugin. The salt bridge between residues E92 and K253 is shown enlarged in the box.

Cytoplasmic Domains Impart Distinct Functional Attributes to SmYidC1 and SmYidC2

An important breakthrough in the field of YidC structure-function occurred when crystal structures of BhYidC2 and *E. coli* YidC (EcYidC) were determined in 2014 (Kumazaki et al., 2014b,c). Both solved structures demonstrated the presence of a hydrophilic groove formed by the five core TMDs, which was proposed as a conserved structural feature of all YidCs. Structural analyses of both species' YidCs further suggested their C1 loops as a primary point of contact for incoming substrates (Kumazaki et al., 2014a). Another unrelated study utilized EcYidC mutants containing segmental deletions of the C1 loop and demonstrated the significance of the second-half of this domain in rescuing a YidC-depletion strain; although this work proposed that the precise sequence of C1 is not essential for EcYidC function (Chen et al., 2014). More recently, Koch and coworkers used formaldehyde cross-linking of *E. coli* cells to demonstrate that the YidC C1 loop interacts with the signal recognition particle

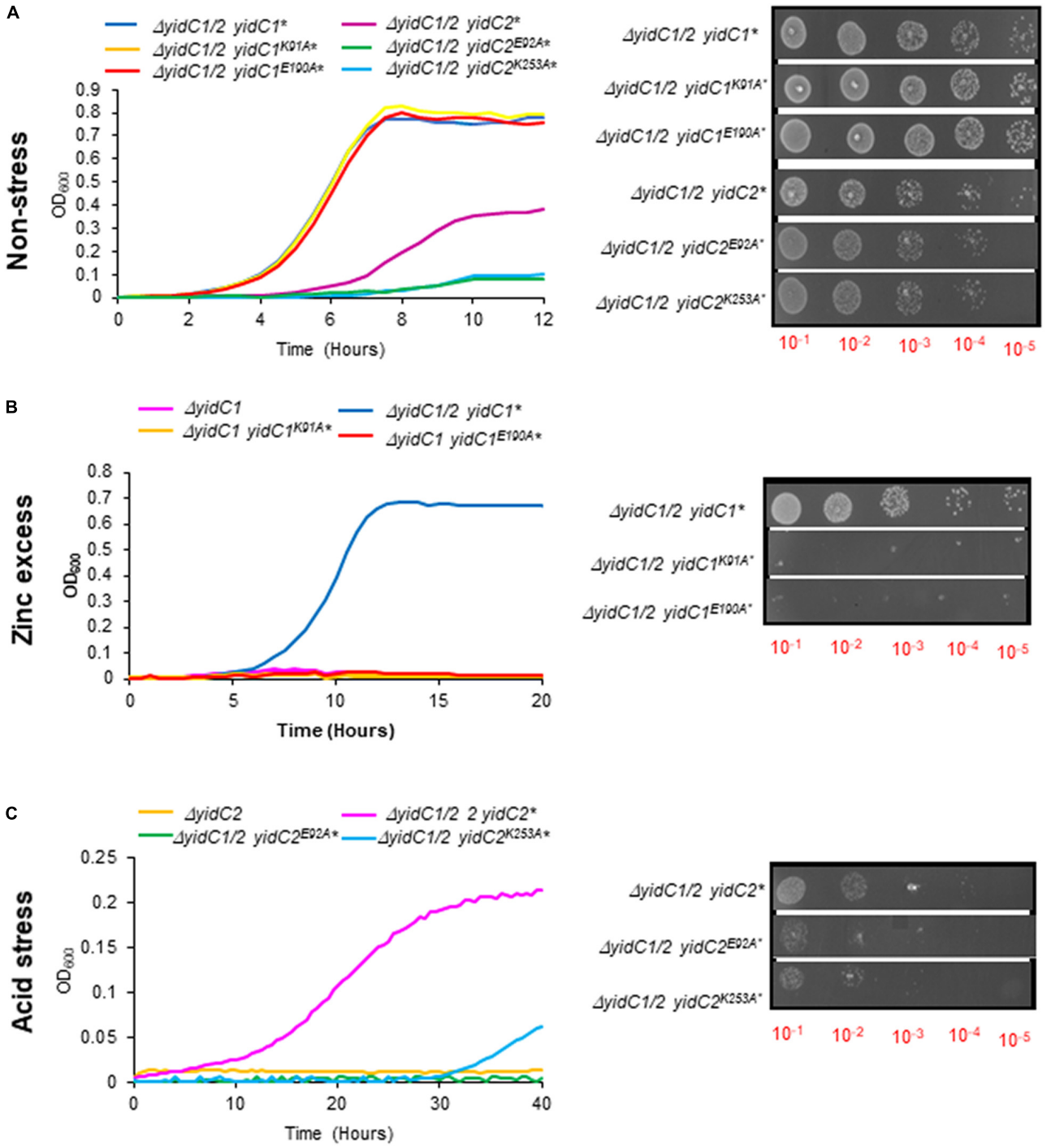

FIGURE 8 | Growth kinetics and efficiency of plating assay of *S. mutans* strains expressing *yidC1* or *yidC2* containing point mutations of residues predicted to contribute to salt bridge formation. Growth of strains complemented by ectopic expression (*) from the *gtfA* locus of unmodified *yidC1, yidC2*, or *yidC1* or *yidC2* containing the indicated point mutations, in a double Δ*yidC1*/Δ*yidC2* background under **(A)** non-stress (THYE, pH 7.0), **(B)** zinc excess (THYE containing 2.5 mM $ZnCl_2$), or **(C)** acid stress (THYE, pH 5.0) conditions.

(SRP), the SRP receptor FtsY, SecY, SecE, and SecG, with a stronger interaction identified with SRP compared to SecYEG (Petriman et al., 2018). Unlike its C1 loop, the BhYidC2 C2 loop was not structurally resolved by X-ray crystallography (Kumazaki et al., 2014c). Molecular dynamic (MD) simulations, however, predicted a contribution of the C2 loop in stabilizing

protein structure, especially in reducing flexibility of the C1 loop by formation of an inter-domain salt bridge between D205 (C2) and K109 (C1) (Harkey et al., 2019). Structural analysis of BhYidC2 also revealed that its C1 loop is assessable to the cytoplasm, while the smaller C2 loop appears to be embedded within the lipid bilayer and probably involved in an interaction with lipid heads.

Since the discovery of dual YidC paralogs in the overwhelming majority of Gram-positive bacteria, it has been of broad interest to understand how they are structurally and functionally distinguished. Distinctive lengths and charge distribution of their cytoplasmic tails is a striking feature. Previous work demonstrated the significance of the SmYidC2 tail with respect to its contribution to acid tolerance; however, the underlying mechanism for this result was not fully understood (Palmer et al., 2012). Driessen and coworkers used purified SmYidC1 and SmYidC2 to demonstrate that both of their tails appear to be involved in interactions with ribosomal proteins; although this work was carried out using *E. coli* ribosomes (Wu et al., 2013). Of note, the longer tails of marine Gram-negative bacteria such as *Rhodopirellula baltica* and *Oceanicaulis alexandrii* interacted with *E. coli* ribosomal proteins, whereas *E. coli* YidC with a shorter C-terminal tail failed to do so (Seitl et al., 2014). We analyzed the respective interactomes of YidC1 and YidC2, including assessment of the binding partners of their C-terminal tails by 2D-difference gel electrophoresis (DIGE) (Lara Vasquez et al., 2021). These data clearly suggested that the isolated C-terminal tails can interact with multiple ribosomal proteins but do not appear to play an important role in recognizing and binding substrates. Characterization of the YidC1/2 protein interactomes showed that of YidC1 to be larger than that of YidC2, and further identified YidC1-SecYEG and YidC2-SRP interactions in *S. mutans* (Lara Vasquez et al., 2021). Bacterial two-hybrid experiments revealed that YidC1 could interact with both SecY and Ffh, while YidC2 could only interact with the SRP protein Ffh (Lara Vasquez et al., 2021). This explained in part, why individual deletion of *yidC2* or *ffh* results in similar growth defects and stress-sensitivity profiles, and co-deletion of *yidC2* and *ffh* is lethal (Hasona et al., 2005; Mishra et al., 2019). Taken together with prior interactome data, and the *in silico* sequence-structure analyses performed in the current study, we hypothesized that their cytoplasmic domains play pivotal roles in conferring functional differences between *S. mutans* YidC1 and YidC2. The data we obtained support this hypothesis.

YidC1 Structure Is More Functionally Resilient That of YidC2

In silico analyses showed higher RMSD values, and therefore greater structural deviations from unmodified YidC1 for most of the chimeric YidC1 variants. Yet strains harboring chimeric YidC1 did not manifest significant growth phenotypes under numerous experimental conditions. This suggests that YidC1 can accommodate multiple structural perturbations without loss of function, or in other words, that its structural malleability is associated with functional plasticity. In contrast, *in silico* analyses of chimeric YidC2 variants showed less structural deviation from unmodified YidC2, with most domain substitutions resulting in impaired YidC2 function as manifested by an inability to support bacterial growth under the conditions tested. This suggests that the more rigid nature of YidC2 compared to YidC1 constrains its ability to mediate insertion of the membrane proteins necessary for bacterial growth and tolerance to environmental stress when its cytoplasmic domains are exchanged for those of YidC1.

YidC1 and YidC2 Cytoplasmic Domains Possess Distinct Intra- and Inter-Domain Interactions

An interesting outcome of the current work was the preference for certain combinations of cytoplasmic domains over others, which was especially notable among the chimeric YidC2 variants. The results of *in silico* analyses of chimeras compared with unmodified YidC1 and YidC2, as evidenced by small (<3 Å) RMSD values, further suggests that certain combinatorial substitutions result in a propensity for the tertiary structure of a given chimera to more closely align with YidC1 or YidC2. In light of *in silico* structure predictions, combined with insight gained from phenotypic assays, we hypothesized that specific interactions between cytoplasmic domains were responsible for particular structure-function attributes. In fact, Moradi and coworkers had proposed that formation of a salt-bridge between the C1 and C2 loops of *B. halodurans* YidC2 appears to stabilize the flexible C1 loop (Harkey et al., 2019). When the SmYidC1 and SmYidC2 cytoplasmic domains were evaluated, both paralogs contained multiple oppositely charged residues within close enough proximity (<3 Å) to form salt-bridges (**Supplementary Table 6**). Most were intra-domain interactions; however, we focused on the two inter-domain interactions identified within YidC1 [K91(C1)-E190(C2)] and YidC2 [E92(C1)-K253(tail)], respectively. Similar to deletion of *yidC2*, the YidC2K253A mutant had a severe growth phenotype. The other three point mutants also recapitulated environmental stress phenotypes associated with *yidC1* or yidC*2* deletion. Hence, the predicted inter-domain salt bridges appear to play important roles in stabilizing YidC1 and YidC2 structures that are necessary for paralog-specific activities.

Impact of YidC1 and YidC2 on Metal Toxicity

An interesting outcome of the current work was the discovery of a novel *yidC1* elimination phenotype. We previously identified pronounced sensitivity to acid, osmotic, or oxidative stress as a result of *yidC2* elimination (Hasona et al., 2005). In contrast, elimination of *yidC1* had far less obvious consequences apart from a modest impact on maturation of surface proteins and hyperadherence to salivary components (Palmer et al., 2012). However, until now a readily assayable clearcut phenotype associated primarily with *yidC1* elimination had not been observed. Our proteomic characterization of *S. mutans* membrane preparations derived from WT and mutant strains, including Δ*yidC1* and Δ*yidC2,* had suggested overlapping, as

well as differential, impacts of elimination of these insertases on the levels of previously characterized, or predicted, membrane-localized metal transporters or regulators (**Supplementary Table 5**; Mishra et al., 2019). Thus, the survival of *S. mutans* Δ*yidC1* and Δ*yidC2* mutants, and the behavior of the ectopic-expression chimeric and control strains, in the presence of excess zinc, iron, and manganese were assessed as part of this work. *S. mutans* contains multiple transporters for Fe(II) including FeoABC, the SMU_995-998 system, and the Mn(II) transporters SloABC and MntH (Paik et al., 2003; Galvao et al., 2015; Ganguly et al., 2018). Deletion of *yidC2* had a more apparent impact on *S. mutans* tolerance to Fe(II) and Mn(II) excess than deletion of *yidC1*, with most YidC2-backbone chimeric proteins being negatively impacted by substitution of YidC1 cytoplasmic domains. However, lack of complete complementation of iron and manganese tolerance by ectopic expression of *yidC2* in a Δ*yidC1*/Δ*yidC2* background suggests the existence of regulatory circuits that will require extensive future study.

While deletion of *yidC2* had a slight impact on zinc tolerance, it did not approach that of *yidC1* deletion. Ectopic expression of *yidC1* in a Δ*yidC1*/Δ*yidC2* background almost completely restored growth in excess Zn(II) to wild-type levels. Proteomic data revealed a pronounced decrease in levels of the putative metal transporter Smu_2057 associated with elimination of *yidC1* compared to *yidC2* (**Supplementary Table 5**). Blast search showed SMU_2057 to be 42% identical and 61% homologous to the *B. subtilis* metal transporting ATPase, PfeT. Mutation of *pfeT* led to improved growth in Zn(II) excess conditions (Gaballa and Helmann, 2002), but the molecular mechanism of the PfeT-dependent increase in growth remains elusive (Guan et al., 2015). It has been proposed to be mediated by mismetallation caused by Zn(II) under aerated conditions when PfeT-dependent iron-efflux is inhibited. The role of SMU_2057 in zinc homeostasis in *S. mutans*, and the potential role of YidC1 in its membrane insertion, will be of much interest in future studies.

Concluding Remarks

In summary, this work successfully revealed distinct functional contributions of cytoplasmic domains to paralog-specific functions of *S. mutans* YidC1 and YidC2. The novel discovery of functionally significant residues within the *S. mutans* YidC1/2 cytoplasmic domains is important, especially since bacterial YidC TMDs have received more attention in prior structure-function studies given their membrane localization and direct involvement in substrate insertion. This newly acquired knowledge will provide additional insights as YidC1/2-specific substrates and relevant interactions with other components of the protein translocation machinery are identified in *S. mutans* and other Gram-positive bacteria.

DATA AVAILABILITY STATEMENT

The original contributions presented in the study are included in the article/**Supplementary Material**, further inquiries can be directed to the corresponding author/s.

AUTHOR CONTRIBUTIONS

SM and LJB conceived the experiments, analyzed the data, and wrote the manuscript. SM performed the experiments and collected data. All authors contributed to the article and approved the submitted version.

FUNDING

This work was supported by NIH NIDCR award DE008007 to LJB.

SUPPLEMENTARY MATERIAL

The Supplementary Material for this article can be found online at: https://www.frontiersin.org/articles/10.3389/fmicb.2021.760873/full#supplementary-material

REFERENCES

Ajdic, D., Mcshan, W. M., Mclaughlin, R. E., Savic, G., Chang, J., Carson, M. B., et al. (2002). Genome sequence of *Streptococcus mutans* UA159, a cariogenic dental pathogen. *Proc. Natl. Acad. Sci. USA* 99, 14434–14439. doi: 10.1073/pnas.172501299

Bagos, P. G., Tsirigos, K. D., Liakopoulos, T. D., and Hamodrakas, S. J. (2008). Prediction of lipoprotein signal peptides in Gram-positive bacteria with a Hidden Markov Model. *J. Proteome Res.* 7, 5082–5093. doi: 10.1021/pr800162c

Ban, X., Lahiri, P., Dhoble, A. S., Li, D., Gu, Z., Li, C., et al. (2019). Evolutionary stability of salt bridges hints its contribution to stability of proteins. *Comput. Struct. Biotechnol. J.* 17, 895–903. doi: 10.1016/j.csbj.2019.06.022

Chandrangsu, P., Rensing, C., and Helmann, J. D. (2017). Metal homeostasis and resistance in bacteria. *Nat. Rev. Microbiol.* 15, 338–350. doi: 10.1038/nrmicro.2017.15

Chen, Y., Shanmugam, S. K., and Dalbey, R. E. (2019). The principles of protein targeting and transport across cell membranes. *Protein J.* 38, 236–248. doi: 10.1007/s10930-019-09847-2

Chen, Y., Soman, R., Shanmugam, S. K., Kuhn, A., and Dalbey, R. E. (2014). The role of the strictly conserved positively charged residue differs among the Gram-positive, Gram-negative, and chloroplast YidC homologs. *J. Biol. Chem.* 289, 35656–35667. doi: 10.1074/jbc.M114.595082

Conrad, B., and Antonarakis, S. E. (2007). Gene duplication: a drive for phenotypic diversity and cause of human disease. *Annu. Rev. Genomics Hum. Genet.* 8, 17–35. doi: 10.1146/annurev.genom.8.021307.110233

Dalbey, R. E., and Kuhn, A. (2015). Membrane insertases are present in all three domains of life. *Structure* 23, 1559–1560. doi: 10.1016/j.str.2015.08.002

Errington, J., Appleby, L., Daniel, R. A., Goodfellow, H., Partridge, S. R., and Yudkin, M. D. (1992). Structure and function of the spoIIIJ gene of *Bacillus subtilis*: a vegetatively expressed gene that is essential for sigma G activity at an intermediate stage of sporulation. *J. Gen. Microbiol.* 138, 2609–2618. doi: 10.1099/00221287-138-12-2609

Gaballa, A., and Helmann, J. D. (2002). A peroxide-induced zinc uptake system plays an important role in protection against oxidative stress in *Bacillus subtilis*. *Mol. Microbiol.* 45, 997–1005. doi: 10.1046/j.1365-2958.2002.03068.x

Galvao, L. C., Miller, J. H., Kajfasz, J. K., Scott-Anne, K., Freires, I. A., Franco, G. C., et al. (2015). Transcriptional and phenotypic characterization of novel

spx-regulated genes in *Streptococcus mutans*. *PLoS One* 10:e0124969. doi: 10.1371/journal.pone.0124969

Ganguly, T., Kajfasz, J. K., Miller, J. H., Rabinowitz, E., Galvao, L. C. C., Rosalen, P. L., et al. (2018). Disruption of a novel iron transport system reverses oxidative stress phenotypes of a dpr mutant strain of streptococcus mutans. *J. Bacteriol.* 2018:200. doi: 10.1128/JB.00062-18

Gasteiger, E., Hoogland, C., Gattiker, A., Duvaud, S., Wilkins, M. R., Appel, R. D., et al. (2005). *The Proteomics Protocols Handbook*. Totowa, N.J: Humana Press.

Gouet, P., Courcelle, E., Stuart, D. I., and Metoz, F. (1999). ESPript: analysis of multiple sequence alignments in PostScript. *Bioinformatics* 15, 305–308. doi: 10.1093/bioinformatics/15.4.305

Guan, G., Pinochet-Barros, A., Gaballa, A., Patel, S. J., Arguello, J. M., and Helmann, J. D. (2015). PfeT, a P1B4 -type ATPase, effluxes ferrous iron and protects Bacillus subtilis against iron intoxication. *Mol. Microbiol.* 98, 787–803. doi: 10.1111/mmi.13158

Hamada, S., and Slade, H. D. (1980). Biology, immunology, and cariogenicity of Streptococcus mutans. *Microbiol. Rev.* 44, 331–384. doi: 10.1128/mr.44.2.331-384.1980

Harkey, T., Govind Kumar, V., Hettige, J., Tabari, S. H., Immadisetty, K., and Moradi, M. (2019). The role of a crystallographically unresolved cytoplasmic loop in stabilizing the bacterial membrane insertase YidC2. *Sci. Rep.* 9:14451. doi: 10.1038/s41598-019-51052-9

Hasona, A., Crowley, P. J., Levesque, C. M., Mair, R. W., Cvitkovitch, D. G., Bleiweis, A. S., et al. (2005). Streptococcal viability and diminished stress tolerance in mutants lacking the signal recognition particle pathway or YidC2. *Proc. Natl. Acad. Sci. USA* 102, 17466–17471. doi: 10.1073/pnas.0508778102

Koch, H. G., Moser, M., and Muller, M. (2003). Signal recognition particle-dependent protein targeting, universal to all kingdoms of life. *Rev. Physiol. Biochem. Pharmacol.* 146, 55–94. doi: 10.1007/s10254-002-0002-9

Kol, S., Nouwen, N., and Driessen, A. J. (2008). The charge distribution in the cytoplasmic loop of subunit C of the F1F0 ATPase is a determinant for YidC targeting. *J. Biol. Chem.* 283, 9871–9877. doi: 10.1074/jbc.M709408200

Krogh, A., Larsson, B., Vonheijne, G., and Sonnhammer, E. L. (2001). Predicting transmembrane protein topology with a hidden Markov model: application to complete genomes. *J. Mol. Biol.* 305, 567–580. doi: 10.1006/jmbi.2000.4315

Kumazaki, K., Chiba, S., Takemoto, M., Furukawa, A., Nishiyama, K., Sugano, Y., et al. (2014a). Structural basis of Sec-independent membrane protein insertion by YidC. *Nature* 509, 516–520. doi: 10.1038/nature13167

Kumazaki, K., Kishimoto, T., Furukawa, A., Mori, H., Tanaka, Y., Dohmae, N., et al. (2014b). Crystal structure of *Escherichia coli* YidC, a membrane protein chaperone and insertase. *Sci. Rep.* 4:7299. doi: 10.1038/srep07299

Kumazaki, K., Tsukazaki, T., Nishizawa, T., Tanaka, Y., Kato, H. E., Nakada-Nakura, Y., et al. (2014c). Crystallization and preliminary X-ray diffraction analysis of YidC, a membrane-protein chaperone and insertase from Bacillus halodurans. *Acta Crystallogr. F Struct. Biol. Commun.* 70, 1056–1060. doi: 10.1107/S2053230X14012540

Kyte, J., and Doolittle, R. F. (1982). A simple method for displaying the hydropathic character of a protein. *J. Mol. Biol.* 157, 105–132. doi: 10.1016/0022-2836(82)90515-0

Lara Vasquez, P., Mishra, S., Kuppuswamy, S. K., Crowley, P. J., and Brady, L. J. (2021). Protein Interactomes of Streptococcus mutans YidC1 and YidC2 Membrane Protein Insertases Suggest SRP pathway-independent- and -dependent functions, respectively. *mSphere* 6:e01308-20. doi: 10.1128/mSphere.01308-20

Lemos, J. A., Palmer, S. R., Zeng, L., Wen, Z. T., Kajfasz, J. K., Freires, I. A., et al. (2019). The Biology of Streptococcus mutans. *Microbiol. Spectr.* 7:512018. doi: 10.1128/9781683670131.ch27

Lewis, N. E., and Brady, L. J. (2015). Breaking the bacterial protein targeting and translocation model: oral organisms as a case in point. *Mol. Oral Microbiol.* 30, 186–197. doi: 10.1111/omi.12088

Lockwood, W. R., Lawson, L. A., Smith, D. L., Mcneil, K. M., and Morrison, F. S. (1974). Streptococcus mutans endocarditis. Report of a case. *Ann. Intern. Med.* 80, 369–370. doi: 10.7326/0003-4819-80-3-369

McGhie, D., Hutchison, J. G., Nye, F., and Ball, A. P. (1977). Infective endocarditis caused by Streptococcus mutans. *Br. Heart J.* 39, 456–458. doi: 10.1136/hrt.39.4.456

Mishra, S., Crowley, P. J., Wright, K. R., Palmer, S. R., Walker, A. R., Datta, S., et al. (2019). Membrane proteomic analysis reveals overlapping and independent functions of Streptococcus mutans Ffh, YidC1, and YidC2. *Mol. Oral Microbiol.* 34, 131–152. doi: 10.1111/omi.12261

Moore, C. M., and Helmann, J. D. (2005). Metal ion homeostasis in *Bacillus subtilis*. *Curr. Opin. Microbiol.* 8, 188–195. doi: 10.1016/j.mib.2005.02.007

Moore, J., Keane, C. T., and Tomkin, G. H. (1977). Streptococcus mutans endocarditis. *Ir. J. Med. Sci.* 146, 144–145. doi: 10.1007/BF03030949

Nomura, R., Nakano, K., Nemoto, H., Fujita, K., Inagaki, S., Takahashi, T., et al. (2006). Isolation and characterization of Streptococcus mutans in heart valve and dental plaque specimens from a patient with infective endocarditis. *J. Med. Microbiol.* 55, 1135–1140. doi: 10.1099/jmm.0.46609-0

Paik, S., Brown, A., Munro, C. L., Cornelissen, C. N., and Kitten, T. (2003). The sloABCR operon of Streptococcus mutans encodes an Mn and Fe transport system required for endocarditis virulence and its Mn-dependent repressor. *J. Bacteriol.* 185, 5967–5975. doi: 10.1128/JB.185.20.5967-5975.2003

Palmer, S. R., Crowley, P. J., Oli, M. W., Ruelf, M. A., Michalek, S. M., and Brady, L. J. (2012). YidC1 and YidC2 are functionally distinct proteins involved in protein secretion, biofilm formation and cariogenicity of Streptococcus mutans. *Microbiology* 158, 1702–1712. doi: 10.1099/mic.0.059139-0

Petersen, T. N., Brunak, S., Vonheijne, G., and Nielsen, H. (2011). SignalP 4.0: discriminating signal peptides from transmembrane regions. *Nat. Methods* 8, 785–786. doi: 10.1038/nmeth.1701

Petriman, N. A., Jauss, B., Hufnagel, A., Franz, L., Sachelaru, I., Drepper, F., et al. (2018). The interaction network of the YidC insertase with the SecYEG translocon, SRP and the SRP receptor FtsY. *Sci. Rep.* 8:578. doi: 10.1038/s41598-017-19019-w

Price, C. E., Otto, A., Fusetti, F., Becher, D., Hecker, M., and Driessen, A. J. (2010). Differential effect of YidC depletion on the membrane proteome of *Escherichia coli* under aerobic and anaerobic growth conditions. *Proteomics* 10, 3235–3247. doi: 10.1002/pmic.201000284

Roy, A., Kucukural, A., and Zhang, Y. (2010). I-TASSER: a unified platform for automated protein structure and function prediction. *Nat. Protoc.* 5, 725–738. doi: 10.1038/nprot.2010.5

Saller, M. J., Otto, A., Berrelkamp-Lahpor, G. A., Becher, D., Hecker, M., and Driessen, A. J. (2011). Bacillus subtilis YqjG is required for genetic competence development. *Proteomics* 11, 270–282. doi: 10.1002/pmic.201000435

Samuelson, J. C., Chen, M., Jiang, F., Moller, I., Wiedmann, M., Kuhn, A., et al. (2000). YidC mediates membrane protein insertion in bacteria. *Nature* 406, 637–641. doi: 10.1038/35020586

Schneider, T. D., and Stephens, R. M. (1990). Sequence logos: a new way to display consensus sequences. *Nucleic Acids Res.* 18, 6097–6100. doi: 10.1093/nar/18.20.6097

Scotti, P. A., Urbanus, M. L., Brunner, J., Degier, J. W., Von Heijne, G., Van Der Does, C., et al. (2000). YidC, the *Escherichia coli* homologue of mitochondrial Oxa1p, is a component of the Sec translocase. *EMBO J.* 19, 542–549. doi: 10.1093/emboj/19.4.542

Seitl, I., Wickles, S., Beckmann, R., Kuhn, A., and Kiefer, D. (2014). The C-terminal regions of YidC from Rhodopirellula baltica and Oceanicaulis alexandrii bind to ribosomes and partially substitute for SRP receptor function in *Escherichia coli*. *Mol. Microbiol.* 91, 408–421. doi: 10.1111/mmi.12465

Shindyalov, I. N., and Bourne, P. E. (1998). Protein structure alignment by incremental combinatorial extension (CE) of the optimal path. *Protein Eng.* 11, 739–747. doi: 10.1093/protein/11.9.739

Smith, J. P., Marymont, J. H., and Schweers, J. H. (1977). Subacute bacterial endocarditis due to Streptococcus mutans. *Am. J. Med. Technol.* 43, 429–432.

Steinberg, R., Knupffer, L., Origi, A., Asti, R., and Koch, H. G. (2018). Co-translational protein targeting in bacteria. *FEMS Microbiol. Lett.* 365:95. doi: 10.1093/femsle/fny095

Stoffel, K. H. A. W. (1993). Tmbase-a database of membrane spanning protein segments. *Biol. Chem. Hoppe. Seyler.* 347:166.

Storz, G., and Imlay, J. A. (1999). Oxidative stress. *Curr. Opin. Microbiol.* 2, 188–194.

Tjalsma, H., Bron, S., and Vandijl, J. M. (2003). Complementary impact of paralogous Oxa1-like proteins of Bacillus subtilis on post-translocational stages in protein secretion. *J. Biol. Chem.* 278, 15622–15632. doi: 10.1074/jbc.M301205200

Urbanus, M. L., Scotti, P. A., Froderberg, L., Saaf, A., Degier, J. W., Brunner, J., et al. (2001). Sec-dependent membrane protein insertion: sequential interaction of nascent FtsQ with SecY and YidC. *EMBO Rep.* 2, 524–529. doi: 10.1093/embo-reports/kve108

van Bloois, E., Janhaan, G., Degier, J. W., Oudega, B., and Luirink, J. (2004). F(1)F(0) ATP synthase subunit c is targeted by the SRP to YidC in the E. coli inner membrane. *FEBS Lett.* 576, 97–100. doi: 10.1016/j.febslet.2004.08.069

van der Laan, M., Nouwen, N., and Driessen, A. J. (2004). SecYEG proteoliposomes catalyze the Deltaphi-dependent membrane insertion of FtsQ. *J. Biol. Chem.* 279, 1659–1664. doi: 10.1074/jbc.M306527200

Vose, J. M., Smith, P. W., Henry, M., and Colan, D. (1987). Recurrent Streptococcus mutans endocarditis. *Am. J. Med.* 82, 630–632. doi: 10.1016/0002-9343(87)90111-2

Williams, M. L., Crowley, P. J., Hasona, A., and Brady, L. J. (2014). YlxM is a newly identified accessory protein that influences the function of signal recognition particle pathway components in Streptococcus mutans. *J. Bacteriol.* 196, 2043–2052. doi: 10.1128/JB.01465-13

Wu, Z. C., De, K. E. Y. Z. E. R., Berrelkamp-Lahpor, G. A., and Driessen, A. J. (2013). Interaction of Streptococcus mutans YidC1 and YidC2 with translating and nontranslating ribosomes. *J. Bacteriol.* 195, 4545–4551. doi: 10.1128/JB.00792-13

Yi, L., Celebi, N., Chen, M., and Dalbey, R. E. (2004). Sec/SRP requirements and energetics of membrane insertion of subunits a, b, and c of the *Escherichia coli* F1F0 ATP synthase. *J. Biol. Chem.* 279, 39260–39267. doi: 10.1074/jbc.M405490200

Zallot, R., Harrison, K. J., Kolaczkowski, B., and Decrecylagard, V. (2016). Functional annotations of paralogs: a blessing and a curse. *Life* 6:39. doi: 10.3390/life6030039

Zhao, H., Sachla, A. J., and Helmann, J. D. (2019). Mutations of the Bacillus subtilis YidC1 (SpoIIIJ) insertase alleviate stress associated with sigmaM-dependent membrane protein overproduction. *PLoS Genet* 15:e1008263. doi: 10.1371/journal.pgen.1008263

Zheng, L., Baumann, U., and Reymond, J. L. (2004). An efficient one-step site-directed and site-saturation mutagenesis protocol. *Nucleic Acids Res.* 32:e115. doi: 10.1093/nar/gnh110

Conflict of Interest: The authors declare that the research was conducted in the absence of any commercial or financial relationships that could be construed as a potential conflict of interest.

Publisher's Note: All claims expressed in this article are solely those of the authors and do not necessarily represent those of their affiliated organizations, or those of the publisher, the editors and the reviewers. Any product that may be evaluated in this article, or claim that may be made by its manufacturer, is not guaranteed or endorsed by the publisher.

frontiers in Microbiology

MINI REVIEW
published: 05 November 2021
doi: 10.3389/fmicb.2021.756136

Roles of Type VI Secretion System in Transport of Metal Ions

Xiaobing Yang[1,2], Hai Liu[3], Yanxiong Zhang[3] and Xihui Shen[4]**

[1] College of Applied Engineering, Henan University of Science and Technology (HAUST), Sanmenxia, China, [2] Medical College, Sanmenxia Vocational Technical School, Sanmenxia, China, [3] Qingyang Longfeng Sponge City Construction Management & Operation Co., Ltd, Qingyang, China, [4] State Key Laboratory of Crop Stress Biology for Arid Areas, Shaanxi Key Laboratory of Agricultural and Environmental Microbiology, College of Life Sciences, Northwest A&F University, Xianyang, China

The type VI secretion system (T6SS) is a transmembrane protein nanomachine employed by many gram-negative bacteria to directly translocate effectors into adjacent cells or the extracellular milieu, showing multiple functions in both interbacterial competition and bacteria-host interactions. Metal ion transport is a newly discovered T6SS function. This review summarizes the identified T6SS functions and highlights the features of metal ion transport mediated by T6SS and discusses its regulation.

Keywords: type VI secretion system, effectors, metal ions, transport, regulation

OPEN ACCESS

Edited by:
Eric Cascales,
Aix-Marseille Université, France

Reviewed by:
Miguel A. Valvano,
Queen's University Belfast, United Kingdom
Jin He,
Huazhong Agricultural University, China

***Correspondence:**
Hai Liu
liuhai@capitalwater.cn
Xihui Shen
xihuishen@nwsuaf.edu.cn

Specialty section:
This article was submitted to Microbial Physiology and Metabolism, a section of the journal Frontiers in Microbiology

Received: *10 August 2021*
Accepted: *12 October 2021*
Published: *05 November 2021*

Citation:
Yang X, Liu H, Zhang Y and Shen X (2021) Roles of Type VI Secretion System in Transport of Metal Ions. Front. Microbiol. 12:756136. doi: 10.3389/fmicb.2021.756136

INTRODUCTION

The type VI secretion system (T6SS) is a transmembrane protein nanomachine employed by many gram-negative bacteria to translocate effectors directly into adjacent target cells or the extracellular milieu (Cianfanelli et al., 2016). T6SS was regarded as virulence-associated secretion apparatus because of its association with pathogenicity (Mougous et al., 2006; Pukatzki et al., 2006). However, subsequent studies have demonstrated T6SS function is involved in multiple physiological and biochemical processes apart from bacterial pathogenesis, such as interbacterial competition (Hood et al., 2010; Chassaing and Cascales, 2018), commensalism or symbiosis (Chow and Mazmanian, 2010), stress response (Weber et al., 2009; Wan et al., 2017), biofilm formation (Zhang et al., 2011; Gallique et al., 2017), and horizontal gene transfer (Borgeaud et al., 2015).

It has been reported that the T6SS function is determined by the loading effectors that can be delivered extracellularly based on energy consumption and load transport (Cianfanelli et al., 2016; Coulthurst, 2019). Many T6SS effectors related to virulence or competition that target the cell wall, membranes, and nucleic acids have been reported (Yang et al., 2018; Song et al., 2021). Several effectors with special activities have also been found. For example, a T6SS dependent effector, YezP, has been reported to combine with Zn^{2+} and contribute to Zn^{2+} transport to deal with environmental stresses (Wang et al., 2015), and subsequent studies confirmed the function of T6SS dependent transport of metal ions (Lin et al., 2017; Si et al., 2017b). This review highlights the features of T6SS-dependent metal ion transport and its regulation.

TYPE VI SECRETION SYSTEM FUNCTIONS FOR METAL IONS TRANSPORT

Metal ions are commonly found in all organisms in association with proteins, such as enzymes, storage proteins, and transcription factors. The metal ions are involved in many crucial biological

Abbreviations: T6SS, type VI secretion system; Azu, azurin.

processes and are necessary for cell survival (Hood and Skaar, 2012). Bacteria have evolved sophisticated acquisition systems, including low- and high-affinity transport systems for scavenging essential chelated or free metals from the environment (Porcheron et al., 2013). As a versatile secretion system widely distributed in Gram-negative bacteria, The T6SS was found to participate in the transport of iron, zinc, copper, manganese, and molybdate, summarized in **Table 1**.

Zinc

Zinc is the second most important transition metal ion in living organisms after iron, playing an essential catalytic and structural role in several proteins involved in DNA replication, glycolysis, pH regulation, amino acid biosynthesis, extracellular peptidoglycan, and low molecular weight thiols (Porcheron et al., 2013). Zinc status is linked to the maintenance of intracellular redox buffering (Andreini et al., 2006). Both the high-affinity transporter ZnuACB and the low-affinity uptake system ZupT mediate zinc uptake across the cytoplasmic membrane (Hantke, 2005). Zinc is an essential nutrient for cells; Excess of zinc is toxic. Therefore, bacterial cells should achieve a delicate balance between ensuring sufficient zinc concentrations to fulfill essential functions while limiting concentration to prevent toxic effects. Zinc homeostasis is mediated by a network of zinc influx and efflux pumps (Wang et al., 2012; Wang and Fierke, 2013).

Wang et al. (2015) reported that the T6SS-4 from *Yersinia pseudotuberculosis* (*Yptb*) can combat multiple adverse stresses and host nutritional immunity, by displaying an unexpected function in transport of Zn^{2+}. Zinc transport is achieved by T6SS-4-mediated secretion of a Zn^{2+}-binding protein substrate, YezP (YPK_3549), which binds Zn^{2+} with high affinity, and represents a novel class of T6SS effector distinct from those extensively studied as bacteriolytic toxins or eukaryotic cell-targeting effectors. Hydroxyl radicals are deleterious reactive oxygen species that are often generated via Fenton chemistry under stress conditions (Mols and Abee, 2011). T6SS-4 was critical to neutralize hydroxyl radicals accumulated under adverse stress conditions, by accumulating Zn^{2+}, which can mitigate hydroxyl radicals to reduce them damage. By mitigating the detrimental hydroxyl radicals induced by multiple stresses, T6SS-4 provided a molecular explanation to the phenomenon of "cross-protection" in which cells subjected to one stress become resistant to distinctly different insults (Isohanni et al., 2013). Consistent with the function of T6SS-4 in combating stress, its expression is regulated by multiple transcription regulators, such as OmpR (Gueguen et al., 2013; Zhang et al., 2013), OxyR (Wang et al., 2015), RovM (Song et al., 2015), RpoS (Guan et al., 2015), and RelA (Yang et al., 2019), all of which respond to various stresses (Song et al., 2015; Zhao et al., 2017; Yang et al., 2019). Both ZntR and Zur, two zinc responsive regulators, are also involved in T6SS-4 regulation by directly binding to its promoter region (Wang et al., 2017; Cai et al., 2021).

The type VI secretion system-4 dependent zinc transport also plays a crucial role in the interactions of pathogenic *Y. pseudotuberculosis* with its mammalian host, as *Y. pseudotuberculosis* T6SS-4 mutants are attenuated in virulence against mice. Especially, mutation of T6SS-4 or *yezP* together with *znuCB* [a classic zinc transporter known to combat host nutritional immunity (Hood et al., 2012; Liu et al., 2012)] resulted in mutants that almost completely lost the virulence against mice, suggesting the importance of T6SS-4 the resistance to host nutritional immunity (Wang et al., 2015). This finding revealed a new mechanism of T6SS in pathogenesis. Further studies on *Burkholderia thailandensis* have revealed the mechanism of zinc ions transport across the membrane through T6SS (Si et al., 2017a). The T6SS-4 in *B. thailandensis* is involved in zinc acquisition via contact-independent secretion of a zinc-scavenging protein, TseZ (BTH_II1884), which cooperates with HmuR, the outer membrane heme transporter for zinc acquisition. T6SS secreted TseZ directly binds zinc ions and interacts with the heme transporter HmuR to transport zinc across the outer membrane. HmuR is a redox-regulated dual functional transporter. Under normal conditions, HmuR is used mainly for the transport of heme-iron; HmuR switches to transport of zinc upon sensing extracellular oxidative stress. Under mild oxidative stress condition, HmuR-mediated zinc transport alone is sufficient to maintain intracellular redox homeostasis. In contrast, under severe oxidative stress challenge, T6SS-4 is fully induced and secretes the proteinaceous zincophore TseZ to enhance the efficiency of HmuR-mediated zinc transport (Si et al., 2017a).

In *Burkholderia pseudomallei*, the T6SS-2 gene cluster also encodes a zinc binding protein (TseZ). TonB-dependent transporters that interact with TseZ and actively transport Zn^{2+} across the outer membrane have also been identified as BhuR (DeShazer, 2019).

TABLE 1 | T6SS dependent ions transport related factors.

Bacteria species	T6SS effector	Membrane transporter	Metal ions	Citation
Y. pseudotuberculosis	YezP		Zinc	Wang et al., 2015
Y. pseudotuberculosis	TssS		Manganese	Zhu et al., 2021
B. thailandensis	TseM	MnoT	Manganese	Si et al., 2017b
B. thailandensis	TseZ	HmuR	Zinc	Si et al., 2017a
B. pseudomallei	TseZ	BhuR	Zinc	DeShazer, 2019
B. pseudomallei	TseM	MnoT	Manganese	DeShazer, 2019
P. aeruginosa	TseF	FptA/OprF	Iron	Lin et al., 2017
P. aeruginosa	Azu	OprC	Copper	Han et al., 2019
P. aeruginosa	ModA	IcmP	Molybdate	Wang et al., 2021
C. necator	TeoL	CubA/CstR	Iron	Li et al., 2021

Manganese

Manganese is also an essential micronutrient for many cellular components or processes, such as lipid, protein, carbohydrate metabolism, transcriptional regulation, and resistance to oxidative stress (Kehres and Maguire, 2003). Manganese plays a crucial role in bacterial iron homeostasis and protection against oxidative damage (Puri et al., 2010). Two manganese ions, $Mn^{2+}$and Mn^{3+}, are found in most organisms. In contrast to Fe^{2+}, free Mn^{2+} is not toxic in a biological environment; thus, it can replace the more reactive Fe^{2+} in Fe^{2+}-containing proteins, reducing oxidative damage to

these proteins (Hood and Skaar, 2012). Manganese can also enhance oxidative stress resistance by serving as a cofactor for ROS-detoxifying enzymes, such as SodA and KatN, or through the formation of non-proteinaceous manganese antioxidants (Aguirre and Culotta, 2012; Barnese et al., 2012). Two major transporters import extracellular manganese across the cytoplasmic membrane: a proton-dependent Nramp-related transport system (MntH) and an ATP-binding cassette transporter (SitABCD and YfeABCD) (Goswami et al., 2001; Forbes and Gros, 2003).

The *B. thailandensis* T6SS-4 plays an important role in survival under oxidative stress by uptake Mn^{2+} through secreting TseM (BTH_II1883). TseM, a T6SS-4-dependent Mn^{2+}-binding effector, is involved in the intracellular accumulation of manganese (Mn^{2+}) under oxidative stress, and an Mn^{2+}-specific TonB-dependent outer membrane transporter MnoT, has been shown to be its interacting partner (Si et al., 2017b). Under high Mn^{2+} conditions, passive diffusion of Mn^{2+} through porins fulfills cellular Mn^{2+} requirements. Low Mn^{2+} triggers the induction of the TonB-dependent outer membrane transporter MnoT for the active transport of Mn^{2+} across the outer membrane. T6SS-4 expression is activated by the conserved oxidative stress regulator OxyR. Activated T6SS-4 secretes TseM into the extracellular milieu to scavenge Mn^{2+} and delivers its Mn^{2+} load to MnoT via direct interaction. The T6SS-MnoT mediated active Mn^{2+} transport system also participates in the interbacterial competition and bacterial virulence. The T6SS-4 provides growth advantage in nutrient-limited environments and is critical for virulence in *Galleria mellonella* larvae (Si et al., 2017b). Similarly, a Mn^{2+}-binding effector (TseM) secreted by T6SS-2, together with its transmembrane transporter MnoT, was used to maintain redox homeostasis via Mn^{2+} acquisition in the *B. pseudomallei* complex (DeShazer, 2019). Recently, *Y. pseudotuberculosis* T6SS-4 was also found to secret a Mn^{2+}-binding micropeptide, TssS, for Mn^{2+} acquisition and oxidative stress resistance. Remarkably, TssS was revealed to be delivered into host cells to inhibit the STING-mediated innate immune response by sequestering Mn^{2+}. This finding provides a new perspective on the role of the T6SS in pathogenesis (Zhu et al., 2021).

Iron

Iron is an essential nutrient for living organisms by acting as a cofactor for a large number of enzymes and regulatory proteins. Although iron is abundant in the Earth's crust, the bioavailability iron is severely restricted due to extremely low solubility under aerobic conditions (Schaible and Kaufmann, 2004; Miethke and Marahiel, 2007). To acquire sufficient iron for growth, bacteria have evolved several strategies, including import of ferrous iron by ATP- or GTP-dependent inner membrane transporters and TonB-ExbB-ExbD-dependent transport of ferric-siderophores, transferrin, haem, or haem-bound proteins through specific outer membrane receptors (Braun, 2001; Hood and Skaar, 2012).

Pseudomonas aeruginosa competes for iron by producing the high affinity siderophores pyoverdine and pyochelin, as well as hemophores, and it can also import xenosiderophores released by other bacteria (Cornelis, 2010). As a *P. aeruginosa* mutant lacking three known iron acquisition systems (PAΔ3Fe) retains the ability to grow in an iron deficient media, a novel iron acquisition pathway coupling the H3-T6SS effector TseF (PA2374), *Pseudomonas* quinolone signal (PQS, 2-heptyl-3-hydroxy-4-quinolone), outer membrane vesicles (OMVs), and the outer membrane receptors FptA and OprF was identified (Lin et al., 2017). TseF does not bind iron, but it interacts with the iron chelating PQS with a high affinity. The PQS molecule has been long known to bind iron with a high affinity but the physiological role of such binding remains unknown (Bredenbruch et al., 2006; Diggle et al., 2006). TseF engages siderophore receptor FptA and the porin OprF for iron acquisition (Nissen-Meyer et al., 1992). Consistent with the biochemical results, both FptA and OprF are required for TseF-mediated iron acquisition. Like the hydrophobic PQS, TseF is incorporated into outer membrane vesicles (OMVs), which have been suggested to play a role in iron acquisition in *P. aeruginosa* by unknown mechanism (Kulp and Kuehn, 2010). The T6SS substrate TseF integrates several molecules previously known to be involved in iron acquisition to transport iron to the cell. The *tseF* gene is present in many bacteria, suggesting wide use of this iron acquisition mechanism. The H3-T6SSpromoters and *tseF* expression for iron acquisition are commonly repressed by the ferric uptake regulator (Fur) for intracellular iron homeostasis (Lin et al., 2017). In *Cupriavidus necator*, T6SS1 secreted TeoL preferentially in association with OMVs through interactions with LPS, which enables bacterial cells to recruit OMVs derived from different species and confers advantages to bacterial cells for iron acquisition (Li et al., 2021).

An iron chelator, pyoverdine, secreted by *Pseudomonas taiwanensis*, can inhibit the growth of the rice bacterial blight pathogen *Xanthomonas oryzae* pv. *oryzae (Xoo)*. T6SS is involved in the secretion of the endogenous iron chelator pyoverdine; however, the mechanism is unknown (Chen et al., 2016). Notably, the regulation of T6SS by Fur or iron has also been reported in *Escherichia coli* (Brunet et al., 2011), *Edwardsiella tarda* (Chakraborty et al., 2011), *Burkholderia mallei,* and *B. pseudomallei* (Burtnick and Brett, 2013), implicating the possible roles of these T6SSs in iron acquisition.

Copper

As one of the most stable divalent transition metals, cupric copper (Cu^{2+}) displays a high affinity for metalloproteins (Waldron and Robinson, 2009). Copper is a catalyzer for electron transfer reactions in bacteria and a cofactor of copper-detoxifying enzymes (Dupont et al., 2011; Hodgkinson and Petris, 2012). Because copper is toxic, intracellular copper levels must be tightly controlled to ensure the homeostasis required for cuproprotein synthesis and prevent toxic effects (Argüello et al., 2013). ComC in *E. coli* represses copper uptake and thus plays an important role in copper homeostasis, and its homologs have been found in many gram-negative bacteria (Rademacher and Masepohl, 2012). For the import of copper, a few cytoplasmic Cu^{2+}-sensing transcriptional regulators (CueR, CsoR, and CopY) (Strausak and Solioz, 1997; Outten et al., 2000; Liu et al., 2007) and periplasmic Cu^{2+}-sensing two-component systems (CopR/S, CusR/S, and PcoR/S) (Rensing and Grass, 2003; Teitzel et al., 2006) have been found to play important roles. However,

copper efflux in pathogenic enterobacteria is more crucial than copper uptake (Nies and Herzberg, 2013). The inner membrane heavy metal pumps (transmembrane P1B-type ATPases) in many gram-negative bacteria are responsible for the exportation of cytoplasmic copper to the periplasm (Klein and Lewinson, 2011).

In *P. aeruginosa*, azurin (Azu) has a high affinity for oxidized Cu^{2+}-bound proteins (Nar et al., 1992; Zhang and Rainey, 2008). Based on an analysis of the *P. aeruginosa* H2-T6SS-dependent secretomes, Azu was characterized as an H2-T6SS-dependent copper (Cu^{2+})-binding effector. OprC, a Cu^{2+}-specific TonB-dependent outer membrane transporter, has been identified as an Azu-interacting partner. Both Azu and OprC are directly regulated by the transcriptional regulator CueR and are induced by low Cu^{2+}concentrations (Han et al., 2019).

Pseudomonas aeruginosa possesses three T6SS loci: H1-, H2-, and H3-T6SSs that provide a fitness advantage in bacterial community competition by delivering toxins to target cells (Mougous et al., 2006; Russell et al., 2011). The identified T6SS-dependent antibacterial toxin effectors include Tse1-Tse3, PldA, TplE, and PldB (Russell et al., 2011; Jiang et al., 2014; Sana et al., 2015). T6SS-mediated Cu acquisition also provides a growth advantage in bacterial competition, indicating the critical role of the Azu-OprC-mediated Cu^{2+} transport system (Han et al., 2019). Like VgrG2b that is secreted by H2-T6SS and shows an anti-eukaryotic function, the H2-T6SS-dependent Cu^{2+} transport system is important for bacterial virulence in the blood and lungs of infected mice (Sana et al., 2015; Han et al., 2019).

Molybdenum

Molybdenum is a trace metal element for nitrate metabolism in many bacteria and exists in the form of its oxyanion, molybdate (MoO_4^{2-}) under natural conditions (Grunden and Shanmugam, 1997). Bacteria acquire molybdate mainly through the high-affinity ATP-binding cassette permease ModABC (Pederick et al., 2014) and non-specific anion importers (Self et al., 2001). The imported MoO_4^{2-}often becomes a part of the Manganese chelating protein molecule to form a molybdenum cofactor, participating in the activity of molybdo-enzymes (Kraft et al., 2011).

In *P. aeruginosa*, the H2-T6SS secreted ModA has been identified as a molybdate-binding protein and mediated molybdate acquisition. Moreover, a ModA partner that participates in molybdate transport has also been identified as IcmP that is an insulin-cleaving metalloproteinase outer membrane protein (Wang et al., 2021). The T6SS-ModA-IcmP system contributes to bacterial virulence and participates in bacterial competition under anaerobic conditions. Studies have shown that the molybdenum homeostasis of *P. aeruginosa* PA1006 is necessary for nitrate utilization, biofilm formation, and virulence (Filiatrault et al., 2013; Tombline et al., 2013). In a mouse model of acute pneumonia, the *P. aeruginosa* Δ*clpV2*,

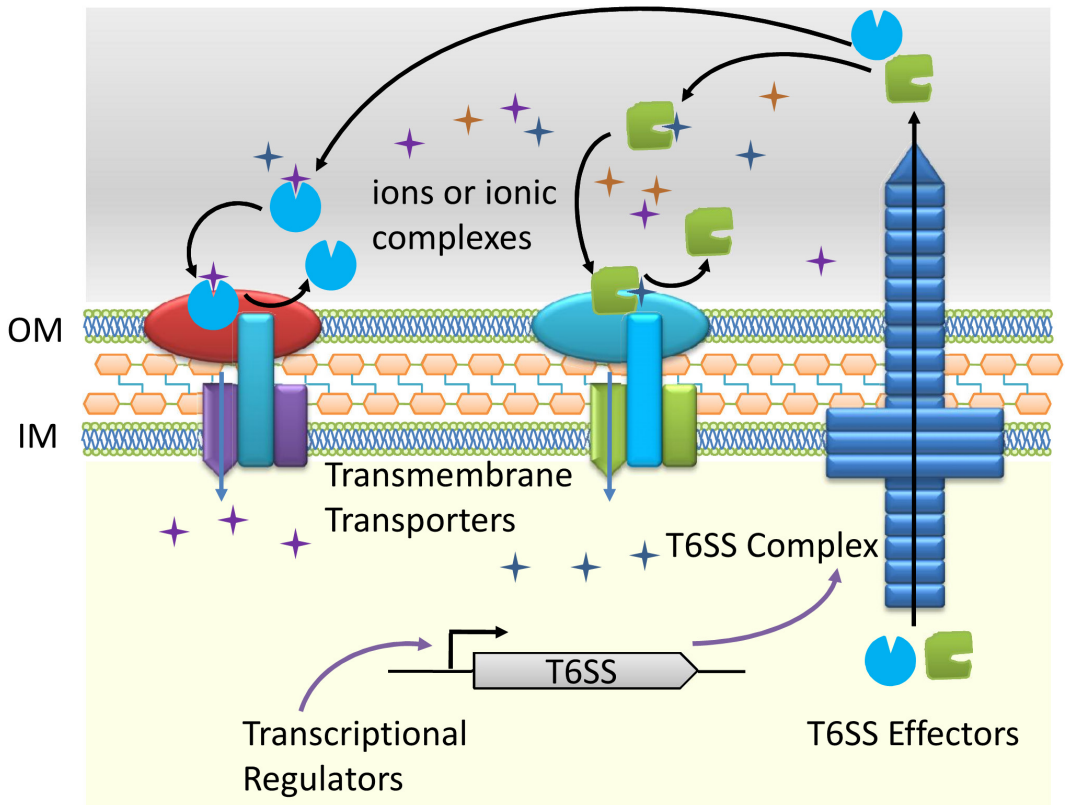

FIGURE 1 | Schematic diagram of the type VI secretion system (T6SS) dependent ions transport.

Δ*modA*, and Δ*anr* mutants exhibited attenuated virulence, indicating that the H2-T6SS-mediated molybdate transport system contributes to the resistance to host nutritional immunity (Wang et al., 2021). Like the previously discovered two H1-T6SS effectors Tse1 and Tse3, which can hydrolyze peptidoglycan and provide a competitive fitness advantage (Russell et al., 2011), H2-T6SS improves bacterial competition by promoting molybdate (MoO_4^{2-}) acquisition under anaerobic conditions (Wang et al., 2021). As a transcriptional regulator, Anr can activate H2-T6SS expression under anaerobic conditions (Wang et al., 2021). Anr in *P. aeruginosa* controls the switch from aerobic to anaerobic growth and plays a pivotal role in adapting to microaerobic or anoxic conditions (Ugidos et al., 2008; Tata et al., 2017).

CONCLUSION

All organisms keep metal homeostasis for physiological demands by sensing small fluctuations in metal levels (Porcheron et al., 2013). Bacteria have developed complex transport systems for each metal whose expression is coordinated by their corresponding regulators (such as Fur, MntR, CueR, and Zur, etc.) (Wakeman and Skaar, 2012). T6SS was a newly found device for bacteria to acquire metal ions, expanding our understanding on sophistication of bacterial metal ion acquisition systems. T6SS participation in metal ion uptake, which assists the bacterial low- and high-affinity transport systems to scavenge from the environment essential metals in chelated or free forms. In addition, the metal ion transport function of T6SS is usually involved in multiple biological processes and is crucial for bacterial survival and host colonization. Traditionally, T6SS is recognized as a contact-dependent molecular machinery. Recent studies revealed that T6SSs play crucial roles in shaping the composition of a microbial population in hosts or environmental niches, either by directly killing competing cells via contact-dependent (Russell et al., 2011) and contact-independent (Song et al., 2021) translocation of toxins, or by competing for essential nutrients via contact-independent secretion of metal ion binding effectors. For example, the T6SS-HmuR-mediated active zinc transport system is involved in a contact-independent bacteria-bacteria competition for nutrients (Si et al., 2017a,b; Han et al., 2019; Wang et al., 2021).

A schematic diagram was used to show the process of metal ions transport through T6SS (**Figure 1**). Briefly, the T6SS dependent effectors bind to specific metal ions or ionic complexes in the environment. Accompanied by a transmembrane ion transporter, the corresponding ions are transferred to the cell. The ions transport process is collaboratively fulfilled by the T6SS effectors and their transmembrane partners. It is worth mentioning that the metal ions transporting function of T6SS is often activated under special circumstances, such as low ions concentrations or environmental stresses and is regulated by multiple transcriptional regulators. So far, it is unknown whether T6SS correlates with metal ions efflux. We believe that ions transport through T6SS expands the range of functions associated with this secretory nanomachines and merits additional studies in other bacteria.

AUTHOR CONTRIBUTIONS

XY, HL, and YZ collected and assessed the references. XS and HL contributed in the proposal and article layout of the review. XY and XS wrote the manuscript. All authors contributed to the article and approved the submitted version.

FUNDING

This work was supported by the grant of National Key R&D Program of China (2018YFA0901200), National Natural Science Foundation of China (31725003 and 31670053), and Comprehensive treatment of Xiaokongtong Gully Project: Research and application of *in situ* greening and soil consolidation technology (QYLF-JSYY-2020029).

REFERENCES

Aguirre, J. D., and Culotta, V. C. (2012). Battles with iron: manganese in oxidative stress protection. *J. Biol. Chem.* 287, 13541–13548. doi: 10.1074/jbc.R111.312181

Andreini, C., Banci, L., Bertini, I., and Rosato, A. (2006). Zinc through the three domains of life. *J. Proteome Res.* 5, 3173–3178. doi: 10.1021/pr0603699

Argüello, J. M., Raimunda, D., and Padilla-Benavides, T. (2013). Mechanisms of copper homeostasis in bacteria. *Front. Cell Infect. Microbiol.* 3:73. doi: 10.3389/fcimb.2013.00073

Barnese, K., Gralla, E. B., Valentine, J. S., and Cabelli, D. E. (2012). Biologically relevant mechanism for catalytic superoxide removal by simple manganese compounds. *Proc. Natl. Acad. Sci. U. S. A.* 109:6892. doi: 10.1073/pnas.1203051109

Borgeaud, S., Metzger, L. C., Scrignari, T., and Blokesch, M. (2015). The type VI secretion system of *Vibrio cholerae* fosters horizontal gene transfer. *Science* 347, 63–67. doi: 10.1126/science.1260064

Braun, V. (2001). Iron uptake mechanisms and their regulation in pathogenic bacteria. *Int. J. Med. Microbiol.* 291, 67–79. doi: 10.1078/1438-4221-00103

Bredenbruch, F., Geffers, R., Nimtz, M., Buer, J., and Haussler, S. (2006). The *Pseudomonas aeruginosa* quinolone signal (PQS) has an iron-chelating activity. *Environ. Microbiol.* 8, 1318–1329. doi: 10.1111/j.1462-2920.2006.01025.x

Brunet, Y. R., Bernard, C. S., Gavioli, M., Lloubes, R., and Cascales, E. (2011). An epigenetic switch involving overlapping fur and DNA methylation optimizes expression of a type VI secretion gene cluster. *PLoS Genet.* 7:e1002205. doi: 10.1371/journal.pgen.1002205

Burtnick, M. N., and Brett, P. J. (2013). Burkholderia mallei and Burkholderia pseudomallei cluster 1 type VI secretion system gene expression is negatively regulated by iron and zinc. *PLoS One* 8:e76767. doi: 10.1371/journal.pone.0076767

Cai, R., Gao, F., Pan, J., Hao, X., Yu, Z., and Qu, Y. (2021). The transcriptional regulator Zur regulates the expression of ZnuABC and T6SS4 in response to stresses in *Yersinia pseudotuberculosis*. *Microbiol. Res.* 249:126787. doi: 10.1016/j.micres.2021.126787

Chakraborty, S., Sivaraman, J., Leung, K. Y., and Mok, Y. K. (2011). Two-component PhoB-PhoR regulatory system and ferric uptake regulator sense phosphate and iron to control virulence genes in type III and VI secretion systems of *Edwardsiella tarda*. *J. Biol. Chem.* 286, 39417–39430. doi: 10.1074/jbc.M111.295188

Chassaing, B., and Cascales, E. (2018). Antibacterial Weapons: targeted Destruction in the Microbiota. *Trends Microbiol.* 26, 329–338. doi: 10.1016/j.tim.2018.01.006

Chen, W. J., Kuo, T. Y., Hsieh, F. C., Chen, P. Y., Wang, C. S., Shih, Y. L., et al. (2016). Involvement of type VI secretion system in secretion of iron

chelator pyoverdine in *Pseudomonas taiwanensis*. *Sci. Rep.* 6:32950. doi: 10.1038/srep32950

Chow, J., and Mazmanian, S. K. (2010). A pathobiont of the microbiota balances host colonization and intestinal inflammation. *Cell Host Microbe* 7, 265–276. doi: 10.1016/j.chom.2010.03.004

Cianfanelli, F. R., Monlezun, L., and Coulthurst, S. J. (2016). Aim, Load, Fire: the Type VI Secretion System, a Bacterial Nanoweapon. *Trends Microbiol.* 24, 51–62. doi: 10.1016/j.tim.2015.10.005

Cornelis, P. (2010). Iron uptake and metabolism in pseudomonads. *Appl. Microbiol. Biotechnol.* 86, 1637–1645. doi: 10.1007/s00253-010-2550-2

Coulthurst, S. (2019). The Type VI secretion system: a versatile bacterial weapon. *Microbiology* 165, 503–515. doi: 10.1099/mic.0.000789

DeShazer, D. (2019). A novel contact-independent T6SS that maintains redox homeostasis via Zn^{2+} and Mn^{2+} acquisition is conserved in the *Burkholderia pseudomallei* complex. *Microbiol. Res.* 226, 48–54. doi: 10.1016/j.micres.2019.05.007

Diggle, S. P., Lumjiaktase, P., Dipilato, F., Winzer, K., Kunakorn, M., Barrett, D. A., et al. (2006). Functional genetic analysis reveals a 2-Alkyl-4-quinolone signaling system in the human pathogen *Burkholderia pseudomallei* and related bacteria. *Chem. Biol.* 13, 701–710. doi: 10.1016/j.chembiol.2006.05.006

Dupont, C. L., Grass, G., and Rensing, C. (2011). Copper toxicity and the origin of bacterial resistance–new insights and applications. *Metallomics* 3, 1109–1118.

Filiatrault, M. J., Tombline, G., Wagner, V. E., Van Alst, N., Rumbaugh, K., Sokol, P., et al. (2013). *Pseudomonas aeruginosa* PA1006, which plays a role in molybdenum homeostasis, is required for nitrate utilization, biofilm formation, and virulence. *PLoS One* 8:e55594. doi: 10.1371/journal.pone.0055594

Forbes, J. R., and Gros, P. (2003). Iron, manganese, and cobalt transport by Nramp1 (Slc11a1) and Nramp2 (Slc11a2) expressed at the plasma membrane. *Blood* 102, 1884–1892. doi: 10.1182/blood-2003-02-0425

Gallique, M., Decoin, V., Barbey, C., Rosay, T., Feuilloley, M. G., Orange, N., et al. (2017). Contribution of the *Pseudomonas* fluorescens MFE01 Type VI Secretion System to Biofilm Formation. *PLoS One* 12:e0170770. doi: 10.1371/journal.pone.0170770

Goswami, T., Bhattacharjee, A., Babal, P., Searle, S., and Moore, E. (2001). Natural-resistance-associated macrophage protein 1 is an H+/bivalent cation antiporter. *Biochem. J.* 354, 511–519. doi: 10.1042/bj3540511

Grunden, A. M., and Shanmugam, K. T. (1997). Molybdate transport and regulation in bacteria. *Arch. Microbiol.* 168, 345–354. doi: 10.1007/s002030050508

Guan, J., Xiao, X., Xu, S., Gao, F., and Wang, J. (2015). Roles of RpoS in *Yersinia pseudotuberculosis* stress survival, motility, biofilm formation and type VI secretion system expression. *J. Microbiol.* 53, 633–642. doi: 10.1007/s12275-015-0099-6

Gueguen, E., Durand, E., Zhang, X. Y., d'Amalric, Q., Journet, L., and Cascales, E. (2013). Expression of a *Yersinia pseudotuberculosis* Type VI Secretion System Is Responsive to Envelope Stresses through the OmpR Transcriptional Activator. *PLoS One* 8:e66615. doi: 10.1371/journal.pone.0066615

Han, Y., Wang, T., Chen, G., Pu, Q., Liu, Q., Zhang, Y., et al. (2019). A *Pseudomonas aeruginosa* type VI secretion system regulated by CueR facilitates copper acquisition. *PLoS Pathog.* 15:e1008198. doi: 10.1371/journal.ppat.1008198

Hantke, K. (2005). Bacterial zinc uptake and regulators. *Curr. Opin. Microbiol.* 8, 196–202. doi: 10.1016/j.mib.2005.02.001

Hodgkinson, V., and Petris, M. J. (2012). Copper homeostasis at the host-pathogen interface. *J. Biol. Chem.* 287, 13549–13555. doi: 10.1074/jbc.R111.316406

Hood, M. I., Mortensen, B. L., Moore, J. L., Zhang, Y., Kehl-Fie, T. E., Sugitani, N., et al. (2012). Identification of an *Acinetobacter baumannii* zinc acquisition system that facilitates resistance to calprotectin-mediated zinc sequestration. *PLoS Pathog.* 8:e1003068. doi: 10.1371/journal.ppat.1003068

Hood, M. I., and Skaar, E. P. (2012). Nutritional immunity: transition metals at the pathogen-host interface. *Nat. Rev. Microbiol.* 10, 525–537. doi: 10.1038/nrmicro2836

Hood, R. D., Singh, P., Hsu, F., Guvener, T., and Carl, M. A. (2010). A type VI secretion system of *Pseudomonas aeruginosa* targets a toxin to bacteria. *Cell Host Microbe* 7, 25–37. doi: 10.1016/j.chom.2009.12.007

Isohanni, P., Huehn, S., Aho, T., Alter, T., and Lyhs, U. (2013). Heat stress adaptation induces cross-protection against lethal acid stress conditions in *Arcobacter butzleri* but not in *Campylobacter jejuni*. *Food Microbiol.* 34, 431–435. doi: 10.1016/j.fm.2013.02.001

Jiang, F., Waterfield, N. R., Yang, J., Yang, G., and Jin, Q. (2014). A *Pseudomonas aeruginosa* type VI secretion phospholipase D effector targets both prokaryotic and eukaryotic cells. *Cell Host Microbe* 15, 600–610. doi: 10.1016/j.chom.2014.04.010

Kehres, D. G., and Maguire, M. E. (2003). Emerging themes in manganese transport, biochemistry and pathogenesis in bacteria. *FEMS Microbiol. Rev.* 27, 263–290. doi: 10.1016/S0168-6445(03)00052-4

Klein, J. S., and Lewinson, O. (2011). Bacterial ATP-driven transporters of transition metals: physiological roles, mechanisms of action, and roles in bacterial virulence. *Metallomics* 3, 1098–1108. doi: 10.1039/c1mt00073j

Kraft, B., Strous, M., and Tegetmeyer, H. E. (2011). Microbial nitrate respiration–genes, enzymes and environmental distribution. *J. Biotechnol.* 155, 104–117. doi: 10.1016/j.jbiotec.2010.12.025

Kulp, A., and Kuehn, M. J. (2010). Biological functions and biogenesis of secreted bacterial outer membrane vesicles. *Annu. Rev. Microbiol.* 64, 163–184. doi: 10.1146/annurev.micro.091208.073413

Li, C., Zhu, L., Wang, D., Wei, Z., Hao, X., Wang, Z., et al. (2021). T6SS secretes an LPS-binding effector to recruit OMVs for exploitative competition and horizontal gene transfer. *ISME J.* doi: 10.1038/s41396-021-01093-8 [Online ahead of print].

Lin, J., Zhang, W., Cheng, J., Yang, X., Zhu, K., Wang, Y., et al. (2017). A *Pseudomonas* T6SS effector recruits PQS-containing outer membrane vesicles for iron acquisition. *Nat. Commun.* 8:14888. doi: 10.1038/ncomms14888

Liu, J. Z., Jellbauer, S., Poe, A. J., Ton, V., Pesciaroli, M., and Kehl-Fie, T. E. (2012). Zinc Sequestration by the Neutrophil Protein Calprotect in Enhances *Salmonella* Growth in the Inflamed Gut. *Cell Host Microbe* 11, 227–239. doi: 10.1016/j.chom.2012.01.017

Liu, T., Ramesh, A., Ma, Z., Ward, S. K., Zhang, L., George, G. N., et al. (2007). CsoR is a novel *Mycobacterium tuberculosis* copper-sensing transcriptional regulator. *Nat. Chem. Biol.* 3, 60–68. doi: 10.1038/nchembio844

Miethke, M., and Marahiel, M. A. (2007). Siderophore-based iron acquisition and pathogen control. *Microbiol. Mol. Biol. Rev.* 71, 413–451.

Mols, M., and Abee, T. (2011). Primary and secondary oxidative stress in *Bacillus*. *Environ. Microbiol.* 13, 1387–1394. doi: 10.1111/j.1462-2920.2011.02433.x

Mougous, J. D., Cuff, M. E., Raunser, S., Shen, A., Zhou, M., Gifford, C. A., et al. (2006). A virulence locus of *Pseudomonas aeruginosa* encodes a protein secretion apparatus. *Science* 312, 1526–1530. doi: 10.1126/science.1128393

Nar, H., Messerschmidt, A., Huber, R., van de Kamp, M., and Canters, G. W. (1992). Crystal structure of *Pseudomonas aeruginosa* apo-azurin at 1.85 A resolution. *FEBS Lett.* 306, 119–124. doi: 10.1016/0014-5793(92)80981-L

Nies, D. H., and Herzberg, M. (2013). A fresh view of the cell biology of copper in enterobacteria. *Mol. Microbiol.* 87, 447–454. doi: 10.1111/mmi.12123

Nissen-Meyer, J., Holo, H., Håvarstein, L. S., Sletten, K., and Nes, I. F. (1992). A novel lactococcal bacteriocin whose activity depends on the complementary action of two peptides. *J. Bacteriol.* 174, 5686–5692.

Outten, F. W., Outten, C. E., Hale, J., and O'Halloran, T. V. (2000). Transcriptional activation of an *Escherichia coli* copper efflux regulon by the chromosomal MerR homologue, cueR. *J. Biol. Chem.* 275, 31024–31029. doi: 10.1074/jbc.M006508200

Pederick, V. G., Eijkelkamp, B. A., Ween, M. P., Begg, S. L., Paton, J. C., and McDevitt, C. A. (2014). Acquisition and role of molybdate in *Pseudomonas aeruginosa*. *Appl. Environ. Microbiol.* 80, 6843–6852.

Porcheron, G., Garenaux, A., Proulx, J., Sabri, M., and Dozois, C. M. (2013). Iron, copper, zinc, and manganese transport and regulation in pathogenic *Enterobacteria*: correlations between strains, site of infection and the relative importance of the different metal transport systems for virulence. *Front. Cell Infect. Microbiol.* 3:90. doi: 10.3389/fcimb.2013.00090

Pukatzki, S., Ma, A. T., Sturtevant, D., Krastins, B., Sarracino, D., Nelson, W. C., et al. (2006). Identification of a conserved bacterial protein secretion system in *Vibrio cholerae* using the Dictyostelium host model system. *Proc. Natl. Acad. Sci. U. S. A.* 103, 1528–1533. doi: 10.1073/pnas.0510322103

Puri, S., Hohle, T. H., and O'Brian, M. R. (2010). Control of bacterial iron homeostasis by manganese. *Proc. Natl. Acad. Sci. U. S. A.* 107, 10691–10695. doi: 10.1073/pnas.1002342107

Rademacher, C., and Masepohl, B. (2012). Copper-responsive gene regulation in bacteria. *Microbiology* 158, 2451–2464. doi: 10.1099/mic.0.058487-0

Rensing, C., and Grass, G. (2003). *Escherichia coli mechanisms of copper homeostasis in a changing environment*. *FEMS Microbiol. Rev.* 27, 197–213. doi: 10.1016/S0168-6445(03)00049-4

Russell, A. B., Hood, R. D., Bui, N. K., LeRoux, M., Vollmer, W., and Mougous, J. D. (2011). Type VI secretion delivers bacteriolytic effectors to target cells. *Nature* 475, 343–347. doi: 10.1038/nature10244

Sana, T. G., Baumann, C., Merdes, A., Soscia, C., Rattei, T., Hachani, A., et al. (2015). Internalization of *Pseudomonas aeruginosa* Strain PAO1 into Epithelial Cells Is Promoted by Interaction of a T6SS Effector with the Microtubule Network. *mBio* 6:e00712. doi: 10.1128/mBio.00712-15

Schaible, U. E., and Kaufmann, S. H. (2004). Iron and microbial infection. *Nat. Rev. Microbiol.* 2, 946–953. doi: 10.1038/nrmicro1046

Self, W. T., Grunden, A. M., Hasona, A., and Shanmugam, K. T. (2001). Molybdate transport. *Res. Microbiol.* 152, 311–321. doi: 10.1016/S0923-2508(01)01202-5

Si, M., Wang, Y., Zhang, B., Zhao, C., Kang, Y., Bai, H., et al. (2017a). The Type VI Secretion System Engages a Redox-Regulated Dual-Functional Heme Transporter for Zinc Acquisition. *Cell Rep.* 20, 949–959. doi: 10.1016/j.celrep.2017.06.081

Si, M., Zhao, C., Burkinshaw, B., Zhang, B., Wei, D., Wang, Y., et al. (2017b). Manganese scavenging and oxidative stress response mediated by type VI secretion system in *Burkholderia thailandensis*. *Proc. Natl. Acad. Sci. U. S. A.* 114, E2233–E2242. doi: 10.1073/pnas.1614902114

Song, L., Pan, J., Yang, Y., Zhang, Z., and Cui, R. (2021). Contact-independent killing mediated by a T6SS effector with intrinsic cell-entry properties. *Nat. Commun.* 12:423. doi: 10.1038/s41467-020-20726-8

Song, Y., Xiao, X., Li, C., Wang, T., Zhao, R., Zhang, W., et al. (2015). The dual transcriptional regulator RovM regulates the expression of AR3- and T6SS4-dependent acid survival systems in response to nutritional status in *Yersinia pseudotuberculosis*. *Environ. Microbiol.* 17, 4631–4645.

Strausak, D., and Solioz, M. (1997). CopY is a copper-inducible repressor of the *Enterococcus hirae* copper ATPases. *J. Biol. Chem.* 272, 8932–8936. doi: 10.1074/jbc.272.14.8932

Tata, M., Amman, F., Pawar, V., Wolfinger, M. T., Weiss, S., Häussler, S., et al. (2017). The Anaerobically Induced sRNA PaiI Affects Denitrification in *Pseudomonas aeruginosa* PA14. *Front. Microbiol.* 8:2312. doi: 10.3389/fmicb.2017.02312

Teitzel, G. M., Geddie, A., De Long, S. K., Kirisits, M. J., Whiteley, M., Parsek, M. R., et al. (2006). Survival and growth in the presence of elevated copper: transcriptional profiling of copper-stressed *Pseudomonas aeruginosa*. *J. Bacteriol.* 188, 7242–7256. doi: 10.1128/JB.00837-06

Tombline, G., Schwingel, J. M., Lapek, J. D. Jr., Friedman, A. E., Darrah, T., Maguire, M., et al. (2013). *Pseudomonas aeruginosa* PA1006 is a persulfide-modified protein that is critical for molybdenum homeostasis. *PLoS One* 8:e55593. doi: 10.1371/journal.pone.0055593

Ugidos, A., Morales, G., Rial, E., Williams, H. D., and Rojo, F. (2008). The coordinate regulation of multiple terminal oxidases by the *Pseudomonas putida* ANR global regulator. *Environ. Microbiol.* 10, 1690–1702. doi: 10.1111/j.1462-2920.2008.01586.x

Wakeman, C. A., and Skaar, E. P. (2012). Metalloregulation of Gram-positive pathogen physiology. *Curr. Opin. Microbiol.* 15, 169–174. doi: 10.1016/j.mib.2011.11.008

Waldron, K. J., and Robinson, N. J. (2009). How do bacterial cells ensure that metalloproteins get the correct metal?. *Nat. Rev. Microbiol.* 7, 25–35. doi: 10.1038/nrmicro2057

Wan, B., Zhang, Q., Ni, J., Li, S., Wen, D., Li, J., et al. (2017). Type VI secretion system contributes to Enterohemorrhagic *Escherichia coli* virulence by secreting catalase against host reactive oxygen species (ROS). *PLoS Pathog.* 13:e1006246. doi: 10.1371/journal.ppat.1006246

Wang, D., and Fierke, C. A. (2013). The BaeSR regulon is involved in defense against zinc toxicity in *E. coli*. *Metallomics* 5, 372–383. doi: 10.1039/c3mt20217h

Wang, D., Hosteen, O., and Fierke, C. A. (2012). ZntR-mediated transcription of zntA responds to nanomolar intracellular free zinc. *J. Inorg. Biochem.* 111, 173–181. doi: 10.1016/j.jinorgbio.2012.02.008

Wang, T., Chen, K., Gao, F., Kang, Y., Chaudhry, M. T., Wang, Z., et al. (2017). ZntR positively regulates T6SS4 expression in *Yersinia pseudotuberculosis*. *J. Microbiol.* 55, 448–456. doi: 10.1007/s12275-017-6540-2

Wang, T., Du, X., Ji, L., Han, Y., Dang, J., Wen, J., et al. (2021). *Pseudomonas aeruginosa* T6SS-mediated molybdate transport contributes to bacterial competition during anaerobiosis. *Cell Rep.* 35:108957. doi: 10.1016/j.celrep.2021.108957

Wang, T., Si, M., Song, Y., Zhu, W., Gao, F., Wang, Y., et al. (2015). Type VI Secretion System Transports Zn^{2+} to Combat Multiple Stresses and Host Immunity. *PLoS Pathog.* 11:e1005020. doi: 10.1371/journal.ppat.1005020

Weber, B., Hasic, M., Chen, C., Wai, S. N., and Milton, D. L. (2009). Type VI secretion modulates quorum sensing and stress response in *Vibrio anguillarum*. *Environ. Microbiol.* 11, 3018–3028.

Yang, X., Long, M., and Shen, X. (2018). Effector(-)Immunity Pairs Provide the T6SS Nanomachine its Offensive and Defensive Capabilities. *Molecules* 23:1009.

Yang, X., Song, Y., Dai, Q., Zhang, H., Song, L., Wang, Z., et al. (2019). The stringent response factor, RelA, positively regulates T6SS4 expression through the RovM/RovA pathway in *Yersinia pseudotuberculosis*. *Microbiol. Res.* 220, 32–41.

Zhang, L., Hinz, A. J., Nadeau, J. P., and Mah, T. F. (2011). *Pseudomonas aeruginosa* tssC1 links type VI secretion and biofilm-specific antibiotic resistance. *J. Bacteriol.* 193, 5510–5513. doi: 10.1128/JB.00268-11

Zhang, W., Wang, Y., Song, Y., Wang, T., and Xu, S. (2013). A type VI secretion system regulated by OmpR in *Yersinia pseudotuberculosis* functions to maintain intracellular pH homeostasis. *Environ. Microbiol.* 15, 557–569. doi: 10.1111/1462-2920.12005

Zhang, X. X., and Rainey, P. B. (2008). Regulation of copper homeostasis in *Pseudomonas fluorescens* SBW25. *Environ. Microbiol.* 10, 3284–3294. doi: 10.1111/j.1462-2920.2008.01720.x

Zhao, R., Song, Y., Dai, Q., Kang, Y., and Pan, J. (2017). A starvation-induced regulator, RovM, acts as a switch for planktonic/biofilm state transition in *Yersinia pseudotuberculosis*. *Sci. Rep.* 7:639.

Zhu, L., Xu, L., Wang, C., Li, C., Li, M., Liu, Q., et al. (2021). T6SS translocates a micropeptide to suppress STING-mediated innate immunity by sequestering manganese. *Proc. Natl. Acad. Sci. U. S. A.* 118:e2103526118.

Conflict of Interest: HL and YZ was employed by the company Qingyang Longfeng Sponge City Construction Management & Operation Co., Ltd.

The remaining authors declare that the research was conducted in the absence of any commercial or financial relationships that could be construed as a potential conflict of interest.

Publisher's Note: All claims expressed in this article are solely those of the authors and do not necessarily represent those of their affiliated organizations, or those of the publisher, the editors and the reviewers. Any product that may be evaluated in this article, or claim that may be made by its manufacturer, is not guaranteed or endorsed by the publisher.

frontiers in Microbiology

REVIEW
published: 30 November 2021
doi: 10.3389/fmicb.2021.782900

Pushing the Envelope: The Mysterious Journey Through the Bacterial Secretory Machinery, and Beyond

*Lucy Troman† and Ian Collinson**

School of Biochemistry, University of Bristol, Bristol, United Kingdom

Gram-negative bacteria are contained by an envelope composed of inner and outer-membranes with the peptidoglycan (PG) layer between them. Protein translocation across the inner membrane for secretion, or insertion into the inner membrane is primarily conducted using the highly conserved, hourglass-shaped channel, SecYEG: the core-complex of the Sec translocon. This transport process is facilitated by interactions with ancillary subcomplex SecDF-YajC (secretion) and YidC (insertion) forming the holo-translocon (HTL). This review recaps the transport process across the inner-membrane and then further explores how delivery and folding into the periplasm or outer-membrane is achieved. It seems very unlikely that proteins are jettisoned into the periplasm and left to their own devices. Indeed, chaperones such as SurA, Skp, DegP are known to play a part in protein folding, quality control and, if necessary degradation. YfgM and PpiD, by their association at the periplasmic surface of the Sec machinery, most probably are also involved in some way. Yet, it is not entirely clear how outer-membrane proteins are smuggled past the proteases and across the PG to the barrel-assembly machinery (BAM) and their final destination. Moreover, how can this be achieved, as is thought, without the input of energy? Recently, we proposed that the Sec and BAM translocons interact with one another, and most likely other factors, to provide a conduit to the periplasm and the outer-membrane. As it happens, numerous other specialized proteins secretion systems also form trans-envelope structures for this very purpose. The direct interaction between components across the envelope raises the prospect of energy coupling from the inner membrane for active transport to the outer-membrane. Indeed, this kind of long-range energy coupling through large inter-membrane assemblies occurs for small molecule import (e.g., nutrient import by the Ton complex) and export (e.g., drug efflux by the AcrAB-TolC complex). This review will consider this hypothetical prospect in the context of outer-membrane protein biogenesis.

Keywords: protein secretion, bacterial envelope biogenesis, SecY translocon, BAM, periplasm, SecDF

OPEN ACCESS

Edited by:
Eric Cascales,
Aix-Marseille Université, France

Reviewed by:
Thomas Brüser,
Leibniz University Hannover, Germany
Etana Padan,
Hebrew College, United States

***Correspondence:**
Ian Collinson
ian.collinson@bristol.ac.uk

†Present address:
Lucy Troman,
Birkbeck, University of London,
London, United Kingdom

Specialty section:
This article was submitted to Microbial Physiology and Metabolism, a section of the journal Frontiers in Microbiology

Received: *24 September 2021*
Accepted: *09 November 2021*
Published: *30 November 2021*

Citation:
Troman L and Collinson I (2021) Pushing the Envelope: The Mysterious Journey Through the Bacterial Secretory Machinery, and Beyond. Front. Microbiol. 12:782900. doi: 10.3389/fmicb.2021.782900

SUMMARY

The Gram-negative bacterial cell envelope is typically composed of inner and outer-membranes with the periplasm sandwiched in between. The inner membrane is the first membrane in contact with the cytoplasm and is therefore central to energy conservation, lipid biosynthesis, protein secretion and transport. The inner membrane itself mostly consists of phospholipids and hydrophobic α-helical proteins. In particular, the inner membrane houses the conserved ubiquitous Sec secretion machinery providing a sophisticated transport pathway for unfolded protein substrates across or into the membrane. Importantly, the inner membrane is necessary for the proton motive force (PMF), which consists of an electrical ($\Delta\Psi$) and chemical (ΔpH) gradient across the inner membrane created by proton transport into the periplasm. Energy conserved in this process can be converted into kinetic movement of several different membrane proteins to assist in transport across the membrane, or to drive energetically unfavorable reactions such as the phosphorylation of adenosine di-phosphate (ADP) to adenosine tri-phosphate (ATP) by ATP synthase. In addition, the PMF powers the rapid rotation of the flagella for movement of the bacterium itself.

The periplasm is a crowded aqueous compartment containing chaperones and proteases for protein quality control and folding, enzymes involved in sugar and amino acid transport and chemotaxis and nucleases preventing uptake of foreign DNA (Weski and Ehrmann, 2012). In addition the periplasm contains the peptidoglycan layer, a structural polymer tethered to the outer-membrane. The role of the peptidoglycan layer is to provide mechanical strength to withstand the cytoplasmic turgor, and maintain the cellular shape. As the name suggests, the peptidoglycan layer is a matrix of glycan strands cross-linked by short peptides; any inhibition to biosynthesis of the peptidoglycans through either mutation or antibiotic inhibition will result in cell lysis (Dezélée and Bricas, 1970).

The primary function of the outer-membrane is to protect the bacteria from the harsh surrounding environment. Additionally, resident membrane proteins are involved in solute and protein translocation and signal transduction. Like the inner membrane, the internal leaflet of is made up of phospholipids, but in bacteria with an outer-membrane the external leaflet of the bilayer is exclusively glycolipids. Unlike the inner membrane, proteins within this outer-membrane environment primarily consist of β-barrels.

CROSSING THE INNER MEMBRANE

Multiple specialized secretion systems have evolved for flagella assembly and for pathogenic contact and protein delivery to host cells (for review see Green and Mecsas, 2016). Many of these systems deploy trans-envelope assemblies to enable uninterrupted protein passage through the periplasm. Most extra-cytosolic proteins, however, are transported through the Sec secretion system (Orfanoudaki and Economou, 2014). This general secretion system spans only the inner membrane and allows transport of unfolded polypeptides destined for the inner membrane, periplasm, or outer-membrane. Unlike the specialized systems, this is highly conserved and abundant through bacteria, as well as archaea and eukaryotes.

The majority of the components for the Sec secretion system were identified through genetic screening experiments in the 1980s (for review see Bieker and Silhavy, 1990). Mutations resulting in a secretion deficiency were dubbed sec alleles, and corresponded to genes for SecY, SecE, SecD, SecF, SecA, and SecB (Emr et al., 1981; Oliver and Beckwith, 1981; Kumamoto and Beckwith, 1983; Riggs et al., 1988). Suppressor mutations causing hyperactive secretion characterized by a lack of sensitivity to the signal sequence mutations—*prl* alleles—corresponded to SecY (*prlA*), SecE (*prlG*), SecG (*prlH*), and SecA (*prlD*) (Oliver and Beckwith, 1981; Schatz and Beckwith, 1990; Schatz et al., 1991; Bost and Belin, 1997).

The first high-resolution structure for the Sec translocon was determined for SecYEG from *Methanococcus jannaschii* (Van Den Berg et al., 2004) allowing the first visualization of a protein conducting channel, in this case at the core of the Sec machinery. Ten transmembrane helices of SecY form two rigid bodies around a central channel with a lateral gate, allowing protein movement across the membrane as well as lateral movement into the phospholipid membrane itself (Van Den Berg et al., 2004; Egea and Stroud, 2010). For transport through the SecY channel the pre-secretory protein must be unfolded (Arkowitz et al., 1993) and this requires a carefully choreographed network of interactions between proteins within the cytoplasm, periplasm and inner membrane to enable efficient translocation of such a broad range of substrates.

The assignment of the pathway for transport across or into the inner-membrane is specified by translation of a short hydrophobic signal sequence on the N-terminus of the secretory/membrane protein (Blobel and Sabatini, 1971; Milstein et al., 1972; Blobel and Dobberstein, 1975). A bespoke toolkit of secretory machinery will ultimately determine the means of translocation of unfolded proteins through and into the membrane. These can loosely be separated as two different pathways.

- *Co-translational translocation:* a translating ribosome nascent chain complex binds to the SecYEG membrane channel usually resulting in membrane insertion.
- *Post-translational/SecA-dependent translocation:* a fully synthesized pre-protein from the cytoplasm is driven through the SecYEG membrane channel using molecular motor SecA, this usually results in membrane translocation into the periplasm.

The hydrophobic signal sequence, preceded by a positive charge at the N-terminus, makes up a recognition site for a range of factors to bind and target the substrate toward the inner membrane (Von Heijne, 1981). Generally, it is the hydrophobicity which then determines whether the pre-protein is transported after or during translation, with more

hydrophobic sequences favoring co-translational translocation and less hydrophobic favoring post-translational translocation (Lee and Bernstein, 2001).

SecA-dependent post-translocation transport across the inner membrane, driven by ATP and the PMF, has been covered in a previous *Frontiers in Microbiology* review (Collinson, 2019). Here we are concerned about what happens after the translocation process. An important aspect of this consideration is the composition of the protein-channel complex. The core-SecYEG complex is necessary and sufficient for protein transport (Brundage et al., 1990), but other factors are known to associate in order to facilitate the reaction. The key point here is that the core complex does not have any appreciable domains at the periplasmic surface. So, on its own SecYEG does not seem to be equipped to effectively manage the release of emerging unfolded polypeptides to secure safe passage to the periplasm or outer-membrane. However, other factors known to associate with the core-complex (the subcomplex SecDF, YidC, YajC, PpiD, YfgM) (Götzke et al., 2014; Schulze et al., 2014; Jauss et al., 2019), possess such exterior domains large enough to be involved in the onward traffic of protein.

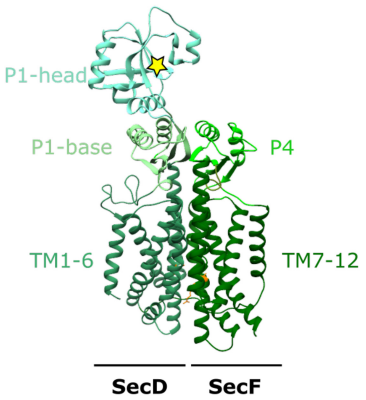

FIGURE 1 | The structure of SecDF. X-ray crystal structure of SecDF in I- form conformation from *Deinococcus radiodurans* R1 PDB:5XANb (Furukawa et al., 2017). TM1-6 from SecD and TM7-12 from SecF make up the 12 TM helices characteristic of the RND superfamily. The periplasmic domains: P1-base and -head in SecD and P4 in SecF, interact to form a domain which moves in response to proton influx through a proton wire (including $SecD_{D519}$ and $SecF_{R247}$; orange) within the membrane domain. The yellow star depicts a hydrophobic pocket within the P1-head of SecD.

THE ANCILLARY SUB-COMPLEX SecDF

Genes encoding both SecD and SecF are co-transcribed within a single operon in *Escherichia coli* (*E. coli*) indicative of the propensity for SecDF complex formation (Gardel et al., 1990). SecDF is not essential in bacteria, but SecDF null strains have heavily impaired translocation leaving them barely viable (Gardel et al., 1990; Pogliano and Beckwith, 1994), whilst the over-expression of SecDF stimulates translocation (Pogliano and Beckwith, 1994). However, the precise mechanism of how SecDF assists translocation is unclear. Early co-immuno precipitation (co-IP) experiments using antibodies for SecG identified SecDF as an interactor with SecYEG as part of a larger complex containing YajC and another protein now identified as YidC (Duong and Wickner, 1997a). This complex was shown to prevent the backsliding of proOmpA translocation intermediates during translocation through the SecYEG channel (Duong and Wickner, 1997b). YajC, SecD and SecF also form a heterotrimer independently of other translocation machinery (Pogliano and Beckwith, 1994).

SecDF is a member of the resistance-nodulation-division (RND) superfamily, containing 12 TM helices, split between SecD and SecF each with 6 TM helices shown in **Figure 1**. SecDF has low homology with other members of the family with the largest differences manifesting in the large and structurally flexible periplasmic domains (P1-head and base and P4), the movement of which is coupled to the movement of protons down their electrostatic and chemical gradient (PMF).

There are multiple high-resolution crystallographic structures solved for the SecDF complex (Tsukazaki et al., 2011; Furukawa et al., 2017, 2018). Each of these differ in both the transmembrane and periplasmic domains, with the most drastic conformational changes observed in the periplasmic domains. The P1 "head" domain of SecD undergoes a 100 degree rotation to move between "F" and "I" forms resulting from a series of smaller conformational changes within the TM region of the complex (Tsukazaki et al., 2011; Furukawa et al., 2017). Cysteine crosslinks "locking" SecDF in this extended I form for crystallographic studies reveal the TM region can accommodate a central channel containing water molecules (Furukawa et al., 2017). This allows the movement of protons across the membrane via a proton wire formed by the water molecules and conserved arginine and aspartate residues. In particular, the deprotonation and reprotonation of a central conserved aspartate residue (D365 in *T. thermophilia*, D519 in *E. coli*) is critical for proton transport. Importantly, this channel is not always present in SecDF but the presence of the channel is likely to be coupled to a series of conformational changes important to the function of SecDF (Furukawa et al., 2017).

A final structural study captured a further more compact state where β-sheets in P1-base and P4 domains rearrange into a single β-barrel within the periplasm; this has been named the "Super-F" form (Furukawa et al., 2018). These movements depend on the interaction between two highly conserved residues at the center of the proton channel in SecDF (in *E. coli* D519 in SecD and R247 in SecF) (Furukawa et al., 2018). Mutagenesis of either of these central residues prevents SecDF reaching this super-F form and "locks" the SecDF into the I form (Furukawa et al., 2018).

The structural studies suggest that proton transport through the membrane is coupled to large conformational changes in the periplasm, which could indeed be involved in protein handling—perhaps for the emergence of polypeptides from the

protein-channel through SecY and subsequent onward passage into the periplasm, or further afield toward the outer-membrane.

MEMBRANE PROTEIN INSERTION AND YidC

Another associate of the core SecYEG complex is the membrane protein YidC—part of the YidC/Oxa1/Alb3 family of membrane "insertases" found across all domains of life. Members of this family are able to act autonomously or cooperatively with other Sec components to facilitate membrane protein assembly. In *E. coli* YidC is thought to function alone for the insertion of small membrane proteins including the c-subunit of F_1F_o-ATP synthase F_oc (Van Der Laan et al., 2004), homopentameric channel protein MscL (Facey et al., 2007), phage coat proteins M13 and Pf3 (Samuelson et al., 2001; Chen et al., 2002), and the tail-anchored membrane protein TssL (Aschtgen et al., 2012). However, it also forms a network of interactions with ribosomes, signal recognition particle (SRP), SecYEG and SecDF where it cooperates to play a much larger role in membrane insertion and membrane protein complex formation. Numerous membrane proteins have been shown to require both YidC and SecY for successful membrane insertion (Nagamori et al., 2004; Celebi et al., 2006; Zhu et al., 2013). Studies from this authors research group even suggest that the small proteins thought to depend only on YidC enter the membrane more efficiently when SecYEG is also present (in the holo-translocon; HTL—see below) (Komar et al., 2016).

Interestingly unlike SecY, members of the YidC/Oxa1/Alb3 family lack any form of channel and instead utilize a conserved helical bundle of only 5 TM helices and a conserved cytoplasmic coiled coil helix. This transmembrane part of YidC is sufficiently conserved across different lifeforms that expression of the family member Alb3 from chloroplasts, Oxa1 from mitochondria in *Saccharomyces cerevisiae*, or Alb4 from Arabidopsis can restore growth in YidC- depleted strains of *E. coli* (Jiang et al., 2002; Van Bloois et al., 2007; Benz et al., 2009). This 5 helical bundle is arranged with a "greasy slide" and a "hydrophilic groove" to interact with both the inner membrane and membrane protein substrate (**Figure 2**). Through a series of both hydrophilic and hydrophobic interactions the activation barrier for membrane protein insertion is reduced resulting in membrane protein insertion.

In addition to the known homology of YidC with Oxa1 and Alb3/4 within mitochondria and chloroplasts (for review see Hennon et al., 2015), recent studies have identified both sequence and structural homology between the prokaryotic YidC and some components of the secretory pathway within eukaryotes (Anghel et al., 2017; Bai et al., 2020; McDowell et al., 2020; Pleiner et al., 2020). Within the conserved endoplasmic reticulum membrane complex (EMC) in eukaryotes TM helices of different Emc components interact to form a YidC-like fold (Bai et al., 2020; Pleiner et al., 2020). Additionally Get1/2 in the guided entry of tail-anchored proteins (GET) pathway in *Saccharomyces cerevisiae*, and the homologous human WRB/CAML both contain hydrophilic grooves analogous to

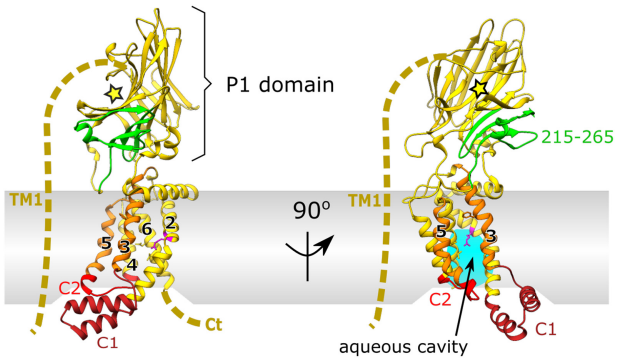

FIGURE 2 | X-ray crystal structure of YidC from *E. coli* PDB:6AL2 (Tanaka et al., 2018). Cytoplasmic loop C1 (dark red) and flexible cytoplasmic C2 loop (red). The conserved 5 helical core of TM2-5 is shown in yellow with hydrophobic, greasy slide helices TM3 and 5 highlighted in orange. Periplasmic domain (P1) is shown in yellow, with the SecF interaction site in green (residues 215–265) and the substrate binding cleft depicted by a yellow star. The unknown structure of non-conserved TM1 and the C-terminus is depicted by a dashed yellow line. Conserved arginine residue (R366) on TM2 of the hydrophilic groove, important for insertion, within the aqueous cavity is shown in magenta.

those in prokaryotic YidC (McDowell et al., 2020). This suggests that the hydrophilic groove within YidC is representative of an evolutionary conserved insertion mechanism for membrane protein substrates.

Unlike many other family members in mitochondria, or Gram-positive bacteria, the Gram-negative counterpart has a large and flexible periplasmic domain (P1; **Figure 2**). Removal of this periplasmic domain in *E. coli* has no effect on its membrane insertion capabilities (Jiang et al., 2003). It is therefore likely that the P1 domain of YidC has a distinct role in *E. coli* not observed elsewhere, e.g., in mitochondrial Oxa1 or Gram-positive SpoIIIJ which lack this domain. Through mutagenesis experiments, residues 215–265 of this region have been identified as the interaction site for SecF of the SecDF subcomplex (shown in green in **Figures 1**, **2**; Xie et al., 2006) although the full function of this domain within the periplasm remains unclear.

The P1 domain has some structural similarities to galactose mutarotase, including a central cleft corresponding to a sugar binding pocket, but lacking the sugar binding motif (Oliver and Paetzel, 2008; Ravaud et al., 2008). In one crystallographic study a polyethelyene glycol (PEG) molecule from the crystallization buffer co-crystallized within the cleft forming extensive hydrophobic interactions with 22 different conserved residues (Ravaud et al., 2008). Notably, PEG molecules have been observed to occupy clefts that naturally bind elongated polymers such as polypeptides in chaperones, or long acyl chains in enzymes and typically form similar interaction networks as that observed within P1 cleft of YidC (Ravaud et al., 2008). Given the hydrophobic binding capabilities of the cleft, the authors of the study suggest a few potential roles for the P1 domain *in vivo*; (*i*) it could interact with the peptidoglycan layer, (*ii*) potentially it could interact with an elongated peptide chain from an interacting protein in the periplasm, or alternatively (*iii*) it

could have a role as a molecular chaperone through interaction with an unfolded polypeptide in the periplasm. Further structural studies have now revealed that this cleft is oriented away from the membrane (Kumazaki et al., 2014), hence interactions with molecules or interacting protein in the periplasm are more likely than with unfolded polypeptide.

THE INTERACTION OF YidC WITH SecYEG AND SecDF

Interactions between YidC and the Sec translocon were first discovered through co-purification with SecYEG (Scotti et al., 2000). These co-purification experiments showed that the over-production of either SecYEG or the SecDF-YajC subcomplex caused an increase in the levels of YidC, implicating a cooperative role in SecDF and SecYEG dependent translocation (Scotti et al., 2000). Subsequent studies revealed the requirement for both SecYEG and YidC in insertion of larger polytopic membrane proteins (Nagamori et al., 2004; Celebi et al., 2006; Zhu et al., 2013). It is now known that YidC forms intimate contacts with the lateral gate and pore ring residues within the channel of SecY (Sachelaru et al., 2013, 2017). This positions it well to receive and facilitate the transition of trans-membrane helices from the channel, *via* the "greasy slide" to the bilayer. Additionally more recent *in vitro* and *in vivo* crosslinking experiments identified the auxiliary TM1 of *E. coli* YidC as a major contact site for interaction with both SecG and SecY (Petriman et al., 2018; **Figure 2**). These also implicate the C1 loop and C2 cytoplasmic domains as major interaction sites with SecY confirming that the hydrophilic cavity of YidC faces the lateral gate of SecY (Petriman et al., 2018).

THE HOLO-TRANSLOCON COMPLEX

The interactions between SecYEG, SecDF-YajC and YidC led to the concept of a large holo-complex: whereby efficient protein secretion and membrane insertion, through the core-complex, is facilitated by associated ancillary factors, respectively SecDF and YidC. This was first recognized through co-immuno-precipitation of SecYEG and SecDF-YajC (Duong and Wickner, 1997a). Much later it was shown that a complex containing SecYEG, SecDF-YajC and YidC could be extracted from native membranes; achieved by SMALPS (styrene maleic anhydride lipid particles) extraction, which retains the lipid bilayer around solubilized membrane proteins (Komar et al., 2016). Balanced over-production of SecYEG, SecDF-YajC and YidC (Bieniossek et al., 2009), enabled the isolation and characterization of the this "holo-translocon" (HTL) (Schulze et al., 2014). The HTL was indeed capable of post-translational ATP and PMF driven transport through SecYEG by SecA, as well as co-translational membrane protein insertion (Schulze et al., 2014).

A low resolution (14 Å) cryo-electron microscopy (cryo-EM) structure allowed the determination of the arrangement of the individual components within the HTL (Botte et al., 2016). This placement used prior knowledge of component interactions, and computational fitting within the density (**Figure 3**; Botte et al., 2016). Efforts to improve the structure, to gain more insights of the interactions between SecYEG and the ancillary factors, have been thwarted by the inherent flexibility (necessary for function) of the assembly.

Interestingly, Martini course-grained (CG) molecular dynamic simulations and small-angle neutron scattering (SANS) experiments revealed a central lipid pool (∼8–29 phospholipids) between SecYEG, YidC and SecDF-YajC (Botte et al., 2016; Martin et al., 2019). Further analysis of the data suggests that both the protein and lipid components of the HTL are highly dynamic. In the former case, this corresponds to movement of SecD between I- and F-forms (**Figure 3D**; Furukawa et al., 2017), and in the latter lipids exchanging between the central pool and the surrounding bilayer (Martin et al., 2019).

This lipid core could create a suitable environment for membrane protein assembly, protected from surrounding membrane proteins which could cause aggregation or proteolysis (**Figure 3E**). This concept is reminiscent of the mechanism deployed by the chaperonin GroEL, which provides an aqueous cavity to promote efficient folding of globular proteins (Ranson et al., 1997; Xu et al., 1997). The likely dynamic nature of this pool would be suited for the accommodation and folding of differently sized membrane proteins on their way to the membrane.

ADDITIONAL ASSOCIATES OF THE Sec MACHINERY

There is a very strong possibility that other factors associate with the translocon. This could be to confer new functionalities, or to regulate and refine protein secretion, insertion and quality-control activities. Additional factors will also be needed for the management of the onward passage of proteins for degradation or for their safe passage through the periplasm.

Membrane tethered periplasmic chaperone PpiD with its partner protein YfgM has been shown to interact with SecY (Götzke et al., 2014; Fürst et al., 2018; Jauss et al., 2019). The interaction sites appear to overlap with the those of YidC at the lateral gate. Thus, these factors might associate to fine tune the properties of the core-SecYEG complex according to the transiting client: YidC for insertion and PpiD/YfgM for periplasmic processing downstream of secretion. These and other complex interaction networks must operate to ensure the versatility of the Sec translocon enabling the effective delivery of a vast quantity and diversity of the proteins across the bacterial envelope.

CROSSING THE PERIPLASM

Proteins exiting through the SecY-channel need to be sorted for delivery and folding into the periplasm or directed to the outer-membrane (**Figure 4**). Irrespective of their final destination the newly transported polypeptide must be maintained in a non-aggregated and non-folded state, or otherwise degraded if things go wrong—e.g., misfolding, channel-blocking, aggregation. In order to achieve this in the very challenging environment of

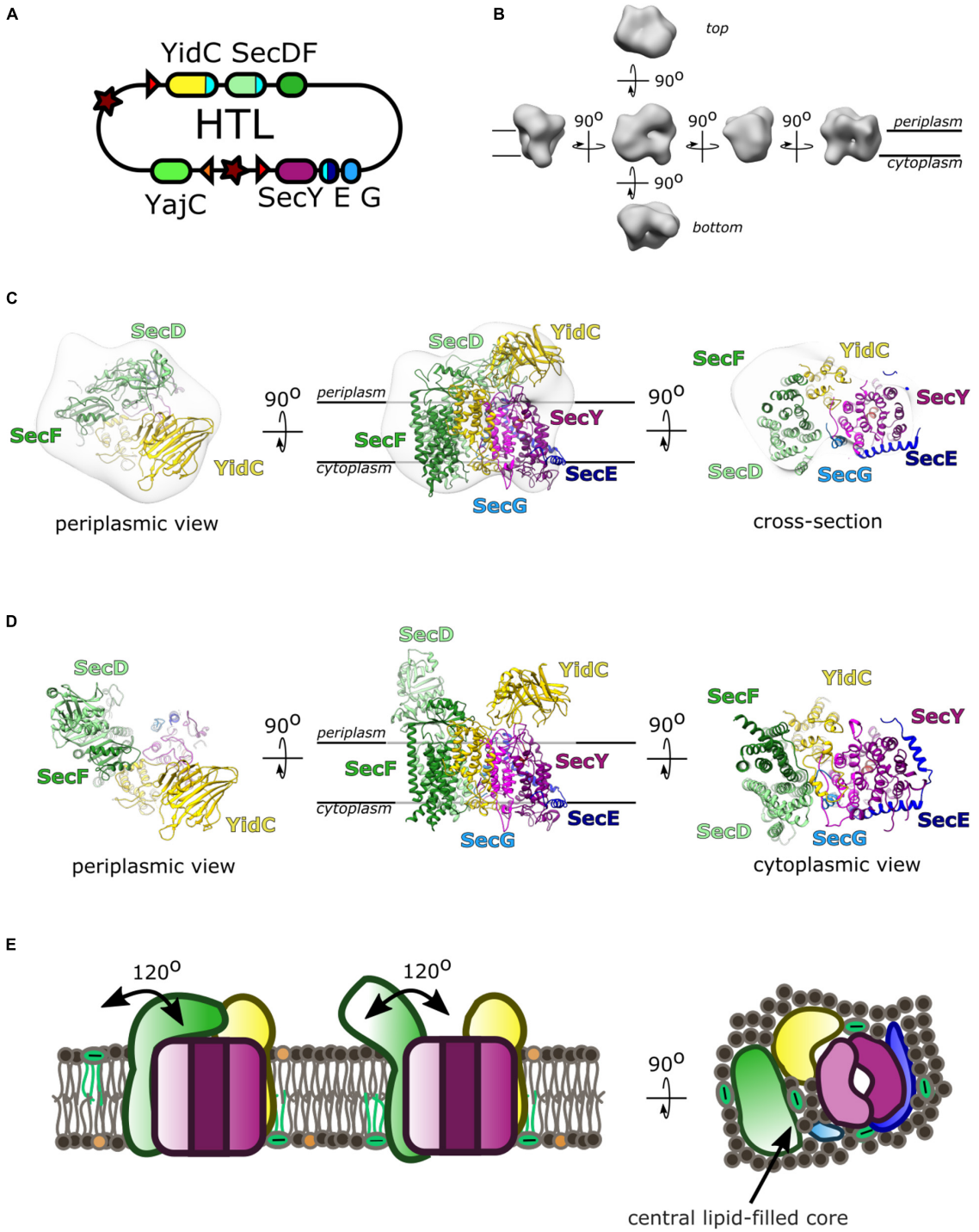

FIGURE 3 | The Holo-translocon of *E. coli*. **(A)** Plasmid system for expression of HTL (Bieniossek et al., 2009). **(B)** 14 Å resolution electron density of HTL in amphipols (EMD:3506; Botte et al., 2016). **(C)** Computational fitting of individual components of HTL to this density (PDB:5MG3 Botte et al., 2016). SecDF (green; SecD P1 domain, light green), YidC (yellow), SecYEG (magenta, dark blue, light blue). **(D)** A suggested alternate conformation of this complex where SecDF periplasmic domain is rotated into the *I*-form (Martin et al., 2019). **(E)** Schematic of HTL depicting SecDF rotation and the central lipid cavity.

the periplasm (Pedebos et al., 2021), a range of periplasmic chaperones have evolved, in the absence of any apparent energy source. SurA and Skp are thought to be the most prominent of these quality control factors, working in conjunction with DegP periplasmic protease (Rizzitello et al., 2001; Sklar et al., 2007; Li et al., 2018). These parallel and redundant pathways provide a

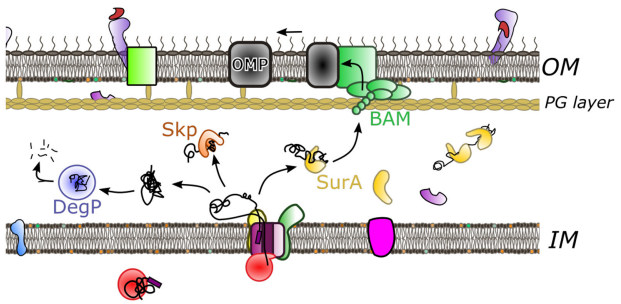

FIGURE 4 | Crossing the periplasm. Following protein translocation through the inner membrane multiple pathways operate during onward passage. The predominant chaperone SurA (yellow) holds the protein in an unfolded state prior to delivery to the outer-membrane through interaction with the BAM complex. Alternatively the chaperone Skp (orange) has aggregate recovery activity. If the peptide misfolds or aggregates DegP protease (blue) will degrade the substrate.

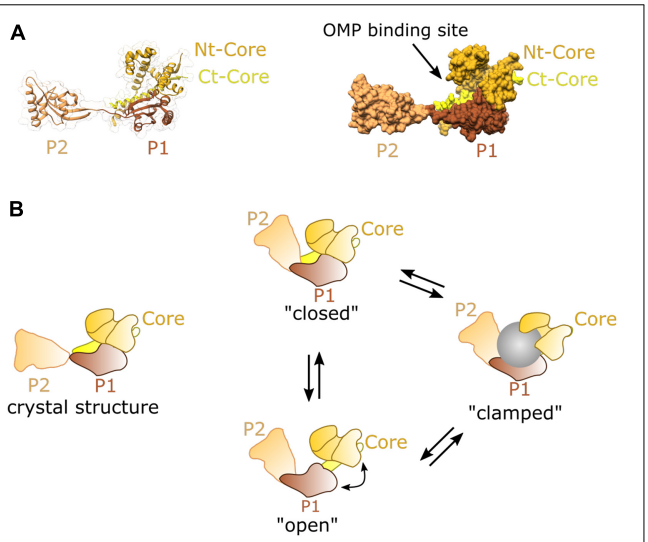

FIGURE 5 | Structure and dynamics of SurA. **(A)** Cartoon (left) and surface (right) representations of the crystal structure of SurA from *E. coli* PDB:1M5Y (Bitto and McKay, 2002). This contains a core domain consisting of the N and C terminal sequences, and P1 and P2 parvulin-like PPIase domains. **(B)** A model of dynamic movements between conformations distinct from the crystal structure as revealed from single molecule FRET experiments, adapted from Calabrese et al. (2020).

robust means to navigate the dense proteinaceous environment. SurA has been shown, by chemical cross-linking, to interact with BamA—the major subunit of the BAM complex, suggestive of a role in the delivery to the outer-membrane (Sklar et al., 2007). Although, how the chaperoned proteins travel beyond the PG layer is unclear.

SurA plays a major role in OMP biogenesis; its deletion leads to OMP assembly defects and changes in outer-membrane composition. This in turn induces the stress response and causes increased susceptibility to external factors such as antibiotics (Lazar and Kolter, 1996; Rouvière and Gross, 1996; Behrens et al., 2001; Justice et al., 2005; Vertommen et al., 2009; Klein et al., 2019). The phenotype is severe, but falls short of lethality—null strains are viable due to redundancy with DegP and Skp (Sklar et al., 2007).

The structure of SurA reveals a core domain split into N- and C- terminal regions, and two parvulin-like peptidylproyl isomerase (PPIase) domains (P1 and P2) (Bitto and McKay, 2002). SurA has a preference for binding aromatic sequences with Ar-X-Ar motif (Bitto and McKay, 2002; Hennecke et al., 2005; Xu et al., 2007), a motif commonly found in C-terminal regions of many OMPs (Behrens-Kneip, 2010; Merdanovic et al., 2011). The site at which these peptide motifs interact with the SurA chaperone has not been identified, but the crystallographic structure reveals an extended crevice within the core of domain which could be involved in the binding and release of the peptide substrate during folding (**Figure 5A**; Bitto and McKay, 2002). Single-molecule FRET experiments indicate that two SurA molecules can bind a single OmpC substrate, but that the stoichiometry may differ depending on the size of the substrate (Li et al., 2018).

Recent studies using FRET and chemical cross-linking, revealed that in solution SurA adopts multiple conformations all of which substantially differ from the crystal structure (**Figure 5B**; Calabrese et al., 2020). Conformational analysis of this data suggests that the three domains of SurA form a cradle around OMP clients protecting them from aggregation (Calabrese et al., 2020). This structural plasticity may be an essential feature of SurA activity, as it is for many other chaperones (Burmann and Hiller, 2015; Suss and Reichmann, 2015). Importantly, the chaperone function of SurA seems to span from early to late stages of the journey forming interactions at both SecYEG (Ureta et al., 2007) and the BAM complex (Hennecke et al., 2005; Sklar et al., 2007; Gunasinghe et al., 2018).

Skp, like SurA, binds a broad range of substrates, sequestering them from the dense and protein-packed periplasmic space (Qu et al., 2007; Wu et al., 2011). Whilst neither SurA or Skp are required for cell viability, cells lacking SurA must contain both Skp and protease DegP, which thereby compensate for the loss of SurA activity (Rizzitello et al., 2001; Sklar et al., 2007).

Unlike SurA which recognizes specific hydrophobic sequences (Bitto and McKay, 2002; Hennecke et al., 2005; Xu et al., 2007), Skp forms a large jellyfish-like trimeric structure (Korndörfer et al., 2004; Walton and Sousa, 2004), interacting with protein substrates through non-specific hydrophobic and electrostatic interactions within a large hydrophobic cavity (Jarchow et al., 2008; Walton et al., 2009; Burmann et al., 2013; Callon et al., 2014; **Figure 6**). For a number of substrates the stoichiometry of Skp to substrate is 1:1 where the chaperone "swallows" the full substrate into the hydrophobic cavity (Bulieris et al., 2003; Qu et al., 2007; Lyu et al., 2012; Burmann et al., 2013) although large substrates can be accommodated by two Skp chaperones if it is too large for just one (Schiffrin et al., 2016). Like SurA, flexibility of Skp is thought to be integral to its function, where it operates as a spring-loaded clamp to wrap its tentacular arms around a range of different sized complexes into its hydrophobic core (Holdbrook et al., 2017).

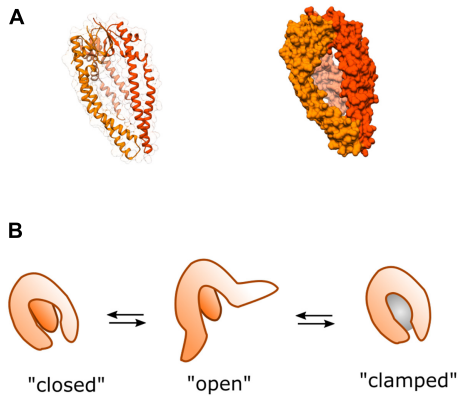

FIGURE 6 | Structure and dynamics of Skp. **(A)** Cartoon (left) and surface (right) representations of the crystal structure of homo-trimeric periplasmic chaperone Skp of *E. coli* PDB:1SG2 (Korndörfer et al., 2004). **(B)** A model of dynamic movements between conformations adapted from Holdbrook et al. (2017). The three tentacular arms function to clamp around substrates of different sizes (represented by the gray sphere) binding them in the hydrophobic core to prevent aggregation, or rescue partially aggregated proteins.

In spite of the functional overlap with SurA, Skp has been shown to possess distinctive characteristics. In contrast to SurA, Skp has been shown to assist with folding of OMPs into the lipid bilayer *in vitro* (Bulieris et al., 2003; Patel et al., 2009; McMorran et al., 2013). Moreover, it has also been shown to be able to recover aggregated OMPs from the periplasm (Li et al., 2018). This activity could become especially important under cellular stress conditions where expression levels of several OMPs are up-regulated causing increased potential for aggregation. This is consistent with the finding that under stress conditions the expression of Skp is upregulated (Sklar et al., 2007), perhaps as a strategy to help prevent OMP aggregation during periods of high demand for outer-membrane biogenesis—e.g., rapid cell growth.

Like SurA, Skp has also been shown to interact with OMP during early stages of the translocation process (Harms et al., 2001). Although, as of yet, no interactions with the Sec or BAM machineries have been demonstrated (Sklar et al., 2007). This is consistent with the suggestion that the role of Skp is more prominent in OMP recovery and that SurA is the more important for OMP transport, although further clarification of their roles within the periplasm is required.

HOLO-TRANSLOCON AND BARREL-ASSEMBLY MACHINERY: INTER-MEMBRANE ASSOCIATION

Even with the assistance of chaperones, it seems improbable that the OMP-chaperone complex can be reliant on diffusion alone for efficient transport through the periplasm. Photo-crosslinking studies (Wang et al., 2016), and more recently biochemical and low-resolution cryo-EM studies (Alvira et al., 2020) have implicated a direct connection between secretory components within the inner and outer-membranes. In particular a low-resolution cryo-EM reveals the interaction between the Sec and BAM translocons (Alvira et al., 2020; **Figure 7**). The assignment of different parts of the density to given complexes was inferred through difference negative stain electron microscopy of multiple subcomplexes with missing components, cross-linking and mass spectrometry. This revealed interactions between both periplasmic domains of HTL (on YidC and SecDF) and the periplasmic domains of BAM.

Mutations in the genes encoding SecDF causing amino acid substitution of an aspartate for an asparagine (approximating a deprotonated neutral aspartate), allow production of the SecDF variant (SecD$_{D519N}$F), with a dysfunctional proton wire in the transmembrane portion of the complex. This version is known to bring about large changes in the conformation of the periplasmic domain P1 of SecDF (see above) (Tsukazaki et al., 2011; Furukawa et al., 2017, 2018). On this basis it is reasonably safe to assume that proton passage through SecD will promote conformational switching back and forth between the 2 states (perhaps similar to the *I*- and *F*-states) as aspartate-519 would alternate between

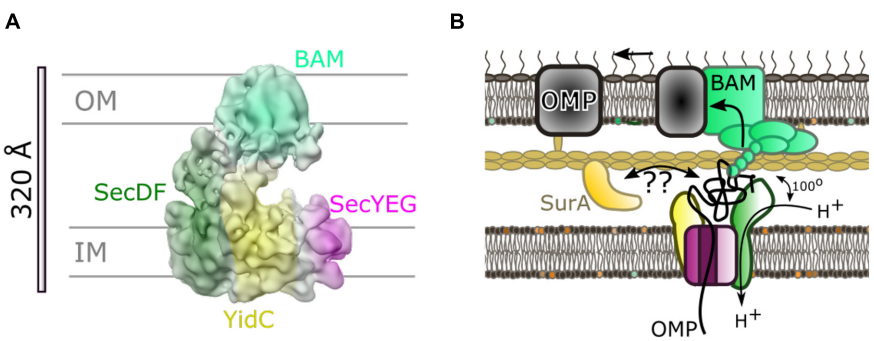

FIGURE 7 | Inter-membrane association of HTL and BAM. **(A)** 14 Å cryo-EM density from Alvira et al. (2020) colored to show locations of BAM (light green) and components of HTL: SecDF (dark green), SecYEG (magenta) and YidC (yellow). **(B)** Cartoon of model for translocation through the HTL-BAM inter-membrane complex adapted from Alvira et al. (2020). Movement of periplasmic domains of SecDF (dark green) has a role in energy transduction of the PMF to the BAM complex for OMP maturation. The precise nature of the involvement of periplasmic chaperones is unknown; SurA is known to interact with OMPs soon after emergence from SecY and also with BAM on the other side of the envelope.

the protonated and deprotonated forms. The analysis of this variant allowed the evaluation of the role of the proton coupled mobility of SecD in the context of its association with BAM, and subsequent OMP maturation. The results found that whilst the interaction with BAM components were unaffected, OMP maturation was considerably inhibited when compared to the wild-type strains, similar to the effect of a SecDF depletion (Alvira et al., 2020).

Previous publications have shown that SecYEG and SecA alone are sufficient for the PMF- and ATP-driven transport through the inner membrane, demonstrating that the SecDF proton driven conformational changes are not required for transport through the inner membrane. It follows that effects of the PMF conferred by SecDF must be important for the down-stream events critical to OMP maturation. Potentially, this could be through a dynamic interaction with the BAM complex (**Figure 7**).

One compelling explanation linking PMF-dependent rearrangement of SecDF to OMP maturation, is that these movements act as a mechanism for energy transduction between the inner and outer-membrane; a concept consistent with observations of other systems. One example of long range energy transduction across the envelope is another RND transporter family member—the multi-drug efflux pump formed by the inter-membrane association of AcrAB (IM) and TolC (OM) (Du et al., 2014; Wang et al., 2017; Chen et al., 2021). Another is the Ton complex for nutrient import (Celia et al., 2016). Other striking parallels even contain homologs of BamA including: (*i*) double membrane spanning translocation and assembly modules (TAM) found in proteobacteria (Selkrig et al., 2012), and (*ii*) the TIC-TOC import machinery of chloroplasts (Chen et al., 2018) contain BamA homologs TamA and TOC75, respectively. The dynamically coupled double-membrane protein transport system suggested between HTL and BAM is therefore far from a novel concept; membrane coupling is a common occurrence within the envelopes of chloroplasts and bacteria, and probably mitochondria as well.

Interestingly, the low-resolution structure for the HTL-BAM complex contains a large periplasmic cavity, with ample room to accommodate periplasmic chaperones. SurA for example, is a known interactor of BamA and may well be stationed here. The obvious question remains about how these chaperones coordinate with HTL alone and with trans-envelope complex HTL-BAM complex in order to manage the lateral efflux of proteins either into the periplasm or the outer-membrane.

There is indeed a lot still to be learnt about the dynamic molecular mechanism and bioenergetics underlying the bacterial general secretory process. This remains true of the early stages of this process—the mechanism of ATP and PMF driven transport across the inner membrane by cytosolic SecA through SecYEG, and even more so for what needs to happen afterward. Knowledge of the early and, in particular, the later stages of this process is critical for our understanding of the fundamental process of bacterial envelope biogenesis. Moreover, future new insights will be critical in the development of strategies to compromise the cell wall toward the development of new anti-bacterials, or as supplements designed to potentiate cytotoxic agents which would otherwise be excluded from the cell.

AUTHOR CONTRIBUTIONS

LT and IC wrote the manuscript. Both authors contributed to the article and approved the submitted version.

ACKNOWLEDGMENTS

We are very grateful to the BBSRC who support our work on bacterial secretion. An SWBio DTP studentship to LT (BB/J014400/1 and BB/M009122/1) and project grants to IC (BB/V001531/1; BB/T006889/1; and BB/S008349/1). Enormous thanks to Tia Salter for meticulous proofreading.

REFERENCES

Alvira, S., Watkins, D. W., Troman, L., Allen, W. J., Lorriman, J. S., Degliesposti, G., et al. (2020). Inter-membrane association of the sec and bam translocons for bacterial outer-membrane biogenesis. *eLife* 9:e60669. doi: 10.7554/eLife.60669

Anghel, S. A., McGilvray, P. T., Hegde, R. S., and Keenan, R. J. (2017). Identification of Oxa1 homologs operating in the eukaryotic endoplasmic reticulum. *Cell Rep.* 21, 3708–3716. doi: 10.1016/j.celrep.2017.12.006

Arkowitz, R. A., Joly, J. C., and Wickner, W. (1993). Translocation can drive the unfolding of a preprotein domain. *EMBO J.* 12, 243–253. doi: 10.1002/j.1460-2075.1993.tb05650.x

Aschtgen, M. S., Zoued, A., Lloubès, R., Journet, L., and Cascales, E. (2012). The C-tail anchored TssL subunit, an essential protein of the enteroaggregative *Escherichia coli* Sci-1 Type VI secretion system, is inserted by YidC. *MicrobiologyOpen* 1, 71–82. doi: 10.1002/mbo3.9

Bai, L., You, Q., Feng, X., Kovach, A., and Li, H. (2020). Structure of the ER membrane complex, a transmembrane-domain insertase. *Nature* 584, 475–478. doi: 10.1038/s41586-020-2389-3

Behrens, S., Maier, R., De Cock, H., Schmid, F. X., and Gross, C. A. (2001). The SurA periplasmic PPIase lacking its parvulin domains functions in vivo and has chaperone activity. *EMBO J.* 20, 285–294. doi: 10.1093/emboj/20.1.285

Behrens-Kneip, S. (2010). The role of SurA factor in outer membrane protein transport and virulence. *Int. J. Med. Microbiol.* 300, 421–428. doi: 10.1016/j.ijmm.2010.04.012

Benz, M., Bals, T., Gügel, I. L., Piotrowski, M., Kuhn, A., Schünemann, D., et al. (2009). Alb4 of arabidopsis promotes assembly and stabilization of a non chlorophyll-binding photosynthetic complex, the CF1CF0-ATP synthase. *Mol. Plant* 2, 1410–1424. doi: 10.1093/mp/ssp095

Bieker, K. L., and Silhavy, T. J. (1990). The genetics of protein secretion in *E. coli*. *Trends Genet.* 6, 329–334. doi: 10.1016/0168-9525(90)90254-4

Bieniossek, C., Nie, Y., Frey, D., Olieric, N., Schaffitzel, C., Collinson, I., et al. (2009). Automated unrestricted multigene recombineering for multiprotein complex production. *Nat. Publ. Group* 6, 447–450. doi: 10.1038/nmeth.1326

Bitto, E., and McKay, D. B. (2002). Crystallographic structure of SurA, a molecular chaperone that facilitates folding of outer membrane porins. *Structure* 10, 1489–1498. doi: 10.1016/S0969-2126(02)00877-8

Blobel, G., and Dobberstein, B. (1975). Transfer of proteins across membranes: I. Presence of proteolytically processed and unprocessed nascent

immunoglobulin light chains on membrane-bound ribosomes of murine myeloma. *J. Cell Biol.* 67, 835–851. doi: 10.1083/jcb.67.3.835

Blobel, G., and Sabatini, D. D. (1971). "Ribosome-Membrane Interaction in Eukaryotic Cells," in *Biomembranes*, ed. L. A. Manson (Boston, MA: Springer), doi: 10.1007/978-1-4684-3330-2_16

Bost, S., and Belin, D. (1997). prl Mutations in the *Escherichia coli* secG gene. *J. Biol. Chem.* 272, 4087–4093. doi: 10.1074/jbc.272.7.4087

Botte, M., Zaccai, N. R., Nijeholt, J. L. À, Martin, R., Knoops, K., Papai, G., et al. (2016). A central cavity within the holo-translocon suggests a mechanism for membrane protein insertion. *Sci. Rep.* 6:38399. doi: 10.1038/srep38399

Brundage, L., Hendrick, J. P., Schiebel, E., Driessen, A. J. M., and Wickner, W. (1990). The purified *E. coli* integral membrane protein SecY E is sufficient for reconstitution of SecA-dependent precursor protein translocation. *Cell* 62, 649–657. doi: 10.1016/0092-8674(90)90111-Q

Bulieris, P. V., Behrens, S., Holst, O., and Kleinschmidt, J. H. (2003). Folding and insertion of the outer membrane protein OmpA is assisted by the chaperone Skp and by lipopolysaccharide. *J. Biol. Chem.* 278, 9092–9099. doi: 10.1074/jbc.M211177200

Burmann, B. M., and Hiller, S. (2015). Chaperones and chaperone-substrate complexes: dynamic playgrounds for NMR spectroscopists. *Prog. Nucl. Magn. Reson. Spectrosc.* 86–87, 41–64. doi: 10.1016/j.pnmrs.2015.02.004

Burmann, B. M., Wang, C., and Hiller, S. (2013). Conformation and dynamics of the periplasmic membrane-protein-chaperone complexes OmpX-Skp and tOmpA-Skp. *Nat. Struct. Mol. Biol.* 20, 1265–1272. doi: 10.1038/nsmb.2677

Calabrese, A. N., Schiffrin, B., Watson, M., Karamanos, T. K., Walko, M., Humes, J. R., et al. (2020). Inter-domain dynamics in the chaperone SurA and multi-site binding to its outer membrane protein clients. *Nat. Commun.* 11:2155. doi: 10.1038/s41467-020-15702-1

Callon, M., Burmann, B. M., and Hiller, S. (2014). Structural mapping of a chaperone-substrate interaction surface. *Angew. Chem. Int. Ed. Engl.* 53, 5069–5072. doi: 10.1002/anie.201310963

Celebi, N., Yi, L., Facey, S. J., Kuhn, A., and Dalbey, R. E. (2006). Membrane biogenesis of subunit II of cytochrome bo oxidase: contrasting requirements for insertion of N-terminal and C-terminal domains. *J. Mol. Biol.* 357, 1428–1436. doi: 10.1016/j.jmb.2006.01.030

Celia, H., Noinaj, N., Zakharov, S. D., Bordignon, E., Botos, I., Santamaria, M., et al. (2016). Structural insight into the role of the Ton complex in energy transduction. *Nature* 538, 60–65. doi: 10.1038/nature19757

Chen, M., Samuelson, J. C., Jiang, F., Muller, M., Kuhn, A., and Dalbey, R. E. (2002). Direct interaction of YidC with the Sec-independent Pf3 coat protein during its membrane protein insertion. *J. Biol. Chem.* 277, 7670–7675. doi: 10.1074/jbc.M110644200

Chen, M., Shi, X., Yu, Z., Fan, G., Serysheva, I. I., Baker, M. L., et al. (2021). In situ structure of the AcrAB-TolC efflux pump at subnanometer resolution. *Structure* doi: 10.1016/j.str.2021.08.008 Online ahead of print

Chen, Y.-L., Chen, L.-J., Chu, C.-C., Huang, P.-K., Wen, J.-R., and Li, H.-M. (2018). TIC236 links the outer and inner membrane translocons of the chloroplast. *Nature* 564, 125–129. doi: 10.1038/s41586-018-0713-y

Collinson, I. (2019). The dynamic ATP-driven mechanism of bacterial protein translocation and the critical role of phospholipids. *Front. Microbiol.* 10:1217. doi: 10.3389/fmicb.2019.01217

Dezélée, P., and Bricas, E. (1970). Structure of the peptidoglycan in *Escherichia coli B* and *Bacillus megaterium* KM. Stereospecific synthesis of two meso-diaminopimelic acid peptides with the tetrapeptide subunit of bacterial cell wall peptidoglycan. *Biochemistry* 9, 823–831. doi: 10.1021/bi00806a015

Du, D., Wang, Z., James, N. R., Voss, J. E., Klimont, E., Ohene-Agyei, T., et al. (2014). Structure of the AcrAB-TolC multidrug efflux pump. *Nature* 509, 512–515. doi: 10.1038/nature13205

Duong, F., and Wickner, W. (1997a). Distinct catalytic roles of the SecYE, SecG and SecDFyajC subunits of preprotein translocase holoenzyme. *EMBO J.* 16, 2756–2768. doi: 10.1093/emboj/16.10.2756

Duong, F., and Wickner, W. (1997b). The SecDFyajC domain of preprotein translocase controls preprotein movement by regulating SecA membrane cycling. *EMBO J.* 16, 4871–4879. doi: 10.1093/emboj/16.16.4871

Egea, P. F., and Stroud, R. M. (2010). Lateral opening of a translocon upon entry of protein suggests the mechanism of insertion into membranes. *Proc. Natl. Acad. Sci. U. S. A.* 107, 17182–17187. doi: 10.1073/pnas.1012556107

Emr, S. D., Hanley-Way, S., and Silhavy, T. J. (1981). Suppressor mutations that restore export of a protein with a defective signal sequence. *Cell* 23, 79–88. doi: 10.1016/0092-8674(81)90272-5

Facey, S. J., Neugebauer, S. A., Krauss, S., and Kuhn, A. (2007). The Mechanosensitive channel protein MscL is targeted by the SRP to the novel YidC membrane insertion pathway of *Escherichia coli*. *J. Mol. Biol.* 365, 995–1004. doi: 10.1016/j.jmb.2006.10.083

Fürst, M., Zhou, Y., Merfort, J., and Müller, M. (2018). Involvement of PpiD in Sec-dependent protein translocation. *Biochim. Biophys. Acta Mol. Cell Res.* 1865, 273–280. doi: 10.1016/j.bbamcr.2017.10.012

Furukawa, A., Nakayama, S., Yoshikaie, K., Tanaka, Y., and Tsukazaki, T. (2018). Remote coupled drastic β-barrel to β-sheet transition of the protein translocation motor. *Structure* 26, 485.e2–489.e2. doi: 10.1016/j.str.2018.01.002

Furukawa, A., Yoshikaie, K., Mori, T., Mori, H., Morimoto, Y. V., Sugano, Y., et al. (2017). Tunnel formation inferred from the I-form structures of the proton-driven protein secretion motor SecDF. *Cell Rep.* 19, 895–901. doi: 10.1016/j.celrep.2017.04.030

Gardel, C., Johnson, K., Jacq, A., and Beckwith, J. (1990). The secD locus of *E. coli* codes for two membrane proteins required for protein export. *EMBO J.* 9, 3209–3216. doi: 10.1002/j.1460-2075.1990.tb07519.x

Götzke, H., Palombo, I., Muheim, C., Perrody, E., Genevaux, P., Kudva, R., et al. (2014). YfgM is an ancillary subunit of the SecYEG translocon in *Escherichia coli*. *J. Biol. Chem.* 289, 19089–19097. doi: 10.1074/jbc.M113.541672

Green, E. R., and Mecsas, J. (2016). Bacterial secretion systems: an overview. *Microbiol. Spectr.* 4, 1–32. doi: 10.1128/microbiolspec.vmbf-0012-2015

Gunasinghe, S. D., Shiota, T., Stubenrauch, C. J., Schulze, K. E., Webb, C. T., Fulcher, A. J., et al. (2018). The WD40 protein BamB mediates coupling of BAM complexes into assembly precincts in the bacterial outer membrane. *Cell Rep.* 23, 2782–2794. doi: 10.1016/j.celrep.2018.04.093

Harms, N., Koningstein, G., Dontje, W., Muller, M., Oudega, B., Luirink, J., et al. (2001). The early interaction of the outer membrane protein PhoE with the periplasmic chaperone Skp occurs at the cytoplasmic membrane. *J. Biol. Chem.* 276, 18804–18811. doi: 10.1074/jbc.M011194200

Hennecke, G., Nolte, J., Volkmer-Engert, R., Schneider-Mergener, J., and Behrens, S. (2005). The periplasmic chaperone SurA exploits two features characteristic of integral outer membrane proteins for selective substrate recognition. *J. Biol. Chem.* 280, 23540–23548. doi: 10.1074/jbc.M413742200

Hennon, S. W., Soman, R., Zhu, L., and Dalbey, R. E. (2015). YidC/Alb3/Oxa1 family of insertases. *J. Biol. Chem.* 290, 14866–14874. doi: 10.1074/jbc.R115.638171

Holdbrook, D. A., Burmann, B. M., Huber, R. G., Petoukhov, M. V., Svergun, D. I., Hiller, S., et al. (2017). A spring-loaded mechanism governs the clamp-like dynamics of the Skp chaperone. *Structure* 25, 1079.e3–1088.e3. doi: 10.1016/j.str.2017.05.018

Jarchow, S., Lück, C., Görg, A., and Skerra, A. (2008). Identification of potential substrate proteins for the periplasmic *Escherichia coli* chaperone Skp. *Proteomics* 8, 4987–4994. doi: 10.1002/pmic.200800288

Jauss, B., Petriman, N. A., Drepper, F., Franz, L., Sachelaru, I., Welte, T., et al. (2019). Noncompetitive binding of PpiD and YidC to the SecYEG translocon expands the global view on the SecYEG interactome in *Escherichia coli*. *J. Biol. Chem.* 294, 19167–19183. doi: 10.1074/jbc.RA119.010686

Jiang, F., Chen, M., Yi, L., De Gier, J. W., Kuhn, A., and Dalbey, R. E. (2003). Defining the regions of *Escherichia coli* YidC that contribute to activity. *J. Biol. Chem.* 278, 48965–48972. doi: 10.1074/jbc.M307362200

Jiang, F., Yi, L., Moore, M., Chen, M., Rohl, T., Van Wijk, K. J., et al. (2002). Chloroplast YidC homolog Albino3 can functionally complement the bacterial YidC depletion strain and promote membrane insertion of both bacterial and chloroplast thylakoid proteins. *J. Biol. Chem.* 277, 19281–19288. doi: 10.1074/jbc.M110857200

Justice, S. S., Justice, S. S., Hunstad, D. A., Hunstad, D. A., Harper, J. R., Harper, J. R., et al. (2005). Periplasmic peptidyl prolyl cis-trans isomerases are not essential for viability, but SurA is required for pilus biogenesis in *Escherichia coli*. *Society* 187, 7680–7686. doi: 10.1128/JB.187.22.7680

Klein, K., Sonnabend, M. S., Frank, L., Leibiger, K., Franz-Wachtel, M., Macek, B., et al. (2019). Deprivation of the periplasmic chaperone SurA reduces virulence and restores antibiotic susceptibility of multidrug-resistant *Pseudomonas aeruginosa*. *Front. Microbiol.* 10:100. doi: 10.3389/fmicb.2019.00100

Komar, J., Alvira, S., Schulze, R., Martin, R., Lycklama A Nijeholt, J., Lee, S., et al. (2016). Membrane protein insertion and assembly by the bacterial holo-translocon SecYEG-SecDF-YajC-YidC. *Biochem. J.* 473, 3341–3354. doi: 10.1042/BCJ20160545

Korndörfer, I. P., Dommel, M. K., and Skerra, A. (2004). Structure of the periplasmic chaperone Skp suggests functional similarity with cytosolic chaperones despite differing architecture. *Nat. Struct. Mol. Biol.* 11, 1015–1020. doi: 10.1038/nsmb828

Kumamoto, C. A., and Beckwith, J. (1983). Mutations in a new gene, secB, cause defective protein localization in *Escherichia coli*. *J. Bacteriol.* 154, 253–260. doi: 10.1128/jb.154.1.253-260.1983

Kumazaki, K., Kishimoto, T., Furukawa, A., Mori, H., Tanaka, Y., Dohmae, N., et al. (2014). Crystal structure of *Escherichia coli* YidC, a membrane protein chaperone and insertase. *Sci. Rep.* 4:7299. doi: 10.1038/srep07299

Lazar, S. W., and Kolter, R. (1996). SurA assists the folding of *Escherichia coli* outer membrane proteins. *J. Bacteriol.* 178, 1770–1773. doi: 10.1128/jb.178.6.1770-1773.1996

Lee, H. C., and Bernstein, H. D. (2001). The targeting pathway of *Escherichia coli* presecretory and integral membrane proteins is specified by the hydrophobicity of the targeting signal. *Proc. Natl. Acad. Sci. U. S. A.* 98, 3471–3476. doi: 10.1073/pnas.051484198

Li, G., He, C., Bu, P., Bi, H., Pan, S., Sun, R., et al. (2018). Single-molecule detection reveals different roles of Skp and SurA as chaperones. *ACS Chem. Biol.* 13, 1082–1089. doi: 10.1021/acschembio.8b00097

Lyu, Z. X., Shao, Q., Gao, Y. Q., and Zhao, X. S. (2012). Direct observation of the uptake of outer membrane proteins by the periplasmic chaperone Skp. *PLoS One* 7:e46068. doi: 10.1371/journal.pone.0046068

Martin, R., Larsen, A. H., Corey, R. A., Midtgaard, S. R., Frielinghaus, H., Schaffitzel, C., et al. (2019). Structure and dynamics of the central lipid pool and proteins of the bacterial holo-translocon. *Biophys. J.* 116, 1931–1940. doi: 10.1016/j.bpj.2019.04.002

McDowell, M. A., Heimes, M., Fiorentino, F., Mehmood, S., Farkas, Á, Coy-Vergara, J., et al. (2020). Structural basis of tail-anchored membrane protein biogenesis by the GET insertase complex. *Mol. Cell* 80, 72–86. doi: 10.1016/j.molcel.2020.08.012

McMorran, L. M., Bartlett, A. I., Huysmans, G. H. M., Radford, S. E., and Brockwell, D. J. (2013). Dissecting the effects of periplasmic chaperones on the in vitro folding of the outer membrane protein PagP. *J. Mol. Biol.* 425, 3178–3191. doi: 10.1016/j.jmb.2013.06.017

Merdanovic, M., Clausen, T., Kaiser, M., Huber, R., and Ehrmann, M. (2011). Protein quality control in the bacterial periplasm. *Annu. Rev. Microbiol.* 65, 149–168. doi: 10.1146/annurev-micro-090110-102925

Milstein, C., Brownlee, G. C., Harrison, T. M., and Mathews, M. B. (1972). A possible precursor of immunoglobulin light chains. *Nature. New Biol.* 239, 117–120. doi: 10.1038/newbio239117a0

Nagamori, S., Smirnova, I. N., and Kaback, H. R. (2004). Role of YidC in folding of polytopic membrane proteins. *J. Cell Biol.* 165, 53–62. doi: 10.1083/jcb.200402067

Oliver, D. B., and Beckwith, J. (1981). *E. coli* mutant pleiotropically defective in the export of secreted proteins. *Cell* 25, 765–772. doi: 10.1016/0092-8674(81)90184-7

Oliver, D. C., and Paetzel, M. (2008). Crystal structure of the major periplasmic domain of the bacterial membrane protein assembly facilitator YidC. *J. Biol. Chem.* 283, 5208–5216. doi: 10.1074/jbc.M708936200

Orfanoudaki, G., and Economou, A. (2014). Proteome-wide subcellular topologies of *E. coli* polypeptides database (STEPdb). *Mol. Cell. Proteomics* 13, 3674–3687. doi: 10.1074/mcp.O114.041137

Patel, G. J., Behrens-Kneip, S., Holst, O., and Kleinschmidt, J. H. (2009). The periplasmic chaperone Skp facilitates targeting, insertion, and folding of OmpA into lipid membranes with a negative membrane surface potential. *Biochemistry* 48, 10235–10245. doi: 10.1021/bi901403c

Pedebos, C., Smith, I. P. S., Boags, A., and Khalid, S. (2021). The hitchhiker's guide to the periplasm: unexpected molecular interactions of polymyxin B1 in *E. coli*. *Structure* 29, 444.e2–456.e2. doi: 10.1016/j.str.2021.01.009

Petriman, N. A., Jauß, B., Hufnagel, A., Franz, L., Sachelaru, I., Drepper, F., et al. (2018). The interaction network of the YidC insertase with the SecYEG translocon, SRP and the SRP receptor FtsY. *Sci. Rep.* 8:578. doi: 10.1038/s41598-017-19019-w

Pleiner, T., Tomaleri, G. P., Januszyk, K., Inglis, A. J., Hazu, M., and Voorhees, R. M. (2020). Structural basis for membrane insertion by the human ER membrane protein complex. *Science* 369, 433–436. doi: 10.1126/science.abb5008

Pogliano, J. A., and Beckwith, J. (1994). SecD and SecF facilitate protein export in *Escherichia coli*. *EMBO J.* 3, 554–561. doi: 10.1002/j.1460-2075.1994.tb06293.x

Qu, J., Mayer, C., Behrens, S., Holst, O., and Kleinschmidt, J. H. (2007). The trimeric periplasmic chaperone Skp of *Escherichia coli* forms 1:1 complexes with outer membrane proteins via hydrophobic and electrostatic interactions. *J. Mol. Biol.* 374, 91–105. doi: 10.1016/j.jmb.2007.09.020

Ranson, N. A., Burston, S. G., and Clarke, A. R. (1997). Binding, encapsulation and ejection: substrate dynamics during a chaperonin-assisted folding reaction. *J. Mol. Biol.* 266, 656–664. doi: 10.1006/jmbi.1996.0815

Ravaud, S., Stjepanovic, G., Wild, K., and Sinning, I. (2008). The crystal structure of the periplasmic domain of the *Escherichia coli* membrane protein insertase YidC contains a substrate binding cleft. *J. Biol. Chem.* 283, 9350–9358. doi: 10.1074/jbc.M710493200

Riggs, P. D., Derman, A. I., and Beckwith, J. (1988). A mutation affecting the regulation of secA-lacZ fusion defines a new sec gene. *Genetics* 118, 571–579. doi: 10.1093/genetics/118.4.571

Rizzitello, A. M. Y. E., Harper, J. R., and Silhavy, T. J. (2001). Genetic evidence for parallel pathways of chaperone activity in the periplasm of *Escherichia coli*. *J. Bacteriol.* 183, 6794–6800. doi: 10.1128/JB.183.23.6794

Rouvière, P. E., and Gross, C. A. (1996). SurA, a periplasmic protein with peptidyl-prolyl isomerase activity, participates in the assembly of outer membrane porins. *Genes Dev.* 10, 3170–3182. doi: 10.1101/gad.10.24.3170

Sachelaru, I., Petriman, N. A., Kudva, R., Kuhn, P., Welte, T., Knapp, B., et al. (2013). YidC occupies the lateral gate of the SecYEG translocon and is sequentially displaced by a nascent membrane protein. *J. Biol. Chem.* 288, 16295–16307. doi: 10.1074/jbc.M112.446583

Sachelaru, I., Winter, L., Knyazev, D. G., Zimmermann, M., Vogt, A., Kuttner, R., et al. (2017). YidC and SecYEG form a heterotetrameric protein translocation channel. *Sci. Rep.* 7:101. doi: 10.1038/s41598-017-00109-8

Samuelson, J. C., Jiang, F., Yi, L., Chen, M., De Gier, J. W., Kuhn, A., et al. (2001). Function of YidC for the insertion of M13 procoat protein in *Escherichia coli*: translocation of mutants that show differences in their membrane potential dependence and Sec requirement. *J. Biol. Chem.* 276, 34847–34852. doi: 10.1074/jbc.M105793200

Schatz, P. J., and Beckwith, J. (1990). Genetic analysis of protein export in *Escherichia coli*. *Annu. Rev. Genet.* 24, 215–248. doi: 10.1146/annurev.ge.24.120190.001243

Schatz, P. J., Bieker, K. L., Ottemann, K. M., Silhavy, T. J., and Beckwith, J. (1991). One of three transmembrane stretches is sufficient for the functioning of the SecE protein, a membrane component of the *E. coli* secretion machinery. *EMBO J.* 10, 1749–1757. doi: 10.1002/j.1460-2075.1991.tb07699.x

Schiffrin, B., Calabrese, A. N., Devine, P. W. A., Harris, S. A., Ashcroft, A. E., Brockwell, D. J., et al. (2016). Skp is a multivalent chaperone of outer-membrane proteins. *Nat. Struct. Mol. Biol.* 23, 786–793. doi: 10.1038/nsmb.3266

Schulze, R. J., Komar, J., Botte, M., Allen, W. J., Whitehouse, S., Gold, V. A. M., et al. (2014). Membrane protein insertion and proton-motive-force-dependent secretion through the bacterial holo-translocon SecYEG-SecDF-YajC-YidC. *Proc. Natl. Acad. Sci. U. S. A.* 111, 4844–4849. doi: 10.1073/pnas.1315901111

Scotti, P. A., Urbanus, M. L., Brunner, J., De Gier, J. W. L., Von Heijne, G., Van Der Does, C., et al. (2000). YidC, the *Escherichia coli* homologue of mitochondrial Oxa1p, is a component of the Sec translocase. *EMBO J.* 19, 542–549. doi: 10.1093/emboj/19.4.542

Selkrig, J., Mosbahi, K., Webb, C. T., Belousoff, M. J., Perry, A. J., Wells, T. J., et al. (2012). Discovery of an archetypal protein transport system in bacterial outer membranes. *Nat. Struct. Mol. Biol.* 19, 506–510, S. doi: 10.1038/nsmb.2261

Sklar, J. G., Wu, T., Kahne, D., and Silhavy, T. J. (2007). Defining the roles of the periplasmic chaperones SurA, Skp, and DegP in *Escherichia coli*. *Genes Dev.* 21, 2473–2484. doi: 10.1101/gad.1581007

Suss, O., and Reichmann, D. (2015). Protein plasticity underlines activation and function of ATP-independent chaperones. *Front. Mol. Biosci.* 2:43. doi: 10.3389/fmolb.2015.00043

Tanaka, Y., Izumioka, A., Abdul Hamid, A., Fujii, A., Haruyama, T., Furukawa, A., et al. (2018). 2.8-Å crystal structure of *Escherichia coli* YidC revealing all core regions, including flexible C2 loop. *Biochem. Biophys. Res. Commun.* 505, 141–145. doi: 10.1016/j.bbrc.2018.09.043

Tsukazaki, T., Mori, H., Echizen, Y., Ishitani, R., Fukai, S., Tanaka, T., et al. (2011). Structure and function of a membrane component SecDF that enhances protein export. *Nature* 474, 235–238. doi: 10.1038/nature09980

Ureta, A. R., Endres, R. G., Wingreen, N. S., and Silhavy, T. J. (2007). Kinetic analysis of the assembly of the outer membrane protein LamB in *Escherichia coli* mutants each lacking a secretion or targeting factor in a different cellular compartment. *J. Bacteriol.* 189, 446–454. doi: 10.1128/JB.01103-06

Van Bloois, E., Koningstein, G., Bauerschmitt, H., Herrmann, J. M., and Luirink, J. (2007). *Saccharomyces cerevisiae* Cox18 complements the essential Sec-independent function of *Escherichia coli* YidC. *FEBS J.* 274, 5704–5713. doi: 10.1111/j.1742-4658.2007.06094.x

Van Den Berg, B., Clemons, W. M., Collinson, I., Modis, Y., Hartmann, E., Harrison, S. C., et al. (2004). X-ray structure of a protein-conducting channel. *Nature* 427, 36–44. doi: 10.1038/nature02218

Van Der Laan, M., Bechduft, P., Kol, S., Nouwen, N., and Driessen, A. J. M. (2004). F1F0 ATP synthase subunit c is a substrate of the novel YidC pathway for membrane protein biogenesis. *J. Cell Biol.* 165, 213–222. doi: 10.1083/jcb.200402100

Vertommen, D., Ruiz, N., Leverrier, P., Silhavy, T. J., and Collet, J. F. (2009). Characterization of the role of the *Escherichia coli* periplasmic chaperone SurA using differential proteomics. *Proteomics* 9, 2432–2443. doi: 10.1002/pmic.200800794

Von Heijne, G. (1981). On the hydrophobic nature of signal sequences. *Eur. J. Biochem.* 116, 419–422. doi: 10.1111/j.1432-1033.1981.tb05351.x

Walton, T. A., and Sousa, M. C. (2004). Crystal structure of Skp, a prefoldin-like chaperone that protects soluble and membrane proteins from aggregation. *Mol. Cell* 15, 367–374. doi: 10.1016/j.molcel.2004.07.023

Walton, T. A., Sandoval, C. M., Fowler, C. A., Pardi, A., and Sousa, M. C. (2009). The cavity-chaperone Skp protects its substrate from aggregation but allows independent folding of substrate domains. *Proc. Natl. Acad. Sci. U. S. A.* 106, 1772–1777. doi: 10.1073/pnas.0809275106

Wang, Y., Wang, R., Jin, F., Liu, Y., Yu, J., Fu, X., et al. (2016). A Supercomplex spanning the inner and outer membranes mediates the biogenesis of β-barrel outer membrane proteins in bacteria. *J. Biol. Chem.* 291, 16720–16729. doi: 10.1074/jbc.M115.710715

Wang, Z., Fan, G., Hryc, C. F., Blaza, J. N., Serysheva, I. I., Schmid, M. F., et al. (2017). An allosteric transport mechanism for the AcrAB-TolC multidrug efflux pump. *eLife* 6:e24905. doi: 10.7554/eLife.24905

Weski, J., and Ehrmann, M. (2012). Genetic analysis of 15 protein folding factors and proteases of the *Escherichia coli* cell envelope. *J. Bacteriol.* 194, 3225–3233. doi: 10.1128/JB.00221-12

Wu, S., Ge, X., Lv, Z., Zhi, Z., Chang, Z., and Zhao, X. S. (2011). Interaction between bacterial outer membrane proteins and periplasmic quality control factors: a kinetic partitioning mechanism. *Biochem. J.* 438, 505–511. doi: 10.1042/BJ20110264

Xie, K., Kiefer, D., Nagler, G., Dalbey, R. E., and Kuhn, A. (2006). Different regions of the nonconserved large periplasmic domain of *Escherichia coli* YidC are involved in the SecF interaction and membrane insertase activity. *Biochemistry* 45, 13401–13408. doi: 10.1021/bi060826z

Xu, X., Wang, S., Hu, Y. X., and McKay, D. B. (2007). The periplasmic bacterial molecular chaperone SurA adapts its structure to bind peptides in different conformations to assert a sequence preference for aromatic residues. *J. Mol. Biol.* 373, 367–381. doi: 10.1016/j.jmb.2007.07.069

Xu, Z., Horwich, A. L., and Sigler, P. B. (1997). The crystal structure of the asymmetric GroEL-GroES-(ADP)7 chaperonin complex. *Nature* 388, 741–750. doi: 10.1038/41944

Zhu, L., Wasey, A., White, S. H., and Dalbey, R. E. (2013). Charge composition features of model single-span membrane proteins that determine selection of YidC and SecYEG translocase pathways in *Escherichia coli*. *J. Biol. Chem.* 288, 7704–7716. doi: 10.1074/jbc.M112.429431

Conflict of Interest: The authors declare that the research was conducted in the absence of any commercial or financial relationships that could be construed as a potential conflict of interest.

Publisher's Note: All claims expressed in this article are solely those of the authors and do not necessarily represent those of their affiliated organizations, or those of the publisher, the editors and the reviewers. Any product that may be evaluated in this article, or claim that may be made by its manufacturer, is not guaranteed or endorsed by the publisher.

frontiers in Microbiology

REVIEW
published: 15 December 2021
doi: 10.3389/fmicb.2021.782673

Secretion Systems in Gram-Negative Bacterial Fish Pathogens

*Sophanit Mekasha and Dirk Linke**

Section for Genetics and Evolutionary Biology, Department of Biosciences, University of Oslo, Oslo, Norway

Bacterial fish pathogens are one of the key challenges in the aquaculture industry, one of the fast-growing industries worldwide. These pathogens rely on arsenal of virulence factors such as toxins, adhesins, effectors and enzymes to promote colonization and infection. Translocation of virulence factors across the membrane to either the extracellular environment or directly into the host cells is performed by single or multiple dedicated secretion systems. These secretion systems are often key to the infection process. They can range from simple single-protein systems to complex injection needles made from dozens of subunits. Here, we review the different types of secretion systems in Gram-negative bacterial fish pathogens and describe their putative roles in pathogenicity. We find that the available information is fragmented and often descriptive, and hope that our overview will help researchers to more systematically learn from the similarities and differences between the virulence factors and secretion systems of the fish-pathogenic species described here.

Keywords: fish pathogen, Gram-negative, fish disease, secretion system, virulence factor, aquaculture

OPEN ACCESS

Edited by:
Eric Cascales,
Aix-Marseille Université, France

Reviewed by:
Dhrubajyoti Nag,
Wayne State University, United States
Carlos J. Blondel,
Andres Bello University, Chile

***Correspondence:**
Dirk Linke
dirk.linke@ibv.uio.no

Specialty section:
This article was submitted to Microbial Physiology and Metabolism, a section of the journal Frontiers in Microbiology

Received: *24 September 2021*
Accepted: *24 November 2021*
Published: *15 December 2021*

Citation:
Mekasha S and Linke D (2021) Secretion Systems in Gram-Negative Bacterial Fish Pathogens. Front. Microbiol. 12:782673. doi: 10.3389/fmicb.2021.782673

INTRODUCTION

Production of cultured fish is one of the fastest-growing sectors of the aquaculture industries. The annual report from the Food and Agriculture Organization of the United Nations indicate that the production reached 179 million tons in 2018 (FAO, 2020). Sustainable production of farmed fish and their commercialization are primarily challenged by the expansion of infectious diseases caused by pathogenic microbes. Bacterial fish pathogens can cause systemic infection where they infect different organs of the fish, or they cause external infections by ulcerating the skin, gills, fin rots and mouth (Bernoth et al., 1997; Mohanty and Sahoo, 2007; Austin and Austin, 2016; Gourzioti et al., 2016; Ina-Salwany et al., 2019). In both cases, the fish cannot be marketed even in cases where the disease is not lethal. Thus, the high global spread of fish diseases causes great economic loss to the aquaculture industry and development of systematic prevention mechanisms is key to its sustainability.

Fish pathogens can infect both edible and ornamental fish species. Some ornamental fish such as zebrafish are used as host model organisms to understand the virulence mechanisms of pathogens in fish in general (Rowe et al., 2014; Nag et al., 2020). This review mainly covers virulence mechanisms of Gram-negative pathogens that target common edible fish. We have also made an attempt to differentiate the virulence factors that are proven to be involved in fish disease from the ones where the evidence is indirect, e.g., inferred from other host examples, and that thus need further investigation.

The composition of the fish microbiota and the presence of pathogens has been evaluated by culture-dependent and/or advanced "omics" techniques for several years. The most prominent

Gram-negative bacterial fish pathogens are distributed across the phyla Proteobacteria and Bacteroidetes (**Figure 1**), and a high number of identified and widely studied pathogens belong to the phylum Proteobacteria. The range of diseases found in fish reflect the diversity of virulence factors and virulence mechanisms utilized by these microbes. In general, bacterial infection is successful when the pathogen can successfully adhere to the host tissue, multiply and invade.

Information obtained from genome sequenced-bacterial strains shows that pathogenic and non-pathogenic fish-associated microbes can be very closely related [**Figure 1**, (Sudheesh et al., 2012)]. Thus, pathogens often acquire unique strategical adaptations specific for their infectious lifestyle that distinguishes them from their close, non-infectious relatives. Such adaptation is often associated with horizontal transfer of gene clusters of virulence genes located on either the chromosome (Naka et al., 2013; Amaro et al., 2015) or the more "flexible" gene pool of plasmids (Naka et al., 2011; Rivas et al., 2011; Amaro et al., 2015). Such blocks of virulence-associated DNA are known as "pathogenicity islands" (PAIs) that promote the pathogenicity of the strains (Hacker and Kaper, 1999; Hacker and Carniel, 2001; Osorio et al., 2015). Loss of potent virulence factors such as secretion systems either reduce or halt bacterial pathogenicity (Stanley et al., 2003; Dacanay et al., 2006; Fadl et al., 2006; Jyot et al., 2011).

Bacterial pathogens rely on the synergistic action of different virulence determinants and on specialized secretion systems to cause disease in susceptible hosts (Finlay and Falkow, 1997; Thanassi and Hultgren, 2000). Initiation of infection is often triggered by adherence of the pathogen to the skin or mucosal surface of the host tissue using attachment mechanisms such as non-fimbrial adhesins (Ostland et al., 1997; Weber et al., 2010; Guardiola et al., 2019), pili or fimbriae (Ho et al., 1990; Mattick, 2002; Gerlach and Hensel, 2007; Craig et al., 2019) which recognize specific receptors. A successful uptake of the pathogen into host cells is then mediated by specific invasion factors (e.g., invasins) which are either membrane anchored proteins of the pathogen or are secreted through specialized secretion systems. Invasins promote translocation of pathogens in host cell [(Meuskens et al., 2019), Yersinia spp.]. Once inside the host, the survival rate of pathogens is modulated by numerous structural and metabolic virulence factors such as capsules and iron acquisition systems, respectively (Lindler et al., 1998; Winkelmann et al., 2002; Hsieh et al., 2003; Møller et al., 2005; Guan et al., 2013; Balado et al., 2018). Encapsulated pathogens are resistant to phagocytosis due to the protective carbohydrate layer that blocks host immune response components from binding to immunogenic membrane proteins of the bacteria (Cress et al., 2014). In many infections, bacterial growth and metabolism is solely limited by the availability of free iron, which is typically completely sequestered in the host organisms. The competition for this limited resource forces pathogens to acquire and use high-affinity siderophore or heme-dependent iron acquisition systems to scavenge iron sequestered in host iron-binding proteins, such as transferrins or hemoglobin. Last but not least, the visible symptoms of disease such as inflammation, bleeding, or lethal shock is typically induced by different toxins. An important toxin is a structural component of Gram-negative pathogens, the lipopolysaccharides, that are a key component of the cell membrane and that exert intense biological effects on the host which may be lethal (Sampath, 2018). In addition to these so-called endotoxins, extracellular toxic proteins known as exotoxins, are produced and secreted by pathogens via specific secretion machinery. Unlike the extensive systemic damage of endotoxins that is mainly based on an adverse immune reaction, exotoxins typically target local tissues and are often restricted to particular cell types or receptors (Cavaillon, 2018). For other virulence factors, their identification and in-depth characterization is fundamental to the development of specific diagnostics and treatment tools. For instance, molecular, structural and biochemical characterizations of genes and proteins involved in secretion systems are useful for discovery of novel treatments for combating pathogenicity in bacteria (Costa et al., 2015; Alteri and Mobley, 2016).

In the case of fish pathogens, the knowledge on virulence factors and disease mechanisms is lagging behind, compared to the often very detailed information available for human pathogens. In this review, we summarize the current knowledge on one class of virulence determinants of fish pathogens, the secretion systems, and on the virulence factors that they secrete. In the course of collecting this information, we noticed that information on the Gram-positive fish pathogens shockingly sparse in this regard. This is why this review focuses on Gram-negative species, that cause most of the more notorious and economically relevant bacterial fish diseases. We hope that this review will be useful for researchers in the field of fish diseases, by providing an overview, and help in the quest to develop vaccines and treatments against fish pathogens that challenge the aquaculture industry worldwide.

Bacterial Secretion Systems

Secretion systems are utilized by bacteria in processes such as growth, motility, pathogenic or symbiotic interactions with their hosts, and formation of microbial communities (Johnson et al., 2014; Costa et al., 2015; Gallique et al., 2017). In pathogenic species, many virulence factors are translocated across the membrane by dedicated secretion systems that are diverse in size, composition and architecture (Costa et al., 2015; Green and Mecsas, 2016).

Gram-negative bacteria possess two phospholipid membranes separated by a periplasmic space accommodating a thin layer of peptidoglycan chain. This creates additional challenges for protein secretion compared to the Gram-positive bacteria that contain only one lipid bilayer encircled by a peptidoglycan layer that forms a thick cell wall (Silhavy et al., 2010). In both Gram-positive and Gram-negative bacteria, two main secretion pathways employed for the secretion of proteins across the cytoplasmic membrane. These are the general secretory (Sec) pathway (Tsirigotaki et al., 2017) and the twin-arginine translocation (Tat) pathway (Palmer and Berks, 2012), where the first translocates unfolded proteins and the latter transports folded proteins. Thus, the two pathways translocate proteins into the periplasm in Gram-negative bacteria and are responsible for extracellular secretion of proteins across the

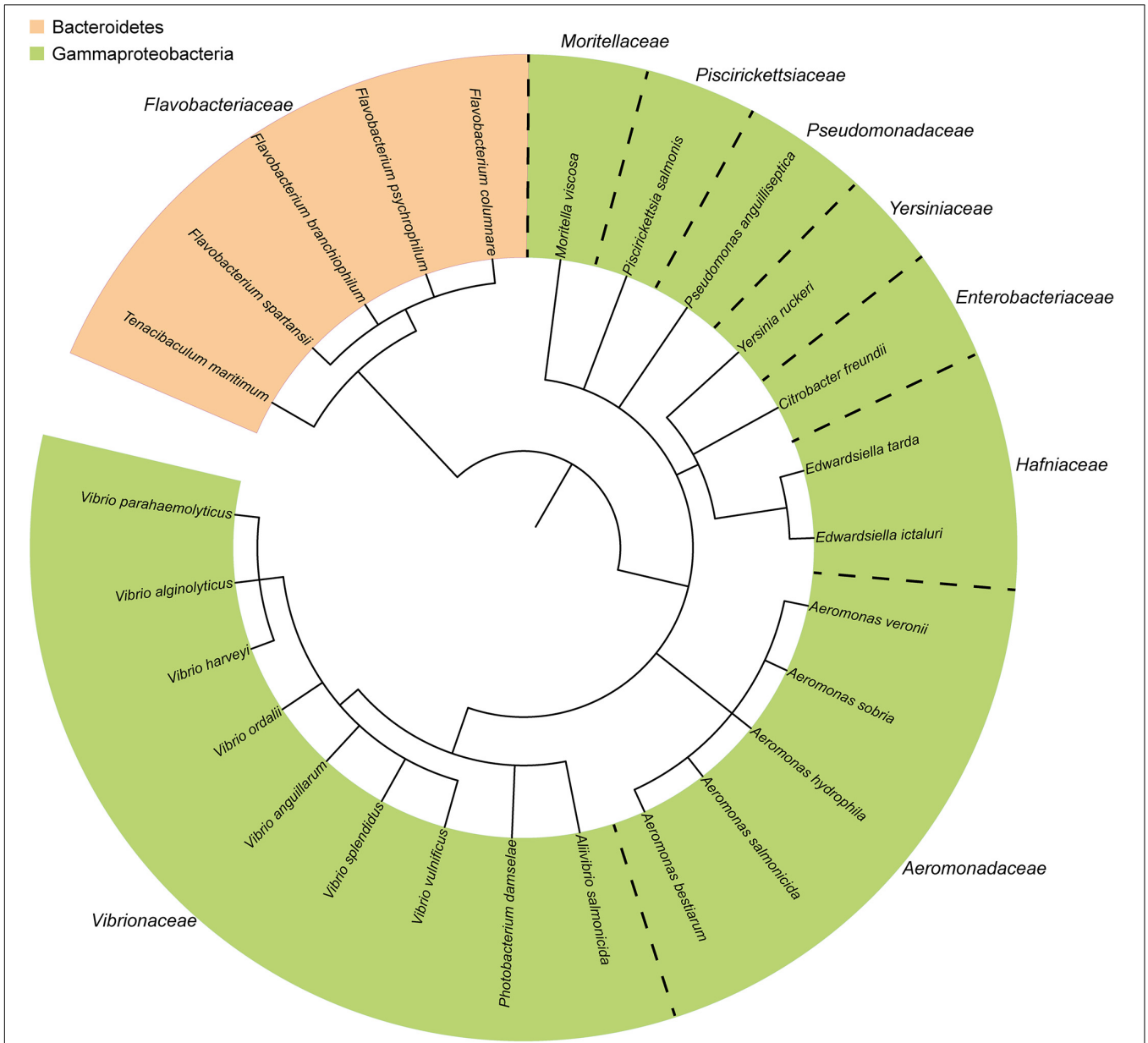

FIGURE 1 | Taxonomic distribution of the most common Gram-negative bacterial fish pathogens. The phylogenetic tree was generated using the phyloT online tool (http://phylot.biobyte.de/), based on annotations from ITOL (http://itol.embl.de/) (Letunic and Bork, 2006).

single plasma membrane in Gram-positive bacteria (Palmer and Berks, 2012; Tsirigotaki et al., 2017). Outside of these two basic secretion pathways, both Gram-positive bacteria and Gram-negative bacteria possess diverse more specialized secretion systems (Green and Mecsas, 2016). It is worth noting that some species classified traditionally as Gram-positive bacteria such as *Mycobacteria* possess a complex additional membrane layer called the mycomembrane (Dulberger et al., 2020). These bacteria possess a specialized secretion system called type VII secretion system (T7SS) that translocates proteins across this complex cell envelope (Rivera-Calzada et al., 2021). The secretion systems of Gram-positive bacteria is out of the scope of the current review. Below, we list individual examples of Gram-negative fish-pathogenic species and their secretion systems and virulence factors, ordered by taxonomy (**Table 1**).

Gram-Negative Bacteria

So far, eight types of Gram-negative bacteria secretion systems (designated as Type I-VI, Type VIII and Type IX or T1SS-T6SS, T8SS and T9SS) have been reported that are classified based on their composition, architecture, function and specificity. There is a multitude of reviews describing the functional and structural features of secretion systems (Gerlach and Hensel, 2007; Costa et al., 2015; Lasica et al., 2017; Burdette et al., 2018;

TABLE 1 | List of common Gram-negative fish pathogens, including taxonomy information, disease type, virulence factors and virulence-related secretion systems obtained from experimental and/or genomic data.

Phylum	Strain	Disease	Virulence factors	Secretion systems (SS)	References
Gram-negatives					
Bacteroidetes	*Flavobacterium columnare*	Columnaris	Adhesins, gliding motility, Fe-acquisition systems, proteases, hemolysins chondroitin sulfate lyase	T9SS, T6SS[iii]	Boyd and Cornelis, 2001; Secades et al., 2001; Stringer-Roth et al., 2002; Kumru et al., 2017; Li et al., 2017; Kunttu et al., 2021
	Flavobacterium psychrophilum	Rainbow trout fry syndrome (RTFS) and cold water disease (CWD)	Adhesins, gliding motility, proteases, hemolysins elastase	T9SS	Ostland et al., 2000; Duchaud et al., 2007; Rochat et al., 2019; Barbier et al., 2020
	Flavobacterium branchiophilum	Gill disease	Adhesins, proteases, toxins	T9SS, T6SS[iii]	Ostland et al., 1997; Touchon et al., 2011; Kumru et al., 2020
	Flavobacterium spartansii	Pathological lesions, systemic infection	Adhesins, gliding motility, hemolysins toxins	T9SS, T6SS[iii]	Chen et al., 2017; Kumru et al., 2020
	Tenacibaculum maritimum	Tenacibaculosis	Adhesins, gliding motility, Fe-acquisition systems, chondroitin sulfate lyase	T9SS	Pérez-Pascual et al., 2017
Proteobacteria	*Vibrio anguillarum*	Vibriosis	Surface-hydrophobicity, Flagella, type IV pili, Fe-acquisition systems, metalloprotease, hemolysins	T2SS, T6SS	Rodkhum et al., 2005; Lopez and Crosa, 2007; Cianciotto and White, 2017
	Vibrio harveyi	Vibriosis	Flagella, non-pilus adhesins, Fe-acquisition systems	T3SS	Zane et al., 2014; Osorio, 2018; Zhang et al., 2021
	Vibrio vulnificus	Warm-water vibriosis	Flagella, Type IV pili, non-pilus adhesins, Fe-acquisition systems, protease, hemolysin, phospholipase	T1SS	Litwin and Byrne, 1998; Valiente et al., 2008; Jang et al., 2017; Guo et al., 2018
	Vibrio parahaemolyticus	Gastroenteritis, wound infections, and septicemia	Fe-acquisition systems, metalloprotease and serine protease, effectors	T2SS, T3SS*, T6SS*	Tanabe et al., 2003; Hiyoshi et al., 2010; Cianciotto and White, 2017; Li L. et al., 2019
	V. alginolyticus		Flagella, Fe-acquisition systems proteases, effectors	T3SS, T6SS	Cai et al., 2007; Wang Q. et al., 2007; Zhao et al., 2010; Salomon et al., 2015
	V. ordalii		Fe-acquisition systems	T3SS	Osorio et al., 2015; Ruiz et al., 2019
	V. splendidus		Flagella, Fe-acquisition systems non-pilus adhesins, effectors	T3SS	Song et al., 2018; Dai et al., 2020; Zhuang et al., 2020, 2021
	Allivibrio salmonicida	Cold-water vibriosis	Surface-hydrophobicity, Fe-acquisition systems, proteases, effectors	T3SS	Espelid et al., 1987; Winkelmann et al., 2002; Frey and Origgi, 2016
	Photobacterium damselae	Photobacteriosis, Skin ulcer	Fe-acquisition systems endopeptidase, toxin hemolysin, lipase, esterase-lipase, phospholipase	T2SS, T3SS	Labella et al., 2010; Rivas et al., 2011; Valderrama et al., 2019
Enterobacterials	*Yersinia ruckeri*	Enteric red mouth (ERM)	Type IV pilus, Fe-acquisition systems, proteases, toxins	T1SS, T4SS, T5SS	Fernández et al., 2002, 2004; Wrobel et al., 2018, 2019
	Edwardsiella ictaruli	Edwardsiellosis	Adhesin, Fe-acquisition system, proteases, effectors	T3SS	Thune et al., 2007; Abayneh et al., 2013; Abdelhamed et al., 2016; Castro et al., 2016
	Edwardsiella tarda (New name: *Edwardsiella piscicida*)	Edwardsiellosis	Adhesin, Fe-acquisition systems hemolysin, proteases, effectors	T3SS, T5SS, T6SS,	Wang X. et al., 2010; Jiao et al., 2010; Hu et al., 2016, 2019; Cheng et al., 2017
	Citrobacter freundii	Gastroenteritis and hemorrhagic septicemia	Adhesin, Fe-acquisition systems	T3SS	Leo et al., 2015; Pan et al., 2021
Aeromonadales	*Aeromonas bestiarum*	Motile Aeromonas septicemia (MAS)	Fe-acquisition systems,	T1SS, T2SS	Ali, 1996
	Aeromonas salmonicida	Furunculosis	Surface hydrophobicity, Fe-acquisition systems, hemolysin, lipase	T1SS, T2SS, T3SS*, T6SS	Titball and Munn, 1981; Burr et al., 2003; Dacanay et al., 2006; Reith et al., 2008; Balado et al., 2015

(Continued)

TABLE 1 | (Continued)

Phylum	Strain	Disease	Virulence factors	Secretion systems (SS)	References
	Aeromonas hydrophila	Motile Aeromonas septicemia (MAS)	Surface hydrophobicity, adhesin, Fe-acquisition systems, hemolysins, proteases	T1SS, T2SS* T3SS, T6SS	Barghouthi et al., 1989b; Chopra et al., 1993; Fadl et al., 2006; Barger et al., 2020
	Aeromonas veronii	Motile Aeromonas septicemia (MAS)	Adhesin, Fe-acquisition systems	T3SS	Namba et al., 2008; Silver and Graf, 2009; Li et al., 2011; Tekedar et al., 2019b
	Aeromonas sobria	Motile Aeromonas septicemia (MAS)	Pili, hemolysin	T1SS, T2SS	Chakraborty et al., 1990
Thiotrichales	*Piscirickettsia salmonis*	Piscirickettsiosis	Adhesin, Fe-acquisition systems, chaperonin, toxins	T3SS, T4SS, T6SS	Rojas et al., 2013; Rozas and Enríquez, 2014; Ortiz-Severín et al., 2019
Alteromonadales	*Moritella viscosa*	Winter ulcer	Flagella, Type IV pili, hemolysin, peptidase	T1SS, T2SS, T6SS	Løvoll et al., 2009; Björnsdóttir, 2011; Bjornsdottir et al., 2012
Pseudomonadales	*Pseudomonas anguilliseptica*	"Red spot disease" also known as "sekiten-byo"	Flagella, capsular antigen	NA	Lönnström et al., 1994; Berthe et al., 1995; López-Romalde et al., 2003a

** Secretion systems where the direct involvement in fish disease still has to be established, as most data was generated with non-fish models. NA, data not available.*

Meuskens et al., 2019; Gorasia et al., 2020), allowing us to skip over the detailed description of each system, and to focus only on features that are relevant to fish pathogens. Extending the list of secretion systems, a recent report proposed the existence of a type X secretion system (T10SS) (Palmer et al., 2021). In short, these specialized secretion systems in Gram-negative bacteria can generally be classified into two categories. The first category includes those spanning both the inner and outer membranes such as the T1SS (Holland et al., 2005; Kanonenberg et al., 2018), T2SS (Nivaskumar and Francetic, 2014), T3SS (Deng et al., 2017), T4SS (Christie et al., 2014), T6SS (Russell et al., 2014a) and T9SS (Lasica et al., 2017; Veith et al., 2017; Gorasia et al., 2020). The second category includes the T5SSs (Meuskens et al., 2019) and T8SS (also known as the curli biogenesis system) (Bhoite et al., 2019; Yan et al., 2020) which span only the outer membrane (OM). This second category, and also the T2SS and T9SS rely on the Sec and Tat pathways to translocate their substrates into the periplasm, while the others are independent and secrete proteins directly from the cytosol into the medium or even into host cells in a single step.

BACTEROIDETES

The phylum Bacteroidetes, also known as Cytophaga-Flexibacter-Bacterioides (CFB), contains diverse anaerobe Gram-negative rods belonging to the *Flavobacteriaceae* family. Bacteroidetes inhabit diverse ecological niches including soil, sediments, oceans and freshwater and are the most predominant members of the animal gut microbiota. They are dominantly commensal and seldomly pathogenic to their host (Thomas et al., 2011; Fierer et al., 2012; An et al., 2013; Sunagawa, 2015; Hahnke et al., 2016).

Flavobacteriaceae

The family *Flavobacteriaceae* is the largest family in the phylum Bacteroidetes, which contains more than ninety genera. This family includes important fish pathogens that belong to the genera *Flavobacterium* and *Tenacibaculum* (McBride, 2014). These pathogens cause severe diseases that impose significant economic losses in the aquaculture industry, and they are commonly isolated from diverse diseased finfish. Common fish pathogens of this family include *Flavobacterium columnare*, *F. psychrophilum*, *F. branchiophilum*, *F. spartansii* and *Tenacibaculum maritimum* (Wakabayashi et al., 1986; Bernardet and Bowman, 2006; Loch and Faisal, 2014; Chen et al., 2017).

Flavobacterium columnare, formerly known as *Flexibacter columnaris* (Bernardet et al., 1996) is an economically important fish pathogen. It is the causative agent of columnaris disease that results in skin lesions, fin erosion and gill necrosis, leading to a high degree of mortality (Declercq et al., 2013). *Flavobacterium psychrophilum*, also considered as an economically important bacteroidetes, causes severe mortality associated with hemorrhagic septicemia (Bernardet and Bowman, 2006). Disease terminologies such as "rainbow trout fry syndrome" (RTFS) and "cold water disease" (CWD) mostly denominate infections caused by *F. psychrophilum* and are based on the susceptibility of rainbow trout fry for these types of infection at temperatures below 10°C (Holt et al., 1989; Nematollahi et al., 2003b). *Flavobacterium branchiophilum* is a causative agent for gill disease, and while it is not usually isolated from internal organs, its severe mortality is associated with hemorrhagic septicemia. The known virulence factors related to this disease involve a cholera-like toxin and several adhesins [discussed below (Touchon et al., 2011)]. *Flavobacterium spartansii*, a recently discovered species that was initially isolated from salmon gills and kidneys causes systemic infection with symptoms such as muscle ulceration, necrotic gills, unilateral exophthalmia and friable kidneys (Loch and Faisal, 2014). *Tenacibaculum maritimum*, formerly known as *Flexibacter maritimus*, is the causative agent for tenacibaculosis, which is an ulcerative disease of marine fish that poses serious threats of economic losses in the aquaculture industry. Tenacibaculosis

cause mostly external symptoms such as skin ulcers, mouth erosion, fin necrosis and rotted tails (Wakabayashi et al., 1986; Pérez-Pascual et al., 2017).

Despite the global challenge of the diseases and the financial losses caused by some members of *Flavobacteriaceae*, research into their mechanisms of pathogenicity is still in its infancy. However, recent studies revealed at least some of the virulence factors that these members of *Flavobacteriaceae* utilize to infect their fish host (Touchon et al., 2011; Chen et al., 2017; Li et al., 2017; Pérez-Pascual et al., 2017; Barbier et al., 2020; Kumru et al., 2020). Among these are genes and proteins responsible for gliding motility, various stress responses, adhesion, and they include secretion systems, degrading enzymes such as proteases, collagenases, polysaccharide lyases, sialidase and hemolysins that are utilized for the invasion and colonization of their host (Duchaud et al., 2007; Touchon et al., 2011; Tekedar et al., 2012; Chen et al., 2017; Pérez-Pascual et al., 2017; Kumru et al., 2020).

Transmission Routes and Adherence

Mucosal surfaces such as skin and gill are primary adhesion sites for several *Flavobacteriaceae* such a *F. columnare*, *F. branchiophilum*, *F. spartansii*, and *T. maritimum*. Several adhesin candidates have been identified, including surface lipopolysaccharides, capsules and fimbriae (Magarinos et al., 1995; Ostland et al., 1997; Klesius et al., 2008; Loch and Faisal, 2014; Pérez-Pascual et al., 2017). In addition, adherence based on hemagglutinins and lectin-like carbohydrates that are part of the capsule are responsible for attachment to gill tissue in *F. columnare* (Decostere et al., 1999; Bernardet and Bowman, 2006). *Flavobacterium psychrophilum* seem to adhere to gill tissue using several leucine-rich repeat proteins, similar to BspA and LrrA of bacteroidetes causing periodontal disease (Sharma et al., 1998; Kondo et al., 2002; Nematollahi et al., 2003a). *Flavobacterium psychrophilum* adheres to stomach and intestinal mucosa in rainbow trout (Nikoskelainen et al., 2001). In both *F. psychrophilum* and *F. columnare* the ability to agglutinate, adhere to, and hemolyze rainbow trout erythrocytes is associated with a sialic acid-binding lectin found in some serotypes of the pathogen (Lorenzen et al., 1997; Møller et al., 2003). The adherence of *F. branchiophilum* on mucosal surfaces of gills is the initial stage of infection in gill disease and this may be facilitated by several adhesin genes horizontally acquired by the pathogen (Ostland et al., 1997; Touchon et al., 2011).

Several adhesins of members of the *Flavobacteriaceae* family are secreted through T9SSs (Touchon et al., 2011; Pérez-Pascual et al., 2017; Barbier et al., 2020; Kunttu et al., 2021). *Flavobacterium columnare*, *F. psychrophilum*, *F. spartansii*, *T. maritimum*, possess genes involved in gliding motility, an active process independent of pili or flagella (Perry, 1973; Alvarez et al., 2006; Touchon et al., 2011; Loch and Faisal, 2014; Pérez-Pascual et al., 2017; Penttinen et al., 2018). *Flavobacterium columnare*, *F. spartansii, T. maritimum* and *F. psychrophilum* contain T9SS-associated genes such as *gld* and *spr*, that are involved in gliding motility. It has been shown that deletion of *gld* genes such as *gldD*, *gldG* and *gldN* not only leads to deficits regarding the ability of gliding motility and adhesion, but also negatively affects biofilm formation and extracellular hemolytic and proteolytic activities, indicating that T9SSs are involved in both gliding motility and secretion of proteins (Sato et al., 2010; Touchon et al., 2011; McBride and Nakane, 2015; Chen et al., 2017; Li et al., 2017; Pérez-Pascual et al., 2017; Barbier et al., 2020; Kumru et al., 2020). Despite the unique gliding motility properties of numerous bacteroidetes, some member species of the family such as *F. branchiophilum*, *T. maritimum* are reported to utilize a non-gliding motility mechanism as they contain pili, fimbriae or pili-like structures on their cell surface (Heo et al., 1990; Rahman et al., 2014).

Survival Mechanisms in the Host

Pathogens have evolved different mechanisms to overcome bacterial competition in order to secure efficient colonization of their host. Among the bacteroidetes, that are the overall most dominant phylum of animal gut microbiota, *F. johnsoniae* is known to possess a unique T6SS named T6SS^{iii} which is directly involved in bacterial competition (Russell et al., 2014b). Similarly, genomic analysis of some strains of *F. branchiophilum*, *F. spartansii*, and *F. columnare* show the presence of T6SS^{iii} coding genes that might be involved in host bacterial competition (Abby et al., 2016; Kumru et al., 2017, 2020).

Furthermore, bacteroidetes evolved diverse survival mechanisms to escape the hostile environments generated by host cells to hinder their colonization. These include defense mechanisms against bacterial pathogens such as the production of reactive oxygen species (ROS) by host macrophages (Secombes, 1996). Bacteroidetes harbor genes encoding superoxide dismutase, catalase-peroxidase, and thiol peroxidase to resist ROS-mediated killing (Duchaud et al., 2007; Chen et al., 2017; Levipan et al., 2018). Iron acquisition systems have been identified in *F. columnare* (Guan et al., 2013; Zhang et al., 2017), *F. psychrophilum* (Møller et al., 2005), *F. spartansii* (Chen et al., 2017), *F. branchiophilum*, and *T. maritimum* (Avendaño-Herrera et al., 2005), whose function is to compete for the limited iron stock in host cells. The uptake of iron-siderophore complexes by bacteroidetes are not fully explored, however, several TonB-dependent outer membrane receptors such as, OmpA related proteins, ferrichrome-iron receptor precursor (FhuA) and ferric uptake receptor (Fur) protein are identified in the genomes of *F. columnare* (Dumpala et al., 2010; Guan et al., 2013), *F. psychrophilum* (Alvarez et al., 2008) *T. maritimum* (Avendaño-Herrera et al., 2005) that may function as iron importer across the outer membrane as is shown for several Gram-negative bacteria (Letain and Postle, 1997; Braun et al., 1998).

Secretion of exopolysaccharides by pathogenic bacteria provides a beneficial environment for survival in the host. *F. columnare* secretes large quantities of exopolysaccharides during infection using polysaccharide exporters that transport polysaccharides from the cytoplasm to the periplasm (Zhang et al., 2017).

Proteases and Their Secretion Systems

Fish-pathogenic flavobacteriaceae isolated from different fish species produce several secreted proteases with elastase, gelatinase, collagenase, and caseinase activities that may

have significant roles in virulence (Bertolini et al., 1994; Dalsgaard and Madsen, 2000; Ostland et al., 2000; Duchaud et al., 2007). The two economically important bacteroidetes *F. psychrophilum* and *F. columnare* cause severe mortality associated with hemorrhagic septicemia and columnaris, respectively, by using multi-factorial virulence factors including the metalloproteases (Griffin, 1987; Secades et al., 2001, 2003). Fpp1 and Fpp2, which are calcium dependent proteases that cleave protein-rich extracellular matrices of connective and muscular tissues during colonization (Secades et al., 2001, 2003). Fpp1 and Fpp2 contain the conserved carboxy terminal domain (CTD-domain) for protein secretion through T9SS, which suggest that the T9SS is the secretion system for these metalloproteases (Li et al., 2017; Barbier et al., 2020).

Virulence-associated collagenases are among the conserved virulence factors in *F. spartansii* (Chen et al., 2017), *F. columnare* (Olivares-Fuster and Arias, 2008), *F. psychrophilum* (Nakayama et al., 2016), and *T, maritimum* (Pérez-Pascual et al., 2017). They are used by the pathogens to disrupt collagen-rich tissues of the host. The specific secretion pathways for these collagenases are yet to be explored, however, different studies show the dependency of secreted proteolytic enzymes on T9SS (Chen et al., 2017; Li et al., 2017; Pérez-Pascual et al., 2017).

Polysaccharide lyases such as Chondroitin AC lyase that degrade complex acidic polysaccharides such as hyaluronic acid and chondroitin sulfates located mainly on the extra-cellar matrix of fish tissues are potential virulence factors in *F. columnare*, where this has been shown *in vivo* using rainbow trout (Stringer-Roth et al., 2002; Li et al., 2017) and in *T. maritimum* where the activity was tested on chondroitin sulfate-supplemented agar (Pérez-Pascual et al., 2017). These enzymes are suggested to initiate and promote infection and are secreted by T9SS: mutational deactivation of a component of T9SS, gldN, in *F. columnare* lead to the loss of the ability to degrade chondroitin (Li et al., 2017; Pérez-Pascual et al., 2017).

Extracellular elastases produced by *F. psychrophilum* may have roles in the digestion of host tissues (Madsen and Dalsgaard, 1998; Nematollahi et al., 2003b; Rochat et al., 2019). Unlike for most other virulence factors of fish-pathogenic flavobacteriaceae the secretion pathway of elastase from *F. psychrophilum* is T9SS-independent (Rochat et al., 2019). Yet, the specific secretion system for the elastase is unidentified.

Glycoproteins are described to be involved in pathogenesis in several pathogenic Gram-negative bacteria (Guerry, 2007), taking part in processes such as cell adhesion and motility (Virji, 1997; Young et al., 2002; Grass et al., 2003; Szymanski et al., 2003). In *F. psychrophilum*, several glycoproteins were previously identified and predicted to promote infection (Merle et al., 2003; Dumetz et al., 2007). An outer membrane glycosyltransferase, FpgA, expressed by *F. psychrophilum* has been shown to promote polysaccharide-mediated gliding motility and bacteria-host cell interactions (Fernández-Gómez et al., 2013; Pérez-Pascual et al., 2015). Mutations in the *fpgA* gene not only impair pathogenicity, but also downregulate expression of the metalloproteases Fpp2 and Fpp1 discussed earlier in this section (Pérez-Pascual et al., 2015). However, neither the secretion apparatus for the metalloproteases Fpp1 and Fpp2 nor its connection to the enzyme FpgA itself is understood.

Hemolysins and Their Secretion Systems

Hemolysins are potent virulence factors for fish pathogens such as *F. psychrophilum*, *F. columnare*, *F. spartansii* and *T. maritimum*. They are involved in the lysis of host erythrocytes and in recovering their hemoglobin-bound iron pool for growth (Avendaño-Herrera et al., 2005; Møller et al., 2005; Högfors-Rönnholm and Wiklund, 2010; Chen et al., 2017; Kayansamruaj et al., 2017). Hemolytic enzymes play a part in the virulence of *F. psychrophilum* (Högfors-Rönnholm and Wiklund, 2010). *F. psychrophilum* contains a putative hemolysin gene, FP0063, with 53% similarity with the hemolysin of *Vibrio anguillarum* VAH5 (see the Vibrio section below). The Vibrio hemolysin has been shown to degrade erythrocytes creating a devastative host cell damage (Rodkhum et al., 2005; Duchaud et al., 2007). Similarly, *F. spartansii* harbors virulence-related hemolysin genes that are vital in pathogenesis process such as tissue damage and sepsis (Chen et al., 2017). *Flavobacterium columnare* contain hemolysin genes that are prominent for pathogenesis (Kayansamruaj et al., 2017; Kumru et al., 2017). *Tenacibaculum maritimum* contains a gene encoding for sphingomyelinase, a toxin directly involved in hemolysis (Oda et al., 2010; Pérez-Pascual et al., 2017). The secretion mechanisms of hemolysins of fish-pathogenic flavobacteriaceae is not yet clear. However, mutations affecting genome regions encoding T9SS responsible for gliding motility, including the examples GldJ, GldK, GldM, and GldN from *F. psychrophilum* led to reduced hemolytic activity, indicating that the secretion of hemolysins is at least indirectly influenced by T9SS (Castillo et al., 2015; Barbier et al., 2020).

Other Protein Toxins and Their Secretion Systems

Flavobacterium spartansii harbors genes encoding for toxin thiol-activated cytolysin (TACY) which possibly modulate or lyse the function of enterocyte membranes through formation of pore (Chen et al., 2017). *Flavobacterium branchiophilum* produces a cholera-like toxin protein, identified as FBFL15_0919 (Touchon et al., 2011), which has high sequence similarity with the cholera toxin (CTA) produced by *V. cholera* and the heat-labile toxin (LTA) produced by enterotoxigenic *Escherichia coli*. The LTA and CTA toxins stimulate adenylate cyclase and provoke the massive loss of fluid and electrolytes through the intestinal epithelium of the host (Sixma et al., 1991; de Haan and Hirst, 2000; Broeck et al., 2007). Similarly, FBFL15_0919 is speculated to disturb the osmoregulatory function of the epithelial cells of the gills. Gill cells are involved in excretion of urea and in uptake of salts, in addition to oxygen uptake (Wilkie, 2002). The exact secretion mechanism for FBFL15_0919 is not yet investigated, however, CTA is reported to be exported by T2SS (Robien et al., 2003).

Despite the availability of genome sequences of fish pathogens such as *F. psychrophilum,* many of the secretion systems for virulence factors that are key to the pathogenesis of other Proteobacteria are not yet described in detail in *Flavobacteriaceae*. Genes for key components for secretion systems from almost all classes have been found in the genomes

of different *Flavobacterium* species, but have not yet been directly linked to virulence experimentally (Kumru et al., 2020). Much more is known about the components for T9SSs (Duchaud et al., 2007). Mutation of genes involved in gliding (the *gld* genes), which are components of the T9SS in *F. johnsonia* (a well-studied member of the fish-pathogenic bacteroidetes) lead not only deterioration of motility but also to significant changes in the secretion of extracellular enzymes (McBride et al., 2003; Braun et al., 2005; Braun and McBride, 2005) strongly suggesting that the T9SS may be the most crucial virulence factor of bacteroidetes. It facilitates pathogenicity through providing multiple virulence tools for successful infection ranging from colonization to host cell disruption processes (Li et al., 2017; Penttinen et al., 2018; Barbier et al., 2020).

PROTEOBACTERIA (CLASS: GAMMAPROTEOBACTERIA)

Vibrionales

The Vibrionales are a separate order within the Proteobacteria that contains only one Family, the *Vibrionacae*. They encompass many important facultative anaerobic fish pathogens, mainly from the genera *Vibrio, Allivibrio* and *Photobacterium*.

Vibrios are rod-shaped ubiquitous and important pathogens to varied marine and freshwater fish species (Rucker, 1959). Vibriosis, one of the common diseases in the aquaculture industry with outbreaks that lead to high mortality of farmed fish, imposes severe negative impacts on productivity, sustainability and profitability. Diverse pathogenic vibrio species have been isolated from diseased fish with vibriosis symptoms that include bruised, red spotted and ulcerated skin, mouth and fin sores, and systemic infection symptoms like tissue necrosis, hemorrhagic muscles, and other bleedings (Buller, 2004; Toranzo et al., 2005). All pathogenic vibrios, including the human-pathogenic *Vibrio cholerae*, are directly connected to aquatic environments. The genome of the vibrios is encompasses two chromosomes, an unusual feature compared to other bacterial genera (Okada et al., 2005). The most common pathogenic vibrio species responsible for fish vibriosis include *V. anguillarum*, *V. harveyi*, *V. vulnificus*, *V. parahaemolyticus*, *V. alginolyticus*, *V. ordalii*, *V. splendidus*, and in addition the species *Allivibrio salmonicida* and *Photobacterium damselae* that are part of closely related *Vibrionacae* genera (Austin B. et al., 2003; Austin and Austin, 2012). *Vibrio cholerae* is able to colonize diverse fish species indicating that fish could be a vector for *V. cholerae*. However, direct pathogenicity of *V. cholerae* to fish is debatable (Halpern and Izhaki, 2017).

Transmission Routes and Adherence

The main routes of transmission for vibriosis include direct contact (entry through skin and/or damaged mucous layers) and oral (ingestion) transmissions (Grisez et al., 1996; Svendsen and Bøgwald, 1997; Jun and Woo, 2003; Weber et al., 2010). The initial stage of infection involves colonization of the skin mucosa and biofilm formation facilitated by exopolysaccharides (Croxatto et al., 2007; Weber et al., 2010). Adherence of the bacteria to host surfaces and survival in the host are particularly determined by the surface hydrophobicity of pathogenic bacteria (Lee and Yii, 1996; Balebona et al., 1998). For instance, *V. anguillarum* and *V. salmonicida* utilize surface hydrophobicity to survival in hosts organism (Horne and Baxendale, 1983; Espelid et al., 1987; Hjelmeland et al., 1988).

Vibrionaceae utilize specific pili or various non-pilus adhesins that facilitate adhesion to host cells and initiate infection. Adhesion can be mediated by flagella in *V. anguillarum*, *V. alginolyticus*, *V. harveyi*, *V. splendidus*, and *V. vulnificus* indicating that motility is key for adhesion in these organisms (Milton et al., 1996; O'Toole et al., 1996; Ormonde et al., 2000; Luo et al., 2016; Dai et al., 2020; Xu et al., 2021). In addition to flagella, the outer membrane protein TolC and NADH oxidase dihydrolipoamide dehydrogenase play pivotal roles in the adhesion of *V. harveyi* and *V. splendidus,* respectively (Dai et al., 2019; Zhu et al., 2019). Experiments performed on non-fish cell lines show other factors including the adhesin *Vp*adF, enolase, capsular polysaccharide, T6SSs, multivalent adhesion molecule 7 (MAM7) and a mannose-sensitive hemagglutinin (MSHA) pilus bind to different receptors to facilitate cell attachment by *V. parahaemolyticus* (Hsieh et al., 2003; Krachler et al., 2011; Yu et al., 2012; O'Boyle et al., 2013; Jiang et al., 2014; Liu and Chen, 2015). A β-pore forming toxin, phobalysin, plays a pivotal role in host cell adherence in *Photobacterium damselae* (Rivas et al., 2015; von Hoven et al., 2018).

Survival mechanisms in the hostOnce inside the host, survival of *Vibrionaceae* is achieved through distinct virulence mechanisms such as regulation of iron acquisition, neutralization of acidic environments, combating oxidative stress, induction of host immune cell death, and immune evasion. *V. vulnificus* neutralizes acidic environments of the host gut and tolerates oxidative stress by converting lysine to cadaverine and CO_2 using lysine decarboxylase and manganese superoxide dismutase (SOD) respectively (Rhee et al., 2002; Kim et al., 2005; Jones and Oliver, 2009). Invasion and inter-microbial competition of *V. cholerae* in the gut of zebrafish is mediated by a T6SS where the syringe-like system plays a role in intensifying the host gut contractions which lead to expulsion of resident microorganisms (Logan et al., 2018).

Several *Vibrionaceae* possess finely regulated and high-affinity siderophore or heme-dependent iron acquisition systems to compete for iron sequestered by iron-binding proteins such as transferrins or in heme in host organisms (Thode et al., 2018; Richard et al., 2019). Siderophore-dependent iron acquisition systems synthesize and secrete siderophores into the environment to chelate ferric iron. The secretion mechanisms for siderophores are not fully understood in the *Vibrionaceae* but a major facilitator superfamily protein (MFS)-mediated efflux pump seems to play an important role (Li and Ma, 2017). No hemophores to chelate iron from hemoproteins have yet been identified in fish-pathogenic species from the *Vibrionaceae* family (Wandersman and Delepelaire, 2004).

Vibrio anguillarum, *V. vulnificus*, *V. ordalii*, *V. harveyi*, *Photobacterium damselae*, *V. parahaemolyticus*, *V. alginolyticus*, *A. salmonicida*, and *V. splendidus* utilize siderophore-mediated iron acquisition systems. The uptake of both ferric-siderophore

complex and heme across the membrane is performed by ABC transporters which utilize TonB complex as energy transducers (Stork et al., 2004; Thode et al., 2018).

Depending on the serotype, *V. anguillarum* produce three distinct iron-uptake systems: anguibactin and its outer membrane receptor FatA (Lopez and Crosa, 2007; López et al., 2007; Naka et al., 2013), piscibactin and its outer membrane receptor FrpA (Balado et al., 2018; Valderrama et al., 2019) and vanchrobactin and its outer membrane transport FvtA (Soengas et al., 2006, 2008; Balado et al., 2008, 2009). Like *Vibrio anguillarum*, *Photobacterium damselae* and *V. ordalii* produce the piscibactin siderophore where the receptor in the former is FrpA and in the latter is unclear (Souto et al., 2012; Ruiz et al., 2019; Valderrama et al., 2019). *Vibrio vulnificus* synthesize vulnibactin and its uptake is mediated by VuuA (Webster and Litwin, 2000; Kim et al., 2006; Alice et al., 2008). *Vibrio harveyi* produce amphi-enterobactin and its uptake receptor FapA (Zane et al., 2014; Naka et al., 2018). *Vibrio parahaemolyticus* produces the siderophore vibrioferrin and its receptor PvuA (Funahashi et al., 2002; Tanabe et al., 2003). Like *V. parahaemolyticus, V. alaginoluticus* contains gene clusters for vibrioferrin biosynthesis (Wang Q. et al., 2007). *Allivibrio salmonicida* utilize bisucaberin that is recognized by BitA (Winkelmann et al., 2002; Kadi et al., 2008). *Vibrio splendidus* utilize a hydroxamate-based siderophore and IutA is proposed as a potential receptor (Song et al., 2018). Besides the siderophore iron acquisition system, *V. vulnificus* directly use heme from hemoglobin as host iron sources, where the uptake of heme is facilitated by outer membrane protein HupA (Litwin and Byrne, 1998). *Vibrio anguillarum* possess a heme-utilizing system where two outer membrane proteins, HuvA and HuvS, perform heme uptake (Mazoy et al., 1996; Mazoy and Lemos, 1996; Mouriño et al., 2005), and where the complex HuvBCD is required for subsequent transport of periplasmic heme into the cytosol (Mouriño et al., 2004).

Proteases and Secretion Systems

Extracellular proteases are associated with the pathogenesis of several *Vibrionacae*. The extracellular zinc metalloproteases EmpA and PrtV of *V. anguillarum* are potent virulence factors with mucinase activities that are required for infecting the gastrointestinal tract of diverse fish species such as salmon, turbot and flounder (Norqvist et al., 1990; Milton et al., 1992; Denkin and Nelson, 1999, 2004; Zhao-lan et al., 2002; Mo et al., 2010; Frans et al., 2011). The secretion of EmpA and PrtV is mediated by a T2SS (Zhang et al., 2006; Rompikuntal et al., 2015). EmpA and PrtV belong to the M4 and M6 family of peptidases, respectively, and are translated in inactive form which passes through a maturation process involving proteolytic cleavages during secretion through the T2SS (Milton et al., 1992; Staroscik et al., 2005; Zhang et al., 2006; Varina et al., 2008; Mo et al., 2010; Rompikuntal et al., 2015). Besides its proteolytic activity, EmpA activates hemolysins promoting disruption of red blood cells in fish (Han et al., 2011). PrtV contains gelatinase, protease and glycosidase activity, and a *prtV* mutant of *V. anguillarum* strain show reduced infection, growth and hemolytic activity in turbot and turbot cell lines (Mo et al., 2010).

Vibrio parahaemolyticus produce multiple extracellular metalloproteases such as the tissue-degrading protease VPM, and the collagenases PrtV and VppC. In addition, serine proteases Vpp1/protease A with cytotoxic activity, VpSP37 with gelatinase activity, and PrtA with hemolytic and cytotoxic activity are produced as virulence factors (Osei-Adjei et al., 2018). Similarly, *V. alginolyticus* produce extracellular alkaline serine protease A and a VppC homolog where the former is an exotoxin and lethal to fish (Takeuchi et al., 1992). *Vibrio vulnificus* produce an extracellular metalloprotease Vvp, however, its involvement in virulence is debatable (Valiente et al., 2008). The secretion mechanisms of these metalloproteases are not yet described.

Hemolysins and Secretion Systems

Six pore-forming hemolysins, Vah1-5 and Rtx, are responsible for disrupting red blood cells leading to hemorrhagic septicemia in *V. anguillarum* (Hirono et al., 1996; Rodkhum et al., 2005). Vah1-5 belong to the HylA hemolysin family (Hirono et al., 1996; Zhang and Austin, 2005). Secretion factors of Vah1-5 from *V. anguillarum* are not documented; however, HylA hemolysins are generally known to be secreted via T1SS (Thomas et al., 2014). Like the metalloproteases EmpA and PrtV of *V. anguillarum*, hemolysins in the HylA family are translated as pre-proteins where the production of mature hemolysins requires multiple processing steps during secretion (Zhang and Austin, 2005). All Vah hemolysins show hemolytic activity on fish erythrocytes, with Vah4 displaying the strongest virulence effects (Rodkhum et al., 2005). RtxA (repeats-in-toxin-A), a multifunctional extracellular protein secreted by diverse Gram-negative fish pathogens, is responsible for cytotoxic and hemolytic attacks in fish (Li L. et al., 2008). The secretion of unfolded Rtxs is performed by a T1SS where folding is initiated only after passage (Linhartova et al., 2018). The expression and secretion of *V. vulnificus* RtxA1 toxin is regulated by a general stress response regulator, RpoS (Guo et al., 2018).

Vibrio parahaemolyticus possess two pathogenic hemolysins, thermostable direct hemolysin (TDH) and TDH-related hemolysin (TRH) (Li L. et al., 2019). *Vibrio parahaemolyticus* possess multiple secretion systems, a T2SS and two T3SSs (T3SS1 and T3SS2) where the T2SS and T3SS2 export the hemolysins. TDH possesses exotoxin roles and secreted through both, the T2SS and T3SS2 (Matsuda et al., 2019). Like TDH, TRH is secreted through both, the T2SS and T3SS2 (Matsuda et al., 2019). The pathogenicity role of T3SS1 of *V. parahaemolyticus* is described below.

Vibrio alginolyticus express the toxic hemolysins Tdh and TLH where the former has hemolytic activity both on mouse and fish and the latter shows both hemolytic and phospholipase activities in zebrafish (Cai et al., 2007; Jia et al., 2010). *Vibrio harveyi* produce a cytotoxic hemolysin VHH with phospholipase B activity, where its native secretion system is not clear; but it has been shown to use T2SS-mediated secretion when recombinantly expressed in *E. coli* (Zhong et al., 2006; Sun et al., 2007). Several extracellular products (ECPs) from *P. damselae* sp. *damselae* that have strong hemolytic, lipase, esterase-lipase and phospholipase activity but weak proteolytic activity are reported to be lethal for fish (Fouz et al., 1993; Labella et al., 2010).

Secretion of Effectors

T3SSs are ubiquitous in Gram-negative pathogens including fish pathogenic *Vibrionaceae* such as *V. parahaemolyticus*, *V. salmonicida, V. alginolyticus*, *V. harveyi and Photobacterium damselae.* They directly deliver both fish and non-fish virulence factors from the pathogen cytosol into host cells where the effect of the virulence factors on fish pathogenesis varies depending on the nature of the *Vibrionaceae* members (Hueck, 1998; Frey and Origgi, 2016; Osorio, 2018).

As mentioned earlier, *V. parahaemolyticus* harbor a set of two T3SSs (T3SS1 and T3SS2) where T3SS1 is related to cytotoxicity and T3SS2 is associated with both cytotoxic and enterotoxic activities in mice (Hiyoshi et al., 2010). Several effectors such as VopQ [that induces autophagy in mammalian cell lines; (Burdette et al., 2009)], VopS [modification of host Rho family GTPases in HeLa cells (Yarbrough et al., 2009)], VopR (unknown function) and VpA0450 [hydrolyzes plasma membrane-located phosphatidylinositol phosphate in human cells (Broberg et al., 2010)] are secreted through T3SS1. Evidence based on non-fish models show that VopA/VopP [inhibits mitogen-activating protein kinase pathway using acetyl transferase, (Trosky et al., 2007; Pan et al., 2021) VopL (induce stress fiber using actin nucleastion (Ham and Orth, 2012)], VopT [Induce cytotoxicity using ADP-ribosylation (Sun and Barbieri, 2003; Barbieri and Sun, 2004)], VopV [facilitate enterotoxicity by F-actin binding/bundling (Hiyoshi et al., 2011)] and VopC [Promote bacterial invasion using deamidase (Zhang et al., 2012)] are secreted through T3SS2 (Ham and Orth, 2012). Additional contributions of T3SS2 to pathogenicity is discussed above in the section on hemolysins.

Effectors of T3SSs in *V. alginolyticus* promote cell death of fish cells (Zhao et al., 2010). Val1686 and Val168 in *V. alginolyticus*, homologous to the T3SS1 effector proteins VoPQ (88 %) and VopS (91 %) of *V. parahaemolyticus*, cause apoptosis in fish cell lines (Osorio, 2018). *V. alginolyticus* harbor two T6SSs, T6SS1 and T6SS2, where T6SS1 secretes multiple effectors such as MIX IV pore- forming effector (Va16152), MIX I (Va01565), LytM, a peptidoglycan hydrolase and lysozyme-like domain (Va01435), OmpA_C (Va01555) and VopQ (Va17542) (Salomon et al., 2015). Also *V. splendidus* produce a virulence effector, Hop, with cytotoxic effects that is secreted by a T3SS (Zhuang et al., 2020, 2021).

Enterobacteriales

Yersiniaceae, *Hafniaceae*, and *Enterobacteriaceae* are three of the seven families classified under the order Enterobacteriales that contain common fish pathogens, causing mild to severe fish diseases.

Yersinia ruckeri is a member of the *Yersiniaceae* family, and strains from different biotypes are reported as causative agents of enteric redmouth disease (ERM). ERM, also known as yersiniosis, dominantly infects salmonids causing serious economic threats to the salmonid aquaculture industry worldwide (Austin D. A. et al., 2003; Fouz et al., 2006; Arias et al., 2007; Wheeler et al., 2009; Calvez et al., 2014; Hjeltnes et al., 2017; Wrobel et al., 2019). *Yersinia ruckeri* is a rod-shaped, nonencapsulated facultative anaerobe (Tobback et al., 2007). Typical symptoms of yersiniosis include septicemia and subsequent development of hemorrhages on the body surface and internal organs (Tobback et al., 2007). Alike some *Yersinia* species infecting other animals and humans, *Y. ruckeri* contain plasmids that encode virulence-related factors such as type IV pilus and T4SS (Wrobel et al., 2018).

Edwardsiella tarda [current name *E. piscicida* (Abayneh et al., 2013)] and *Edwardsiella ictaruli* belong to the genus Edwardsiella within the *Hafniaceae* family. They are economically important fish pathogens predominant in aquaculture industries worldwide (Thune et al., 1993; Mohanty and Sahoo, 2007). Edwardsiellosis is the general term used for the septicemic diseases caused by *E. tarda* and *E. ictaluri* leading to severe skin, muscle and internal organ lesions and causing high levels of mortality (Ewing et al., 1965; Abbott and Janda, 2006; Kerie et al., 2019). *Edwardsiella tarda* is a. short, mostly motile and rod-shaped facultative anaerobe that infects wide ranges of fish species (Matsuyama et al., 2005; Park et al., 2012). *Edwardsiella ictaruli* is a short and pleomorphic rod-shaped, motile species that is primarily recognized as a causative agent of enteric septicemia of catfish species. *E. ictaluri* was isolated from kidney and livers of several catfish with signs of enteric septicemia (Hawke et al., 1981). *Edwardsiella tarda* and *E. ictaruli* share common virulence strategies (see below).

Citrobacter freundii a member of the genus Citrobacter, is a long, rod shaped, facultative anaerobic bacterium of the family *Enterobacteriaceae*. Several *C. freundii* strains contain flagella used for locomotion while some are non-motile. *Citrobacter freundii* is closely related to *E.coli* and *Salmonella* and is prevalent in diverse ecological niches such as soil, water, sewage, food and the gut of animals including humans (Knirel et al., 2002; Murray et al., 2010; Abbott, 2011; Bandeira Junior et al., 2018). *Citrobacter freundii*, a causative agent of gastroenteritis and hemorrhagic septicemia, is a common pathogen of diverse freshwater fish where infected fish show symptoms such as skin ulceration, systemic infectious signs on the liver, kidney, muscles and gills (Jeremić et al., 2003; Baldissera et al., 2018; Sun et al., 2018).

Transmission Routes and Adherence

Host cell adherence by *Y. ruckeri* is promoted through the pathogen's variable motility that depends on the presence and absence of flagella (Davies and Frerichs, 1989). Bacterial adherence in *Y. ruckeri* may also involve type IV pili, a hair-like multi-subunit surface appendage which its function is not restricted to surface biding and twitching motility, but also DNA-uptake, and micro-colony or biofilm formation (Mattick, 2002; Craig et al., 2019).

Experimental evidence shows that the site of entry for virulent *E. tarda* and *E. ictaluri* are gills, gastrointestinal tract and body surface (Ling et al., 2001; Pirarat et al., 2016). *Edwardsiella tarda* is shown to involve actin and microtubules for entry to host cells (Ling et al., 2001; Sui et al., 2017). Motility is critical during the initial phase of colonization for several aquaculture pathogens (Ormonde et al., 2000). Two types, motile and non-motile strains, of *E. tarda* exist where there is apparent differences in the pathogenicity between these variants (Park et al., 2012), however, the difference in colonization mechanisms of these variants are

not clear. Furthermore, secretion systems such as T3SS and T6SS play pivotal roles in adherence and cell-diffusion (Tan et al., 2005; Park et al., 2012). For instance, EvpP, a component of T6SS, is shown to control the internalization process in invasion suggesting that this secretion system plays a key role in the pathogenesis of *E. tarda* (Wang X. et al., 2009).

The site of infection of *C. freundii* are the mucosal layers of the intestine which suffer severe damage during infection (Pan et al., 2021). A whole genome analysis of *C. freundii* indicates the presence of multiple virulence factors that are potentially involved in colonization and in-host cell survival. *C. freundii* displays strong adhesion to the hepatic fish cell line L8824 and can cause distinctive lesions known as A/E lesions (Pan et al., 2021), similar to A/E lesions caused by *E.coli* on the intestinal mucosa. This effect requires strong attachment of the pathogen to the surface of the enterocyte and involves a T3SS which injects multiple effector proteins into the cell (Wong et al., 2011; Hartland and Leong, 2013). An adhesin named EaeA of *C. freundii* has previously been identified as key element for colonization in mice but its role in colonization of fish is not clear (Schauer and Falkow, 1993). EaeA itself is an autotransporter, a member of the type Vc secretion systems (Leo et al., 2015).

Survival mechanisms in the hostIt is crucial for pathogens to avoid host defense mechanisms, in order to survive, proliferate and maintain infection in the host. Key to *Y. ruckeri* survival, growth and pathogenicity in the host is its iron acquisition system that produces an enterobactin-like siderophore known as ruckerbactin; the gene encoding ruckerbactin is upregulated during infection (Fernández et al., 2004; Tobback et al., 2007). The secretion and uptake systems for ruckerbactin and ferric-ruckerbactin, respectively, are not yet elucidated in detail, however, the ruckerbactin receptor has a high degree of similarity with the ferrichrysobactin receptor of *Dickeya dadantii* (Fernández et al., 2004).

Edwardsiella tarda has evolved several mechanisms to survive immune responses. One of these mechanisms involves the neutralization of reactive oxygen species using redox enzymes such as superoxide dismutase (SodB) and catalase KatB (Han et al., 2006). *Edwardsiella tarda* has the ability to survive in host serum, to resist acidic milieu and to replicate in phagocytes with the help of a serum-induced, putative hydrogenase protein named Sip2 (Li and Sun, 2018). In serum, the complement system has a significant role in host defense against infection via mechanisms involving both innate and adaptive immunity (Walport, 2001; Merle et al., 2015). Activation of the complement system lead to bacterial membrane damage and subsequent lyses using membrane attack complex (MAC) (Endo et al., 2006; Sarma and Ward, 2011). *Edwardsiella tarda* has the ability to evade the bactericidal effect of host serum through blocking the activation of the complement using the zinc metalloprotease Sip1 (Zhou et al., 2015). Besides, serum enhances the tricarboxylic acid cycle of *E. tarda* which increases membrane potential and decreases the formation of MAC, leading to serum resistance (Cheng et al., 2017). Furthermore, the chaperone protein HtpG is shown to help *E. tarda* to cope with stress conditions during infection (Dang et al., 2011).

Like *E. tarda*, *E. ictaluri* has the ability to survive and grow within host macrophages (Miyazaki and Plumb, 1985; Baldwin and Newton, 1993; Pirarat et al., 2016). A T3SS translocates several effectors from *E. tarda* and *E. ictaluri* directly into the host cytoplasm, where they have essential roles for internal replication and virulence (Dubytska et al., 2016). The T3SS of *E. tarda* plays important roles in phagocyte survival, in host proliferation and virulence (Tan et al., 2005). For instance, the T3SS effector EseJ facilitates cell proliferation in host cells by inhibiting the oxidative stress produced by host macrophages (Xie et al., 2015). Like the T3SS, a T6SS has a pivotal role in survival and replication of *E. tarda* in host epithelial cells and phagocytes (Park et al., 2012). However, the mechanisms of the two secretion systems are antagonistic, where the T3SS promotes bacterial replication in host cells while the T6SS protects the pathogens from attack by the activated innate immune system through suppressing replication (Xie et al., 2015; Hu et al., 2019).

Iron acquisition systems such as siderophore biosynthesis and iron uptake systems are necessary for pathogenicity of *E. tarda* (Castro et al., 2016). The genome of *E. tarda* contains genes encoding for multiple factors putatively involved in iron utilization including ferric uptake regulator, ferric reductase, ferritin and TonB (Wang Q. et al., 2009). It also includes a gene cluster sharing high similarity to the *pvsABCDE-psuA-pvuA* operon which encodes proteins for synthesis and utilization of vibrioferrin siderophore of the two fish pathogen vibrios *V. parahaemolyticus* and *V. alginolyticus* (Tanabe et al., 2003; Wang Q. et al., 2007).

In contrary, there are no dedicated siderophore biosynthesis genes detected in the genome of *E. ictaluri* (Santander et al., 2012), however, the pathogen carries a ferric hydroxamate uptake (Fhu) system involved in uptake of hydroxamate-type siderophores. Experimental evidence shows that the Fhu-system is indeed involved in pathogenicity, suggesting that the system may be utilized to uptake hydroxamates secreted by other bacteria (Abdelhamed et al., 2016). In addition, the genome of *E. ictaluri* contains an alternative ferric uptake system (afuABC) and the general TonB energy transducing system (TonB-ExbB-ExbD) which may be involved in iron uptake (Abdelhamed et al., 2013, 2017). Furthermore, *E. ictaluri* utilizes a Fur-regulated heme-hemoglobin uptake system (Santander et al., 2012).

In addition to the siderophore-dependent systems, *E. tarda* can utilize hemin, hemoglobin and hematin as iron sources (Abbott and Janda, 2006). A heme utilization operon in its genome that encodes for three proteins identified as $HutW_{Et}$, $HutX_{Et}$ and $HutZ_{Et}$ is highly similar to the heme utilization operon in *V. cholera* (Shi et al., 2019). In *V. cholera* $HutX_{Vc}$ functions as an electron carrier to the heme-degrading $HutZ_{Vc}$ while $HutW_{Vc}$ may be a reductase for $HuyZ_{Vc}$ (Sekine et al., 2016). $HutZ_{Et}$ has been shown to be involved in biofilm formation and motility (Shi et al., 2019). Furthermore, *E. tarda* produce an iron-mediated hemolysin that is released under iron-limited conditions (Janda and Abbott, 1993; Hirono et al., 1997). All in all, iron depletion in host cells is a signal for pathogens to turn on the expression of virulence genes. The ferric uptake regulator (Fur) protein senses iron depletion in, for example, *E. tarda* to regulate expression of key virulence factors such

as T3SS and T6SS through secretion regulator protein EsrC (Chakraborty et al., 2011).

Citrobacter freundii harbor genes that could be utilized in diverse mechanisms and virulence factors to maintain infection, including a T3SS that plays a crucial role in the injection of effector proteins such as HopAJ2 family member that mediate survival against host immune response (Galán et al., 2014; Pan et al., 2021). Iron acquisition in *C. freundii* is facilitated by FepE, a component of the ferric enterobactin siderophore transport system (Wang et al., 2019). In addition to the siderophore-dependent iron transport system, an hemophore-mediated heme uptake apparatus is present that includes an outer membrane channel protein HasF (Létoffé et al., 2001). In addition, surface lipopolysaccharides (LPS) of some serogroups of *C. freundii* have been shown to play vital roles in colonization and host survival (Denkin and Nelson, 1999).

Proteases and Their Secretion Systems

Yersinia ruckeri produce a serralysin metalloprotease named Yrp1 that is secreted via an ATP-dependent T1SS composed of three genes, *yrpD-F,* and a protease inhibitor *inh*. Yip1 seems to have pivotal roles in the development of ERM due to its ability to disrupt several extracellular matrix proteins of fish such as laminin and fibronectin, and proteins important in muscle function such as actin and myosin (Fernández et al., 2002). Furthermore, *Y. ruckeri* produce two additional peptidases, YrpA and YrpB encoded by the *yrpAB* operon. Toxicity tests indicate that at least YrpA is involved in *Y. ruckeri* pathogenicity, as deletion of the gene encoding YrpA drastically reduces the virulence of the bacteria (Navais et al., 2014).

Edwardsiella tarda produce multiple virulence-related proteases that are engaged in diverse processes of infection. For instance, the above mentioned zinc metalloprotease Sip1 of *E. tarda* is secreted to effectively prevent complement-mediated serum killing through blocking the activation of the complement system (Zhou et al., 2015). A serine protease autotransporter Tsh_{ET}, which is a temperature-sensitive hemagglutinin, belongs to the Type V secretion systems (T5SS) and contributes to the virulence of *E. tarda*. Tsh has multiple functions; mutations in the *tsh* gene led to hindrance of biofilm growth, reduction of resistance against serum killing, impairment of the ability to block the host immune response, and attenuation of tissue invasion and cellular infectivity (Hu et al., 2016). In addition, the periplasmic serine protease $DegP_{ET}$ is presumably involved in virulence of *E. tarda*, similar to DegP in *Salmonella enterica*, *Streptococcus pyogenes* and *Legionella* (Johnson et al., 1991; Jones et al., 2001, 2002; Pedersen et al., 2001; Wilson et al., 2006; Flannagan et al., 2007; Jiao et al., 2010).

Hemolysins and Their Secretion Systems

The gene cluster *yhlBA* of *Y. ruckeri* encodes for a hemolysin (YhlA) and a protein involved in its secretion/activation (YhlB). The expression of YhlA is upregulated in iron-limited conditions suggesting that the hemolysin may be directly involved in acquisition of iron from the host cell (Fernández et al., 2007; Wrobel et al., 2019). Both *yhlA* and *yhlB* genes have high sequence similarity with a type Vb secretion system with hemolysin activity in *Serratia* sp. (Wrobel et al., 2019).

Edwardsiella tarda produce two different hemolysins, the iron-mediated cell associated hemolysin EthA, secreted under iron limited conditions, and an extracellular pore-forming hemolysin district from EthA (Janda and Abbott, 1993; Chen et al., 1996; Hirono et al., 1997). Similar to the hemolysin YhlA of *Y. ruckeri* and its activation/secretion protein YhlB (described above), the hemolysin EthA from *E. tarda* needs an activation/secretion protein EthB encoded in an operon. EthA and EthB, are prevalent in hemolytic *E. tarda* strains isolated from diseased fish (Hirono et al., 1997) which may indicate that they are among the key virulence mechanisms utilized by the pathogenic *E. tarda*.

Polysaccharide Degrading Enzymes

Chondroitinases are involved in the pathogenicity of infectious bacteria (Schaechter et al., 1993). Chondroitinase activity is known to be virulence factor in *Edwardsiella* spp. including *E. tarda* and *E. ictaruli.* These species produce chondroitinase that mediates cartilage degradation in the process of invasion (Waltman et al., 1986; Shotts and Cooper, 1996). The Sialidase NanA from *E. tarda* also promotes tissue invasion, and mutations of the gene encoding for the enzyme led to drastic attenuation of the pathogen, by limiting its ability for invasion and colonization (Jin et al., 2012).

Secretion of Other Toxin Proteins or Toxins and Their Secretion Pathway

Distinct strains of *Y. ruckeri* produce TcpA, a Toll/interleukin-1 (TIR) domain containing protein that inhibits Toll-like receptor signaling and promotes immune evasion. TcpA is also known to increase tissue damage in fish. The gene for TcpA is located adjacent to a T4SS gene cluster which may indicate that the secretion of TcpA is related to this T4SS (Liu et al., 2019). As discussed above, T3SS are a crucial and multipurpose system in *E. tarda* and *E. ictaluri*. The T3SS of *E. tarda* belongs to the Ssa-Esc family which includes T3SS encoded by Salmonella pathogenicity island 2 (SPI-2) in *Salmonella enterica* serover Typhimurium, the causative agent of foodborne illness worldwide (Anderson and Kendall, 2017). The core components of the T3SS are encoded by 34 genes, where all obtain different functions (Tan et al., 2005; Sadarangani et al., 2013). Among these are the three translocon proteins EseB, EseC and EseD that are essential for delivery of effectors into host cells (Tan et al., 2005).

Aeromonadales

The order Aeromonadales contains only two families, the *Succinivibrionaceae* and the *Aeromonadaceae*. Species of the family *Aeromonadaceae* are known to cause acute hemorrhagic septicemia in fish (Colwell et al., 1986; Stackebrandt and Hespell, 2006). *Aeromonas* species, ubiquitous in aquatic environments, are classified into two groups; motile mesophilic aeromonads with optimal growth temperature around 37°C, and non-motile psychrophilic strains with an optimal growth temperature range of 22–28°C where the latter are cold-water fish pathogens. *Aeromonas bestiarum*, *Aeromonas sobria*, *Aeromonas hydrophila*

and *Aeromonas veronii,* all categorized as motile and mesophilic, are responsible for motile *Aeromonas* septicemia (MAS), an acute hemorrhagic septicemia, or for chronic skin ulcers (Ali, 1996; Stratev and Odeyemi, 2017). *Aeromonas salmonicida* comprising both non-motile psychrophilic and motile mesophilic strains is a causative agent for systemic furunculosis, a disease that causes sepsis, hemorrhages, muscle lesions, inflammation of the lower intestine, spleen enlargement, and death in freshwater fish populations (Beaz-Hidalgo and Figueras, 2013). Genome information of diverse *Aeromonas* species is available and indicates specialized pathogenic mechanisms (Seshadri et al., 2006; Reith et al., 2008; Li et al., 2011; Beaz-Hidalgo and Figueras, 2013). Virulence by *Aeromonas* is a complex succession of processes, where successful infection requires potential for the formation of biofilms, production and secretion of virulence factors such as adhesins, proteases, hemolysins, lipases, DNases and effector proteins as well as regulation of virulence factors through quorum sensing (Allan and Stevenson, 1981; Cahill, 1990; Thornley et al., 1997; Beaz-Hidalgo and Figueras, 2013).

Transmission Routes and Adherence

The important initial infection sites for *Aeromonas* such as *A. salmonicida* include skin, gills and the gastrointestinal tract (Ringø et al., 2004; Bartkova et al., 2017). Tissue invasion in the gastrointestinal tract is mediated by extracellular virulence factors that are utilized to damage the tissue (Ringø et al., 2004). Adhesion, a prerequisite for successful colonization by pathogens, is executed by different factors in *Aeromonas species*. Outer membrane proteins such as OmpA and AHA1 function as adhesins in *A. veronii* and *A. hydrophila* (Fang et al., 2004; Namba et al., 2008). A tight adherence system (TaD) is present in the majority of *A. hydrophila* strains (Tekedar et al., 2019a). *A. hydrophila* and *A. sobria* use pili (Lallier and Daigneault, 1984; Ho et al., 1990), lipopolysaccharides (LPS) is used by *A. hydrophila* (Merino et al., 1996), and cell-associated lectins are used by *A. veronii* (Guzman-Murillo et al., 2000) to bind to host cells and tissues. Paracrystalline surface protein layers in *A. salmonicida* and *A. hydrophila* display significant hydrophobicity and contribute to adhesion (Chu et al., 1991; Beveridge et al., 1997).

Survival Mechanism in the Host

Survival of *A. salmonicida* and *A. hydrophila* in the host is achieved by S-layers that bind to extracellular matrix components such as laminin, fibronectin and vibronectin providing resistance to serum killing and protease digestion (Beveridge et al., 1997; Noonan and Trust, 1997). Most *Aeromonas* sequester iron from their hosts through utilization of siderophore-dependent or siderophore-independent (heme-binding) mechanisms (Byers et al., 1991; Reith et al., 2008; Lange et al., 2020). The siderophore-dependent mechanisms rely on the synthesis of enterobactin or amonabactin and some *A. salmonicida* species are capable of synthesizing anguibactin-like siderophores (Barghouthi et al., 1989a,b; Byers et al., 1991; Telford and Raymond, 1998; Reith et al., 2008). *Allivibrio salmonicida* and *A. hydrophila* synthesize both ferric and heme iron acquisition systems (Ishiguro et al., 1986; Najimi et al., 2008b). In most cases, two catechol siderophores; acinetobactin and amonabactin, are produced simultaneously (Balado et al., 2015) and their uptake is facilitated by the TonB-dependent outer membrane proteins FstB and FstC that function as receptors for ferric-acinetobactin and ferric-amonabactin, respectively (Balado et al., 2017; Rey-Varela et al., 2019). Ferric-siderophore uptake is mediated by FstA in some species of *A. bestiarum* and *A. salmonicida* (Beaz-Hidalgo et al., 2008, 2013). An multifunctional amonabactin receptor of *A. hydrophila* is reported to transport several different siderophores across the membrane (Stintzi and Raymond, 2000). Heme uptake is performed by the membrane receptors HgpB in *A. veronii* and HutA in *A. salmonicida* and *A. hydrophila*, (Najimi et al., 2008a; Maltz et al., 2015).

Virulence Factors and Their Secretion Systems

Aeromonas utilize several secretion systems such as the sec-dependent systems T1SS, T2SS, and the sec independent T3SS and T6SS to transport virulence factors, toxins and effectors for infecting diverse fish species (Burr et al., 2002; Tekedar et al., 2019b). The T1SS and T2SS are prominent in almost all *Aeromonas* species, and a T3SS is detected in species such as *A. salmonicida*, *A. hydrophila*, and *A. veronii* (Citterio and Biavasco, 2015; Tekedar et al., 2019b; Barger et al., 2020). A T6SS was detected for the first time in the genomes of *A. hydrophila* and *A. salmonicida* (Seshadri et al., 2006; Reith et al., 2008).

Proteases and Their Secretion Systems

Proteases are among the main virulence factors in *Aeromonas* (Sakai, 1985). Three types of proteases, metalloproteases, acetylcholinesterases and serineproteases are produced by *Aeromonas* (Seshadri et al., 2006). Both metallo- and serine proteases are secreted trough a T2SS by *A. hydrophila* (Sandkvist, 2001). A serine protease (AspA) as well as a glycerophospholipid:cholesterol acetyltransferase (GCAT; a lipase; see below) are secreted by *A. salmonicida* and were previously thought to be main virulence determinants (Buckley et al., 1982; Lee and Ellis, 1990; Whitby et al., 1992; Coleman and Whitby, 1993; Bernoth et al., 1997), however, it has later been shown that their deletion has minor effects on pathogenicity (Vipond et al., 1998).

Hemolysins and Their Secretion Systems

The presence of hemolytic capability in *Aeromonas* is associated with the development of lesions and mortality in fish species such as rainbow trout (Ellis et al., 1988). *Aeromonas* species such as *A. hydrophila* produce α-hemolysin (HlyA), a pivotal virulence factor causing cell-rounding and apoptosis (Tekedar et al., 2019a). HlyA is an Rtx-type toxin that are known to be secreted through T1SS in *Vibrio* species (Boardman and Satchell, 2004). Other pore-forming Hemolysins including H-lysin, T-lysin, salmolysin, ASH1, ASH3 and ASH4 are produced by *A. salmonicida* to lyse erythrocytes (Titball and Munn, 1981, 1985; Nomura et al., 1988; Hirono and Aoki, 1993). Secretion mechanisms of most of the hemolysins discussed here are not yet investigated. However, mutation of a T2SS in *A. hydrophila* led to impaired hemolytic activity suggesting that the T2SS may be one of a secretion mechanism for at least some

hemolysins in some members of the *Aeromonas* species (Barger et al., 2020). Aerolysin, a hemolysin, is a cytolytic pore-forming toxin produced by *A. hydrophila*, *A. salmonicida* and *A. sobria* (Chakraborty et al., 1990; Wilmsen et al., 1990; Hirono and Aoki, 1993; Fivaz et al., 2001) which binds to host cells and leads to increased membrane permeability. Aerolysin from *A. hydrophila* is known to be secreted through a T2SS (Ast et al., 2002).

Lipases and Their Secretion Systems

Glycerophospholipid:cholesterol acetyltransferase (GCAT) is an unusual lipase involved in the pathogenicity of *A. salmonicida* (Lee and Ellis, 1990). Combinations of GCAT and lipopolysaccharide (LPS) from *A. salmonicida* have lethal effects on salmon and rainbow trout (Røsjø et al., 1993; Lachmann et al., 1998). Glycerophospholipid:cholesterol acetyltransferase is secreted through T2SS (Sandkvist, 2001).

Elastase and Their Secretion Systems

The role of elastases from numerous bacterial pathogens as virulence factor is well documented (Kamath et al., 1998; Cascón et al., 2000; Bleves et al., 2010; Li J. et al., 2019). Among these, an extracellular elastase AhyB produced by *A. hydrophila* has high elastolytic activity in non-fish model and is essential for pathogenicity (Cascón et al., 2000). AhyB is secreted through T2SS (Cascón et al., 2000; Barger et al., 2020).

DNase and Their Secretion Systems

A DNase produced and secreted through a T2SS is present in the genome of *A. hydrophila* (Sandkvist, 2001), which is not yet fully characterized but is predicted to have an impact in virulence.

Toxins and Their Secretion Systems

An extracellular ADP-ribosylating toxin (AexT) is produced by *A. salmonicida*, similar to the mechanism of Exoenzyme S (ExoS) in *Pseudomonas aeruginosa* (Yahr et al., 1996a,b) to modify host cell proteins hence induce disease. One example of this is AexT from *A. salmonicida* (Burr et al., 2003; Dacanay et al., 2006) where experimental evidence confirmed that this ADP-ribosylating toxin is directly translocated into the host cytosol by T3SS, similar to its *P. aeruginosa* homolog ExoS (Yahr et al., 1996a,b; Braun et al., 2002; Dacanay et al., 2006; Silver and Graf, 2009).

Effectors and Their Secretion Systems

T3SSs are generally considered as a key virulence factor in many bacterial pathogens including *Aeromonas* due to their needle structure enabling injection of specific toxins directly into the host cytosol (Vilches et al., 2004; Dacanay et al., 2006; Coburn et al., 2007; Fast et al., 2009; Austin and Austin, 2016). Several T3SS effectors of *Aeromonas* are reported to affect the host immune response. AopH and AopO are effectors secreted by *A. salmonicida* that are secreted via the T3SS and that are highly similar to the effector proteins YopH and YopO from *Yersinia* species that influence cytoskeleton functions. YopH dephosphorylates tyrosines in focal adhesion proteins while YopO modulate the function of Rho GTPase to impair its roles in gene transcription, regulate actin cytoskeleton, control cell cycle and intracellular vesicle transport (Aepfelbacher, 2004). AopP is injected directly into host cells via T3SS to influence the host inflammatory response through inhibiting the nuclear factor- κB (NF-κB) signaling pathway (Fehr et al., 2006; Frey and Origgi, 2016). Other T3SS effector proteins such as the inositol polyphosphate 5-phosphatase Ati2 (Dallaire-Dufresne et al., 2013), HrpJ or BopN-like effector protein (AopN) (Nagamatsu et al., 2009; Crabill et al., 2012; Bergh and Frey, 2014), and ExsE of *A. salmonicida* have been shown to down-regulate host inflammatory responses (Bergh and Frey, 2014). In contrast to this, Aerolysin produced by *A. hydrophila* is secreted by a T2SS (Sandkvist, 2001).

The T3SS in *A. salmonicida* can be lost through genome modifications triggered by mobile elements such as insertion sequence (IS) elements when the bacteria are grown at temperatures exceeding 25°C, changing the strain phenotype from virulent to non-virulent (Tanaka et al., 2012, 2017). Whole genome analysis of 33 strains of *A. hydrophila* indicate the presence of T3SS, and mutation of two of the T3SS genes *aopB* (a translator) and *aopD* (a transmembrane protein) decreases cytotoxicity in carp epithelial cells, reduces virulence in blue gourami and increases phagocytosis (Yu et al., 2004). However, some hyper-virulent strains of *A. hydrophila* lack core components of the T3SS, which may indicate that these pathogens have an alternative secretion mechanism for virulence factors (Hossain et al., 2013; Pang et al., 2015).

Others Fish Pathogens From the Proteobacteria

Thiotrichales

Piscirickettsia salmonis, a member of Piscirickettsiaceae family, genus Piscirickettsia is the causative agent of piscirickettsiosis, also known as salmon rickettsial syndrome (SRS), a disease with high mortality that affects several seawater fish species. *P. salmonis* is non-motile, aerobic, encapsulated and pleomorphic (Fryer et al., 1990, 1992). *Piscirickettsia salmonis* is an intracellular pathogen causing remarkable economic loss in the aquaculture industry worldwide (Rozas and Enríquez, 2014; Figueroa et al., 2019). Diseased fish are dark in color, anemic where their kidney is swollen and the liver develops lesions (Fryer et al., 1992).

Transmission Routes and Adherence

The main routes of entry of *P. salmonis* in rainbow trout is through skin and gills (Smith et al., 1999). Studies on *P. salmonis* adherence and mode of invasion using fish eggs show that the pathogen attaches to the ova by means of membrane extension which allows penetration into the cell (Larenas et al., 2003). *P. salmonis* replicates within membrane-bound cytoplasmic vacuoles in host cells (Fryer et al., 1992). In stress conditions, *P. salmonis* form a biofilm-like cell aggregate that disintegrates when treated with cellulase, which indicates the presence of polysaccharides that are common for biofilm formation (Marshall et al., 2012). In addition, some lectins show strong binding to the biofilm-like structure, which confirms the presence of an exopolysaccharide (Rozas and Enríquez, 2014).

Piscirickettsia salmonis is capable of growing and surviving in fish macrophages where the bacteria are partially enclosed into vacuole membrane vesicles which escape destruction within

phagolysosomes (Almendras and Fuentealba, 1997; McCarthy et al., 2005, 2008). *Piscirickettsia salmonis* possess genes belonging to the Dot/Icm-type IV secretion system (T4SS) which is a type of secretion system utilized as major virulence mechanism in related intracellular pathogens such as *Legionella pneumophila* and *Coxiella burnetii* where the system is used for intracellular survival and replication (Thomas et al., 2020). It is shown that *P. salmonis*-containing vacuoles do not fuse with lysosomes, which suggests the presence of bacteria-mediated interference with the endosomal maturation process to ensure bacterial survival. This process depends on the Dot/Icm-type IV secretion system that delivers effector proteins into the host cytosol (Rozas and Enríquez, 2014; Zúñiga et al., 2020). As an additional virulence factor, *P. salmonis* contains lipopolysaccharides with endotoxin activity (Cvitanich et al., 1991). Moreover, *P. salmonis*-infected fish show a downregulation of genes involved in the adaptive immune response (Tacchi et al., 2011).

The molecular virulence mechanisms of *P. salmonis* are poorly described. However, it is known that extracellular extracts of *P. salmonis* contain products with cytotoxic and exotoxin effects (Rojas et al., 2013). Outer membrane vesicles containing several outer membrane proteins are released by *P. salmonis* during intracellular replication, including OmpA, which is involved in biofilm formation, adherence or invasion in other species. The chaperonin Hsep60, which is a cytoplasmic component but has been shown to be secreted by some pathogenic bacteria (Garduño et al., 1998; González-López et al., 2013) is presumably involved in adherence to host cell membranes (Ensgraber and Loos, 1992; Huesca et al., 1996). The chaperone HtpG that is involved in pathogenesis of *E. tarda* (Dang et al., 2011) is detected in the vacuoles during *P. salmonis* infections (Oliver et al., 2016).

Genome analysis of *P. salmonis* shows the presence of several other potential virulence factors (Ortiz-Severín et al., 2019). These include a Phospholipase D-like domain protein similar to the toxin Ymt from *Yersinia pestis* (Otsuka, 2016); three PipB2 pentapeptide repeate-containing proteins that potentially contribute to replication in intracellular vesicles as described for their homologs in *Salmonella enterica* (Knodler and Steele-Mortimer, 2005), an ATPase related to the flhG ATPase of *Campylobacter fetus*, which is part of the flagellar apparatus (Henderson et al., 2020), and a glutamate-1-semialdehyde-2,1-aminomutase whose *Haemophilus somnus* homolog is incolved in heme-dependent iron uptake (Villarreal, 2008).

Alteromonadales

Moritella viscosa, a member of *Moritellaceae* family, is a rod-shaped psychotrophic bacterium that is a main causative agent of winter ulcer, a cold season disease that infects a wide variety of salmonid fish in sea water. Diseased fish shown swelled skin, and develop lesions, hemorrhages and tissue necrosis. The mortality rate of winter ulcer is relatively low but the disease represents a significant fish welfare problem (Bruno et al., 1998; Løvoll et al., 2009).

Adherence of *M. viscosa* to various mucosal surface has been reported (Tunsjø et al., 2009). Gills are reported as the site of entry of *M. viscosa* from where the pathogens penetrate further into muscles, kidney, spleen and liver, a sign that the pathogen can cause systemic infections (Løvoll et al., 2009). The genome of *M. viscosa* comprises both flagella and type IV pili system genes. Adherence to fish cells is facilitated by flagella and higher level of adherence is recoded at low temperature. During adhesion by *M. viscosa*, aggregation of F-actin microfilaments of the cell line CHSE was observed and the host cell membrane disrupted (Tunsjø et al., 2009).

Moritella viscosa seem to survive in the host using escape mechanisms that suppress immune responses and help to evade the host immune system (Løvoll et al., 2009). *Moritella viscosa* contains lipopolysaccharides (LPS) and other outer membrane antigens with potential to protect the pathogen in host cells (Heidarsdottir et al., 2008). *Moritella viscosa* uses a metallopeptidase, MvP1 (see below for details) that is involved in invasion and dispersion of the pathogen (Bjornsdottir et al., 2009).

The virulence mechanisms of *M. viscosa* have not been extensively studied. The extracellular products (ECP) of the pathogen contain several secreted virulence factors with both cytotoxic and hemolytic activities that lead to the disease phenotype in Atlantic salmon (Bjornsdottir et al., 2009). The ECP contains enzymes and toxins (Benediktsdóttir and Heidarsdóttir, 2007). Genome analysis of *M. viscosa* shows the presence of three types of secretion systems: T1SS, T2SS and T6SS. In addition, vesicle-like structures have been observed by electro-microscopy (Tunsjø et al., 2009; Bjornsdottir et al., 2012).

The metallopeptidase MvP1 is an extracellular protease secreted by *M. viscosa*, formerly identified as vibrolysin with virulence related activities. By itself it is non-lethal to salmon at low concentrations. But MvP1 causes severe hemorrhages and degrades host tissues leading to necrosis, and affecting adhesion. MvP1 is suggested to be involved in invasion and dispersion in the host (Bjornsdottir et al., 2009; Björnsdóttir, 2011).

Virulence-related genes detected in several *M. viscosa* strains include the T6SS ATPase (clpV) and hemolysis co-regulated proteins (hcp) (Bjornsdottir et al., 2012) as well as Bacterioferritin homologs, which are known to enhance *Pseudomonas putida* survival in iron depleted environments (Chen et al., 2010). Further examples include a Hemagglutinin (hemG), a lectin that is produced during cell aggregation (Romeo et al., 1986) and a multifunctional autoprocessing repeats-in-toxin (martxA) from the RTX family of toxins that are secreted via a T1SS (Satchell, 2007).

Pseudomonadales

Pseudomonas anguilliseptica, is a rod-shaped and flagellated member of the *Pseudomonadaceae* family (Palleroni, 2010). *Pseudomonas anguilliseptica* is a known pathogen and a serious threat to the production of a variety of fish species cultured in marine and brackish water in different parts of the world (Stewart et al., 1983; Wiklund and Bylund, 1990; Toranzo and Barja, 1993; Lönnström et al., 1994; Berthe et al., 1995; Fernández et al., 2002; Austin and Austin, 2016). The pathogen causes a disease named "red spot disease" also known as "sekiten-byo," a hemorrhagic septicemia that was first discovered in Japan (Wakabayashi and Egusa, 1972). The disease caused by *P. anguilliseptica* is sometimes associated to winter disease; however,

this is considered as misrepresentation as some authors consider winter disease as multifactorial condition linked with cold and stressful environments (Tort et al., 1998; Contessi et al., 2006).

Despite the seriousness of the threat of *P. anguilliseptica* to the aquaculture industry worldwide, knowledge on virulence mechanisms of this pathogen is scarce. The site of entry for *P. anguilliseptica* is not clear, but the presence of flagella indicates that the pathogen has the capacity for motility and host cell adhesion (Berthe et al., 1995). *P. anguilliseptica* possesses capsular (K) antigens, which was first observed in a case of eel infection. This antigen may be used for escaping complement mediated killing by fish serum (Nakai, 1985; López-Romalde et al., 2003b).

DISCUSSION

This review can only give a glimpse on the many variations of protein secretion in commercially relevant fish pathogens. Molecular information is extremely scarce in many cases, despite the importance of the diseases caused. Part of this problem is that in most cases, the researchers working with fish diseases by tradition are not molecular biologists, but veterinarians more interested in the treatment of acute conditions using traditional antimicrobial therapies. Vaccine development in the aquaculture industry is also not based on molecular targets and studies, but rather relies on heat-killed bacterial extracts for cost reasons. The information is even more scarce for Gram-positive fish pathogens, where almost all molecular information on virulence mechanisms is only inferred from closely related human-pathogenic species. This is especially true for fish diseases with very broad and general symptoms that are hard to connect to a single pathogenic species or strain, such as streptococcosis, that is caused by diverse *Streptococcus* species depending on the host fish (Buller, 2004). A notable exception is *Mycobacterium marinum*, the causative agent of fish tuberculosis, that has received a lot of attention because it infects the model species zebrafish and thus makes a formidable model system for the study of human tuberculosis disease mechanisms (Bouz and Al Hasawi, 2018).

We strongly believe that a better molecular understanding of protein secretion in fish pathogens can help to develop more targeted therapies for the aquaculture industry, with the aim to avoid the use of antibiotics in aquatic habitats, and hope that this overview helps interested researchers in their quest to develop new vaccines or drugs.

AUTHOR CONTRIBUTIONS

SM wrote the manuscript. DL edited the manuscript. Both authors contributed to the article and approved the submitted version.

FUNDING

This work was supported by the Research Council of Norway, grant 302723.

REFERENCES

Abayneh, T., Colquhoun, D. J., and Sørum, H. (2013). *Edwardsiella piscicida* sp. nov., a novel species pathogenic to fish. *J. Appl. Microbiol.* 114, 644–654. doi: 10.1111/jam.12080

Abbott, S. L. (2011). *Klebsiella, Enterobacter*, *Citrobacter, Serratia, Plesiomonas, And Other Enterobacteriaceae*, *Manual Clinical Microbiology*, 10th Edn. Washington, DC: American Society of Microbiology, 639–657.

Abbott, S. L., and Janda, J. M. (2006). The genus edwardsiella. *Prokaryotes* 6, 72–89. doi: 10.1007/0-387-30746-x_4

Abby, S. S., Cury, J., Guglielmini, J., Néron, B., Touchon, M., and Rocha, E. P. C. (2016). Identification of protein secretion systems in bacterial genomes. *Sci. Rep.* 6:23080.

Abdelhamed, H., Lawrence, M. L., and Karsi, A. (2017). The role of TonB gene in edwardsiella ictaluri virulence. *Front. Physiol.* 8:1066. doi: 10.3389/fphys.2017.01066

Abdelhamed, H., Lu, J., Lawrence, M. L., and Karsi, A. (2016). Ferric hydroxamate uptake system contributes to *Edwardsiella ictaluri* virulence. *Microb. Pathog.* 100, 195–200. doi: 10.1016/j.micpath.2016.09.018

Abdelhamed, H., Lu, J., Shaheen, A., Abbass, A., Lawrence, M. L., and Karsi, A. (2013). Construction and evaluation of an *Edwardsiella ictaluri* fhuC mutant. *Vet. Microbiol.* 162, 858–865. doi: 10.1016/j.vetmic.2012.11.006

Aepfelbacher, M. (2004). Modulation of Rho GTPases by type III secretion system translocated effectors of Yersinia. *Rev. Physio. Biochem. Pharmacol.* 152, 65–77. doi: 10.1007/s10254-004-0035-3

Ali, A. (1996). *Aeromonas bestiarum* sp. nov. (formerly genomospecies DNA group 2 A. hydrophila), a new species isolated from non-human sources. *Med. Microbiol. Lett.* 5, 156–165.

Alice, A. F., Naka, H., and Crosa, J. H. (2008). Global gene expression as a function of the iron status of the bacterial cell: influence of differentially expressed genes in the virulence of the human pathogen *Vibrio vulnificus*. *Infect. Immun.* 76, 4019–4037. doi: 10.1128/IAI.00208-08

Allan, B. J., and Stevenson, R. M. W. (1981). Extracellular virulence factors of *Aeromonas hydrophila* in fish infections. *Can. J. Microbiol.* 27, 1114–1122. doi: 10.1139/m81-174

Almendras, F. E., and Fuentealba, I. C. (1997). Salmonid rickettsial septicemia caused by *Piscirickettsia salmonis*: a review. *Dis. Aquat. Org.* 29, 137–144. doi: 10.3354/dao029137

Alteri, C. J., and Mobley, H. L. T. (2016). The versatile type VI secretion system . *Microbiol. Spectr* 4. doi: 10.1128/microbiolspec.VMBF-0026-2015

Alvarez, B., Alvarez, J., Menendez, A., and Guijarro, J. A. (2008). A mutant in one of two exbD loci of a TonB system in *Flavobacterium psychrophilum* shows attenuated virulence and confers protection against cold water disease. *Microbiology* 154, 1144–1151. doi: 10.1099/mic.0.2007/010900-0

Alvarez, B., Secades, P., Prieto, M., McBride, M. J., and Guijarro, J. A. (2006). A mutation in Flavobacterium psychrophilum tlpB inhibits gliding motility and induces biofilm formation. *Appl. Environ. Microbiol.* 72, 4044–4053. doi: 10.1128/AEM.00128-06

Amaro, C., Sanjuán, E., Fouz, B., Pajuelo, D., Lee, C. T., Hor, L. I., et al. (2015). The Fish Pathogen *Vibrio vulnificus* biotype 2: epidemiology, phylogeny, and virulence factors involved in warm-water vibriosis. *Microbiol. Spectr.* 3. doi: 10.1128/microbiolspec.VE-0005-2014

An, S., Couteau, C., Luo, F., Neveu, J., and DuBow, M. S. (2013). Bacterial diversity of surface sand samples from the gobi and taklamaken deserts. *Microb. Ecol.* 66, 850–860. doi: 10.1007/s00248-013-0276-2

Anderson, C. J., and Kendall, M. M. (2017). *Salmonella enterica* serovar typhimurium strategies for host adaptation. *Front. Microbiol.* 8:1983. doi: 10.3389/fmicb.2017.01983

Arias, C. R., Olivares-Fuster, O., Hayden, K., Shoemaker, C. A., Grizzle, J. M., and Klesius, P. H. (2007). First report of *Yersinia ruckeri* biotype 2 in the USA. *J. Aquat. Anim. Health* 19, 35–40. doi: 10.1577/H06-011.1

Ast, V. M. I, Schoenhofen, C., Langen, G. R., Stratilo, C. W., Chamberlain, M. D., and Howard, S. P. (2002). Expression of the ExeAB complex of *Aeromonas hydrophila* is required for the localization and assembly of the ExeD secretion port multimer. *Mol. Microbiol.* 44, 217–231. doi: 10.1046/j.1365-2958.2002.02870.x

Austin, B., and Austin, D. A. (2012). *Bacterial Fish Pathogens*. Cham: Springer.

Austin, B., and Austin, D. A. (2016). *Bacterial Fish Pathogens: Disease Of Farmed And Wild Fish*. Cham: Springer.

Austin, B., Pride, A. C., and Rhodie, G. A. (2003). Association of a bacteriophage with virulence in *Vibrio harveyi*. *J. Fish. Dis.* 26, 55–58. doi: 10.1046/j.1365-2761.2003.00413.x

Austin, D. A., Robertson, P. A., and Austin, B. (2003). Recovery of a new biogroup of *Yersinia ruckeri* from diseased rainbow trout (*Oncorhynchus mykiss*, Walbaum). *Syst. Appl. Microbiol.* 26, 127–131. doi: 10.1078/072320203322337416

Avendaño-Herrera, R., Toranzo, A. E., Romalde, J. L., Lemos, M. L., and Magariños, B. (2005). Iron uptake mechanisms in the fish pathogen *Tenacibaculum maritimum*. *Appl. Environ. Microbiol.* 71, 6947–6953. doi: 10.1128/AEM.71.11.6947-6953.2005

Balado, M., Lages, M. A., Fuentes-Monteverde, J. C., Martínez-Matamoros, D., Rodríguez, J., Jiménez, C., et al. (2018). The siderophore piscibactin is a relevant virulence factor for *Vibrio anguillarum* favored at low temperatures. *Front. Microbiol.* 9:1766. doi: 10.3389/fmicb.2018.01766

Balado, M., Osorio, C. R., and Lemos, M. L. (2008). Biosynthetic and regulatory elements involved in the production of the siderophore vanchrobactin in *Vibrio anguillarum*. *Microbiology* 154, 1400–1413. doi: 10.1099/mic.0.2008/016618-0

Balado, M., Osorio, C. R., and Lemos, M. L. (2009). FvtA is the receptor for the siderophore vanchrobactin in *Vibrio anguillarum*: utility as a route of entry for vanchrobactin analogues. *Appl. Environ. Microbiol.* 75, 2775–2783. doi: 10.1128/AEM.02897-08

Balado, M., Segade, Y., Rey, D., Osorio, C. R., Rodríguez, J., Lemos, M. L., et al. (2017). Identification of the ferric-acinetobactin outer membrane receptor in *Aeromonas salmonicida* subsp. salmonicida and structure–activity relationships of synthetic acinetobactin analogues. *ACS Chem. Biol.* 12, 479–493. doi: 10.1021/acschembio.6b00805

Balado, M., Souto, A., Vences, A., Careaga, V. P., Valderrama, K., Segade, Y., et al. (2015). Two catechol siderophores, acinetobactin and amonabactin, are simultaneously produced by *Aeromonas salmonicida* subsp. *salmonicida* sharing part of the biosynthetic pathway. *ACS Chem. Biol.* 10, 2850–2860. doi: 10.1021/acschembio.5b00624

Baldissera, M. D., Souza, C. F., Junior, G. B., Moreira, K. L. S., da Veiga, M. L., da Rocha, M. I. U. M., et al. (2018). Citrobacter freundii impairs the phosphoryl transfer network in the gills of *Rhamdia quelen*: impairment of bioenergetics homeostasis. *Microb. Pathog.* 117, 157–161. doi: 10.1016/j.micpath.2018.02.040

Baldwin, T. J., and Newton, J. C. (1993). Pathogenesis of enteric septicemia of channel catfish, caused by *Edwardsiella ictaluri*: bacteriologic and light and electron microscopic findings. *J. Aquat. Anim. Health* 5, 189–198. doi: 10.1577/1548-8667(1993)005<0189:poesoc>2.3.co;2

Balebona, M. C., Andreu, M. J., Bordas, M. A., Zorrilla, I., Moriñigo, M. A., and Borrego, J. J. (1998). Pathogenicity of *Vibrio alginolyticus* for cultured gilthead sea bream (*Sparus aurata* L.). *Appl. Environ. Microbiol.* 64, 4269–4275. doi: 10.1128/AEM.64.11.4269-4275.1998

Bandeira Junior, G., Dos Santos, A. C., Souza, C. F., Baldissera, M. D., Moreira, K., da Veiga, M. L., et al. (2018). *Citrobacter freundii* infection in silver catfish (*Rhamdia quelen*): hematological and histological alterations. *Microb. Pathog.* 125, 276–280. doi: 10.1016/j.micpath.2018.09.038

Barbier, P., Rochat, T., Mohammed, H. H., Wiens, G. D., Bernardet, J.-F., Halpern, D., et al. (2020). The type IX secretion system is required for virulence of the fish pathogen *Flavobacterium psychrophilum*. *Appl. Environ. Microbiol.* 86:e01769–17.

Barbieri, J. T., and Sun, J. (2004). *Pseudomonas aeruginosa* exos and exot. *Rev. Physiol. Biochem. Pharmacol.* 152, 79–92. doi: 10.1007/s10254-004-0031-7

Barger, P. C., Liles, M. R., and Newton, J. C. (2020). Type II secretion is essential for virulence of the emerging fish pathogen, hypervirulent *Aeromonas hydrophila*. *Front. Vet. Sci.* 7:706. doi: 10.3389/fvets.2020.574113

Barghouthi, S., Young, R., Olson, M. O., Arceneaux, J. E., Clem, L. W., and Byers, B. R. (1989b). Amonabactin, a novel tryptophan-or phenylalanine-containing phenolate siderophore in *Aeromonas hydrophila*. *J. Bacteriol.* 171, 1811–1816. doi: 10.1128/jb.171.4.1811-1816.1989

Barghouthi, S., Young, R., Arceneaux, J. E. L., and Byers, B. R. (1989a). Physiological control of amonabactin biosynthesis in *Aeromonas hydrophila*. *Biol. Metals* 2, 155–160. doi: 10.1007/BF01142554

Bartkova, S., Kokotovic, B., and Dalsgaard, I. (2017). Infection routes of *Aeromonas salmonicida* in rainbow trout monitored in vivo by real-time bioluminescence imaging. *J. Fish Dis.* 40, 73–82. doi: 10.1111/jfd.12491

Beaz-Hidalgo, R., and Figueras, M. J. (2013). *Aeromonas* spp. whole genomes and virulence factors implicated in fish disease. *J. Fish Dis.* 36, 371–388. doi: 10.1111/jfd.12025

Beaz-Hidalgo, R., Latif-Eugenín, F., and Figueras, M. J. (2013). The improved PCR of the fstA (ferric siderophore receptor) gene differentiates the fish pathogen *Aeromonas salmonicida* from other *Aeromonas* species. *Vet. Microbiol.* 166, 659–663. doi: 10.1016/j.vetmic.2013.06.028

Beaz-Hidalgo, R., Magi, G. E., Balboa, S., Barja, J. L., and Romalde, J. L. (2008). Development of a PCR protocol for the detection of *Aeromonas salmonicida* in fish by amplification of the fstA (ferric siderophore receptor) gene. *Vet. Microbiol.* 128, 386–394. doi: 10.1016/j.vetmic.2007.10.004

Benediktsdóttir, E., and Heidarsdóttir, K. J. (2007). Growth and lysis of the fish pathogen *Moritella viscosa*. *Lett. Appl. Microbiol.* 45, 115–120. doi: 10.1111/j.1472-765X.2007.02161.x

Bergh, P. V., and Frey, J. (2014). *Aeromonas salmonicida* subsp. salmonicida in the light of its type-three secretion system. *Microb. Biotechnol.* 7, 381–400. doi: 10.1111/1751-7915.12091

Bernardet, J. F., and Bowman, J. P. (2006). The genus flavobacterium. *Prokaryotes* 7, 481–531.

Bernardet, J.-F., Segers, P., Vancanneyt, M., Berthe, F., Kersters, K., and Vandamme, P. (1996). Cutting a gordian knot: emended classification and description of the genus *Flavobacterium*, emended description of the family *Flavobacteriaceae*, and proposal of *Flavobacterium hydatis* nom. nov. (basonym, *Cytophaga* aquatilis Strohl and Tait 1978). *Int. J. Syst. Evol. Microbiol.* 46, 128–148. doi: 10.1099/00207713-46-1-128

Bernoth, E. M., Ellis, A. E., Midtlyng, P. J., Olivier, G., and Smith, P. (1997). *Furunculosis: Multidisciplinary Fish Disease Research*. Amsterdam: Elsevier.

Berthe, F. C. J., Michel, C., and Bernardet, J.-F. (1995). Identification of *Pseudomonas* anguilliseptica isolated from several fish species in France. *Dis. Aquat. Org.* 21, 151–155.

Bertolini, J. M., Wakabayashi, H., Watral, V. G., Whipple, M. J., and Rohovec, J. S. (1994). Electrophoretic detection of proteases from selected strains of *Flexibacter psychrophilus* and assessment of their variability. *J. Aquat. Anim. Health* 6, 224–233. doi: 10.1577/1548-8667(1994)006<0224:edopfs>2.3.co;2

Beveridge, T. J., Pouwels, P. H., Sára, M., Kotiranta, A., Lounatmaa, K., Kari, K., et al. (1997). Functions of S-layers. *FEMS Microbiol. Rev.* 20, 99–149.

Bhoite, S., van Gerven, N., Chapman, M. R., Remaut, H., Sandkvist, M., Cascales, E., et al. (2019). Curli biogenesis: bacterial amyloid assembly by the Type VIII secretion pathway. *EcoSal Plus* 8. doi: 10.1128/ecosalplus.ESP-0037-2018

Björnsdóttir, B. (2011). *Moritella viscosa Virulence – Extracellular Products And Host-Pathogen Interaction*. Ph.D. thesis. Reykjavík: University of Iceland.

Bjornsdottir, B., Fridjonsson, O. H., Magnusdottir, S., Andresdottir, V., Hreggvidsson, G. O., and Gudmundsdottir, B. K. (2009). Characterisation of an extracellular vibriolysin of the fish pathogen *Moritella viscosa*. *Vet. Microbiol.* 136, 326–334. doi: 10.1016/j.vetmic.2008.11.020

Bjornsdottir, B., Hjerde, E., Bragason, B. T., Gudmundsdottir, T., Willassen, N. P., and Gudmundsdottir, B. K. (2012). Identification of type VI secretion systems in *Moritella viscosa*. *Vet. Microbiol.* 158, 436–442.

Bleves, S., Viarre, V., Salacha, R., Michel, G. P. F., Filloux, A., and Voulhoux, R. (2010). Protein secretion systems in *Pseudomonas aeruginosa*: a wealth of pathogenic weapons. *Int. J. Med. Microbiol.* 300, 534–543. doi: 10.1016/j.ijmm.2010.08.005

Boardman, B. K., and Satchell, K. J. F. (2004). *Vibrio cholerae* strains with mutations in an atypical type I secretion system accumulate RTX toxin intracellularly. *J. Bacteriol.* 186, 8137–8143. doi: 10.1128/JB.186.23.8137-8143.2004

Bouz, G., and Al Hasawi, N. (2018). The zebrafish model of tuberculosis – no lungs needed. *Crit. Rev. Microbiol.* 44, 779–792. doi: 10.1080/1040841x.2018.1523132

Boyd, A. P., and Cornelis, G. R. (2001). "Chapter 6 – *yersinia*," in *Principles Of Bacterial Pathogenesis*, ed. E. A. Groisman (San Diego, CA: Academic Press), 227–264.

Braun, M., Stuber, K., Schlatter, Y., Wahli, T., Kuhnert, P., and Frey, J. (2002). Characterization of an ADP-ribosyltransferase toxin (AexT) from *Aeromonas salmonicida* subsp. salmonicida. *J. Bacteriol.* 184, 1851–1858. doi: 10.1128/JB.184.7.1851-1858.2002

Braun, T. F., and McBride, M. J. (2005). *Flavobacterium johnsoniae* GldJ is a lipoprotein that is required for gliding motility. *J. Bacteriol.* 187, 2628–2637. doi: 10.1128/JB.187.8.2628-2637.2005

Braun, T. F., Khubbar, M. K., Saffarini, D. A., and McBride, M. J. (2005). *Flavobacterium johnsoniae* gliding motility genes identified by mariner mutagenesis. *J. Bacteriol.* 187, 6943–6952. doi: 10.1128/JB.187.20.6943-6952.2005

Braun, V., Hantke, K., and Koester, W. (1998). Bacterial iron transport: mechanisms, genetics, and regulation. *Met. Ions Biol. Syst.* 35, 67–146.

Broberg, C. A., Zhang, L., Gonzalez, H., Laskowski-Arce, M. A., and Orth, K. (2010). A Vibrio effector protein is an inositol phosphatase and disrupts host cell membrane integrity. *Science* 329, 1660–1662. doi: 10.1126/science.1192850

Broeck, D. V., Horvath, C., and De Wolf, M. J. (2007). *Vibrio cholerae*: cholera toxin. *Internat. J. Biochem. Cell Biol.* 39, 1771–1775. doi: 10.1016/j.biocel.2007.07.005

Bruno, D. W., Griffiths, J., Petrie, J., and Hastings, T. S. (1998). *Vibrio viscosus* in farmed Atlantic salmon *Salmo salar* in Scotland: field and experimental observations. *Dis. Aquat. Org.* 34, 161–166. doi: 10.3354/dao034161

Buckley, J. T., Halasa, L. N., and MacIntyre, S. (1982). Purification and partial characterization of a bacterial phospholipid: cholesterol acyltransferase. *J. Biol. Chem.* 257, 3320–3325.

Buller, N. B. (2004). *Bacteria From Fish And Other Aquatic Animals: A Practical Identification Manual*. Wallingford: CABI.

Burdette, D. L., Seemann, J., and Orth, K. (2009). Vibrio VopQ induces PI3-kinase-independent autophagy and antagonizes phagocytosis. *Mol. Microbiol.* 73, 639–649. doi: 10.1111/j.1365-2958.2009.06798.x

Burdette, L. A., Leach, S. A., Wong, H. T., and Tullman-Ercek, D. (2018). Developing Gram-negative bacteria for the secretion of heterologous proteins. *Microb. Cell Fact.* 17, 196–196.

Burr, S. E., Stuber, K., and Frey, J. (2003). The ADP-ribosylating toxin, AexT, from *Aeromonas salmonicida* subsp. *salmonicida* is translocated via a type III secretion pathway. *J. Bacteriol.* 185, 6583–6591. doi: 10.1128/JB.185.22.6583-6591.2003

Burr, S. E., Stuber, K., Wahli, T., and Frey, J. (2002). Evidence for a type III secretion system in *Aeromonas salmonicida* subsp. *salmonicida*. *J. Bacteriol.* 184, 5966–5970. doi: 10.1128/jb.184.21.5966-5970.2002

Byers, B. R., Massad, G., Barghouthi, S., and Arceneaux, J. E. (1991). Iron acquisition and virulence in the motile aeromonads: siderophore-dependent and -independent systems. *Experientia* 47, 416–418.

Cahill, M. M. (1990). A review virulence factors in motile *Aeromonas* species. *J. Appl. Bacteriol.* 69, 1–16. doi: 10.1501/vetfak_0000000684

Cai, S. H., Wu, Z. H., Jian, J. C., and Lu, Y. S. (2007). Cloning and expression of gene encoding the thermostable direct hemolysin from *Vibrio alginolyticus* strain HY9901, the causative agent of vibriosis of crimson snapper (*Lutjanus erythopterus*). *J. Appl. Microbiol.* 103, 289–296. doi: 10.1111/j.1365-2672.2006.03250.x

Calvez, S., Gantelet, H., Blanc, G., Douet, D. G., and Daniel, P. (2014). *Yersinia ruckeri* Biotypes 1 and 2 in France: presence and antibiotic susceptibility. *Dis. Aquat. Organ.* 109, 117–126. doi: 10.3354/dao02725

Cascón, A., Yugueros, J., Temprano, A., Sánchez, M., Hernanz, C., Luengo, J. M., et al. (2000). A major secreted elastase is essential for pathogenicity of *Aeromonas hydrophila*. *Infect. Immun.* 68, 3233–3241. doi: 10.1128/IAI.68.6.3233-3241.2000

Castillo, D., Christiansen, R. H., Dalsgaard, I., Madsen, L., and Middelboe, M. (2015). Bacteriophage resistance mechanisms in the fish pathogen *Flavobacterium psychrophilum*: linking genomic mutations to changes in bacterial virulence factors. *Appl. Environ. Microbiol.* 81, 1157–1167. doi: 10.1128/AEM.03699-14

Castro, N., Osorio, C. R., Buján, N., Fuentes, J. C., Rodríguez, J., Romero, M., et al. (2016). Insights into the virulence-related genes of *Edwardsiella tarda* isolated from turbot in Europe: genetic homogeneity and evidence for vibrioferrin production. *J. Fish Dis.* 39, 565–576. doi: 10.1111/jfd.12389

Cavaillon, J. M. (2018). Exotoxins and endotoxins: inducers of inflammatory cytokines. *Toxicon* 149, 45–53. doi: 10.1016/j.toxicon.2017.10.016

Chakraborty, S., Sivaraman, J., Leung, K. Y., and Mok, Y.-K. (2011). Two-component PhoB-PhoR regulatory system and ferric uptake regulator sense phosphate and iron to control virulence genes in type III and VI secretion systems of *Edwardsiella tarda*. *J. Biol. Chem.* 286, 39417–39430. doi: 10.1074/jbc.M111.295188

Chakraborty, T., Schmid, A., Notermans, S., and Benz, R. (1990). Aerolysin of *Aeromonas sobria*: evidence for formation of ion-permeable channels and comparison with alpha-toxin of *Staphylococcus aureus*. *Infect. Immun.* 58, 2127–2132. doi: 10.1128/iai.58.7.2127-2132.1990

Chen, J. D., Lai, S. Y., and Huang, S. L. (1996). Molecular cloning, characterization, and sequencing of the hemolysin gene from *Edwardsiella tarda*. *Arch. Microbiol.* 165, 9–17. doi: 10.1007/s002030050290

Chen, S., Bleam, W. F., and Hickey, W. J. (2010). Molecular analysis of two bacterioferritin genes, bfralpha; and bfrbeta, in the model rhizobacterium *Pseudomonas putida* KT2440. *Appl. Environ. Microbiol.* 76, 5335–5343. doi: 10.1128/AEM.00215-10

Chen, S., Blom, J., Loch, T. P., Faisal, M., and Walker, E. D. (2017). The emerging fish pathogen *Flavobacterium spartansii* isolated from *Chinook salmon*: comparative genome analysis and molecular manipulation. *Front. Microbiol.* 8:2339. doi: 10.3389/fmicb.2017.02339

Cheng, Z.-X., Gong, Q.-Y., Wang, Z., Chen, Z.-G., Ye, J.-Z., Li, J., et al. (2017). *Edwardsiella tarda* tunes tricarboxylic acid cycle to evade complement-mediated killing. *Front. Immunol.* 8:1706. doi: 10.3389/fimmu.2017.01706

Chopra, A. K., Houston, C. W., Peterson, J. W., and Jin, G.-F. (1993). Cloning, expression, and sequence analysis of a cytolytic enterotoxin gene from *Aeromonas hydrophila*. *Can. J. Microbiol.* 39, 513–523. doi: 10.1139/m93-073

Christie, P. J., Whitaker, N., and González-Rivera, C. (2014). Mechanism and structure of the bacterial type IV secretion systems. *Biochim. Biophys. Acta Mol. Cell Res.* 1843, 1578–1591.

Chu, S., Cavaignac, S., Feutrier, J., Phipps, B. M., Kostrzynska, M., Kay, W. W., et al. (1991). Structure of the tetragonal surface virulence array protein and gene of *Aeromonas salmonicida*. *J. Biol. Chem.* 266, 15258–15265.

Cianciotto, N. P., and White, R. C. (2017). Expanding role of type II secretion in bacterial pathogenesis and beyond. *Infect. Immun.* 85:e00014–e17.

Citterio, B., and Biavasco, F. (2015). *Aeromonas hydrophila* virulence. *Virulence* 6, 417–418.

Coburn, B., Sekirov, I., and Finlay, B. B. (2007). Type III secretion systems and disease. *Clin. Microbiol. Rev.* 20, 535–549.

Coleman, G., and Whitby, P. W. (1993). A comparison of the amino acid sequence of the serine protease of the fish pathogen *Aeromonas salmonicida* subsp. *salmonicida* with those of other subtilisin-type enzymes relative to their substrate-binding sites. *J. Gen. Microbiol.* 139, 245–249. doi: 10.1099/00221287-139-2-245

Colwell, R. R., MacDonell, M. T., and De Ley, J. (1986). Proposal to recognize the family *Aeromonadaceae fam*. nov. *Int. J. Syst. Evol Microbiol.* 36, 473–477.

Contessi, B., Volpatti, D., Gusmani, L., and Galeotti, M. (2006). Evaluation of immunological parameters in farmed gilthead sea bream, *Sparus aurata* L., before and during outbreaks of 'winter syndrome'. *J. Fish Dis.* 29, 683–690. doi: 10.1111/j.1365-2761.2006.00765.x

Costa, T. R. D., Felisberto-Rodrigues, C., Meir, A., Prevost, M. S., Redzej, A., Trokter, M., et al. (2015). Secretion systems in Gram-negative bacteria: structural and mechanistic insights. *Nat. Rev. Microbiol.* 13, 343–359. doi: 10.1038/nrmicro3456

Crabill, E., Karpisek, A., and Alfano, J. R. (2012). The *Pseudomonas syringae* HrpJ protein controls the secretion of type III translocator proteins and has a virulence role inside plant cells. *Mol. Microbiol.* 85, 225–238. doi: 10.1111/j.1365-2958.2012.08097.x

Craig, L., Forest, K. T., and Maier, B. (2019). Type IV pili: dynamics, biophysics and functional consequences. *Nat. Rev. Microbiol.* 17, 429–440. doi: 10.1038/s41579-019-0195-4

Cress, B. F., Englaender, J. A., He, W., Kasper, D., Linhardt, R. J., and Koffas, M. A. G. (2014). Masquerading microbial pathogens: capsular polysaccharides mimic host-tissue molecules. *FEMS Microbiol. Rev.* 38, 660–697. doi: 10.1111/1574-6976.12056

Croxatto, A., Lauritz, J., Chen, C., and Milton, D. L. (2007). *Vibrio anguillarum* colonization of rainbow trout integument requires a DNA locus involved in exopolysaccharide transport and biosynthesis. *Environ. Microbiol.* 9, 370–382. doi: 10.1111/j.1462-2920.2006.01147.x

Cvitanich, J. D., Garaten, O., and Smith, C. E. (1991). The isolation of a rickettsia-like organism causing disease and mortality in *Chilean salmonids* and its confirmation by Koch's postulate. *J. Fish Dis.* 14, 121–145. doi: 10.1111/j.1365-2761.1991.tb00584.x

Dacanay, A., Knickle, L., Solanky, K. S., Boyd, J. M., Walter, J. A., Brown, L. L., et al. (2006). Contribution of the type III secretion system (TTSS) to virulence of *Aeromonas salmonicida* subsp. *salmonicida*. *Microbiology* 152, 1847–1856. doi: 10.1099/mic.0.28768-0

Dai, F., Li, Y., Shao, Y., Li, C., and Zhang, W. (2020). FliC of *Vibrio splendidus*-related strain involved in adhesion to *Apostichopus japonicus*. *Microb. Pathog.* 149:104503. doi: 10.1016/j.micpath.2020.104503

Dai, F., Zhang, W., Zhuang, Q., Shao, Y., Zhao, X., Lv, Z., et al. (2019). Dihydrolipoamide dehydrogenase of *Vibrio splendidus* is involved in adhesion to *Apostichopus japonicus*. *Virulence* 10, 839–848. doi: 10.1080/21505594.2019.1682761

Dallaire-Dufresne, S., Barbeau, X., Sarty, D., Tanaka, K. H., Denoncourt, A. M., Lagüe, P., et al. (2013). *Aeromonas salmonicida* Ati2 is an effector protein of the type three secretion system. *Microbiology* 159, 1937–1945. doi: 10.1099/mic.0.067959-0

Dalsgaard, I., and Madsen, L. (2000). Bacterial pathogens in rainbow trout, *Oncorhynchus mykiss* (Walbaum), reared at Danish freshwater farms. *J. Fish Dis.* 23, 199–209. doi: 10.1046/j.1365-2761.2000.00242.x

Dang, W., Hu, Y., and Sun, L. (2011). HtpG is involved in the pathogenesis of *Edwardsiella tarda*. *Vet. Microbiol.* 152, 394–400. doi: 10.1016/j.vetmic.2011.05.030

Davies, R. L., and Frerichs, G. N. (1989). Morphological and biochemical differences among isolates of *Yersinia ruckeri* obtained from wide geographical areas. *J. Fish Dis.* 12, 357–365.

de Haan, L., and Hirst, T. R. (2000). Cholera toxin and related enterotoxins: a cell biological and immunological perspective. *J. Nat. Toxins* 9, 281–297.

Declercq, A. M., Haesebrouck, F., Van den Broeck, W., Bossier, P., and Decostere, A. (2013). Columnaris disease in fish: a review with emphasis on bacterium-host interactions. *Vet. Res.* 44:27. doi: 10.1186/1297-9716-44-27

Decostere, A., Haesebrouck, F., Van Driessche, E., Charlier, G., and Ducatelle, R. (1999). Characterization of the adhesion of *Flavobacterium columnare* (*Flexibacter columnaris*) to gill tissue. *J. Fish Dis.* 22, 465–474.

Deng, W., Marshall, N. C., Rowland, J. L., McCoy, J. M., Worrall, L. J., Santos, A. S., et al. (2017). Assembly, structure, function and regulation of type III secretion systems. *Nat. Rev. Microbiol.* 15, 323–337. doi: 10.1038/nrmicro.2017.20

Denkin, S. M., and Nelson, D. R. (1999). Induction of protease activity in *Vibrio anguillarum* by gastrointestinal mucus. *Appl. Environ. Microbiol.* 65, 3555–3560. doi: 10.1128/AEM.65.8.3555-3560.1999

Denkin, S. M., and Nelson, D. R. (2004). Regulation of *Vibrio anguillarum* empA metalloprotease expression and its role in virulence. *Appl. Environ. Microbiol.* 70, 4193–4204. doi: 10.1128/AEM.70.7.4193-4204.2004

Dubytska, L. P., Rogge, M. L., Thune, R. L., and Blokesch, M. (2016). Identification and characterization of putative translocated effector proteins of the *Edwardsiella ictaluri* Type III secretion system. *mSphere* 1:e00039–e16. doi: 10.1128/mSphere.00039-16

Duchaud, E., Boussaha, M., Loux, V., Bernardet, J. F., Michel, C., Kerouault, B., et al. (2007). Complete genome sequence of the fish pathogen *Flavobacterium psychrophilum*. *Nat. Biotechnol.* 25, 763–769. doi: 10.1038/nbt1313

Dulberger, C. L., Rubin, E. J., and Boutte, C. C. (2020). The mycobacterial cell envelope — a moving target. *Nat. Rev. microbiol.* 18, 47–59. doi: 10.1038/s41579-019-0273-7

Dumetz, F., LaPatra, S. E., Duchaud, E., Claverol, S., and Le Henaff, M. (2007). The *Flavobacterium psychrophilum* OmpA, an outer membrane glycoprotein, induces a humoral response in rainbow trout. *J. Appl. Microbiol.* 103, 1461–1470. doi: 10.1111/j.1365-2672.2007.03359.x

Dumpala, P. R., Gülsoy, N., Lawrence, M. L., and Karsi, A. (2010). Proteomic analysis of the fish pathogen *Flavobacterium columnare*. *Proteome Sci.* 8, 26–26.

Ellis, A. E., Burrows, A. S., and Stapleton, K. J. (1988). Lack of relationship between virulence of *Aeromonas salmonicida* and the putative virulence factors: a-layer, extracellular proteases and extracellular haemolysins. *J. Fish Dis.* 11, 309–323. doi: 10.1111/j.1365-2761.1988.tb01227.x

Endo, Y., Takahashi, M., and Fujita, T. (2006). Lectin complement system and pattern recognition. *Immunobiology* 211, 283–293. doi: 10.1016/j.imbio.2006.01.003

Ensgraber, M., and Loos, M. (1992). A 66-kilodalton heat shock protein of *Salmonella* typhimurium is responsible for binding of the bacterium to intestinal mucus. *Infect. Immun.* 60, 3072–3078. doi: 10.1128/iai.60.8.3072-3078.1992

Espelid, S., Hjelmeland, K., and Jørgensen, T. (1987). The specificity of *Atlantic salmon* antibodies made against the fish pathogen *Vibrio salmonicida*, establishing the surface protein VS-P1 as the dominating antigen. *Dev. Comp. Immunol.* 11, 529–537. doi: 10.1016/0145-305x(87)90042-5

Ewing, W. H., Mcwhorter, A. C., Escobar, M. R., and Lubin, A. H. (1965). Edwardsiella, a new genus of *Enterobacteriaceae* based on a new species. *E. tarda*. *Int. J. Syst. Evol. Microbiol.* 15, 33–38. doi: 10.1099/00207713-15-1-33

Fadl, A. A., Galindo, C. L., Sha, J., Erova, T. E., Houston, C. W., Olano, J. P., et al. (2006). Deletion of the genes encoding the type III secretion system and cytotoxic enterotoxin alters host responses to *Aeromonas hydrophila* infection. *Microb. Pathog.* 40, 198–210. doi: 10.1016/j.micpath.2006.01.003

Fang, H. M., Ge, R., and Sin, Y. M. (2004). Cloning, characterisation and expression of *Aeromonas hydrophila* major adhesin. *Fish Shellfish Immunol.* 16, 645–658. doi: 10.1016/j.fsi.2003.10.003

FAO (2020). *The State Of World Fisheries And Aquaculture (SOFIA) 2020*. Rome: FAO.

Fast, M. D., Tse, B., Boyd, J. M., and Johnson, S. C. (2009). Mutations in the *Aeromonas salmonicida* subsp. *salmonicida* type III secretion system affect *Atlantic salmon* leucocyte activation and downstream immune responses. *Fish Shellfish Immunol.* 27, 721–728. doi: 10.1016/j.fsi.2009.09.009

Fehr, D., Casanova, C., Liverman, A., Blazkova, H., Orth, K., Dobbelaere, D., et al. (2006). AopP, a type III effector protein of *Aeromonas salmonicida*, inhibits the NF-κB signalling pathway. *Microbiology* 152, 2809–2818. doi: 10.1099/mic.0.28889-0

Fernández, L., Márquez, I., and Guijarro, J. A. (2004). Identification of specific in vivo-induced (ivi) genes in *Yersinia ruckeri* and analysis of ruckerbactin, a catecholate siderophore iron acquisition system. *Appl. Environ. Microbiol.* 70, 5199–5207. doi: 10.1128/aem.70.9.5199-5207.2004

Fernández, L., Prieto, M., and Guijarro, J. A. (2007). The iron- and temperature-regulated haemolysin YhlA is a virulence factor of *Yersinia ruckeri*. *Microbiology* 153, 483–489. doi: 10.1099/mic.0.29284-0

Fernández, L., Secades, P., Lopez, J. R., Márquez, I., and Guijarro, J. A. (2002). Isolation and analysis of a protease gene with an ABC transport system in the fish pathogen *Yersinia ruckeri*: insertional mutagenesis and involvement in virulence. *Microbiology* 148, 2233–2243. doi: 10.1099/00221287-148-7-2233

Fernández-Gómez, B., Richter, M., Schüler, M., Pinhassi, J., Acinas, S. G., González, J. M., et al. (2013). Ecology of marine Bacteroidetes: a comparative genomics approach. *ISME J.* 7, 1026–1037. doi: 10.1038/ismej.2012.169

Fierer, N., Leff, J. W., Adams, B. J., Nielsen, U. N., Bates, S. T., Lauber, C. L., et al. (2012). Cross-biome metagenomic analyses of soil microbial communities and their functional attributes. *Proc. Natl. Acad. Sci. U.S.A.* 109, 21390–21395. doi: 10.1073/pnas.1215210110

Figueroa, J., Cárcamo, J., Yañez, A., Olavarria, V., Ruiz, P., Manríquez, R., et al. (2019). Addressing viral and bacterial threats to salmon farming in Chile: historical contexts and perspectives for management and control. *Rev. Aquac.* 11, 299–324.

Finlay, B. B., and Falkow, S. (1997). Common themes in microbial pathogenicity revisited. *Microbiol. Mol. Biol. Rev.* 61, 136–169. doi: 10.1128/mmbr.61.2.136-169.1997

Fivaz, M., Abrami, L., Tsitrin, Y., and Van Der Goot, F. G. (2001). Aerolysin from *Aeromonas hydrophila* and related toxins. *Curr. Top. Microbiol. Immunol.* 257, 35–52. doi: 10.1007/978-3-642-56508-3_3

Flannagan, R. S., Aubert, D., Kooi, C., Sokol, P. A., and Valvano, M. A. (2007). Burkholderia cenocepacia requires a periplasmic HtrA protease for growth under thermal and osmotic stress and for survival in vivo. *Infect. Immun.* 75, 1679–1689. doi: 10.1128/IAI.01581-06

Fouz, B., Barja, J. L., Amaro, C., Rivas, C., and Toranzo, A. E. (1993). Toxicity of the extracellular products of *Vibrio damsela* isolated from diseased fish. *Curr. Microbiol.* 27, 341–347. doi: 10.3354/dao02275

Fouz, B., Zarza, C., and Amaro, C. (2006). First description of non-motile *Yersinia ruckeri* serovar I strains causing disease in rainbow trout, *Oncorhynchus mykiss* (Walbaum), cultured in Spain. *J. Fish Dis.* 29, 339–346. doi: 10.1111/j.1365-2761.2006.00723.x

Frans, I., Michiels, C. W., Bossier, P., Willems, K. A., Lievens, B., and Rediers, H. (2011). *Vibrio anguillarum* as a fish pathogen: virulence factors, diagnosis and prevention. *J. Fish Dis.* 34, 643–661. doi: 10.1111/j.1365-2761.2011.01279.x

Frey, J., and Origgi, F. C. (2016). Type III secretion system of *Aeromonas salmonicida* undermining the host's immune response. *Front. Mar. Sci.* 3:130. doi: 10.3389/fmars.2016.00130

Fryer, J. L., Lannan, C. N., Garces, L. H., Larenas, J. J., and Smith, P. A. (1990). Isolation of a rickettsiales-like organism from diseased coho salmon (*Oncorhynchus kisutch*) in Chile. *Fish Pathol.* 25, 107–114. doi: 10.3147/jsfp.25.107

Fryer, J., Lannan, C., Giovannoni, S., and Wood, N. (1992). *Piscirickettsia salmonis* gen. nov., sp. nov., the causative agent of an epizootic disease in salmonid fishes. *Int. J. Syst. Evol. Microbiol.* 42, 120–126. doi: 10.1099/00207713-42-1-120

Funahashi, T., Moriya, K., Uemura, S., Miyoshi, S. I., Shinoda, S., Narimatsu, S., et al. (2002). Identification and characterization of pvuA, a gene encoding the ferric vibrioferrin receptor protein in *Vibrio parahaemolyticus*. *J. Bacteriol.* 184, 936–946. doi: 10.1128/jb.184.4.936-946.2002

Galán, J. E., Lara-Tejero, M., Marlovits, T. C., and Wagner, S. (2014). Bacterial type III secretion systems: specialized nanomachines for protein delivery into target cells. *Annu. Rev. Microbiol.* 68, 415–438. doi: 10.1146/annurev-micro-092412-155725

Gallique, M., Decoin, V., Barbey, C., Rosay, T., Feuilloley, M. G. J., Orange, N., et al. (2017). Contribution of the *Pseudomonas fluorescens* MFE01 type VI secretion system to biofilm formation. *PLoS One* 12:e0170770. doi: 10.1371/journal.pone.0170770

Garduño, R. A., Faulkner, G., Trevors, M. A., Vats, N., and Hoffman, P. S. (1998). Immunolocalization of Hsp60 in *Legionella pneumophila*. *J. Bacteriol.* 180, 505–513. doi: 10.1128/jb.180.3.505-513.1998

Gerlach, R. G., and Hensel, M. (2007). Protein secretion systems and adhesins: the molecular armory of Gram-negative pathogens. *Int. J. Med. Microbiol.* 297, 401–415. doi: 10.1016/j.ijmm.2007.03.017

González-López, M. A., Velázquez-Guadarrama, N., Romero-Espejel, M. E., and Olivares-Trejo, J. D. (2013). *Helicobacter* pylori secretes the chaperonin GroEL (HSP60), which binds iron. *FEBS Lett.* 587, 1823–1828. doi: 10.1016/j.febslet.2013.04.048

Gorasia, D. G., Veith, P. D., and Reynolds, E. C. (2020). The Type IX secretion system: advances in structure, function and organisation. *Microorganisms* 8:1173. doi: 10.3390/microorganisms8081173

Gourzioti, E., Kolygas, M. N., Athanassopoulou, F., and Babili, V. (2016). Tenacibaculosis in aquaculture farmed marine fish. *J. Hell. Vet. Medical Soc.* 67, 21–32. doi: 10.12681/jhvms.15620

Grass, S., Buscher, A. Z., Swords, W. E., Apicella, M. A., Barenkamp, S. J., Ozchlewski, N., et al. (2003). The *Haemophilus influenzae* HMW1 adhesin is glycosylated in a process that requires HMW1C and phosphoglucomutase, an enzyme involved in lipooligosaccharide biosynthesis. *Mol. Microbiol.* 48, 737–751. doi: 10.1046/j.1365-2958.2003.03450.x

Green, E. R., and Mecsas, J. (2016). Bacterial secretion systems: an overview. *Microbiol. Spectr.* 4. doi: 10.1128/microbiolspec.VMBF-0012-2015

Griffin, B. R. (1987). Columnaris disease: recent advances in research. *Aquac. Mag.* 13, 48–50.

Grisez, L., Sorgeloos, P., and Ollevier, F. (1996). Mode of infection and spread of *Vibrio anguillarum* in turbot *Scophthalmus maximus* larvae after oral challenge through live feed. *Dis. Aqu. Org.* 26, 181–187.

Guan, L., Santander, J., Mellata, M., Zhang, Y., and Curtiss, R. I. (2013). Identification of an iron acquisition machinery in *Flavobacterium columnare*. *Dis. Aquat. Organ.* 106, 129–138. doi: 10.3354/dao02635

Guardiola, F. A., Mabrok, M., Machado, M., Azeredo, R., Afonso, A., Esteban, M. A., et al. (2019). Mucosal and systemic immune responses in *Senegalese sole* (*Solea senegalensis* Kaup) bath challenged with *Tenacibaculum maritimum*: a time-course study. *Fish Shellfish Immunol.* 87, 744–754. doi: 10.1016/j.fsi.2019.02.015

Guerry, P. (2007). Campylobacter flagella: not just for motility. *Trends Microbiol.* 15, 456–461.

Guo, R. H., Lim, J. Y., My, D.N. Tra, Jo, S. J., Park, J. U., Rhee, J. H., et al. (2018). *Vibrio vulnificus* RtxA1 toxin expression upon contact with host cells is RpoS-dependent. *Front. Cell. Infect. Microbiol* 8:70. doi: 10.3389/fcimb.2018.00070

Guzman-Murillo, M., Merino-Contreras, M. L., and Ascencio, F. (2000). Interaction between *Aeromonas veronii* and epithelial cells of spotted sand bass (*Paralabrax maculatofasciatus*) in culture. *J. Appl. Microbiol.* 88, 897–906. doi: 10.1046/j.1365-2672.2000.01061.x

Hacker, J., and Carniel, E. (2001). Ecological fitness, genomic islands and bacterial pathogenicity. *EMBO Rep.* 2, 376–381. doi: 10.1093/embo-reports/kve097

Hacker, J., and Kaper, J. B. (1999). "The concept of pathogenicity islands, pathogenicity islands and other mobile virulence elements," in *Pathogenicity Islands and Other Mobile Virulence Elements*, eds J. B. Kaper and J. Hacker (Washington, DC: ASM Press), 1–11. doi: 10.1128/9781555818173.ch1

Hahnke, R. L., Meier-Kolthoff, J. P., García-López, M., Mukherjee, S., Huntemann, M., Ivanova, N. N., et al. (2016). Genome-based taxonomic classification of bacteroidetes. *Front. Microbiol.* 7:2003. doi: 10.3389/fmicb.2016.02003

Halpern, M., and Izhaki, I. (2017). Fish as hosts of *Vibrio cholerae*. *Front. Microbiol.* 8:282. doi: 10.3389/fmicb.2017.00282

Ham, H., and Orth, K. (2012). The role of type III secretion system 2 in *Vibrio parahaemolyticus* pathogenicity. *J. Microbiol.* 50, 719–725. doi: 10.1007/s12275-012-2550-2

Han, H. J., Kim, D. H., Lee, D. C., Kim, S. M., and Park, S. I. (2006). Pathogenicity of *Edwardsiella tarda* to olive flounder, *Paralichthys olivaceus* (temminck & schlegel). *J. Fish Dis.* 29, 601–609. doi: 10.1111/j.1365-2761.2006.00754.x

Han, Y., Mo, Z., Xiao, P., Hao, B., Li, J., and Yang, G. (2011). Characterization of EmpA protease in *Vibrio anguillarum* M3. *J. Ocean Univ. China* 10, 379–384. doi: 10.1007/s11802-011-1781-x

Hartland, E., and Leong, J. (2013). Enteropathogenic and enterohemorrhagic *E. coli*: ecology, pathogenesis, and evolution. *Front. Cell. Infect. Microbiol.* 3:15. doi: 10.3389/fcimb.2013.00015

Hawke, J. P., McWhorter, A. C., Steigerwalt, A. G., and Brenner, D. J. (1981). *Edwardsiella ictaluri* sp. nov., the causative agent of enteric septicemia of catfish. *Int. J. Syst. Evol. Microbiol.* 31, 396–400. doi: 10.1099/00207713-31-4-396

Heidarsdottir, K. J., Gravningen, K., and Benediktsdottir, E. (2008). Antigen profiles of the fish pathogen *Moritella viscosa* and protection in fish. *J. Appl. Microbiol.* 104, 944–951. doi: 10.1111/j.1365-2672.2007.03639.x

Henderson, L. D., Matthews-Palmer, T. R. S., Gulbronson, C. J., Ribardo, D. A., Beeby, M., Hendrixson, D. R., et al. (2020). Diversification of *Campylobacter jejuni* flagellar C-ring composition impacts its structure and function in motility, flagellar assembly, and cellular processes. *mBio* 11:e02286–19. doi: 10.1128/mBio.02286-19

Heo, G. J., Wakabayashi, H., and Watabe, S. (1990). Purification and characterization of pili from *Flavobacterium branchiophila*. *Fish Pathol.* 25, 21–27. doi: 10.3147/jsfp.25.21

Hirono, I., and Aoki, T. (1993). Cloning and characterization of three hemolysin genes from *Aeromonas salmonicida*. *Microb. Pathog.* 15, 269–282. doi: 10.1006/mpat.1993.1077

Hirono, I., Masuda, T., and Aoki, T. (1996). Cloning and detection of the hemolysin gene of *Vibrio anguillarum*. *Microb. Pathog.* 21, 173–182. doi: 10.1006/mpat.1996.0052

Hirono, I., Tange, N., and Aoki, T. (1997). Iron-regulated haemolysin gene from *Edwardsiella tarda*. *Mol. Microbiol.* 24, 851–856. doi: 10.1046/j.1365-2958.1997.3971760.x

Hiyoshi, H., Kodama, T., Iida, T., and Honda, T. (2010). Contribution of *Vibrio parahaemolyticus* virulence factors to cytotoxicity, enterotoxicity, and lethality in mice. *Infect. Immun.* 78, 1772–1780. doi: 10.1128/IAI.01051-09

Hiyoshi, H., Kodama, T., Saito, K., Gotoh, K., Matsuda, S., Akeda, Y., et al. (2011). VopV, an F-actin-binding Type III secretion effector, is required for *Vibrio parahaemolyticus*-induced enterotoxicity. *Cell Host Microbe* 10, 401–409. doi: 10.1016/j.chom.2011.08.014

Hjelmeland, K., Stensvaag, K., Jørgensen, T., and Espelid, S. (1988). Isolation and characterization of a surface layer antigen from *Vibrio salmonicida*. *J. Fish Dis.* 11, 197–205. doi: 10.1111/j.1365-2761.1988.tb00540.x

Hjeltnes, B., Bang-Jensen, B., Bornø, G., Haukaas, A., and Walde, C. (2017). *The Health Situation In Norwegian Aquaculture 2016*. Oslo: The Norwegian Veterinary Institute, 127.

Ho, A. S., Mietzner, T. A., Smith, A. J., and Schoolnik, G. K. (1990). The pili of *Aeromonas hydrophila*: identification of an environmentally regulated "mini pilin". *J. Exp. Med.* 172, 795–806. doi: 10.1084/jem.172.3.795

Högfors-Rönnholm, E., and Wiklund, T. (2010). Hemolytic activity in *Flavobacterium psychrophilum* is a contact-dependent, two-step mechanism

and differently expressed in smooth and rough phenotypes. *Microb. Pathog.* 49, 369–375. doi: 10.1016/j.micpath.2010.08.002

Holland, I. B., Schmitt, L., and Young, J. (2005). Type 1 protein secretion in bacteria, the ABC-transporter dependent pathway (Review). *Mol. Membr. Biol.* 22, 29–39. doi: 10.1080/09687860500042013

Holt, R. A., Amandi, A., Rohovec, J. S., and Fryer, J. L. (1989). Relation of water temperature to bacterial cold-water disease in coho salmon, chinook salmon, and rainbow trout. *J. Aquat. Anim. Health* 1, 94–101.

Horne, M. T., and Baxendale, A. (1983). The adhesion of *Vibrio anguillarum* to host tissues and its role in pathogenesis. *J. Fish Dis.* 6, 461–471. doi: 10.1111/j.1365-2761.1983.tb00100.x

Hossain, M. J., Waldbieser, G. C., Sun, D., Capps, N. K., Hemstreet, W. B., Carlisle, K., et al. (2013). Implication of lateral genetic transfer in the emergence of *Aeromonas hydrophila* isolates of epidemic outbreaks in channel catfish. *PLoS One* 8:e80943. doi: 10.1371/journal.pone.0080943

Hsieh, Y. C., Liang, S. M., Tsai, W. L., Chen, Y. H., Liu, T. Y., and Liang, C. M. (2003). Study of capsular polysaccharide from *Vibrio parahaemolyticus*. *Infect. Immun.* 71, 3329–3336. doi: 10.1128/iai.71.6.3329-3336.2003

Hu, T., Chen, R., Zhang, L., Wang, Z., Yang, D., Zhang, Y., et al. (2019). Balanced role of T3SS and T6SS in contribution to the full virulence of *Edwardsiella piscicida*. *Fish Shellfish Immunol.* 93, 871–878. doi: 10.1016/j.fsi.2019.08.014

Hu, Y. H., Zhou, H. Z., Jin, Q. W., and Zhang, J. (2016). The serine protease autotransporter Tsh contributes to the virulence of *Edwardsiella tarda*. *Vet. Microbiol.* 189, 68–74. doi: 10.1016/j.vetmic.2016.04.021

Hueck, C. J. (1998). Type III protein secretion systems in bacterial pathogens of animals and plants. *Microbiol. Mol. Biol Rev.* 62, 379–433.

Huesca, M., Borgia, S., Hoffman, P., and Lingwood, C. A. (1996). Acidic pH changes receptor binding specificity of *Helicobacter* pylori: a binary adhesion model in which surface heat shock (stress) proteins mediate sulfatide recognition in gastric colonization. *Infect. Immun.* 64, 2643–2648. doi: 10.1128/iai.64.7.2643-2648.1996

Ina-Salwany, M. Y., Al-saari, N., Mohamad, A., Mursidi, F. A., Mohd-Aris, A., Amal, M. N. A., et al. (2019). Vibriosis in fish: a review on disease development and prevention. *J. Aqu. Anim. Health* 31, 3–22. doi: 10.1002/aah.10045

Ishiguro, E. E., Ainsworth, T., Kay, W. W., and Trust, T. J. (1986). Heme requirement for growth of fastidious atypical strains of *Aeromonas salmonicida*. *Appl. Environ. Microbiol.* 51, 668–670. doi: 10.1128/aem.51.3.668-670.1986

Janda, J. M., and Abbott, S. L. (1993). Expression of an iron-regulated hemolysin by *Edwardsiella tarda*. *FEMS Microbiol. Lett.* 111, 275–280.

Jang, K. K., Lee, Z. W., Kim, B., Jung, Y. H., Han, H. J., Kim, M. H., et al. (2017). Identification and characterization of *Vibrio vulnificus* plpA encoding a phospholipase A2 essential for pathogenesis. *J. Biol. Chem.* 292, 17129–17143. doi: 10.1074/jbc.M117.791657

Jeremić, S., Jakić-Dimić, D., and Veljović, L. J. (2003). *Citrobacter freundii* as a cause of disease in fish. *Acta Vet.* 53, 399–410. doi: 10.2298/avb0306399j

Jia, A., Woo, N. Y., and Zhang, X. H. (2010). Expression, purification, and characterization of thermolabile hemolysin (TLH) from *Vibrio alginolyticus*. *Dis. Aquat. Organ.* 90, 121–127. doi: 10.3354/dao02225

Jiang, W., Han, X., Wang, Q., Li, X., Yi, L., Liu, Y., et al. (2014). *Vibrio parahaemolyticus* enolase is an adhesion-related factor that binds plasminogen and functions as a protective antigen. *Appl. Microbiol. Biotechnol.* 98, 4937–4948. doi: 10.1007/s00253-013-5471-z

Jiao, X. D., Zhang, M., Cheng, S., and Sun, L. (2010). Analysis of *Edwardsiella tarda* DegP, a serine protease and a protective immunogen. *Fish Shellfish Immunol.* 28, 672–677. doi: 10.1016/j.fsi.2010.01.004

Jin, R. P., Hu, Y. H., Sun, B. G., Zhang, X. H., and Sun, L. (2012). *Edwardsiella tarda* sialidase: pathogenicity involvement and vaccine potential. *Fish Shellfish Immunol.* 33, 514–521. doi: 10.1016/j.fsi.2012.06.002

Johnson, K., Charles, I., Dougan, G., Pickard, D., O'gaora, P., Costa, G., et al. (1991). The role of a stress-response protein in *Salmonella typhimurium* virulence. *Mol. Microbiol.* 5, 401–407.

Johnson, T. L., Fong, J. C., Rule, C., Rogers, A., Yildiz, F. H., and Sandkvist, M. (2014). The Type II secretion system delivers matrix proteins for biofilm formation by *Vibrio cholerae*. *J. Bacteriol.* 196, 4245–4252. doi: 10.1128/JB.01944-14

Jones, C. H., Bolken, T. C., Jones, K. F., Zeller, G. O., and Hruby, D. E. (2001). Conserved DegP protease in gram-positive bacteria is essential for thermal and oxidative tolerance and full virulence in *Streptococcus pyogenes*. *Infect. Immun.* 69, 5538–5545. doi: 10.1128/IAI.69.9.5538-5545.2001

Jones, C. H., Dexter, P., Evans, A. K., Liu, C., Hultgren, S. J., and Hruby, D. E. (2002). *Escherichia coli* DegP protease cleaves between paired hydrophobic residues in a natural substrate: the PapA pilin. *J. Bacteriol.* 184, 5762–5771. doi: 10.1128/JB.184.20.5762-5771.2002

Jones, M. K., and Oliver, J. D. (2009). *Vibrio vulnificus*: disease and pathogenesis. *Infect. Immun.* 77, 1723–1733.

Jun, L., and Woo, N. Y. S. (2003). Pathogenicity of *vibrios* in fish: an overview. *J. Ocean Univ. Qingdao* 2, 117–128. doi: 10.1007/s11802-003-0039-7

Jyot, J., Balloy, V., Jouvion, G., Verma, A., Touqui, L., Huerre, M., et al. (2011). Type II secretion system of *Pseudomonas aeruginosa*: in vivo evidence of a significant role in death due to lung infection. *J. Infect. Dis.* 203, 1369–1377. doi: 10.1093/infdis/jir045

Kadi, N., Song, L., and Challis, G. L. (2008). Bisucaberin biosynthesis: an adenylating domain of the BibC multi-enzyme catalyzes cyclodimerization of N-hydroxy-N-succinylcadaverine. *Chem. Commun.* 41, 5119–5121. doi: 10.1039/b813029a

Kamath, S., Kapatral, V., and Chakrabarty, A. M. (1998). Cellular function of elastase in *Pseudomonas aeruginosa*: role in the cleavage of nucleoside diphosphate kinase and in alginate synthesis. *Mol. Microbiol.* 30, 933–941. doi: 10.1046/j.1365-2958.1998.01121.x

Kanonenberg, K., Spitz, O., Erenburg, I. N., Beer, T., and Schmitt, L. (2018). Type I secretion system—it takes three and a substrate. *FEMS Microbiol. Lett.* 365. doi: 10.1093/femsle/fny094

Kayansamruaj, P., Dong, H. T., Hirono, I., Kondo, H., Senapin, S., and Rodkhum, C. (2017). Comparative genome analysis of fish pathogen *Flavobacterium columnare* reveals extensive sequence diversity within the species. *Infect. Genet. Evol.* 54, 7–17. doi: 10.1016/j.meegid.2017.06.012

Kerie, Y., Nuru, A., and Abayneh, T. (2019). *Edwardsiella* species infection in fish population and its status in *Ethiopia*. *Fish. Aquac. J.* 10, 1–7.

Kim, C. M., Park, R. Y., Park, J. H., Sun, H. Y., Bai, Y. H., Ryu, P. Y., et al. (2006). *Vibrio vulnificus* vulnibactin, but not metalloprotease VvpE, is essentially required for iron-uptake from human holotransferrin. *Biol. Pharm. Bull.* 29, 911–918. doi: 10.1248/bpb.29.911

Kim, J. S., Sung, M. H., Kho, D. H., and Lee, J. K. (2005). Induction of manganese-containing superoxide dismutase is required for acid tolerance in *Vibrio vulnificus*. *J. Bacteriol.* 187, 5984–5995. doi: 10.1128/JB.187.17.5984-5995.2005

Klesius, P. H., Shoemaker, C. A., and Evans, J. J. (2008). *Flavobacterium columnare* chemotaxis to channel catfish mucus. *FEMS Microbiol. Lett.* 288, 216–220. doi: 10.1111/j.1574-6968.2008.01348.x

Knirel, Y. A., Kocharova, N. A., Bystrova, O. V., Katzenellenbogen, E., and Gamian, A. (2002). Structures and serology of the O-specific polysaccharides of bacteria of the genus Citrobacter. *Arch. Immunol. Ther. Exp.* 50, 379–392.

Knodler, L. A., and Steele-Mortimer, O. (2005). The *Salmonella* effector PipB2 affects late endosome/lysosome distribution to mediate Sif extension. *Mol. Biol. Cell* 16, 4108–4123. doi: 10.1091/mbc.e05-04-0367

Kondo, M., Kawai, K., Kurohara, K., and Oshima, S. I. (2002). Adherence of *Flavobacterium psychrophilum* on the body surface of the ayu *Plecoglossus altivelis*. *Microb. Infect.* 4, 279–283. doi: 10.1016/s1286-4579(02)01539-3

Krachler, A. M., Ham, H., and Orth, K. (2011). Outer membrane adhesion factor multivalent adhesion molecule 7 initiates host cell binding during infection by gram-negative pathogens. *Proc. Natl. Acad. Sci. U.S.A.* 108, 11614–11619. doi: 10.1073/pnas.1102360108

Kumru, S., Tekedar, H. C., Blom, J., Lawrence, M. L., and Karsi, A. (2020). Genomic diversity in flavobacterial pathogens of aquatic origin. *Microb. Pathog.* 142:104053. doi: 10.1016/j.micpath.2020.104053

Kumru, S., Tekedar, H. C., Gulsoy, N., Waldbieser, G. C., Lawrence, M. L., and Karsi, A. (2017). Comparative analysis of the *Flavobacterium columnare* genomovar I and II genomes. *Front. Microbiol.* 8:1375. doi: 10.3389/fmicb.2017.01375

Kunttu, H. M. T., Runtuvuori-Salmela, A., Sundell, K., Wiklund, T., Middelboe, M., Landor, L., et al. (2021). Bacteriophage resistance affects *Flavobacterium columnare* virulence partly via mutations in genes related to gliding motility and the Type IX secretion system. *Appl. Environ. Microbiol* 87:e00812–e821. doi: 10.1128/AEM.00812-21

Labella, A., Sanchez-Montes, N., Berbel, C., Aparicio, M., Castro, D., Manchado, M., et al. (2010). Toxicity of *Photobacterium damselae* subsp. *damselae* strains

isolated from new cultured marine fish. *Dis. Aquat. Organ.* 92, 31–40. doi: 10.3354/dao02275

Lachmann, I., Wagner, U., Hädge, D., and Drössler, K. (1998). Generation and preliminary characterisation of monoclonal antibodies directed to glycerophospholipid: cholesterol acyltransferase (GCAT) native epitopes of *Aeromonas salmonicida*. *Dis. Aquat. Org.* 33, 73–75. doi: 10.3354/dao033073

Lallier, R., and Daigneault, P. (1984). Antigenic differentiation of pili from non-virulent and fish-pathogenic strains of *Aeromonas hydrophila*. *J. Fish Dis.* 7, 509–512. doi: 10.1111/j.1365-2761.1984.tb01177.x

Lange, M. D., Abernathy, J., Shoemaker, C. A., Zhang, D., Kirby, A., Peatman, E., et al. (2020). Proteome analysis of virulent *Aeromonas hydrophila* reveals the upregulation of iron acquisition systems in the presence of a xenosiderophore. *FEMS Microbiol. Lett.* 367:fnaa169. doi: 10.1093/femsle/fnaa169

Larenas, J. J., Bartholomew, J., Troncoso, O., Fernández, S., Ledezma, H., Sandoval, N., et al. (2003). Experimental vertical transmission of *Piscirickettsia salmonis* and in vitro study of attachment and mode of entrance into the fish ovum. *Dis. Aquat. Org.* 56, 25–30. doi: 10.3354/dao056025

Lasica, A. M., Ksiazek, M., Madej, M., and Potempa, J. (2017). The Type IX secretion system (T9SS): highlights and recent insights into its structure and function. *Front. Cell. Infect. Microbiol.* 7:215. doi: 10.3389/fcimb.2017.00215

Lee, K. K., and Ellis, A. E. (1990). Glycerophospholipid: cholesterol acyltransferase complexed with lipopolysaccharide (LPS) is a major lethal exotoxin and cytolysin of *Aeromonas salmonicida*: LPS stabilizes and enhances toxicity of the enzyme. *J. Bacteriol.* 172, 5382–5393. doi: 10.1128/jb.172.9.5382-5393.1990

Lee, K. K., and Yii, K. C. (1996). A comparison of three methods for assaying hydrophobicity of pathogenic *vibrios*. *Lett. Appl. Microbiol.* 23, 343–346.

Leo, J. C., Oberhettinger, P., Schütz, M., and Linke, D. (2015). The inverse autotransporter family: intimin, invasin and related proteins. *Int. J. Med. Microbiol.* 305, 276–282.

Letain, T. E., and Postle, K. (1997). TonB protein appears to transduce energy by shuttling between the cytoplasmic membrane and the outer membrane in *Escherichia coli*. *Mol. Microbiol.* 24, 271–283. doi: 10.1046/j.1365-2958.1997.3331703.x

Létoffé, S., Deniau, C., Wolff, N., Dassa, E., Delepelaire, P., Lecroisey, A., et al. (2001). Haemophore-mediated bacterial haem transport: evidence for a common or overlapping site for haem-free and haem-loaded haemophore on its specific outer membrane receptor. *Mol. Microbiol.* 41, 439–450. doi: 10.1046/j.1365-2958.2001.02530.x

Letunic, I., and Bork, P. (2006). Interactive tree of life (iTOL): an online tool for phylogenetic tree display and annotation. *Bioinformatics* 23, 127–128. doi: 10.1093/bioinformatics/btl529

Levipan, H. A., Quezada, J., and Avendaño-Herrera, R. (2018). Stress tolerance-related genetic traits of fish pathogen *Flavobacterium psychrophilum* in a mature biofilm. *Front. Microbiol.* 9:18. doi: 10.3389/fmicb.2018.00018

Li, J., Ramezanpour, M., Fong, S. A., Cooksley, C., Murphy, J., Suzuki, M., et al. (2019). *Pseudomonas aeruginosa* exoprotein-induced barrier disruption correlates with elastase activity and marks chronic rhinosinusitis severity. *Front. Cell. Infect. Microbiol.* 9:38. doi: 10.3389/fcimb.2019.00038

Li, L., Meng, H., Gu, D., Li, Y., and Jia, M. (2019). Molecular mechanisms of *Vibrio parahaemolyticus* pathogenesis. *Microbiol. Res.* 222, 43–51.

Li, L., Rock, J. L., and Nelson, D. R. (2008). Identification and characterization of a repeat-in-toxin gene cluster in *Vibrio anguillarum*. *Infect. Immun.* 76, 2620–2632. doi: 10.1128/IAI.01308-07

Li, M. F., and Sun, L. (2018). *Edwardsiella tarda* Sip2: a serum-induced protein that is essential to serum survival, acid resistance, intracellular replication, and host infection. *Front. Microbiol.* 9:1084. doi: 10.3389/fmicb.2018.01084

Li, N., Zhu, Y., LaFrentz, B. R., Evenhuis, J. P., Hunnicutt, D. W., Conrad, R. A., et al. (2017). The Type IX secretion system is required for virulence of the fish pathogen *Flavobacterium columnare*. *Appl. Environ. Microbiol.* 83:e01769–17.

Li, Y., and Ma, Q. (2017). Iron acquisition strategies of *Vibrio anguillarum*. *Front. Cell. Infect. Microbiol.* 7:342. doi: 10.3389/fcimb.2017.00342

Li, Y., Liu, Y., Zhou, Z., Huang, H., Ren, Y., Zhang, Y., et al. (2011). Complete genome sequence of *Aeromonas veronii* strain B565. *J. Bacteriol.* 193, 3389–3390. doi: 10.1128/JB.00347-11

Lindler, L. E., Plano, G. V., Burland, V., Mayhew, G. F., and Blattner, F. R. (1998). Complete DNA sequence and detailed analysis of the *Yersinia pestis* KIM5 plasmid encoding murine toxin and capsular antigen. *Infect. Immun.* 66, 5731–5742. doi: 10.1128/IAI.66.12.5731-5742.1998

Ling, S. H. M., Wang, X. H., Lim, T. M., and Leung, K. Y. (2001). Green fluorescent protein-tagged *Edwardsiella tarda* reveals portal of entry in fish. *FEMS Microbiol. Lett.* 194, 239–243. doi: 10.1111/j.1574-6968.2001.tb09476.x

Linhartova, I., Osicka, R., Bumba, L., Masin, J., and Sebo, P. (2018). "Repeats-in-toxin (RTX) toxins: a review," in *Microbiology Toxins*, eds B. Stiles, A. Alape-Girón, J. D. Dubreuil, M. Mandal, and P. Gopalakrishnakone (Dordrecht: Springer Netherlands), 353–381. doi: 10.1007/978-94-007-6449-1_13

Litwin, C. M., and Byrne, B. L. (1998). Cloning and characterization of an outer membrane protein of *Vibrio vulnificus* required for heme utilization: regulation of expression and determination of the gene sequence. *Infect. Immun.* 66, 3134–3141. doi: 10.1128/IAI.66.7.3134-3141.1998

Liu, M., and Chen, S. (2015). A novel adhesive factor contributing to the virulence of *Vibrio parahaemolyticus*. *Sci. Rep.* 5:14449. doi: 10.1038/srep14449

Liu, T., Wang, E., Wei, W., Wang, K., Yang, Q., and Ai, X. (2019). TcpA, a novel *Yersinia ruckeri* TIR-containing virulent protein mediates immune evasion by targeting MyD88 adaptors. *Fish Shellfish Immunol.* 94, 58–65. doi: 10.1016/j.fsi.2019.08.069

Loch, T. P., and Faisal, M. (2014). *Flavobacterium spartansii* sp. nov., a pathogen of fishes, and emended descriptions of *Flavobacterium aquidurense* and *Flavobacterium araucananum*. *Int. J. Syst. Evol. Microbiol.* 64, 406–412. doi: 10.1099/ijs.0.051433-0

Logan, S. L., Thomas, J., Yan, J., Baker, R. P., Shields, D. S., Xavier, J. B., et al. (2018). The *Vibrio cholerae* type VI secretion system can modulate host intestinal mechanics to displace gut bacterial symbionts. *Proc. Natl. Acad. Sci. U.S.A.* 115, E3779–E3787. doi: 10.1073/pnas.1720133115

Lönnström, L., Wiklund, T., and Bylund, G. (1994). *Pseudomonas* anguilliseptica isolated from *Baltic herring* Clupea harengus membras with eye lesions. *Dis. Aquat. Org.* 18, 143–147.

López, C. S., Alice, A. F., Chakraborty, R., and Crosa, J. H. (2007). Identification of amino acid residues required for ferric-anguibactin transport in the outer-membrane receptor FatA of *Vibrio anguillarum*. *Microbiology* 153, 570–584. doi: 10.1099/mic.0.2006/001735-0

Lopez, C. S., and Crosa, J. H. (2007). Characterization of ferric-anguibactin transport in *Vibrio anguillarum*. *Biometals* 20:393. doi: 10.1007/s10534-007-9084-9

López-Romalde, S., Magariños, B., Núñez, S., Toranzo, A. E., and Romalde, J. L. (2003a). Phenotypic and genetic characterization of *Pseudomonas anguilliseptica* strains isolated from fish. *J. Aquat. Anim. Health* 15, 39–47.

López-Romalde, S., Magariños, B., Ravelo, C., Toranzo, A. E., and Romalde, J. L. (2003b). Existence of two O-serotypes in the fish pathogen *Pseudomonas anguilliseptica*. *Vet. Microbiol.* 94, 325–333. doi: 10.1016/s0378-1135(03)00124-x

Lorenzen, E., Dalsgaard, I., and Bernardet, J. F. (1997). Characterization of isolates of *Flavobacterium psychrophilum* associated with coldwater disease or rainbow trout fry syndrome I: phenotypic and genomic studies. *Dis. Aquat. Org.* 31, 197–208.

Løvoll, M., Wiik-Nielsen, C. R., Tunsjø, H. S., Colquhoun, D., Lunder, T., Sørum, H., et al. (2009). Atlantic salmon bath challenged with *Moritella viscosa*-pathogen invasion and host response. *Fish Shellfish Immunol.* 26, 877–884. doi: 10.1016/j.fsi.2009.03.019

Luo, G., Huang, L., Su, Y., Qin, Y., Xu, X., Zhao, L., et al. (2016). flrA, flrB and flrC regulate adhesion by controlling the expression of critical virulence genes in *Vibrio alginolyticus*. *Emerg. Microbes Infect.* 5, 1–11. doi: 10.1038/emi.2016.82

Madsen, L., and Dalsgaard, I. (1998). "Characterization of *Flavobacterium psychrophilum*; comparison of proteolytic activity and virulence of strains isolated from rainbow trout (*Oncorhynchus mykiss*)," in *Methodology in Fish Diseases Research*, eds A. C. Barnes, G. A. Davidson, M. P. Hiney, and D. McIntosh (Aberdeen: Fisheries Research Services), 45–52.

Magarinos, B., Pazos, F., Santos, Y., Romalde, J. L., and Toranzo, A. E. (1995). Response of *Pasteurella piscicida* and *Flexibacter maritimus* to skin mucus of marine fish. *Dis. Aquat. Org.* 21, 103–108. doi: 10.3354/dao021103

Maltz, M., Levarge, B., and Graf, J. (2015). Identification of iron and heme utilization genes in *Aeromonas* and their role in the colonization of the leech digestive tract. *Front. Microbiol.* 6:763. doi: 10.3389/fmicb.2015.00763

Marshall, S. H., Gómez, F. A., Ramírez, R., Nilo, L., and Henríquez, V. (2012). Biofilm generation by *Piscirickettsia salmonis* under growth stress conditions: a putative in vivo survival/persistence strategy in marine environments. *Res. Microbiol.* 163, 557–566. doi: 10.1016/j.resmic.2012.08.002

Matsuda, S., Okada, R., Tandhavanant, S., Hiyoshi, H., Gotoh, K., Iida, T., et al. (2019). Export of a *Vibrio parahaemolyticus* toxin by the Sec and Type III secretion machineries in tandem. *Nat. Microbiol.* 4, 781–788. doi: 10.1038/s41564-019-0368-y

Matsuyama, T., Kamaishi, T., Ooseko, N., Kurohara, K., and Iida, T. (2005). Pathogenicity of motile and non-motile *Edwardsiella tarda* to some marine fish. *Fish Pathol.* 40, 133–135. doi: 10.3147/jsfp.40.133

Mattick, J. S. (2002). Type IV pili and twitching motility. *Annu. Rev. Microbiol.* 56, 289–314. doi: 10.1146/annurev.micro.56.012302.160938

Mazoy, R., and Lemos, M. L. (1996). Identification of heme-binding proteins in the cell membranes of *Vibrio anguillarum*. *FEMS Microbiol. Lett.* 135, 265–270. doi: 10.1111/j.1574-6968.1996.tb07999.x

Mazoy, R., Vázquez, F., and Lemos, M. L. (1996). Isolation of heme-binding proteins from *Vibrio anguillarum* using affinity chromatography. *FEMS Microbiol. Lett.* 141, 19–23. doi: 10.1111/j.1574-6968.1996.tb08357.x

McBride, M. J. (2014). "The family flavobacteriaceae," in *The Prokaryotes: Other Major Lineages Of Bacteria And The Archaea*, eds E. Rosenberg, E. F. DeLong, S. Lory, E. Stackebrandt, and F. Thompson (Berlin: Springer), 643–676.

McBride, M. J., and Nakane, D. (2015). Flavobacterium gliding motility and the Type IX secretion system. *Curr. Opin. Microbiol.* 28, 72–77.

McBride, M. J., Braun, T. F., and Brust, J. L. (2003). *Flavobacterium johnsoniae* GldH is a lipoprotein that is required for gliding motility and chitin utilization. *J. Bacteriol.* 185, 6648–6657. doi: 10.1128/jb.185.22.6648-6657.2003

McCarthy, U., Steiropoulos, N. A., Thompson, K. D., Adams, A., Ellis, A. E., and Ferguson, H. W. (2005). Confirmation of *Piscirickettsia salmonis* as a pathogen in European sea bass *Dicentrarchus labrax* and phylogenetic comparison with salmonid strains. *Dis. Aquat. Org.* 64, 107–119. doi: 10.3354/dao064107

McCarthy, ÚM., Bron, J. E., Brown, L., Pourahmad, F., Bricknell, I. R., Thompson, K. D., et al. (2008). Survival and replication of *Piscirickettsia salmonis* in rainbow trout head kidney macrophages. *Fish Shellfish Immunol* 25, 477–484. doi: 10.1016/j.fsi.2008.07.005

Merino, S., Rubires, X., Aguilar, A., and Tomás. (1996). The O:34-antigen lipopolysaccharide as an adhesin in *Aeromonas hydrophila*. *FEMS Microbiol. Lett* 139, 97–101. doi: 10.1111/j.1574-6968.1996.tb08186.x

Merle, C., Faure, D., Urdaci, M. C., and Le Henaff, M. (2003). Purification and characterization of a membrane glycoprotein from the fish pathogen *Flavobacterium psychrophilum*. *J. Appl. Microbiol.* 94, 1120–1127.

Merle, N. S., Church, S. E., Fremeaux-Bacchi, V., and Roumenina, L. T. (2015). Complement system part I–molecular mechanisms of activation and regulation. *Front. Immunol.* 6:262. doi: 10.3389/fimmu.2015.00262

Meuskens, I., Saragliadis, A., Leo, J. C., and Linke, D. (2019). Type V secretion systems: an overview of passenger domain functions. *Front. Microbiol.* 10:1163. doi: 10.3389/fmicb.2019.01163

Milton, D. L., Norqvist, A., and Wolf-Watz, H. (1992). Cloning of a metalloprotease gene involved in the virulence mechanism of *Vibrio anguillarum*. *J. Bacteriol.* 174, 7235–7244. doi: 10.1128/jb.174.22.7235-7244.1992

Milton, D. L., O'Toole, R., Horstedt, P., and Wolf-Watz, H. (1996). Flagellin A is essential for the virulence of *Vibrio anguillarum*. *J. Bacteriol.* 178, 1310–1319. doi: 10.1128/jb.178.5.1310-1319.1996

Miyazaki, T., and Plumb, J. A. (1985). Histopathology of *Edwardsiella ictaluri* in channel catfish, *Ictalurus punctatus* (Rafinesque). *J. Fish Dis.* 8, 389–392. doi: 10.1111/j.1365-2761.1985.tb00961.x

Mo, Z., Guo, D., Mao, Y., Ye, X., Zou, Y., Xiao, P., et al. (2010). Identification and characterization of the *Vibrio anguillarum* prtV gene encoding a new metalloprotease. *Chin. J. Oceanol. Limnol.* 28, 55–61. doi: 10.1007/s00343-010-9246-4

Mohanty, B. R., and Sahoo, P. K. (2007). Edwardsiellosis in fish: a brief review. *J. Biosci.* 32, 1331–1344. doi: 10.1007/s12038-007-0143-8

Møller, J. D., Ellis, A. E., Barnes, A. C., and Dalsgaard, I. (2005). Iron acquisition mechanisms of *Flavobacterium psychrophilum*. *J. Fish Dis.* 28, 391–398.

Møller, J. D., Larsen, J. L., Madsen, L., and Dalsgaard, I. (2003). Involvement of a sialic acid-binding lectin with hemagglutination and hydrophobicity of *Flavobacterium psychrophilum*. *Appl. Environ. Microbiol.* 69, 5275–5280. doi: 10.1128/AEM.69.9.5275-5280.2003

Mouriño, S., Osorio, C. R., and Lemos, M. L. (2004). Characterization of heme uptake cluster genes in the fish pathogen *Vibrio anguillarum*. *J. Bacteriol.* 186, 6159–6167. doi: 10.1128/JB.186.18.6159-6167.2004

Mouriño, S., Rodríguez-Ares, I., Osorio, C. R., and Lemos, M. L. (2005). Genetic variability of the heme uptake system among different strains of the fish pathogen *Vibrio anguillarum*: identification of a new heme receptor. *Appl. Environ. Microbiol.* 71, 8434–8441. doi: 10.1128/AEM.71.12.8434-8441.2005

Murray, P. R., Holmes, B., and Aucken, H. M. (2010). "Citrobacter, *Enterobacter*, klebsiella, plesiomonas, serratia, and other members of the *Enterobacteriaceae*," in *Topley & Wilson's Microbiology and Microbial Infections*, eds H. E. Jensen and F. W. Chandler (Hoboken, NJ: John Wiley & Sons Ltd).

Nag, D., Farr, D. A., Walton, M. G., and Withey, J. H. (2020). Zebrafish models for *Pathogenic Vibrios*. *J. Bacteriol.* 202:e00165–20.

Nagamatsu, K., Kuwae, A., Konaka, T., Nagai, S., Yoshida, S., Eguchi, M., et al. (2009). *Bordetella* evades the host immune system by inducing IL-10 through a type III effector. *BopN. J. Exp. Med.* 206, 3073–3088. doi: 10.1084/jem.20090494

Najimi, M., Lemos, M. L., and Osorio, C. R. (2008b). Identification of siderophore biosynthesis genes essential for growth of *Aeromonas salmonicida* under iron limitation conditions. *Appl. Environ. Microbiol.* 74, 2341–2348. doi: 10.1128/AEM.02728-07

Najimi, M., Lemos, M. L., and Osorio, C. R. (2008a). Identification of heme uptake genes in the fish pathogen *Aeromonas salmonicida* subsp. *salmonicida*. *Arch. Microbiol.* 190, 439–449. doi: 10.1007/s00203-008-0391-5

Naka, H., Actis, L. A., and Crosa, J. H. (2013). The anguibactin biosynthesis and transport genes are encoded in the chromosome of *Vibrio harveyi*: a possible evolutionary origin for the pJM1 plasmid-encoded system of *Vibrio anguillarum*? *Microbiologyopen* 2, 182–194. doi: 10.1002/mbo3.65

Naka, H., Dias, G. M., Thompson, C. C., Dubay, C., Thompson, F. L., and Crosa, J. H. (2011). Complete genome sequence of the marine fish pathogen *Vibrio anguillarum* harboring the pJM1 virulence plasmid and genomic comparison with other virulent strains of *V. anguillarum* and *V. ordalii*. *Infect. Immun.* 79, 2889–2900. doi: 10.1128/IAI.05138-11

Naka, H., Reitz, Z. L., Jelowicki, A. M., Butler, A., and Haygood, M. G. (2018). Amphi-enterobactin commonly produced among *Vibrio campbellii* and *Vibrio harveyi* strains can be taken up by a novel outer membrane protein FapA that also can transport canonical Fe(III)-enterobactin. *J. Biol. Inorg. Chem.* 23, 1009–1022. doi: 10.1007/s00775-018-1601-5

Nakai, T. (1985). Resistance of *Pseudomonas anguilliseptica* [an eel pathogen] to bactericidal action of fish serum. *Bull. Jpn. Soc. Sci. Fish.* 51, 1431–1436. doi: 10.2331/suisan.51.1431

Nakayama, H., Tanaka, K. H., Teramura, N., and Hattori, S. (2016). Expression of collagenase in *Flavobacterium psychrophilum* isolated from cold-water disease-affected ayu (*Plecoglossus altivelis*). *Biosci. Biotechnol. Biochem.* 80, 135–144. doi: 10.1080/09168451.2015.1079477

Namba, A., Mano, N., Takano, H., Beppu, T., Ueda, K., and Hirose, H. (2008). OmpA is an adhesion factor of *Aeromonas veronii*, an optimistic pathogen that habituates in carp intestinal tract. *J. Appl. Microbiol.* 105, 1441–1451. doi: 10.1111/j.1365-2672.2008.03883.x

Navais, R., Méndez, J., Pérez-Pascual, D., Cascales, D., and Guijarro, J. A. (2014). The yrpAB operon of *Yersinia ruckeri* encoding two putative U32 peptidases is involved in virulence and induced under microaerobic conditions. *Virulence* 5, 619–624. doi: 10.4161/viru.29363

Nematollahi, A., Decostere, A., Pasmans, F., and Haesebrouck, F. (2003b). *Flavobacterium psychrophilum* infections in salmonid fish. *J. Fish Dis.* 26, 563–574. doi: 10.1046/j.1365-2761.2003.00488.x

Nematollahi, A., Decostere, A., Pasmans, F., Ducatelle, R., and Haesebrouck, F. (2003a). Adhesion of high and low virulence *Flavobacterium psychrophilum* strains to isolated gill arches of rainbow trout *Oncorhynchus mykiss*. *Dis. Aquat. Org.* 55, 101–107. doi: 10.3354/dao055101

Nikoskelainen, S., Salminen, S., Bylund, G., and Ouwehand, A. C. (2001). Characterization of the properties of human-and dairy-derived probiotics for prevention of infectious diseases in fish. *Appl. Environ. Microbiol.* 67, 2430–2435. doi: 10.1128/AEM.67.6.2430-2435.2001

Nivaskumar, M., and Francetic, O. (2014). Type II secretion system: a magic beanstalk or a protein escalator. *Biochim. Biophys. Acta Mol. Cell Res.* 1843, 1568–1577. doi: 10.1016/j.bbamcr.2013.12.020

Nomura, S., Fujino, M., Yamakawa, M., and Kawahara, E. (1988). Purification and characterization of salmolysin, an extracellular hemolytic toxin from *Aeromonas salmonicida*. *J. Bacteriol.* 170, 3694–3702. doi: 10.1128/jb.170.8.3694-3702.1988

Noonan, B., and Trust, T. J. (1997). The synthesis, secretion and role in virulence of the paracrystalline surface protein layers of *Aeromonas salmonicida* and *A. hydrophila*. *FEMS Microbiol. Lett.* 154, 1–7. doi: 10.1111/j.1574-6968.1997.tb12616.x

Norqvist, A., Norrman, B., and Wolf-Watz, H. (1990). Identification and characterization of a zinc metalloprotease associated with invasion by the fish pathogen *Vibrio anguillarum*. *Infect. Immun.* 58, 3731–3736. doi: 10.1128/iai.58.11.3731-3736.1990

O'Boyle, N., Houeix, B., Kilcoyne, M., Joshi, L., and Boyd, A. (2013). The MSHA pilus of *Vibrio parahaemolyticus* has lectin functionality and enables TTSS-mediated pathogenicity. *Int. J. Med. Microbiol.* 303, 563–573. doi: 10.1016/j.ijmm.2013.07.010

Oda, M., Takahashi, M., Matsuno, T., Uoo, K., Nagahama, M., and Sakurai, J. (2010). Hemolysis induced by *Bacillus cereus* sphingomyelinase. *Biochim. Biophys. Acta* 1798, 1073–1080. doi: 10.1016/j.bbamem.2010.03.004

Okada, K., Iida, T., Kita-Tsukamoto, K., and Honda, T. (2005). *Vibrios* commonly possess two chromosomes. *J. Bacteriol.* 187, 752–757. doi: 10.1128/JB.187.2.752-757.2005

Olivares-Fuster, O., and Arias, C. R. (2008). Use of suppressive subtractive hybridization to identify *Flavobacterium columnare* DNA sequences not shared with *Flavobacterium johnsoniae*. *Lett. Appl. Microbiol.* 46, 605–612. doi: 10.1111/j.1472-765X.2008.02366.x

Oliver, C., Valenzuela, K., Hernández, M., Sandoval, R., Haro, R. E., Avendaño-Herrera, R., et al. (2016). Characterization and pathogenic role of outer membrane vesicles produced by the fish pathogen *Piscirickettsia salmonis* under in vitro conditions. *Vet. Microbiol.* 184, 94–101. doi: 10.1016/j.vetmic.2015.09.012

Ormonde, P., Hörstedt, P., O'Toole, R., and Milton, D. L. (2000). Role of motility in adherence to and invasion of a fish cell line by *Vibrio anguillarum*. *J. Bacteriol.* 182, 2326–2328. doi: 10.1128/JB.182.8.2326-2328.2000

Ortiz-Severín, J., Travisany, D., Maass, A., Chávez, F. P., and Cambiazo, V. (2019). Piscirickettsia salmonis cryptic plasmids: source of mobile DNA and virulence factors. *Pathogens* 8:269. doi: 10.3390/pathogens8040269

Osei-Adjei, G., Huang, X., and Zhang, Y. (2018). The extracellular proteases produced by *Vibrio parahaemolyticus*. *World J. Microbiol. Biotechnol.* 34:68. doi: 10.1007/s11274-018-2453-4

Osorio, C. R. (2018). T3SS effectors in vibrios: homology in sequence, diversity in biological functions? *Virulence* 9, 721–723. doi: 10.1080/21505594.2018.1435965

Osorio, C. R., Rivas, A. J., Balado, M., Fuentes-Monteverde, J. C., Rodríguez, J., Jiménez, C., et al. (2015). A transmissible plasmid-borne pathogenicity island confers piscibactin biosynthesis in the fish pathogen *Photobacterium damselae* subsp. piscicida. *Appl. Environ. Microbiol.* 81, 5867–5879. doi: 10.1128/AEM.01580-15

Ostland, V. E., Byrne, P. J., Hoover, G., and Ferguson, H. W. (2000). Necrotic myositis of rainbow trout, *Oncorhynchus mykiss* (Walbaum): proteolytic characteristics of a crude extracellular preparation from *Flavobacterium psychrophilum*. *J. Fish Dis.* 23, 329–336. doi: 10.1046/j.1365-2761.2000.00251.x

Ostland, V. E., Lumsden, J. S., MacPhee, D. D., Derksen, J. A., and Ferguson, H. W. (1997). Inhibition of the attachment of *Flavobacterium branchiophilum* to the gills of rainbow trout *Oncorhynchus Mykiss* (Walbaum). *J. Fish Dis.* 20, 109–117. doi: 10.1046/j.1365-2761.1997.d01-113.x

O'Toole, R., Milton, D. L., and Wolf-Watz, H. (1996). Chemotactic motility is required for invasion of the host by the fish pathogen *Vibrio anguillarum*. *Mol. Microbiol.* 19, 625–637. doi: 10.1046/j.1365-2958.1996.412927.x

Otsuka, Y. (2016). Prokaryotic toxin–antitoxin systems: novel regulations of the toxins. *Curr. Genet.* 62, 379–382.

Palleroni, N. J. (2010). The *Pseudomonas* story. *Environ. Microbiol.* 12, 1377–1383.

Palmer, T., and Berks, B. C. (2012). The twin-arginine translocation (Tat) protein export pathway. *Nat. Rev. Microbiol.* 10, 483–496. doi: 10.1038/nrmicro2814

Palmer, T., Finney, A. J., Saha, C. K., Atkinson, G. C., and Sargent, F. (2021). A holin/peptidoglycan hydrolase-dependent protein secretion system. *Mol. Microbiol.* 115, 345–355. doi: 10.1111/mmi.14599

Pan, L., Yang, Y., Peng, Y., Li, D., Khan, T. A., Chen, P., et al. (2021). The novel pathogenic *Citrobacter freundii* (CFC202) isolated from diseased crucian carp (*Carassius auratus*) and its ghost vaccine as a new prophylactic strategy against infection. *Aquaculture* 533:736190.

Pang, M., Jiang, J., Xie, X., Wu, Y., Dong, Y., Kwok, A. H. Y., et al. (2015). Novel insights into the pathogenicity of epidemic *Aeromonas hydrophila* ST251 clones from comparative genomics. *Sci. Rep.* 5, 1–15. doi: 10.1038/srep09833

Park, S. B., Aoki, T., and Jung, T. S. (2012). Pathogenesis of and strategies for preventing *Edwardsiella tarda* infection in fish. *Vet. Res.* 43:67.

Pedersen, L. L., Radulic, M., Doric, M., and Kwaik, Y. A. (2001). HtrA homologue of *Legionella pneumophila*: an indispensable element for intracellular infection of mammalian but not protozoan cells. *Infect. Immun.* 69, 2569–2579. doi: 10.1128/IAI.69.4.2569-2579.2001

Penttinen, R., Hoikkala, V., and Sundberg, L. R. (2018). Gliding motility and expression of motility-related genes in spreading and non-spreading colonies of *Flavobacterium columnare*. *Front. Microbiol.* 9:525. doi: 10.3389/fmicb.2018.00525

Pérez-Pascual, D., Gómez, E., and Guijarro, J. A. (2015). Lack of a type-2 glycosyltransferase in the fish pathogen *Flavobacterium psychrophilum* determines pleiotropic changes and loss of virulence. *Vet. Res.* 46:1. doi: 10.1186/s13567-014-0124-5

Pérez-Pascual, D., Lunazzi, A., Magdelenat, G., Rouy, Z., Roulet, A., Lopez-Roques, C., et al. (2017). The complete genome sequence of the fish pathogen *Tenacibaculum maritimum* provides insights into virulence mechanisms. *Front. Microbiol.* 8:1542. doi: 10.3389/fmicb.2017.01542

Perry, L. B. (1973). Gliding motility in some non-spreading flexibacteria. *J. Appl. Bacteriol.* 36, 227–232. doi: 10.1111/j.1365-2672.1973.tb04095.x

Pirarat, N., Ooi, E. L., Thompson, K. D., Thinh, N. H., Maita, M., and Katagiri, T. (2016). Examination of entry portal and pathogenesis of *Edwardsiella ictaluri* infection in striped catfish, *Pangasianodon hypophthalmus*. *Aquaculture* 464, 279–285. doi: 10.1016/j.aquaculture.2016.06.043

Rahman, T., Suga, K., Kanai, K., and Sugihara, Y. (2014). Biological and serological characterization of a non-gliding strain of *Tenacibaculum maritimum* isolated from a diseased puffer fish *Takifugu rubripes*. *Fish Pathol.* 49, 121–129. doi: 10.3147/jsfp.49.121

Reith, M. E., Singh, R. K., Curtis, B., Boyd, J. M., Bouevitch, A., Kimball, J., et al. (2008). The genome of *Aeromonas salmonicida* subsp. *salmonicida* A449: insights into the evolution of a fish pathogen. *BMC Genomics* 9:427. doi: 10.1186/1471-2164-9-427

Rey-Varela, D., Cisneros-Sureda, J., Balado, M., Rodríguez, J., Lemos, M. L., and Jiménez, C. (2019). The outer membrane protein FstC of *Aeromonas salmonicida* subsp. *salmonicida* acts as receptor for amonabactin siderophores and displays a wide ligand plasticity. Structure–activity relationships of synthetic amonabactin analogues. *ACS Infect. Dis.* 5, 1936–1951. doi: 10.1021/acsinfecdis.9b00274

Rhee, J. E., Rhee, J. H., Ryu, P. Y., and Choi, S. H. (2002). Identification of the cadBA operon from *Vibrio vulnificus* and its influence on survival to acid stress. *FEMS Microbiol. Lett.* 208, 245–251. doi: 10.1111/j.1574-6968.2002.tb11089.x

Richard, K. L., Kelley, B. R., and Johnson, J. G. (2019). Heme uptake and utilization by gram-negative bacterial pathogens. *Front. Cell. Infect. Microbiol.* 9:81. doi: 10.3389/fcimb.2019.00081

Ringø, E., Jutfelt, F., Kanapathippillai, P., Bakken, Y., Sundell, K., Glette, J., et al. (2004). Damaging effect of the fish pathogen *Aeromonas salmonicida* ssp. salmonicida on intestinal enterocytes of *Atlantic salmon* (*Salmo salar* L.). *Cell Tissue Res.* 318, 305–311. doi: 10.1007/s00441-004-0934-2

Rivas, A. J., Balado, M., Lemos, M. L., and Osorio, C. R. (2011). The *Photobacterium damselae* subsp. *damselae* hemolysins damselysin and HlyA are encoded within a new virulence plasmid. *Infect. Immun.* 79, 4617–4627. doi: 10.1128/IAI.05436-11

Rivas, A. J., Hoven, G. V., Neukirch, C., Meyenburg, M., Qin, Q., Füser, S., et al. (2015). Phobalysin, a small beta-pore-forming toxin of *Photobacterium damselae* subsp. *damselae*. *Infect. Immun.* 83, 4335–4348. doi: 10.1128/IAI.00277-15

Rivera-Calzada, A., Famelis, N., Llorca, O., and Geibel, S. (2021). Type VII secretion systems: structure, functions and transport models. *Nat. Rev. Microbiol.* 19, 567–584.

Robien, M. A., Krumm, B. E., Sandkvist, M., and Hol, W. G. J. (2003). Crystal structure of the extracellular protein secretion NTPase EpsE of *Vibrio cholerae*. *J. Mol. Biol.* 333, 657–674. doi: 10.1016/j.jmb.2003.07.015

Rochat, T., Pérez-Pascual, D., Nilsen, H., Carpentier, M., Bridel, S., Bernardet, J. F., et al. (2019). Identification of a novel elastin-degrading enzyme from

the fish pathogen *Flavobacterium psychrophilum*. *Appl. Environ. Microbiol.* 85:e02535–18. doi: 10.1128/AEM.02535-18

Rodkhum, C., Hirono, I., Crosa, J. H., and Aoki, T. (2005). Four novel hemolysin genes of *Vibrio anguillarum* and their virulence to rainbow trout. *Microb. Pathog.* 39, 109–119. doi: 10.1016/j.micpath.2005.06.004

Rojas, M. E., Galleguillos, M., Diaz, S., Machuca, A., Carbonero, A., and Smith, P. A. (2013). Evidence of exotoxin secretion of *Piscirickettsia salmonis*, the causative agent of piscirickettsiosis. *J. Fish Dis.* 36, 703–709. doi: 10.1111/jfd.12019

Romeo, J. M., Esmon, B., and Zusman, D. R. (1986). Nucleotide sequence of the myxobacterial hemagglutinin gene contains four homologous domains. *Proc. Natl. Acad. Sci. U.S.A.* 83, 6332–6336. doi: 10.1073/pnas.83.17.6332

Rompikuntal, P. K., Vdovikova, S., Duperthuy, M., Johnson, T. L., Åhlund, M., Lundmark, R., et al. (2015). Outer membrane vesicle-mediated export of processed PrtV protease from *Vibrio cholerae*. *PLoS One* 10:e0134098. doi: 10.1371/journal.pone.0134098

Røsjø, C., Salte, R., Thomassen, M. S., and Eggset, G. (1993). Glycerophospholipid:cholesterol acyltransferase complexed with lipopolysaccharide (GCAT-LPS) of *Aeromonas salmonicida* produces lysophospholipids in salmonid red cell membranes: a probable haemolytic mechanism. *J. Fish Dis.* 16, 87–99. doi: 10.1111/j.1365-2761.1993.tb00852.x

Rowe, H. M., Withey, J. H., and Neely, M. N. (2014). Zebrafish as a model for zoonotic aquatic pathogens. *Dev. Comp. Immunol.* 46, 96–107.

Rozas, M., and Enríquez, R. (2014). *Piscirickettsiosis* and *Piscirickettsia salmonis* in fish: a review. *J. Fish Dis.* 37, 163–188.

Rucker, R. R. (1959). *Vibrio* infections among marine and fresh-water fish. *Prog. Fish Cult.* 21, 22–25.

Ruiz, P., Balado, M., Fuentes-Monteverde, J. C., Toranzo, A. E., Rodríguez, J., Jiménez, C., et al. (2019). The fish pathogen *Vibrio ordalii* under iron deprivation produces the siderophore piscibactin. *Microorganisms* 7:313. doi: 10.3390/microorganisms7090313

Russell, A. B., Peterson, S. B., and Mougous, J. D. (2014a). Type VI secretion system effectors: poisons with a purpose. *Nat. Rev. Microbiol.* 12, 137–148.

Russell, A. B., Wexler, A. G., Harding, B. N., Whitney, J. C., Bohn, A. J., Goo, Y. A., et al. (2014b). A Type VI secretion-related pathway in Bacteroidetes mediates interbacterial antagonism. *Cell Host Microbe* 16, 227–236.

Sadarangani, V., Datta, S., and Arunachalam, M. (2013). New players in the same old game: a system level in silico study to predict Type III secretion system and effector proteins in bacterial genomes reveals common themes in T3SS mediated pathogenesis. *BMC Res. Notes* 6:297. doi: 10.1186/1756-0500-6-297

Sakai, D. K. (1985). Loss of virulence in a protease-deficient mutant of *Aeromonas salmonicida*. *Infect. Immun.* 48, 146–152.

Salomon, D., Klimko, J. A., Trudgian, D. C., Kinch, L. N., Grishin, N. V., Mirzaei, H., et al. (2015). Type VI secretion system toxins horizontally shared between marine bacteria. *PLoS Pathog.* 11:e1005128. doi: 10.1371/journal.ppat.1005128

Sampath, V. P. (2018). Bacterial endotoxin-lipopolysaccharide; structure, function and its role in immunity in vertebrates and invertebrates. *Agric. Nat. Resour.* 52, 115–120.

Sandkvist, M. (2001). Type II secretion and pathogenesis. *Infect. Immun.* 69, 3523–3535.

Santander, J., Golden, G., Wanda, S. Y., and Curtiss, R. R. (2012). Fur-regulated iron uptake system of *Edwardsiella ictaluri* and its influence on pathogenesis and immunogenicity in the catfish host. *Infect. Immun.* 80, 2689–2703.

Sarma, J. V., and Ward, P. A. (2011). The complement system. *Cell Tissue Res.* 343, 227–235.

Satchell, K. J. F. (2007). MARTX, multifunctional autoprocessing repeats-in-toxin toxins. *Infect. Immun.* 75, 5079–5084.

Sato, K., Naito, M., Yukitake, H., Hirakawa, H., Shoji, M., McBride, M. J., et al. (2010). A protein secretion system linked to bacteroidete gliding motility and pathogenesis. *Proc. Natl. Acad. Sci. U.S.A.* 107, 276–281.

Schaechter, M., Medoff, G., and Eisenstein, B. I. (1993). *Mechanisms Of Microbial Disease*. Philadelphia, PA: Lippincott Williams & Wilkins.

Schauer, D. B., and Falkow, S. (1993). Attaching and effacing locus of a *Citrobacter freundii* biotype that causes transmissible murine colonic hyperplasia. *Infect. Immun.* 61, 2486–2492.

Secades, P., Alvarez, B., and Guijarro, J. A. (2001). Purification and characterization of a psychrophilic, calcium-induced, growth-phase-dependent metalloprotease from the fish pathogen *Flavobacterium psychrophilum*. *Appl. Environ. Microbiol.* 67, 2436–2444.

Secades, P., Alvarez, B., and Guijarro, J. A. (2003). Purification and properties of a new psychrophilic metalloprotease (Fpp2) in the fish pathogen *Flavobacterium psychrophilum*. *FEMS Microbiol. Lett.* 226, 273–279.

Secombes, C. J. (1996). The nonspecific immune system: cellular defenses. *Fish Immune Syst.* 15, 63–103.

Sekine, Y., Tanzawa, T., Tanaka, Y., Ishimori, K., and Uchida, T. (2016). Cytoplasmic heme-binding protein (HutX) from *Vibrio cholerae* is an intracellular heme transport protein for the heme-degrading enzyme, HutZ. *Biochemistry* 55, 884–893.

Seshadri, R., Joseph, S. W., Chopra, A. K., Sha, J., Shaw, J., Graf, J., et al. (2006). Genome sequence of *Aeromonas hydrophila* ATCC 7966T: jack of all trades. *J. Bacteriol.* 188, 8272–8282.

Sharma, A., Sojar, H. T., Glurich, I., Honma, K., Kuramitsu, H. K., and Genco, R. J. (1998). Cloning, expression, and sequencing of a cell surface antigen containing a leucine-rich repeat motif from *Bacteroides* forsythus ATCC 43037. *Infect. Immun.* 66, 5703–5710.

Shi, Y. J., Fang, Q. J., Huang, H. Q., Gong, C. G., and Hu, Y. H. (2019). HutZ is required for biofilm formation and contributes to the pathogenicity of *Edwardsiella piscicida*. *Vet. Res.* 50:76.

Shotts, E. B. Jr., and Cooper, I. R. K. (1996). Chondroitinase Attenuated *Edwardsiella Ictaluri* And A Vaccine For Prevention Of Enteric Septicemia (ES) In Fish, United States Patent 5536658.

Silhavy, T. J., Kahne, D., and Walker, S. (2010). The bacterial cell envelope. *Cold Spring Harb. Perspect. Biol.* 2:a000414.

Silver, A. C., and Graf, J. (2009). Prevalence of genes encoding the type three secretion system and the effectors AexT and AexU in the *Aeromonas veronii* group. *DNA Cell Biol.* 28, 383–388.

Sixma, T. K., Pronk, S. E., Kalk, K. H., Wartna, E. S., van Zanten, B. A. M., Witholt, B., et al. (1991). Crystal structure of a cholera toxin-related heat-labile enterotoxin from *E. coli*. *Nature* 351, 371–377.

Smith, P. A., Pizarro, P., Ojeda, P., Contreras, J., Oyanedel, S., and Larenas, J. (1999). Routes of entry of *Piscirickettsia salmonis* in rainbow trout *Oncorhynchus mykiss*. *Dis. Aquat. Org.* 37, 165–172.

Soengas, R. G., Anta, C., Espada, A., Paz, V., Ares, I. R., Balado, M., et al. (2006). Structural characterization of vanchrobactin, a new catechol siderophore produced by the fish pathogen *Vibrio anguillarum* serotype O2. *Tetrahedron Lett.* 47, 7113–7116.

Soengas, R. G., Larrosa, M., Balado, M., Rodríguez, J., Lemos, M. L., and Jiménez, C. (2008). Synthesis and biological activity of analogues of vanchrobactin, a siderophore from *Vibrio anguillarum* serotype O2. *Org. Biomol. Chem.* 6, 1278–1287.

Song, T., Liu, H., Lv, T., Zhao, X., Shao, Y., Han, Q., et al. (2018). Characteristics of the iron uptake-related process of a pathogenic *Vibrio splendidus* strain associated with massive mortalities of the sea cucumber *Apostichopus japonicus*. *J. Invertebr. Pathol.* 155, 25–31.

Souto, A., Montaos, M. A., Rivas, A. J., Balado, M., Osorio, C. R., Rodríguez, J., et al. (2012). Structure and biosynthetic assembly of piscibactin, a siderophore from *Photobacterium damselae* subsp. *piscicida*, predicted from genome analysis. *Eur. J. Org. Chem.* 2012, 5693–5700.

Stackebrandt, E., and Hespell, R. (2006). The family succinivibrionaceae. *Prokaryotes* 3, 419–429.

Stanley, S. A., Raghavan, S., Hwang, W. W., and Cox, J. S. (2003). Acute infection and macrophage subversion by *Mycobacterium tuberculosis* require a specialized secretion system. *Proc. Natl. Acad. Sci. U.S.A.* 100, 13001–13006.

Staroscik, A. M., Denkin, S. M., and Nelson, D. R. (2005). Regulation of the *Vibrio anguillarum* metalloprotease EmpA by posttranslational modification. *J. Bacteriol.* 187, 2257–2260.

Stewart, D. J., Woldemariam, K., Dear, G., and Mochaba, F. M. (1983). An outbreak of 'Sekiten-byo' among cultured European eels, *Anguilla anguilla* L., in Scotland. *J. Fish Dis.* 6, 75–76.

Stintzi, A., and Raymond, K. N. (2000). Amonabactin-mediated iron acquisition from transferrin and lactoferrin by *Aeromonas hydrophila*: direct measurement of individual microscopic rate constants. *J. Biol. Inorg. Chem.* 5, 57–66.

Stork, M., Lorenzo, M. D., Mouriño, S., Osorio, C. R., Lemos, M. L., and Crosa, J. H. (2004). Two tonB systems function in iron transport in *Vibrio anguillarum*, but only one is essential for virulence. *Infect. Immun.* 72, 7326–7329.

Stratev, D., and Odeyemi, O. A. (2017). An overview of motile *Aeromonas septicaemia* management. *Aquac. Int.* 25, 1095–1105.

Stringer-Roth, K. M., Yunghans, W., and Caslake, L. F. (2002). Differences in chondroitin AC lyase activity of *Flavobacterium columnare* isolates. *J. Fish Dis.* 25, 687–691.

Sudheesh, P. S., Al-Ghabshi, A., Al-Mazrooei, N., and Al-Habsi, S. (2012). Comparative pathogenomics of bacteria causing infectious diseases in fish. *Int. J. Evol. Biol.* 2012:457264.

Sui, Z. H., Xu, H., Wang, H., Jiang, S., Chi, H., and Sun, L. (2017). Intracellular trafficking pathways of *Edwardsiella tarda*: from clathrin-and caveolin-mediated endocytosis to endosome and lysosome. *Front. Cell. Infect. Microbiol.* 7:400. doi: 10.3389/fcimb.2017.00400

Sun, B. G., Zhang, X. H., Tang, X., Wang, S., Zhong, Y., Chen, J., et al. (2007). A single residue change in Vibrio harveyi hemolysin results in the loss of phospholipase and hemolytic activities and pathogenicity for turbot (*Scophthalmus maximus*). *J. Bacteriol.* 189, 2575–2579.

Sun, H. Y., Cao, X. H., Jiang, Y. F., Ni, L. Y., Mo, Z. Q., Qin, Q. W., et al. (2018). Outbreak of a novel disease associated with *Citrobacter freundii* infection in freshwater cultured stingray, *Potamotrygon motoro*. *Aquaculture* 492, 35–39.

Sun, J., and Barbieri, J. T. (2003). *Pseudomonas aeruginosa* ExoT ADP-ribosylates CT10 regulator of kinase (Crk) proteins. *J. Biol. Chem.* 278, 32794–32800.

Sunagawa, S. (2015). Ocean plankton: structure and function of the global ocean 793 microbiome. *Science* 348:794.

Svendsen, Y. S., and Bøgwald, J. (1997). Influence of artificial wound and non-intact mucus layer on mortality of *Atlantic salmon* (*Salmo salar*) following a bath challenge with *Vibrio anguillarum* and *Aeromonas salmonicida*. *Fish Shellfish Immun.* 7, 317–325.

Szymanski, C. M., Michael, F. S., Jarrell, H. C., Li, J., Gilbert, M., Larocque, S., et al. (2003). Detection of conserved N-linked glycans and phase-variable lipooligosaccharides and capsules from campylobacter cells by mass spectrometry and high resolution magic angle spinning NMR spectroscopy. *J. Biol. Chem.* 278, 24509–24520.

Tacchi, L., Bron, J. E., Taggart, J. B., Secombes, C. J., Bickerdike, R., Adler, M. A., et al. (2011). Multiple tissue transcriptomic responses to *Piscirickettsia salmonis* in *Atlantic salmon* (*Salmo salar*). *Physiol. Genomics* 43, 1241–1254.

Takeuchi, H., Shibano, Y., Morihara, K., Fukushima, J., Inami, S., Keil, B., et al. (1992). Structural gene and complete amino acid sequence of *Vibrio alginolyticus* collagenase. *Biochem. J.* 281(Pt 3), 703–708.

Tan, Y. P., Zheng, J., Tung, S. L., Rosenshine, I., and Leung, K. Y. (2005). Role of type III secretion in *Edwardsiella tarda* virulence. *Microbiology* 151, 2301–2313.

Tanabe, T., Funahashi, T., Nakao, H., Miyoshi, S. I., Shinoda, S., and Yamamoto, S. (2003). Identification and characterization of genes required for biosynthesis and transport of the siderophore vibrioferrin in *Vibrio parahaemolyticus*. *J. Bacteriol.* 185, 6938–6949.

Tanaka, K. H., Dallaire-Dufresne, S., Daher, R. K., Frenette, M., and Charette, S. J. (2012). An insertion sequence-dependent plasmid rearrangement in *Aeromonas salmonicida* causes the loss of the type three secretion system. *PLoS One* 7:e33725.

Tanaka, K. H., Vincent, A. T., Emond-Rheault, J. G., Adamczuk, M., Frenette, M., and Charette, S. J. (2017). Plasmid composition in *Aeromonas salmonicida* subsp. *salmonicida* 01-B526 unravels unsuspected type three secretion system loss patterns. *BMC Genom.* 18:528. doi: 10.1186/s12864-017-3921-1

Tekedar, H. C., Karsi, A., Gillaspy, A. F., Dyer, D. W., Benton, N. R., Zaitshik, J., et al. (2012). Genome sequence of the fish pathogen *Flavobacterium columnare* ATCC 49512. *J. Bacteriol.* 194, 2763–2764.

Tekedar, H. C., Kumru, S., Blom, J., Perkins, A. D., Griffin, M. J., Abdelhamed, H., et al. (2019b). Comparative genomics of *Aeromonas veronii*: identification of a pathotype impacting aquaculture globally. *PLoS One* 14:e0221018. doi: 10.1371/journal.pone.0221018

Tekedar, H. C., Abdelhamed, H., Kumru, S., Blom, J., Karsi, A., and Lawrence, M. L. (2019a). Comparative genomics of *Aeromonas hydrophila* secretion systems and mutational analysis of hcp1 and vgrG1 genes from T6SS. *Front. Microbiol.* 9:3216. doi: 10.3389/fmicb.2018.03216

Telford, J. R., and Raymond, K. N. (1998). Coordination chemistry of the amonabactins, bis(catecholate) siderophores from *Aeromonas hydrophila*(1). *Inorg. Chem.* 37, 4578–4583.

Thanassi, D. G., and Hultgren, S. J. (2000). Multiple pathways allow protein secretion across the bacterial outer membrane. *Curr. Opin. Cell Biol.* 12, 420–430.

Thode, S. K., Rojek, E., Kozlowski, M., Ahmad, R., and Haugen, P. (2018). Distribution of siderophore gene systems on a *Vibrionaceae phylogeny*: database searches, phylogenetic analyses and evolutionary perspectives. *PLoS One* 13:e0191860. doi: 10.1371/journal.pone.0191860

Thomas, D. R., Newton, P., Lau, N., and Newton, H. J. (2020). Interfering with autophagy: the opposing strategies deployed by *Legionella pneumophila* and *Coxiella burnetii* effector proteins. *Front. Cell. Infect. Microbiol.* 10:599762. doi: 10.3389/fcimb.2020.599762

Thomas, F., Hehemann, J. H., Rebuffet, E., Czjzek, M., and Michel, G. (2011). Environmental and gut bacteroidetes: the food connection. *Front. Microbiol.* 2:93. doi: 10.3389/fmicb.2011.00093

Thomas, S., Holland, B. I., and Schmitt, L. (2014). The type 1 secretion pathway — the hemolysin system and beyond. *Biochim. Biophys. Acta Mol. Cell Res.* 1843, 1629–1641.

Thornley, J. P., Shaw, J. G., Gryllos, A. I., and Eley, A. (1997). Virulence properties of clinically significant *Aeromonas* species: evidence for pathogenicity. *Rev. Med. Microbiol.* 8, 61–72.

Thune, R. L., Fernandez, D. H., Benoit, J. L., Kelly-Smith, M., Rogge, M. L., Booth, N. J., et al. (2007). Signature-tagged mutagenesis of *Edwardsiella ictaluri* identifies virulence-related genes, including a *Salmonella* pathogenicity island 2 class of Type III secretion systems. *Appl. Environ. Microbiol.* 73, 7934–7946.

Thune, R. L., Stanley, L. A., and Cooper, R. K. (1993). Pathogenesis of gram-negative bacterial infections in warmwater fish. *Annu. Rev. Fish Dis.* 3, 37–68.

Titball, R. W., and Munn, C. B. (1985). The purification and some properties of H-lysin from *Aeromonas salmonicida*. *J. Gen. Microbiol.* 131, 1603–1609.

Titball, R., and Munn, C. (1981). Evidence for two haemolytic activities from *Aeromonas salmonicida*. *FEMS Microbiol. Lett.* 12, 27–30.

Tobback, E., Decostere, A., Hermans, K., Haesebrouck, F., and Chiers, K. (2007). *Yersinia ruckeri* infections in salmonid fish. *J. Fish Dis.* 30, 257–268.

Toranzo, A. E., and Barja, J. L. (1993). Virulence factors of bacteria pathogenic for coldwater fish. *Annu. Rev. Fish Dis.* 3, 5–36.

Toranzo, A. E., Magariños, B., and Romalde, J. L. (2005). A review of the main bacterial fish diseases in mariculture systems. *Aquaculture* 246, 37–61.

Tort, L., Padros, F., Rotllant, J., and Crespo, S. (1998). Winter syndrome in the gilthead sea bream *Sparus aurata*. Immunological and histopathological features. *Fish Shellfish Immunol.* 8, 37–47.

Touchon, M., Barbier, P., Bernardet, J. F., Loux, V., Vacherie, B., Barbe, V., et al. (2011). Complete genome sequence of the fish pathogen *Flavobacterium branchiophilum*. *Appl. Environ. Microbiol.* 77, 7656–7662.

Trosky, J. E., Li, Y., Mukherjee, S., Keitany, G., Ball, H., and Orth, K. (2007). VopA inhibits ATP binding by acetylating the catalytic loop of MAPK kinases. *J. Biol. Chem.* 282, 34299–34305.

Tsirigotaki, A., De Geyter, J., Šoštaric', N., Economou, A., and Karamanou, S. (2017). Protein export through the bacterial Sec pathway. *Nat. Rev. Microbiol* 15, 21–36.

Tunsjø, H. S., Paulsen, S. M., Berg, K., Sørum, H., and L'Abée-Lund, T. M. (2009). The winter ulcer bacterium *Moritella viscosa* demonstrates adhesion and cytotoxicity in a fish cell model. *Microb. Pathog.* 47, 134–142.

Valderrama, K., Balado, M., Rey-Varela, D., Rodríguez, J., Vila-Sanjurjo, A., Jiménez, C., et al. (2019). Outer membrane protein FrpA, the siderophore piscibactin receptor of *Photobacterium damselae* subsp. piscicida, as a subunit vaccine against photobacteriosis in sole (*Solea senegalensis*). *Fish Shellfish Immunol.* 94, 723–729.

Valiente, E., Lee, C. T., Lamas, J., Hor, L., and Amaro, C. (2008). Role of the virulence plasmid pR99 and the metalloprotease Vvp in resistance of *Vibrio vulnificus* serovar E to eel innate immunity. *Fish Shellfish Immunol.* 24, 134–141.

Varina, M., Denkin, S. M., Staroscik, A. M., and Nelson, D. R. (2008). Identification and characterization of Epp, the secreted processing protease for the *Vibrio anguillarum* EmpA metalloprotease. *J. Bacteriol.* 190, 6589–6597.

Veith, P. D., Glew, M. D., Gorasia, D. G., and Reynolds, E. C. (2017). Type IX secretion: the generation of bacterial cell surface coatings involved in virulence, gliding motility and the degradation of complex biopolymers. *Mol. Microbiol.* 106, 35–53.

Vilches, S., Urgell, C., Merino, S., Chacón, M. R., Soler, L., Castro-Escarpulli, G., et al. (2004). Complete Type III secretion system of a mesophilic *Aeromonas hydrophila* Strain. *Appl. Environ. Microbiol.* 70, 6914–6919.

Villarreal, L. P. (2008). *Origin of Group Identity: Viruses, Addiction And Cooperation*. Berlin: Springer Science & Business Media.

Vipond, R., Bricknell, R. I., Durant, E., Bowden, T. J., Ellis, A. E., Smith, M., et al. (1998). Defined deletion mutants demonstrate that the major secreted toxins are not essential for the virulence of *Aeromonas salmonicida*. *Infect. Immun.* 66, 1990–1998.

Virji, M. (1997). Post-translational modifications of meningococcal pili. Identification of common substituents: glycans and α-glycerophosphate-a review. *Gene* 192, 141–147.

von Hoven, G., Neukirch, C., Meyenburg, M., Schmidt, S., Vences, A., Osorio, C. R., et al. (2018). Cytotoxin- and chemotaxis-genes cooperate to promote adhesion of *Photobacterium damselae* subsp. damselae. *Front. Microbiol.* 9:2996. doi: 10.3389/fmicb.2018.02996

Wakabayashi, H., and Egusa, S. (1972). Characteristics of a *Pseudomonas* sp. from an epizootic of pond-cultured eels (*Anguilla japonica*). *Bull. Jpn. Soc. Sci. Fish.* 38, 577–587.

Wakabayashi, H., Hikida, M., and Masumura, K. (1986). *Flexibacter maritimus* sp. nov., a pathogen of marine fishes. *Int. J. Syst. Evol. Microbiol.* 36, 396–398.

Walport, M. J. (2001). Complement. First of two parts. *N. Engl. J. Med.* 344, 1058–1066.

Waltman, W. D., Shotts, E. B., and Hsu, T. C. (1986). Biochemical characteristics of *Edwardsiella ictaluri*. *Appl. Environ. Microbiol.* 51, 101–104.

Wandersman, C., and Delepelaire, P. (2004). Bacterial iron sources: from siderophores to hemophores. *Annu. Rev. Microbiol.* 58, 611–647.

Wang, H., Zeng, X., Mo, Y., He, B., Lin, H., and Lin, J. (2019). Enterobactin-specific antibodies induced by a novel enterobactin conjugate vaccine. *Appl. Environ. Microbiol.* 85:e00358–19.

Wang, Q., Liu, Q., Ma, Y., Zhou, L., and Zhang, Y. (2007). Isolation, sequencing and characterization of cluster genes involved in the biosynthesis and utilization of the siderophore of marine fish pathogen *Vibrio alginolyticus*. *Arch. Microbiol.* 188, 433–439.

Wang, Q., Yang, M., Xiao, J., Wu, H., Wang, X., Lv, Y., et al. (2009). Genome sequence of the versatile fish pathogen *Edwardsiella tarda* provides insights into its adaptation to broad host ranges and intracellular niches. *PLoS One* 4:e7646. doi: 10.1371/journal.pone.0007646

Wang, X., Wang, Q., Xiao, J., Liu, Q., Wu, H., and Zhang, Y. (2010). Hemolysin EthA in *Edwardsiella tarda* is essential for fish invasion in vivo and in vitro and regulated by two-component system EsrA-EsrB and nucleoid protein HhaEt. *Fish Shellfish Immunol.* 29, 1082–1091.

Wang, X., Wang, Q., Xiao, J., Liu, Q., Wu, H., Xu, L., et al. (2009). *Edwardsiella tarda* T6SS component evpP is regulated by esrB and iron, and plays essential roles in the invasion of fish. *Fish. Shellfish Immunol.* 27, 469–477.

Weber, B., Chen, C., and Milton, D. L. (2010). Colonization of fish skin is vital for *Vibrio anguillarum* to cause disease. *Environ. Microbiol. Rep.* 2, 133–139.

Webster, A. C., and Litwin, C. M. (2000). Cloning and characterization of vuuA, a gene encoding the *Vibrio vulnificus* ferric vulnibactin receptor. *Infect. Immun.* 68, 526–534.

Wheeler, R. W., Davies, R. L., Dalsgaard, I., Garcia, J., Welch, T. J., Wagley, S., et al. (2009). *Yersinia ruckeri* biotype 2 isolates from mainland Europe and the UK likely represent different clonal groups. *Dis. Aquat. Organ.* 84, 25–33.

Whitby, P., Landon, M., and Coleman, G. (1992). The cloning and nucleotide sequence of the serine protease gene (aspA) of *Aeromonas salmonicida* ssp. salmonicida. *FEMS Microbiol. Lett.* 78, 65–71.

Wiklund, T., and Bylund, G. (1990). *Pseudomonas* anguilliseptica as a pathogen of salmonid fish in Finland. *Dis. Aqu. Org.* 8, 13–19.

Wilkie, M. P. (2002). Ammonia excretion and urea handling by fish gills: present understanding and future research challenges. *J. Exp. Zool.* 293, 284–301.

Wilmsen, H. U., Pattus, F., and Buckley, J. T. (1990). Aerolysin, a hemolysin from *Aeromonas hydrophila*, forms voltage-gated channels in planar lipid bilayers. *J. Membr. Biol.* 115, 71–81.

Wilson, R. L., Brown, L. L., Kirkwood-Watts, D., Warren, T. K., Lund, S. A., King, D. S., et al. (2006). *Listeria monocytogenes* 10403S HtrA is necessary for resistance to cellular stress and virulence. *Infect. Immun.* 74, 765–768.

Winkelmann, G., Schmid, D. G., Nicholson, G., Jung, G., and Colquhoun, D. J. (2002). Bisucaberin–a dihydroxamate siderophore isolated from *Vibrio salmonicida*, an important pathogen of farmed Atlantic salmon (*Salmo salar*). *Biometals* 15, 153–160.

Wong, A. R. C., Pearson, J. S., Bright, M. D., Munera, D., Robinson, K. S., Lee, S. F., et al. (2011). Enteropathogenic and enterohaemorrhagic *Escherichia coli*: even more subversive elements. *Mol. Microbiol.* 80, 1420–1438.

Wrobel, A., Leo, J. C., and Linke, D. (2019). Overcoming fish defences: the virulence factors of *Yersinia ruckeri*. *Genes (Basel)* 10:700.

Wrobel, A., Ottoni, C., Leo, J. C., and Linke, D. (2018). pYR4 from a Norwegian isolate of *Yersinia ruckeri* is a putative virulence plasmid encoding both a Type IV pilus and a Type IV secretion system. *Front. Cell. Infect. Microbiol.* 8:373. doi: 10.3389/fcimb.2018.00373

Xie, H. X., Lu, J. F., Zhou, Y., Yi, J., Yu, X. J., Leung, K. Y., et al. (2015). Identification and functional characterization of the novel *Edwardsiella tarda* effector EseJ. *Infect. Immun.* 83, 1650–1660.

Xu, X., Li, H., Qi, X., Chen, Y., Qin, Y., Zheng, J., et al. (2021). cheA, cheB, cheR, cheV, and cheY are involved in regulating the adhesion of *Vibrio harveyi*. *Front. Cell. Infect. Microbiol.* 10:591751. doi: 10.3389/fcimb.2020.591751

Yahr, T. L., Barbieri, J. T., and Frank, D. W. (1996a). Genetic relationship between the 53- and 49-kilodalton forms of exoenzyme S from *Pseudomonas aeruginosa*. *J. Bacteriol.* 178, 1412–1419.

Yahr, T. L., Goranson, J., and Frank, D. W. (1996b). Exoenzyme S of *Pseudomonas aeruginosa* is secreted by a type III pathway. *Mol. Microbiol.* 22, 991–1003.

Yan, Z., Yin, M., Chen, J., and Li, X. (2020). Assembly and substrate recognition of curli biogenesis system. *Nat. Commun.* 11:241.

Yarbrough, M. L., Li, Y., Kinch, L. N., Grishin, N. V., Ball, H. L., and Orth, K. (2009). AMPylation of Rho GTPases by *Vibrio* VopS disrupts effector binding and downstream signaling. *Science* 323, 269–272.

Young, N. M., Brisson, J. R., Kelly, J., Watson, D. C., Tessier, L., Lanthier, P. H., et al. (2002). Structure of the N-linked glycan present on multiple glycoproteins in the Gram-negative bacterium, *Campylobacter jejuni*. *J. Biol. Chem.* 277, 42530–42539.

Yu, H. B., Rao, P. S. S., Lee, H. C., Vilches, S., Merino, S., Tomas, J. M., et al. (2004). A type III secretion system is required for *Aeromonas hydrophila* AH-1 pathogenesis. *Infect. Immun.* 72, 1248–1256.

Yu, Y., Yang, H., Li, J., Zhang, P., Wu, B., Zhu, B., et al. (2012). Putative Type VI secretion systems of *Vibrio parahaemolyticus* contribute to adhesion to cultured cell monolayers. *Arch. Microbiol.* 194, 827–835.

Zane, H. K., Naka, H., Rosconi, F., Sandy, M., Haygood, M. G., and Butler, A. (2014). Biosynthesis of amphi-enterobactin siderophores by *Vibrio harveyi* BAA-1116: identification of a bifunctional nonribosomal peptide synthetase condensation domain. *J. Am. Chem. Soc.* 136, 5615–5618.

Zhang, F., Chen, J., Chi, Z., and Wu, L. F. (2006). Expression and processing of *Vibrio anguillarum* zinc-metalloprotease in *Escherichia coli*. *Arch. Microbiol.* 186, 11–20.

Zhang, L., Krachler, A. M., Broberg, C. A., Li, Y., Mirzaei, H., Gilpin, C. J., et al. (2012). Type III effector VopC mediates invasion for *Vibrio* species. *Cell Rep.* 1, 453–460.

Zhang, X. H., and Austin, B. (2005). Haemolysins in *Vibrio* species. *J. Appl. Microbiol.* 98, 1011–1019.

Zhang, Y., Deng, Y., Feng, J., Guo, Z., Chen, H., Wang, B., et al. (2021). Functional characterization of VscCD, an important component of the Type III secretion system of *Vibrio harveyi*. *Microb. Pathog.* 157:104965.

Zhang, Y., Zhao, L., Chen, W., Huang, Y., Yang, L., Sarathbabu, V., et al. (2017). Complete genome sequence analysis of the fish pathogen *Flavobacterium columnare* provides insights into antibiotic resistance and pathogenicity related genes. *Microb. Pathog.* 111, 203–211.

Zhao, Z., Chen, C., Hu, C. Q., Ren, C. H., Zhao, J. J., Zhang, L. P., et al. (2010). The Type III secretion system of *Vibrio alginolyticus* induces rapid apoptosis, cell rounding and osmotic lysis of fish cells. *Microbiology* 156, 2864–2872.

Zhao-lan, M., Shi-yong, C., and Pei-jun, Z. (2002). Properties of proteolytic toxin of *Vibrio anguilolarum* from diseased flounder. *Chin. J. Oceanol. Limnol.* 20, 316–322.

Zhong, Y., Zhang, X. H., Chen, J., Chi, Z., Sun, B., Li, Y., et al. (2006). Overexpression, purification, characterization, and pathogenicity of *Vibrio harveyi* hemolysin VHH. *Infect. Immun.* 74, 6001–6005.

Zhou, Z.-J., Sun, B. G., and Sun, L. (2015). *Edwardsiella tarda* Sip1: A serum-induced zinc metalloprotease that is essential to serum resistance and host infection. *Vet. Microbiol.* 177, 332–340.

Zhu, Z., Dong, C., Weng, S., and He, J. (2019). Identification of outer membrane protein TolC as the major adhesin and potential vaccine candidate for *Vibrio harveyi* in hybrid grouper, *Epinephelus fuscoguttatus* (♀) × *E. lanceolatus* (♂). *Fish Shellfish Immunol.* 86, 143–151.

Zhuang, Q., Dai, F., Shao, Y., Li, C., and Zhang, W. (2021). vscN encodes a Type III secretion system ATPase in *Vibrio splendidus* AJ01 that contributes to pathogenicity and Hop secretion. *Aquaculture* 533: 736228.

Zhuang, Q., Dai, F., Zhao, X., Shao, Y., Guo, M., Lv, Z., et al. (2020). Cloning and characterization of the virulence factor Hop from *Vibrio splendidus*. *Microb. Pathog.* 139:103900.

Zúñiga, A., Aravena, P., Pulgar, R., Travisany, D., Ortiz-Severín, J., Chávez, F. P., et al. (2020). Transcriptomic changes of *Piscirickettsia salmonis* during intracellular growth in a salmon macrophage-like cell line. *Front. Cell. Infect. Microbiol.* 9:426. doi: 10.3389/fcimb.2019.00426

Conflict of Interest: The authors declare that the research was conducted in the absence of any commercial or financial relationships that could be construed as a potential conflict of interest.

Publisher's Note: All claims expressed in this article are solely those of the authors and do not necessarily represent those of their affiliated organizations, or those of the publisher, the editors and the reviewers. Any product that may be evaluated in this article, or claim that may be made by its manufacturer, is not guaranteed or endorsed by the publisher.

frontiers in Microbiology

MINI REVIEW
published: 15 December 2021
doi: 10.3389/fmicb.2021.762582

The Impact of *Bartonella* VirB/VirD4 Type IV Secretion System Effectors on Eukaryotic Host Cells

*Katja Fromm and Christoph Dehio**

Biozentrum, University of Basel, Basel, Switzerland

Bartonella spp. are facultative intracellular pathogens that infect a wide range of mammalian hosts including humans. The VirB/VirD4 type IV secretion system (T4SS) is a key virulence factor utilized to translocate *Bartonella* effector proteins (Beps) into host cells in order to subvert their functions. Crucial for effector translocation is the C-terminal Bep intracellular delivery (BID) domain that together with a positively charged tail sequence forms a bipartite translocation signal. Multiple BID domains also evolved secondary effector functions within host cells. The majority of Beps possess an N-terminal filamentation induced by cAMP (FIC) domain and a central connecting oligonucleotide binding (OB) fold. FIC domains typically mediate AMPylation or related post-translational modifications of target proteins. Some Beps harbor other functional modules, such as tandem-repeated tyrosine-phosphorylation (EPIYA-related) motifs. Within host cells the EPIYA-related motifs are phosphorylated, which facilitates the interaction with host signaling proteins. In this review, we will summarize our current knowledge on the molecular functions of the different domains present in Beps and highlight examples of Bep-dependent host cell modulation.

Keywords: host-pathogen interaction, bacterial pathogenesis, type IV secretion system (T4SS), VirB/VirD4, bacterial effector protein, *Bartonella* effector protein (Bep)

OPEN ACCESS

Edited by:
Eric Cascales,
Aix-Marseille Université, France

Reviewed by:
Rishi Drolia,
Purdue University, United States
Ethel Bayer-Santos,
University of São Paulo, Brazil

***Correspondence:**
Christoph Dehio
christoph.dehio@unibas.ch

Specialty section:
This article was submitted to Microbial Physiology and Metabolism, a section of the journal Frontiers in Microbiology

Received: *22 August 2021*
Accepted: *29 October 2021*
Published: *15 December 2021*

Citation:
Fromm K and Dehio C (2021) The Impact of Bartonella VirB/VirD4 Type IV Secretion System Effectors on Eukaryotic Host Cells. Front. Microbiol. 12:762582. doi: 10.3389/fmicb.2021.762582

INTRODUCTION

Bacterial type IV secretion systems (T4SSs) are multi-protein complexes embedded in the cell envelopes of bacteria and some archaea. These systems enable the translocation of macromolecules across membranes, such as uptake of extracellular DNA and translocation of protein effectors into recipient cells (Christie et al., 2014; Waksman, 2019; Costa et al., 2020). T4SSs are essential for the pathogenicity of many bacteria infecting humans and other mammals, such as *Helicobacter pylori*, *Legionella pneumophila*, *Brucella* spp. or *Bartonella* spp. (Cascales and Christie, 2003). Based on structural characteristics T4SS can be categorized into T4AS and T4BS systems. T4AS are composed of 12 subunits termed VirB1-11 and VirD4 according to the nomenclature of the paradigmatic VirB/VirD4 T4SS of the plant pathogen *Agrobacterium tumefaciens* (Waksman, 2019). VirB2-11 assemble the translocation channel spanning through the inner and outer membranes. Typically, the membrane-bound ATPase VirD4, also termed type IV secretion (T4S) coupling protein (T4CP), recognizes T4S substrates prior to translocation. The majority of the T4S substrates contain signals at their C-termini consisting of a few positively charged or hydrophobic residues (Christie et al., 2014).

However, some T4S substrates form a larger structural scaffold as translocation signal. These include the R1-plasmid encoded relaxase TraI (Redzej et al., 2013) and the effector proteins of *Bartonella* spp. (Schulein et al., 2005).

Bartonellae are Gram-negative facultative intracellular pathogens, which infect various mammals including humans. These bacteria are transmitted by blood-sucking arthropods such as fleas, sand flies or lice. The current model suggests that the bacteria are superficially inoculated into the dermis (e.g., through scratching) followed by the colonization of two sequential niches, the "dermal niche" and the "blood-seeding niche" (Okujava et al., 2014; Siamer and Dehio, 2015; **Figure 1**). In the dermal stage of infection, the bacteria might hijack migratory cells, such as dendritic cells or macrophages, to reach the "blood-seeding niche." In this niche, the bacteria colonize endothelial cells and possibly other cell types. Subsequently, *Bartonella* seed into the blood stream where they cause a long-lasting intraerythrocytic bacteremia, an infection stage restricted to the natural reservoir host (Schulein et al., 2001; Harms and Dehio, 2012; Pulliainen and Dehio, 2012).

The genus *Bartonella* can be divided into three phylogenetic clades: *Bartonella apis* and *Bartonella tamiae*, which occupy ancestral positions and the Eubartonellae, which are further divided into four distinct lineages (Engel et al., 2011; Guy et al., 2013). *Bartonella anchashensis* of lineage 1 and all members of lineages 3 and 4 harbor a VirB/VirD4 T4SS (Harms et al., 2017). The VirB/VirD4 T4SS in *Bartonella* is essential for successful host colonization. T4SS-deficient mutants of *Bartonella tribocorum*, Δ*virB4* or Δ*virD4*, failed to invade the blood stream in an experimental rat infection model (Schulein and Dehio, 2002). Multiple *in vitro* studies with the major human pathogen *Bartonella henselae* showed that *Bartonella* effector proteins (Beps) are translocated *via* the VirB/VirD4 T4SS into different host cells belonging to the "dermal" and the "blood-seeding niche." Inside the host cells, Beps target various components to modulate the immune response and to subvert host cellular functions to the benefit of the pathogen (Schulein et al., 2005; Schmid M. C. et al., 2006; Okujava et al., 2014; Sorg et al., 2020; Marlaire and Dehio, 2021; **Figure 1**).

In this review, we will discuss recent advances made concerning the functional role of Beps during host colonization. We will focus on the structural and functional aspects of different domains present in Beps with regard to the subversion of host cellular function.

DOMAIN ARCHITECTURE OF *BARTONELLA* EFFECTOR PROTEINS

Bartonella effector proteins display a modular domain architecture (**Figure 1**). The majority of the Beps possess an N-terminal filamentation induced by cAMP (FIC) domain followed by a central connecting oligonucleotide binding (OB) fold and a C-terminal Bep intracellular delivery (BID) domain (Engel et al., 2011; Harms et al., 2017). Instead of the FIC domain, some effectors harbor tandem-repeated tyrosine phosphorylation motifs (pY) and/or additional BID domains (Wagner and Dehio, 2019; **Figure 1**). While the C-terminal BID domains function as a conserved T4S signal, some BID domains also acquired secondary effector functions within eukaryotic host cells (Truttmann et al., 2011a; Pulliainen et al., 2012; Okujava et al., 2014).

The different domain architectures suggest that Beps evolved from a single ancestral effector with a FIC-OB-BID structure *via* independent gene duplication and recombination events. Diverse Bep repertoires arose in the three distinct lineages resulting in Bep197-234 in *Bartonella ancashensis* of lineage 1, Bep1-10 in bacteria of lineage 3, and BepA-I in lineage 4 (Harms et al., 2017).

STRUCTURAL FEATURES OF BID DOMAINS

Bartonella effector proteins are recognized by the VirB/VirD4 T4SS *via* a bipartite translocation signal composed of the approximately 100-aa-long BID domain and a short positively charged C-terminal tail (Schulein et al., 2005; Stanger et al., 2017). BID domains are sequence-variable but adopt a conserved structural fold consisting of an anti-parallel four-helix bundle topped with a hook (Stanger et al., 2017; Wagner et al., 2019). The conserved fold and the elongated shape of the BID domains might be crucial features for the secretion signal. In addition, the surface charge distribution of BID domains is also to some degree conserved, displaying two positively charged areas separated by one negatively charged patch (Stanger et al., 2017; Wagner et al., 2019). The conserved fold of the BID domains might be essential for the secretion *via* the VirB/VirD4 T4SS, while the highly variable sequence might enable the acquisition of secondary functions.

BID Domain-Mediated Host Cell Modulations

The secondary evolved functions of some BID domains are essential for host colonization at various stages of the infection cycle. These functions include dissemination within the host, bacterial uptake through induction of stress fiber formation and inhibition of apoptosis.

Bartonella spp. supposedly infect dendritic cells during the dermal stage of infection in order to reach the "blood-seeding niche." BepE was shown to promote the migratory capability of dendritic cells indicating that the bacteria exploit these cells as Trojan horses in order to reach the blood stream. Further, dissemination of *B. tribocorum* into the blood stream depends on the function of BepE (Okujava et al., 2014). BepE of *B. henselae* harbors a pY-domain and two BID domains (Wagner et al., 2019). Although, the pY motif of BepE interacts with several host proteins (Selbach et al., 2009), the dissemination of the bacteria into the blood stream exclusively relies on the BID domains. *In vitro* assays demonstrated that the terminal BID domain of BepE was required to safeguard dendritic cells from damage triggered by BepC (Okujava et al., 2014; **Figure 2**).

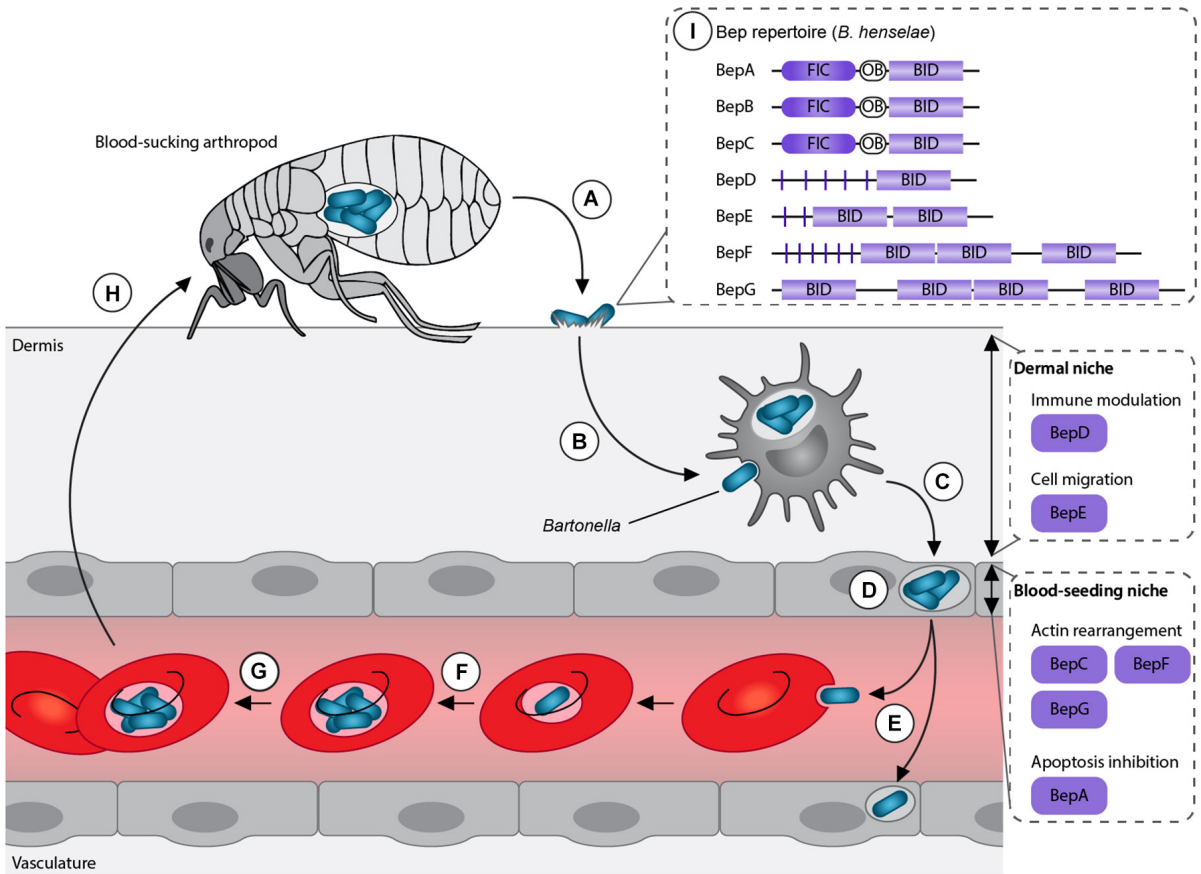

FIGURE 1 | Model of *Bartonella* life cycle. **(A)** Bartonellae replicate inside the midgut of their arthropod vector and are secreted with their feces. **(B)** After inoculation into the dermis, the bacteria colonize the "dermal niche," which most likely includes dendritic cells. During this infection stage, the downregulation of the immune response mediated by BepD might play an essential role. **(C)** Migratory immune cells are considered to disseminate the bacteria to the "blood-seeding niche," a process that seems to depend on BepE. **(D)** Inside the "blood-seeding niche," the bacteria likely colonize endothelial cells, which might require the action of BepC, BepF, BepG, and BepA. **(E)** From the "blood-seeding niche" Bartonellae are disseminated into the blood stream, where they invade erythrocytes. **(F)** The bacteria undergo replication and **(G)** persist until **(H)** they can be taken up during the next blood meal by another arthropod. **(I)** Representative *Bartonella* effector protein (Bep) repertoire of the model organism *B. henselae*. Adapted from Siamer and Dehio (2015).

A recent publication demonstrated that the BID domains of BepE (*Bartonella quintana*) are ubiquitinated and trigger selective autophagy inside the host cells. Interestingly, BepE of *B. henselae* was not ubiquitinated (Wang et al., 2019). These data indicate that orthologous Beps can vary between *Bartonella* species. Future studies should aim to clarify whether the assigned functional differences are relevant in a pathogen- or host-specific context.

B. henselae invades endothelial cells either individually by endocytosis or as bacterial aggregate through the formation of the so-called invasome. This unique cellular structure is induced by F-actin rearrangements and stress fiber formation (Dehio, 1999). The invasome formation depends on the VirB/VirD4 T4SS and is induced by either BepG or the combined action of BepC and BepF (Schmid et al., 2004; Rhomberg et al., 2009; Truttmann et al., 2011b). BepF of *B. henselae* contains three BID domains. The two non-terminal BID domains trigger the invasome formation (together with BepC), while the third BID domain is negligible in this process (Truttmann et al., 2011a; **Figure 2**). BepG consists of solely four BID domains connected *via* short linker sequences, hence it is likely that at least one of them induces the invasome formation (Rhomberg et al., 2009).

B. henselae and *B. quintana* promote the proliferation of human endothelial cells by inhibiting apoptosis (Kirby and Nekorchuk, 2002; Schmid M. C. et al., 2006; Pulliainen et al., 2012). The anti-apoptotic activity depends on the BID domain of BepA, which interacts with the catalytic subunit C2 of the human adenylyl cyclase 7 (AC7) (Pulliainen et al., 2012). AC7 is a plasma membrane-bound protein that regulates cAMP synthesis (Sadana and Dessauer, 2009). The interaction of BepA with C2 likely enhances the association with the C1 subunit and thereby potentiates cAMP production. The elevated cAMP-levels and consecutive upregulation of gene expression then leads to the inhibition of apoptosis (Pulliainen et al., 2012; **Figure 2**). It is believed that the bacteria undergo several rounds of replication within "primary" or "blood-seeding niche" before invading the blood stream (Schulein et al., 2001). Inhibition of endothelial cell death might therefore be crucial for host colonization.

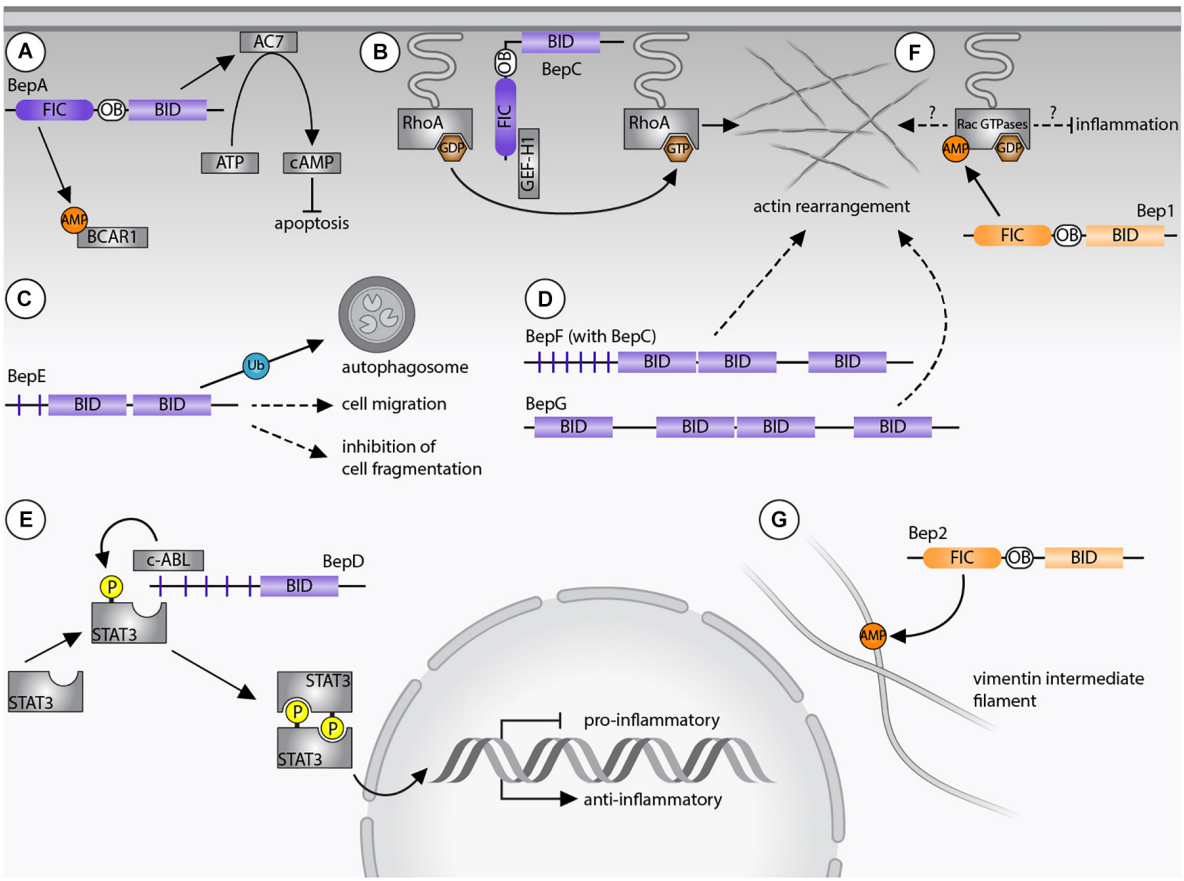

FIGURE 2 | *Bartonella* effector protein-mediated subversion of host cellular functions. **(A)** BepA AMPylates breast cancer anti-estrogen resistance protein 1 (BCAR1) *via* its filamentation induced by cAMP (FIC) domain and interacts with adenylyl cyclase 7 (AC7) *via* its Bep intracellular delivery (BID) domain. The AC7-mediated conversion of ATP to cAMP results in inhibition of apoptosis. **(B)** BepC recruits GEF-H1 *via* its FIC domain to activate the RhoA pathway. **(C)** BepE is required for the dissemination within the mammalian host and promotes cell migration. The BID domain of BepE of *B. quintana* becomes ubiquitinated inside host cells and is degraded by autophagy. **(D)** BepG or BepF together with BepC induce stress fiber formation resulting in the formation of the invasome. **(E)** Upregulation of an anti-inflammatory immune response depends on the pY-domain of BepD, which provides a binding platform for the SH2 domain containing proteins c-ABL and STAT3. Due to close proximity, STAT3 becomes phosphorylated by c-ABL and triggers gene expression of IL-10. **(F)** Bep1 AMPylates the GDP-bound Rac-subfamily of GTPases. **(G)** Bep2 AMPylates the vimentin intermediate filaments. Dashed arrows indicate currently unknown target proteins, continuous arrows display interactions with confirmed targets. *Bartonella* effector proteins (Beps) of lineage 4 of are displayed in purple, Beps of lineage 3 Bartonellae are shown in orange.

Interestingly, the BepA ortholog of *B. tribocorum* did not display anti-apoptotic activity (Schmid D. et al., 2006), indicating again that orthologous Beps can fulfill divergent functions in the infection process.

EVOLUTIONARY DIVERSIFICATION OF FIC DOMAIN-CONTAINING *BARTONELLA* EFFECTOR PROTEINS

FIC domains are characterized by a helical topology and a conserved FIC signature motif. The canonical signature motif [HPFx(D/E)GNGRxxR] comprises a catalytic histidine and residues involved in adenosine triphosphate (ATP) binding. This motif is strictly required for catalyzing the AMPylation reaction, a post-translational modification that involves the transfer of an adenosine monophosphate (AMP) moiety from ATP onto target proteins (Engel et al., 2012; Roy and Cherfils, 2015; Harms et al., 2016). While most FIC domain-containing proteins harbor a canonical FIC signature motif, several others also carry non-canonical FIC signature motifs, which may mediate different post-translational modifications (Mukherjee et al., 2011; Castro-Roa et al., 2013; Roy and Cherfils, 2015). The deAMPylating activity of some FIC enzymes was also demonstrated (Perera et al., 2019; Veyron et al., 2019). Additionally, FIC domains contain a β-hairpin, commonly also referred to as "flap," which is involved in substrate binding (Xiao et al., 2010). Comparison of crystal structures of FIC domains of various Beps revealed a highly conserved conformation. However, the flap region is less conserved, which may relate to the individual target spectra of different FIC enzymes. Based on the canonical FIC signature motif, it was speculated that around half of the investigated Beps might represent AMP transferases, such as Bep1, Bep2 and BepA (Schirmer et al., 2021).

AMPylating FIC Domain-Containing *Bartonella* Effector Proteins

FIC domains containing a canonical FIC signature motif are likely AMPylators, but their targets are diverse. BepA of *B. henselae* AMPylates the breast cancer anti-estrogen resistance protein 1 (BCAR1) (Gulen et al., 2020) and additional unidentified proteins (Palanivelu et al., 2011).

Bep2 AMPylates the intermediate filament protein vimentin (Pieles et al., 2014), while the closely related Bep1 AMPylates Rho family GTPases. Similarly, FIC domain-containing effectors of other pathogens are known to AMPylate Rho GTPases to regulate the cytoskeleton or the immune response of mammalian host cells. Prominent examples are IbpA of *Histophilus somni* and VopS of *Vibrio parahaemolyticus* (Yarbrough et al., 2009; Mattoo et al., 2011). AMPylation of those GTPases blocks downstream signaling cascades and ultimately leads to a collapse of the cytoskeleton and cell death (Roy and Cherfils, 2015). What distinguishes Bep1 of *Bartonella rochalimae* from these FIC enzymes with broad target spectrum is the selectivity for the Rac-subfamily of Rho GTPases (i.e., Rac1/2/3 and RhoG). As such, Bep1 is the first bacterial effector selectively targeting Rac-subfamily GTPases without affecting the Rho GTPase Cdc42. Bep1 modifies Y32 of Rac1, a residue involved in GTP binding, limiting its physiological targets to GDP-bound GTPases (Dietz et al., 2021; **Figure 2**).

The target selectivity of Bep1 is based on a short insert of six residues in the flap loop of the FIC domain. A modeled complex between the FIC domain of Bep1 and Rac2 revealed that the extended flap of Bep1 interacts with the nucleotide-binding G4 motif [(K/Q)xD] and the following Rho-insert helix of Rac2. Crucial for the target selectivity of Bep1 are two identified salt bridges between a conserved lysine residue in the G4 motif and a glutamate in the Rho-insert. These residues are only present in the Rac-subfamily GTPases (Dietz et al., 2021). The Bep1 target selectivity might play a critical role for the evasion of the innate immune response. In fact, inhibition of Rac1 and Rac2 decreases the production of reactive oxygen species (ROS), which interferes with clearance of bacterial infections (Kurkchubasche et al., 2001; Bhattacharyya et al., 2014). In contrast, inhibition of RhoA, as for example by IbpA or VopS, triggers the activation of the pyrin inflammasome resulting in an inflammatory type of programmed cell death called pyroptosis (Xu et al., 2014; Heilig and Broz, 2018). Thus, inhibition of Rac GTPases but avoiding RhoA inhibition may be crucial for *Bartonella* to evade the innate immune response and to establish chronic infections. However, experiments showing the Bep1-specific inhibition of Rac-subfamily GTPases inside host cells are still missing.

Functions of Non-canonical FIC Domains

BepC contains a non-canonical FIC signature motif, which differs from the canonical motif by the replacement of an acetic residue (D/E) by a lysine. This FIC domain should thus be devoid of AMPylation activity, but might encode a different enzymatic activity. Recently, the molecular mechanism underlying BepC-dependent stress fiber formation has been uncovered. After translocation into host cells, BepC localizes to the plasma membrane *via* its BID domain. Immunoprecipitation revealed that BepC interacts with GEF-H1 *via* its FIC domain. GEF-H1 is a guanine nucleotide exchange (GEF) factor that remains inactive when bound to microtubules. Upon release, GEF-H1 activates the RhoA pathway. The interaction of BepC and GEF-H1 might not depend on post-translational modifications. Extensive mutagenesis of the conserved non-canonical FIC motif of BepC did not interfere with stress fiber formation. Rather, the BepC-triggered relocalization of GEF-H1 to the plasma membrane leads to activation of RhoA by exchanging GDP to GTP (**Figure 2**). In turn, the downstream Rho kinase ROCK is activated and induces stress fiber formation (Marlaire and Dehio, 2021; Wang et al., 2021).

pY DOMAIN-DEPENDENT MODULATION OF THE INNATE IMMUNE RESPONSE

In order to colonize their hosts pathogens evolved various mechanisms to modulate the innate immune response (Reddick and Alto, 2014). The transcription factor Signal Transducer and Activator of Transcription 3 (STAT3), a central regulator of inflammation, mediates the switch from a pro- to an anti-inflammatory immune response (Hillmer et al., 2016; Huynh et al., 2019). In response to cytokine signaling, Janus kinases (JAKs) phosphorylate STAT3 on Y705, causing its dimerization and translocation into the nucleus, where it activates gene transcription (Huynh et al., 2019). Alternatively, STAT3 becomes phosphorylated by the Abelson tyrosine kinase (c-ABL) (Allen et al., 2011). The canonical JAK-STAT3 signaling pathway controls the expression of pro-inflammatory cytokines (e.g., IL-6, TNF-α) and anti-inflammatory cytokines (like IL-10) (Williams et al., 2004; Melillo et al., 2010). Recent evidence suggests that pathogens evolved strategies to modulate innate immunity by STAT3 activation (Gibbs et al., 2020; Panagi et al., 2020).

BepD promotes an anti-inflammatory response through an exceptional pathway for STAT3 activation. BepD of *B. henselae* harbors two almost identical tyrosine phosphorylation domains (pY and pY'), each with nine EPIYA-related motifs which were originally identified in CagA of *H. pylori* (Backert and Selbach, 2005; Hayashi et al., 2013). Inside host cells, tyrosine phosphorylation of the respective EPIYA-related motifs enables interaction with SH2-domain containing proteins (Selbach et al., 2009; Sorg et al., 2020). c-ABL and STAT3 were identified as interaction partners of BepD. Moreover, STAT3 was found to be phosphorylated on Y705. Interestingly, the BepD-dependent activation of STAT3 occurred independently of autocrine or paracrine cytokine signaling. Accordingly, JAKs, which integrate pro- and anti-inflammatory cytokine signaling to phosphorylate STAT3, were not required for BepD-dependent STAT3 activation. Instead, c-ABL recruited to the phosphorylated EPIYA motifs of BepD triggered the phosphorylation of STAT3 on Y705. Through the activation of STAT3, BepD impairs the pro-inflammatory response and promotes secretion of the anti-inflammatory cytokine IL-10 (Sorg et al., 2020; **Figure 2**). This mechanism

might be important for *Bartonella* to modulate innate immune cells encountered in the dermal niche.

CONCLUDING REMARKS AND OPEN QUESTIONS

The stealth infection strategy of *Bartonella* requires precise modulation of the host cellular function in order to invade the blood stream. Throughout the different stages of infection, the translocation of Beps *via* the VirB/VirD4 T4SS into various host cells favors the pathogenicity of the bacteria (**Figure 1**). BepD and BepE seem to support the progress from the dermal site of infection towards the "blood-seeding niche" by downregulating the innate immune response and safeguarding the migratory capacity of hijacked cells against deleterious effects by BepC. Colonization of endothelial cells is enhanced by the combined action of BepG and BepC together with BepF, which induce internalization of bacterial aggregates. BepA inhibits apoptosis of endothelial cells, which constitute the "blood-seeding niche."

Most information concerning the function of Beps was gathered using the cat-adapted strain *B. henselae* that incidentally infects humans but not rodents. However, an experimental model to study the infection of cats is rather laborious (Chomel et al., 1996; Foil et al., 1998). Therefore, *in vivo* studies in the natural host were often conducted with rodent-specific strains (Boulouis et al., 2001; Schulein and Dehio, 2002). However, *in vitro* infection protocols to study the effector function of rodent-specific strains are missing. *Bartonella* species translocate individual cocktails of Beps into the host cells possibly affecting different host cellular processes (Harms et al., 2017). While different orthologs of BepD share a conserved function (Sorg et al., 2020), other Beps seem to differ in a species-specific context, as for example BepA and BepE (Schmid D. et al., 2006; Wang et al., 2019). Suitable *in vitro* and *in vivo* models using the same *Bartonella* species will be necessary to study the role of Beps in the natural host.

Despite the progress made to elucidate the function of lineage 4 Beps, less is known about Beps from lineage 3. Bep1 and Bep2 AMPylate several host proteins that potentially affect the cytoskeleton (**Figure 2**). However, *in vitro* or *in vivo* assays demonstrating their function inside host cells or a suitable model organism to study *Bartonella* species of lineage 3 are still missing.

Next to the need to solve the functions of several uncharacterized Beps, the translocation mechanism through the VirB/VirD4 T4SS should be also investigated in more detail. The BID domain and the positively charged tail are essential for the secretion of Beps *via* the T4SS (Schulein et al., 2005; Schmid M. C. et al., 2006), however, structural information resolving the interaction of Beps with the T4CP is still missing. Future work should aim to determine key residues of BID domains mediating the interaction with VirD4.

AUTHOR CONTRIBUTIONS

KF designed the figures. KF and CD wrote the manuscript. Both authors contributed to the article and approved the submitted version.

FUNDING

This work was supported by grants 310030B_201273 to CD from the Swiss National Science Foundation and a "Fellowship for Excellence" to KF by the Werner Siemens-Foundation.

ACKNOWLEDGMENTS

We would like to thank Lena Siewert, Markus Huber, and Jaroslaw Sedzicki for critical reading of the manuscript.

REFERENCES

Allen, J. C., Talab, F., Zuzel, M., Lin, K., and Slupsky, J. R. (2011). c-Abl regulates Mcl-1 gene expression in chronic lymphocytic leukemia cells. *Blood* 117, 2414–2422. doi: 10.1182/blood-2010-08-301176

Backert, S., and Selbach, M. (2005). Tyrosine-phosphorylated bacterial effector proteins: the enemies within. *Trends Microbiol.* 13, 476–484. doi: 10.1016/j.tim.2005.08.002

Bhattacharyya, A., Chattopadhyay, R., Mitra, S., and Crowe, S. E. (2014). Oxidative stress: an essential factor in the pathogenesis of gastrointestinal mucosal diseases. *Physiol. Rev.* 94, 329–354.

Boulouis, H. J., Barrat, F., Bermond, D., Bernex, F., Thibault, D., Heller, R., et al. (2001). Kinetics of *Bartonella birtlesii* infection in experimentally infected mice and pathogenic effect on reproductive functions. *Infect. Immun.* 69, 5313–5317. doi: 10.1128/IAI.69.9.5313-5317.2001

Cascales, E., and Christie, P. J. (2003). The versatile bacterial type IV secretion systems. *Nat. Rev. Microbiol.* 1, 137–149. doi: 10.1038/nrmicro753

Castro-Roa, D., Garcia-Pino, A., De Gieter, S., Van Nuland, N. A. J., Loris, R., and Zenkin, N. (2013). The Fic protein Doc uses an inverted substrate to phosphorylate and inactivate EF-Tu. *Nat. Chem. Biol.* 9, 811–817. doi: 10.1038/nchembio.1364

Chomel, B. B., Kasten, R. W., Floyd-Hawkins, K., Chi, B., Yamamoto, K., Roberts-Wilson, J., et al. (1996). Experimental transmission of *Bartonella henselae* by the cat flea. *J. Clin. Microbiol.* 34, 1952–1956. doi: 10.1128/jcm.34.8.1952-1956.1996

Christie, P. J., Whitaker, N., and Gonzalez-Rivera, C. (2014). Mechanism and structure of the bacterial type IV secretion systems. *Biochim. Biophys. Acta* 1843, 1578–1591.

Costa, T. R. D., Harb, L., Khara, P., Zeng, L., Hu, B., and Christie, P. J. (2020). Type IV secretion systems: advances in structure, function, and activation. *Mol. Microbiol.* 115, 436–452.

Dehio, C. (1999). Interactions of *Bartonella henselae* with vascular endothelial cells. *Curr. Opin. Microbiol.* 2, 78–82. doi: 10.1016/s1369-5274(99)80013-7

Dietz, N., Huber, M., Sorg, I., Goepfert, A., Harms, A., Schirmer, T., et al. (2021). Structural basis for selective AMPylation of Rac-subfamily GTPases by *Bartonella* effector protein 1 (Bep1). *Proc. Natl. Acad. Sci. U.S.A.* 118:e2023245118. doi: 10.1073/pnas.2023245118

Engel, P., Goepfert, A., Stanger, F. V., Harms, A., Schmidt, A., Schirmer, T., et al. (2012). Adenylylation control by intra- or intermolecular active-site obstruction in Fic proteins. *Nature* 482, 107–110. doi: 10.1038/nature10729

Engel, P., Salzburger, W., Liesch, M., Chang, C. C., Maruyama, S., Lanz, C., et al. (2011). Parallel evolution of a type IV secretion system in radiating lineages

of the host-restricted bacterial pathogen *Bartonella*. *PLoS Genet.* 7:e1001296. doi: 10.1371/journal.pgen.1001296

Foil, L., Andress, E., Freeland, R. L., Roy, A. F., Rutledge, R., Triche, P. C., et al. (1998). Experimental infection of domestic cats with *Bartonella henselae* by inoculation of *Ctenocephalides felis* (Siphonaptera: Pulicidae) feces. *J. Med. Entomol.* 35, 625–628. doi: 10.1093/jmedent/35.5.625

Gibbs, K. D., Washington, E. J., Jaslow, S. L., Bourgeois, J. S., Foster, M. W., Guo, R., et al. (2020). The *Salmonella* secreted effector SarA/SteE mimics cytokine receptor signaling to activate STAT3. *Cell Host Microbe* 27, 129–139.e124. doi: 10.1016/j.chom.2019.11.012

Gulen, B., Rosselin, M., Fauser, J., Albers, M. F., Pett, C., Krisp, C., et al. (2020). Identification of targets of AMPylating Fic enzymes by co-substrate-mediated covalent capture. *Nat. Chem.* 12, 732–739. doi: 10.1038/s41557-020-0484-6

Guy, L., Nystedt, B., Toft, C., Zaremba-Niedzwiedzka, K., Berglund, E. C., Granberg, F., et al. (2013). A gene transfer agent and a dynamic repertoire of secretion systems hold the keys to the explosive radiation of the emerging pathogen *Bartonella*. *PLoS Genet.* 9:e1003393. doi: 10.1371/journal.pgen.1003393

Harms, A., and Dehio, C. (2012). Intruders below the radar: molecular pathogenesis of *Bartonella* spp. *Clin. Microbiol. Rev.* 25, 42–78. doi: 10.1128/CMR.05009-11

Harms, A., Segers, F. H., Quebatte, M., Mistl, C., Manfredi, P., Korner, J., et al. (2017). Evolutionary dynamics of pathoadaptation revealed by three independent acquisitions of the VirB/D4 Type IV secretion system in *Bartonella*. *Genome Biol. Evol.* 9, 761–776. doi: 10.1093/gbe/evx042

Harms, A., Stanger, F. V., and Dehio, C. (2016). Biological diversity and molecular plasticity of FIC domain proteins. *Annu. Rev. Microbiol.* 70, 341–360. doi: 10.1146/annurev-micro-102215-095245

Hayashi, T., Morohashi, H., and Hatakeyama, M. (2013). Bacterial EPIYA effectors–where do they come from? What are they? Where are they going? *Cell Microbiol.* 15, 377–385. doi: 10.1111/cmi.12040

Heilig, R., and Broz, P. (2018). Function and mechanism of the pyrin inflammasome. *Eur. J. Immunol.* 48, 230–238. doi: 10.1002/eji.201746947

Hillmer, E. J., Zhang, H., Li, H. S., and Watowich, S. S. (2016). STAT3 signaling in immunity. *Cytokine Growth Fact. Rev.* 31, 1–15. doi: 10.1016/j.cytogfr.2016.05.001

Huynh, J., Chand, A., Gough, D., and Ernst, M. (2019). Therapeutically exploiting STAT3 activity in cancer - using tissue repair as a road map. *Nat. Rev. Cancer* 19, 82–96. doi: 10.1038/s41568-018-0090-8

Kirby, J. E., and Nekorchuk, D. M. (2002). *Bartonella*-associated endothelial proliferation depends on inhibition of apoptosis. *Proc. Natl. Acad. Sci. U.S.A.* 99, 4656–4661. doi: 10.1073/pnas.072292699

Kurkchubasche, A. G., Panepinto, J. A., Tracy, T. F. Jr., Thurman, G. W., and Ambruso, D. R. (2001). Clinical features of a human Rac2 mutation: a complex neutrophil dysfunction disease. *J. Pediatr.* 139, 141–147. doi: 10.1067/mpd.2001.114718

Marlaire, S., and Dehio, C. (2021). *Bartonella* effector protein C mediates actin stress fiber formation via recruitment of GEF-H1 to the plasma membrane. *PLoS Pathog.* 17:e1008548. doi: 10.1371/journal.ppat.1008548

Mattoo, S., Durrant, E., Chen, M. J., Xiao, J., Lazar, C. S., Manning, G., et al. (2011). Comparative analysis of Histophilus somni immunoglobulin-binding protein A (IbpA) with other fic domain-containing enzymes reveals differences in substrate and nucleotide specificities. *J. Biol. Chem.* 286, 32834–32842. doi: 10.1074/jbc.M111.227603

Melillo, J. A., Song, L., Bhagat, G., Blazquez, A. B., Plumlee, C. R., Lee, C., et al. (2010). Dendritic cell (DC)-specific targeting reveals Stat3 as a negative regulator of DC function. *J. Immunol.* 184, 2638–2645. doi: 10.4049/jimmunol.0902960

Mukherjee, S., Liu, X., Arasaki, K., Mcdonough, J., Galan, J. E., and Roy, C. R. (2011). Modulation of Rab GTPase function by a protein phosphocholine transferase. *Nature* 477, 103–106. doi: 10.1038/nature10335

Okujava, R., Guye, P., Lu, Y. Y., Mistl, C., Polus, F., Vayssier-Taussat, M., et al. (2014). A translocated effector required for *Bartonella* dissemination from derma to blood safeguards migratory host cells from damage by co-translocated effectors. *PLoS Pathog.* 10:e1004187. doi: 10.1371/journal.ppat.1004187

Palanivelu, D. V., Goepfert, A., Meury, M., Guye, P., Dehio, C., and Schirmer, T. (2011). Fic domain-catalyzed adenylylation: insight provided by the structural analysis of the type IV secretion system effector BepA. *Protein Sci.* 20, 492–499. doi: 10.1002/pro.581

Panagi, I., Jennings, E., Zeng, J., Gunster, R. A., Stones, C. D., Mak, H., et al. (2020). *Salmonella* effector SteE converts the mammalian serine/Threonine kinase GSK3 into a Tyrosine kinase to direct macrophage polarization. *Cell Host Microbe* 27, 41–53.e46. doi: 10.1016/j.chom.2019.11.002

Perera, L. A., Rato, C., Yan, Y., Neidhardt, L., Mclaughlin, S. H., Read, R. J., et al. (2019). An oligomeric state-dependent switch in the ER enzyme FICD regulates AMPylation and deAMPylation of BiP. *EMBO J.* 38:e102177.

Pieles, K., Glatter, T., Harms, A., Schmidt, A., and Dehio, C. (2014). An experimental strategy for the identification of AMPylation targets from complex protein samples. *Proteomics* 14, 1048–1052. doi: 10.1002/pmic.201300470

Pulliainen, A. T., and Dehio, C. (2012). Persistence of *Bartonella* spp. stealth pathogens: from subclinical infections to vasoproliferative tumor formation. *FEMS Microbiol. Rev.* 36, 563–599. doi: 10.1111/j.1574-6976.2012.00324.x

Pulliainen, A. T., Pieles, K., Brand, C. S., Hauert, B., Bohm, A., Quebatte, M., et al. (2012). Bacterial effector binds host cell adenylyl cyclase to potentiate Galphas-dependent cAMP production. *Proc. Natl. Acad. Sci. U.S.A.* 109, 9581–9586. doi: 10.1073/pnas.1117651109

Reddick, L. E., and Alto, N. M. (2014). Bacteria fighting back: how pathogens target and subvert the host innate immune system. *Mol. Cell* 54, 321–328. doi: 10.1016/j.molcel.2014.03.010

Redzej, A., Ilangovan, A., Lang, S., Gruber, C. J., Topf, M., Zangger, K., et al. (2013). Structure of a translocation signal domain mediating conjugative transfer by type IV secretion systems. *Mol. Microbiol.* 89, 324–333. doi: 10.1111/mmi.12275

Rhomberg, T. A., Truttmann, M. C., Guye, P., Ellner, Y., and Dehio, C. (2009). A translocated protein of *Bartonella henselae* interferes with endocytic uptake of individual bacteria and triggers uptake of large bacterial aggregates via the invasome. *Cell Microbiol.* 11, 927–945. doi: 10.1111/j.1462-5822.2009.01302.x

Roy, C. R., and Cherfils, J. (2015). Structure and function of Fic proteins. *Nat. Rev. Microbiol.* 13, 631–640.

Sadana, R., and Dessauer, C. W. (2009). Physiological roles for G protein-regulated adenylyl cyclase isoforms: insights from knockout and overexpression studies. *Neurosignals* 17, 5–22. doi: 10.1159/000166277

Schirmer, T., De Beer, T. A. P., Tamegger, S., Harms, A., Dietz, N., Dranow, D. M., et al. (2021). Evolutionary diversification of host-targeted *Bartonella* effectors proteins derived from a conserved FicTA toxin-antitoxin module. *Microorganisms* 9:1645. doi: 10.3390/microorganisms9081645

Schmid, D., Dengjel, J., Schoor, O., Stevanovic, S., and Munz, C. (2006). Autophagy in innate and adaptive immunity against intracellular pathogens. *J. Mol. Med.* 84, 194–202. doi: 10.1007/s00109-005-0014-4

Schmid, M. C., Scheidegger, F., Dehio, M., Balmelle-Devaux, N., Schulein, R., Guye, P., et al. (2006). A translocated bacterial protein protects vascular endothelial cells from apoptosis. *PLoS Pathog.* 2:e115. doi: 10.1371/journal.ppat.0020115

Schmid, M. C., Schulein, R., Dehio, M., Denecker, G., Carena, I., and Dehio, C. (2004). The VirB type IV secretion system of *Bartonella henselae* mediates invasion, proinflammatory activation and antiapoptotic protection of endothelial cells. *Mol. Microbiol.* 52, 81–92. doi: 10.1111/j.1365-2958.2003.03964.x

Schulein, R., and Dehio, C. (2002). The VirB/VirD4 type IV secretion system of *Bartonella* is essential for establishing intraerythrocytic infection. *Mol. Microbiol.* 46, 1053–1067. doi: 10.1046/j.1365-2958.2002.03208.x

Schulein, R., Guye, P., Rhomberg, T. A., Schmid, M. C., Schroder, G., Vergunst, A. C., et al. (2005). A bipartite signal mediates the transfer of type IV secretion substrates of *Bartonella henselae* into human cells. *Proc. Natl. Acad. Sci. U.S.A.* 102, 856–861. doi: 10.1073/pnas.0406796102

Schulein, R., Seubert, A., Gille, C., Lanz, C., Hansmann, Y., Piemont, Y., et al. (2001). Invasion and persistent intracellular colonization of erythrocytes. A unique parasitic strategy of the emerging pathogen *Bartonella*. *J. Exp. Med.* 193, 1077–1086. doi: 10.1084/jem.193.9.1077

Selbach, M., Paul, F. E., Brandt, S., Guye, P., Daumke, O., Backert, S., et al. (2009). Host cell interactome of tyrosine-phosphorylated bacterial proteins. *Cell Host Microbe* 5, 397–403. doi: 10.1016/j.chom.2009.03.004

Siamer, S., and Dehio, C. (2015). New insights into the role of Bartonella effector proteins in pathogenesis. *Curr. Opin. Microbiol.* 23, 80–85. doi: 10.1016/j.mib.2014.11.007

Sorg, I., Schmutz, C., Lu, Y. Y., Fromm, K., Siewert, L. K., Bogli, A., et al. (2020). A *Bartonella* effector acts as signaling hub for intrinsic STAT3 activation to trigger anti-inflammatory responses. *Cell Host Microbe* 27, 476–485.e477. doi: 10.1016/j.chom.2020.01.015

Stanger, F. V., De Beer, T. A. P., Dranow, D. M., Schirmer, T., Phan, I., and Dehio, C. (2017). The BID domain of Type IV secretion substrates forms a conserved four-helix bundle topped with a hook. *Structure* 25, 203–211. doi: 10.1016/j.str.2016.10.010

Truttmann, M. C., Guye, P., and Dehio, C. (2011a). BID-F1 and BID-F2 domains of *Bartonella henselae* effector protein BepF trigger together with BepC the formation of invasome structures. *PLoS One* 6:e25106. doi: 10.1371/journal.pone.0025106

Truttmann, M. C., Rhomberg, T. A., and Dehio, C. (2011b). Combined action of the type IV secretion effector proteins BepC and BepF promotes invasome formation of *Bartonella henselae* on endothelial and epithelial cells. *Cell Microbiol.* 13, 284–299. doi: 10.1111/j.1462-5822.2010.01535.x

Veyron, S., Oliva, G., Rolando, M., Buchrieser, C., Peyroche, G., and Cherfils, J. (2019). A Ca(2+)-regulated deAMPylation switch in human and bacterial FIC proteins. *Nat. Commun.* 10:1142. doi: 10.1038/s41467-019-09023-1

Wagner, A., and Dehio, C. (2019). Role of distinct Type-IV-secretion systems and secreted effector sets in host adaptation by pathogenic *Bartonella* species. *Cell Microbiol.* 21:e13004. doi: 10.1111/cmi.13004

Wagner, A., Tittes, C., and Dehio, C. (2019). Versatility of the BID domain: conserved function as Type-IV-secretion-signal and secondarily evolved effector functions within *Bartonella*-infected host cells. *Front. Microbiol.* 10:921. doi: 10.3389/fmicb.2019.00921

Waksman, G. (2019). From conjugation to T4S systems in Gram-negative bacteria: a mechanistic biology perspective. *EMBO Rep.* 20:e47012. doi: 10.15252/embr.201847012

Wang, C., Fu, J., Wang, M., Cai, Y., Hua, X., Du, Y., et al. (2019). *Bartonella* quintana type IV secretion effector BepE-induced selective autophagy by conjugation with K63 polyubiquitin chain. *Cell Microbiol.* 21:e12984. doi: 10.1111/cmi.12984

Wang, C., Zhang, H., Fu, J., Wang, M., Cai, Y., Ding, T., et al. (2021). *Bartonella* type IV secretion effector BepC induces stress fiber formation through activation of GEF-H1. *PLoS Pathog.* 17:e1009065. doi: 10.1371/journal.ppat.1009065

Williams, L., Bradley, L., Smith, A., and Foxwell, B. (2004). Signal transducer and activator of transcription 3 is the dominant mediator of the anti-inflammatory effects of IL-10 in human macrophages. *J. Immunol.* 172, 567–576. doi: 10.4049/jimmunol.172.1.567

Xiao, J., Worby, C. A., Mattoo, S., Sankaran, B., and Dixon, J. E. (2010). Structural basis of Fic-mediated adenylylation. *Nat. Struct. Mol. Biol.* 17, 1004–1010. doi: 10.1038/nsmb.1867

Xu, H., Yang, J., Gao, W., Li, L., Li, P., Zhang, L., et al. (2014). Innate immune sensing of bacterial modifications of Rho GTPases by the Pyrin inflammasome. *Nature* 513, 237–241. doi: 10.1038/nature13449

Yarbrough, M. L., Li, Y., Kinch, L. N., Grishin, N. V., Ball, H. L., and Orth, K. (2009). AMPylation of Rho GTPases by Vibrio VopS disrupts effector binding and downstream signaling. *Science* 323, 269–272. doi: 10.1126/science.1166382

Conflict of Interest: The authors declare that the research was conducted in the absence of any commercial or financial relationships that could be construed as a potential conflict of interest.

Publisher's Note: All claims expressed in this article are solely those of the authors and do not necessarily represent those of their affiliated organizations, or those of the publisher, the editors and the reviewers. Any product that may be evaluated in this article, or claim that may be made by its manufacturer, is not guaranteed or endorsed by the publisher.

frontiers in Microbiology

ORIGINAL RESEARCH
published: 16 December 2021
doi: 10.3389/fmicb.2021.784483

Expression, Localization, and Protein Interactions of the Partitioning Proteins in the Gonococcal Type IV Secretion System

*Melanie M. Callaghan[1], Birgit Koch[2], Kathleen T. Hackett[1], Amy K. Klimowicz[1], Ryan E. Schaub[1], Natalio Krasnogor[2] and Joseph P. Dillard[1]**

[1]Department of Medical Microbiology and Immunology, University of Wisconsin-Madison, Madison, WI, United States, [2]Interdisciplinary Computing and Complex BioSystems (ICOS), Newcastle University, Newcastle upon Tyne, United Kingdom

Partitioning proteins are well studied as molecular organizers of chromosome and plasmid segregation during division, however little is known about the roles partitioning proteins can play within type IV secretion systems. The single-stranded DNA (ssDNA)-secreting gonococcal T4SS has two partitioning proteins, ParA and ParB. These proteins work in collaboration with the relaxase TraI as essential facilitators of type IV secretion. Bacterial two-hybrid experiments identified interactions between each partitioning protein and the relaxase. Subcellular fractionation demonstrated that ParA is found in the cellular membrane, whereas ParB is primarily in the membrane, but some of the protein is in the soluble fraction. Since TraI is known to be membrane-associated, these data suggest that the gonococcal relaxosome is a membrane-associated complex. In addition, we found that translation of ParA and ParB is controlled by an RNA switch. Different mutations within the stem-loop sequence predicted to alter folding of this RNA structure greatly increased or decreased levels of the partitioning proteins.

Keywords: ***Neisseria gonorrhoeae*** **(GC), relaxosome, riboswitch, protein–protein interaction, subcellular loalization**

OPEN ACCESS

Edited by:
Eric Cascales,
Aix-Marseille Université, France

Reviewed by:
Jose Antonio Ibarra,
Instituto Politécnico Nacional (IPN), Mexico
William Shafer,
Emory University, United States

****Correspondence:***
Joseph P. Dillard
jpdillard@wisc.edu

Specialty section:
This article was submitted to Microbial Physiology and Metabolism, a section of the journal Frontiers in Microbiology

Received: *27 September 2021*
Accepted: *24 November 2021*
Published: *16 December 2021*

Citation:
Callaghan MM, Koch B, Hackett KT, Klimowicz AK, Schaub RE, Krasnogor N and Dillard JP (2021) Expression, Localization, and Protein Interactions of the Partitioning Proteins in the Gonococcal Type IV Secretion System. Front. Microbiol. 12:784483. doi: 10.3389/fmicb.2021.784483

INTRODUCTION

The human-restricted bacterial pathogen *Neisseria gonorrhoeae* is responsible for causing the sexually-transmitted infection gonorrhea, colonizing mucosal surfaces and causing both highly inflammatory and asymptomatic infections. In 2019, over 600,000 new cases of gonorrhea infection were reported to the Centers for Disease Control (Centers for Disease Control and Prevention, 2021); this is likely an underestimate due to the prevalence of asymptomatic infections. Antibiotic resistance in gonorrhea infections has continued to rise since the 1950s and represents an urgent worldwide health concern (Centers for Disease Control and Prevention, 2019).

A majority (60–80%) of gonococcal isolates contain the 59 kb gonococcal genetic island (GGI), which encodes a type IV secretion system (T4SS; Dillard and Seifert, 2001; Hamilton and Dillard, 2006; Shockey, 2019). The gonococcal T4SS is unique in that it secretes single-stranded DNA (ssDNA) into the extracellular space independent of cell–cell contact. Due to the natural transformability of *N. gonorrhoeae* at all stages of growth, this active DNA release

can facilitate horizontal gene transfer (Dillard and Seifert, 2001; Hamilton and Dillard, 2006; Salgado-Pabón et al., 2007; Shockey, 2019). Regulation of gonococcal T4SS expression and activity is only beginning to be understood (Ramsey et al., 2015; Callaghan et al., 2021).

The GGI encodes homologues of many known T4SS proteins, providing a basis for modeling activity in this system (Hamilton et al., 2005). While many of these proteins have been further characterized, two that have not yet been addressed are the partitioning proteins, ParA and ParB (Jain et al., 2012; Kohler et al., 2013; Ramsey et al., 2014).

Partitioning proteins are found on most bacterial chromosomes and many plasmids, often as a matched pair (Bignell and Thomas, 2001). These types of proteins play a role in localizing chromosome or plasmid DNA during the process of cell division, ensuring non-random distribution of DNA molecules into daughter cells. Canonically, ParA homologues are ATPases and ParB homologues are DNA-binding proteins. Often these proteins interact with each other as a cognate pair, and ParB interacts with DNA in a sequence-specific manner (Lin and Grossman, 1998; Bignell and Thomas, 2001; Atmakuri et al., 2007).

There is limited information on the function of partitioning proteins as components of a T4SS. In the R1 plasmid conjugation system in *Escherichia coli*, ParR binds a centromere-like DNA sequence, *parC*, to facilitate the physical placement of the DNA. A recent study has shown that in this system, the association of the cognate pair of partitioning proteins ParM and ParR with the relaxase TraI, the coupling protein TraD, and the cell membrane contribute to the assembly of the apparatus and initiation of conjugative transfer (Gruber et al., 2016). In the chromosomally encoded VirB/D4 T4SS of *Agrobacterium tumefaciens*, the ParA and ParB homologues VirC1 and VirC2, respectively, interact at the cellular poles to direct relaxosome formation and DNA substrate localization. The VirC1-DNA interaction is also sequence-specific; facilitated by VirC2, VirC1 binds a DNA sequence called *overdrive* (Atmakuri et al., 2007).

In the gonococcal T4SS, both *parA* and *parB* are essential for T4SS-mediated DNA secretion to occur (Hamilton et al., 2005; Pachulec et al., 2014). They are co-transcribed in an operon of the GGI distant from the other T4SS genes and near the *difA* site (**Figure 1A**). The *parAB* operon is transcribed at high levels compared to the rest of the characterized GGI (Pachulec et al., 2014; Ramsey et al., 2015). There is a large region of genes of unknown function between the partitioning proteins and the rest of the known T4SS protein homologues, and this region is dispensable for secretion (Pachulec et al., 2014; Callaghan et al., 2017). Little is known about the gonococcal T4SS ParAB, except that both are necessary for T4S and ParA has a conserved ATPase domain with a Walker A box that is also necessary for DNA secretion (Hamilton et al., 2005; Pachulec et al., 2014).

More is known about the regulation of T4SS expression in gonococci, and RNA-mediated mechanisms are recently emerging as the regulatory network is probed (Ramsey et al., 2015; Callaghan et al., 2021). Several sRNAs have been identified within the GGI and have yet to be functionally characterized (Remmele et al., 2014). Recent work has also implicated the Fur regulon in regulating some aspects of T4SS expression (Callaghan et al., 2021), and this regulon is known to utilize sRNA intermediates to control iron-responsive genes (Mellin et al., 2007; Yu et al., 2016). The GGI encodes an RNA switch in the *traH* 5′ untranslated region (UTR) which controls protein expression from the P_{traH}-derived transcript (Ramsey et al., 2015). This RNA switch adopts an energetically favorable structure with two stem-loops that occludes the Shine-Dalgarno sequence and *traH* start codon. However, an alternate secondary structure becomes more energetically favorable if the upstream portion of the first stem-loop is unavailable for binding. This alternate structure is a single stem-loop that leaves the start site available for binding (Ramsey et al., 2015).

We have characterized ParAB in the gonococcal T4SS by investigating expression, protein interactions, and localization of the partitioning proteins. Our data suggest that ParAB protein expression is tightly controlled by an RNA switch. We present evidence for ParA-TraI and ParB-TraI interactions, supporting a ParAB-TraI relaxosome that initiates T4S. Finally, localization studies indicate the ParAB are unusual among partitioning proteins in that they associate with the bacterial cytoplasmic membrane.

MATERIALS AND METHODS

Bacterial Strains and Growth Conditions

Neisseria gonorrhoeae MS11 and derivative strains were grown on GCB agar plates with Kellogg's supplements or in GCBL medium with 0.042% sodium bicarbonate and Kellogg's supplements ("cGCBL"; Kellogg et al., 1963; Morse and Bartenstein, 1974) at 37°C.

Strain Building

Plasmids for this study (**Table 1**) were generated by PCR amplification of *N. gonorrhoeae* MS11 chromosomal DNA with primers listed in **Table 2**, followed by restriction digest with listed enzymes (**Table 2**). Purified, digested inserts and vectors were ligated overnight with T4 DNA ligase. Ligations were transformed in TAM1 *E. coli* (Active Motif).

To construct pAKK128 and pAKK129, primers iga-end-out and lacZ937-R were used to PCR-amplify the *parAB* promoter region and ~1kb of the 5′ region of *lacZ* from MMC545 (wild-type SLs) and MMC546 ($SL_{\Delta BC}$) chromosomal DNA. The PCR products were digested with ClaI (upstream of the promoter region) and XhoI (within *lacZ*), resulting in ~0.9-kb fragments that contained the *parAB* promoter with either the wild-type stem-loops or mutant stem-loops fused to the first 839bp of *lacZ*. pMR115+1, which contains the full *lacZ* gene fused to a different promoter, was digested with ClaI and XhoI. The PCR products were ligated into the digested plasmid and transformed into *E. coli* TAM1, generating pAKK128 (wild-type SLs-*lacZ*) and pAKK129 ($SL_{\Delta BC}$ -*lacZ*). The constructs were confirmed by sequencing.

Plasmid pMMC25 was made using site-directed mutagenesis to alter the −10 promoter element of *NcngR_093* from TACGCT to **G**ACG**GA**: two fragments were amplified from the MS11 chromosome using primers (1) nc093_sdmF1 + nc093R1 and (2) nc093F1 + nc093_sdmR1. Base pair changes are shown in bold (**Table 2**). Fragments were purified and then used in

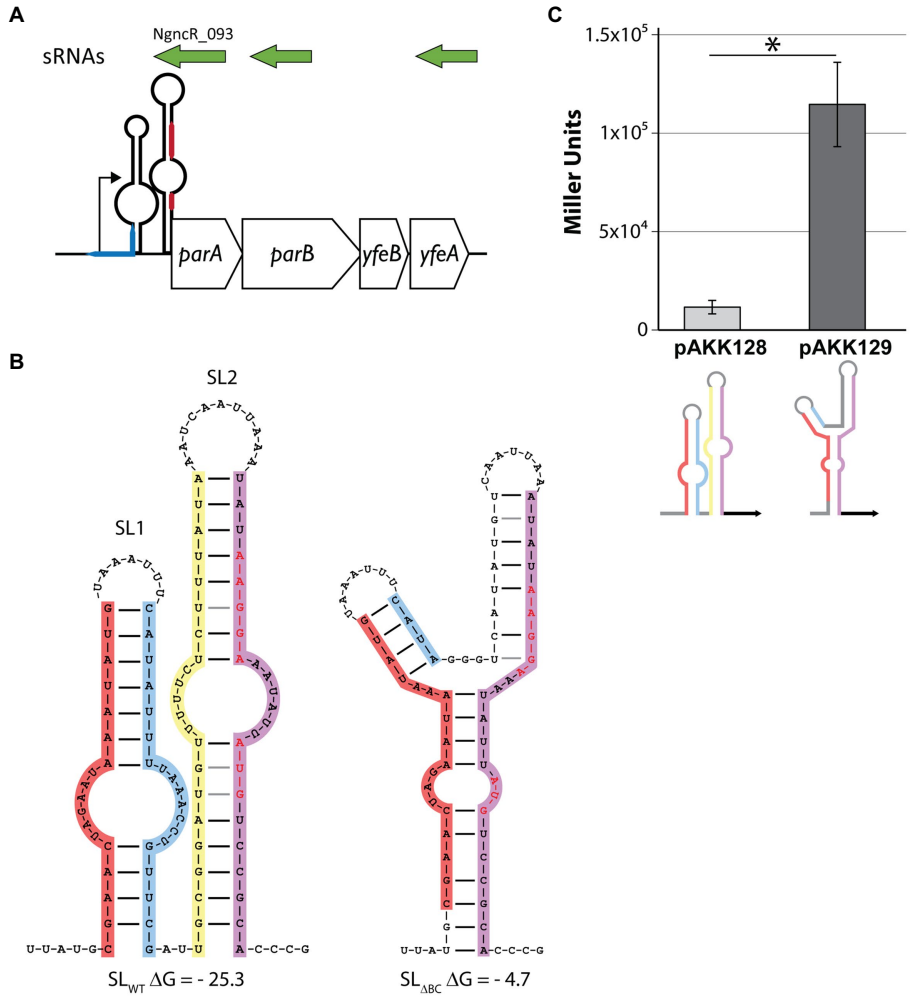

FIGURE 1 | Disruption of the stem-loops in the *parA* 5′UTR increases translation of LacZ. **(A)** Schematic depicting the *parA* operon. sRNAs (green) were detected by Remmele et al. (2014). The blue line represents the *difA* site. The red line represents the Shine-Dalgarno sequence (top) and *parA* start codon (bottom). Note that *parA* 5′UTR is not to scale. **(B)** Predicted secondary structures of wild-type and mutant stem-loops. Shine-Dalgarno sequence and start codon are shown in red letters. Left: wild-type sequence. Leg A (red), leg B (blue), leg C (yellow), leg D (purple). Right: deletion of legs B and C ($SL_{\Delta BC}$). **(C)** *Escherichia coli* expressing LacZ translational fusions with either the wild-type (pAKK128) or $SL_{\Delta BC}$ (pAKK129) $5'UTR_{parA}$ constructs on plasmids were assayed for β-galactosidase activity. The disrupted stem-loop construct allows for >10-fold higher β-galactosidase activity, demonstrating a clear role for the native stem-loop structure in controlling protein levels. *$p < 0.01$ by Student's *t* test compared to SL_{WT} ($p = 0.0012$).

equal parts as the template for a secondary PCR with primers nc093F1 + nc093R1. pIDN1 vector and purified secondary PCR product were digested with SacI/XhoI and ligated together with T4 DNA ligase before transformation into TAM1 *E. coli*.

Gonococcal strains were generated by spot transformation on GCB agar plates (Callaghan and Dillard, 2019). All strains are derived from MS11. **Table 3** specifies transformations for this study as (transforming DNA) x (parent strain).

Gonococcal transformations with pMMC38 were re-streaked for screening on GCB agar plates containing 2 μg/ml chloramphenicol (Cm2). The fastest-growing colonies from Cm2 plates were re-streaked to GCB + Cm10 plates, from which single colonies were isolated for PCR screening and sequence confirmation.

Synthetic DNA gene blocks were used to transform GC directly by spot transformation and introduce new constructs by homologous recombination at the *iga*/*trpB* complementation locus. Gonococci transformed by gene blocks were re-streaked onto GCB + 40 μg/ml X-gal agar plates. For MMC545 and MMC564, white colonies were chosen for PCR screening and sequence confirmation. For MMC546, blue colonies were chosen.

Construction of BACTH constructs is described in the "BACTH assays" section, below.

Real-Time PCR

RNA isolation and qRT-PCR were performed as described in (Ramsey et al., 2015), using SYBR green reagents. When comparing MS11 and KH655, RNA isolation was performed using TRIzol and the Zymo Direct-zol RNA Miniprep kit. DNase and cDNA preparation were unchanged. Quantitation

TABLE 1 | Plasmid constructs used in this study.

Plasmid	Description	Vector	Source/References
pMMC17	*parA′-FLAG3* intermediate	pMR100	This work
pMMC18	*parA′-FLAG3*	pMMC17	This work
pMMC20	*parB′-FLAG3* intermediate	pMR100	This work
pMMC21	*parB′-FLAG3*	pMMC20	This work
pMMC25	*NgncR_093* promoter mutant	pIDN1	This work
pMMC38	*NgncR_093* O/E (IPTG inducible) at *aspC/lctP*	pKH37	This work
pAKK128	SL_{WT}-*lacZ* translational fusion	pMR115 + 1	This work
pAKK129	$SL_{\Delta BC}$-*lacZ* translational fusion	pMR115 + 1	This work
pIDN1	Cloning vector (Erm^R)		Hamilton et al., 2001
pKH37	*cat* at *aspC/lctP*		Ramsey et al., 2012
pKH502	$SL_{\Delta BC}$		This work
pMR100	FLAG3 tagging vector		Ramsey et al., 2014
BACTH constructs			
Plasmid	**Vector**	**Primer pair[a]**	**References**
T18 $TraD_N$	pUT18CT	3/4	This study
$TraD_N$ T18	pUT18	3/5	This study
$TraD_N$ T25	p25N	3/5	This study
T25 $TraD_N$	pKT25	3/4	This study
$TraI_N$ T18	pUT18	6/7	This study
$TraI_N$ T25	p25N	6/7	This study
$TraL_N$ T18	pUT18		Koch et al., 2020
$TraL_N$ T25	p25N		Koch et al., 2020
T18 $TraE_N$	pUT18C		Koch et al., 2020
T25 $TraE_N$	pKT25		Koch et al., 2020
T18 $TraB_N$	pUT18C		Koch et al., 2020
T25 $TraB_N$	pKT25		Koch et al., 2020
T25 $TraC_N$	pKT25		Koch et al., 2020
Tra_NC T25	p25N		Koch et al., 2020
T18 $TraC_N$	pUT18C		Koch et al., 2020
$TraC_N$ T18	pUT18		Koch et al., 2020
$TraG_N$ T25	p25N		Koch et al., 2020
$TraG_N$ T18	pUT18		Koch et al., 2020
$ParB_N$ T18	pUT18	49/51	This study
$ParB_N$ T25	p25N	49/51	This study
T18 $ParB_N$	pUT18C	49/50	This study
T25 $ParB_N$	pKT25	49/50	This study
$ParA_N$ T18	pUT18	52/53	This study
T25 $ParA_N$	pKT25	52/53	This study
$ParA_N$ T25	p25N	52/54	This study
T18 $ParA_N$	pUT18C	52/54	This study
T18 $TraB_F$	pUT18C		Koch et al., 2020
T25 $TraB_F$	pKT25		Koch et al., 2020
T18 $TraE_F$	pUT18C		Koch et al., 2020
T25 $TraE_F$	pKT25		Koch et al., 2020
$TraC_F$ T18	pUT18		Koch et al., 2020
$TraC_F$ T25	p25N		Koch et al., 2020
T18 $TraC_F$	pUT18C		Koch et al., 2020
T25 $TraC_F$	pKT25		Koch et al., 2020
$TraI_F$ T18	pUT18	82/84	This study
$TraI_F$ T25	p25N	82/84	This study
T18 $TraI_F$	pUT18C	82/83	This study
T25 $TraI_F$	pKT25	82/83	This study
$SopA_F$ T18	pUT18	76/78	This study
$SopA_F$ T25	p25N	76/78	This study
T18 $SopA_F$	pUT18C	76/77	This study
T25 $SopA_F$	pKT25	76/77	This study
$SopB_F$ T18	pUT18	79/81	This study
$SopB_F$ T25	p25N	79/81	This study
T18 $SopB_F$	pUT18C	79/80	This study
T25 $SopB_F$	pKT25	79/80	This study

(Continued)

TABLE 1 | Continued

BACTH vectors	Antibiotic resistance marker	Source/References
p25N	Kan	Claessen et al., 2008
pUT18C	Amp	Karimova et al., 2001
pUT18	Amp	Karimova et al., 2001
pKT25	Kan	Karimova et al., 2001

[a]*See Table 2, primers for BACTH constructs.*

was achieved by the $\Delta\Delta C_T$ method or with standard curves from MS11 genomic DNA, and Student's *t* tests determined significance following previous studies (Applied Biosystems, 1997; Yuan et al., 2006). Primers are listed in **Table 2**.

Western Blotting

Western blots were performed on PVDF membranes against the FLAG epitope, with the exception of **Supplementary Figure S4** (described below). After protein transfer, membranes were blocked with 5% milk in 1X TBS + 0.1% Tween 20 (TBST). M2 Mouse α-FLAG primary antibody (Sigma Aldrich) was used at a concentration of 1:20,000 in TBST. Goat α-mouse secondary antibody (Santa Cruz Biotechnology) was also diluted 1:20,000 for use. Samples containing 6 µg protein were loaded per lane unless otherwise noted. Protein amounts were determined using the Bradford assay (Bio-Rad). All blots were visualized using the LI-COR Odyssey® Fc imaging system. For subcellular fractionation samples, α-CAT (Sigma) was used at 1:14,000 and α-SecY (Genscript) at 1:5,000. Horseradish peroxidase-conjugated secondary antibody mouse α-rabbit (Santa Cruz Biotechnology) was used at 1:20,000 dilution.

The western blot for the subcellular fractionation experiment shown in **Supplementary Figure S4** used 4 µg protein per lane, and was transferred onto a nitrocellulose membrane. Blocking and primary antibodies were performed as above. LtgA was detected using 1:5,000 mouse monoclonal α-LtgA (final concentration ~0.17 µg/ml) primary antibody. 800CW goat α-mouse secondary antibody was used to detect ParA-FLAG3, ParB-FLAG3, and LtgA, 680RD goat α-rabbit secondary antibody was used to detect SecY and CAT.

Metabolite Screening

A non-piliated variant of *N. gonorrhoeae* strain MMC545 was grown from freezer stocks on GCB plates overnight. Colonies were swabbed into cGCBL to start 3 ml cultures at $OD_{540} = 0.25$, and cultures were grown to mid-log phase (2 h). Cultures were diluted back to $OD_{540} = 0.3$ with cGCBL and aliquoted into the Biolog Phenotype Microarrays (PMs) with pipetting to resuspend the desiccated compounds of interest. We tested PMs 5, 8, 9, 10, 12, 13, 15, 16 (Biolog, #12141, 12,183, 12,161, 12,212, 12,213, 12,215, 12,216, respectively). We performed *in vivo* β-galactosidase assays by incubating these plates in the Biotek Synergy HT plate reader for 12 h at 37°C with agitation. OD_{492}, OD_{540}, and OD_{660} reads were taken every 30 min. According to Tang et al., normalized β-galactosidase activity was calculated as $\frac{OD_{630}indigo}{OD_{492}cell\ density} = \frac{a \times OD_{492} - OD_{630}}{b \times OD_{630} - OD_{492}}$, where $a = 0.762$, the correction factor for cell density and $b = 0.267$, the correction factor for indigo. To calculate the correction factor a, OD_{492} and OD_{630} were measured for non-piliated MMC545 gonococcal cultures during 16.5 h growth in a blank Biolog plate (six wells, $n = 204$ data points). Plotting OD_{630} as a function of OD_{492} yielded a linear relationship with $R = 0.977$, and the slope of the linear line of best fit is the correction factor *a* (Tang et al., 2013).

Disk Diffusion

GCB agar plates of piliated MMC545 were grown 16–20 h at 37°C, 5% CO_2, then swabbed into 2–4 ml cGCBL. Dilutions of 10^{-4}–10^{-5} (80 µl) were spread plated on GCB + 40 µg ml^{-1} X-gal plates. Atop the spread culture, a 0.25-inch disk (Hardy Diagnostics) was placed and saturated with 10 µl of the compound of interest. Colony color was assessed after 36–48 h of incubation at 37°C with 5% CO_2 and colony color was visually assessed 36–48 h later.

BACTH Assays

GGI genes were PCR amplified from MS11 chromosomal DNA using primers specified in **Table 2**. PCR products and vectors were restriction enzyme digested (specified in **Table 2**, "Enzyme" column) and ligated. BACTH vectors are specified in **Table 1**. Final plasmids were confirmed by DNA sequencing. Plasmids of interest were co-transformed into *E. coli* BTH101 and plated on LB agar plates with 0.5 mM IPTG, 40 µg/ml Xgal, and appropriate antibiotic selection (**Table 1**, antibiotic selection needed for both co-transformed plasmids). Plates were incubated 40–48 h at 30°C before assessing blue colony color. Antibiotics were used at the following concentrations: 100 µg/ml ampicillin, 50 µg/ml kanamycin. For β-galactosidase assays using BACTH constructs, cells were grown overnight at 30°C in LB with appropriate antibiotics and 0.5 mM IPTG and β-galactosidase activities were measured as described by Miller (1972).

β-Galactosidase Assays

Neisseria gonorrhoeae assays were performed according to Ramsey et al. (2015). Briefly, *N. gonorrhoeae* was grown overnight on GCB plates and swabbed into cGCBL at an $OD_{540} \sim 0.25$. After 3 h of aerated growth by rotation, 0.5 ml samples were collected for protein quantification. Cultures were chilled for 20 min on ice, then cells were collected from 2 ml samples by centrifugation, resuspended in 400 µl Z buffer (Miller, 1972) containing 0.002% SDS (Ramsey et al., 2015), aliquoted into 96 well plates, and exposed to ONPG

TABLE 2 | Primers used in this study.

Primers			
Primer name	**Sequence (5′–3′)**	**Assembly**	**Plasmid**
parA_SpeIF	GTCGACTAGTATGTCCGCACCCGTAATATTG	SpeI/SmaI T4 ligation	pMMC17
parA_SmaIR2	AGTTCCCGGGTGATTGCACCTCCTTTTG		
parB_HindIIIF	CGTCAAGCTTATGAATTTGGACCAAAATAAAGC	HindIII/XhoI T4 ligation	pMMC18
parB′_XhoIR	GAGTCTCGAGGCATGGGAAAGTTTGAATGC		
parB_SpeIF	GTCGACTAGTACAGAAGAACCTGCG	SpeI/SmaI T4 ligation	pMMC20
parB_SmaIR	ATCACCCGGGCTCCTCACTCTTAGC		
parBflank_SalIF	GTGCGTCGACCTGAGCACACAGTAC	HindIII/XhoI T4 ligation	pMMC21
parBflank_XhoIR	ATGACTCGAGCTCTGAAACAGAACC		
nc093_sdmF1	GCTTTGGCAGCAGGAACTGC**G**ACG**GA**TAACAATTTACGTCTG	Site-directed mutagenesis	pMMC25
nc093_sdmR1	CAGACGTAAATTGTTA**TC**CGT**C**GCAGTTCCTGCTGCCAAAGC		
nc093F1	CATAGAGCTCGCCCCGAGAAGGAGTATCC		
nc093R1	CAGTCTCGAGCTGCATTCCCAATACATAC		
iga-end-out	ATGTGGGCGGTAAATCCTTC		
lacZ937-R	ACAGTTTCGGGTTTTCGACG		
rpoB-RT-F	TGCCGTACATGGCGGAC		
rpoB-RT-R	ATACGGGAAGGTACGCCCA		
traD-RT-F	GCGCGAAAACATGAGATTGA		
traD-RT-R	CCATGCCGATTTCCGAGTTA		
traK-RT-F	GAAGCAGCAGTATTGGCTTCGCAA		
traK-RT-R	ATTGATGCCCATATCGCCGGTAGT		
traH-RT-F	GCAATGGGAAAACTGGGTTC		
traH-RT-R	TTATCGGCTTCATGGACAAGG		
parA-RT-F	GCCTGCTTTGCCCAATTATG	Note: amplify both *parA* and *NcngR_093*	
parA-RT-R	AATTGAGGCATCGGGATACG		
parA-RT2-F	TTCCACGCAGGTTCTTCTG	Note: amplify only *parA*	
parA-RT2-R	AAGAGTCCCGGTTCATTGTC		
Primers for BACTH constructs			
Primer number	**Sequence (5′–3′)**	**Enzyme**	
3	GCTACTCTAGAGATGAGTGCCCACTTCCCTGAAAAC	XbaI	
4	CTACGGTACCCGTTAGACGGCATAACTACTTCCCTCCGT	KpnI	
5	CTACGGTACCCGGACGGCATAACTACTTCCCTCCGTA	KpnI	
6	CAAGATCTAGAGATGAAAACAAGCCTTCTCACTATTG	XbaI	
7	GCTACGAATTCGATTTTTGTTCCATTACTAATAAGTCG	EcoRI	
49	GGAAGGATCCCATGAATTTGGACCAAAATAAA	BamHI	
50	GCTACGAATTCTTACTCCTCACTCTTAGCTCC	EcoRI	
51	GCTACGAATTCGACTCCTCACTCTTAGCTCCC	EcoRI	
52	GGAAGGATCCCATGTCCGCACCCGTAATATTG	BamHI	
53	GCTACGAATTCTCATGATTGCACCTCCTTTTG	EcoRI	
54	GCTACGAATTCGATGATTGCACCTCCTTTTGCAG	EcoRI	
76	GGAAGGATCCCATGTTCAGAATGAAACTCATGGAAAC	BamHI	
77	GCTACGAATTCTTATCTAATCTCCCAGCGTGGTTT	EcoRI	
78	GCTACGAATTCGATCTAATCTCCCAGCGTGGTTT	EcoRI	
79	GGAAGGATCCCATGAAGCGTGCGCCTGTTAT	BamHI	
80	GCTACGAATTCTCAGGGTGCTGGCTTTTCAA	EcoRI	
81	GCTACGAATTCGAGGGTGCTGGCTTTTCAAGTT	EcoRI	
82	GGAAGGATCCCATGATGAGTATTGCGCAGGT	BamHI	
83	GCTACGAATTCTCAGTCTCCACCCAGG	EcoRI	
84	GCTACGAATTCGAGTCTCCACCCAGGGTT	EcoRI	

Underlined sequence indicates restriction enzyme cut site. Mutated bases are indicated in bold.

at final concentration of 0.92 mg/ml. Protein concentration was assessed by Bradford assay and substituted for optical density to calculate the output in Miller units (Miller, 1972). Absorbance measurements were taken using a BioTek Synergy HT plate reader. For *E. coli* carrying pAKK128 or pAKK129, overnight cultures were diluted to an OD_{600} of 0.25 in LB with 25 μg/ml chloramphenicol and grown at 37°C for 3 h with rotation. The OD_{600} of the cultures was measured. The cultures were placed on ice for 20 min, and then 1 ml was pelleted and the cells resuspended in 1 ml of Z buffer. A 10 μl volume of the cell suspension was mixed with 990 μl of Z buffer, then 40 μl of chloroform was added, and the samples were vortexed. Samples were incubated at 28°C for 5 min. Three 100 μl aliquots of each sample were placed in a flat bottom 96-well plate. A volume of 30 μl of ONPG (4 mg/ml) was added to each well, and the OD_{420} and OD_{550} were measured every 5 min. β-gal units were calculated using the Miller equation.

TABLE 3 | Bacterial strains used in this study.

***Neisseria gonorrhoeae* strains**		
Strain name	**Description**	**Source/References**
MMC538	*parA′-FLAG3*	This work
MMC542	pMMC18 x MS11 ΔSL-*parA′-FLAG3*	This work
MMC543	pKH502 x MMC538 ΔSL-*parA′-FLAG3*, *cat*	This work
MMC544	pKH37 x MMC542 $P_{Ngnc093}$ -10 mutant	This work
MMC545	pMMC25 x MS11 P_{opaB}-SL_{WT}-*lacZ*	This work
MMC546	parA-lacZ WT3 gene block x MR664 (MS11 background) P_{opaB}-$SL_{\Delta BC}$-*lacZ*	This work
MMC547	parA-lacZ mut2 gene block x MR661 (MS11 background) *parB′-FLAG3*	This work
MMC548	pMMC21 x MS11 ΔSL-*parB′-FLAG3*	This work
MMC549	pMMC21 x KH655 ΔSL-*parA′-FLAG3, cat*	This work
MMC550	pKH37 x MMC548 $P_{Ngnc093}$ -10 mutant, *parA′-FLAG3*	This work
MMC557	pMMC18 x MMC544 *parA′-FLAG3,* P_{aTc}-*NgncR_093*	This work
MMC558	pMMC38 x MMC547 *parB′-FLAG3*, P_{aTc}-*NgncR_093*	This work
MMC562	pMMC38 x MMC538 P_{opaB}-SL-*lacZ*, P_{aTc}-*NgncR_093*	This work
MMC563	pMMC38 x MMC545 P_{opaB}-ΔSL-*lacZ*, P_{aTc}-*NgncR_093*	This work
MMC564	pMMC38 x MMC546 P_{opaB}-SL1mut5-*lacZ*	This work
MS11	parA-lacZ mut3 gene block x MMC546 Wild type *N. gonorrhoeae*	Swanson, 1972
KH655	ΔSL*parA*	This work
MR661	pKH502 x MS11 MS11 locked *pilE*, WT SL*traH – lacZ* at *iga/trpB*	Ramsey et al., 2015
MR664	MS11 locked *pilE*, SL*traH-*$_{\Delta A}$ *– lacZ* at *iga/trpB*	Ramsey et al., 2015
***E. coli* strains**		
E. coli TAM1	Used for cloning for all non-BACTH constructs. *mcrA* Δ(*mrr-hsdRMS-mcrBC*) Φ*80lacZ*ΔM15 Δ*lacX74 recA1 araD139* Δ(*ara-leu*)*7697 galU galK rpsL endA1 nupG*	Active Motif
E. coli 10-beta	Used for cloning in BACTH vectors. Δ(*ara-leu*) *7697 araD139 fhuA* Δ*lacX74 galK16 galE15 e14-* Φ*80dlacZ*Δ*M15 recA1 relA1 endA1 nupG rpsL* (Str^R) *rph spoT1* Δ(*mrr-hsdRMS-mcrBC*)	New England Biolabs
BTH101	Used for BACTH assays. (F-, *cya-99*, *araD139*, *galE15*, *galK16*, *rpsL1* (*Str r*), *hsdR2*, *mcrA1*, *mcrB1*)	Euromedex

Subcellular Fractionation

Isolation of soluble and total membrane fractions was performed according to Ramsey et al. (2014) with the following modifications: at least four 3 ml cultures of each strain were grown for each fractionation experiment. Washed cell pellets were resuspended in 0.5 ml 0.01 M Tris–HCl (pH 7.0) before sonication. Samples were sonicated for a total of 50-, 10-s intervals with ≥30 s on ice between each pulse. Ultracentrifugation was performed at 65,000 rpm in a Beckman TLA110 rotor for 1.5 h.

Outer membrane samples were also prepared as described in (Ramsey et al., 2014), although for this study cells were harvested from six gonococcal cultures, 4 ml each, in cGCBL

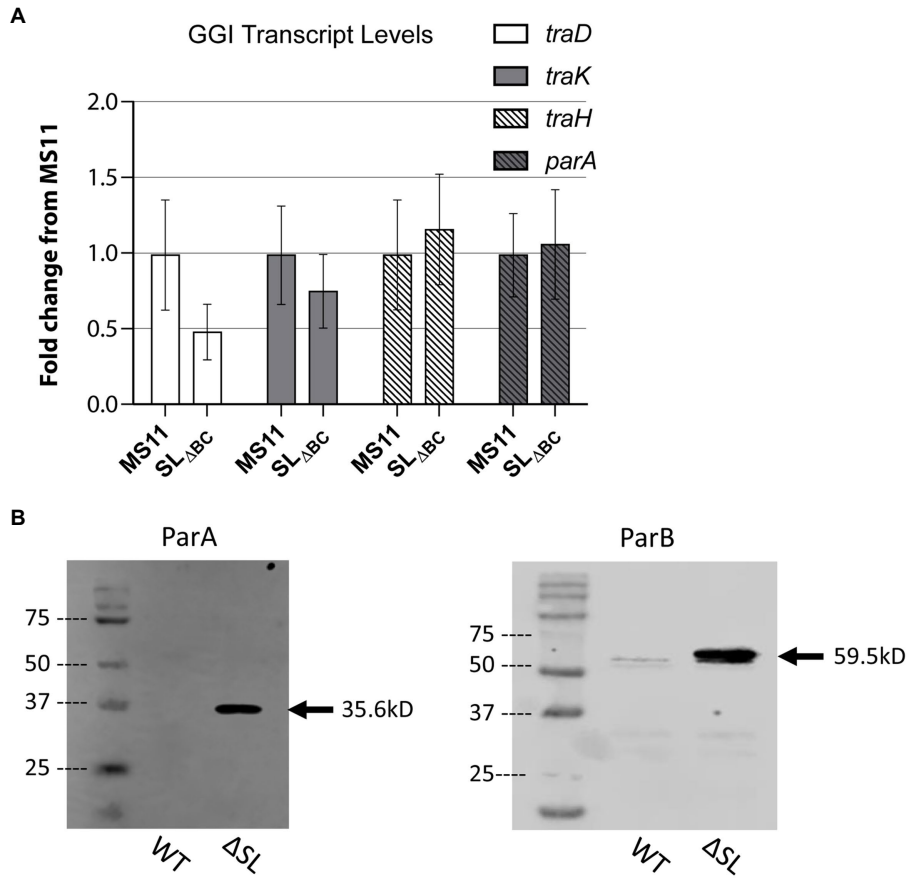

FIGURE 2 | Stem-loop structure controls ParAB expression. **(A)** qRT-PCR measuring GGI transcript levels for T4SS genes in wild-type *Neisseria gonorrhoeae* strain MS11 and $SL_{\Delta BC}$ mutant (KH655). Data shown are three replicates normalized to *rpoB*. Error bars are 95% confidence intervals. No significant differences by Student's *t* test comparing ΔC_T values ($p = 0.48$, 0.72, 0.88, and 0.93 for *traD*, *traK*, *traH*, and *parA*, respectively). **(B)** Western blots of ParA-FLAG3 and ParB-FLAG3 comparing expression in wild type and $SL_{\Delta BC}$ expression. Arrow indicates the expected band size.

grown from $OD_{540} = 0.25$ for 3 h. Cells were collected by centrifugation at 10,000 rpm for 10 min at 4°C and washed once with cold PBS before proceeding.

RESULTS

Stem-Loop Structure Dictates Protein Expression of ParA and ParB

Investigations of the expression of the gonococcal T4SS have begun to reveal a complex regulatory network, with transcriptional, translational, and post-translational mechanisms all at play (Pachulec et al., 2014; Ramsey et al., 2014, 2015; Callaghan et al., 2021). Quantitative transcript data indicate that for both the *traH* operon (*traH*, *traG*, and *atlA*) and the *parA* operon (containing *parA* and *parB*), transcripts are readily detected *in vitro*. However, proteins encoded on the *traH* operon are difficult to detect and attempts to visualize ParA and ParB expression have yet to be reported (Ramsey et al., 2015). The expression of TraH and TraG was shown to be controlled by an RNA switch, and we report here that *parA* uses a similar switch. We discovered a putative pair of stem-loops in the 5′ UTR of *parA*, by manual curation of intergenic GGI regions. The stem-loop proximal to the promoter ("SL2") occludes the translational start site (TSS) and Shine-Dalgarno sequence of the *parA* operon mRNA (**Figures 1A**,**B**). We were unable to identify an energetically favorable alternate secondary structure that releases any part of the ribosome binding site (RBS) in the *parAB* 5′UTR secondary structure.

To determine the necessity of the stem-loop structure for regulation, we deleted the inner portion of the stem-loop sequence. By removing the inside "leg" of each stem (legs B and C, creating "$SL_{\Delta BC}$") the formation of the secondary structure becomes much less favorable, increasing the Gibbs free energy (ΔG) of the structure from −25.3 to −4.68 kcal/mol (**Figure 1B**). This deletion also removes the bases that pair with the TSS "AUG" in the wild-type structure, leaving it more easily accessible. We cloned the wild-type and $SL_{\Delta BC}$ 5′UTR_{parA} constructs into *E. coli* plasmids, making translational fusions with a *lacZ* reporter. The fusions were made such that the *lacZ* start codon and subsequent coding sequence replaced those of *parA*. The wild-type 5′UTR resulted in low levels of LacZ activity, whereas

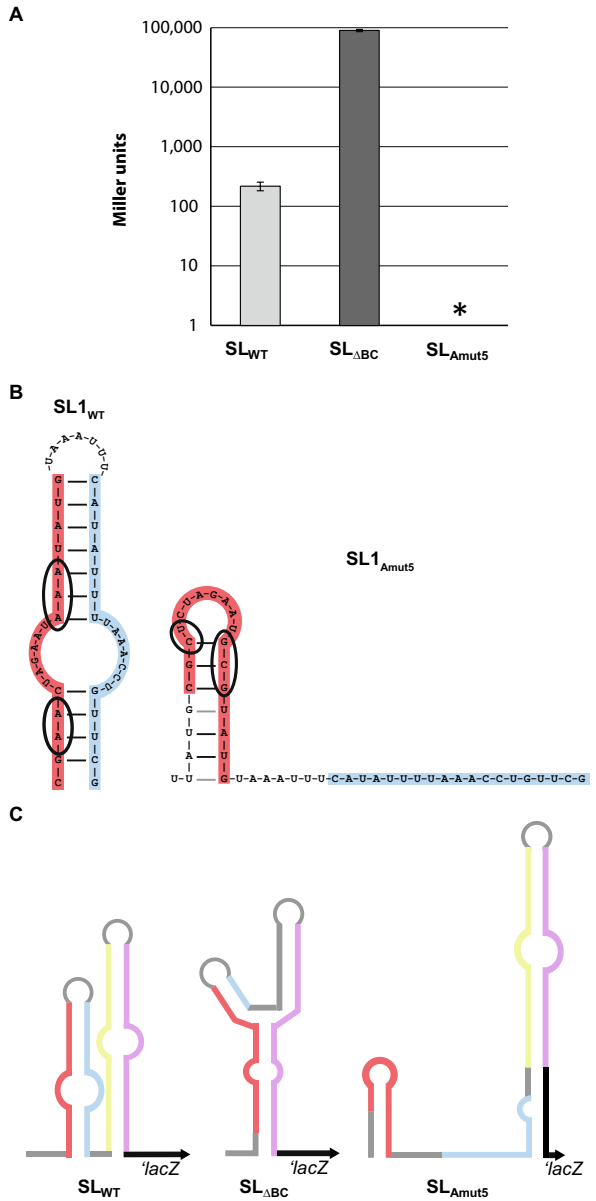

FIGURE 3 | Genetic manipulation to up- and down-regulate protein expression. **(A)** Five base pair changes introduced to SL1 (left) lead to altered predicted secondary structure of the stem-loop region (right). Mutated bases are circled in wild-type and mutated SL1 diagram. **(B)** β-galactosidase assays of wild-type, $SL_{\Delta BC}$, and SL_{Amut5} LacZ reporters. Data shown is averaged from three separate experiments. Note that the y-axis is in log scale. Error bars are SDs. *$p < 0.05$ by Student's *t* test compared to SL_{WT} ($SL_{\Delta BC}$: $p = 0.14$; SL_{Amut5}: $p = 0.00085$). **(C)** Schematic of LacZ reporter constructs. Note that *lacZ* is involved in pairing with SL_{Amut5}, as *parA* is also predicted to do.

the $SL_{\Delta BC}$ mutant gave approximately 10-fold increased levels (**Figure 1C**). These data indicate that the stem-loop structures are functional in gene regulation and can perform such regulation in the absence of gonococcal-specific factors.

We introduced the $SL_{\Delta BC}$ mutation into *N. gonorrhoeae* and examined effects on transcription and translation. We measured relative transcript abundance using qRT-PCR to test for transcriptional effects, looking for direct effects on *parA* or possible indirect effects on other T4SS genes. The $SL_{\Delta BC}$ deletion did not significantly alter transcript levels for any of the four tested genes, one gene from each of the four GGI operons necessary for secretion (operon 1: *traD*, operon 2: *traK*, operon 3: *traH*, terminal operon: *parA*; **Figure 2A**). This result suggests that the secondary structure is not a determinant of transcription activity nor mRNA stability for *parA*, nor does it affect transcript levels for genes in other T4SS operons.

Since SL2 would occlude the ribosome binding site and start codon of the *parA* mRNA, we next asked whether the stem-loops control protein expression. To detect the partitioning proteins by western blot, we added a FLAG3 epitope tag (three repeat copies of the FLAG epitope tag in tandem) to the C-terminus of either ParA or ParB by making genetic changes at the native loci. The epitope-tagged constructs were introduced into both wild-type gonococci (MS11) and the stem-loop deletion strain. In the wild-type background, ParA-FLAG3 was undetectable by western blot, and ParB-FLAG3 was very faintly visible. However, in the stem-loop mutant strains, expression of both proteins was greatly increased and easily visualized *via* western blotting against the FLAG epitope (**Figure 2B**). The control of ParB translation by a switch regulating ParA expression is possible because the start codon of *parB* overlaps the stop codon of *parA*, making it likely that *parA* and *parB* are translationally coupled like many of the gonococcal T4SS genes (Hamilton et al., 2005). We conclude that the stem-loops in the *parA* 5′UTR control protein expression from the *parA-parB* mRNA, revealing a putative riboswitch mechanism of control.

Stem-Loop 1 Contributes to Riboswitch Architecture

For screening and semi-quantitative assessment of protein expression in *N. gonorrhoeae*, we introduced stem-loop – LacZ reporter constructs into the *iga/trpB* complementation locus on the gonococcal chromosome. We fused the *lacZ* gene to either the wild-type stem-loops (MMC545) or the stem-loop deletion sequence $SL_{\Delta BC}$ (MMC546) such that the *lacZ* translational start site is the native *parA* start site, normally occluded by the wild-type stem-loop structure. This construct was placed under the control of the *opaB* promoter, which is constitutively active in gonococci. β-galactosidase assays with these strains confirmed that the wild-type stem-loops expressed little LacZ protein whereas the stem-loop deletion mutant allows ample LacZ expression, increasing LacZ expression approximately 400-fold (**Figure 3A**).

Since no alternate structure for the 5′-UTR was identified, and the translation start site for ParA lies entirely on SL2 leg D, we questioned whether SL1 was playing a role in stem-loop-mediated regulation. To probe the utility of SL 1 in this system, we created a LacZ reporter strain with five base pair changes in SL1 leg A (SL_{Amut5}), predicted to make folding of stem-loop 1 less favorable ($\Delta G_{SL1\text{-}WT} = -8.3$ kcal/mol, $\Delta G_{SL1\text{-}Amut5} = -2.8$ kcal/mol; **Figure 3B**). Surprisingly, these mutations abolished β-galactosidase activity to undetectable levels, below

wild-type levels (**Figure 3A**), indicating a role for SL1 in structure and/or stability of the RNA secondary structure.

Sequence predictions of the mRNA containing SL_{Amut5} indicate a propensity for SL2 to elongate in the absence of strong SL1 folding (**Figure 3C**). At its native locus, a portion of SL1 leg B is able to pair with the beginning of the *parA* gene, creating six new base pairings and extending SL2. In the *lacZ* reporter constructs, SL2 is also predicted to elongate by pairing bases of SL1 leg B with the beginning of the *lacZ*, forming seven new base pairings in a slightly different configuration (**Figure 3C**). The predicted secondary structures of SL2-*parA* and SL2-*lacZ* are very similar, with $\Delta G = -18.5$ and -19.1, respectively. The elongated SL2 structure has a more favorable free energy of folding (predicted ΔG_{SL2} decreases by 4.7 kcal/mol in the *lacZ* constructs, 2.8 kcal/mol in the *parA* constructs when it adopts the elongated conformation), which could explain the decreased protein output from the SL_{Amut5} construct.

Thus, it seems plausible that SL1 contributes to the formation of the wild-type SL2, and prevents the extension of SL2 into a longer and more stable structure. The wild-type stem-loop structure allows for a limited amount of protein expression – far lower than we observe in the complete disruption of these structures, but still detectable by β-galactosidase assay (**Figure 3A**). However, the formation of a structure with an even tighter occlusion of the ribosome binding site, as we observe in the absence of proper SL1 folding, introduces the possibility that binding of an unknown element of SL1 leg A could be a mechanism to completely abolish protein expression of ParAB. These stem-loop mutation results suggest a protein regulation system that can be finely tuned, both increasing and decreasing translation as the cell responds to environmental stimuli.

Identification of Candidate Activators for ParAB Expression in Gonococci

If the 5′UTR sequence is a switch, what are its biologically relevant activators? We saw two potential avenues for RNA switch activation. Firstly, ligand binding could induce conformational changes that make the RBS more accessible to the ribosome. Alternatively, but not exclusively, an sRNA could interact with the stem-loops to alter their structure and allow translation initiation.

The sRNA *NgncR_093* Does Not Affect the RNA Switch

An RNA-Seq analysis by Remmele et al. (2014) identified several sRNAs within the GGI (Remmele et al., 2014). One such sRNA, NgncR_093, overlaps most of the *parA* gene beginning at base 664 (of the total 898 bp of *parA*) and continues, antiparallel, to cover the promoter and stem-loop regions (**Figure 1A**). Based on the reported transcription start site of NgncR_093, we mutated the predicted promoter sequence in wild-type gonococci to change two of the critical −10 residues using site-directed mutagenesis (**Supplementary Figure S1A**). This mutation did not alter *parA* transcript levels (**Supplementary Figure S1B**). We introduced the same NgncR_093 promoter mutations into the ParA-FLAG3 native expression strain and performed western blotting against the FLAG epitope tag. ParA was not detected in either the wild type or the NgncR_093 promoter mutant strain (data not shown).

Next, we asked if overexpression of NgncR_093 might alter ParAB expression, hypothesizing that the sRNA may bind to and alter the stem-loop structure of the *parAB* mRNA. We expressed NgncR_093 from a distant locus under inducible control of the *lac* promoter in the stem-loop-*lacZ* gonococcal reporter strains. Expression of NgncR_093 did not affect β-galactosidase activity in either the wild-type or mutant stem-loop reporters (**Supplementary Figure S1C**). Although the presence of the sRNA did not affect ParAB expression, it is still possible that local NgncR_093 transcriptional activity influences the RNA switch.

Screen for Metabolite Activators

We used Biolog Phenotype MicroArrays (PMs) to do a high-throughput screen for compounds that might activate expression from the RNA switch in strain MMC545, where the *parA* transcript is constitutively expressed and a LacZ reporter has been fused to the stem-loops. Based on the normalized β-galactosidase activity detection protocol of Tang et al. (2013), untreated plates were used to determine the correction factor for cell density and measure normalized β-galactosidase activity in control strains. MMC545 was then grown in PMs, where it was exposed to a panel of over 700 different metabolites. Several compounds increased LacZ expression in this screen. We identified the 11 compounds that yielded the highest normalized β-galactosidase activity (**Supplementary Figure S2**) and pursued further testing with these compounds.

As a method of verification, disk diffusion with promising compounds was performed using the wild-type stem-loop LacZ reporter construct. The following compounds were tested in X-gal disk diffusion assays: 100 mM adenine (in DMSO), 100 mM histidine, 100 mM glycine, 500 mM sodium phosphate buffer pH 7.0, 500 mM EDTA, 100 mM $CuSO_4$, 500 mM sodium sulfate, 60% v/v sodium lactate solution, 100 mM 6-mercaptopurine (in DMSO), 100 mM $CrCl_3$, and 100 mM His-His dipeptide (H-His-His-OH trifluoroacetate salt, Bachem). Only copper sulfate ($CuSO_4$) had any visible effect on colony color (data not shown). Although the magnitude of activation by copper seen in the Biolog assays or on plates is only moderate, this finding aligns with other instances of copper-dependent enhancement of T4SS protein expression, described in (Callaghan et al., 2021).

The ParA and ParB Encoded on the GGI Are Not Homologous to Known Cognate Pairs of Partitioning Proteins

The specific roles or mechanisms of partitioning activity have not been extensively explored in the gonococcal T4SS. Although we have built hypotheses around findings in other systems, there is ample variation in how these proteins function (Atmakuri et al., 2007; Lutkenhaus, 2012; Gruber et al., 2016). We decided to begin characterizing these proteins by looking at sequence homology, interaction partners, and localization.

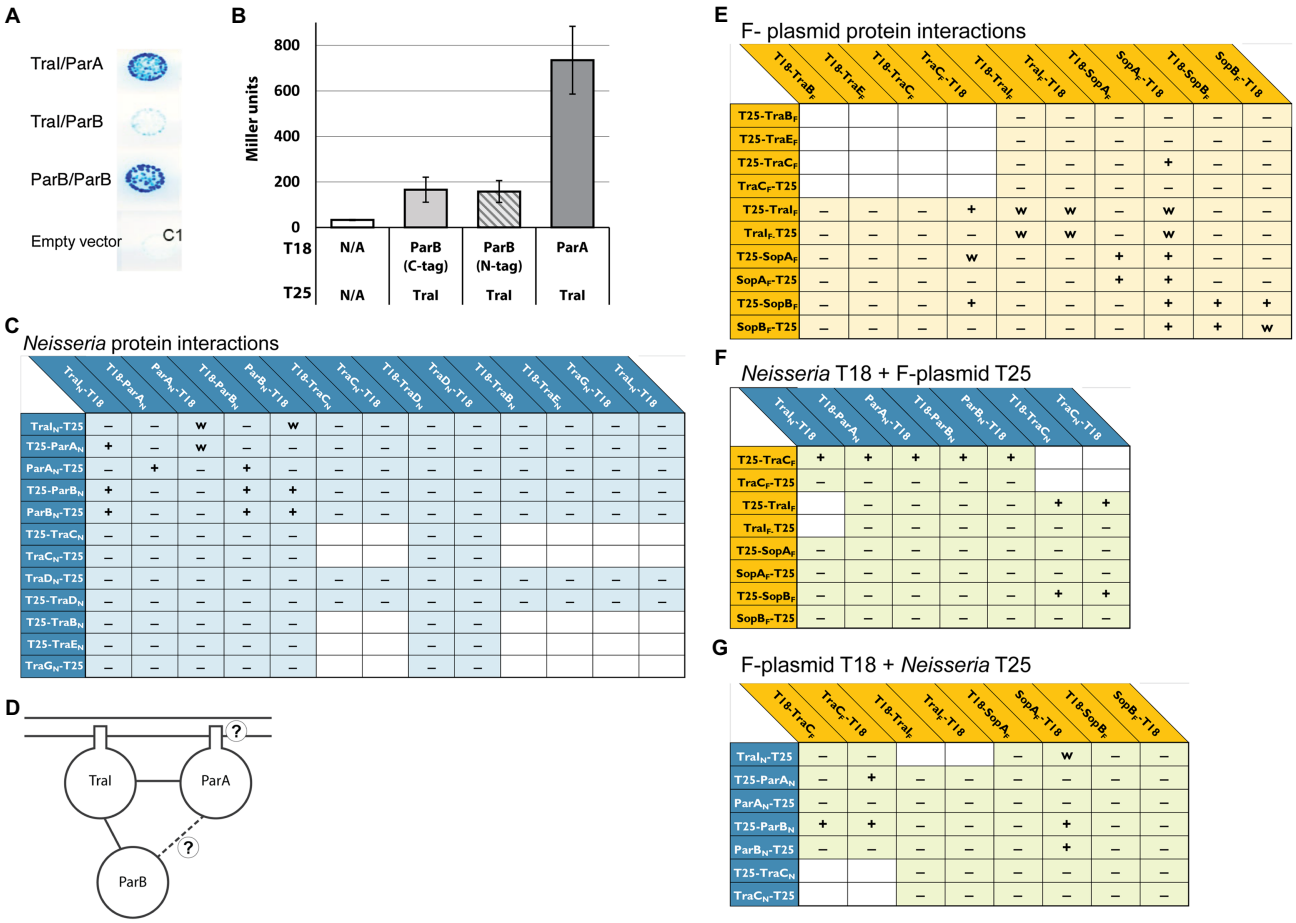

FIGURE 4 | Bacterial two-hybrid interactions formed between *Neisseria* ParAB and TraI proteins. **(A)** Scanned image of an agar plate with colonies of *E. coli* BTH101 transformants carrying plasmids encoding the proteins indicated in the order T18/T25. C1 is an empty vector control: pUT18C/pKT25. **(B)** β-galactosidase assay testing expression from ParB-TraI and ParA-TraI interactions in BACTH constructs. Left to right: pUT18C/pKT25, pUT18TraI/pKT25ParB, pUT18TraI/p25NParB, pUT18TraI/pKT25ParA. Data shown are three replicates, error bars are SDs. **(C)** Interactions between *N. gonorrhoeae* ParA, ParB, and TraI with cytoplasmic and transmembrane proteins from *N. gonorrhoeae* T4SS. **(D)** Schematic drawing of all interactions identified between ParA, ParB, and TraI. **(E)** Interactions between F-plasmid homologues of the gonococcal T4SS. **(F,G)** Interactions between *Neisseria* and F-plasmid proteins. +, –, and w indicate interaction, no interaction, and weak interaction, respectively, tested in this study. Interactions tested in previous studies have been omitted. The placement of T18 and T25 relative to the protein name indicates N- or C-terminal fusion. T18 or T25 indicate that the gene encoding the protein was cloned into the BACTH vectors.

Interestingly, the ParA and ParB encoded on the GGI may not be cognate partners. ParA contains a conserved domain from the P-loop NTPase superfamily of proteins, which are found abundantly in protein and DNA localization roles (Pfam accession cl38936; Marchler-Bauer et al., 2017; El-Gebali et al., 2019; **Supplementary Figure S3**). ParAB cognate pairs are canonically found adjacently encoded, which is indeed the case for the GGI (Bignell and Thomas, 2001; Hamilton et al., 2005; Pachulec et al., 2014; **Figure 1A**). On the other hand, the gonococcal ParB contains a conserved domain from the ParB family protein of the *Pseudomonas fluorescens* Pf-5 genetic island-1 (PFGI_1) class of integrating conjugative elements (Pfam superfamily cl26723, family TIGR03764; Marchler-Bauer et al., 2017; El-Gebali et al., 2019; **Supplementary Figure S3**). The founding members of this protein family are not encoded in immediate proximity to a ParA partner (Klockgether et al., 2004; Paulsen et al., 2005), and of the 41 protein architectures in the CDART database, only five have an adjacent P-loop NTPase (Pfam cl38936) domain (Geer et al., 2002). Consistent with this finding, neither nucleotide alignment search nor translated nucleotide alignment searches using the basic local alignment search tool (BLAST) identified homology of the *N. gonorrhoeae parAB* gene region to sequence from any organism outside of the *Neisseriaceae* family in which both *parA* and *parB* homologues were present, although *parA* and *parB* are individually homologous to many genes within their respective families (Altschul et al., 1990). Thus, while each gonococcal protein is likely to fit the role for one half of a partitioning protein pair, it is unclear whether these two proteins work together as a cognate pair, nor whether the GGI-encoded *parA* and *parB* were evolutionarily acquired as a unit.

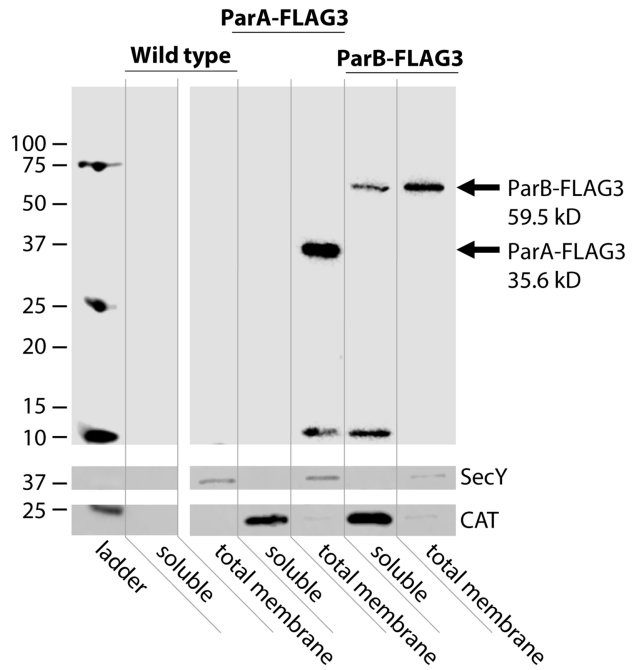

FIGURE 5 | Subcellular fractionation of ParA and ParB. Western blot against the FLAG epitope to detect ParA-FLAG3 and ParB-FLAG3 expressed from the native locus in the $SL_{\Delta BC}$ strain background. The inner membrane protein SecY is a total membrane fraction control, CAT is a cytosolic control (Ramsey et al., 2014).

ParA and ParB Interact With the Relaxase, TraI

We used a Bacterial Two-Hybrid (BACTH) system to test for direct interactions between ParA and ParB with the other predicted cytoplasmic and transmembrane proteins of the gonococcal T4SS. This system uses two fragments, T18 and T25, of the catalytic domain of *Bortedella pertussis* adenylate cyclase, fused to the N- or C-terminal end of two proteins of interest. If an interaction between the proteins of interest brings T18 and T25 into sufficient proximity, functional complementation results in cAMP synthesis inducing transcriptional activation of the lactose operon (Karimova et al., 2001; Battesti and Bouveret, 2012). Using this system functional complementation can therefore be detected on agar plates with X-gal or by β-galactosidase assay. We tagged ParA and ParB with either T18 or T25 at both the N- and C-termini. These constructs were tested for interactions with the N- and C-termini of the other cytoplasmic and transmembrane gonococcal T4SS proteins: TraI, TraC, TraB, TraD, TraE, TraG, and TraL. Transmembrane proteins were tagged at the N- or C-terminus based on predicted topology, such that the tag will be cytosolic (Koch et al., 2020). This large screen identified only two definite interactions for each ParA and ParB: each protein gave a positive interaction result with itself and with TraI, the T4SS relaxase. Only one combination of fusion proteins indicated an interaction between ParA and ParB directly: ParA-T25 interacted with T18-ParB, but none of the other combinations gave a positive result (**Figures 4A–C**).

Gonococcal Relaxosome Components Can Form Interactions With *E. coli* F-Plasmid Proteins

The plasmid partitioning proteins of F-plasmid, SopA and SopB, constitute a Walker-type ATPase (SopA) and DNA-binding partner (SopB; Watanabe et al., 1992; Schumacher and Funnell, 2005). We used the BACTH system to test for interactions between F-plasmid SopAB and TraI, looking to gain information on where the gonococcal system parallels or differs from better-characterized T4SSs. Additionally, we used this system to ask whether our gonococcal proteins of interest were able to interact with their counterparts in the F-plasmid system.

We created both N- and C-terminal fusions of SopA, SopB, and TraI from F-plasmid with the T18 and T25 fragments and tested them for interactions amongst themselves and with elements of the putative gonococcal relaxosome, as well as the cytoplasmic ATPase TraC (a homologue of VirB4, the most conserved element across T4SSs; Alvarez-Martinez and Christie, 2009; Guglielmini et al., 2013; Koch et al., 2020). For clarity, F-plasmid proteins will be specified by "F" (e.g., $TraI_F$) and *Neisseria* proteins by "N" (e.g., $TraI_N$) for these constructs. Apart from the expected dimerizations for the $SopA_F$ and $SopB_F$ proteins and the expected $SopA_F$/$SopB_F$ interaction (Bartosik et al., 2014), we observed a weak $TraI_F$ dimerization and weak $SopA_F$/$TraI_F$ interactions (**Figure 4D**). For unknown reasons co-expression of a plasmid expressing $TraC_F$ and a plasmid expressing ParB, TraI and in particular ParA homologues led to a decreased cell number in overnight cultures.

Interactions between F-plasmid partners helped confirm the utility of our approach and identified a parallel relaxase-partitioning protein interaction. Several mixed interactions have been reported between proteins of the F-plasmid and gonococcal systems previously, however none testing elements of the putative gonococcal relaxosome (Koch et al., 2020). The following cross-system interactions were observed, however in none of these cases were the proteins seen interacting in all possible N- and C-terminal or T18- and T25-terminal configurations: $TraC_F$-$ParA_N$ (3 of 8 potential interactions) and $TraC_F$-$ParB_N$ (4 of 8 potential interactions), $SopA_F$-$ParB_N$ (2 of 4 potential interactions), $SopB_F$-$TraC_N$ (2 of 4 potential interactions) and $TraI_F$-$TraC_N$ (2 of 4 potential interactions; **Figures 4E,F**).

Subcellular Localization of ParA and ParB

To better understand where the partitioning proteins act to facilitate DNA secretion, subcellular fractionation of FLAG3-tagged ParA and ParB was used to separate soluble from membrane-associated proteins. Strains used for the fractionation studies had the stem-loop deletion in the native site *parA* 5′UTR to overexpress ParAB and allow visualization on western blots. These strains also had the chloramphenicol acetyltransferase gene *cat* expressed at the *aspC*/*lctP* complementation site, to be used as a cytosolic protein control (Ramsey et al., 2014). Based on sequence predictions, we expected both proteins to be entirely cytosolic (Bernsel et al., 2009). However, western blotting against the FLAG epitope revealed that ParA fractionated exclusively with the membrane fraction of culture lysates.

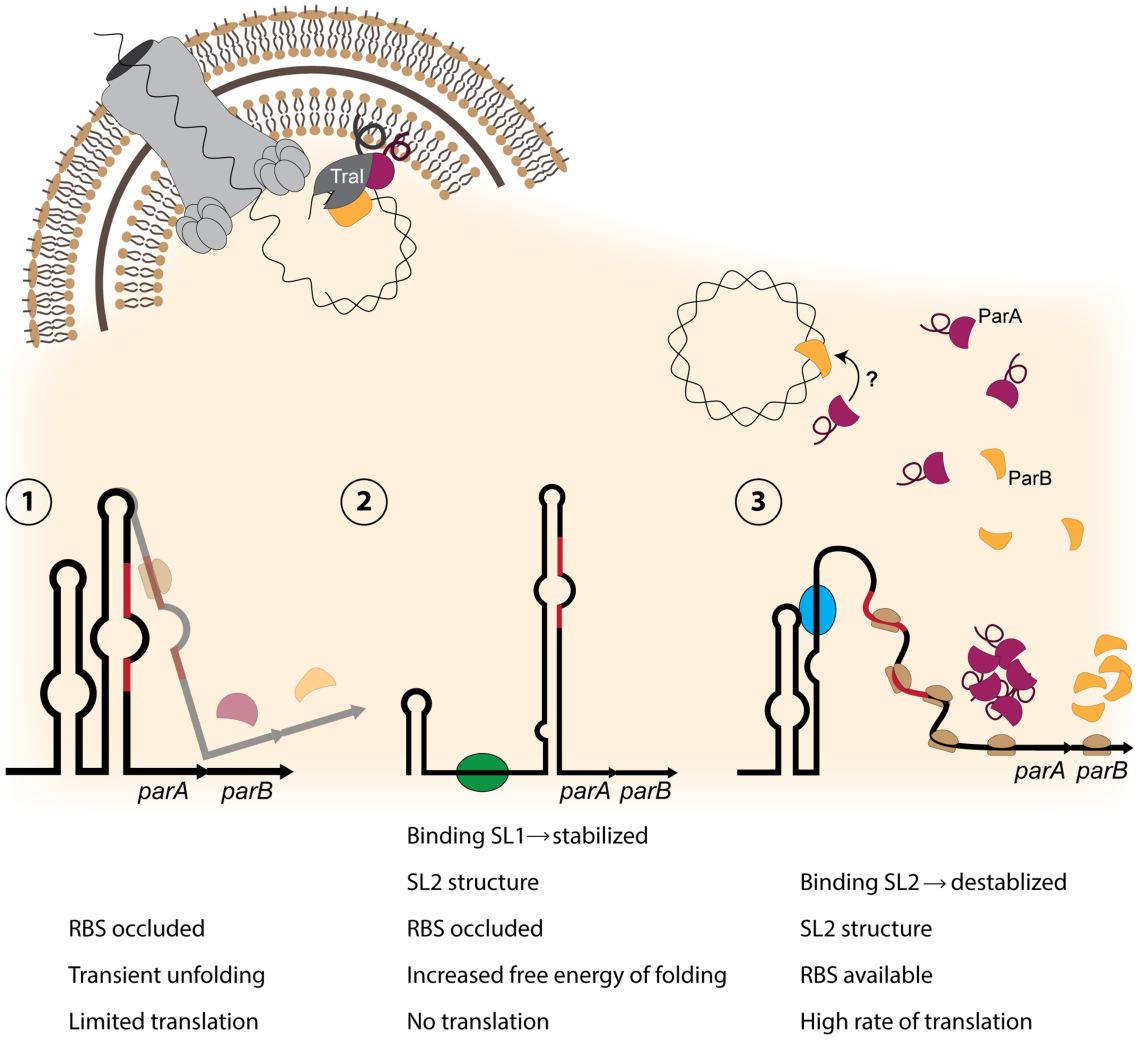

FIGURE 6 | Model of partitioning protein activity in the gonococcal T4SS. (1) The *parAB* transcript contains an RNA-switch consisting of two stem-loops, with stem-loop 2 (SL2) occluding the Shine-Dalgarno sequence and the start codon (red regions) from binding the ribosome. Only a small amount of translation occurs. (2) If stem-loop 1 is destabilized, possibly by a protein or sRNA (green oval) binding to SL1 sequence, SL2 forms an extended structure, preventing translation. (3) If SL2 is destabilized by a factor (blue oval) binding within the SL2 sequence, a high rate of translation can occur. Production of ParA (burgundy) and ParB (yellow) allows for relaxosome formation with ParB binding chromosomal DNA (top right). It is possible that ParA binds ParB. ParA and TraI (dark gray) associate with the inner membrane through amphipathic alpha-helix regions (looped line), and ParB binds TraI. TraI nicks the DNA, and it may be transported into the medium through the T4SS apparatus (top left).

Furthermore, ParB is present in both the soluble and membrane fractions, with the membrane fraction having greater ParB signal than the soluble fraction (**Figure 5**). Isolation of outer membrane proteins from the total membrane fraction revealed no ParA or ParB in the outer membrane, indicating that both proteins associate with the inner membrane (**Supplementary Figure S4**).

DISCUSSION

The partitioning proteins ParA and ParB of the gonococcal T4SS are integral to ssDNA secretion. Canonically, partitioning proteins act in cognate pairs to accurately segregate chromosomes and/or plasmids. However, gonococcal ParA and ParB are not an obvious cognate pair; while they are encoded adjacent to one another on the same operon, their conserved domains exhibit homology to differing classes of partitioning proteins. We found limited evidence to support a direct ParA-ParB interaction. We did find evidence that both ParA and ParB interact with themselves and the relaxase TraI, supporting the existing hypothesis that a ParAB-TraI relaxosome facilitates DNA nicking during the initiation of secretion. These results suggest that ParA and ParB might function in a novel way, working to initiate secretion by associating with TraI without interacting with one another.

Fractionation experiments indicate an association of both partitioning proteins with the bacterial inner membrane. These results were surprising because the canonical action of partitioning proteins led us to expect that at least one of these proteins will associate with DNA in the cytosol. Sequence-based analysis

using the SignalP 5.0 and TOPCONS algorithms predicted no probable transmembrane domains in either protein and a low likelihood signal peptide in ParA (Bernsel et al., 2009; Juan et al., 2019). Examination of the N-terminal region of ParA with the Helical Wheel generator program EMBOSS pepwheel[1] suggests that amino acids 21–28 may form an amphipathic alpha-helix that could interact with the membrane.

Our finding that ParA and ParB both interact with TraI provides an alternate explanation to membrane or transmembrane ParAB proteins; TraI associates with the inner membrane *via* an amphipathic helix and fractionates with cellular membranes (Salgado-Pabón et al., 2007). Disruption of this helix causes TraI to fractionate with the soluble proteins (Salgado-Pabón et al., 2007). Thus ParA and ParB might each bind to membrane-associated TraI, and the three proteins may form a relaxosome complex at the inner membrane (**Figures 4B**, **6**).

If the entire relaxosome assembles at the inner membrane, we are left with new questions about substrate localization. How does the relaxosome recruit chromosomal DNA for nicking, and what caused this novel localization to develop in the gonococcal T4SS? Although the chromosome is cytosolic, perhaps transient association with the membrane is sufficient to allow interaction with a membrane-associated relaxosome. Alternatively, more aligned with other T4SS partitioning systems, the key may lie in the dual-localization of ParB in both the cytosol and membrane fraction. As the DNA-binding entity, we may speculate that the role of recruitment falls to ParB, which complexes the DNA to be nicked with our membrane-associated TraI, and (directly or indirectly) works in conjugation with ParA ATPase activity to initiate secretion (**Figure 6**).

Several instances of stem-loop-mediated regulation have been reported in the pathogenic *Neisseria* (Loh et al., 2013; Ramsey et al., 2015; Masters et al., 2016). We grow this body of literature by presenting a previously unknown RNA switch upstream of *parA* that contributes to the regulation of the gonococcal T4SS by controlling the expression of the partitioning proteins ParAB. The *parAB* switch consists of two stem-loops, which we have termed SL1 and SL2. Folding of SL2 occludes the Shine-Dalgarno sequence and the start codon of the *parA* mRNA. Complete disruption of both stem-loops greatly increases ParAB protein expression, whereas disruption of SL1 formation abolishes protein expression. We did not observe any effects from promoter disruption or ectopic overexpression of NgncR_093, the sRNA overlapping *parA* and the stem-loop region. Thus the function of this sRNA remains a mystery.

Stem-loop structure could be manipulated by a variety of mechanisms to effectively control protein expression. Since significant disruption of the secondary structure allows huge amounts of protein expression, a classic riboswitch mechanism in which ligand binding causes conformation change to allow expression seems likely. The potential to turn expression entirely "off" introduces more complexity and nuance to this system. Perhaps the folding of SL1 keeps the extended SL2 from becoming energetically favorable, maintaining low levels of ParAB expression (**Figure 6**). However, there may be other factors at play; stabilization of SL1 could act as a mechanism to allow or increase protein expression under certain conditions. Identification of regulatory elements here is challenging; because laboratory GGI expression is very different than in the human host – relevant ligands, sRNAs, and/or proteins may not be expressed *in vitro* (Callaghan et al., 2021).

Together, our data suggest that the *parAB* RNA switch can be finely tuned, allowing for precise control of ParAB expression at the translational level. We speculate that since ParAB activity in the relaxosome results in chromosomal nicking, and potentially initiates the ssDNA secretion process, the expression of these proteins needs to be tightly regulated to prevent unnecessary DNA damage by the relaxase and wasteful ATP-dependent secretion when it has no benefit to the bacterial cell or population. Additionally, extracellular DNA can elicit robust host immune responses, so careful regulation to avoid DNA secretion when evading the host immune system may be paramount to T4SS regulation (Hemmi et al., 2000).

A large-scale metabolite screen identified several compounds as potential activators of the RNA switch. Of these, we confirmed modest, concentration-dependent upregulation from copper sulfate. Copper has been shown to alter T4SS protein expression previously, and this activation was speculated to occur when gonococci are in the macrophage phagosome (Callaghan et al., 2021). This finding opens a line of inquiry regarding copper binding or indirect activation of the RNA switch. More extensive testing is required to fully characterize this newly reported regulatory element. Riboswitch ligands vary widely, including proteins, sRNAs, tRNAs, metals and metabolites. Temperature and pH-responsive riboswitches have also been described (Winkler and Breaker, 2005; Nechooshtan et al., 2009; Loh et al., 2013; Sherwood and Henkin, 2016).

The *parAB* stem-loop regulator is the second RNA switch identified on the GGI; there is also a stem-loop structure upstream of *traH* that can form an alternate fold to activate protein expression (Ramsey et al., 2015). The activator(s) of the *traH* switch has not yet been identified. The occurrence of two stem-loop-based regulatory mechanisms in the 59 kb space of the GGI raises specific questions about mechanisms of T4SS regulation, but also broader questions regarding the levels of regulation and interplay between regulatory mechanisms at different sites of the GGI.

DATA AVAILABILITY STATEMENT

The original contributions presented in the study are included in the article/**Supplementary Material**; further inquiries can be directed to the corresponding author.

AUTHOR CONTRIBUTIONS

MC, AK, and JD: conceptualization. BK, KH, and AK: methodology. MC, BK, KH, AK, and RS: investigation. MC: writing – original draft. JD, MC, BK, KH, AK, and NK: writing – review and editing. JD and NK: supervision and funding. All authors contributed to the article and approved the submitted version.

[1]https://www.bioinformatics.nl/cgi-bin/emboss/pepwheel

FUNDING

This work was funded by NIH grant R01AI047958. BK and NK were funded by the EPSRC (EP/N031962/1) and a Royal Academy of Engineering Chair in Emerging Technologies award.

SUPPLEMENTARY MATERIAL

The Supplementary Material for this article can be found online at: https://www.frontiersin.org/articless/10.3389/fmicb.2021.784483/full#supplementary-material

REFERENCES

Altschul, S., Gish, W., Miller, W., Myers, E., and Lipman, D. J. (1990). Basic local alignment search tool. *J. Mol. Biol.* 215, 403–410. doi: 10.1016/S0022-2836(05)80360-2

Alvarez-Martinez, C. E., and Christie, P. J. (2009). Biological diversity of prokaryotic type IV secretion systems. *Microbiol. Mol. Biol. Rev.* 73, 775–808. doi: 10.1128/MMBR.00023-09

Applied Biosystems (1997). User Bulletin #2 Relative Quantitation of Gene Expression Introduction. Foster City, CA.

Atmakuri, K., Cascales, E., Burton, O. T., Banta, L. M., and Christie, P. J. (2007). *Agrobacterium* ParA/MinD-like VirC1 spatially coordinates early conjugative DNA transfer reactions. *EMBO J.* 26, 2540–2551. doi: 10.1038/sj.emboj.7601696

Bartosik, A. A., Glabski, K., Jecz, P., Lasocki, K., Mikosa, M., Plochocka, D., et al. (2014). Dissection of the region of *Pseudomonas aeruginosa* ParA that is important for dimerization and interactions with its partner ParB. *Microbiology* 160, 2406–2420. doi: 10.1099/mic.0.081216-0

Battesti, A., and Bouveret, E. (2012). The bacterial two-hybrid system based on adenylate cyclase reconstitution in *Escherichia coli*. *Methods* 58, 325–334. doi: 10.1016/j.ymeth.2012.07.018

Bernsel, A., Viklun, H., Hennerdal, A., and Elofsson, A. (2009). TOPCONS: consensus prediction of membrane protein topology. *Nucleic Acids Res.* 37, W465–W468. doi: 10.1093/nar/gkp363

Bignell, C., and Thomas, C. M. (2001). The bacterial ParA-ParB partitioning proteins. *J. Biotechnol.* 91, 1–34. doi: 10.1016/S0168-1656(01)00293-0

Callaghan, M. M., and Dillard, J. P. (2019). Transformation in *Neisseria gonorrhoeae*. *Methods Mol. Biol.* 1997, 143–162. doi: 10.1007/978-1-4939-9496-0_10

Callaghan, M. M., Heilers, J., van der Does, C., and Dillard, J. P. (2017). "Secretion of chromosomal DNA by the *Neisseria gonorrhoeae* type IV secretion system," in *Current Topics in Microbiology and Immunology: Type IV Secretion in Gram-Negative and Gram-Positive Bacteria*. eds. S. Backert and E. Grohmann. 413th ed (Cham, Switzerland: Springer), 323–345.

Callaghan, M. M., Klimowicz, A. K., Shockey, A. C., Kane, J., Pepperell, C. S., and Dillard, J. P. (2021). Transcriptional and translational responsiveness of the *Neisseria gonorrhoeae* type IV secretion system to conditions of host infections. *Infect. Immun.* 89:e0051921. doi: 10.1128/IAI.00519-21

Centers for Disease Control and Prevention (2019). Sexually Transmitted Disease Surveillance 2018. Atlanta, Georgia.

Centers for Disease Control and Prevention (2021). Sexually Transmitted Disease Surveillance 2019: Gonococcal Isolate Surveillance Project (GISP) Supplement & Profiles. Atlanta, Georgia.

Claessen, D., Emmins, R., Hamoen, L. W., Daniel, R. A., Errington, J., and Edwards, D. H. (2008). Control of the cell elongation-division cycle by shuttling of PBP1 protein in *Bacillus subtilis*. *Mol. Microbiol.* 68, 1029–1046. doi: 10.1111/j.1365-2958.2008.06210.x

Dillard, J. P., and Seifert, H. S. (2001). A variable genetic island specific for *Neisseria gonorrhoeae* is involved in providing DNA for natural transformation and is found more often in disseminated infection isolates. *Mol. Microbiol.* 41, 263–277. doi: 10.1046/j.1365-2958.2001.02520.x

El-Gebali, S., Mistry, J., Bateman, A., Eddy, S. R., Luciani, A., Potter, S. C., et al. (2019). The Pfam protein families database in 2019. *Nucleic Acids Res.* 47, D427–D432. doi: 10.1093/nar/gky995

Geer, L. Y., Domrachev, M., Lipman, D. J., and Bryant, S. H. (2002). CDART: protein homology by domain architecture. *Genome Res.* 12, 1619–1623. doi: 10.1101/gr.278202

Gruber, C. J., Lang, S., Rajendra, V. K. H., Nuk, M., Raffl, S., Schildbach, J. F., et al. (2016). Conjugative DNA transfer is enhanced by plasmid R1 partitioning proteins. *Front. Mol. Biosci.* 3:32. doi: 10.3389/fmolb.2016.00032

Guglielmini, J., De La Cruz, F., and Rocha, E. P. C. (2013). Evolution of conjugation and type IV secretion systems. *Mol. Biol. Evol.* 30, 315–331. doi: 10.1093/molbev/mss221

Hamilton, H. L., and Dillard, J. P. (2006). Natural transformation of *Neisseria gonorrhoeae*: from DNA donation to homologous recombination. *Mol. Microbiol.* 59, 376–385. doi: 10.1111/j.1365-2958.2005.04964.x

Hamilton, H. L., Domínguez, N. M., Schwartz, K. J., Hackett, K. T., and Dillard, J. P. (2005). *Neisseria gonorrhoeae* secretes chromosomal DNA via a novel type IV secretion system. *Mol. Microbiol.* 55, 1704–1721. doi: 10.1111/j.1365-2958.2005.04521.x

Hamilton, H. L., Schwartz, K. J., and Dillard, J. P. (2001). Insertion-duplication mutagenesis of *Neisseria*: use in characterization of DNA transfer genes in the gonococcal genetic island. *J. Bacteriol.* 183, 4718–4726. doi: 10.1128/JB.183.16.4718-4726.2001

Hemmi, H., Takeuchi, O., Kawai, T., Kaisho, T., Sato, S., Sanjo, H., et al. (2000). A toll-like receptor recognizes bacterial DNA. *Nature* 408, 740–745. doi: 10.1038/35047123

Jain, S., Zweig, M., Peeters, E., Siewering, K., Hackett, K. T., Dillard, J. P., et al. (2012). Characterization of the single stranded DNA binding protein SsbB encoded in the gonoccocal genetic island. *PLoS One* 7:e35285. doi: 10.1371/journal.pone.0035285

Juan, J. A. A., Tsirigos, K. D., Sønderby, C. K., Petersen, T. N., Winther, O., Brunak, S., et al. (2019). SignalP 5.0 improves signal peptide predictions using deep neural networks. *Nat. Biotechnol.* 37, 420–423. doi: 10.1038/s41587-019-0036-z

Karimova, G., Ullmann, A., and Ladant, D. (2001). Protein-protein interaction between *Bacillus stearothermophilus* tyrosyl-tRNA synthetase subdomains revealed by a bacterial two-hybrid system. *J. Mol. Microbiol. Biotechnol.* 3, 73–82.

Kellogg, D. S., Peacock, W. L., Deacon, W. E., Brown, L., and Pirkle, D. I. (1963). *Neisseria gonorrhoeae*. I. virulence genetically linked to clonal variation. *J. Bacteriol.* 85, 1274–1279. doi: 10.1128/jb.85.6.1274-1279.1963

Klockgether, J., Reva, O., Larbig, K., and Tümmler, B. (2004). Sequence analysis of the mobile genome island pKLC102 of *Pseudomonas aeruginosa* C. *J. Bacteriol.* 186, 518–534. doi: 10.1128/JB.186.2.518-534.2004

Koch, B., Callaghan, M. M., Tellechea-Luzardo, J., Seeger, A. Y., Dillard, J. P., and Krasnogor, N. (2020). Protein interactions within and between two F-type type IV secretion systems. *Mol. Microbiol.* 114, 823–838. doi: 10.1111/mmi.14582

Kohler, P. L., Chan, Y. A., Hackett, K. T., Turner, N., Holly, L. H., Cloud-Hansen, C., et al. (2013). Mating pair formation homologue TraG is a variable membrane protein essential for contact-independent type IV secretion of chromosomal DNA by *Neisseria gonorrhoeae*. *J. Bacteriol.* 195, 1666–1679. doi: 10.1128/JB.02098-12

Lin, D. C. H., and Grossman, A. D. (1998). Identification and characterization of a bacterial chromosome partitioning site. *Cell* 92, 675–685. doi: 10.1016/S0092-8674(00)81135-6

Loh, E., Kugelberg, E., Tracy, A., Zhang, Q., Gollan, B., Ewles, H., et al. (2013). Temperature triggers immune evasion by *Neisseria meningitidis*. *Nature* 502, 237–240. doi: 10.1038/nature12616

Lutkenhaus, J. (2012). The ParA/MinD family puts things in their place. *Trends Microbiol.* 20, 411–418. doi: 10.1016/j.tim.2012.05.002

Marchler-Bauer, A., Bo, Y., Han, L., He, J., Lanczycki, C. J., Lu, S., et al. (2017). CDD/SPARCLE: functional classification of proteins via subfamily domain architectures. *Nucleic Acids Res.* 45, D200–D203. doi: 10.1093/nar/gkw1129

Masters, T. L., Wachter, J., and Hill, S. A. (2016). Loop structures in the 5′ untranslated region and antisense RNA mediate *pilE* gene expression in *Neisseria gonorrhoeae*. *Microbiology* 162, 2005–2016. doi: 10.1099/mic.0.000369

Mellin, J. R., Goswami, S., Grogan, S., Tjaden, B., and Genco, C. A. (2007). A novel Fur- and iron-regulated small RNA, NrrF, is required for indirect

Fur-mediated regulation of the *sdhA* and *sdhC* genes in *Neisseria meningitidis*. *J. Bacteriol.* 189, 3686–3694. doi: 10.1128/JB.01890-06

Miller, J.H. (1972). *Experiments in Molecular Genetics*. Cold Spring Harbor Laboratory, Cold Spring Harbor, NY.

Morse, S. A., and Bartenstein, L. (1974). Factors affecting autolysis of *Neisseria gonorrhoeae*. *Proc. Soc. Exp. Biol. Med.* 145, 1418–1421. doi: 10.3181/00379727-145-38025

Nechooshtan, G., Elgrably-weiss, M., Sheaffer, A., Westhof, E., and Altuvia, S. (2009). A pH-responsive riboregulator. *Genes Dev.* 23, 2650–2662. doi: 10.1101/gad.552209

Pachulec, E., Siewering, K., Bender, T., Heller, E.-M., Salgado-Pabón, W., Schmoller, S. K., et al. (2014). Functional analysis of the gonococcal genetic island of *Neisseria gonorrhoeae*. *PLoS One* 9:e109613. doi: 10.1371/journal.pone.0109613

Paulsen, I. T., Press, C. M., Ravel, J., Kobayashi, D. Y., Myers, G. S. A., Mavrodi, D. V., et al. (2005). Complete genome sequence of the plant commensal *Pseudomonas fluorescens* Pf-5. *Nat. Biotechnol.* 23, 873–878. doi: 10.1038/nbt1110

Ramsey, M. E., Bender, T., Klimowicz, A. K., Hackett, K. T., Yamamoto, A., Jolicoeur, A., et al. (2015). Targeted mutagenesis of intergenic regions in the *Neisseria gonorrhoeae* gonococcal genetic island reveals multiple regulatory mechanisms controlling type IV secretion. *Mol. Microbiol.* 97, 1168–1185. doi: 10.1111/mmi.13094

Ramsey, M. E., Hackett, K. T., Bender, T., Kotha, C., van der Does, C., and Dillard, J. P. (2014). TraK and TraB are conserved outer membrane proteins of the *Neisseria gonorrhoeae* type IV secretion system and are expressed at low levels in wild-type cells. *J. Bacteriol.* 196, 2954–2968. doi: 10.1128/JB.01825-14

Ramsey, M. E., Hackett, K. T., Kotha, C., and Dillard, J. P. (2012). New complementation constructs for inducible and constitutive gene expression in *Neisseria gonorrhoeae* and *Neisseria meningitidis*. *Appl. Environ. Microbiol.* 78, 3068–3078. doi: 10.1128/AEM.07871-11

Remmele, C. W., Xian, Y., Albrecht, M., Faulstich, M., Fraunholz, M., Heinrichs, E., et al. (2014). Transcriptional landscape and essential genes of *Neisseria gonorrhoeae*. *Nucleic Acids Res.* 42, 10579–10595. doi: 10.1093/nar/gku762

Salgado-Pabón, W., Jain, S., Turner, N., van der Does, C., and Dillard, J. P. (2007). A novel relaxase homologue is involved in chromosomal DNA processing for type IV secretion in *Neisseria gonorrhoeae*. *Mol. Microbiol.* 66, 930–947. doi: 10.1111/j.1365-2958.2007.05966.x.A

Schumacher, M. A., and Funnell, B. E. (2005). Structures of ParB bound to DNA reveal mechanism of partition complex formation. *Nature* 438, 516–519. doi: 10.1038/nature04149

Sherwood, A. V., and Henkin, T. M. (2016). Riboswitch-mediated gene regulation: novel RNA architectures dictate gene expression responses. *Annu. Rev. Microbiol.* 70, 361–374. doi: 10.1146/annurev-micro-091014-104306

Shockey, A.C. (2019). Genomics of Bacterial Pathogens across Evolutionary Scales. Ph.D. thesis. University of Wisconsin-Madison.

Swanson, J. (1972). Studies on gonococcus infection II: freeze-fracture, freeze-etch studies on gonococci. *J. Exp. Med.* 136, 1258–1271. doi: 10.1084/jem.136.5.1258

Tang, K., Zhang, Y., Yu, M., Shi, X., Coenye, T., Bossier, P., et al. (2013). Evaluation of a new high-throughput method for identifying quorum quenching bacteria. *Sci. Rep.* 3, 1–9. doi: 10.1038/srep02935

Watanabe, E., Wachi, M., Yamasaki, M., and Nagai, K. (1992). ATPase activity of SopA, a protein essential for active partitioning of F plasmid. *Mol. Gen. Genet.* 234, 346–352. doi: 10.1007/BF00538693

Winkler, W. C., and Breaker, R. R. (2005). Regulation of bacterial gene expression by riboswitches. *Annu. Rev. Microbiol.* 59, 487–517. doi: 10.1146/annurev.micro.59.030804.121336

Yu, C., McClure, R., Nudel, K., Daou, N., and Genco, C. A. (2016). Characterization of the *Neisseria gonorrhoeae* iron and Fur regulatory network. *J. Bacteriol.* 198, 2180–2191. doi: 10.1128/JB.00166-16

Yuan, J. S., Reed, A., Chen, F., and Stewart, C. N. (2006). Statistical analysis of real-time PCR data. *BMC Bioinform.* 7:85. doi: 10.1186/1471-2105-7-85

Conflict of Interest: The authors declare that the research was conducted in the absence of any commercial or financial relationships that could be construed as a potential conflict of interest.

Publisher's Note: All claims expressed in this article are solely those of the authors and do not necessarily represent those of their affiliated organizations, or those of the publisher, the editors and the reviewers. Any product that may be evaluated in this article, or claim that may be made by its manufacturer, is not guaranteed or endorsed by the publisher.

frontiers in Microbiology

ORIGINAL RESEARCH
published: 11 January 2022
doi: 10.3389/fmicb.2021.781960

Oligomerization of the FliF Domains Suggests a Coordinated Assembly of the Bacterial Flagellum MS Ring

Giuseppina Mariano[1,2†], Raquel Faba-Rodriguez[2†], Soi Bui[1], Weilong Zhao[1], James Ross[3], Svetomir B. Tzokov[2] and Julien R. C. Bergeron[1,2]*

[1]Randall Division of Cell and Molecular Biophysics, King's College London, London, United Kingdom, [2]Department of Molecular Biology and Biotechnology, University of Sheffield, Sheffield, United Kingdom, [3]Department of Biochemistry, University of British Columbia, Vancouver, BC, Canada

The bacterial flagellum is a complex, self-assembling macromolecular machine that powers bacterial motility. It plays diverse roles in bacterial virulence, including aiding in colonization and dissemination during infection. The flagellum consists of a filamentous structure protruding from the cell, and of the basal body, a large assembly that spans the cell envelope. The basal body is comprised of over 20 different proteins forming several concentric ring structures, termed the M- S- L- P- and C-rings, respectively. In particular, the MS rings are formed by a single protein FliF, which consists of two trans-membrane helices anchoring it to the inner membrane and surrounding a large periplasmic domain. Assembly of the MS ring, through oligomerization of FliF, is one of the first steps of basal body assembly. Previous computational analysis had shown that the periplasmic region of FliF consists of three structurally similar domains, termed Ring-Building Motif (RBM)1, RBM2, and RBM3. The structure of the MS-ring has been reported recently, and unexpectedly shown that these three domains adopt different symmetries, with RBM3 having a 34-mer stoichiometry, while RBM2 adopts two distinct positions in the complex, including a 23-mer ring. This observation raises some important question on the assembly of the MS ring, and the formation of this symmetry mismatch within a single protein. In this study, we analyze the oligomerization of the individual RBM domains in isolation, in the *Salmonella enterica* serovar Typhimurium FliF ortholog. We demonstrate that the periplasmic domain of FliF assembles into the MS ring, in the absence of the trans-membrane helices. We also report that the RBM2 and RBM3 domains oligomerize into ring structures, but not RBM1. Intriguingly, we observe that a construct encompassing RBM1 and RBM2 is monomeric, suggesting that RBM1 interacts with RBM2, and inhibits its oligomerization. However, this inhibition is lifted by the addition of RBM3. Collectively, this data suggest a mechanism for the controlled assembly of the MS ring.

Keywords: bacteria, flagellum, *Salmonella*, cryo-EM, structure

OPEN ACCESS

Edited by:
Eric Cascales,
Aix-Marseille Université, France

Reviewed by:
Andreas Diepold,
Max Planck Institute for Terrestrial Microbiology, Germany
Kelly Hughes,
The University of Utah, United States

****Correspondence:***
Julien R. C. Bergeron
julien.bergeron@kcl.ac.uk

†Present address:
Giuseppina Mariano,
Microbes in Health and Disease Theme, Newcastle University Biosciences Institute, Newcastle University, Newcastle upon Tyne, United Kingdom
Raquel Faba-Rodriguez,
Peak Proteins Ltd., Mereside, United Kingdom

Specialty section:
This article was submitted to Microbial Physiology and Metabolism, a section of the journal Frontiers in Microbiology

Received: *23 September 2021*
Accepted: *08 December 2021*
Published: *11 January 2022*

Citation:
Mariano G, Faba-Rodriguez R, Bui S, Zhao W, Ross J, Tzokov SB and Bergeron JRC (2022) Oligomerization of the FliF Domains Suggests a Coordinated Assembly of the Bacterial Flagellum MS Ring. Front. Microbiol. 12:781960. doi: 10.3389/fmicb.2021.781960

INTRODUCTION

The flagellum is a complex macromolecular motor, whose role is to allow swimming motility, through the rotation of a long filament at the bacterium cell surface. The flagellum is employed by many bacteria to swim in liquid environments (Minamino and Imada, 2015), but it also represents an important virulence factor, playing central roles in cell adhesion and invasion, secretion of other virulence factors, and biofilm formation (Duan et al., 2013). The bacterial flagellum can be divided into four major regions: Embedded in the inner membrane, the rotor and stator complexes are responsible for inducing filament rotation, using the proton motor force or sodium gradient (depending on the bacterial species; Berg, 2003; Li et al., 2011). The basal body is the region that spans the cell envelope, and includes consecutive ring-like structures, termed M (membrane)- S (supramembrane)- L (lipopolysaccharide)- P (peptidoglycan)- and C (cytoplasm)-rings; the hook is a bended structure that protrudes from the basal body on the cell surface; and the filament is a long (up to several micrometer) tubular structure of >20,000s copies of a singular protein, the flagellin (Nakamura and Minamino, 2019).

The M- and S-rings are formed by the protein FliF, a ~60 kDa protein, embedded in the cytoplasmic membrane through two trans-membrane helices (**Figure 1A**). It oligomerizes into a circular membrane-spanning complex, forming the fundamental scaffold for flagellar structure and assembly (Minamino et al., 2008). In-between the two transmembrane helices, FliF possesses a large periplasmic region consisting of three globular domains termed Ring-Building Domains (RBM1, RBM2, and RBM3, respectively; **Figure 1A**; Bergeron, 2016). Those RBMs possess a common fold (Spreter et al., 2009), and show structural homology with components of the Type III Secretion System (T3SS) injectisome, and in particular RBM1 and RBM2 have sequence similarity with the T3SS protein SctJ (Yip et al., 2005; Bergeron et al., 2015; Bergeron, 2016). Conversely, RBM3 shows homology to the SpoIIIAG protein (Bergeron, 2016; Zeytuni et al., 2017), a macromolecular complex involved in spore formation.

On the cytosolic side, FliF binds to the protein FliG, part of the C-ring (Kubori et al., 1992; Levenson et al., 2012), *via* its C-terminus. This interaction is necessary for flagellum assembly (Li and Sourjik, 2011; Morimoto et al., 2014). FliG, together with FliM and FliN, form the C-ring, and are responsible for switching of the rotation between clockwise and counterclockwise (Morimoto and Minamino, 2014; Minamino and Imada, 2015).

The assembly of the flagellar motor has been mainly investigated in the model systems *Escherichia coli* and *Salmonella enterica* serovar Typhimurium. In these peritrichously flagellated bacteria, the initial component to form is the MS-ring, followed by the C-, P-, and L-rings. A T3SS-like export apparatus is recruited by interaction with the MS-ring and is responsible for secretion of the single components of the rod, hook, and filament, which are then assembled outside the cytoplasm (Minamino et al., 2008; Minamino and Imada, 2015; Nakamura and Minamino, 2019).

While the MS-ring formation occurs early during flagellar biogenesis, it remains unclear which factors are needed for its recruitment and assembly. In *E. coli,* FliF was not able to efficiently self-oligomerize and assemble at the membrane when expressed at its physiological levels. Instead, it was suggested that the basal body assembly in *E. coli* is a cooperative process where FlhA firstly assembles to the membrane and subsequently recruits FliF through direct interaction, further aided by FliG and both FlhA and FliG (Li and Sourjik, 2011). In contrast, in *S.* Typhimurium it was observed that FliF overexpression led to spontaneous assembly of MS-ring structures (Suzuki et al., 2004; Kawamoto and Namba, 2017; Kawamoto et al., 2020; Johnson et al., 2021) whereas in *Vibrio alginolyticus* the same behavior was not observed (Terashima et al., 2020). Furthermore, co-expression of FlhF and FliG promotes formation of MS-rings in *V. alginolyticus* (Terashima et al., 2020). These findings are in agreement with previous studies where it was highlighted that FlhF and FlhG are involved

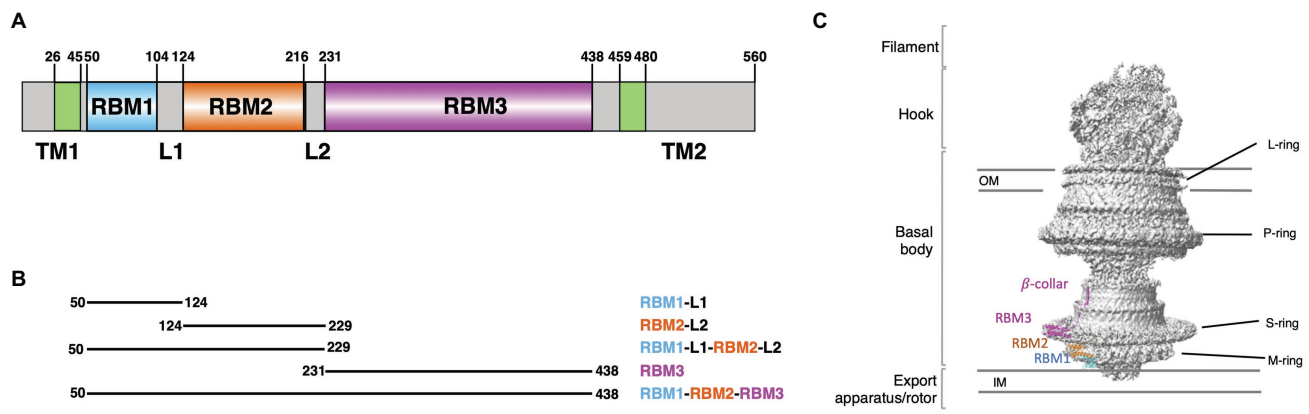

FIGURE 1 | *Salmonella typhimurium* FliF domain organization. **(A)** Schematic representation of the domain composition and their boundaries in FliF. **(B)** Summary of the constructs, encompassing distinct FliF regions, used in this study. **(C)** Structure of FliF (PDB: 6SNC, 7CIK), in cartoon representation, placed in the corresponding region of the bacterial flagellum basal body electron density map.

in regulation of flagellar localization and assembly in species with polar flagella and in some peritrichous species such as *Bacillus subtilis* (Kazmierczak and Hendrixson, 2013). FlhG is a MinD-like ATPase, and interacts with components of the C-ring, FliM, FliN, and FliY (Schuhmacher et al., 2015a,b). Upon interaction with these proteins, FlhG promotes their interaction and assembly with FliG (Schuhmacher et al., 2015a,b). FlhF is a SRP-type GTPase that localizes at the cell pole to positively regulate the localization and formation of the flagellum by recruiting FliF (Green et al., 2009; Terashima et al., 2020), whereas FlhG acts as a negative regulator of flagellar assembly through interaction with FlhF (Kusumoto et al., 2008; Kojima et al., 2020).

The structure of FliF in isolation was recently determined, and revealed that the RBM3 has a symmetry that can vary from C32 to C35, with the majority of particles displaying a C33 symmetry (Johnson et al., 2020). Astonishingly, this study showed that RBM2 forms rings with a 21 or 22-fold symmetry, localized at the inner part of the M-ring (Johnson et al., 2020), revealing a symmetry mismatch between the domains. RBM1 was not resolved in these structures. Subsequently, it was shown that the prevalent symmetry for the basal body is C34 and that the RBM2 adopts preferentially a C23 symmetry at the internal face of the M-ring (Kawamoto et al., 2020). The cryo-EM structure of the intact basal body further confirmed that the RBM3 unambiguously displays a C34 symmetry (Kawamoto et al., 2020; Johnson et al., 2021). Nonetheless, these structures raise the question of how this protein can form an oligomeric assembly with different symmetries in different domains, and how their assembly is coordinated.

Here, we studied the oligomerization of the different FliF domains in isolation. We show that a construct encompassing RBM1, RMB2, and RBM3, but lacking the two trans-membrane helices, is still able to form the proper MS ring assembly, in the *S.* Typhimurium ortholog (but not the *Helicobacter* one). We demonstrate that the RBM2 and RBM3 domains oligomerize in isolation, and form ring-like structures, with symmetry corresponding to that of these domains within the basal body. In contrast, RBM1 in isolation is strictly monomeric. Intriguingly, we also report that a construct encompassing both RBM1 and RBM2 is monomeric, suggesting that within this construct, RBM1 prevents RBM2's oligomerization. Finally, ectopic addition of RBM3 promotes the oligomerization of the RBM1-RBM2 construct, reversing the inhibition of RBM2 oligomerization by RBM1. Taken together, these results suggest that the oligomerization of FliF is coordinated and allows us to propose a model for the regulated formation of the MS ring to the final, correct assembly.

MATERIALS AND METHODS

Protein Expression and Purification

The gene coding for FliF encompassing RBM1, RBM2, and RBM3 ($FliF_{50–438}$) was synthesized (Bio Basic), and cloned into the pET-28a vector, to include with a Thrombin-cleavable N-terminal His_6 tag. Other FliF constructs (see **Figure 1B**) were generated by site-directed mutagenesis, using the aforementioned construct as a template.

For protein over-expression, the corresponding plasmids were transformed into *E. coli* BL21 DE3 cells and grown at 25°C at 160 rpm overnight in ZYM-5052 auto-induction media (1% Tryptone, 0.5% Yeast Extract, 25 mM Na_2HPO_4, 25 mM KH_2PO_4, 50 mM NH_4Cl, 5 mM Na_2SO_4, 2 mM $MgSO_4$, 0.5% glycerol, 0.05% glucose, and 0.2% α-lactose) for 16 h. Following induction, cells were centrifuged at 5,000 × *g* and pellets resuspended in buffer A containing 50 mM Hepes pH 8.0, 500 mM NaCl, and 20 mM imidazole. Cells were lysed by sonication following addition of cOmplete™ EDTA-free protease inhibitor (Sigma) and debris removed by centrifugation at 14,000 × *g* for 45 min. The cleared supernatant was applied onto a 5 ml HisPure™ Ni-NTA resin (Thermo Scientific) gravity-based column equilibrated with 10 column volumes of buffer A. Proteins were eluted with a two step-gradient elution containing 50 and 500 mM imidazole, respectively. Fractions containing purified FliF RBM2 ($FliF_{124–229}$) were further purified by size exclusion chromatography (SEC) using a Superdex 200 10/300 column (GE Healthcare) in a buffer containing 50 mM Hepes pH 9.0 and 500 mM NaCl. Purified FliF RBM1-RBM2 ($FliF_{50–229}$) and RBM3 ($FliF_{231–438}$) were applied to a Superdex 200 10/300 column and to a Superose 6 10/300 column (GE Healthcare), respectively, in a buffer containing 50 mM Hepes pH 8.0 and 500 mM NaCl.

SEC-MALS Analysis

Samples were run through a standard bore, 5 µ 300 Å SEC column (Wyatt), using an infinityII HPLC (Agilent), in buffer containing 20 mM HEPES pH 7.0, 150 mM NaCl, and 1 mM DTT. MALS and DRI data were obtained using the DAWN and Optilab detectors, respectively (Wyatt), and analyzed with the Dynamics software (Wyatt) to determine the molecular mass.

Negative-Stain Grid Preparation and EM Data Acquisition

For negative-stain EM experiments, 5 µl of purified protein, at a concentration of 0.2 mg/ml were applied onto glow-discharged carbon-coated copper grids, and incubated at 20°C for 2 min. The grids were then washed in deionized water, and incubated with 1% Uranyl Formate for 30 s. For the titration experiments, FliF RBM1-RBM2 ($FliF_{50–229}$) and RBM3 ($FliF_{231–438}$) were mixed at 1:1 ratio; and RBM2 ($FliF_{124–229}$) was kept at a constant concentration of 0.2 mg/ml, while RBM1 ($FliF_{50–124}$) was added at different ratios, respectively.

Images were acquired on a Technai T12 Spirit TEM (Thermo Fisher) equipped with an Orius SC-1000 camera (Gatan). For FliF RBM2 ($FliF_{124–229}$) domain, images were acquired at a 49 k magnification with a defocus range of −0.5 to −1.0 µm. For FliF RBM3 ($FliF_{231–438}$) domain, images were acquired at a 30 k magnification with a defocus range of −0.5 to −1.0 µm.

Cryo-EM Grid Preparation, Data Collection, and Data Processing

About 5 µl of protein at a concentration of 10 mg/ml, in 50 mM Hepes (pH 9.0) and 150 mM NaCl, was applied

onto glow-discharged 300 mesh Quantifoil R1.2/1.3 grids. Grids were then blotted for 10 s at 80% humidity, and plunged into liquid ethane, using a Leica EM-GP plunge freezer.

For RBM2 ($FliF_{124–229}$), micrographs were collected on a 300 kV Titan Krios microscope equipped with a Gatan K3 camera. 10,053 movies were recorded with a pixel size of 0.85 Å and an exposure of 1 $e^-/Å^2$/frame for 40–50 frames. For RBM1-RBM2-RBM3 ($FliF_{50–438}$), micrographs were collected on a 200 kV Tecnai Arctica equipped with a Falcon 3 camera. A total of 2,540 movies were collected using a pixel size of 2.03 Å and an exposure of 0.8 $e^-/Å^2$/frame over 50 frames.

Data processing was performed in RELION 3.1 (Scheres, 2020). Motion correction was performed with MotionCor2 (Zheng et al., 2017). CTF parameters were estimated with CTFFIND4 (Rohou and Grigorieff, 2015). For RBM2 ($FliF_{124–229}$), 2,000 micrographs were manually picked and used for training a model for particle picking in crYOLO 1.5 (Wagner et al., 2019). The trained model was then used for automated particle picking for the whole dataset and box files were imported on RELION 3.1 for particle extraction. A total of ~2,000,000 particles were extracted with a 230 pixels box. Extracted particle were subjected to multiple rounds of 2D classification to filter top views that allowed evaluation of symmetry. For RBM1-RBM2-RBM3 ($FliF_{50–438}$), automated picking was instead performed within RELION 3.1, and a total of 129.000 particles were extracted with a box size of 220 pixels.

Sequence Analysis and Model Docking

The co-evolution analysis between RBM1 ($FliF_{50–124}$), and RBM2 ($FliF_{124–229}$) was performed with the RaptorX Complex Contact prediction server (Zeng et al., 2018), using default parameters. To model the interaction between RBM1 ($FliF_{50–124}$), and RBM2 ($FliF_{124–229}$) based on the co-evolution data, we first generated a homology model of the *S.* Typhimurium RBM1, based on the *A. aeolicus* RBM1-RBM2 crystal structure (PDB ID: 7CIK, **Figure 1C**). We then employed the HADDOCK 2.4 server to predict the structure of a complex formed between this homology model and the RBM2 structure (from PDB ID 6SD4), with all the co-evolving residues with a score above 0.4 included as active residues in the interaction. About 200 decoys were modeled, which could be classified in 10 clusters, three of which were very similar, with identical interaction interfaces and RMSD < 4A. These included the lowest-energy model, and combined represented 55 decoys, suggesting that it is likely close to the real complex structure.

RESULTS

Oligomerization of Individual Domains of FliF

Previous studies had shown that when purified in isolation, the *S.* Typhimurium FliF adopted its oligomeric state, including an unusual symmetry mismatch between RBM2 and RBM3 (Johnson et al., 2020; Kawamoto et al., 2020), suggesting a complex folding and assembly pathway for the MS ring. This observation prompted us to investigate if the individual RBMs could oligomerize on their own.

To this end, we engineered a series of constructs that encompassed one or several RBMs (**Figure 1B**; **Table 1**). For each construct, the correspondent protein was purified, and its oligomerization propensity was analyzed by SEC (**Table 1**; **Figure 2A**; **Supplementary Figure S1**).

As shown on **Figure 2A**, a construct encompassing RBM1, RBM2, and RBM3 ($FliF_{50–438}$) forms a high-order oligomer, stable by SEC. Negative-stain EM (ns-EM) analysis revealed that the protein possessed ring-like features (**Figure 2C**), similar to that of the full-length protein. This demonstrates that the TM helices of FliF are dispensable for its oligomeric assembly. These findings are perhaps not surprising, considering that in some bacterial species, the T3SS equivalent of FliF, SctJ, lacks a N-terminal TM helix (Crepin et al., 2005; Yip et al., 2005). Nonetheless, SctJ also possesses a C-terminal palmytoilation site, not present in FliF, and required for membrane localization and assembly.

We however note that the protein is prone to aggregation, with multiple MS rings assembling from the side opposing the collar region, suggesting that some hydrophobic surfaces, possibly facing the membrane, are exposed in the absence of the TM helices. Indeed, SEC-MALS analysis confirmed that FliF from *S.* Typhimurium ($StFliF_{50–438}$) self-oligomerized in a complex with an apparent mass of ~10 MDa (**Supplementary Figure S2A**), significantly larger than the FliF 34-mer. This is consistent with the ns-TEM experiment reported above (**Figure 2C**), which showed that most of the $StFliF_{50–438}$ oligomers were sticking together.

Next, we observed that constructs encompassing RBM2 ($FliF_{124–229}$) or RBM3 ($FliF_{231–438}$) also formed higher-order

TABLE 1 | List of *S.* Typhimurium constructs used in this study, with their corresponding predicted MW, and that calculated by their SEC elution volume.

Domain	Construct boundaries	Monomer MW (KDa)	Oligomeric state of the purified protein	Elution volume (Ve, ml)	Apparent (by SEC) molecular weight (KDa)	Predicted molecular weight (KDa)
RBM1 + L1	50–124	8.13	Monomer	18.90	7.56	8.13
RBM2 + L2	124–229	11.21	Oligomer	9.35	390.15	257.83
RBM1 + L1 + RBM2 + L2	50–229	19.25	Monomer	17.65	11.93	19.25
RBM3	231–438	22.50	Oligomer	8.66	868.80	765.00
RBM1 + RBM2 + RBM3	50–438	41.87	Oligomer	8.27	1046.44	1422.56
Full length	1–560	63.95	-	-	-	-

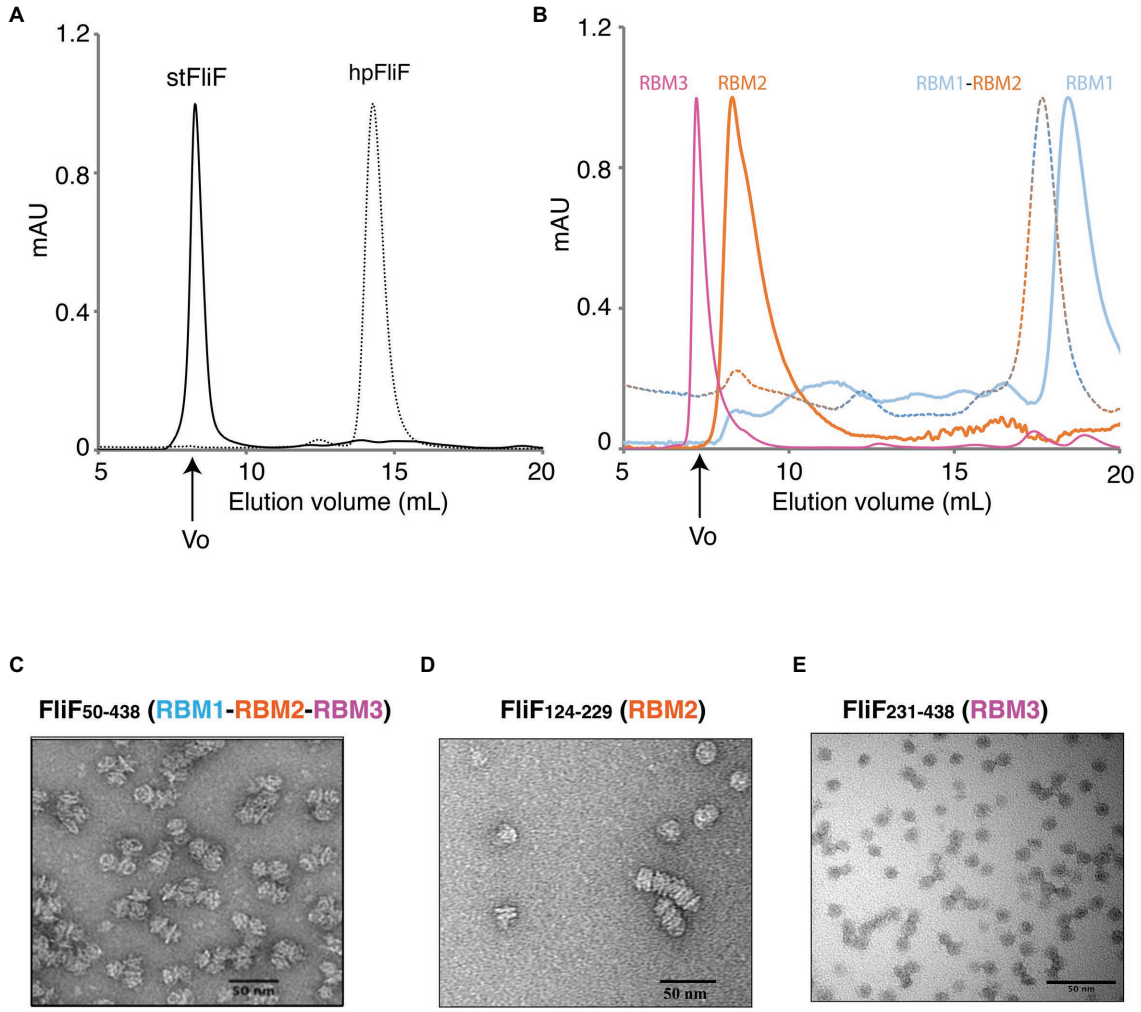

FIGURE 2 | Oligomerization of the FliF domains. **(A)** Size exclusion chromatography (SEC) UV trace of constructs encompassing the entire periplasmic regions of *S.* typhimurium FliF and *Helicobacter pylori* FliF. **(B)** SEC UV trace of constructs encompassing the individual domains of *S. typhimurium* FliF **(C–E)** Negative stain analysis of **(C)** RBM1-RBM2-RBM3 ($FliF_{50–438}$), **(D)** RBM2 ($FliF_{124–229}$), and **(E)** RBM3 ($FliF_{231–438}$). RBM1-RBM2-RBM3 and RBM2 show mostly side views, while RBM3 mainly displays top views.

oligomers in isolation (**Figure 2B**). Negative-stain EM analysis confirmed that they adopted ring-like structures (**Figures 2D,E**), consistent with their architecture within the native MS ring. In the instance of RBM2 ($FliF_{124–229}$), we note that the ring-like structures exhibited a tendency to cluster together, forming lines of disks (**Figure 2D**). It is noteworthy that in the T3SS FliF homolog SctJ, previous biochemical studies have shown that RBM2 is monomeric, and requires the L1 linker to oligomerize in isolation (Bergeron et al., 2015).

In contrast to RBM2 ($FliF_{124–229}$) and RBM3 ($FliF_{231–438}$), we observed that the construct encompassing RBM1 ($FliF_{50–124}$) was strictly monomeric in isolation (**Figure 2B**; **Table 1**). Collectively, these results demonstrate that in *S.* Typhimurium, the TM helices of FliF are dispensable for its oligomeric assembly, and that RBM2 and RBM3, but not RBM1, can form oligomeric rings in isolation.

While we observed that RBM1-RBM2-RBM3 ($FliF_{50–438}$) in *S.* Typhimurium spontaneously oligomerized, previous studies have shown that in other non-peritrichous organisms, such as *V. alginolyticus*, FliF required additional flagellum components, such as FhlF, to efficiently assemble MS-rings (Terashima et al., 2020). For this reason, we investigated the oligomeric state of FliF in another non-peritrichous organism, *Helicobacter pylori*. We observed that *H. pylori* RBM1-RBM2-RBM3 ($HpFliF_{51–427}$) eluted from the gel filtration column much later than $StFliF_{50–438}$, consistent with a monomeric protein (**Figure 2A**). SEC-MALS analysis was used to measure the molecular weight of this purified protein (**Supplementary Figure S2B**), which was measured to be ~41 kDa, very close to the predicted molecular weight of a single monomer (42 kDa). This result suggests that in *H. pylori*, FliF requires additional factors to trigger oligomerization, as also reported in other non-peritrichous organisms (Dasgupta et al., 2003; Hendrixson and DiRita, 2003).

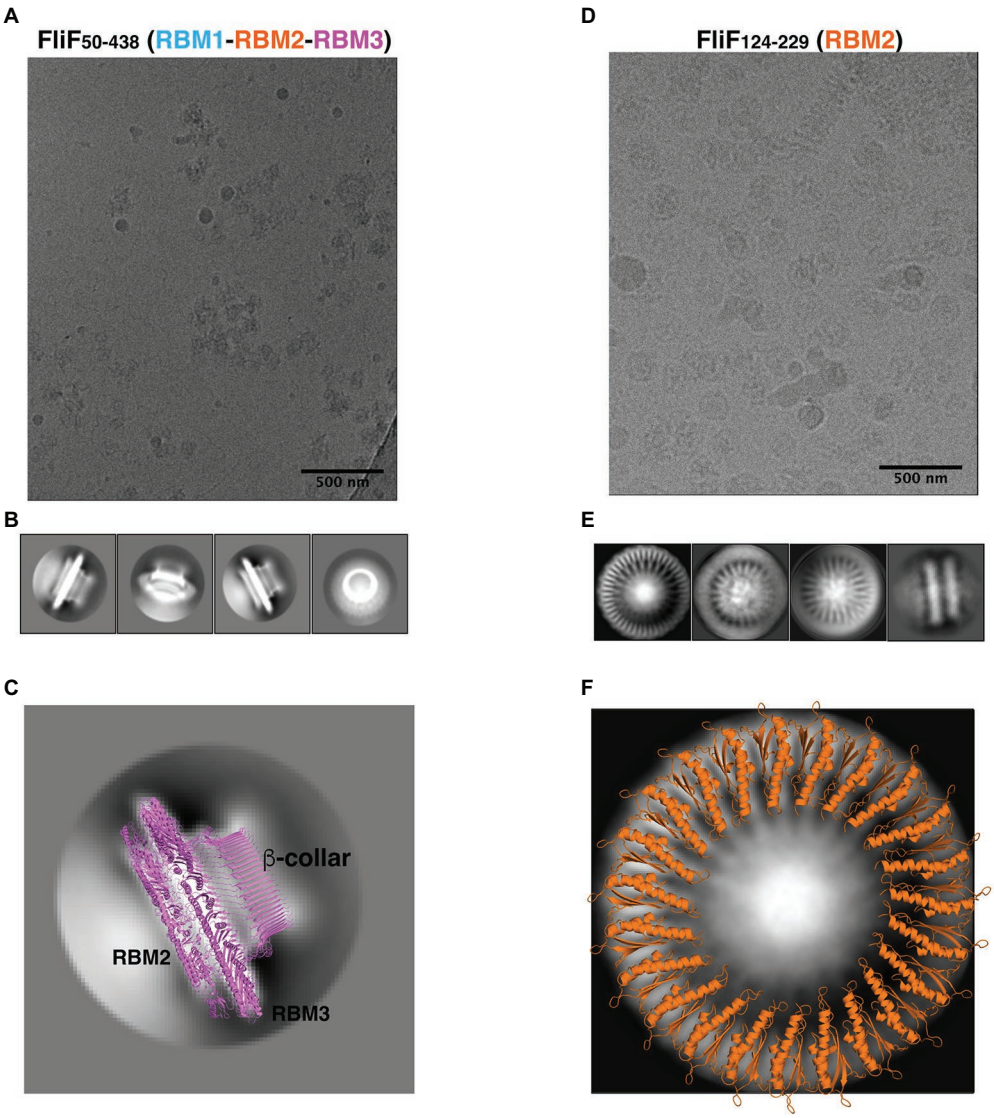

FIGURE 3 | FliF RBM2 and RBM3 stoichiometry. **(A)** Cryo-electron micrograph and **(B)** selected 2D classes of RBM1-RBM2-RBM3 ($FliF_{50–438}$). **(C)** A 2D class from a side view of RBM1-RBM2-RBM3 is shown, overlayed to a cartoon representation of the 33-mer FliF structure (PDBID: 6SD1). The majority of particles is side view, and matches the architecture of intact FliF. **(D)** Cryo-electron micrograph, and **(E)** selected 2D classes of RBM2 ($FliF_{124–229}$). Particles show top views and some filaments that consist of aggregation of single RBM2 disks. **(F)** A 2D class of a RBM2 top view is shown, overlayed to a cartoon model of the 23-mer RBM2 inner ring structure (from PDBID: 7BK0).

Cryo-EM Analysis of the FliF RBM2 and RBM3

The structures of FliF revealed a range of stoichiometries, from 32 to 34 for RBM3, and 21 or 22 for RBM2, with an extra 11–12 RBM2 domains in a distinct orientation relative to RBM3, and facing outward (Johnson et al., 2020). Subsequent structures of this protein in the intact basal body demonstrated that the true stoichiometries are 34 and 23, respectively (Kawamoto et al., 2020; Johnson et al., 2021). This prompted us to use cryo-EM to characterize the oligomeric constructs described above, to confirm that they match the structure of the native FliF oligomer, and determine the stoichiometry of the individual domains.

As shown on **Figure 3A**, the FliF construct encompassing RBM1, RBM2, and RBM3 ($FliF_{50–438}$) was readily incorporated into ice, which allowed us to collect a cryo-EM dataset. Because of the high level of aggregation (see above), we picked particles from this data manually, and used these to generate 2D classes (**Figure 3B**). These 2D classes are highly similar to that of the MS ring in isolation, with density for RBM2, RBM3, and the **β**-collar clearly visible (**Figure 3C**). Diffuse density below RBM2 is also visible, and was also seen in previously-reported 2D classes of the full MS ring, corresponding to density for dynamic RBM1 domains.

While most particles were attributed to 2D classes corresponding to side-views of the complex, a subset (~10%)

corresponded to top views (**Figure 3B**, far right). Notably, in this class, we were able to clearly identify a 33-fold symmetry (**Supplementary Figure S3A**). This is in agreement with the structure of FliF in isolation, reported previously (Johnson et al., 2020), where RBM3 adopts a 33-mer stoichiometry in the majority of particles. Further work will be required to determine if our construct also adopts a range of stoichiometries.

Next, we used cryo-EM to characterize the RBM2 ($FliF_{124–229}$) oligomer. This protein was also readily incorporated into ice (**Figure 3D**), and we were able to collect a cryo-EM dataset. We attempted automated particle picking using a range of tools, but only cryOLO (Wagner et al., 2019) was able to pick both side and top views, in particular as the side views consisted of long aggregation of disks (see above). Using these particles, we generated 2D classes in Relion (Scheres, 2012; **Figure 3E**). These confirmed that this protein had a pathological level of preferred orientation, with most particles visible from the top of the ring, and very few tilted or side views, with the side views clustered together, as seen in negative stain (see above). This precluded high-resolution structure determination but allowed us to exploit the top views to infer the symmetry of the particles.

In the intact FliF structure in isolation, RBM2 forms two rings: one inner ring with 21 subunits, and one outer ring with nine subunits. As shown on **Figure 3F**, we can observe on these 2D classes clear density for the two helices of RBM2, notably with a 23-fold symmetry (**Supplementary Figure S3B**). Additional classification, using a larger top-view dataset would be required if this sample is heterogeneous and includes a range of symmetries, as observed for the intact FliF. Nonetheless, this demonstrates that the oligomers obtained for our RBM2 construct ($FliF_{124–229}$) correspond to the inner ring alone, and does not include the outer ring.

Finally, we note that in the RBM2 ($FliF_{124–229}$) 2D classes, some density is visible in the center of the ring, which cannot be interpreted with the current structures of FliF. We propose that this density likely corresponds to some undetermined chemical that was co-purified with the protein. Further work will be necessary to determine the nature of this additional density.

Collectively, these observations confirm that the FliF transmembrane helices are not required for it to adopt its native MS-ring architecture. In addition, we show that both the RBM2 and RBM3 of FliF adopt their native oligomeric conformation in isolation.

RBM1 Prevents the Oligomerization of RBM2, and This Effect Is Counteracted by RBM3

Previous work on the T3SS FliF homologue SctJ had shown that RBM2 self-oligomerizes, similarly to FliF, but that this oligomerization is repressed in the presence of RBM1 (Bergeron et al., 2015, 2018). We therefore sought to verify if the RBM1 of FliF played a similar role. To that end, we engineered a FliF construct that encompassed both RBM1 and RBM2 ($FliF_{50–229}$). As shown on **Figure 2A**, SEC analysis demonstrated that the resulting protein was strictly monomeric (**Figure 1B**; **Table 1**). This suggests that RBM1 prevents RBM2 from oligomerizing on its own.

In order to determine how RBM1 could inhibit RBM2 domains to oligomerize, we first performed co-evolution analysis to determine amino-acid residues that were potentially involved into the interaction between RBM1 and RBM2, using RaptorX Complex Contact prediction server (Zeng et al., 2018). As shown in **Supplementary Figure S4A**, several regions of the protein, largely corresponding to the β-strands, showed significant co-evolution scores. Next, we employed the HADDOCK docking server to model the interaction between the two domains, using these residues as restraints in the docking process. This led to a cluster of models with low energy score, where the two domains had their β-sheet facing each other (**Supplementary Figure S4B**), in agreement with the co-evolution analysis. Furthermore, overlay of this model onto the RBM2 23-mer structure had RBM1 in the position of an adjacent RBM2 molecule (**Supplementary Figure S4C**), providing a potential explanation of how the intramolecular contacts between RBM1 and RBM2 sterically obstruct the RBM2 oligomerization. This is consistent with our observation that the RBM2 oligomerization is inhibited by RBM1.

This effect mentioned above was observed in the context on a RBM1-RBM2 construct. This led to the question of whether the addition of ectopic RBM1 ($FliF_{50–124}$) onto assembled RBM2 ($FliF_{124–229}$) rings promoted their dissociation. To verify this, we titrated purified RBM1 ($FliF_{50–124}$) against oligomeric RBM2 ($FliF_{124–229}$) and used ns-EM to investigate if the ectopic addition of RBM1 disrupted the RBM2 oligomers (see above). As shown on **Supplementary Figure S5**, we observed no changes in the architecture or density of the RBM2 oligomers, even in large excess of RBM1. This observation demonstrates that once the RBM2 ring is formed, it can no longer be disrupted by RBM1, and suggests that in the context of the RBM1-RBM2 ($FliF_{50–229}$) construct, RBM1 prevents RBM2 oligomerization by binding to the ring oligomerization interface.

Given that RBM1-RBM2 ($FliF_{50–229}$) was shown to be strictly monomeric, while RBM1-RBM2-RBM3 ($FliF_{50–438}$) assembled into the MS ring (**Figure 2**; **Table 1**), we further investigated whether addition to RBM3 ($FliF_{231–438}$) would prompt RBM1-RBM2 ($FliF_{50–229}$) to oligomerize. To this end, purified RBM1-RBM2 ($FliF_{50–229}$) and RBM3 ($FliF_{231–438}$) were mixed (**Figure 4A**), and ns-EM was employed to test the formation of the intact MS ring. Surprisingly, while we observed presence of ring-like structures formed by RBM3 ($FliF_{231–438}$) alone, we also observed the presence of long tubular structures (**Figure 4B**). These are distinct in appearance from the lines of disks observed for our RBM2 construct (see **Figure 2C**), but also to the RBM1-RBM2-RBM3 oligomers (See **Figure 2B**). These tubular structures are reminiscent in the supercoil arrangement observed in the crystal structure of the *E. coli* SctJ orthologue (Yip et al., 2005). Indeed, projection of the crystallographic symmetry-generated SctJ supercoiled structure looked strikingly similar to the tubular structures we observed for our RBM1-RBM2 construct in the presence of RBM3 added ectopically (**Figure 4B**; **Supplementary Figure S6**). We therefore propose that these tubular structures correspond to RBM1-RBM2 oligomers, in a supercoiled arrangement, and are likely capped by RBM3. This interpretation would however require to be experimentally

verified. Nonetheless, this observation suggests that while RBM1-RBM2 exists as a monomer, addition of RBM3 is the determinant factor that pushes toward assembly of FliF into an oligomeric state.

Collectively, these results suggest an intricate set of interactions between the different FliF domains; with RBM1 binding to RBM2 to prevent its oligomerization, and RBM3 acting to prevent this interaction.

DISCUSSION

The MS-ring assembly is one of the first steps that occur during biogenesis of the flagellum (Minamino et al., 2008). The MS-ring then functions as a scaffold to recruit the C-ring through the interaction of FliF with FliG (Li and Sourjik, 2011; Morimoto et al., 2014) and the export apparatus (Minamino et al., 2008; Minamino and Imada, 2015; Nakamura and Minamino, 2019). Despite this central role in flagellum assembly, the process and regulation underlying the MS-ring folding remain unknown. A deeper understanding of the FliF folding process has become increasingly important in light of the recent structural studies that have reported the existence of distinct symmetries within the MS-ring, which could serve multiple functions (Johnson et al., 2020, 2021; Kawamoto et al., 2020; Takekawa et al., 2021).

Indeed recent structural analyses have highlighted that the MS-ring symmetry can adopt a range of oligomeric states, with a mismatched symmetry between RBM2 and RBM3 (Johnson et al., 2020). While initially this suggested that RBM3 adopted a range of stoichiometries that range from 32 to 34 subunits, and that RBM2 formed either 21 or 22-mer (Johnson et al., 2020), in subsequent studies it was consistently observed that RBM3 was a 34-mer and RBM2 was a 23-mer (Kawamoto et al., 2020; Johnson et al., 2021). The symmetry mismatch between RBM2 and RBM3, together with the different symmetries detected in the existing studies suggests the existence of a complex process that regulates the folding and biogenesis of the MS-ring. In this study, we aimed to determine the mechanism underlining the complex folding of FliF, by analyzing the oligomeric state of the different domains of FliF.

Here, we show that in a construct encompassing FliF RBM1, RBM2, and RBM3 is able to assemble to form MS-rings, wherein RBM3 displays a 33-mer stoichiometry. Additionally, our data reveal that RBM2 is able to form rings with a 23-mer stoichiometry. These correspond to the main stoichiometry observed for FliF in isolation. Conversely, we observe that a construct encompassing RBM1-RBM2-RBM3 ($HpFliF_{51–427}$) from *H. pylori* yields a monomeric protein. These findings show similarities with what was observed for FliF in *V. alginolyticus*, where its proper oligomerization required additional factors and suggest the existence of a different regulation of the MS-ring assembly for non-peritrichous organisms (Terashima et al., 2020).

Indeed, our data demonstrate that a construct encompassing RBM1 and RBM2 is monomeric, contrary to a construct encompassing RBM2 only. Since the addition of RBM1 to already formed RBM2 rings does not show any changes, we propose

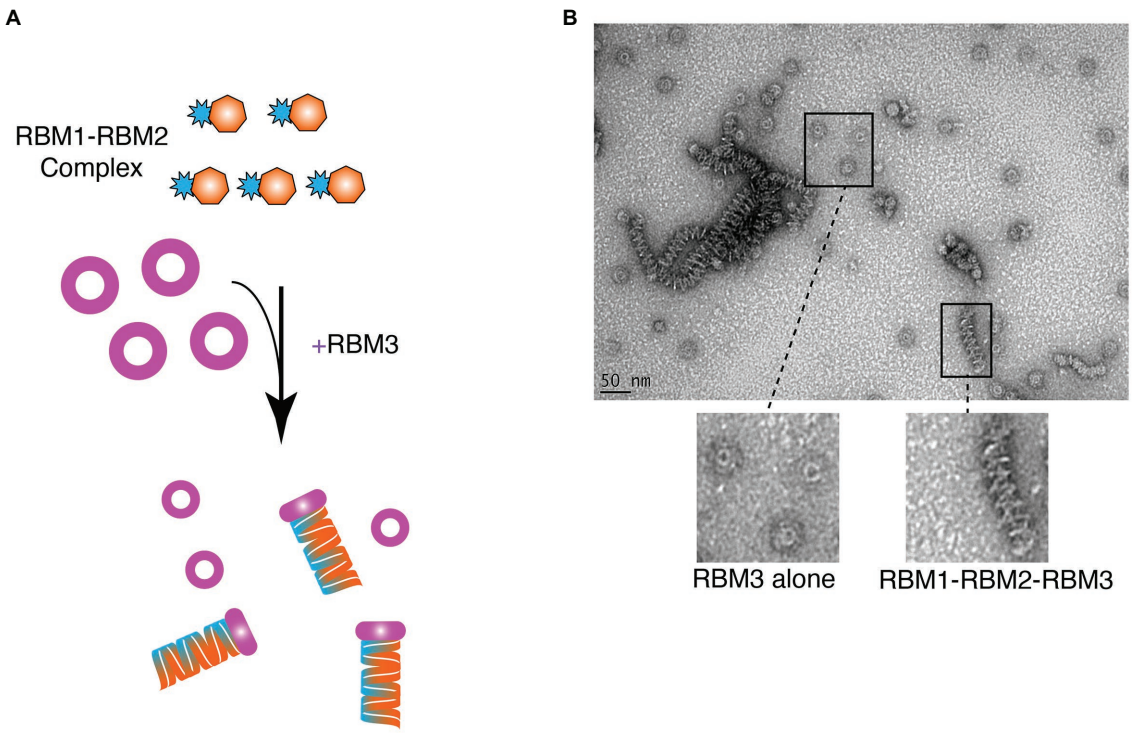

FIGURE 4 | Ring-Building Motif (RBM)3 induces oligomerization of the RBM1-RBM2 construct. **(A)** Schematic representation of the experiment. RBM1-RBM2 ($FliF_{50–229}$) was mixed with RBM3 ($FliF_{231–438}$) oligomers and imaged by negative stain EM. **(B)** Negative stain electron micrograph of the RBM3 and RBM1-RBM2 mixture. Ring-like structures, representative ofRBM3alone, are visible, as well as tubular structures that are likely composed of stacks RBM1-RBM2-RBM3 rings.

that RBM1 prevents the RMB2 oligomerization by binding to, and thus occluding, its oligomerization interface. Additionally, we also show that addition of RBM3 to monomeric RBM1-RBM2 causes formation of tubular structures, which we attribute to RBM1-RBM2 adopting a superhelical fold, similarly to SctJ (Yip et al., 2005), possibly capped by RBM3. This in turn suggests that RBM3 interacts with the RBM1-RBM2 construct in a way that dislodges RBM1 and allows RBM2 to oligomerize.

Based on this, we propose the following mechanism for MS ring assembly: Upon membrane insertion by the SEC pathway, FliF is a monomer; the interaction between RBM1 and the oligomerization interface on RBM2 retains FliF in a monomeric state (**Figure 5A**). Next, while RBM1 still prevents RBM2 molecules from associating, RBM3 oligomerization initiates (**Figure 5B**), imposing an overall 34-mer stoichiometry to the complex. Assembled RBM3 rings can subsequently disrupt RBM1 from RBM2 oligomerization interface, and RBM2 rings start forming (**Figure 5C**). These form 23-mer rings, but because the overall stoichiometry is imposed by the initial RBM3 oligomerization, 11 RBM2 domains are left on the outside. Therefore, we propose that the role of RBM1-mediated inhibition of RBM2 oligomerization in the FliF assembly process allows RBM3 rings to form and drive the MS-ring biogenesis process, determining the right stoichiometry for all the sub-assemblies. This leads to the formation of the intact MS-ring, with its symmetry mismatch between RBM2 and RBM3 (**Figure 5D**).

The concept that the three periplasmic domains RBM1-RBM2-RBM3 of FliF provide regulation of its oligomerization, thus guaranteeing the right stoichiometry of the MS-ring and the consequent correct assembly of the basal body, is not foreign. Indeed a similar regulation has been proposed in the evolutionarily-related T3SS secretion apparatus (Yip et al., 2005; Bergeron et al., 2015, 2018; Bergeron, 2016). There, the model suggests that the SctJ linker between RBM1 and RBM2 interacts with

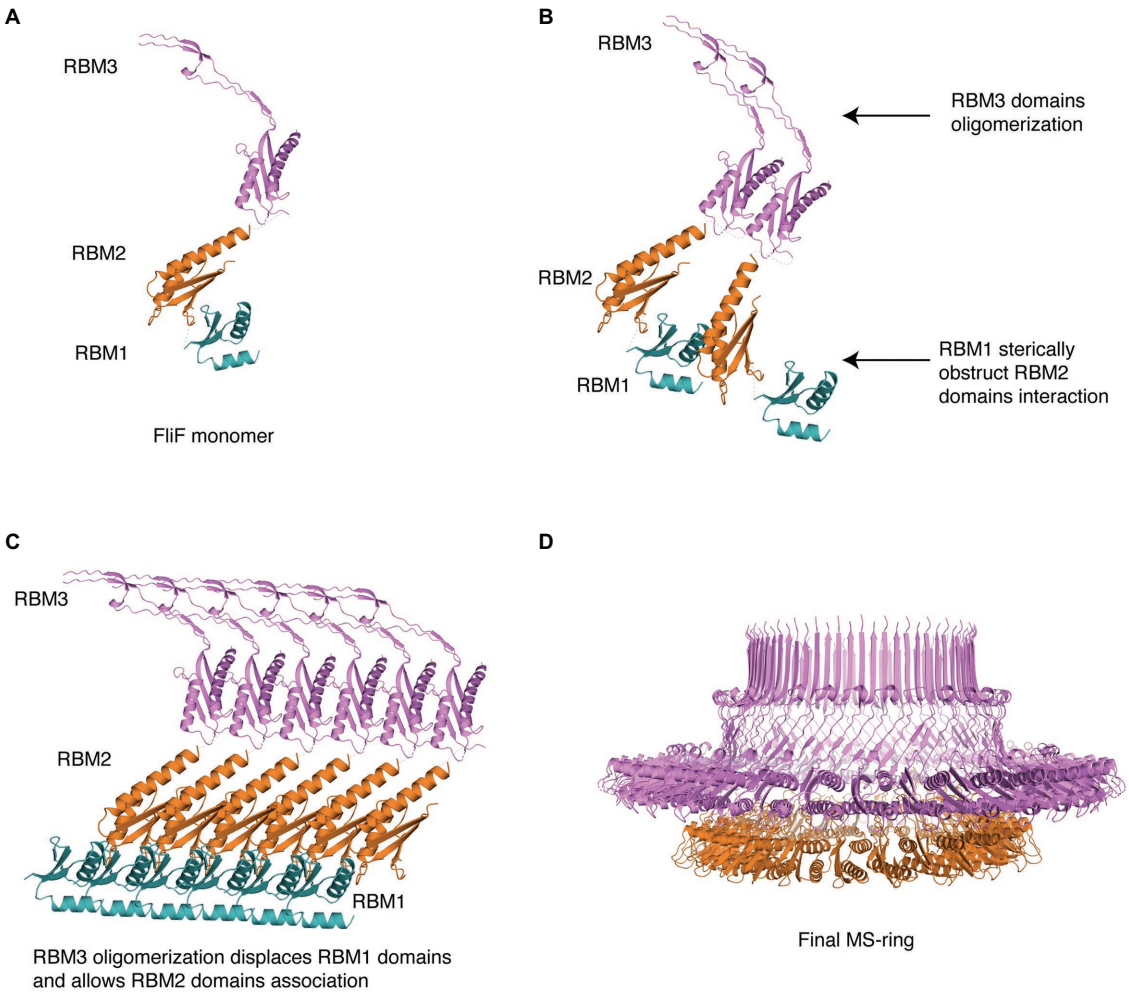

FIGURE 5 | Structural representation of the proposed MS-ring assembly process. Cartoon representations of each domain, colored as in **Figure 1**, are used. **(A)** As it gets exported to the membrane *via* the Sec pathway, FliF is monomeric, **(B)** The presence of adjacent FliF molecules allows RBM3 to drive the oligomerization process, establishing the 34-mer stoichiometry. The contacts between RBM1 and RBM2 prevent RBM2 to oligomerize. **(C)** At completion of RBM3 oligomerization, RBM1 is displaced from RBM2, allowing RBM2 domains from different FliF molecules to come into contact and assemble, forming a 23-mer. The remaining 11 RBM2 domains sit outside this ring. **(D)** In the final stage, the MS-ring reaches the final correct conformation, with asymmetry mismatch between RBM2 and RBM3.

RBM1 with hydrophobic interaction, keeping SctJ in a monomeric state (Bergeron et al., 2015, 2018). Upon dissociation of the linker region from RBM1, SctJ subunits can associate, and establish a series of interactions between their respective RBM1-RBM2 domains, as well as with the linker region (Bergeron et al., 2015, 2018). SctD molecules subsequently insert between two adjacent SctJ subunits, and SctJ-SctD heterodimers can finally oligomerize to form the finalized rings (Bergeron et al., 2015, 2018). Our data show that while in FliF, RBM1 and RBM3 can provide regulation of RBM2 oligomerization; it appears that the process is opposite to what observed in SctJ.

The functional implication for this difference is not known; however, it is tempting to speculate that it might be related to a regulatory process, to fine-tune the assembly and/or disassembly of these complexes. Notably, most T3SS complexes are required only in the context of an interaction with target cell membranes, and it is therefore likely to have a disassembly pathway (although this has not been observed directly). In contrast, the bacterial flagellum plays multiple roles in the bacterial cell, beyond motility, including cellular localization, and regulation of cell division (Chaban et al., 2015). Therefore it is likely a much more stable complex, with the basal body constantly anchored at the cell pole in many (but probably not all) bacterial species. The difference observed between the T3SS and flagellar inner-membrane components could reflect these distinct properties. Further investigation, combining biochemical characterization and *in vivo* assays, in both systems and in a range of bacterial species, would be required to decipher this.

It is worth to note that for SctJ the regulation role was pin-pointed to the linker region, and notably to a conserved phenylalanine residue, necessary for RBM2 oligomerization, and controlled by the isomerization of a proline residue. In this study, the FliF RBM2 construct we used does not encompass the linker between RBM1 and RBM2, and thus, it appears that this linker does not play a critical role in FliF oligomerization. In addition, the aforementioned Phe or Pro residues are not conserved in the corresponding region of FliF (Bergeron, 2016; Bergeron et al., 2018), further supporting the distinction between FliF and SctJ.

The biogenesis of the flagellum is a hierarchical process that initiated with the insertion of the Type III export apparatus and the assembly of the MS-ring. The remaining flagellar components are then secreted through the export apparatus to build up the final flagellar structure (Yonekura et al., 2002; Macnab, 2003). The levels of regulation of this process are complex, relying on the hierarchical and timely transcription of the distinct components of the flagellum, which are transcribed in different groups according to their role in the flagellar structure (Kutsukake et al., 1990; Dasgupta et al., 2003). In a similar fashion, it is possible to speculate that RBM1 and RBM3-mediated control over the oligomerization and assembly of the MS-ring will provide an additional level of complexity to the flagellum biogenesis.

Several studies have shown that the regulation process involves different factors between peritrichous and polar flagella. Namely, FlhF and FlhG are not present in *E. coli* and *S.* Typhimurium but are necessary for flagellar synthesis and localization in a number of species (Pandza et al., 2000; Hendrixson and DiRita, 2003; Niehus et al., 2004; Kusumoto et al., 2008; Schuhmacher et al., 2015a). Interestingly, FlhF and FlhG were found to antagonistically influence the levels of expression of the distinct groups of genes involved in flagellum synthesis (Dasgupta et al., 2003; Hendrixson and DiRita, 2003). It is also noteworthy that in some species carrying FlhF and FlhG, FliF was found to remain in a monomeric state *in vitro* and oligomerization occurred only in presence of FlhF and FliG (Terashima et al., 2020). In this study, we reported that FliF in *H. pylori* exists in a monomeric state *in vitro.* In other non-peritrichous organisms, such as *V. alginolyticus,* FliF requires additional factors to efficiently form MS-rings structures (Terashima et al., 2020). Given the non-peritrichous nature of the flagella of these two organisms, it is possible to speculate that in *H. pylori* FliF may also require FlhF or other additional factors to trigger its oligomerization, suggesting distinct assembly models between peritrichous and mono/amphitrichous bacteria, which will require further investigation.

Conversely, in *S.* Typhimurium, it has been shown that FliF can oligomerize spontaneously (Minamino et al., 2008; Johnson et al., 2020). Nevertheless, distinct regulation strategies were also found between peritrichous flagella. Indeed, FhlA was shown to firstly assemble at the membrane of *E. coli* and to be pivotal for FliF recruitment (Li and Sourjik, 2011).

These observations underline that different, multi-faceted mechanisms of regulations exist for correct assembly of the flagellar machinery between species and that control of FliF oligomerization in *S.* Typhimurium, provided by FliF own domains, adds a new level of complexity to the modulation of the flagellum biogenesis.

Ultimately, characterization of the differences in the assembly of the flagellum between species will provide a better understanding of the molecular elements that determine regulation of the flagellum.

DATA AVAILABILITY STATEMENT

The original contributions presented in the study are included in the article/**Supplementary Material**, further inquiries can be directed to the corresponding author.

AUTHOR CONTRIBUTIONS

RF-R and JR cloned the various constructs. GM, RF-R, SB, WZ, and JR purified the proteins. GM and RF-R performed the negative-stain EM and cryo-EM analyses, and processed the cryo-EM data, with help from SBT. JRCB conceptualized the project. GM and JRCB wrote the manuscript, with contributions from all authors. All authors contributed to the article and approved the submitted version.

FUNDING

This work was funded by a UBC Centre for Blood Research Post-doctoral transition award, and by a United Kingdom Biotechnology and Biological Sciences Research Council (BBSRC) grant (BB/R009759/2), both to JRCB. Cryo-EM data were collected at the UK national Electron Bio-Imaging center (eBIC),

proposal EM19709-1, and at the University of Sheffield FoS Electron Microscopy Facility.

ACKNOWLEDGMENTS

We are grateful to Natalie Strynadka for use of her laboratory at the initial stage of the project, and to Susan Lea, Emily Furlong, and Steven Johnson for useful discussion on the FliF symmetry. We thank John Hall (Wyatt) for assistance with the SEC-MALS data collection and analysis.

SUPPLEMENTARY MATERIAL

The Supplementary Material for this article can be found online at: https://www.frontiersin.org/articles/10.3389/fmicb.2021.781960/full#supplementary-material

REFERENCES

Berg, H. C. (2003). The rotary motor of bacterial flagella. *Annu. Rev. Biochem.* 72, 19–54. doi: 10.1146/annurev.biochem.72.121801.161737

Bergeron, J. R. C. (2016). Structural modeling of the flagellum MS ring protein FliF reveals similarities to the type III secretion system and sporulation complex. *PeerJ* 4:e1718. doi: 10.7717/peerj.1718

Bergeron, J. R. C., Brockerman, J. A., Vuckovic, M., Deng, W., Okon, M., Finlay, B. B., et al. (2018). Characterization of the two conformations adopted by the T3SS inner-membrane protein PrgK. *Protein Sci.* 27, 1680–1691. doi: 10.1002/pro.3447

Bergeron, J. R. C., Worrall, L. J., De, S., Sgourakis, N. G., Cheung, A. H., Lameignere, E., et al. (2015). The modular structure of the inner-membrane ring component PrgK facilitates assembly of the type III secretion system basal body. *Structure* 23, 161–172. doi: 10.1016/j.str.2014.10.021

Chaban, B., Hughes, H. V., and Beeby, M. (2015). The flagellum in bacterial pathogens: for motility and a whole lot more. *Semin. Cell Dev. Biol.* 46, 91–103. doi: 10.1016/j.semcdb.2015.10.032

Crepin, V. F., Prasannan, S., Shaw, R. K., Wilson, R. K., Creasey, E., Abe, C. M., et al. (2005). Structural and functional studies of the enteropathogenic Escherichia coli type III needle complex protein EscJ. *Mol. Microbiol.* 55, 1658–1670. doi: 10.1111/j.1365-2958.2005.04508.x

Dasgupta, N., Wolfgang, M. C., Goodman, A. L., Arora, S. K., Jyot, J., Lory, S., et al. (2003). A four-tiered transcriptional regulatory circuit controls flagellar biogenesis in *Pseudomonas aeruginosa*. *Mol. Microbiol.* 50, 809–824. doi: 10.1046/j.1365-2958.2003.03740.x

Duan, Q., Zhou, M., Zhu, L., and Zhu, G. (2013). Flagella and bacterial pathogenicity. *J. Basic Microbiol.* 53, 1–8. doi: 10.1002/jobm.201100335

Green, J. C. D., Kahramanoglou, C., Rahman, A., Pender, A. M. C., Charbonnel, N., and Fraser, G. M. (2009). Recruitment of the earliest component of the bacterial flagellum to the old cell division pole by a membrane-associated signal recognition particle family GTP-binding protein. *J. Mol. Biol.* 391, 679–690. doi: 10.1016/j.jmb.2009.05.075

Hendrixson, D. R., and DiRita, V. J. (2003). Transcription of sigma54-dependent but not sigma28-dependent flagellar genes in *Campylobacter jejuni* is associated with formation of the flagellar secretory apparatus. *Mol. Microbiol.* 50, 687–702. doi: 10.1046/j.1365-2958.2003.03731.x

Johnson, S., Fong, Y. H., Deme, J. C., Furlong, E. J., Kuhlen, L., and Lea, S. M. (2020). Symmetry mismatch in the MS-ring of the bacterial flagellar rotor explains the structural coordination of secretion and rotation. *Nat. Microbiol.* 5, 966–975. doi: 10.1038/s41564-020-0703-3

Johnson, S., Furlong, E. J., Deme, J. C., Nord, A. L., Caesar, J. J. E., Chevance, F. F. V., et al. (2021). Molecular structure of the intact bacterial flagellar basal body. *Nat. Microbiol.* 6, 712–721. doi: 10.1038/s41564-021-00895-y

Kawamoto, A., Miyata, T., Makino, F., Kinoshita, M., Minamino, T., Imada, K., et al. (2020). Native structure of flagellar MS ring is formed by 34 subunits with 23-fold and 11-fold subsymmetries. bioRxiv [Preprint]. doi: 10.1101/2020.10.11.334888

Kawamoto, A., and Namba, K. (2017). Structural study of the bacterial flagellar basal body by electron cryomicroscopy and image analysis. *Methods Mol. Biol.* 1593, 119–131. doi: 10.1007/978-1-4939-6927-2_9

Kazmierczak, B. I., and Hendrixson, D. R. (2013). Spatial and numerical regulation of flagellar biosynthesis in polarly flagellated bacteria. *Mol. Microbiol.* 88, 655–663. doi: 10.1111/mmi.12221

Kojima, S., Terashima, H., and Homma, M. (2020). Regulation of the single polar flagellar biogenesis. *Biomol. Ther.* 10:533. doi: 10.3390/biom10040533

Kubori, T., Shimamoto, N., Yamaguchi, S., Namba, K., and Aizawa, S. (1992). Morphological pathway of flagellar assembly in *Salmonella* typhimurium. *J. Mol. Biol.* 226, 433–446. doi: 10.1016/0022-2836(92)90958-m

Kusumoto, A., Shinohara, A., Terashima, H., Kojima, S., Yakushi, T., and Homma, M. (2008). Collaboration of FlhF and FlhG to regulate polar-flagella number and localization in *Vibrio alginolyticus*. *Microbiology* 154, 1390–1399. doi: 10.1099/mic.0.2007/012641-0

Kutsukake, K., Ohya, Y., and Iino, T. (1990). Transcriptional analysis of the flagellar regulon of *Salmonella typhimurium*. *J. Bacteriol.* 172, 741–747. doi: 10.1128/jb.172.2.741-747.1990

Levenson, R., Zhou, H., and Dahlquist, F. W. (2012). Structural insights into the interaction between the bacterial flagellar motor proteins FliF and FliG. *Biochemistry* 51, 5052–5060. doi: 10.1021/bi3004582

Li, N., Kojima, S., and Homma, M. (2011). Sodium-driven motor of the polar flagellum in marine bacteria vibrio. *Genes Cells* 16, 985–999. doi: 10.1111/j.1365-2443.2011.01545.x

Li, H., and Sourjik, V. (2011). Assembly and stability of flagellar motor in *Escherichia coli*. *Mol. Microbiol.* 80, 886–899. doi: 10.1111/j.1365-2958.2011.07557.x

Macnab, R. M. (2003). How bacteria assemble flagella. *Annu. Rev. Microbiol.* 57, 77–100. doi: 10.1146/annurev.micro.57.030502.090832

Minamino, T., and Imada, K. (2015). The bacterial flagellar motor and its structural diversity. *Trends Microbiol.* 23, 267–274. doi: 10.1016/j.tim.2014.12.011

Minamino, T., Imada, K., and Namba, K. (2008). Molecular motors of the bacterial flagella. *Curr. Opin. Struct. Biol.* 18, 693–701. doi: 10.1016/j.sbi.2008.09.006

Morimoto, Y. V., Ito, M., Hiraoka, K. D., Che, Y.-S., Bai, F., Kami-Ike, N., et al. (2014). Assembly and stoichiometry of FliF and FlhA in *Salmonella* flagellar basal body. *Mol. Microbiol.* 91, 1214–1226. doi: 10.1111/mmi.12529

Morimoto, Y. V., and Minamino, T. (2014). Structure and function of the bi-directional bacterial flagellar motor. *Biomol. Ther.* 4, 217–234. doi: 10.3390/biom4010217

Nakamura, S., and Minamino, T. (2019). Flagella-driven motility of bacteria. *Biomol. Ther.* 9:279. doi: 10.3390/biom9070279

Niehus, E., Gressmann, H., Ye, F., Schlapbach, R., Dehio, M., Dehio, C., et al. (2004). Genome-wide analysis of transcriptional hierarchy and feedback regulation in the flagellar system of *Helicobacter pylori*. *Mol. Microbiol.* 52, 947–961. doi: 10.1111/j.1365-2958.2004.04006.x

Pandza, S., Baetens, M., Park, C. H., Au, T., Keyhan, M., and Matin, A. (2000). The G-protein FlhF has a role in polar flagellar placement and general stress response induction in *Pseudomonas putida*. *Mol. Microbiol.* 36, 414–423. doi: 10.1046/j.1365-2958.2000.01859.x

Rohou, A., and Grigorieff, N. (2015). CTFFIND4: fast and accurate defocus estimation from electron micrographs. *J. Struct. Biol.* 192, 216–221. doi: 10.1016/j.jsb.2015.08.008

Scheres, S. H. W. (2012). RELION: implementation of a Bayesian approach to cryo-EM structure determination. *J. Struct. Biol.* 180, 519–530. doi: 10.1016/j.jsb.2012.09.006

Scheres, S. H. W. (2020). Amyloid structure determination in RELION-3.1. *Acta Crystallogr. Sect. F Struct. Biol. Cryst. Commun.* 76, 94–101. doi: 10.1107/S2059798319016577

Schuhmacher, J. S., Rossmann, F., Dempwolff, F., Knauer, C., Altegoer, F., Steinchen, W., et al. (2015a). MinD-like ATPase FlhG effects location and number of bacterial flagella during C-ring assembly. *Proc. Natl. Acad. Sci. U. S. A.* 112, 3092–3097. doi: 10.1073/pnas.1419388112

Schuhmacher, J. S., Thormann, K. M., and Bange, G. (2015b). How bacteria maintain location and number of flagella? *FEMS Microbiol. Rev.* 39, 812–822. doi: 10.1093/femsre/fuv034

Spreter, T., Yip, C. K., Sanowar, S., André, I., Kimbrough, T. G., Vuckovic, M., et al. (2009). A conserved structural motif mediates formation of the periplasmic rings in the type III secretion system. *Nat. Struct. Mol. Biol.* 16, 468–476. doi: 10.1038/nsmb.1603

Suzuki, H., Yonekura, K., and Namba, K. (2004). Structure of the rotor of the bacterial flagellar motor revealed by electron cryomicroscopy and single-particle image analysis. *J. Mol. Biol.* 337, 105–113. doi: 10.1016/j.jmb.2004.01.034

Takekawa, N., Kawamoto, A., Sakuma, M., Kato, T., Kojima, S., Kinoshita, M., et al. (2021). Two distinct conformations in 34 FliF subunits generate three different symmetries within the flagellar MS-ring. *MBio* 12:e03199-20. doi: 10.1128/mBio.03199-20

Terashima, H., Hirano, K., Inoue, Y., Tokano, T., Kawamoto, A., Kato, T., et al. (2020). Assembly mechanism of a supramolecular MS-ring complex to initiate bacterial flagellar biogenesis in vibrio species. *J. Bacteriol.* 202:e00236-20. doi: 10.1128/JB.00236-20

Wagner, T., Merino, F., Stabrin, M., Moriya, T., Antoni, C., Apelbaum, A., et al. (2019). SPHIRE-crYOLO is a fast and accurate fully automated particle picker for cryo-EM. *Commun. Biol.* 2, 218–213. doi: 10.1038/s42003-019-0437-z

Yip, C. K., Kimbrough, T. G., Felise, H. B., Vuckovic, M., Thomas, N. A., Pfuetzner, R. A., et al. (2005). Structural characterization of the molecular platform for type III secretion system assembly. *Nature* 435, 702–707. doi: 10.1038/nature03554

Yonekura, K., Maki-Yonekura, S., and Namba, K. (2002). Growth mechanism of the bacterial flagellar filament. *Res. Microbiol.* 153, 191–197. doi: 10.1016/s0923-2508(02)01308-6

Zeng, H., Wang, S., Zhou, T., Zhao, F., Li, X., Wu, Q., et al. (2018). ComplexContact: a web server for inter-protein contact prediction using deep learning. *Nucleic Acids Res.* 46, W432–W437. doi: 10.1093/nar/gky420

Zeytuni, N., Hong, C., Flanagan, K. A., Worrall, L. J., Theiltges, K. A., Vuckovic, M., et al. (2017). Near-atomic resolution cryoelectron microscopy structure of the 30-fold homooligomeric SpoIIIAG channel essential to spore formation in *Bacillus subtilis*. *Proc. Natl. Acad. Sci. U. S. A.* 114, E7073–E7081. doi: 10.1073/pnas.1704310114

Zheng, S. Q., Palovcak, E., Armache, J.-P., Verba, K. A., Cheng, Y., and Agard, D. A. (2017). MotionCor2: anisotropic correction of beam-induced motion for improved cryo-electron microscopy. *Nat. Methods* 14, 331–332. doi: 10.1038/nmeth.4193

Conflict of Interest: The authors declare that the research was conducted in the absence of any commercial or financial relationships that could be construed as a potential conflict of interest.

Publisher's Note: All claims expressed in this article are solely those of the authors and do not necessarily represent those of their affiliated organizations, or those of the publisher, the editors and the reviewers. Any product that may be evaluated in this article, or claim that may be made by its manufacturer, is not guaranteed or endorsed by the publisher.

frontiers in Microbiology

ORIGINAL RESEARCH
published: 01 February 2022
doi: 10.3389/fmicb.2021.738818

The Trimeric Autotransporter Adhesin YadA of *Yersinia enterocolitica* Serotype O:9 Binds Glycan Moieties

*Ina Meuskens[1], Juan Leva-Bueno[2], Paul Millner[2], Monika Schütz[3], Sally A. Peyman[4] and Dirk Linke[1]**

[1] Section for Genetics and Evolutionary Biology, Department of Biosciences, University of Oslo, Oslo, Norway, [2] Faculty of Biological Sciences, School of Biomedical Sciences, University of Leeds, Leeds, United Kingdom, [3] Interfakultäres Institut für Mikrobiologie und Infektionsmedizin Tübingen (IMIT), Institut für Medizinische Mikrobiologie und Hygiene, Universität Tübingen, Tübingen, Germany, [4] Molecular and Nanoscale Physics Group, Department of Physics and Astronomy, University of Leeds, Leeds, United Kingdom

Yersinia adhesin A (YadA) is a key virulence factor of *Yersinia enterocolitica* and *Yersinia pseudotuberculosis*. YadA is a trimeric autotransporter adhesin, a class of adhesins that have been shown to enable many Gram-negative pathogens to adhere to/interact with the host extracellular matrix proteins such as collagen, vitronectin, and fibronectin. Here, we show for the first time that YadA of *Yersinia enterocolitica* serotype O:9 not only interacts with proteinaceous surface molecules but can also attach directly to glycan moieties. We show that YadA from *Y. enterocolitica* serotype O:9 does not interact with the vitronectin protein itself but exclusively with its N-linked glycans. We also show that YadA can target other glycan moieties as found in heparin, for example. So far, little is known about specific interactions between bacterial autotransporter adhesins and glycans. This could potentially lead to new antimicrobial treatment strategies, as well as diagnostic applications.

Keywords: trimeric autotransporter adhesin, bacterial adhesion, virulence, extracellular matrix (ECM), adhesion, glycan

OPEN ACCESS

Edited by:
Eric Cascales, Aix-Marseille Université, France

Reviewed by:
Amit Kumar, Laboratory Corporation of America Holdings (LabCorp), United States
Jyl S. Matson, University of Toledo, United States

****Correspondence:***
Dirk Linke
dirk.linke@ibv.uio.no

Specialty section:
This article was submitted to Microbial Physiology and Metabolism, a section of the journal Frontiers in Microbiology

Received: *09 July 2021*
Accepted: *06 December 2021*
Published: *01 February 2022*

Citation:
Meuskens I, Leva-Bueno J, Millner P, Schütz M, Peyman SA and Linke D (2022) The Trimeric Autotransporter Adhesin YadA of Yersinia enterocolitica Serotype O:9 Binds Glycan Moieties. Front. Microbiol. 12:738818. doi: 10.3389/fmicb.2021.738818

INTRODUCTION

Yersinia adhesin A (YadA), a type Vc trimeric autotransporter adhesin of *Yersinia* spp. is crucial for virulence. YadA is encoded on a virulence plasmid, the pYV plasmid. Expression of the YadA gene is temperature controlled, and upon a temperature shift to 37°C, once the bacterium enters the host, the expression of YadA is initiated (Toivanen and Skurnik, 1992).

YadA is a surface-exposed adhesin that is anchored in the bacterial outer membrane *via* a trimeric β-barrel domain (Shahid et al., 2015). The passenger domain of YadA, a trimeric coiled-coil stalk, and an N-terminal β-roll head domain are channeled through the barrel in an unfolded state during the autotransport process (Chauhan et al., 2019). Upon autotransport, the passenger domain starts folding, building a rigid structure protruding toward the outside of the cell (Chauhan et al., 2019). Here, the head domain has been shown to be responsible for many of YadA's adhesion properties (Leo et al., 2008; Mühlenkamp et al., 2015).

While YadA is typically classified as an adhesin that aids in pathogen–host interactions *via* interactions with the extracellular matrix (ECM) (Tamm et al., 1993; Westerlund and Korhonen, 1993; Leo et al., 2008; Keller et al., 2015), YadA has also been shown to be involved in immune evasion (Tamm et al., 1993; Westerlund and Korhonen, 1993; Grosskinsky et al., 2007; Leo et al., 2008; Schindler et al., 2012; Keller et al., 2015). YadA-knockout mutants are avirulent (Pepe et al., 1995; Schütz et al., 2010). This is only partially due to the adhesion properties of YadA as *Yersinia* spp. have additional adhesins which can replace its function (Mallick et al., 2012; Chauhan et al., 2016). During an infection with *Yersinia enterocolitica*, YadA is involved in surface adhesion and has been shown to interact with a variety of proteinaceous ECM molecules such as collagen, fibronectin, and vitronectin (Vn) (Tertti et al., 1992; Schulze-Koops et al., 1993; Leo et al., 2008; Mühlenkamp et al., 2017). The interaction with ECM varies in strength and depends on environmental shear forces (Müller et al., 2011). While the YadA head domain is conserved among *Yersinia* species, some *Y. enterocolitica* strains and *Yersinia pseudotuberculosis* exhibit an additional stretch of approximately 31 residues at the N-terminus of each monomer of the YadA head domain (**Figure 1A**). This stretch has been shown to be responsible for Vn binding (Mühlenkamp et al., 2017).

Vn has been described as an incidental component of the ECM (Leavesley et al., 2013). The ECM is a matrix composed of a variety of proteins, such as collagen, fibronectin, and laminin, and also proteoglycans and glycosaminoglycans (GAGs) forming a hydrogel. This matrix surrounds cellular components of the cell surface and provides strength and elasticity (Frantz et al., 2010). Vn is an approximately 75 kDa glycoprotein involved in tissue repair. It is heavily glycosylated, exhibiting three N-linked glycans (N86, N169, and N242) (Hwang et al., 2014). Vn shows great flexibility, and its conformational state is greatly dependent on interaction partners such as heparin (Izumi et al., 1989; Stockmann et al., 1993). The ability of Vn to associate with GAGs like heparin and heparan sulfate, which are in turn part of the ECM, contributes to the function of Vn in tissue repair (Leavesley et al., 2013). The ECM and its components are an attractive binding target for *Y. enterocolitica* and *Y. pseudotuberculosis* as surface adhesion is crucial for subsequent tissue invasion (Pepe et al., 1995).

Here, we report that YadA from *Y. enterocolitica* strain E40, serotype O:9 ($YadA_{O:9}$) interacts with Vn *via* its glycosylations. We furthermore show that $YadA_{O:9}$ can directly interact with heparin. Up until now, an interaction with glycan moieties like the glycosylations of ECM proteins or GAGs has not been described for YadA.

MATERIALS AND METHODS

Plasmids and Constructs

Plasmids and constructs used in this study are listed in **Table 1**, and sequences can be found in the supplements (**Table 1**). Constructs made in this study were cloned using the Gibson assembly (Gibson et al., 2009).

Bacterial Strains and Growth Conditions

Bacteria were cultivated in Lysogeny broth (LB, Miller formulation). For whole-cell assays with fluorescence detection, *Escherichia coli* Top10 *glmS*:sfGFP (AS75) was used and grown in the presence of arabinose (Saragliadis and Linke, 2019). For protein purification, genes encoding the proteins of interest were expressed in *E. coli* BL21 (DE3) Gold. Generally, bacteria were grown at 37°C to the desired OD_{600}. During overexpression, the temperature was shifted to 23°C after induction.

YadA Head Domain Purification

pASK-IBA3_$YadA_{O:8/O:9}$ was transformed into *E. coli* BL21 (DE3) Gold and grown on ampicillin plates. A single colony was inoculated into 20 ml of LB medium supplemented with 100 μg/ml ampicillin and grown at 37°C overnight (o/n). The following day, a 2 L subculture was prepared and grown in a home-built fermentation system (a system where air is bubbling through bottles of growth medium that stand in a temperature-controlled water bath) until an OD_{600} of 0.5–0.7 was reached. The temperature was shifted to 23°C, and expression was induced with 0.2 μg/ml anhydrotetracycline (AHTC). Protein expression was allowed for 16 h. The culture was harvested by centrifugation at 4,000 × *g*. Afterward, the pellet was resuspended in Tris-buffered saline (TBS) buffer (20 mM Tris pH 7.5, 300 mM NaCl, 20 mM imidazole) with 8 μg/ml lysozyme and a pinch of DNAse. The suspension was subjected to cell lysis using a French press after addition of a HALT protease inhibitor mix (1:500, Thermo Fisher Scientific; 1861278). The lysate was centrifuged for 1 h at 69,600 × *g*, and the supernatant was then filtered through a 0.2 μm filter and subjected to Ni-NTA affinity chromatography (Cytiva, 17531901). As YadA with C-terminal His_6-tag elutes at high imidazole concentrations (160–500 mM), the protein was pure enough for binding experiments after Ni-affinity chromatography. The protein was subjected to dialysis against TBS buffer (20 mM Tris pH 7.5, 150 mM NaCl).

Vitronectin Binding Experiments With Whole Bacteria

E. coli AS75 with pASK-Iba4C_$YadA_{O:8}$ or pASK-Iba4C_$YadA_{O:9}$ was grown o/n in LB medium supplemented with 0.02% (w/v) arabinose and 100 μg/ml ampicillin. The next day, the cultures were diluted 1:100 in 20 ml LB medium supplemented as before and grown at 37°C to an OD_{600} of 0.5. YadA expression was then induced by the addition of AHTC to a final concentration of 0.2 μg/ml and grown for another 3 h at 37°C. YadA expression was checked for by visual inspection for auto-aggregation (Trunk et al., 2018). In the meantime, clear flat-bottom 96-well plates were coated with 100 μl of a 10 μg/ml Vn solution, from either plasma (Gibco, PHE0011), recombinantly expressed in HEK cell cultures (Merck/Millipore, SRP3186), or *E. coli* (Thermo Fisher Scientific, A14700), by incubation for 1 h at room temperature (RT). The Vn solution was discarded from the plates, and the wells were washed three times with TBS (20 mM Tris

TABLE 1 | Constructs used in this study.

Construct	Resistance	Source strain	Source
pASK-IBA4C_YadA$_{O:8}$	Chloramphenicol	*Y. enterocolitica* O:8 WA-314	Mühlenkamp et al., 2017
pASK-IBA4C_YadA$_{O:9}$	Chloramphenicol	*Y. enterocolitica* O:9 E40	Mühlenkamp et al., 2017
pASK-IBA3_YadA$_{O:9}$_head domain	Ampicillin	*Y. enterocolitica* O:8 WA-314	This study (supplement)
pASK-IBA3_YadA$_{O:9}$_head domain	Ampicillin	*Y. enterocolitica* O:9 E40	This study (supplement)

pH 7.5, 150 mM NaCl). Afterward, the wells were blocked using 3% bovine serum albumin (BSA) in TBS. The bacteria were then harvested, washed twice with TBS, and resuspended in TBS with 0.1% BSA to achieve an OD_{600} of 0.2. One hundred microliters of the bacterial suspension was added per well and incubated for 1 h at RT. After that, the wells were washed three times using TBS. Lastly, the wells were filled with 100 µl TBS buffer, and fluorescence was measured using an excitation wavelength of 488 nm and recording the emission at 533 nm (BioTek Synergy H). For experiments with deglycosylated Vn, the experiment was performed the same way, but deglycosylated Vn (see section "Deglycosylation of Vitronectin") was used for coating.

Vitronectin Binding Experiments With Purified YadA Head Domains

A clear 96-well plate was coated with Vn and blocked as described before (section "Vitronectin Binding Experiments With Whole Bacteria"). Then 100 µl of a 10 µg/ml YadA solution in 0.1% (w/v) BSA in TBS (20 mM Tris pH 7.5, 150 mM NaCl) was added to the wells and incubated for 1 h at RT. After the wells were washed twice with 0.1% BSA in TBS and once with TBS with Tween-20 (TBS-T), Ni-horseradish peroxidase (HRP) conjugates were used for the detection of bound, His_6-tagged YadA. One hundred microliters of a Ni-HRP conjugate solution at a final concentration of 5 µg/ml (Thermo Fisher Scientific, 15165) was incubated for 1 h at RT in 3% BSA in TBS per well. This was discarded, and the wells were washed three times with TBS-T and once with TBS. Binding was detected using 150 µl of a 1 mg/ml ABTS solution in ABTS buffer (2.43 ml of 100 mM citric acid, 2.57 ml of 200 mM Na_2HPO_4, 5.0 ml H_2O, 10 µl H_2O_2) (Thermo Fisher Scientific, 34026; VWR, ICNA0219502305). The color development was stopped by adding 100 µl of 1% (w/v) SDS after incubation at RT, and the absorption was measured at 405 nm in a BioTek Synergy H plate reader.

Deglycosylation of Vitronectin

For deglycosylation of Vn, 20 µg of Vn from the respective sources (in water) was mixed with 2 µg of the glycopeptidase PNGase F (500 U) (Promega, V4831) and incubated at 37°C for 19 h. The non-deglycosylated control samples of Cn were incubated at 37°C for 19 h, omitting the PNGase F. For PNGase F control samples, 2 µl of PNGase F was added to water and incubated as described before. Successful deglycosylation was checked for on a SDS-PAGE gel with subsequent silver staining (Nesterenko et al., 1994).

Heparin Inhibition Assay Using Microscopy

Glass coverslips were coated with 50 µl Vn (10 µg/ml) at 4°C o/n. An o/n culture of *E. coli* AS75 harboring pASK-IBA4C_YadA$_{O:8/O:9}$ was inoculated into LB supplemented with 20 µg/ml chloramphenicol and 0.02% w/v arabinose. The next day, the culture was diluted 1:100 in the same broth, and the culture was grown to OD_{600} of 0.5 followed by induction with 0.2 µg/ml AHTC and *yadA* expression for 3 h at 37°C. In the meantime, Vn-coated coverslips were incubated with TBS or 100 µM heparin-disaccharide I-S (Merck, H9267-1MG) for 1 h at RT where applicable. After that, all coverslips were blocked with 3% (w/v) BSA in TBS for 1 h at RT. One hundred microliters of 5×10^8 bacteria in suspension were centrifuged at 4,000 × g for 5 min and resuspended in either TBS (20 mM Tris pH 7.5, 150 mM NaCl) or 100 µM heparin-disaccharide in TBS and incubated for 1 h at RT. After that, the bacteria were centrifuged down again and washed three times in 100 µl TBS. Finally, the bacteria were resuspended in 1 ml 3% BSA in TBS. Three hundred microliters of the bacteria was added to the coverslips and incubated for 30 min at RT. The supernatant was discarded, and the coverslips were washed three times with TBS and fixed with 500 µl of 4% (w/v) paraformaldehyde in TBS for 20 min at RT. Finally, the coverslips were mounted in 5 µl ProLong Glass Antifade Mountant (Invitrogen, P36980) and dried o/n. Microscopy was performed using a fluorescent microscope (Zeiss Axioplan 2) and a 100× oil immersion objective. For quantification, images were converted into binary files, and the area of the particles was calculated using Fiji (**Supplementary Figure 3**). Mean areas were plotted including the standard error of the mean.

Disaggregation Experiments Using Microscopy

An o/n culture of *E. coli* AS75 harboring pASK-IBA4C_YadA$_{O:8/O:9}$ was inoculated into LB supplemented with 100 µg/ml ampicillin and 0.02% (w/v) arabinose. The next day, the culture was diluted 1:100 in the same broth and grown to OD_{600} of 0.5 followed by induction with 0.2 µg/ml AHTC and *yadA* expression for 3 h at 37°C. The culture was diluted to an OD_{600} of 1.0, and 50 µl was centrifuged down at 4,000 × *g* for 5 min. The pellets were then resuspended in 50 µl TBS or TBS supplemented with 100 µM heparin-disaccharide (Merck, H9267-1MG). This was incubated at 37°C in a shaking incubator for 30 min. Five microliters of each solution was wet-mounted onto microscope slides, and the edges were sealed using a CoverGrip coverslip sealant (Biotium, 23005). Microscopy was

performed using a fluorescence microscope (Zeiss Axioplan 2) and a ×100 oil immersion objective. For quantification, images were converted into binary files, and the particle sizes were calculated using Fiji (**Supplementary Figure 4**). The area of each individual particle was plotted in a column scatter plot.

Dot Blots for Heparin Binding to YadA Head Domains

Nitrocellulose membranes were cut and transferred into a six-well plate. Three 2 μl drops of a 700 μg/ml purified $YadA_{O:8}$ or $YadA_{O:9}$ solution were applied onto the membrane and air-dried. Then, the membrane was blocked with 5% BSA in TBS-T (20 mM Tris pH 7.5, 150 mM NaCl, 0.2% Tween-20) for 1 h at RT. Five hundred microliters of a 100 μM biotinylated heparin (Merck, B9806-10MG) solution in TBS-T was incubated on the membrane for 1 h at RT. The membrane was washed three times with TBS-T and afterward incubated with 500 μl of 1:10,000 diluted Strep-Tactin–HRP conjugate (IBA Lifesciences, 2-1502-001) in 5% BSA in TBS-T for 30 min at RT. After the membrane was washed three times with TBS-T and once with TBS (20 mM Tris pH 7.5, 150 mM NaCl), a 500 μl ECL reagent (Thermo Fisher Scientific, 320106) was added, and the membrane was immediately imaged using a Kodak Image Station 4000R.

Heparin Binding Assay Using Bacteria

An o/n culture of *E. coli* AS75 pASK-IBA4C_$YadA_{O:8/O:9}$ was grown in the presence of 0.2% (w/v) arabinose and 100 μg/ml ampicillin. This culture was diluted 1:100 the next morning and grown to an OD_{600} of 0.5. YadA full-length expression was induced by addition of 0.2 μg/ml AHTC. Expression was allowed for 3 h at 37°C. Uninduced bacteria were used as a control. The bacteria were diluted to an OD_{600} of 0.2, spun down, and resuspended in phosphate-buffered saline (PBS). One hundred microliters of that bacterial solution was pipetted into 96-well plates and centrifuged at 4,000 × *g*. After that, 100 μl of a 10 μg/ml biotinylated heparin (Merck, B9806-10MG) solution in 3% (w/v) BSA in TBS was added and incubated at RT for 0.5 h. The plate was washed three times with TBS. The plate was centrifuged as before after every wash before discarding the washing buffer. Strep-Tactin–HRP conjugates (IBA Lifesciences, 2-1502-001) at 1:1,000 in 3% (w/v) BSA in TBS were added and incubated for 30 min at RT. The plate was washed as described before. The ABTS solution was prepared, and color development was stopped as described before. Wells that did not contain any bacteria were used as background controls. Absorbance at 405 nm was measured in a plate reader (BioTek Synergy H).

Binding Assay Using Purified YadA Head Domains

One hundred microliters of 10 μg/ml YadA in TBS was coated into a 96-well plate by incubation at RT for 1 h. The plate was washed three times with 200 μl TBS (20 mM Tris pH 7.5, 150 mM NaCl) and blocked using 200 μl of 3% BSA in TBS. Afterward, 100 μl of biotinylated heparin dilution (0–6.75 μg/ml) in TBS was added to the wells and incubated for 1 h at RT. The wells were washed three times with TBS as described above and blocked with 3% BSA in TBS for 1 h at RT. Strep-Tactin–HRP (IBA Lifesciences, 2-1502-001) at 1:1,000 was added in 3% BSA in TBS and incubated for 1 h at RT. The wells were washed again as described earlier, and an ABTS solution was used for detection as described before. After color development, the reaction was stopped by adding 100 μl of a 1% SDS solution. Absorbance at 405 nm was measured in a plate reader (BioTek Synergy H).

Binding Assay Using Immobilized Heparin on Impedimetric Nanobiosensors

Biosensor Fabrication

Gold screen-printed electrodes (BVT-AC1.W1.RS.Dw2) from BVT Technologies were employed for biosensor fabrication. The electrodes were pre-treated by washing with 97% v/v ethanol for 30 min, rinsed with deionized water, and dried with N_2. Twenty-five microliters of 2.5 mM octopamine in 10 mM phosphate buffer pH 7.2 was spread across the working electrode and electro-polymerized for two cycles at a scan rate of 100 mV/s from +0.0 to +1.6 V. The electrodes were rinsed with 10 mM PBS and dried with Ar. The electrodes were functionalized by binding of biotinylated NeutrAvidin (Ahmed et al., 2013). After that, 10 μl of a 1 mg/ml biotinylated heparin was coated onto the surface for 1 h at RT. The surface was washed with 10 mM PBS and dried with Ar.

Electrochemical Impedance Spectroscopy Measurements and Data Treatment

For binding measurements, 10 μl of *E. coli* AS75 expressing either $YadA_{O:8}$ or $YadA_{O:9}$ full length at OD_{600} of 2, 0.2, and 0.02 was applied to the working electrodes and incubated for 30 min at RT. Blanks were acquired by measuring 10 mM phosphate buffer, omitting the bacteria. Electrical impedance measurements were carried out in a three-cell system of a PalmSens4 potentiostat, galvanostat, and frequency response analyzer (PalmSens BV, Netherland), adding 10 mM $[Fe(CN)6]^{3-/4-}$ in 10 mM PBS pH 7.2 onto the electrodes. EIS measurements were recorded at 0 V over a frequency range of 5–0.1 Hz, with a modulation voltage of + 10 mV. Measurements corresponding to finite Warburg impedances were excluded from the Nyquist plots (Nguyen and Breitkopf, 2018). PSTrace (5.8) was used to record the EIS measurements. Metrohm Autolab Nova 2.1.4. was used to fit the Nyquist plots into Randles' equivalent circuits. From the fitting, the charge-transfer resistance (Rct) was obtained. The biosensor was assessed before and after analyte addition. Changes in Rct (%) were obtained to analytically assess bacterial binding with Equation 1:

$$\textbf{Change in Rct(\%)} = (\textbf{Rct}_{\textbf{analyte}} - \textbf{Rct}_{\textbf{zero}})/\textbf{Rct}_{\textbf{zero}} \cdot \textbf{100} \quad (1)$$

All experiments were replicated $n \geq 6$. Layer-by-layer construction can be found in **Supplementary Figure 2**.

Statistical Analysis

For binding data analysis, data are shown as means ± SD and were analyzed using a one-way ANOVA including Tukey's test. For data plotting and statistical analysis, OriginPro and "R" were used. For microscopy analysis, mean particle areas ± SEM were plotted. As the particles sizes were not normally distributed, non-parametric testing including a Kruskal–Wallis test and subsequent Wilcox testing were applied to test for significance. Significance levels are indicated in the graphs with $p < 0.05$ (*), $p < 0.01$ (**), or $p < 0.001$ (***).

RESULTS

Head Domain of YadA From *Y. enterocolitica* Serotype O:9 Binds to Vitronectin Isolated From Plasma and HEK Cells but Not to Vitronectin Produced in *E. coli*

We first aimed to describe the molecular details of the interaction between the YadA head domain of *Y. enterocolitica* serotype O:9 ($YadA_{O:9}$) and Vn. $YadA_{O:9}$ harbors an additional, N-terminal, 31-residue stretch (**Figure 1A**) that has been described to interact with Vn (Mühlenkamp et al., 2017). We started out replicating the experiments done by Mühlenkamp et al. (2017). For these enzyme-linked immunosorbent assay (ELISA)-like binding experiments, Vn from different sources was used. Vn purified from plasma (Vn_{plasma}), Vn expressed in HEK cell culture (Vn_{HEK}), and Vn recombinantly expressed in *E. coli* (Vn_{Ec}) were tested for their capacity to be bound by *E. coli* expressing either full-length $YadA_{O:8}$ or $YadA_{O:9}$ (**Figure 1B**). Additionally, Vn binding by purified YadA head domains was tested (**Figure 1C**). We reasoned that, if YadA indeed bound to a conserved sequence within Vn, the binding should happen irrespective of the origin of Vn and only with $YadA_{O:9}$. Indeed, the whole-cell assays show that only $YadA_{O:9}$-expressing bacteria bound to Vn_{plasma} and Vn_{HEK} (**Figure 1B**). Binding between Vn_{Ec} and $YadA_{O:9}$ could not be observed. Bacteria expressing $YadA_{O:8}$ did not bind to either Vn variant (**Figure 1B**). These findings were corroborated by assays using purified YadA head domains. While we observed some binding of purified $YadA_{O:8}$ to Vn_{plasma}, no binding to Vn_{HEK} and Vn_{Ec} was observed (**Figure 1C**). The weak binding of purified $YadA_{O:8}$ can be explained by Vn_{plasma} being contaminated with other proteins (**Supplementary Figure 1**). $YadA_{O:9}$ on the other hand showed clear binding to all Vn variants, with reduced binding to Vn_{Ec}. Based on these findings, we sought to investigate the difference between $YadA_{O:9}$ binding to $Vn_{plasma/HEK}$ and binding to Vn_{Ec}.

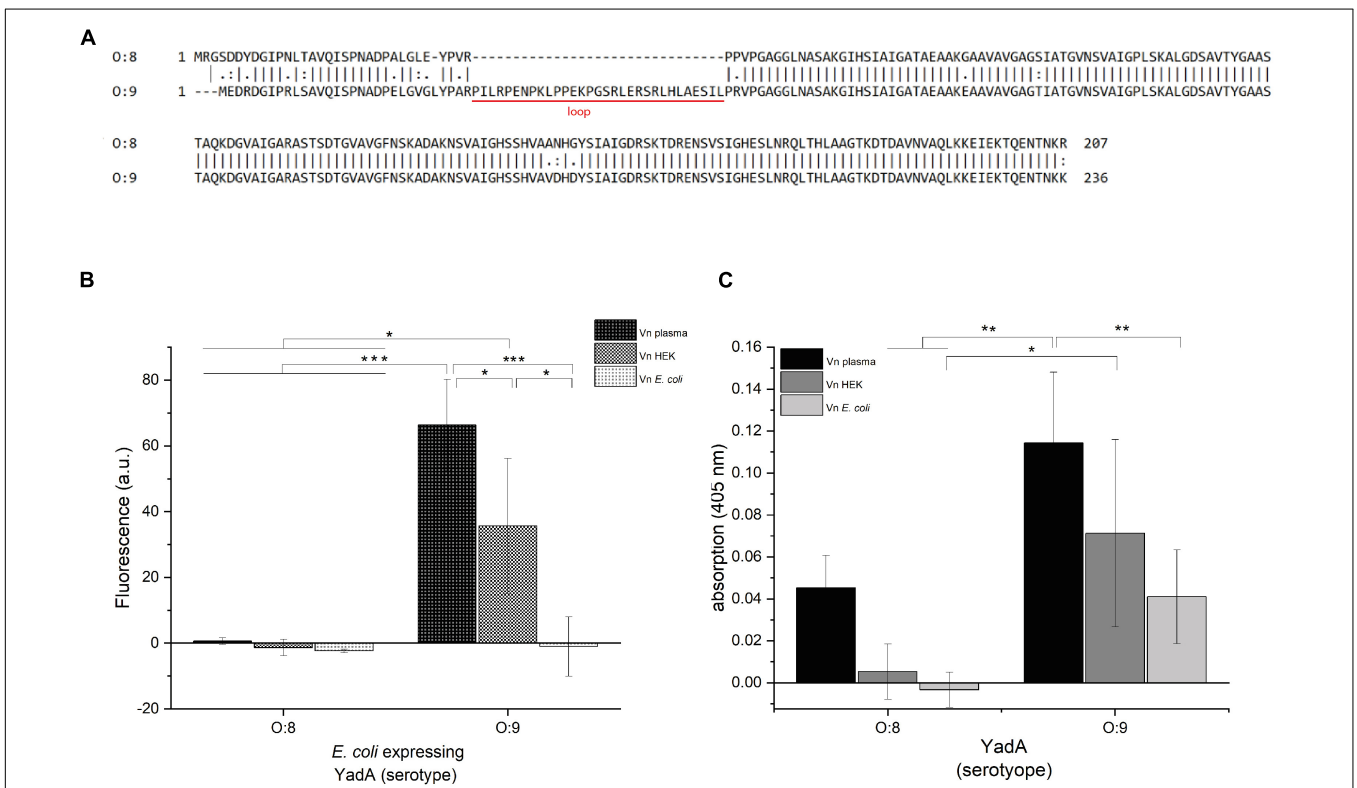

FIGURE 1 | $YadA_{O:9}$ binds to Vn_{plasma} and Vn_{HEK} but shows reduced binding to Vn_{Ec}. **(A)** Alignment of the N-terminal head domains of the YadA head domain from *Y. enterocolitica* serotypes O:8 and O:9. The alignments include the head domain of YadA, the neck region, and the first 20 residues of the coiled-coil stalk domain. $YadA_{O:9}$ has an insertion of 31 residues toward the N-terminus of the head domain. **(B)** Whole-cell binding assay to Vn using *E. coli* expressing either $YadA_{O:8}$ or $YadA_{O:9}$. **(C)** Vn binding assay with purified $YadA_{O:8}$ and $YadA_{O:9}$ head domains. Significance levels are indicated with $*p < 0.05$, $**p < 0.01$, $***p < 0.001$.

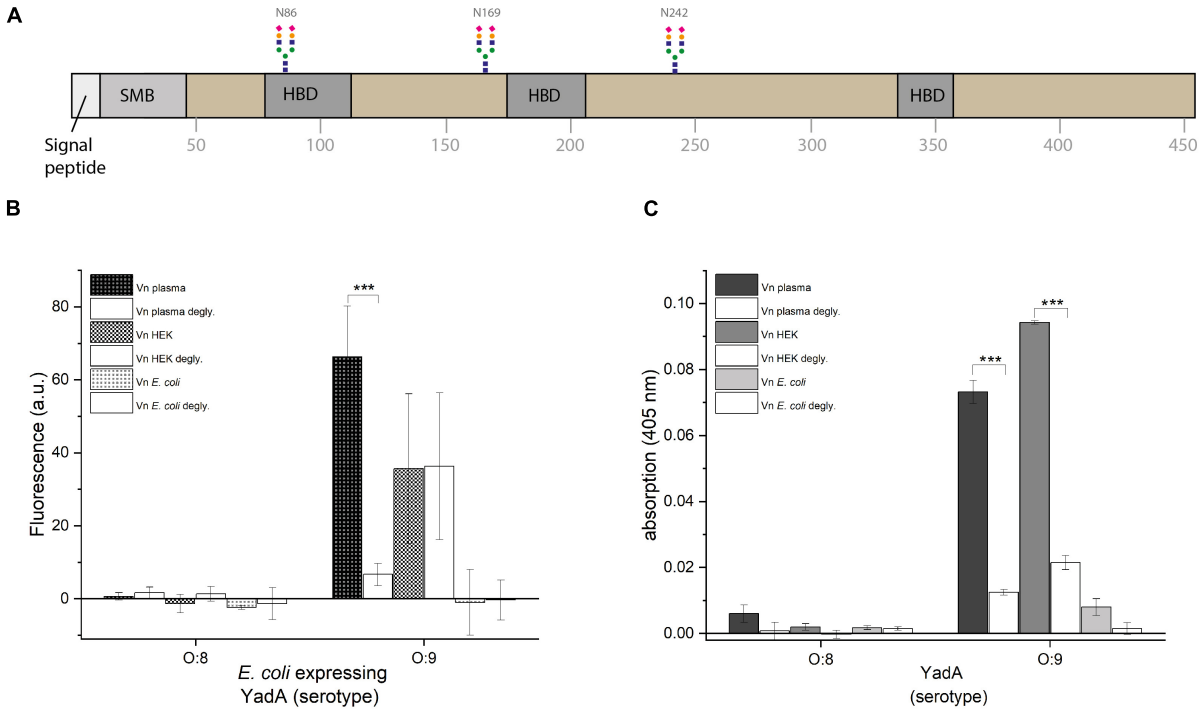

FIGURE 2 | YadA$_{O:9}$ binding to deglycosylated Vn is reduced. **(A)** Schematic representation of full-length Vn. Vn has three N-linked glycosylations in positions N86, N169, and N242. **(B)** Whole-cell binding assay to glycosylated and deglycosylated Vn. **(C)** Binding assay using purified YadA head domains to glycosylated and deglycosylated Vn. Significance levels are indicated with $^{*}p < 0.05$, $^{**}p < 0.01$, $^{***}p < 0.001$.

The Head Domain of YadA From *Y. enterocolitica* Serotype O:9 Only Binds Glycosylated Vitronectin

Due to the observation that YadA$_{O:9}$ binds Vn$_{plasma}$ and Vn$_{HEK}$ but shows at least reduced binding to Vn$_{Ec}$, we wanted to investigate whether YadA$_{O:9}$ actually binds a stretch within Vn or whether it either recognized a folded binding site or the glycosylations of Vn. Vn is heavily glycosylated with at least three N-linked glycans at residues N86, N169, and N242 (**Figure 2A**). As eukaryotic proteins recombinantly expressed in *E. coli* are usually not glycosylated, we first tested the latter hypothesis. We used PNGase F, a glycopeptidase that selectively removes glycans directly at the N-linkage by cleaving the glycosidic bond between asparagine and the core GlcNAc. With the deglycosylated Vn, the binding assays were repeated to see whether binding could be abrogated by removal of the N-linked glycosylations. In **Figure 2B**, the fluorescence-based whole-cell assay using *E. coli* AS75 expressing either full-length YadA$_{O:8}$ or full-length YadA$_{O:9}$ is shown. No binding was observed with cells expressing YadA$_{O:8}$, which fits the hypothesis, as the postulated Vn binding stretch is not present in YadA from *Y. enterocolitica* serotype O:8. In the case of binding of bacteria expressing full-length YadA$_{O:9}$, a clear difference in binding to Vn$_{plasma}$ was observed between the glycosylated Vn$_{plasma}$ and deglycosylated Vn$_{plasma}$ (**Figure 2B**). For Vn$_{HEK}$, no change in binding of YadA$_{O:9}$-expressing *E. coli* AS75 before and after glycosylation was observed. We can at this point not say as to why no change was observed for bacterial binding of Vn$_{HEK}$ compared to deglycosylated Vn$_{HEK}$. Vn$_{Ec}$ was bound in neither the glycosylated nor the deglycosylated state. While this supported our hypothesis that the glycan residues of Vn might be involved in the YadA$_{O:9}$–Vn interaction rather than the proteinaceous part of Vn, we also repeated the binding assay using purified YadA head domains from both serotypes of *Y. enterocolitica* (**Figure 2C**). While, as expected, YadA$_{O:8}$ did not bind to Vn-coated plates, neither to the untreated nor to the deglycosylated version, YadA$_{O:9}$ bound to both untreated Vn$_{plasma}$ and untreated Vn$_{HEK}$ (**Figure 2C**). Untreated Vn$_{Ec}$ was not bound as already shown in **Figure 1C**. After deglycosylation with PNGase F, neither Vn$_{plasma}$ nor Vn$_{HEK}$ was bound by YadA$_{O:9}$ anymore, further supporting our hypothesis of YadA$_{O:9}$ interacting with the N-linked glycans.

Binding of YadA$_{O:9}$ to Heparin Abrogates the YadA$_{O:9}$–Vitronectin Interaction

Heparin was described to abrogate the interaction between Vn and YadA$_{O:9}$ (Mühlenkamp et al., 2017). We next wanted to investigate whether the potential YadA$_{O:9}$ glycan interaction might be the cause for this observation. It was hypothesized before that heparin blocks the YadA binding site on Vn. As in the globular state, the heparin binding site in Vn is mostly hidden inside the core of the protein; this seemed unlikely to be the reason for YadA$_{O:9}$ binding inhibition

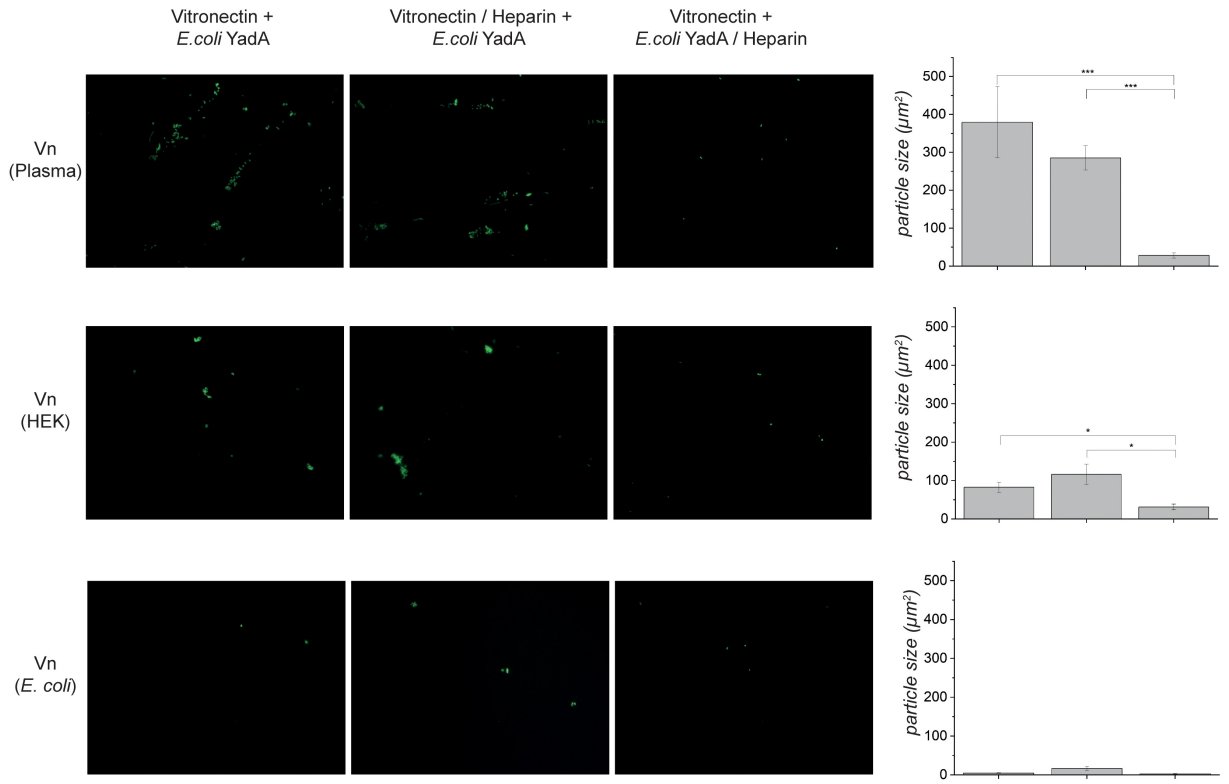

FIGURE 3 | Binding of *E. coli* expressing YadA$_{O:9}$ is reduced when the bacteria are preincubated with heparin-disaccharide. Vn from different sources was coated onto coverslips, and binding of fluorescence *E. coli* expressing YadA$_{O:9}$ was measured (left column). Images in the middle column show micrographs of Vn-coated coverslips that were preincubated with 100 μM heparin-disaccharide. Afterward, binding of fluorescent *E. coli* expressing YadA$_{O:9}$ was monitored. When Vn was coated and binding of fluorescent *E. coli* expressing YadA$_{O:9}$ that were preincubated with heparin was (column 3) reduced, adhesion was measured for both Vn$_{plasma}$ and Vn$_{HEK}$. *E. coli* expressing YadA$_{O:9}$ did only weakly bind to Vn$_{Ec}$ as already observed in previous experiments. In the last column, the mean area of particles (μm^2) ± SEM was calculated and plotted as bar graphs. Significance levels are indicated with $^*p < 0.05$, $^{**}p < 0.01$, $^{***}p < 0.001$.

(Hayashi et al., 1985; Izumi et al., 1989; Zhuang et al., 1996; Leavesley et al., 2013). Coverslips were coated with untreated Vn$_{plasma}$, Vn$_{HEK}$, or Vn$_{Ec}$. YadA$_{O:9}$ (full length)-expressing, fluorescent bacteria were checked for binding (**Figure 3**, left column). To check for the influence of heparin on this interaction, we also prepared samples where we either preincubated Vn with heparin (**Figure 3**, middle column) or preincubated YadA$_{O:9}$-expressing bacteria with heparin (**Figure 3**, right column). In the fluorescence microscopy adhesion assay, we observed only minimal adhesion of bacteria to Vn$_{Ec}$ (**Figure 3**, bottom row). When coverslips had been coated with Vn$_{plasma}$ or Vn$_{HEK}$, adhesion was observed only in the absence of heparin. In cases where Vn was preincubated with heparin, bacteria expressing YadA$_{O:9}$ adhered to Vn to a comparable level as in the untreated samples (**Figure 3**, left and middle columns). When YadA$_{O:9}$-expressing bacteria were preincubated with heparin, reduced binding to untreated Vn$_{plasma}$ and Vn$_{HEK}$ was observed (**Figure 3**, right column). Quantifications of the area of the particles reflect the tendencies seen in the experiment, where preincubation of the bacteria expressing YadA$_{O:9}$ with heparin seems to reduce binding to Vn whereas preincubation of Vn with heparin did not change the adhesion of YadA$_{O:9}$-expressing bacteria. This observation further strengthened our hypothesis that the YadA Vn-binding loop aids in adhesion of YadA$_{O:9}$ to glycan moieties.

The Head Domain of YadA From *Y. enterocolitica* Serotype O:9 Prefers Heparin Binding Over Autoaggregation

YadA, as an adhesin, is involved in autoaggregation, which has been described as an important mechanism for immune evasion during infection as well as for biofilm formation (Trunk et al., 2018). We have observed earlier that the interaction with other adhesin targets, such as ECM molecules, interferes with autoaggregation (manuscript in preparation). We thus wanted to investigate what effect heparin might have on autoaggregation mediated by YadA$_{O:9}$. We expressed YadA$_{O:8}$ or YadA$_{O:9}$ full length in fluorescent *E. coli* AS75 and allowed for autoaggregation of these samples. Uninduced samples served as a control. Half of the samples were then preincubated with heparin-disaccharide. The uninduced samples did not show any autoaggregation behavior, either in the presence or in the absence of heparin (**Figure 4**, rows 1 and 3). The induced YadA$_{O:8}$ samples autoaggregated to similar degrees both in the absence and in the presence of heparin (**Figure 4**, row 2). Fluorescent bacteria

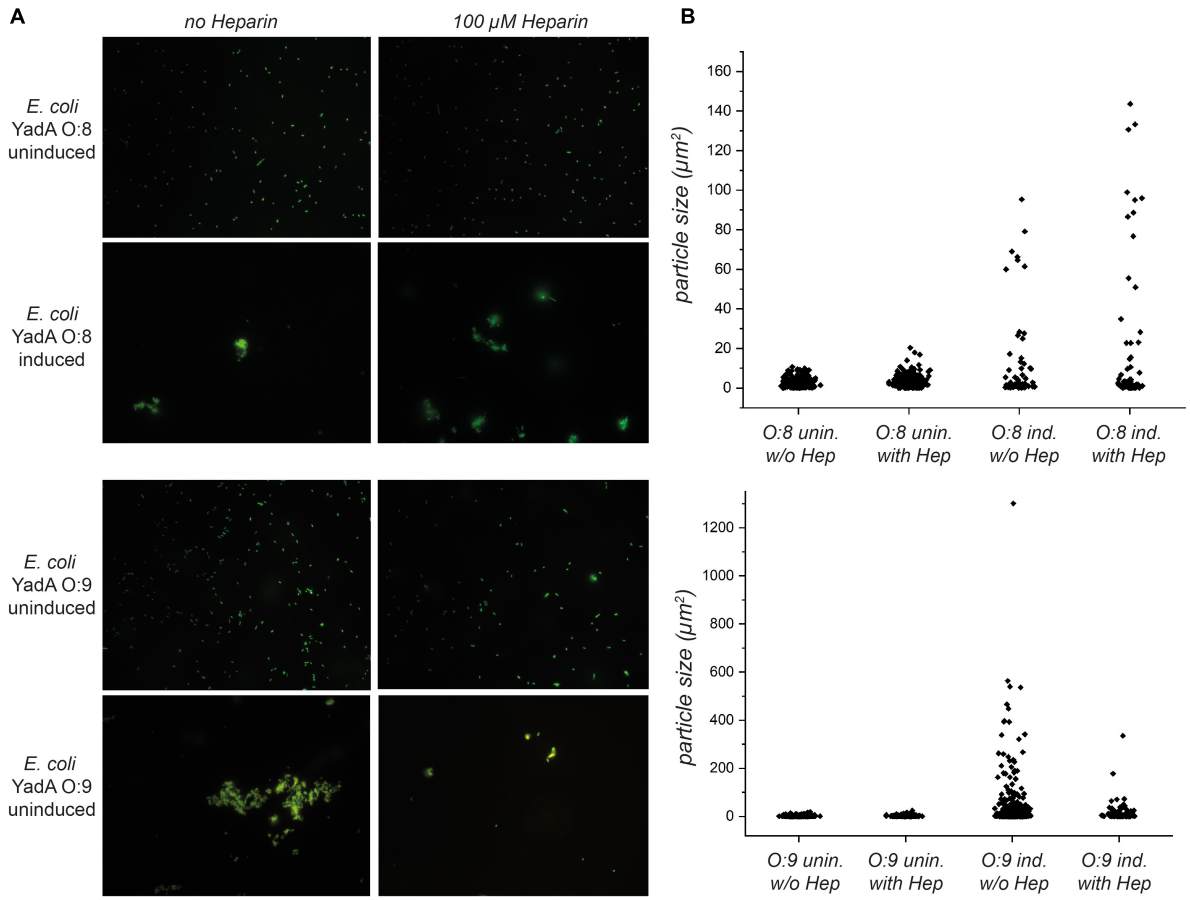

FIGURE 4 | Autoaggregation of *E. coli* expressing YadA$_{O:9}$ in the presence of 100 µM heparin-disaccharide is reduced. **(A)** In the upper row, uninduced bacteria expressing YadA$_{O:8}$ in the presence and absence of heparin-disaccharide are shown. Uninduced bacteria (no YadA$_{O:8}$ expressed) were used as a negative control for aggregation. After induction, *E. coli* expressing YadA$_{O:8}$ show autoaggregation (row 2). In rows 3 and 4, the autoaggregation behavior of *E. coli* expressing YadA$_{O:9}$ was tested in the presence and absence of 100 µM heparin-disaccharide. Uninduced *E. coli* expressing YadA$_{O:9}$ are shown in row 3, and induced samples are shown in row 4. **(B)** Quantifications of the area of the particles are shown in the bar scatter plots for *E. coli* expressing YadA$_{O:8}$ samples in the upper graph and *E. coli* expressing YadA$_{O:9}$ samples in the lower graph.

expressing YadA$_{O:9}$ showed autoaggregation in the absence of heparin but reduced autoaggregation in the presence of heparin (**Figure 4**, lower row). This indicates that, indeed, heparin binding of YadA$_{O:9}$ dissolves the autoaggregation tendencies caused by surface expression of YadA$_{O:9}$. The dispersion of particles sizes (µm^2) is shown in **Figure 4B**. The scatter plots reflect the difference in aggregate (particle) sizes. A reduction in area between aggregates of *E. coli* expressing YadA$_{O:9}$ with and without addition of heparin-disaccharide can be seen shifting from large aggregates to smaller aggregates or fully disaggregated samples.

YadA Directly Binds Heparin

To test for a direct interaction between YadA$_{O:9}$ and heparin, we used *E. coli* AS75 cells expressing either YadA$_{O:8}$ or YadA$_{O:9}$. The bacteria were immobilized in a 96-well plate to capture biotinylated heparin. Bound biotinylated heparin was detected using Strep-Tactin–HRP. While no binding of biotinylated heparin to YadA$_{O:8}$-expressing bacteria was observed, bacteria expressing YadA$_{O:9}$ clearly showed heparin binding (**Figure 5A**). To support these results, we used electrochemical impedance measurements to measure bacterial binding to a heparin-coated surface. Biotinylated heparin was coated onto a biosensor using matrix-embedded NeutrAvidin (Ahmed et al., 2013). The change in impedance was then measured upon binding of *E. coli* AS75 expressing either YadA$_{O:8}$ or YadA$_{O:9}$ (**Figure 5B**). Please note that negative binding values are due to stronger adhesion of *E. coli* expressing YadA$_{O:8/O:9}$ to uncoated electrodes that were used as a background and subtracted. While, for uninduced *E. coli* AS75 and *E. coli* expressing YadA$_{O:8}$, no change in impedance was observed, we could clearly measure binding of *E. coli* expressing YadA$_{O:9}$ by a significant change of impedance (**Figure 5B**). We then aimed to test for binding of heparin to purified YadA head domains. A dot blot using immobilized YadA$_{O:8}$ and YadA$_{O:9}$ head domains to detect binding of biotinylated heparin was performed. While no heparin binding was observed for either the buffer control or the YadA$_{O:8}$ head domain, a signal could be observed for the binding of

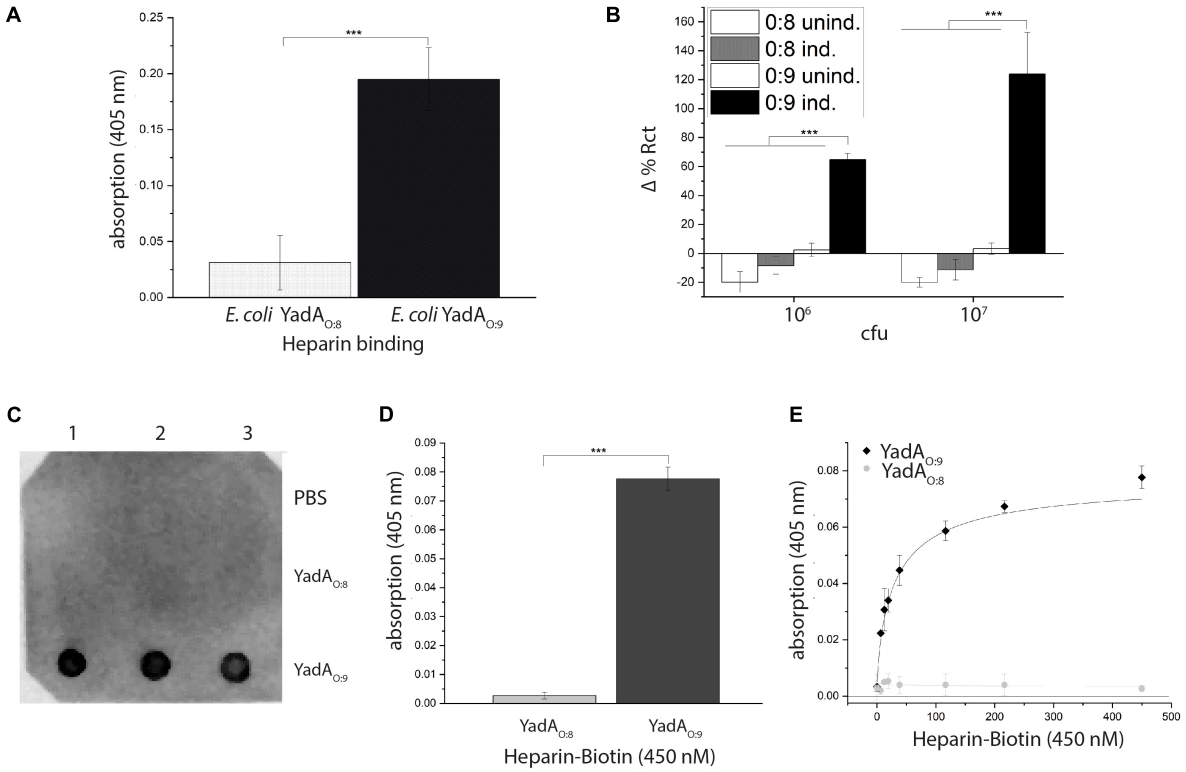

FIGURE 5 | YadA$_{O:9}$ directly binds to heparin. **(A)** Whole-cell binding assay of heparin to *E. coli* expressing YadA$_{O:8}$ or YadA$_{O:9}$ shows binding of YadA$_{O:9}$-expressing bacterial binding to heparin. **(B)** Impedimetric biosensor experiment showing the adhesion of bacteria expressing YadA$_{O:8}$ or YadA$_{O:9}$ to surface-coated heparin. **(C)** Dot blot using immobilized YadA$_{O:8}$ or YadA$_{O:9}$ head domains shows direct binding to biotinylated heparin. **(D)** ELISA-like binding assay using immobilized YadA head domains to capture biotinylated heparin. **(E)** ELISA-like binding assay showing the interaction between immobilized, purified YadA head domains and biotinylated heparin in a concentration-dependent manner. Significance levels are indicated with $^{*}p < 0.05$, $^{**}p < 0.01$, $^{***}p < 0.001$.

biotinylated heparin to the immobilized YadA$_{O:9}$ head domain (**Figure 5C**). To quantify the binding, we immobilized the head domains of YadA$_{O:8}$ and YadA$_{O:9}$ in a 96-well plate and tested for binding at various concentrations. We observed that at 450 μg/ml of heparin, binding between YadA$_{O:8}$ or YadA$_{O:9}$ head domains and heparin is significantly different (**Figures 5D,E**). Repeating the assay with a dilution series of biotinylated heparin allowed us to investigate the concentration dependency of the binding. Using a fifth-party logistics fit, we estimate the (apparent) K_D to be approximately 30 nM. Furthermore, this experiment allows for an estimation of the binding ratio between YadA$_{O:9}$ and biotinylated heparin. The binding ratio is estimated to be 1:1 (YadA$_{O:9}$ monomer to biotinylated heparin). We can at this point not claim an accurate K_D or binding ratio as heparin varies in length but averages at 15 kDa (Shriver et al., 2012).

DISCUSSION

With this work, we present evidence that a 31-residue loop insertion specifically found in YadA$_{O:9}$ is responsible for the interaction between YadA$_{O:9}$ and glycan moieties. All experiments presented in this work were done using YadA from *Y. enterocolitica* strains WA-314 (serotype O:8) or E40 (serotype O:9). While Vn binding results published previously indicate that all *Y. enterocolitica* strains of serotype O:9 harbor this N-terminal 31-residue loop (Mühlenkamp et al., 2017), we cannot be sure that the presence or absence of this loop correlates with the serotypes in all cases. To our knowledge, sequence variations of YadA have never been reported to contribute directly to serotyping.

This loop region aids in the interaction between YadA$_{O:9}$ and the glycosylated host protein Vn as well as heparin, which, like Vn, is part of the ECM. We show that this interaction is not specific for one type of glycan residue but rather for a variety of glycans. This is supported by the observation that YadA$_{O:9}$ interacts not only with the glycan residues of the glycoprotein Vn but also with the carbohydrate polymer heparin. Interactions with glycans are employed by many pathogens for adhesion and invasion, especially in viruses (Marks et al., 2001; Guan et al., 2017; Sorin et al., 2021). Also, bacterial virulence factors like UpaB and Pili have been shown to interact with the glycosylations of glycoproteins and GAGs (Rajas et al., 2017; Paxman et al., 2019; Sauer et al., 2019; Vizarraga et al., 2021). To our knowledge, this is the first time that a trimeric autotransporter adhesin is described to bind glycans.

While it has been established in earlier work that YadA$_{O:9}$ interacts directly with human Vn (Mühlenkamp et al., 2017), we show that recombinant Vn expressed in *E. coli* is not bound by YadA$_{O:9}$. Eukaryotic proteins expressed in *E. coli* often lack glycosylations, as *E. coli* does not possess the glycosyltransferases and glycosidases present in eukaryotes (Sahdev et al., 2008; Khow and Suntrarachun, 2012). We further show in deglycosylation experiments that properly deglycosylated Vn was not bound by YadA$_{O:9}$ any longer. This, and the fact that binding does not occur when using YadA$_{O:8}$, further supports our model that the YadA$_{O:9}$ loop is responsible for interactions with glycans. Furthermore, as Mühlenkamp et al. (2017) had described that heparin could inhibit the interaction between YadA$_{O:9}$ and Vn, we set out to investigate whether heparin binding to Vn was actually the reason for this inhibition or whether a more direct interaction of heparin with YadA$_{O:9}$ was the reason for this effect. While Vn indeed harbors a heparin binding site, this site is hidden in globular Vn (Izumi et al., 1989). We thus checked for binding of fluorescent *E. coli* expressing full-length YadA$_{O:9}$ after preincubating either Vn with heparin-disaccharide or after preincubating fluorescent *E. coli* expressing YadA$_{O:9}$ with heparin-disaccharide. Heparin preincubation of fluorescent *E. coli* expressing YadA$_{O:9}$ inhibited Vn interaction, while preincubation of Vn with heparin-disaccharide did not. This is in agreement with literature stating that only 2% of the overall plasma Vn is present in a heparin-binding-competent state (Izumi et al., 1989), as well as with our model stating that the YadA$_{O:9}$ 31-aa loop might be responsible for glycan binding. Furthermore, heparin-disaccharide was able to dissolve the YadA-mediated autoaggregation of bacteria expressing YadA$_{O:9}$, which again indicates that there might be a direct interaction between heparin and YadA$_{O:9}$. Finally, we were able to directly show the interaction using YadA$_{O:9}$-expressing *E. coli* as well as purified YadA$_{O:9}$ head domains in dot blots and ELISA-like assays. When looking at the YadA$_{O:9}$ sequence, one can see that the loop contains seven positively charged residues (Arg and Lys). We hypothesize that the interaction between YadA$_{O:9}$ could be explained by charge interactions with these residues, as the terminal sugar of the glycosylation of Vn is in most cases negatively charged sialic acid (Hwang et al., 2014). In heparin, sulfate moieties render this oligosaccharide heavily negatively charged (Rabenstein, 2002). It is worth noting that many known heparin binding motifs exhibit multiple, evenly spaced basic residues (Capila and Linhardt, 2002). Overall, we thus suggest that electrostatic interactions between the positively charged YadA$_{O:9}$ loop residues and negatively charged functional groups on glycans are key to the binding affinity between YadA$_{O:9}$ and glycans.

In terms of biological relevance, we hypothesize the interaction with YadA$_{O:9}$ to be an additional mechanism for binding to host cell surfaces. As many secreted eukaryotic proteins are glycosylated for protein stability in the extracellular space (Varki et al., 2009), glycosylated ECM proteins could make a prime adhesion target during infection. Furthermore, a major group of molecules found in the ECM are GAGs such as heparin and heparan sulfate (Frantz et al., 2010). In addition to glycan adhesion being beneficial for the pathogen, it can conceptually be used in diagnostic workflows, e.g., to enrich pathogens from biological samples and potentially to develop anti-infective drugs. As glycans play a crucial role in pathogen adhesion, they have been used previously as therapeutics. Examples are the use of D-mannose in the treatment of urinary tract infections or of glycan derivatives to treat influenza (Domenici et al., 2016; Rustmeier et al., 2019; Weiss et al., 2020).

DATA AVAILABILITY STATEMENT

The original contributions presented in the study are included in the article/**Supplementary Material**, further inquiries can be directed to the corresponding author.

AUTHOR CONTRIBUTIONS

IM: data acquisition, data visualization, methodology, writing of the original draft, and project conceptualization. JL-B: data acquisition, methodology, data visualization, and draft writing and review. PM, MS, and SP: conceptualization, and draft review and editing. DL: project administration, project conceptualization, and draft writing and editing. All authors contributed to the article and approved the submitted version.

FUNDING

This work was funded by the Horizon 2020 Innovative Training Network "ViBrANT" (to DL, SP, and PM) (funding ID: 765042). Contributions by the University of Oslo are gratefully acknowledged.

ACKNOWLEDGMENTS

We thank D. Hatlem and Ana Lucía Campaña (University of Oslo) for helpful discussions and T. Späth (Institute for Medical Microbiology, Tubingen) for technical assistance. We thank Kristian Prydz for helpful discussions concerning this manuscript. We furthermore thank the imaging platform (NorMIC), especially Frode Miltzow Skjeldal, for help with the image analysis and quantification.

SUPPLEMENTARY MATERIAL

The Supplementary Material for this article can be found online at: https://www.frontiersin.org/articles/10.3389/fmicb.2021.738818/full#supplementary-material

REFERENCES

Ahmed, A., Rushworth, J. V., Wright, J. D., and Millner, P. A. (2013). Novel impedimetric immunosensor for detection of pathogenic bacteria *Streptococcus pyogenes* in human Saliva. *Anal. Chem.* 85, 12118–12125. doi: 10.1021/ac403253j

Capila, I., and Linhardt, R. J. (2002). Heparin-protein-wechselwirkungen. *Angew. Chem.* 114, 426–450. doi: 10.1002/1521-3757(20020201)114:3<426::aid-ange426>3.0.co;2-q

Chauhan, N., Hatlem, D., Orwick-Rydmark, M., Schneider, K., Floetenmeyer, M., van Rossum, B., et al. (2019). Insights into the autotransport process of a trimeric autotransporter, Yersinia Adhesin A (YadA). *Mol. Microbiol.* 111, 844–862. doi: 10.1111/mmi.14195

Chauhan, N., Wrobel, A., Skurnik, M., and Leo, J. C. (2016). Yersinia adhesins: an arsenal for infection. *Proteomics Clin. Appl.* 10, 949–963. doi: 10.1002/prca.201600012

Domenici, L., Monti, M., Bracchi, C., Giorgini, M., Colagiovanni, V., Muzii, L., et al. (2016). D-mannose: a promising support for acute urinary tract infections in women. A pilot study. *Eur. Rev. Med. Pharmacol. Sci.* 20, 2920–2925.

Frantz, C., Stewart, K. M., and Weaver, V. M. (2010). The extracellular matrix at a glance. *J. Cell Sci.* 123, 4195–4200. doi: 10.1242/jcs.023820

Gibson, D. G., Young, L., Chuang, R. Y., Venter, J. C., Hutchison, C. A. III, and Smith, H. O. (2009). Enzymatic assembly of DNA molecules up to several hundred kilobases. *Nat. Methods* 6, 343–345. doi: 10.1038/nmeth.1318

Grosskinsky, U., Schütz, M., Fritz, M., Schmid, Y., Lamparter, M. C., Szczesny, P., et al. (2007). A conserved glycine residue of trimeric autotransporter domains plays a key role in Yersinia adhesin a autotransport. *J. Bacteriol.* 189, 9011–9019. doi: 10.1128/JB.00985-07

Guan, J., Bywaters, S. M., Brendle, S. A., Ashley, R. E., Makhov, A. M., Conway, J. F., et al. (2017). Cryoelectron microscopy maps of human papillomavirus 16 reveal L2 densities and heparin binding site. *Structure* 25, 253–263. doi: 10.1016/j.str.2016.12.001

Hayashi, M., Akama, T., Kono, I., and Kashiwagi, H. (1985). Activation of vitronectin (serum spreading factor) binding of heparin by denaturing agents. *J. Biochem.* 98, 1135–1138. doi: 10.1093/oxfordjournals.jbchem.a135363

Hwang, H., Lee, J. Y., Lee, H. K., Park, G. W., Jeong, H. K., Moon, M. H., et al. (2014). In-depth analysis of site-specific n-glycosylation in vitronectin from human plasma by tandem mass spectrometry with immunoprecipitation. *Anal. Bioanal. Chem.* 406, 7999–8011. doi: 10.1007/s00216-014-8226-5

Izumi, M., Yamada, K. M., and Hayashi, M. (1989). Vitronectin exists in two structurally and functionally distinct forms in human plasma. *Biochim. Biophys. Acta Gen. Subj.* 990, 101–108. doi: 10.1016/S0304-4165(89)80019-4

Keller, B., Mühlenkamp, M., Deuschle, E., Siegfried, A., Mössner, S., Schade, J., et al. (2015). Yersinia enterocolitica exploits different pathways to accomplish adhesion and toxin injection into host cells. *Cell. Microbiol.* 17, 1179–1204. doi: 10.1111/cmi.12429

Khow, O., and Suntrarachun, S. (2012). Strategies for production of active eukaryotic proteins in bacterial expression system. *Asian Pac. J. Trop. Biomed.* 2, 159–162. doi: 10.1016/S2221-1691(11)60213-X

Leavesley, D. I., Kashyap, A. S., Croll, T., Sivaramakrishnan, M., Shokoohmand, A., Hollier, B. G., et al. (2013). Vitronectin - master controller or micromanager? *IUBMB Life* 65, 807–818. doi: 10.1002/iub.1203

Leo, J. C., Elovaara, H., Brodsky, B., Skurnik, M., and Goldman, A. (2008). The Yersinia Adhesin YadA binds to a collagenous triple-helical conformation but without sequence specificity. *Protein Eng. Design Sel.* 21, 475–484. doi: 10.1093/protein/gzn025

Mallick, E. M., Brady, M. J., Luperchio, S. A., Vanguri, V. K., Magoun, L., Liu, H., et al. (2012). Allele- and Tir-independent functions of intimin in diverse animal infection models. *Front. Microbiol.* 3:11. doi: 10.3389/fmicb.2012.00011

Marks, R. M., Lu, H., Sundaresan, R., Toida, T., Suzuki, A., Imanari, T., et al. (2001). Probing the interaction of dengue virus envelope protein with heparin: assessment of glycosaminoglycan-derived inhibitors. *J. Med. Chem.* 44, 2178–2187. doi: 10.1021/jm000412i

Mühlenkamp, M., Oberhettinger, P., Leo, J. C., Linke, D., and Schütz, M. S. (2015). Yersinia Adhesin A (YadA) - beauty & beast. *Int. J. Med. Microbiol.* 305, 252–258. doi: 10.1016/j.ijmm.2014.12.008

Mühlenkamp, M. C., Hallström, T. I, Autenrieth, B., Bohn, E., Linke, D., Rinker, J., et al. (2017). Vitronectin binds to a specific stretch within the head region of Yersinia Adhesin a and thereby modulates yersinia enterocolitica host interaction. *J. Innate Immun.* 9, 33–51. doi: 10.1159/000449200

Müller, N. F., Kaiser, P. O., Linke, D., Schwarz, H., Riess, T., Schäfer, A., et al. (2011). *Trimeric Autotransporter Adhesin*-dependent adherence of *Bartonella henselae*, *Bartonella quintana*, and *Yersinia enterocolitica* to Matrix components and endothelial cells under static and dynamic flow conditions. *Infect. Immun.* 79, 2544–2553. doi: 10.1128/IAI.01309-10

Nesterenko, M. V., Tilley, M., and Upton, S. J. (1994). A simple modification of blum's silver stain method allows for 30 minite detection of proteins in polyacrylamide gels. *J. Biochem. Biophys. Methods* 28, 239–242. doi: 10.1016/0165-022x(94)90020-5

Nguyen, T. Q., and Breitkopf, C. (2018). Determination of diffusion coefficients using impedance spectroscopy data. *J. Electrochem. Soc.* 165, E826–E831. doi: 10.1149/2.1151814jes

Paxman, J. J., Lo, A. W., Sullivan, M. J., Panjikar, S., Kuiper, M., Whitten, A. E., et al. (2019). Unique structural features of a bacterial autotransporter adhesin suggest mechanisms for interaction with host macromolecules. *Nat. Commun.* 10, 1–12. doi: 10.1038/s41467-019-09814-6

Pepe, J. C., Wachtel, M. R., Wagar, E., and Miller, V. L. (1995). Pathogenesis of defined invasion mutants of *Yersinia enterocolitica* in a BALB/c mouse model of infection. *Infect. Immun.* 63, 4837–4848. doi: 10.1128/iai.63.12.4837-4848.1995

Rabenstein, D. L. (2002). Heparin and heparan sulfate: structure and function. *Nat. Prod. Rep.* 19, 312–331. doi: 10.1039/b100916h

Rajas, O., Quirós, L. M., Ortega, M., Vazquez-Espinosa, E., Merayo-Lloves, J., Vazquez, F., et al. (2017). Glycosaminoglycans are involved in bacterial adherence to lung cells. *BMC Infect. Dis.* 17:319. doi: 10.1186/s12879-017-2418-5

Rustmeier, N. H., Strebl, M., and Stehle, T. (2019). The symmetry of viral sialic acid binding sites-implications for antiviral strategies. *Viruses* 11, 1–15. doi: 10.3390/v11100947

Sahdev, S., Khattar, S. K., and Saini, K. S. (2008). Production of active eukaryotic proteins through bacterial expression systems: a review of the existing biotechnology strategies. *Mol. Cell. Biochem.* 307, 249–264. doi: 10.1007/s11010-007-9603-6

Saragliadis, A., and Linke, D. (2019). Assay development for the discovery of small-molecule inhibitors of YadA adhesion to collagen. *Cell Surface* 5:100025. doi: 10.1016/j.tcsw.2019.100025

Sauer, M. M., Jakob, R. P., Luber, T., Canonica, F., Navarra, G., Ernst, B., et al. (2019). Binding of the bacterial Adhesin FimH to its natural, multivalent high-mannose type glycan targets. *J. Am. Chem. Soc.* 141, 936–944. doi: 10.1021/jacs.8b10736

Schindler, M. K. H., Schutz, M. S., Muhlenkamp, M. C., Rooijakkers, S. H. M., Hallstrom, T., Zipfel, P. F., et al. (2012). *Yersinia enterocolitica* YadA mediates complement evasion by recruitment and inactivation of C3 products. *J. Immunol.* 189, 4900–4908. doi: 10.4049/jimmunol.1201383

Schulze-Koops, H., Burkhardt, H., Heesemann, J., Kirsch, T., Swoboda, B., Bull, C., et al. (1993). Outer membrane protein YadA of enteropathogenic yersiniae mediates specific binding to cellular but not plasma fibronectin. *Infect. Immun.* 61, 2513–2519. doi: 10.1098/rspb.2017.0729

Schütz, M., Weiss, E. M., Schindler, M., Hallström, T., Zipfel, P. F., Linke, D., et al. (2010). Trimer stability of YadA is critical for virulence of *Yersinia enterocolitica*. *Infect. Immun.* 78, 2677–2690. doi: 10.1128/IAI.01350-09

Shahid, S. A., Nagaraj, M., Chauhan, N., Franks, T. W., Bardiaux, B., Habeck, M., et al. (2015). Solid-state NMR study of the YadA Membrane-anchor domain in the bacterial outer membrane. *Angew. Chem. Int. Edn.* 54, 12602–12606. doi: 10.1002/anie.201505506

Shriver, Z., Capila, I., Venkataraman, G., and Sasisekharan, R. (2012). Heparin and heparan sulfate: analyzing structure amd microheterogeneity. *Handb. Exp. Pharmacol.* 207, 159–176. doi: 10.1007/978-3-642-23056-1_3

Sorin, M. N., Kuhn, J., Stasiak, A. C., and Stehle, T. (2021). Structural insight into non-enveloped virus binding to glycosaminoglycan receptors: a review. *Viruses* 13, 1–11. doi: 10.3390/v13050800

Stockmann, A., Hess, S., Declerck, P., Timpl, R., and Preissner, K. T. (1993). Multimeric vitronectin. Identification and characterization of conformation-dependent self-association of the adhesive protein. *J. Biol. Chem.* 268, 22874–22882. doi: 10.1016/s0021-9258(18)41608-0

Tamm, A., Tarkkanen, A. M., Korhonen, T. K., Kuusela, P., Toivanen, P., and Skurnik, M. (1993). Hydrophobic domains affect the collagen-binding specificity and surface polymerization as well as the virulence potential of the YadA Protein of *Yersinia enterocolitica*. *Mol. Microbiol.* 10, 995–1011. doi: 10.1111/j.1365-2958.1993.tb00971.x

Tertti, R., Skurnik, M., Vartio, T., and Kuusela, P. (1992). Adhesion protein YadA of *Yersinia* species mediates binding of bacteria to fibronectin. *Infect. Immun.* 60, 3021–3024. doi: 10.1128/iai.60.7.3021-3024.1992

Toivanen, P., and Skurnik, M. (1992). LcrF is the temperature-regulated activator of the YadA gene of *Yersinia enterocolitica* and *Yersinia pseudotuberculosis*. *J. Bacteriol.* 174, 2047–2051. doi: 10.1128/jb.174.6.2047-2051.1992

Trunk, T., Khalil, H. S., and Leo, J. C. (2018). Bacterial autoaggregation. *AIMS Microbiol.* 4, 140–164. doi: 10.3934/microbiol.2018.1.140

Varki, A., Esko, J. D., and Colley, K. J. (2009). *Essentials of Glycobiology*, 2nd Edn. Cold Spring Harbor, NY: Cold Spring Harbor Laboratory Press.

Vizarraga, D., Torres-Puig, S., Aparicio, D., and Pich, O. Q. (2021). The sialoglycan binding adhesins of *Mycoplasma genitalium* and *Mycoplasma pneumoniae*. *Trend Microbiol.* 29, 477–481. doi: 10.1016/j.tim.2021.01.011

Weiss, G. L., Stanisich, J. J., Sauer, M. M., Lin, C.-W., Eras, J., Zyla, D. S., et al. (2020). Filaments in urinary tract infections. *Science* 369, 1005–1010. doi: 10.1126/science.aaz9866

Westerlund, B., and Korhonen, T. K. (1993). Bacterial proteins binding to the mammalian extracellular matrix. *Mol. Microbiol.* 9, 687–694. doi: 10.1111/j.1365-2958.1993.tb01729.x

Zhuang, P., Li, H., Williams, J. G., Wagner, N. V., Seiffert, D., and Peterson, C. B. (1996). Characterization of the denaturation and renaturation of human plasma vitronectin II. Investigation into the mechanism of formation of multimers. *J. Biol. Chem.* 271, 14333–14343. doi: 10.1074/jbc.271.24.14333

Conflict of Interest: The authors declare that the research was conducted in the absence of any commercial or financial relationships that could be construed as a potential conflict of interest.

Publisher's Note: All claims expressed in this article are solely those of the authors and do not necessarily represent those of their affiliated organizations, or those of the publisher, the editors and the reviewers. Any product that may be evaluated in this article, or claim that may be made by its manufacturer, is not guaranteed or endorsed by the publisher.

frontiers in Microbiology

ORIGINAL RESEARCH
published: 10 February 2022
doi: 10.3389/fmicb.2022.811932

Identification of Type VI Secretion Systems Effector Proteins That Contribute to Interbacterial Competition in *Salmonella* Dublin

*Fernando A. Amaya[1†], Carlos J. Blondel[2†], María F. Barros-Infante[3], Dácil Rivera[4], Andrea I. Moreno-Switt[5,6], Carlos A. Santiviago[1]*and David Pezoa[3]**

[1]*Laboratorio de Microbiología, Departamento de Bioquímica y Biología Molecular, Facultad de Ciencias Químicas y Farmacéuticas, Universidad de Chile, Santiago, Chile,* [2]*Instituto de Ciencias Biomédicas, Facultad de Medicina y Facultad de Ciencias de la Vida, Universidad Andrés Bello, Santiago, Chile,* [3]*Escuela de Medicina Veterinaria, Facultad de Ciencias, Universidad Mayor, Santiago, Chile,* [4]*Escuela de Medicina Veterinaria, Facultad de Ciencias de la Vida, Universidad Andrés Bello, Santiago, Chile,* [5]*Escuela de Medicina Veterinaria, Facultad de Agronomía e Ingeniería Forestal, Facultad de Ciencias Biológicas y Facultad de Medicina, Pontificia Universidad Católica de Chile, Santiago, Chile,* [6]*Millennium Initiative on Collaborative Research on Bacterial Resistance (MICROB-R), Santiago, Chile*

OPEN ACCESS

Edited by:
Eric Cascales,
Aix-Marseille Université, France

Reviewed by:
Qiyao Wang,
East China University of Science and Technology, China
Casey Fowler,
University of Alberta, Canada

***Correspondence:**
Carlos A. Santiviago
csantiviago@ciq.uchile.cl
David Pezoa
david.pezoa@umayor.cl

[†]These authors have contributed equally to this work and share first authorship

Specialty section:
This article was submitted to Microbial Physiology and Metabolism, a section of the journal Frontiers in Microbiology

Received: *09 November 2021*
Accepted: *04 January 2022*
Published: *10 February 2022*

Citation:
Amaya FA, Blondel CJ, Barros-Infante MF, Rivera D, Moreno-Switt AI, Santiviago CA and Pezoa D (2022) Identification of Type VI Secretion Systems Effector Proteins That Contribute to Interbacterial Competition in Salmonella Dublin. Front. Microbiol. 13:811932. doi: 10.3389/fmicb.2022.811932

The Type VI Secretion System (T6SS) is a multiprotein device that has emerged as an important fitness and virulence factor for many Gram-negative bacteria through the injection of effector proteins into prokaryotic or eukaryotic cells *via* a contractile mechanism. While some effector proteins specifically target bacterial or eukaryotic cells, others can target both types of cells (trans-kingdom effectors). In *Salmonella*, five T6SS gene clusters have been identified within pathogenicity islands SPI-6, SPI-19, SPI-20, SPI-21, and SPI-22, which are differentially distributed among serotypes. *Salmonella enterica* serotype Dublin (*S*. Dublin) is a cattle-adapted pathogen that harbors both $T6SS_{SPI-6}$ and $T6SS_{SPI-19}$. Interestingly, while both systems have been linked to virulence and host colonization in *S.* Dublin, an antibacterial activity has not been detected for $T6SS_{SPI-6}$ in this serotype. In addition, there is limited information regarding the repertoire of effector proteins encoded within $T6SS_{SPI-6}$ and $T6SS_{SPI-19}$ gene clusters in *S.* Dublin. In the present study, we demonstrate that $T6SS_{SPI-6}$ and $T6SS_{SPI-19}$ of *S.* Dublin CT_02021853 contribute to interbacterial competition. Bioinformatic and comparative genomic analyses allowed us to identify genes encoding three candidate antibacterial effectors located within SPI-6 and two candidate effectors located within SPI-19. Each antibacterial effector gene is located upstream of a gene encoding a hypothetic immunity protein, thus conforming an effector/immunity (E/I) module. Of note, the genes encoding these effectors and immunity proteins are widely distributed in *Salmonella* genomes, suggesting a relevant role in interbacterial competition and virulence. Finally, we demonstrate that E/I modules SED_RS01930/SED_RS01935 (encoded in SPI-6), SED_RS06235/SED_RS06230, and SED_RS06335/SED_RS06340 (both encoded in SPI-19) contribute to interbacterial competition in *S.* Dublin CT_02021853.

Keywords: *Salmonella* Dublin, interbacterial competition, T6SS, effector, immunity protein

INTRODUCTION

Salmonellosis is a foodborne bacterial disease caused by different serotypes of *Salmonella enterica* (GBD-2017 et al., 2019). Worldwide, this illness is linked to 95.1 million cases of gastroenteritis per year (GBD-2017 et al., 2019). The genus *Salmonella* includes more than 2,600 serotypes (also referred to as serovars) distributed between species *S. enterica* and *S. bongori* (Issenhuth-Jeanjean et al., 2014), which differ in clinical signs and host range (Uzzau et al., 2000). *Salmonella enterica* serotype Dublin (*S.* Dublin) represents a cattle-adapted pathogen that can lead to serious economic problems in bovine production, where it causes a severe systemic disease (Hoelzer et al., 2011; Nielsen et al., 2013). In addition, *S.* Dublin may constitute a serious risk for public health due to ingestion of contaminated milk by the human population (Small and Sharp, 1979; Fierer, 1983).

The Type VI Secretion System (T6SS) has emerged as an important fitness and virulence factor for many Gram-negative bacteria (Records, 2011; Basler, 2015; Alteri and Mobley, 2016; Cianfanelli et al., 2016; Navarro-Garcia et al., 2019). The T6SS is a molecular nanomachine consisting of three main complexes: a contractile tail, a membrane complex, and a baseplate (Aschtgen et al., 2008; Zoued et al., 2014; Durand et al., 2015; Brunet et al., 2015b; Logger et al., 2016; Nazarov et al., 2018; Rapisarda et al., 2019; Yin et al., 2019). The contractile tail is composed of an internal tube generated by the polymerization of a hexameric protein called Hcp, where a needle-shaped VgrG protein trimer is assembled at the tip. VgrG proteins are often associated with proteins harboring a N-terminal PAAR motif that sharpen the tip (Ballister et al., 2008; Shneider et al., 2013; Brunet et al., 2014, 2015b; Douzi et al., 2014; Zoued et al., 2014; Renault et al., 2018). The internal tube is surrounded by a contractile sheath formed by the polymerization of TssB and TssC subunits (Leiman et al., 2009; Basler, 2015; Durand et al., 2015). Contraction of the sheath provides the energy required for the injection of effector proteins that are confined within the Hcp tube, bound to VgrG and/or associated with PAAR proteins (Silverman et al., 2013). Secreted effectors are delivered fused to VgrG and/or PAAR proteins (evolved or specialized effectors) or through non-covalent interaction with some core components (cargo effectors) (Durand et al., 2014; Whitney et al., 2014; Diniz and Coulthurst, 2015; Ma et al., 2017b; Pissaridou et al., 2018). Notably, both antibacterial and antieukaryotic effector proteins have been identified (Feria and Valvano, 2020; Hernandez et al., 2020), highlighting the role of T6SSs as key players in processes, such as interbacterial competition and host–pathogen interaction (Ma and Mekalanos, 2010; Russell et al., 2012, 2013; Koskiniemi et al., 2013; Miyata et al., 2013; Srikannathasan et al., 2013; Whitney et al., 2013; Egan et al., 2015; Bondage et al., 2016; Flaugnatti et al., 2016; Tang et al., 2018; Ting et al., 2018; Ahmad et al., 2019; Berni et al., 2019; Coulthurst, 2019; Jana et al., 2019; Mariano et al., 2019; Wood et al., 2020). Antibacterial effectors include, among others, those targeting the peptide or glycosidic bonds of peptidoglycan (Ma and Mekalanos, 2010; Russell et al., 2012; Srikannathasan et al., 2013; Whitney et al., 2013; Berni et al., 2019; Wood et al., 2019), or the FtsZ cell division ring (Ting et al., 2018). These antibacterial effectors are usually encoded along with their cognate immunity proteins in bicistronic elements known as effector/immunity (E/I) modules. Immunity proteins bind tightly and specifically to their cognate effector preventing self-intoxication and killing of sibling cells (Russell et al., 2012). Antieukaryotic effectors include, among others, those targeting the actin or microtubule cytoskeleton networks, the endoplasmic reticulum, lipid membranes, and others that activate the AIM2 inflammasome and decrease the levels of reactive oxygen species contributing to survival in macrophages (Pukatzki et al., 2007; Ma et al., 2009; Ma and Mekalanos, 2010; Miyata et al., 2011; Zheng et al., 2011; Durand et al., 2012; Lindgren et al., 2013; Schwarz et al., 2014; Heisler et al., 2015; Sana et al., 2015; Aubert et al., 2016; Jiang et al., 2016; Ray et al., 2017; Dutta et al., 2019; Tan et al., 2019; Wood et al., 2019). In addition, effectors presenting both antibacterial and antieukaryotic activity (defined as trans-kingdom effectors) include, among others, those targeting conserved molecules (e.g., NAD) or macromolecules (e.g., DNA and phospholipids), or those forming pores in biological membranes (Whitney et al., 2015; Tang et al., 2018; Ahmad et al., 2019).

In *Salmonella*, five T6SS gene clusters have been identified within pathogenicity islands SPI-6, SPI-19, SPI-20, SPI-21, and SPI-22 (Blondel et al., 2009; Fookes et al., 2011). These T6SSs are distributed in four different evolutionary lineages: $T6SS_{SPI-6}$ belongs to subtype i3, $T6SS_{SPI-19}$ to subtype i1, $T6SS_{SPI-20}$ and $T6SS_{SPI-21}$ to subtype i2, and $T6SS_{SPI-22}$ to subtype i4a (Bao et al., 2019). In addition to their distinct evolutionary origin, these five T6SS clusters are differentially distributed among distinct serotypes, subspecies, and species of *Salmonella* (Blondel et al., 2009; Fookes et al., 2011).

Notably, while both $T6SS_{SPI-6}$ and $T6SS_{SPI-19}$ have been linked to antibacterial competition, virulence, and host colonization in different *Salmonella* serotypes (Blondel et al., 2010, 2013; Libby et al., 2010; Wang et al., 2011, 2019; Mulder et al., 2012; Pezoa et al., 2013; Koskiniemi et al., 2014; Brunet et al., 2015a; Sana et al., 2016; Schroll et al., 2019; Sibinelli-Sousa et al., 2020; Xian et al., 2020), there is limited information regarding the effector proteins encoded within the corresponding gene clusters among different *Salmonella* serotypes. Furthermore, the contribution of both T6SSs to these phenotypes seems to differ between strains within the same serotype (Schroll et al., 2019). This appears to be the case for different *S.* Dublin strains. While $T6SS_{SPI-19}$ has been shown to be dispensable for colonization of either chickens or mice by *S.* Dublin CT_02021853 (Pezoa et al., 2014), it has been shown to be required for efficient intestinal colonization of mice by *S.* Dublin 2229 (Schroll et al., 2019). Furthermore, it has been reported that $T6SS_{SPI-19}$ of *S.* Dublin 2229 contributes to interbacterial competition (Schroll et al., 2019), reminiscent of what has been shown

for $T6SS_{SPI-6}$ of *S.* Typhimurium (Brunet et al., 2015a; Sana et al., 2016). Interestingly, the contribution of $T6SS_{SPI-6}$ to interbacterial competition has not been assessed in *S.* Dublin and there is a lack of information regarding the presence of antibacterial and/or antieukaryotic effector proteins encoded in the SPI-6 and SPI-19 T6SS gene clusters present in this serotype.

In the present study, we evaluated the contribution of $T6SS_{SPI-6}$ and $T6SS_{SPI-19}$ to interbacterial competition by *S.* Dublin CT_02021853 and performed an *in silico* analysis of both T6SS gene clusters to identify putative effector and cognate immunity proteins. First, we observed that *S.* Dublin CT_02021853 outcompeted a susceptible *Escherichia coli* strain in the presence of bile salts, as reported in the case of *S.* Dublin 2229 (Schroll et al., 2019). In addition, we found that both $T6SS_{SPI-6}$ and $T6SS_{SPI-19}$ contribute to interbacterial competition by this strain. Subsequently, a comprehensive bioinformatic analysis identified five high-confidence potential new effector and immunity proteins encoded within SPI-6 and SPI-19 T6SS gene clusters in *S.* Dublin CT_02021853. The bioinformatic analysis was based on four distinct criteria, including prediction of E/I modules by the Bastion6 prediction pipeline, identification of conserved domains and motifs linked to known T6SS effectors, and remote homology prediction by the HHpred HMM-HMM prediction pipeline. Finally, we confirmed the participation of E/I modules SED_RS01930/SED_RS01935, SED_RS06235/SED_RS06230, and SED_RS06335/SED_RS06340 of *S.* Dublin CT_02021853 in interbacterial competition.

MATERIALS AND METHODS

Bacterial Strains and Growth Conditions

The bacterial strains used in this study are listed in **Table 1**. Bacteria were routinely grown in Luria-Bertani (LB) broth (10 g/L tryptone, 5 g/L yeast extract, 5 g/L NaCl) at 37°C with aeration. LB broth was supplemented with ampicillin (Amp; 100 μg/ml), kanamycin (Kan; 50 μg/ml), chloramphenicol (Cam; 20 μg/ml), or nalidixic acid (Nal; 15 μg/ml), as needed. LB medium was solidified by addition of agar (15 g/L). For interbacterial competition assays bacteria were incubated on MacConkey agar plates at 37°C for 24 h.

Standard DNA Techniques

Plasmid DNA was isolated using the "QIAprep Spin Miniprep Kit" (QIAGEN, MD, United States). PCR products were purified using the "QIAquick PCR Purification Kit" (QIAGEN, MD, United States). DNA samples were analyzed by electrophoresis in 1% agarose gels and were visualized under UV light after RedGel (Biotium, CA, United States) staining. Primers were designed using the "Vector NTI Advance 11.0" software (Invitrogen, CA, United States) and are listed in **Table 2**. PCR products were amplified in a "MultiGene TC9600-G" thermal cycler (LabNet, NJ, United States). PCR reaction mixes contained 1X buffer, 2 mM $MgCl_2$, 100 nM dNTPs, 100 nM of each primer, 100 ng of template DNA and 0.5–1 U of HiFi DNA pol (KAPA, MA, United States). Standard conditions for amplification were: 2 min at 95°C, followed by 30–35 cycles of 94°C for 45 s, 55°C for 30 s, and 72°C for a suitable time (1 min/kb) according to DNA polymerase processivity, and a final extension step at 72°C for 5 min.

TABLE 1 | Bacterial strains and plasmids used in this study.

Strains	Features	Source or reference
Escherichia coli		
DH5α	F^- Φ80Δ*lacZ*(M15) Δ(*lacZYA-argF*)*U169* deoR *recA1 endA1 hsdR17*(r_k^-, m_k^+) *phoA supE44 thi-1 gyrA96 relA1* λ^-	Laboratory collection
***Salmonella* Dublin**		
CT_02021853	Wild-type strain	Laboratory collection
$\Delta T6SS_{SPI-6}$	CT_02021853 Δ(SED_RS01790-SED_RS25725)::Kan	This study
$\Delta T6SS_{SPI-19}$	CT_02021853 Δ(SED_RS06220-SED_RS06380)::Kan	This study
$\Delta T6SS_{SPI-6}$ $\Delta T6SS_{SPI-19}$	CT_02021853 Δ(SED_RS01790-SED_RS25725)::FRT Δ(SED_RS06220-SED_RS06380)::Cam	This study
Δ*phoN*::Kan	CT_02021853 Δ(SED_RS22655)::Kan	This study
Δ(SED_RS01930)::FRT Δ*phoN*::Kan	CT_02021853 Δ(SED_RS01930)::FRT Δ(SED_RS22655)::Kan	This study
Δ(SED_RS01930)::FRT Δ*phoN*::Cam	CT_02021853 Δ(SED_RS01930)::FRT Δ(SED_RS22655)::Cam	This study
Δ(SED_RS01930-SED_RS01935)::FRT Δ*phoN*::Cam	CT_02021853 Δ(SED_RS01930-SED_RS01935)::FRT Δ(SED_RS22655)::Cam	This study
Δ(SED_RS06235)::FRT Δ*phoN*::Kan	CT_02021853 Δ(SED_RS06235)::FRT Δ(SED_RS22655)::Kan	This study
Δ(SED_RS06235)::FRT Δ*phoN*::Cam	CT_02021853 Δ(SED_RS06235)::FRT Δ(SED_RS22655)::Cam	This study
Δ(SED_RS06235-SED_RS06230)::FRT Δ*phoN*::Cam	CT_02021853 Δ(SED_RS06235-SED_RS06230)::FRT Δ(SED_RS22655)::Cam	This study
Δ(SED_RS06335)::FRT Δ*phoN*::Kan	CT_02021853 Δ(SED_RS06335)::FRT Δ(SED_RS22655)::Kan	This study
Δ(SED_RS06335)::FRT Δ*phoN*::Cam	CT_02021853 Δ(SED_RS06335)::FRT Δ(SED_RS22655)::Cam	This study
Δ(SED_RS06335-SED_RS06340)::FRT Δ*phoN*::Cam	CT_02021853 Δ(SED_RS06335-SED_RS06340)::FRT Δ(SED_RS22655)::Cam	This study
Plasmids		
pKD46	*bla* P_{BAD} *bet gam exo oriR101*(TS), Amp^R	Datsenko and Wanner, 2000
pCP20	*bla cat cI857* λP_R *flp oriR101*(TS), Cam^R, Amp^R	Cherepanov and Wackernagel, 1995
pCLF2	Red-swap redesigned vector, Cam^R	GenBank HM047089
pCLF4	Red-swap redesigned vector, Kan^R	GenBank EU629214

TABLE 2 | Primers used in this study.

Primer	Sequence[a]
SPI-6_T6SS_(H1 + P1)	AGGGTGTTTTTATACATCCTGTGAAGTAAAAAAAACCGTA*GTGTAGGCTGGAGCTGCTTC*
SPI-6_T6SS_(H2 + P2)	GTGAACATGGCACATTAATTTGAAGCAGCTCTCATCCGGT*CATATGAATATCCTCCTTAG*
SPI-6_T6SS_Out5	CCGAAGTGTATCTGGCGATGA
SPI-19_T6SS_(H1 + P1)	TAGCTGAATTGCAATATGCGAAAAAAGCCGAGCTTGATGACAAAC*GTGTAGGCTGGAGCTGCTTC*
SPI-19_T6SS_(H2 + P2)	AAGCATCTTCAATAATCACGGGTATAAATGCTTACACTCTTTATC*CATATGAATATCCTCCTTAG*
SPI-19_T6SS_Out5	ATCCGGCATGTTCTTGCG
SED_RS01930_(H1 + P1)	CAACGACTGCATGACGATGCACCGGGAGCCGGGCGGCGAAG*TGCAGGCTGGAGCTGCTTC*
SED_RS01930_(H2 + P2)	TCATCAAGAGTCATGATATTGGCCTTTGAGGTTTGGATGGC*ATATGAATATCCTCCTTAG*
SED_RS01935_(H2 + P2)	CCGGCTGTCATTATATCTTATCTGATACTGAAAAACCAAAC*ATATGAATATCCTCCTTAG*
SED_RS01930_Out5	ACCTTCAATACAGCCCCACA
SED_RS06235_(H1 + P1)	AGGGTTGCACATGGTAAATCGCACAGCATCGGCACACAAAG*TGCAGGCTGGAGCTGCTTC*
SED_RS06235_(H2 + P2)	CTTGTAAACGTTATTTACTCTCATCTGCGACAATGAGAGC*CATATGAATATCCTCCTTAG*
SED_RS06230_(H2 + P2)	ATAATAACCTCTATATATAATCGTTAAGCCATTTTATTTG*CATATGAATATCCTCCTTAG*
SED_RS06235_Out5	TTTCTCGATTGCGCATGTAGTC
SED_RS06335_(H1 + P1)	AGAAATAAAGATGAGCGGAAAACCAGCGGCGCGTCAGGGC*GTGCAGGCTGGAGCTGCTTC*
SED_RS06335_(H2 + P2)	ATCTTTATCATCAGTATTTCATCCTTGGTGGGATTCCCATC*ATATGAATATCCTCCTTAG*
SED_RS06340_(H2 + P2)	CTATGAAATATTAGTGATTATCTTCATATATATATATTCT*CATATGAATATCCTCCTTAG*
SED_RS06335_Out5	GCGGTATTTTTCTGAACGGCA
phoN_SDu_(H1 + P1)	GTGAGTCTTTATGAAAAGTCGTTATTTAGTATTTTTTCTA*GTGCAGGCTGGAGCTGCTTC*
phoN_SDu_(H2 + P2)	ACTTTCACCTTCAGTAATTAAGTTCGGGGTGATCTTCTTT*CATATGAATATCCTCCTTAG*
phoN_SDu_Out5	TTGCCTGATCCGGAGTGA
K1	CAGTCATAGCCGAATAGCCT
C3	CAGCTGAACGGTCTGGTTATAGG

[a]*Italics indicate the region that anneals to the 5′ or 3′ end of the antibiotic resistance cassette used for the mutagenesis.*

Construction of *Salmonella* Dublin Mutant Strains

Derivatives of *S.* Dublin CT_02021853 with deletions of single genes or gene clusters were constructed by the one-step inactivation procedure using the Lambda Red recombination system (Datsenko and Wanner, 2000), with modifications (Santiviago et al., 2009). The oligonucleotides used for mutagenesis (**Table 2**) were designed with 40 bases at the 5′ ends identical to the ends of the corresponding deletion, and 20 bases at the 3′ ends that anneal with the 5′ or 3′ end of a Cam or Kan resistance cassette flanked by Flp recombinase target (FRT) sites present in plasmids pCLF2 (GenBank accession number HM047089) and pCLF4 (GenBank accession number EU629214.1), respectively. These plasmids were used as templates for the corresponding amplification of PCR products. *S.* Dublin CT_02021853 carrying the plasmid pKD46, which expresses the Lambda Red recombination system, was grown to an OD_{600nm} of 0.6 at 30°C in LB broth supplemented with Amp and L-arabinose (10 mM). Then, bacteria were made electrocompetent by serial washes with ice-cold, sterile 15% glycerol and transformed by electroporation with 500–600 ng of each PCR product. Transformants were selected on LB agar supplemented with the corresponding antibiotic at 37°C. Correct allelic replacement in each mutant was confirmed by PCR amplification using specific forward primers (Out5) together with reverse primer K1 (that hybridizes within the Kan resistance cassette) or reverse primer C3 (that hybridizes within the Cam resistance cassette; **Table 2**).

When required, the antibiotic resistance cassette was removed by transforming each mutant with the temperature-sensitive plasmid pCP20, which encodes the Flp recombinase (Cherepanov and Wackernagel, 1995). Transformants were selected at 30°C on LB agar plates containing Amp. A few colonies were streaked two consecutive times at 37°C on LB agar plates and tested for the loss of the antibiotic resistance cassettes and pCP20 by patching them on LB agar plates containing Kan or Cam plus Amp. The absence of the antibiotic resistance cassette was confirmed by PCR amplification using primers flanking the sites of substitution (**Table 2**). Finally, to differentiate between *S.* Dublin strains in our interbacterial competition assays, a Kan or Cam resistance cassette was incorporated at a neutral position (i.e., replacing the ORF of *phoN* gene) in the chromosome of the attacker or the prey strain, respectively. To do this, phage P22 HT 105-1 *int*-201 was used to transduce mutant alleles Δ*phoN*::Kan and Δ*phoN*::Cam into the corresponding mutant strains harboring unmarked deletions of genes encoding effectors or E/I protein pairs.

Interbacterial Competition Assays

Competition assays were performed as described (Ma et al., 2018), with modifications. Briefly, attacker and prey bacteria were grown overnight in LB broth at 37°C. An aliquot (1 ml) of each culture was spun down, and the supernatant was discarded. Each bacterial pellet was washed three times in PBS, adjusted to an OD_{600nm} of 0.5, and mixed at a 1:1 (attacker/prey) ratio. Then, 25 µl of the mixture was incubated at 37°C for 24 h in triplicate on MacConkey agar plates, a condition reported to induce the expression of T6SS gene clusters in *Salmonella* (Schroll et al., 2019). After incubation, the bacterial mixtures were scraped from the plates and resuspended in 1 ml of PBS, and CFU were determined by plating of serial dilutions on LB agar supplemented with suitable antibiotics. Statistical significance was determined using a one-way ANOVA followed by Tukey's multiple comparisons test using GraphPad Prism 9.0 software.

Bioinformatics Analyses

To identify putative T6SS effectors encoded within SPI-6 and SPI-19 in *S.* Dublin CT_02021853, each ORF of both pathogenicity islands was analyzed with the Bastion6 pipeline (Wang et al., 2018) excluding those encoding the 13 structural components of the T6SS. ORFs presenting a Bastion6 score ≥ 0.7 were considered as putative T6SS effectors. Each Bastion6 prediction was also analyzed to determine if it was part of a bicistron encoding a putative immunity protein [i.e., a small protein with potential signal peptides (SignalP) and/or transmembrane domains (TMHMM)] with the Operon-Mapper web server (Taboada et al., 2018). Identification of conserved functional domains and motifs was performed using the PROSITE, NCBI-CDD, Motif-finder, and Pfam databases (Kanehisa et al., 2002; Sigrist et al., 2013; Finn et al., 2014; Lu et al., 2019) with the GenomeNet search engine. An e-value cutoff score of 0.01 was used. Finally, for each putative effector and immunity protein identified, a biochemical functional prediction was performed *via* HMM homology searches using the HHpred HMM-HMM comparison tool (Zimmermann et al., 2017).

Sequence and Phylogenetic Analysis

Identification of T6SS effector orthologs was carried out using the DNA sequence of each effector/immunity module in BLASTn analyses using publicly available bacterial genome sequences of the NCBI database (January 2021). An 80% identity and 80% sequence coverage threshold were used to select positive matches. Sequence conservation was analyzed by multiple sequence alignments using MAFFT (Katoh et al., 2017) and T-Coffee Expresso (Notredame et al., 2000) and visualized by ESPript 3 (Robert and Gouet, 2014). Comparative genomic analysis of T6SS gene clusters was performed using the multiple aligner Mauve (Darling et al., 2004) and EasyFig v2.2.2 (Sullivan et al., 2011). Nucleotide sequences were analyzed by the sequence visualization and annotation tool Artemis version 18 (Rutherford et al., 2000).

RESULTS AND DISCUSSION

The T6SSs Encoded in SPI-6 and SPI-19 Contribute to Interbacterial Competition by *S.* Dublin CT_02021853

To determine the contribution of $T6SS_{SPI-6}$ and $T6SS_{SPI-19}$ to interbacterial competition by *S.* Dublin CT_02021853, we performed a competition assay in MacConkey agar as it has been shown that bile salts upregulate the expression of T6SS-related genes in *S.* Typhimurium and *S.* Dublin strains (Brunet et al., 2015a; Sana et al., 2016; Schroll et al., 2019). We decided to use mutant strains lacking the complete SPI-6 and/or SPI-19 T6SS gene clusters rather than single mutants in key structural components to avoid potential cross-complementation between components of both T6SS gene clusters as reported in other systems (Santos et al., 2020). We observed that the *E. coli* DH5α prey strain was significantly outcompeted after coincubation with *S.* Dublin CT_02021853. Of note, the ability of derivative strains $\Delta T6SS_{SPI-6}$ and $\Delta T6SS_{SPI-19}$ to outcompete the *E. coli* prey strain was similar to the wild-type strain, recovering 1,000-fold lower CFU of *E. coli* after coincubation (**Figure 1**). Remarkably, the ability of a $\Delta T6SS_{SPI-6}$ $\Delta T6SS_{SPI-19}$ double mutant to outcompete the *E. coli* prey strain was 100-fold lower than the wild-type strain and derivative strains $\Delta T6SS_{SPI-6}$ and $\Delta T6SS_{SPI-19}$ (**Figure 1**). These results indicate that $T6SS_{SPI-6}$ and $T6SS_{SPI-19}$ provide a competitive advantage to *S.* Dublin CT_02021853 over *E. coli* DH5α. Furthermore, having both T6SS systems does not provide an additive advantage over having only one, revealing a functional redundancy between both systems.

The SPI-6 of *S.* Dublin CT_02021853 Encodes 3 Novel Putative T6SS Effector Proteins

S. Dublin CT_02021853 encodes 3 out of 4 antibacterial E/I pairs, as well as the two orphan immunity proteins, previously described in the SPI-6 T6SS gene cluster of *S. enterica* (**Figure 2A**): (i) Tae2/TaeI2 E/I pair (SED_RS26190/SED_RS01845) present in different *Salmonella* serotypes (Russell et al., 2012), (ii) the RHS_{main} (SED_RS01910) effector protein (Koskiniemi et al., 2014), and (iii) the Tlde1/Tldi1 E/I pair (SED_RS01895/SED_RS01890; Sibinelli-Sousa et al., 2020). In contrast, *S.* Dublin CT_02021853 does not encode the Tae4/Tai4 and RHS_{orphan}/RhsI E/I pairs described in *S.* Typhimurium 14028s (Blondel et al., 2009; Koskiniemi et al., 2014; **Figure 2A**).

To gain insight into the T6SS-dependent antibacterial activity of *S.* Dublin, we performed bioinformatic and comparative genomic analyses to identify potential novel T6SS effector proteins and their cognate immunity proteins. To do this, each ORF encoded within the SPI-6 T6SS gene cluster of *S.* Dublin CT_02021853 was analyzed based on four criteria, including: (i) analysis by the Bastion6 prediction pipeline (a bioinformatics tool that predicts T6SS effectors based on amino acids sequence profile, evolutionary information, and physicochemical properties); (ii) bioinformatic analysis to identify the presence of putative immunity proteins through detection of signal peptide (SignalP), transmembrane domains (TMHMM), and operon prediction (Operon-mapper; Taboada et al., 2018); (iii) identification of conserved domains and motifs linked to known T6SS effectors (PROSITE, NCBI-CDD, Motif-finder, and Pfam databases); and (iv) functional predictions *via* HMM homology searches using the HHpred HMM-HMM prediction pipeline (Zimmermann et al., 2017). In addition, we analyzed the SPI-6 T6SS gene cluster to identify potential unannotated ORFs which could encode putative effectors and cognate immunity proteins. Our analysis identified three potential E/I pairs encoded within this T6SS gene cluster of *S.* Dublin CT_02021853 (**Figure 2B**; **Table 3**).

First, we identified an unannotated ORF located between the SED_RS24320 and SED_RS24325 ORFs. This novel ORF (Bastion6 score = 0,873) encodes a 210 amino acid protein with a predicted endonuclease RHS-HNHc protein domain (**Figure 2B**; **Table 3**). The presence of the HNHc endonuclease domain suggests that this putative protein harbors DNase

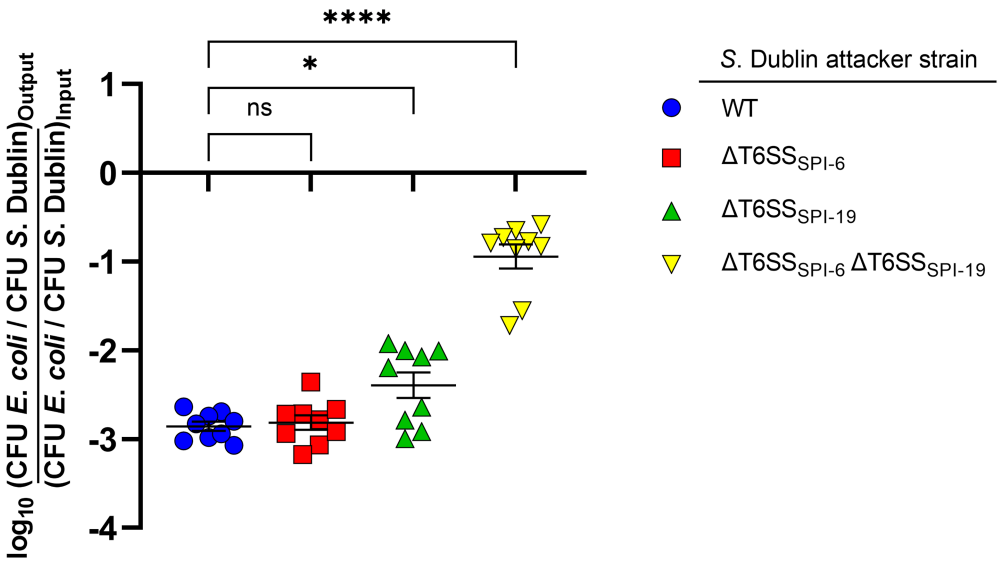

FIGURE 1 | Contribution of $T6SS_{SPI-6}$ and $T6SS_{SPI-19}$ to interbacterial competition by *S.* Dublin strain CT_02021853. Wild-type and mutant strains $\Delta T6SS_{SPI-6}$, $\Delta T6SS_{SPI-19}$, and $\Delta T6SS_{SPI-6}$ $\Delta T6SS_{SPI-19}$ of *S.* Dublin CT_02021853 were mixed at a ratio of 1:1 (attacker/prey) with *Escherichia coli* DH5α. Then, 25 μl of the mixture was incubated at 37°C for 24 h in triplicate on MacConkey agar plates. Bacterial counts recovered from each competition assay were calculated by plating serial 10-fold dilutions on LB agar plates with the appropriate antibiotics (Nal in the case of *E. coli* and Kan or Cam in the case of *S.* Dublin strains). Data show the ratio of *E. coli* CFU (prey) to *S.* Dublin CFU (attacker) normalized to the inoculum ratio and expressed as $\log_{10}$. Error bars indicate standard error. Statistical significance was determined using a one-way ANOVA followed by Tukey's multiple comparisons test (*$p < 0.05$; ****$p < 0.0001$; ns, not significant).

activity, as described for other antibacterial and antieukaryote T6SS effector proteins (Ma et al., 2017a,b). SED_RS24325 is predicted to be co-transcribed with the downstream ORF SED_RS26565, suggesting that this latter ORF is the cognate immunity protein of the putative novel effector.

A second putative effector protein was predicted to be encoded by SED_RS1930. This ORF (Bastion6 score = 0,909) encodes a large 924 amino acid protein with both a RHS and an Ntox47 protein domain, involved in degrading target cell RNA (Zhang et al., 2012). It should be noted that the Ntox47 protein domain of SED_RS1930 has similarity to the Ntox47 domain of RHS_{orphan} protein of *S.* Typhimurium 14028s (**Figure 2B**). Since RHS orphan proteins have been linked to recombination events between RHS elements generating $RHS_{main\text{-}orphan}$ chimeras (Koskiniemi et al., 2014), it is plausible that SED_RS1930 was generated through one of such events.

Finally, a third effector protein was predicted to be encoded in SED_RS24315. This ORF (Bastion6 score = 0,733) encodes a small 113 amino acid protein with similarity to bacterial polymorphic toxins in the Tox-URI2 family, a DNAse protein domain that has been linked to RHS-CT proteins exported by the T6SS (Zhang et al., 2012; Jamet and Nassif, 2015; Ma et al., 2017b). SED_RS24315 is predicted to be co-transcribed with SED_RS01915, suggesting that this latter ORF encodes the cognate immunity protein of the putative effector. Interestingly, the ORF just upstream of SED_RS24315 encodes the RHS_{main} protein (SED_RS01910). Taking into account that there are RHS proteins with C-terminal Tox-URI2 domains (Zhang et al., 2012; Ma et al., 2017b), it is possible that SED_RS01910 and SED_RS24315 were at some point a single ORF that was later split due to the accumulation of nonsense mutations.

Many T6SS-associated RHS proteins have C-terminal endonuclease effector domains, which degrade DNA or RNA in the target cell (Zhang et al., 2012). Interestingly, RHS proteins have YD-peptide repeats, which fold into a large β-cage structure that encapsulates and protects the C-terminal toxin domain and highly increase T6SS secretion efficiency (Donato et al., 2020), which could explain why many T6SS effectors are associated with RHS elements.

The SPI-19 of *S.* Dublin CT_02021853 Encodes 2 Putative T6SS Effector Proteins

As mentioned, no effector protein has been described to be encoded within the SPI-19 T6SS gene cluster in *Salmonella*, despite its clear contribution to intestinal colonization and antibacterial activity (Blondel et al., 2010; Pezoa et al., 2014; Schroll et al., 2019; Xian et al., 2020). To identify novel T6SS effector proteins encoded within SPI-19, we performed bioinformatic analyses of each ORF included in this T6SS gene cluster of *S.* Dublin CT_02021853. In addition, we performed a comparative analysis of this T6SS gene cluster with the SPI-19 T6SS gene cluster of *S.* Gallinarum SG9, as $T6SS_{SPI-19}$ activity in this strain causes cytotoxicity to primary macrophages from hens (Schroll et al., 2019).

Our analysis identified two putative T6SS effector proteins encoded in SPI-19 (**Figure 3**; **Table 4**), that are conserved in *S.* Gallinarum SG9 (**Figure 3A**). The first putative effector corresponds to SED_RS06335 (Bastion6 score = 0,939), an RHS protein that harbors an N-terminal PAAR domain and a C-terminal M91 metallopeptidase domain (**Figure 3B**). Our analysis showed that SED_RS06335 is part of a bicistronic unit with SED_RS06340.

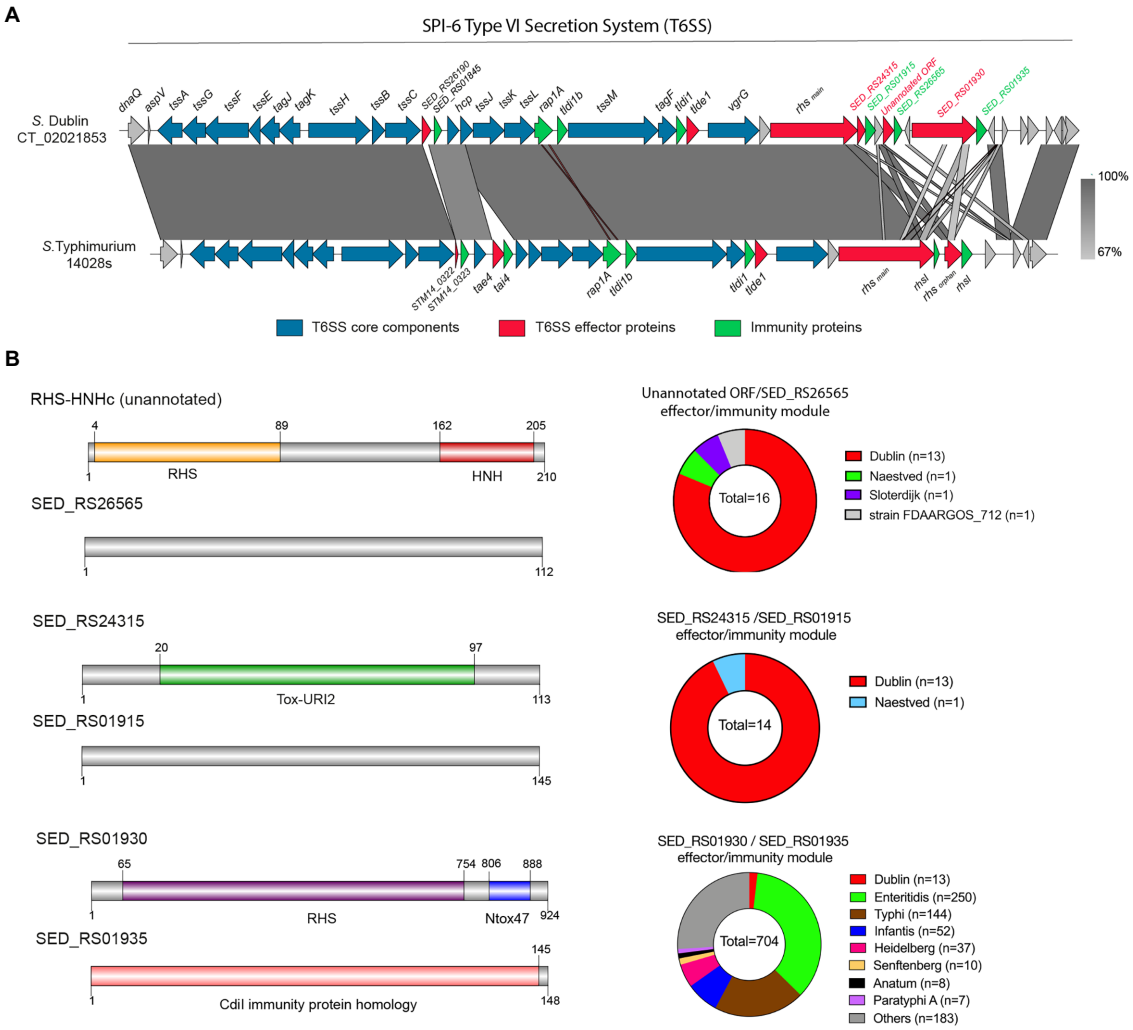

FIGURE 2 | The SPI-6 T6SS gene cluster encodes novel putative Type VI Secretion Systems (T6SS) effector proteins. **(A)** Comparative genomic analysis of the SPI-6 T6SS cluster of *S.* Dublin CT_02021853 and *S.* Typhimurium 14028s. BLASTn sequence alignment was performed and visualized using EasyFig (Sullivan et al., 2011). **(B)** Schematic representation and distribution among *Salmonella* genomes of each novel effector and immunity protein identified. Names of genes encoding novel effectors and immunity proteins are highlighted in red and green, respectively. Homologs for each component were identified by BLASTn analyses as described in Materials and Methods.

TABLE 3 | Novel predicted T6SS effectors and cognate immunity proteins encoded in SPI-6 of *Salmonella* Dublin CT_02021853.

	T6SS effector genes				Cognate T6SS immunity protein genes	
ORF (old locus annotation)	**Size (aa)**	**Bastion6 T6SE (Score)**	**Target cell**	**Predicted activity/ Domain**	**ORF/Upstream or downstream[a]**	**TM or signal peptide/Domain[b]**
Unannotated ORF	210	0,873	Prokaryotic	DNase/RHS-HNH	SED_RS26565/ Downstream	No/No
SED_RS01930 (SeD_A0317)	924	0,909	Prokaryotic	RNase/RHS-Ntox47	SED_RS01935/ Downstream	No/Cdi immunity protein homolog
SED_RS24315	113	0,733	Prokaryotic	DNase/Tox-URI2	SED_RS01915/ Downstream	No/No

[a]*This column indicates if the putative immunity protein gene (ORF) is encoded upstream or downstream the corresponding T6SS effector in a bicistronic unit.*
[b]*Presence or absence of transmembrane domains (TM) or a signal peptide and protein domains present in the putative immunity protein genes.*

This latter ORF encodes a 110 amino acid protein with a transmembrane domain that may correspond to the cognate immunity protein of SED_RS06335. A comparative analysis with the SPI-19 T6SS gene cluster of *S.* Gallinarum SG9 revealed the presence of two copies of genes encoding this PAAR-RHS effector protein in this strain (SG9_1071 and SG9_1075; **Figure 3A**). Interestingly, a M91 metallopeptidase domain is present in the trans-kingdom effector VgrG2b of *Pseudomonas aeruginosa* (Wood et al., 2019). This M91 domain of VgrG2b has been shown to be involved in the internalization of *P. aeruginosa* into host cells by interacting with the host gamma-tubulin ring complex (Sana et al., 2015) and in the antibacterial activity of the H2-T6SS (Wood et al., 2019). Our analysis of SED_RS06335 showed the presence of the HEXXH motif typically found in the catalytic site of metallopeptidases (**Supplementary Figure S1**).

Besides SED_RS06335, our bioinformatic analysis also identified another effector protein encoded within the SPI-19 T6SS gene cluster in *S.* Dublin CT_02021853. This putative effector protein is encoded in SED_RS06235 (Bastion6 score = 0,711). This ORF encodes a 290 amino acid protein with a predicted LysM domain (IPR018392) at its C-terminus. This domain is present in several T6SS effector proteins and has been linked to peptidoglycan hydrolase activity (Fitzsimons et al., 2018), suggesting that SED_RS06235 is a novel T6SS amidase effector protein with antibacterial activity. Indeed, HHPred analysis revealed the presence of a transglycosylase domain in the N-terminal region of SED_RS06235, which is consistent with the notion that this ORF encodes an antibacterial effector protein. Our analysis also revealed that SED_RS06235 is part of a bicistronic unit along with SED_RS06230. This ORF encodes a 146 amino acid protein with a periplasmic-targeting signal peptide. A sequence analysis revealed that SED_RS06230 harbors the LprI PFAM domain (PF07007). This domain is found in LprI, a *Mycobacterium tuberculosis* protein which functions as a lysozyme inhibitor (Sethi et al., 2016). This suggests that SED_RS06235/SED_RS06230 corresponds to a LysM/LysMI E/I pair. Interestingly, the LysM effector of *S.* Enteritidis (SEN1001) has been linked to the ability of the bacteria to colonize the murine host and survive within infected macrophages (Silva et al., 2012). Since SPI-19 has a large internal deletion that inactivated the $T6SS_{SPI-19}$ in *S.* Enteritidis, the mechanism involved in these processes remains unknown.

The Identified Putative T6SS Effector and Immunity Proteins Are Widely Distributed in *Salmonella* Genomes

The identification of five putative T6SS effector proteins encoded within SPI-6 and SPI-19 T6SS gene clusters of

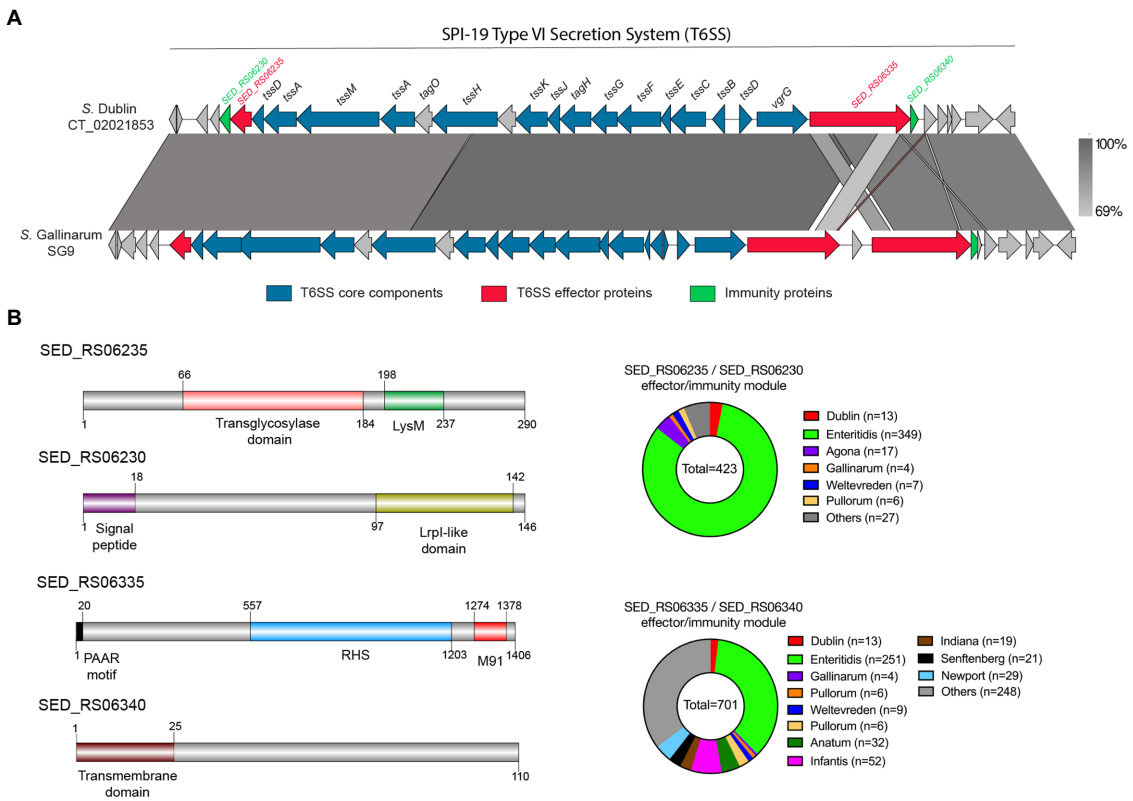

FIGURE 3 | The SPI-19 T6SS gene cluster encodes novel putative T6SS effector proteins. **(A)** Comparative genomic analysis of the SPI-19 T6SS cluster of *S.* Dublin CT_02021853 and *S.* Gallinarum SG9. BLASTn sequence alignment was performed and visualized using EasyFig (Sullivan et al., 2011). **(B)** Schematic representation and distribution among *Salmonella* genomes of each novel effector and immunity protein identified. Names of genes encoding novel effectors and immunity proteins are highlighted in red and green, respectively. Homologs for each component were identified by BLASTn analyses as described in Materials and Methods.

TABLE 4 | Novel predicted T6SS effectors and cognate immunity proteins encoded in SPI-19 of *Salmonella* Dublin CT_02021853.

T6SS effector genes					Cognate T6SS immunity protein genes	
ORF (old locus annotation)	**Size (aa)**	**Bastion6 T6SE (Score)**	**Target cell**	**Predicted activity/ Domain**	**ORF/Upstream or downstream[a]**	**TM or signal peptide/Domain[b]**
SED_RS06235 (SeD_A1215)	290	0,711	Prokaryotic	Peptidoglycan hydrolase/LysM	SED_RS06230/ Downstream	Signal peptide (Sec/SPI)/Lysozyme inhibitor domain (LprI)
SED_RS06335 (SeD_A1235)	1,406	0,939	Prokaryotic	Peptidoglycan hydrolase/PAAR-RHS-Peptidase_M91	SED_RS06340/ Downstream	1 TM/No

[a]*This column indicates if the putative immunity protein gene (ORF) is encoded upstream or downstream the corresponding T6SS effector in a bicistronic unit.*
[b]*Presence or absence of transmembrane domains (TM) or a signal peptide and protein domains present in the putative immunity protein genes.*

S. Dublin CT_02021853 prompted us to investigate the presence and distribution of these proteins in *Salmonella*. To this end, the sequence of each E/I module identified in this study was used in BLASTn searches using publicly available bacterial genome sequences and the distribution of each effector protein was determined (**Figures 2B, 3B**; **Supplementary Table S1**).

The analysis of the three putative effector proteins encoded in SPI-6 showed that only a small number of genomes harbors the unannotated E/I module SED_RS24315/SED_RS01915, and they were almost restricted to *S.* Dublin strains (**Figure 2B**). In contrast, the SED_RS01930/SED_RS01935 E/I module was found in the genome of most *Salmonella* serotypes that harbor SPI-6, including a large number of *S.* Enteritidis strains (33%). Of note, *S.* Enteritidis strains harbor an internal deletion within the SPI-6 T6SS gene cluster that is located upstream of the SED_RS01930/SED_RS01935 E/I module (Blondel et al., 2009).

The two putative effector proteins encoded in SPI-19 that we identified were also widely distributed among *Salmonella* serotypes (**Figure 3B**). Our analysis showed that the SED_RS06235/SED_RS06230 E/I module is present in the genome of strains of every *Salmonella* serotype harboring SPI-19. However, the SED_RS06335/SED_RS06340 E/I module was found in a larger number of *Salmonella* genomes, including those not previously described to carry SPI-19 (**Supplementary Table S1**). As in the case of the SED_RS01930/SED_RS01935 E/I pair encoded in SPI-6, a large number of *S.* Enteritidis strains were also found to encode the two $T6SS_{SPI-19}$ effector proteins identified in this study. Although *S.* Enteritidis strains harbor large deletions within SPI-6 and SPI-19 that most likely make the corresponding T6SSs non-functional (Blondel et al., 2009), the presence of multiple E/I modules in these clusters suggests that *S.* Enteritidis retains immunity to many $T6SS_{SPI-6}$ and $T6SS_{SPI-19}$ effector proteins.

Contribution of Selected E/I Modules to Interbacterial Competition in *S.* Dublin CT_02021853

We aimed to evaluate if a selected group of E/I modules identified by our bioinformatic analysis contribute to interbacterial competition in *S.* Dublin. To this end, we chose E/I modules SED_RS01930/SED_RS01935 (located in SPI-6), SED_RS06235/SED_RS06230, and SED_RS06335/SED_RS06340 (both located in SPI-19) and generated non-polar deletion mutants of either the effector-encoding gene or the whole E/I module in *S.* Dublin CT_02021853. Next, we performed interbacterial competition assays using different combinations of attacker and prey strains. Noteworthy, in all three E/I modules analyzed we observed that the survival of the mutant lacking the effector-encoding gene (and keeping intact the gene encoding the cognate immunity protein) was not affected after coincubation with the wild-type strain (**Figure 4**). These results indicate that each immunity protein is able to counteract the toxic activity of the cognate effector protein delivered by the attacker. In contrast, the survival of the mutant lacking the whole E/I module was reduced after coincubation with the wild-type strain. In fact, single mutants lacking E/I module SED_RS01930/SED_RS01935, SED_RS06235/SED_RS06230, and SED_RS06335/SED_RS06340 were recovered 2-, 1.5-, and 2.4-fold less than the wild-type after coincubation, respectively (**Figure 4**). Finally, the survival of mutants lacking either the effector-encoding gene or the corresponding E/I module were identical when they were coincubated (**Figure 4**). These results confirm that modules SED_RS01930/SED_RS01935, SED_RS06235/SED_RS06230, and SED_RS06335/SED_RS06340 contribute to interbacterial competition mediated by either $T6SS_{SPI-6}$ or $T6SS_{SPI-19}$ in *S.* Dublin CT_02021853. Also, these results indicate that SED_RS01930, SED_RS06235, and SED_RS06335 encode functional effector proteins, while SED_RS01935, SED_RS06230, and SED_RS06340 encode their cognate immunity proteins. Further experimental evidence is required to fully confirm that each identified effector protein is secreted *via* $T6SS_{SPI-6}$ and/or $T6SS_{SPI-19}$.

CONCLUSIONS

Altogether, our results indicate that both $T6SS_{SPI-6}$ and $T6SS_{SPI-19}$ contribute to interbacterial competition by *S.* Dublin CT_02021853. We identified novel effector proteins and cognate immunity proteins encoded in SPI-6 and SPI-19 T6SS gene clusters and confirmed the contribution of three novel E/I pairs to interbacterial competition in *S.* Dublin CT_02021853. The biochemical characterization of the putative effector proteins identified is currently undergoing in our laboratory.

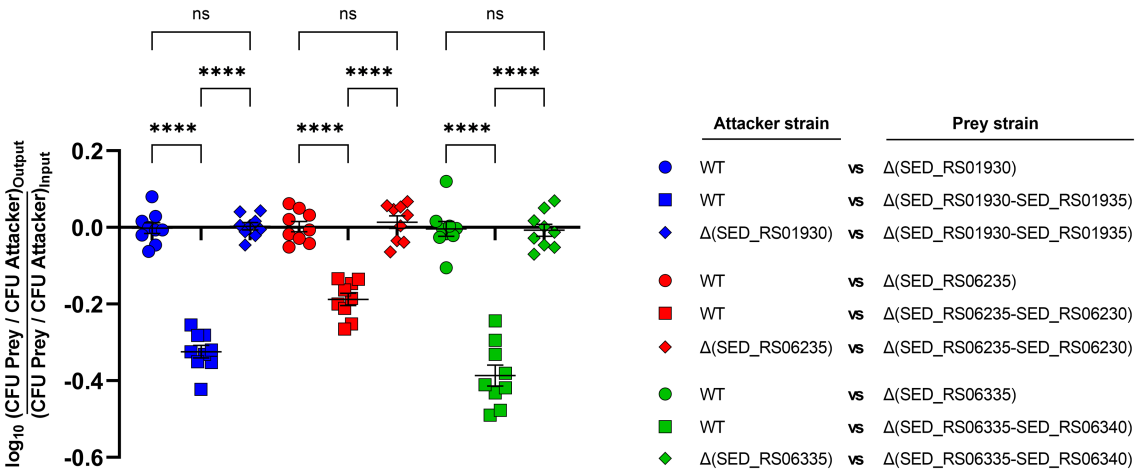

FIGURE 4 | Contribution of selected effectors and effector/immunity protein pairs to interbacterial competition in *S.* Dublin. Bacterial suspensions of attacker and prey strains adjusted to an OD_{600nm} of 0.5 were mixed at a 1:1 ratio. Then, 25 µl of the mixture was incubated at 37°C for 24 h in triplicate on MacConkey agar plates. Bacterial counts recovered from each competition assay were calculated by plating serial 10-fold dilutions on LB agar plates with the appropriate antibiotics (Kan in the case of the attacker strain and Cam in the case of the prey strain). Data show the prey to attacker CFU ratio normalized to the inoculum and expressed as $\log_{10}$. Error bars indicate standard error. Statistical significance was determined using a one-way ANOVA followed by Tukey's multiple comparisons test (****$p < 0.0001$; ns, not significant).

The question of why *S.* Dublin acquired and maintained two distinct and functional T6SSs remains unanswered. We and others have proposed that the presence of multiple T6SSs could contribute to *Salmonella* fitness in different environments and/or hosts. Thus, the presence of putative antibacterial T6SS effector proteins suggests that *S.* Dublin may use them to differentially target bacterial cells within the cattle microbiota. Additional studies are required to confirm this hypothesis.

DATA AVAILABILITY STATEMENT

The original contributions presented in the study are included in the article/**Supplementary Material**; further inquiries can be directed to the corresponding authors.

AUTHOR CONTRIBUTIONS

FA, CB, CS, and DP: conceptualization, formal analysis, validation, writing-original draft preparation, and writing-review and editing. FA, CB, MB-I, DR, CS, and DP: methodology and investigation. CB, CS, AM-S, and DP: resources, project administration, and funding acquisition. CS and DP: supervision. FA, CB, and DP: visualization. All authors read and approved the final manuscript.

FUNDING

This work was supported by FONDECYT grant 1181167, ANID Millennium Science Initiative/Millennium Initiative for Collaborative Research on Bacterial Resistance, MICROB-R, NCN17_081. CS was supported by FONDECYT grants 1171844, and 1212075. CB was supported by FONDECYT grant 1201805, ECOS-ANID ECOS200037, and HHMI-Gulbenkian International Research Scholar grant #55008749. FA was supported by CONICYT/ANID fellowship 21191925.

ACKNOWLEDGMENTS

We thank Andrea Sabag for technical assistance.

SUPPLEMENTARY MATERIAL

The Supplementary Material for this article can be found online at: https://www.frontiersin.org/articles/10.3389/fmicb.2022.811932/full#supplementary-material

REFERENCES

Ahmad, S., Wang, B., Walker, M. D., Tran, H.-K. R., Stogios, P. J., Savchenko, A., et al. (2019). An interbacterial toxin inhibits target cell growth by synthesizing (p)ppApp. *Nature* 575, 674–678. doi: 10.1038/s41586-019-1735-9

Alteri, C. J., and Mobley, H. L. T. (2016). "The versatile type VI secretion system," in *Virulence Mechanisms of Bacterial Pathogens*. (Washington, DC, USA: ASM Press), 337–356.

Aschtgen, M.-S., Bernard, C. S., Bentzmann, S. D., Lloubès, R., and Cascales, E. (2008). SciN is an outer membrane lipoprotein required for type VI secretion in enteroaggregative *Escherichia coli*. *J. Bacteriol.* 190, 7523–7531. doi: 10.1128/jb.00945-08

Aubert, D. F., Xu, H., Yang, J., Shi, X., Gao, W., Li, L., et al. (2016). A *Burkholderia* type VI effector deamidates rho GTPases to activate the pyrin inflammasome and trigger inflammation. *Cell Host Microbe* 19, 664–674. doi: 10.1016/j.chom.2016.04.004

Ballister, E. R., Lai, A. H., Zuckermann, R. N., Cheng, Y., and Mougous, J. D. (2008). In vitro self-assembly of tailorable nanotubes from a simple protein building block. *Proc. Natl. Acad. Sci. U.S.A.* 105, 3733–3738. doi: 10.1073/pnas.0712247105

Bao, H., Zhao, J.-H., Zhu, S., Wang, S., Zhang, J., Wang, X.-Y., et al. (2019). Genetic diversity and evolutionary features of type VI secretion systems in *Salmonella*. *Future Microbiol.* 14, 139–154. doi: 10.2217/fmb-2018-0260

Basler, M. (2015). Type VI secretion system: secretion by a contractile nanomachine. *Philos. Trans. R. Soc. Lond. B Biol. Sci.* 370:20150021. doi: 10.1098/rstb.2015.0021

Berni, B., Soscia, C., Djermoun, S., Ize, B., and Bleves, S. (2019). A type VI secretion system trans-kingdom effector is required for the delivery of a novel antibacterial toxin in *Pseudomonas aeruginosa*. *Front. Microbiol.* 10:1218. doi: 10.3389/fmicb.2019.01218

Blondel, C. J., Jiménez, J. C., Contreras, I., and Santiviago, C. A. (2009). Comparative genomic analysis uncovers 3 novel loci encoding type six secretion systems differentially distributed in *Salmonella* serotypes. *BMC Genomics* 10:354. doi: 10.1186/1471-2164-10-354

Blondel, C. J., Jiménez, J. C., Leiva, L. E., Alvarez, S. A., Pinto, B. I., Contreras, F., et al. (2013). The type VI secretion system encoded in *Salmonella* pathogenicity island 19 is required for *Salmonella enterica* serotype Gallinarum survival within infected macrophages. *Infect. Immun.* 81, 1207–1220. doi: 10.1128/iai.01165-12

Blondel, C. J., Yang, H.-J., Castro, B., Chiang, S., Toro, C. S., Zaldívar, M., et al. (2010). Contribution of the type VI secretion system encoded in SPI-19 to chicken colonization by *Salmonella enterica* serotypes Gallinarum and Enteritidis. *PLoS One* 5:e11724. doi: 10.1371/journal.pone.0011724

Bondage, D. D., Lin, J.-S., Ma, L.-S., Kuo, C.-H., and Lai, E.-M. (2016). VgrG C terminus confers the type VI effector transport specificity and is required for binding with PAAR and adaptor–effector complex. *Proc. Natl. Acad. Sci. U.S.A.* 113, E3931–E3940. doi: 10.1073/pnas.1600428113

Brunet, Y. R., Hénin, J., Celia, H., and Cascales, E. (2014). Type VI secretion and bacteriophage tail tubes share a common assembly pathway. *EMBO Rep.* 15, 315–321. doi: 10.1002/embr.201337936

Brunet, Y. R., Khodr, A., Logger, L., Aussel, L., Mignot, T., Rimsky, S., et al. (2015a). H-NS silencing of the *Salmonella* Pathogenicity Island 6-encoded type VI secretion system limits *Salmonella enterica* serovar Typhimurium interbacterial killing. *Infect. Immun.* 83, 2738–2750. doi: 10.1128/iai.00198-15

Brunet, Y. R., Zoued, A., Boyer, F., Douzi, B., and Cascales, E. (2015b). The type VI secretion TssEFGK-VgrG phage-like baseplate is recruited to the TssJLM membrane complex via multiple contacts and serves as assembly platform for tail tube/sheath polymerization. *PLoS Genet.* 11:e1005545. doi: 10.1371/journal.pgen.1005545

Cherepanov, P. P., and Wackernagel, W. (1995). Gene disruption in *Escherichia coli*: TcR and KmR cassettes with the option of Flp-catalyzed excision of the antibiotic-resistance determinant. *Gene* 158, 9–14. doi: 10.1016/0378-1119(95)00193-a

Cianfanelli, F. R., Monlezun, L., and Coulthurst, S. J. (2016). Aim, load, fire: the type VI secretion system, a bacterial nanoweapon. *Trends Microbiol.* 24, 51–62. doi: 10.1016/j.tim.2015.10.005

Coulthurst, S. (2019). The type VI secretion system: a versatile bacterial weapon. *Microbiology* 165, 503–515. doi: 10.1099/mic.0.000789

Darling, A. C. E., Mau, B., Blattner, F. R., and Perna, N. T. (2004). Mauve: multiple alignment of conserved genomic sequence with rearrangements. *Genome Res.* 14, 1394–1403. doi: 10.1101/gr.2289704

Datsenko, K. A., and Wanner, B. L. (2000). One-step inactivation of chromosomal genes in *Escherichia coli* K-12 using PCR products. *Proc. Natl. Acad. Sci. U.S.A.* 97, 6640–6645. doi: 10.1073/pnas.120163297

Diniz, J. A., and Coulthurst, S. J. (2015). Intraspecies competition in *Serratia marcescens* is mediated by type VI-secreted Rhs effectors and a conserved effector-associated accessory protein. *J. Bacteriol.* 197, 2350–2360. doi: 10.1128/jb.00199-15

Donato, S. L., Beck, C. M., Garza-Sánchez, F., Jensen, S. J., Ruhe, Z. C., Cunningham, D. A., et al. (2020). The β-encapsulation cage of rearrangement hotspot (Rhs) effectors is required for type VI secretion. *Proc. Natl. Acad. Sci. U.S.A.* 117, 33540–33548. doi: 10.1073/pnas.1919350117

Douzi, B., Spinelli, S., Blangy, S., Roussel, A., Durand, E., Brunet, Y. R., et al. (2014). Crystal structure and self-interaction of the type VI secretion tail-tube protein from enteroaggregative *Escherichia coli*. *PLoS One* 9:e86918. doi: 10.1371/journal.pone.0086918

Durand, E., Cambillau, C., Cascales, E., and Journet, L. (2014). VgrG, Tae, Tle, and beyond: the versatile arsenal of type VI secretion effectors. *Trends Microbiol.* 22, 498–507. doi: 10.1016/j.tim.2014.06.004

Durand, E., Derrez, E., Audoly, G., Spinelli, S., Ortiz-Lombardia, M., Raoult, D., et al. (2012). Crystal structure of the VgrG1 actin cross-linking domain of the *Vibrio cholerae* type VI secretion system. *J. Biol. Chem.* 287, 38190–38199. doi: 10.1074/jbc.m112.390153

Durand, E., Nguyen, V. S., Zoued, A., Logger, L., Péhau-Arnaudet, G., Aschtgen, M.-S., et al. (2015). Biogenesis and structure of a type VI secretion membrane core complex. *Nature* 523, 555–560. doi: 10.1038/nature14667

Dutta, P., Jijumon, A. S., Mazumder, M., Dileep, D., Mukhopadhyay, A. K., Gourinath, S., et al. (2019). Presence of actin binding motif in VgrG-1 toxin of *Vibrio cholerae* reveals the molecular mechanism of actin cross-linking. *Int. J. Biol. Macromol.* 133, 775–785. doi: 10.1016/j.ijbiomac.2019.04.026

Egan, F., Reen, F. J., and O'Gara, F. (2015). Tle distribution and diversity in metagenomic datasets reveal niche specialization. *Environ. Microbiol. Rep.* 7, 194–203. doi: 10.1111/1758-2229.12222

Feria, J. M., and Valvano, M. A. (2020). An overview of anti-eukaryotic T6SS effectors. *Front. Cell. Infect. Microbiol.* 10:584751. doi: 10.3389/fcimb.2020.584751

Fierer, J. (1983). Invasive *Salmonella* Dublin infections associated with drinking raw milk. *West. J. Med.* 138, 665–669.

Finn, R. D., Bateman, A., Clements, J., Coggill, P., Eberhardt, R. Y., Eddy, S. R., et al. (2014). Pfam: the protein families database. *Nucleic Acids Res.* 42, D222–D230. doi: 10.1093/nar/gkt1223

Fitzsimons, T. C., Lewis, J. M., Wright, A., Kleifeld, O., Schittenhelm, R. B., Powell, D., et al. (2018). Identification of novel *Acinetobacter baumannii* type VI secretion system antibacterial effector and immunity pairs. *Infect. Immun.* 86, e00297–e00318. doi: 10.1128/iai.00297-18

Flaugnatti, N., Le, T. T. H., Canaan, S., Aschtgen, M., Nguyen, V. S., Blangy, S., et al. (2016). A phospholipase A1 antibacterial type VI secretion effector interacts directly with the C-terminal domain of the VgrG spike protein for delivery. *Mol. Microbiol.* 99, 1099–1118. doi: 10.1111/mmi.13292

Fookes, M., Schroeder, G. N., Langridge, G. C., Blondel, C. J., Mammina, C., Connor, T. R., et al. (2011). *Salmonella bongori* provides insights into the evolution of the salmonellae. *PLoS Pathog.* 7:e1002191. doi: 10.1371/journal.ppat.1002191

GBD-2017, Stanaway, J. D., Parisi, A., Sarkar, K., Blacker, B. F., Reiner, R. C., et al. (2019). The global burden of non-typhoidal *Salmonella* invasive disease: a systematic analysis for the global burden of disease study 2017. *Lancet Infect. Dis.* 19, 1312–1324. doi: 10.1016/s1473-3099(19)30418-9

Heisler, D. B., Kudryashova, E., Grinevich, D. O., Suarez, C., Winkelman, J. D., Birukov, K. G., et al. (2015). ACD toxin–produced actin oligomers poison formin-controlled actin polymerization. *Science* 349, 535–539. doi: 10.1126/science.aab4090

Hernandez, R. E., Gallegos-Monterrosa, R., and Coulthurst, S. J. (2020). Type VI secretion system effector proteins: effective weapons for bacterial competitiveness. *Cell. Microbiol.* 22:e13241. doi: 10.1111/cmi.13241

Hoelzer, K., Switt, A. I. M., and Wiedmann, M. (2011). Animal contact as a source of human non-typhoidal salmonellosis. *Vet. Res.* 42:34. doi: 10.1186/1297-9716-42-34

Issenhuth-Jeanjean, S., Roggentin, P., Mikoleit, M., Guibourdenche, M., de Pinna, E., Nair, S., et al. (2014). Supplement 2008–2010 (no. 48) to the White–Kauffmann–Le Minor scheme. *Res. Microbiol.* 165, 526–530. doi: 10.1016/j.resmic.2014.07.004

Jamet, A., and Nassif, X. (2015). New players in the toxin field: polymorphic toxin systems in bacteria. *mBio* 6, e00285–e00315. doi: 10.1128/mbio.00285-15

Jana, B., Fridman, C. M., Bosis, E., and Salomon, D. (2019). A modular effector with a DNase domain and a marker for T6SS substrates. *Nat. Commun.* 10:3595. doi: 10.1038/s41467-019-11546-6

Jiang, F., Wang, X., Wang, B., Chen, L., Zhao, Z., Waterfield, N. R., et al. (2016). The *Pseudomonas aeruginosa* type VI secretion PGAP1-like effector induces host autophagy by activating endoplasmic reticulum stress. *Cell Rep.* 16, 1502–1509. doi: 10.1016/j.celrep.2016.07.012

Kanehisa, M., Goto, S., Kawashima, S., and Nakaya, A. (2002). The KEGG databases at GenomeNet. *Nucleic Acids Res.* 30, 42–46. doi: 10.1093/nar/30.1.42

Katoh, K., Rozewicki, J., and Yamada, K. D. (2017). MAFFT online service: multiple sequence alignment, interactive sequence choice and visualization. *Brief. Bioinform.* 20, 1160–1166. doi: 10.1093/bib/bbx108

Koskiniemi, S., Garza-Sánchez, F., Sandegren, L., Webb, J. S., Braaten, B. A., Poole, S. J., et al. (2014). Selection of orphan Rhs toxin expression in evolved *Salmonella enterica* serovar Typhimurium. *PLoS Genet.* 10:e1004255. doi: 10.1371/journal.pgen.1004255

Koskiniemi, S., Lamoureux, J. G., Nikolakakis, K. C., t'Kint de Roodenbeke, C., Kaplan, M. D., Low, D. A., et al. (2013). Rhs proteins from diverse bacteria mediate intercellular competition. *Proc. Natl. Acad. Sci. U.S.A.* 110, 7032–7037. doi: 10.1073/pnas.1300627110

Leiman, P. G., Basler, M., Ramagopal, U. A., Bonanno, J. B., Sauder, J. M., Pukatzki, S., et al. (2009). Type VI secretion apparatus and phage tail-associated protein complexes share a common evolutionary origin. *Proc. Natl. Acad. Sci. U.S.A.* 106, 4154–4159. doi: 10.1073/pnas.0813360106

Libby, S. J., Brehm, M. A., Greiner, D. L., Shultz, L. D., McClelland, M., Smith, K. D., et al. (2010). Humanized nonobese diabetic-*scid IL2rγ*^{null} mice are susceptible to lethal *Salmonella* Typhi infection. *Proc. Natl. Acad. Sci. U.S.A.* 107, 15589–15594. doi: 10.1073/pnas.1005566107

Lindgren, M., Bröms, J. E., Meyer, L., Golovliov, I., and Sjöstedt, A. (2013). The *Francisella tularensis* LVS Δ*pdpC* mutant exhibits a unique phenotype during intracellular infection. *BMC Microbiol.* 13:20. doi: 10.1186/1471-2180-13-20

Logger, L., Aschtgen, M.-S., Guérin, M., Cascales, E., and Durand, E. (2016). Molecular dissection of the interface between the type VI secretion TssM cytoplasmic domain and the TssG baseplate component. *J. Mol. Biol.* 428, 4424–4437. doi: 10.1016/j.jmb.2016.08.032

Lu, S., Wang, J., Chitsaz, F., Derbyshire, M. K., Geer, R. C., Gonzales, N. R., et al. (2019). CDD/SPARCLE: the conserved domain database in 2020. *Nucleic Acids Res.* 48, D265–D268. doi: 10.1093/nar/gkz991

Ma, A. T., McAuley, S., Pukatzki, S., and Mekalanos, J. J. (2009). Translocation of a *Vibrio cholerae* type VI secretion effector requires bacterial endocytosis by host cells. *Cell Host Microbe* 5, 234–243. doi: 10.1016/j.chom.2009.02.005

Ma, A. T., and Mekalanos, J. J. (2010). In vivo actin cross-linking induced by *Vibrio cholerae* type VI secretion system is associated with intestinal inflammation. *Proc. Natl. Acad. Sci. U.S.A.* 107, 4365–4370. doi: 10.1073/pnas.0915156107

Ma, J., Pan, Z., Huang, J., Sun, M., Lu, C., and Yao, H. (2017a). The Hcp proteins fused with diverse extended-toxin domains represent a novel pattern of antibacterial effectors in type VI secretion systems. *Virulence* 8, 1189–1202. doi: 10.1080/21505594.2017.1279374

Ma, J., Sun, M., Dong, W., Pan, Z., Lu, C., and Yao, H. (2017b). PAAR-Rhs proteins harbor various C-terminal toxins to diversify the antibacterial pathways of type VI secretion systems. *Environ. Microbiol.* 19, 345–360. doi: 10.1111/1462-2920.13621

Ma, J., Sun, M., Pan, Z., Lu, C., and Yao, H. (2018). Diverse toxic effectors are harbored by *vgrG* islands for interbacterial antagonism in type VI secretion system. *Biochim. Biophys. Acta Gen. Subj.* 1862, 1635–1643. doi: 10.1016/j.bbagen.2018.04.010

Mariano, G., Trunk, K., Williams, D. J., Monlezun, L., Strahl, H., Pitt, S. J., et al. (2019). A family of type VI secretion system effector proteins that form ion-selective pores. *Nat. Commun.* 10:5484. doi: 10.1038/s41467-019-13439-0

Miyata, S. T., Kitaoka, M., Brooks, T. M., McAuley, S. B., and Pukatzki, S. (2011). *Vibrio cholerae* requires the type VI secretion system virulence factor VasX to kill *Dictyostelium discoideum*. *Infect. Immun.* 79, 2941–2949. doi: 10.1128/iai.01266-10

Miyata, S. T., Unterweger, D., Rudko, S. P., and Pukatzki, S. (2013). Dual expression profile of type VI secretion system immunity genes protects pandemic *Vibrio cholerae*. *PLoS Pathog.* 9:e1003752. doi: 10.1371/journal.ppat.1003752

Mulder, D. T., Cooper, C. A., and Coombes, B. K. (2012). Type VI secretion system-associated gene clusters contribute to pathogenesis of *Salmonella enterica* serovar Typhimurium. *Infect. Immun.* 80, 1996–2007. doi: 10.1128/iai.06205-11

Navarro-Garcia, F., Ruiz-Perez, F., Cataldi, Á., and Larzábal, M. (2019). Type VI secretion system in pathogenic *Escherichia coli*: structure, role in virulence, and acquisition. *Front. Microbiol.* 10:1965. doi: 10.3389/fmicb.2019.01965

Nazarov, S., Schneider, J. P., Brackmann, M., Goldie, K. N., Stahlberg, H., and Basler, M. (2018). Cryo-EM reconstruction of type VI secretion system baseplate and sheath distal end. *EMBO J.* 37:e97103. doi: 10.15252/embj.201797103

Nielsen, T. D., Kudahl, A. B., Østergaard, S., and Nielsen, L. R. (2013). Gross margin losses due to *Salmonella* Dublin infection in Danish dairy cattle herds estimated by simulation modelling. *Prev. Vet. Med.* 111, 51–62. doi: 10.1016/j.prevetmed.2013.03.011

Notredame, C., Higgins, D. G., and Heringa, J. (2000). T-coffee: a novel method for fast and accurate multiple sequence alignment. *J. Mol. Biol.* 302, 205–217. doi: 10.1006/jmbi.2000.4042

Pezoa, D., Blondel, C. J., Silva, C. A., Yang, H.-J., Andrews-Polymenis, H., Santiviago, C. A., et al. (2014). Only one of the two type VI secretion systems encoded in the *Salmonella enterica* serotype Dublin genome is involved in colonization of the avian and murine hosts. *Vet. Res.* 45:2. doi: 10.1186/1297-9716-45-2

Pezoa, D., Yang, H.-J., Blondel, C. J., Santiviago, C. A., Andrews-Polymenis, H. L., and Contreras, I. (2013). The type VI secretion system encoded in SPI-6 plays a role in gastrointestinal colonization and systemic spread of *Salmonella enterica* serovar Typhimurium in the chicken. *PLoS One* 8:e63917. doi: 10.1371/journal.pone.0063917

Pissaridou, P., Allsopp, L. P., Wettstadt, S., Howard, S. A., Mavridou, D. A. I., and Filloux, A. (2018). The *Pseudomonas aeruginosa* T6SS-VgrG1b spike is topped by a PAAR protein eliciting DNA damage to bacterial competitors. *Proc. Natl. Acad. Sci. U.S.A.* 115, 12519–12524. doi: 10.1073/pnas.1814181115

Pukatzki, S., Ma, A. T., Revel, A. T., Sturtevant, D., and Mekalanos, J. J. (2007). Type VI secretion system translocates a phage tail spike-like protein into target cells where it cross-links actin. *Proc. Natl. Acad. Sci. U.S.A.* 104, 15508–15513. doi: 10.1073/pnas.0706532104

Rapisarda, C., Cherrak, Y., Kooger, R., Schmidt, V., Pellarin, R., Logger, L., et al. (2019). In situ and high-resolution cryo-EM structure of a bacterial type VI secretion system membrane complex. *EMBO J.* 38:e100886. doi: 10.15252/embj.2018100886

Ray, A., Schwartz, N., de Santos, M. S., Zhang, J., Orth, K., and Salomon, D. (2017). Type VI secretion system MIX-effectors carry both antibacterial and anti-eukaryotic activities. *EMBO Rep.* 18, 1978–1990. doi: 10.15252/embr.201744226

Records, A. R. (2011). The type VI secretion system: a multipurpose delivery system with a phage-Like machinery. *Mol. Plant-Microbe Interact.* 24, 751–757. doi: 10.1094/mpmi-11-10-0262

Renault, M. G., Beas, J. Z., Douzi, B., Chabalier, M., Zoued, A., Brunet, Y. R., et al. (2018). The gp27-like hub of VgrG serves as adaptor to promote Hcp tube assembly. *J. Mol. Biol.* 430, 3143–3156. doi: 10.1016/j.jmb.2018.07.018

Robert, X., and Gouet, P. (2014). Deciphering key features in protein structures with the new ENDscript server. *Nucleic Acids Res.* 42, W320–W324. doi: 10.1093/nar/gku316

Russell, A. B., LeRoux, M., Hathazi, K., Agnello, D. M., Ishikawa, T., Wiggins, P. A., et al. (2013). Diverse type VI secretion phospholipases are functionally plastic antibacterial effectors. *Nature* 496, 508–512. doi: 10.1038/nature12074

Russell, A. B., Singh, P., Brittnacher, M., Bui, N. K., Hood, R. D., Carl, M. A., et al. (2012). A widespread bacterial type VI secretion effector superfamily identified using a heuristic approach. *Cell Host Microbe* 11, 538–549. doi: 10.1016/j.chom.2012.04.007

Rutherford, K., Parkhill, J., Crook, J., Horsnell, T., Rice, P., Rajandream, M.-A., et al. (2000). Artemis: sequence visualization and annotation. *Bioinformatics* 16, 944–945. doi: 10.1093/bioinformatics/16.10.944

Sana, T. G., Baumann, C., Merdes, A., Soscia, C., Rattei, T., Hachani, A., et al. (2015). Internalization of *Pseudomonas aeruginosa* strain PAO1 into epithelial cells is promoted by interaction of a T6SS effector with the microtubule network. *mBio* 6, e00712–e00715. doi: 10.1128/mbio.00712-15

Sana, T. G., Flaugnatti, N., Lugo, K. A., Lam, L. H., Jacobson, A., Baylot, V., et al. (2016). *Salmonella* Typhimurium utilizes a T6SS-mediated antibacterial weapon to establish in the host gut. *Proc. Natl. Acad. Sci. U.S.A.* 113, E5044–E5051. doi: 10.1073/pnas.1608858113

Santiviago, C. A., Reynolds, M. M., Porwollik, S., Choi, S.-H., Long, F., Andrews-Polymenis, H. L., et al. (2009). Analysis of pools of targeted *Salmonella* deletion mutants identifies novel genes affecting fitness during competitive infection in mice. *PLoS Pathog.* 5:e1000477. doi: 10.1371/journal.ppat.1000477

Santos, M. N. M., Cho, S.-T., Wu, C.-F., Chang, C.-J., Kuo, C.-H., and Lai, E.-M. (2020). Redundancy and specificity of type VI secretion *vgrG* loci in antibacterial activity of *Agrobacterium tumefaciens* 1D1609 strain. *Front. Microbiol.* 10:3004. doi: 10.3389/fmicb.2019.03004

Schroll, C., Huang, K., Ahmed, S., Kristensen, B. M., Pors, S. E., Jelsbak, L., et al. (2019). The SPI-19 encoded type-six secretion-systems (T6SS) of *Salmonella enterica* serovars Gallinarum and Dublin play different roles during infection. *Vet. Microbiol.* 230, 23–31. doi: 10.1016/j.vetmic.2019.01.006

Schwarz, S., Singh, P., Robertson, J. D., LeRoux, M., Skerrett, S. J., Goodlett, D. R., et al. (2014). VgrG-5 is a *Burkholderia* type VI secretion system-exported protein required for multinucleated giant cell formation and virulence. *Infect. Immun.* 82, 1445–1452. doi: 10.1128/iai.01368-13

Sethi, D., Mahajan, S., Singh, C., Lama, A., Hade, M. D., Gupta, P., et al. (2016). Lipoprotein LprI of *Mycobacterium tuberculosis* acts as a lysozyme inhibitor. *J. Biol. Chem.* 291, 2938–2953. doi: 10.1074/jbc.m115.662593

Shneider, M. M., Buth, S. A., Ho, B. T., Basler, M., Mekalanos, J. J., and Leiman, P. G. (2013). PAAR-repeat proteins sharpen and diversify the type VI secretion system spike. *Nature* 500, 350–353. doi: 10.1038/nature12453

Sibinelli-Sousa, S., Hespanhol, J. T., Nicastro, G. G., Matsuyama, B. Y., Mesnage, S., Patel, A., et al. (2020). A family of T6SS antibacterial effectors related to l,d-transpeptidases targets the peptidoglycan. *Cell Rep.* 31:107813. doi: 10.1016/j.celrep.2020.107813

Sigrist, C. J. A., de Castro, E., Cerutti, L., Cuche, B. A., Hulo, N., Bridge, A., et al. (2013). New and continuing developments at PROSITE. *Nucleic Acids Res.* 41, D344–D347. doi: 10.1093/nar/gks1067

Silva, C. A., Blondel, C. J., Quezada, C. P., Porwollik, S., Andrews-Polymenis, H. L., Toro, C. S., et al. (2012). Infection of mice by *Salmonella enterica* serovar Enteritidis involves additional genes that are absent in the genome of serovar Typhimurium. *Infect. Immun.* 80, 839–849. doi: 10.1128/iai.05497-11

Silverman, J. M., Agnello, D. M., Zheng, H., Andrews, B. T., Li, M., Catalano, C. E., et al. (2013). Haemolysin coregulated protein is an exported receptor and chaperone of type VI secretion substrates. *Mol. Cell* 51, 584–593. doi: 10.1016/j.molcel.2013.07.025

Small, R. G., and Sharp, J. C. M. (1979). A milk-borne outbreak due to *Salmonella* Dublin. *J. Hyg.* 82, 95–100. doi: 10.1017/s0022172400025511

Srikannathasan, V., English, G., Bui, N. K., Trunk, K., O'Rourke, P. E. F., Rao, V. A., et al. (2013). Structural basis for type VI secreted peptidoglycan dl-endopeptidase function, specificity and neutralization in *Serratia marcescens*. *Acta Crystallogr. D Biol. Crystallogr.* 69, 2468–2482. doi: 10.1107/s0907444913022725

Sullivan, M. J., Petty, N. K., and Beatson, S. A. (2011). Easyfig: a genome comparison visualizer. *Bioinformatics* 27, 1009–1010. doi: 10.1093/bioinformatics/btr039

Taboada, B., Estrada, K., Ciria, R., and Merino, E. (2018). Operon-mapper: a web server for precise operon identification in bacterial and archaeal genomes. *Bioinformatics* 34, 4118–4120. doi: 10.1093/bioinformatics/bty496

Tan, J., Yang, D., Wang, Z., Zheng, X., Zhang, Y., and Liu, Q. (2019). EvpP inhibits neutrophils recruitment via Jnk-caspy inflammasome signaling in vivo. *Fish Shellfish Immunol.* 92, 851–860. doi: 10.1016/j.fsi.2019.05.051

Tang, J. Y., Bullen, N. P., Ahmad, S., and Whitney, J. C. (2018). Diverse NADase effector families mediate interbacterial antagonism via the type VI secretion system. *J. Biol. Chem.* 293, 1504–1514. doi: 10.1074/jbc.ra117.000178

Ting, S.-Y., Bosch, D. E., Mangiameli, S. M., Radey, M. C., Huang, S., Park, Y.-J., et al. (2018). Bifunctional immunity proteins protect bacteria against FtsZ-targeting ADP-Ribosylating toxins. *Cell* 175, 1380.e14–1392.e14. doi: 10.1016/j.cell.2018.09.037

Uzzau, S., Brown, D. J., Wallis, T., Rubino, S., Leori, G., Bernard, S., et al. (2000). Host adapted serotypes of *Salmonella enterica*. *Epidemiol. Infect.* 125, 229–255. doi: 10.1017/s0950268899004379

Wang, M., Luo, Z., Du, H., Xu, S., Ni, B., Zhang, H., et al. (2011). Molecular characterization of a functional type VI secretion system in *Salmonella enterica* serovar Typhi. *Curr. Microbiol.* 63, 22–31. doi: 10.1007/s00284-011-9935-z

Wang, J., Yang, B., Leier, A., Marquez-Lago, T. T., Hayashida, M., Rocker, A., et al. (2018). Bastion6: a bioinformatics approach for accurate prediction of type VI secreted effectors. *Bioinformatics* 34, 2546–2555. doi: 10.1093/bioinformatics/bty155

Wang, S., Yang, D., Wu, X., Yi, Z., Wang, Y., Xin, S., et al. (2019). The ferric uptake regulator represses type VI secretion system function by binding directly to the *clpV* promoter in *Salmonella enterica* serovar Typhimurium. *Infect. Immun.* 87, e00562–19. doi: 10.1128/iai.00562-19

Whitney, J. C., Beck, C. M., Goo, Y. A., Russell, A. B., Harding, B. N., Leon, J. A. D., et al. (2014). Genetically distinct pathways guide effector export through the type VI secretion system. *Mol. Microbiol.* 92, 529–542. doi: 10.1111/mmi.12571

Whitney, J. C., Chou, S., Russell, A. B., Biboy, J., Gardiner, T. E., Ferrin, M. A., et al. (2013). Identification, structure, and function of a novel type VI secretion peptidoglycan glycoside hydrolase effector-immunity pair. *J. Biol. Chem.* 288, 26616–26624. doi: 10.1074/jbc.m113.488320

Whitney, J. C., Quentin, D., Sawai, S., LeRoux, M., Harding, B. N., Ledvina, H. E., et al. (2015). An interbacterial $NAD(P)^+$ glycohydrolase toxin requires elongation factor Tu for delivery to target cells. *Cell* 163, 607–619. doi: 10.1016/j.cell.2015.09.027

Wood, T. E., Aksoy, E., and Hachani, A. (2020). From welfare to warfare: the arbitration of host-microbiota interplay by the type VI secretion system. *Front. Cell. Infect. Microbiol.* 10:587948. doi: 10.3389/fcimb.2020.587948

Wood, T. E., Howard, S. A., Förster, A., Nolan, L. M., Manoli, E., Bullen, N. P., et al. (2019). The *Pseudomonas aeruginosa* T6SS delivers a periplasmic toxin that disrupts bacterial cell morphology. *Cell Rep.* 29, 187.e7–201.e7. doi: 10.1016/j.celrep.2019.08.094

Xian, H., Yuan, Y., Yin, C., Wang, Z., Ji, R., Chu, C., et al. (2020). The SPI-19 encoded T6SS is required for *Salmonella* Pullorum survival within avian macrophages and initial colonization in chicken dependent on inhibition of host immune response. *Vet. Microbiol.* 250:108867. doi: 10.1016/j.vetmic.2020.108867

Yin, M., Yan, Z., and Li, X. (2019). Architecture of type VI secretion system membrane core complex. *Cell Res.* 29, 251–253. doi: 10.1038/s41422-018-0130-7

Zhang, D., de Souza, R. F., Anantharaman, V., Iyer, L. M., and Aravind, L. (2012). Polymorphic toxin systems: comprehensive characterization of trafficking modes, processing, mechanisms of action, immunity and ecology using comparative genomics. *Biol. Direct* 7:18. doi: 10.1186/1745-6150-7-18

Zheng, J., Ho, B., and Mekalanos, J. J. (2011). Genetic analysis of anti-amoebae and anti-bacterial activities of the type VI secretion system in *Vibrio cholerae*. *PLoS One* 6:e23876. doi: 10.1371/journal.pone.0023876

Zimmermann, L., Stephens, A., Nam, S.-Z., Rau, D., Kübler, J., Lozajic, M., et al. (2017). A completely reimplemented MPI bioinformatics toolkit with a new HHpred server at its core. *J. Mol. Biol.* 430, 2237–2243. doi: 10.1016/j.jmb.2017.12.007

Zoued, A., Brunet, Y. R., Durand, E., Aschtgen, M.-S., Logger, L., Douzi, B., et al. (2014). Architecture and assembly of the type VI secretion system. *Biochim. Biophys. Acta Mol. Cell Res.* 1843, 1664–1673. doi: 10.1016/j.bbamcr.2014.03.018

Conflict of Interest: The authors declare that the research was conducted in the absence of any commercial or financial relationships that could be construed as a potential conflict of interest.

Publisher's Note: All claims expressed in this article are solely those of the authors and do not necessarily represent those of their affiliated organizations, or those of the publisher, the editors and the reviewers. Any product that may be evaluated in this article, or claim that may be made by its manufacturer, is not guaranteed or endorsed by the publisher.

frontiers | Frontiers in Microbiology

ORIGINAL RESEARCH
published: 29 April 2022
doi: 10.3389/fmicb.2022.800366

A Surface Exposed, Two-Domain Lipoprotein Cargo of a Type XI Secretion System Promotes Colonization of Host Intestinal Epithelia Expressing Glycans

Alex S. Grossman[1†], Cristian A. Escobar[2†], Erin J. Mans[1†], Nicholas C. Mucci[1], Terra J. Mauer[2], Katarina A. Jones[3], Cameron C. Moore[1], Paul E. Abraham[4], Robert L. Hettich[4], Liesel Schneider[5], Shawn R. Campagna[4,6,7], Katrina T. Forest[2] and Heidi Goodrich-Blair[1,2]**

[1] Department of Microbiology, The University of Tennessee, Knoxville, Knoxville, TN, United States, [2] Department of Bacteriology, The University of Wisconsin–Madison, Madison, WI, United States, [3] Department of Chemistry, The University of Tennessee, Knoxville, Knoxville, TN, United States, [4] Biosciences Division, Oak Ridge National Laboratory, Oak Ridge, TN, United States, [5] Department of Animal Sciences, The University of Tennessee, Knoxville, Knoxville, TN, United States, [6] Biological and Small Molecule Mass Spectrometry Core, The University of Tennessee, Knoxville, Knoxville, TN, United States, [7] The University of Tennessee Oak Ridge Innovation Institute, Knoxville, TN, United States

OPEN ACCESS

Edited by:
Eric Cascales,
Aix-Marseille Université, France

Reviewed by:
Trevor F. Moraes,
University of Toronto, Canada
Olivera Francetic,
Institut Pasteur, France

***Correspondence:**
Heidi Goodrich-Blair
hgblair@utk.edu
Katrina T. Forest
forest@bact.wisc.edu

[†] These authors have contributed equally to this work

Specialty section:
This article was submitted to Microbial Physiology and Metabolism, a section of the journal Frontiers in Microbiology

Received: 09 November 2021
Accepted: 07 March 2022
Published: 29 April 2022

Citation:
Grossman AS, Escobar CA, Mans EJ, Mucci NC, Mauer TJ, Jones KA, Moore CC, Abraham PE, Hettich RL, Schneider L, Campagna SR, Forest KT and Goodrich-Blair H (2022) A Surface Exposed, Two-Domain Lipoprotein Cargo of a Type XI Secretion System Promotes Colonization of Host Intestinal Epithelia Expressing Glycans. Front. Microbiol. 13:800366. doi: 10.3389/fmicb.2022.800366

The only known required component of the newly described Type XI secretion system (TXISS) is an outer membrane protein (OMP) of the DUF560 family. $TXISS_{OMPs}$ are broadly distributed across proteobacteria, but properties of the cargo proteins they secrete are largely unexplored. We report biophysical, histochemical, and phenotypic evidence that *Xenorhabdus nematophila* NilC is surface exposed. Biophysical data and structure predictions indicate that NilC is a two-domain protein with a C-terminal, 8-stranded β-barrel. This structure has been noted as a common feature of TXISS effectors and may be important for interactions with the $TXISS_{OMP}$. The NilC N-terminal domain is more enigmatic, but our results indicate it is ordered and forms a β-sheet structure, and bioinformatics suggest structural similarities to carbohydrate-binding proteins. *X. nematophila* NilC and its presumptive $TXISS_{OMP}$ partner NilB are required for colonizing the anterior intestine of *Steinernema carpocapsae* nematodes: the receptacle of free-living, infective juveniles and the anterior intestinal cecum (AIC) in juveniles and adults. We show that, in adult nematodes, the AIC expresses a Wheat Germ Agglutinin (WGA)-reactive material, indicating the presence of *N*-acetylglucosamine or *N*-acetylneuraminic acid sugars on the AIC surface. A role for this material in colonization is supported by the fact that exogenous addition of WGA can inhibit AIC colonization by *X. nematophila*. Conversely, the addition of exogenous purified NilC increases the frequency with which *X. nematophila* is observed at the AIC, demonstrating that abundant extracellular NilC can enhance colonization. NilC may facilitate *X. nematophila* adherence to the nematode intestinal surface by binding to host glycans, it might support *X. nematophila* nutrition by cleaving sugars from the host surface, or it might help protect *X. nematophila* from nematode host immunity. Proteomic and metabolomic analyses of wild type *X. nematophila* compared to those

lacking *nilB* and *nilC* revealed differences in cell wall and secreted polysaccharide metabolic pathways. Additionally, purified NilC is capable of binding peptidoglycan, suggesting that periplasmic NilC may interact with the bacterial cell wall. Overall, these findings support a model that NilB-regulated surface exposure of NilC mediates interactions between *X. nematophila* and host surface glycans during colonization. This is a previously unknown function for a TXISS.

Keywords: type XI secretion, symbiosis, Slam, lipidation, proteomics, metabolomics, NMR

INTRODUCTION

Bacteria rely on secretion systems to convey proteins across membranes to the cell surface and extracellular environment. In host-associated bacteria, such effector proteins, which can include surface-exposed lipoproteins, mediate acquisition of nutrients, signaling interactions with host cells, mechanical interactions with host surfaces, and specificity in host range. These processes make effector proteins potential targets for pharmaceutical treatment and vaccine development (Konovalova and Silhavy, 2015; Wilson and Bernstein, 2016; Kinkead et al., 2018). Bacterial lipoproteins are classified by N-terminal lipidation at a cysteine residue but, otherwise, are diverse in sequence, function, and subcellular localization. The mechanisms by which certain classes of proteins, including lipoproteins, are targeted to and oriented within the outer-membrane are still largely unknown. The newly described type XI secretion system (TXISS), comprising an outer membrane protein (OMP) containing a DUF560 (a domain of unknown function 560), is broadly distributed among proteobacteria and mediates translocation of lipoprotein and a soluble protein cargo across the outer membrane (Heungens et al., 2002; Bhasin et al., 2012; Hooda et al., 2017; Grossman et al., 2021).

A sequence-similarity-based network analysis provided functionally relevant categorization of these TXISS OMPs, hereafter referred to as $TXISS_{OMPs}$, into 10 clusters. Cluster 1, which contains the largest number of $TXISS_{OMPs}$, was further refined into three subclusters: A, B, and C. Clusters 1A and 1B contain the few characterized TXISS OMPs, and its members predominantly are encoded by microbes isolated from animals (Grossman et al., 2021). *Neisseria meningitidis* Slam1 and Slam2 are $TXISS_{OMPs}$ responsible for secretion of transferrin-, lactoferrin-, factor H- or hemoglobin/haptoglobin-binding lipoproteins. *X. nematophila* HrpB and *Acinetobacter baumanii* HsmA are $TXISS_{OMPs}$ that secrete the soluble (non-lipidated) hemophores HrpC and HrpA, respectively. *Xenorhabdus nematophila* NilB is a $TXISS_{OMP}$ that, along with the associated lipoprotein NilC, is necessary for mutualistic colonization of the nematode *Steinernema carpocapsae* (Cowles and Goodrich-Blair, 2008; Hooda et al., 2016, 2017; Fantappie et al., 2017; da Silva et al., 2019; Bateman et al., 2021; Grossman et al., 2021).

Current evidence indicates $TXISS_{OMPs}$ have specificity for their cargo. When expressed in *Escherichia coli* BL21-C43, *Neisseria* TXISS-1A homologs Slam1 and Slam2 do not translocate each other's cargo proteins, nor can Slam1 translocate the *E. coli* periplasmic lipoprotein PgaB (Hooda et al., 2016). TXISS cargo proteins for which there are known structures (TbpB, LbpB, fHbp, HupA) have limited sequence similarity but a common organization of an N-terminal effector domain and a C-terminal 8-stranded β-barrel that may direct a cargo for secretion (Hooda et al., 2017). The TbpB C-terminal β-barrel is the first part of the cargo protein to be surface exposed during secretion (Hooda et al., 2016), which may indicate this domain initiates interactions with $TXISS_{OMPs}$. Hooda et al. (2017) suggested that, in contrast to the common C-terminal β-barrel, the N-terminal regions of TXISS cargo proteins are variable. This suggests a general conceptual framework in which the cargo C-terminus is necessary for its interaction with a $TXISS_{OMP}$, while the N-terminus encodes the host interaction (or other) effector domain.

An *X. nematophila* $TXISS_{OMP}$, NilB, is encoded near an outer membrane lipoprotein NilC on a locus known as Symbiosis Region 1 (SR1) (Heungens et al., 2002; Cowles and Goodrich-Blair, 2004; Bhasin et al., 2012). In *X. nematophila,* the SR1 locus, which encodes both *nilB* and *nilC,* is necessary and sufficient for normal levels of colonization of *S. carpocapsae* intestines (Heungens et al., 2002; Cowles and Goodrich-Blair, 2008; Chaston et al., 2013). *nilB* and *nilC* are not organized in an operon and have two different promoter sequences, but they are coordinately downregulated at the transcriptional level by the transcription factors NilR and Lrp in a synergistic manner (Cowles and Goodrich-Blair, 2006). Although NilB and NilC function in *S. carpocapsae* colonization is well-established, their cellular and molecular functions remain unclear. Given that NilB is a member of the $TXISS_{OMP}$ family that facilitates the surface exposure of target lipoproteins, we considered the model that it functions to facilitate NilC surface exposure, and that NilC is a host-interaction effector. We describe here experiments to determine if NilB and NilC form a $TXISS_{OMP}$–host interaction effector pair by determining if NilC lipoprotein can be surface exposed, if NilB facilitates NilC lipoprotein surface exposure, and what effector activity one or both of them might have with respect to host interactions.

RESULTS

NilB Facilitates NilC Surface Exposure During Heterologous Expression in *Escherichia coli*

To determine if NilC is a cargo protein for NilB, we monitored NilC surface exposure during heterologous expression

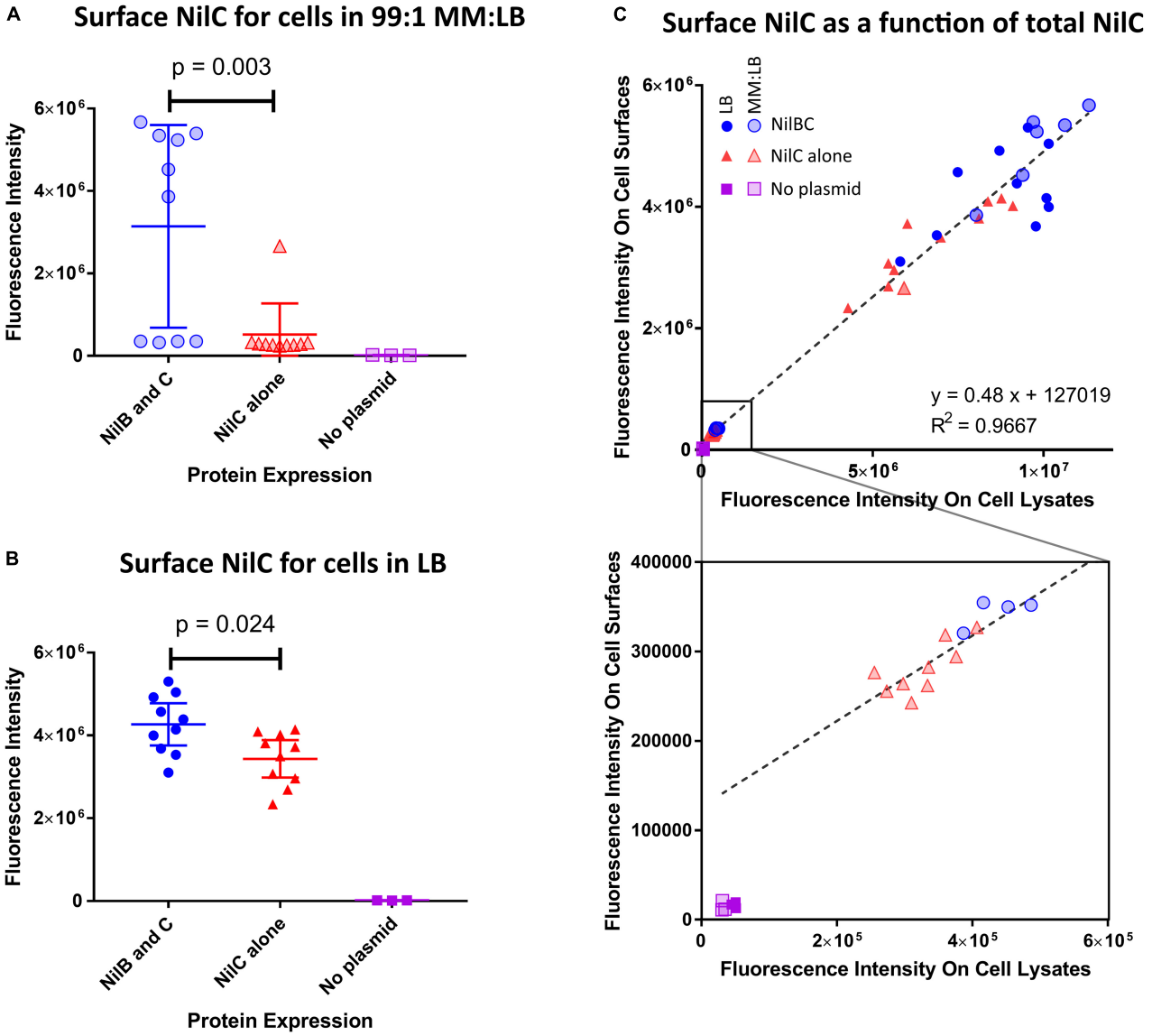

FIGURE 1 | NilB positively influences the amount of NilC present on the surface of *E. coli* when co-expressed. *E. coli* BL21 DE3 C43 was transformed with pET-Duet-1 plasmids carrying *nilC* alone (red triangles) or both *nilC* and *nilB* (blue circles) under control of the inducible T7 polymerase promoter. A no-plasmid control (purple squares) was included to account for a potential cross-reacting signal. Surface exposure of NilC was quantified by immunofluorescence with anti-NilC antibody dot blotting of cells grown in LB [**(B,C)** solid symbols], or MM:LB [**(A,C)** transparent symbols]. *p*-values were determined *via* one-way ANOVA with Tukey's multiple comparison. Total cellular levels of NilC were quantified by immunoblotting whole cell lysates from the same samples and surface NilC as a function of total cellular NilC is shown in **(C).** A linear regression of data from both media conditions revealed that total NilC expression was a strong predictor of surface exposure of NilC (R-squared = 0.9667). The bottom graph provides an expanded view of the region of the top graph indicated with a square.

in *Escherichia coli,* with and without co-expression with NilB. We constructed plasmids in which expression of *nilC* and, when present, *nilB* are under control of an IPTG-inducible T7 RNA polymerase (see section "Materials and Methods"). NilC surface exposure experiments were conducted by immuno-dot blotting with an anti-NilC antibody. As expected, *E. coli* without an expression plasmid did not react with the antibody. For NilC-expressing strains, we found that NilC was present on the surface of *E. coli* at significantly higher levels in the presence of NilB than in its absence after cultivation in either LB (**Figure 1B** and **Supplementary Figure 1**) or a minimal glucose medium supplemented with 1% LB (MM:LB) (**Figure 1A**). When considering all treatments together, we noted a positive correlation between the total amount of NilC expressed and the amount on the cell surface. This indicates that NilC can efficiently reach the *E. coli* cell surface even in the absence of NilB (**Figure 1C**). However, when NilC was expressed alone, its levels on the cell surface were 16.5% or 80% of those observed when co-expressed with NilB, during incubation in MM:LB or LB, respectively, indicating that NilB enhances the surface

exposure of NilC. Furthermore, supernatants of induced *E. coli* cells expressing *nilC* with or without *nilB* did not have NilC levels detectable by the immuno-dot-blotting assay, indicating that cell lysis does not explain the surface NilC levels detected (**Supplementary Figure 2**). These data indicate that the presence of NilB supports greater overall levels of NilC expression in *E. coli* and that, like its $TXISS_{OMP}$ family relatives, NilB facilitates surface exposure of its cargo: NilC lipoprotein. NilC surface exposure enhancement by, rather than complete dependence on, NilB $TXISS_{OMP}$ is similar to the relationship between *N. meningitidis* fHbp and its $TXISS_{OMP}$, Slam1. In either *E. coli* or *N. meningitides*, the fHbp lipoprotein can be surface exposed even in the absence of Slam1, particularly when expressed at high levels, but fHbp surface levels are elevated in the presence of Slam1 (Hooda et al., 2016; Fantappie et al., 2017; da Silva et al., 2019).

NilC Is a Two-Domain Protein With a Predicted C-Terminal, 8-Stranded β-Barrel

Given these data that indicate NilC is a surface exposed cargo protein for the NilB $TXISS_{OMP}$, we sought to understand its molecular properties and biological function. Our investigation of the structural and biophysical characteristics of NilC required purified protein. A recombinant NilC soluble domain ($NilC_{22-282}$) with a C-terminal 6X-His tag was expressed in *E. coli* and purified by nickel affinity and size exclusion chromatographies. The C-terminal His-tag did not impede the ability of NilC to function in colonization when it was expressed instead of the native sequence in *X. nematophila* (**Supplementary Figure 3**). The purified protein is remarkably highly soluble, remaining in solution until at least 80 mg/ml. Secondary structure prediction based on the NilC amino acid sequence indicates a protein that is largely random coil (∼71–74%) with only ∼24% of the protein predicted to form β-strand and little to no α-helix predicted (∼0–4%) (**Figure 2A**). This prediction was corroborated by circular dichroism (CD). The $NilC_{22-282}$ CD spectrum is noteworthy for the fact that it has apparently no characteristic negative signal of α-helix (208 and 222 nm) or β-strand (218 nm) secondary structure elements (**Figure 2B**). On the other hand, the NilC spectrum has a positive band centered at 200 nm, which indicates it is not completely unfolded, as disordered proteins have a negative band at 195 nm. We suspected that a negative signal at 218 nm for β-strand might be masked in the experimental spectra by the high concentration of random coil with a positive signal at a nearby wavelength. CD spectrum deconvolution using CONTIN and BeStSel algorithms supported this interpretation and indicates a β-strand content between 43 and 49%, with no significant presence of α-helix (∼2%).

Tertiary structure predictions of NilC – both *via* well-established remote homology modeling in Phyre2 (Kelley et al., 2015) or *via* neural net analysis as implemented in RoseTTAFold (Baek et al., 2021), AlphaFold2 (Jumper et al., 2021), and their combined implementation in ColabFold (Mirdita et al., 2021) – predict with high statistical significance the 8-stranded C-terminal β barrel of the TX1SS targeting domain. The structure of this domain is robustly modeled using *Haemophilus haemolyticus* hemophilin (PDB: 6OM5) as a template (Latham et al., 2020). The N-terminal effector domain, on the other hand, is poorly defined even by these recent powerful structure prediction methods, although all models of the N-terminal domain have a large fraction of random coil, ∼7 β-strands or extended segments without well-defined secondary structure, and, essentially, no α-helical content (**Figure 2C**). These predictions are an excellent match to our experimental measurements. Intriguingly, a surface electrostatic calculation of the model with the highest amount of secondary structure shows a large non-polar patch, an unexpected feature for a protein so readily soluble (**Figure 2D**). Indeed, because the first 40 amino acids of the mature NilC sequence contain a high fraction of glycine and proline, we surmised they might be highly disordered. We thus created a second NilC construct, and expressed and purified $NilC_{62-282}$. This protein is significantly less soluble than $NilC_{22-282}$, bolstering the hypothesis that this N-terminal extension may protect the hydrophobic patch of purified $NilC_{22-282}$ in solution. We also noticed an unusually high concentration of tyrosine in the primary sequence, with 12 Tyr in the first 133 amino acids of the secreted protein (9%) (**Supplementary Figure 4C**). Tyrosine is an important element in sugar-binding sites for its aromatic stacking and, to a lesser extent, -OH hydrogen bond-donating abilities (Quiocho, 1986; Weis and Drickamer, 1996; Hudson et al., 2015; Banno et al., 2017). The only homologs of *X. nematophila nilC* identified to date occur in two other species (of ∼23 with sequenced genomes) of nematode-associated *Xenorhabdus: X. innexi* and *X. stockiae*, both of which also contain the associated *nilB* gene (Grossman et al., 2021) (**Supplementary Figures 4A,B**). In each case, the NilC polypeptide is predicted to be a two-domain protein with a C-terminal barrel and conserved tyrosines at positions 75 and 77 of the mature sequence in the N-terminal presumed effector domain (**Supplementary Figure 4C**). Both of these tyrosines occur within a region predicted to be a β-strand (**Figures 2A,C**).

To further our experimental characterization of $NilC_{22-282}$, we collected a 2D ^{1}H-^{15}N HSQC spectrum of ^{15}N labeled protein. The nuclear magnetic resonance (NMR) spectrum shows good signal dispersion, covering a range of more than 4 ppm on the proton axis, indicating NilC is well-folded under the conditions used (Felli and Pierattelli, 2015; **Supplementary Figure 5**). The most intense peaks, which are collapsed into the center of the spectrum, imply that some parts of the protein are highly flexible. Finally, we carried out limited protease digestion of $NilC_{22-282}$ in order to experimentally investigate the potential for stable subdomains. Several fragments of sizes between 12 and 27 kDa are relatively stable intermediate breakdown products of NilC (**Supplementary Figure 6A**). Mass spectrometry of the peptide mixture after partial digestion identified the prominent fragment as having a mass of approximately 12,358 Da (**Supplementary Figure 6B**). Mapping of this mass onto the possible array of all Proteinase K partial digestion fragments provides insight into the folded core of NilC. This mass corresponds to the C-terminal barrel without its last strand, implying once again that the two

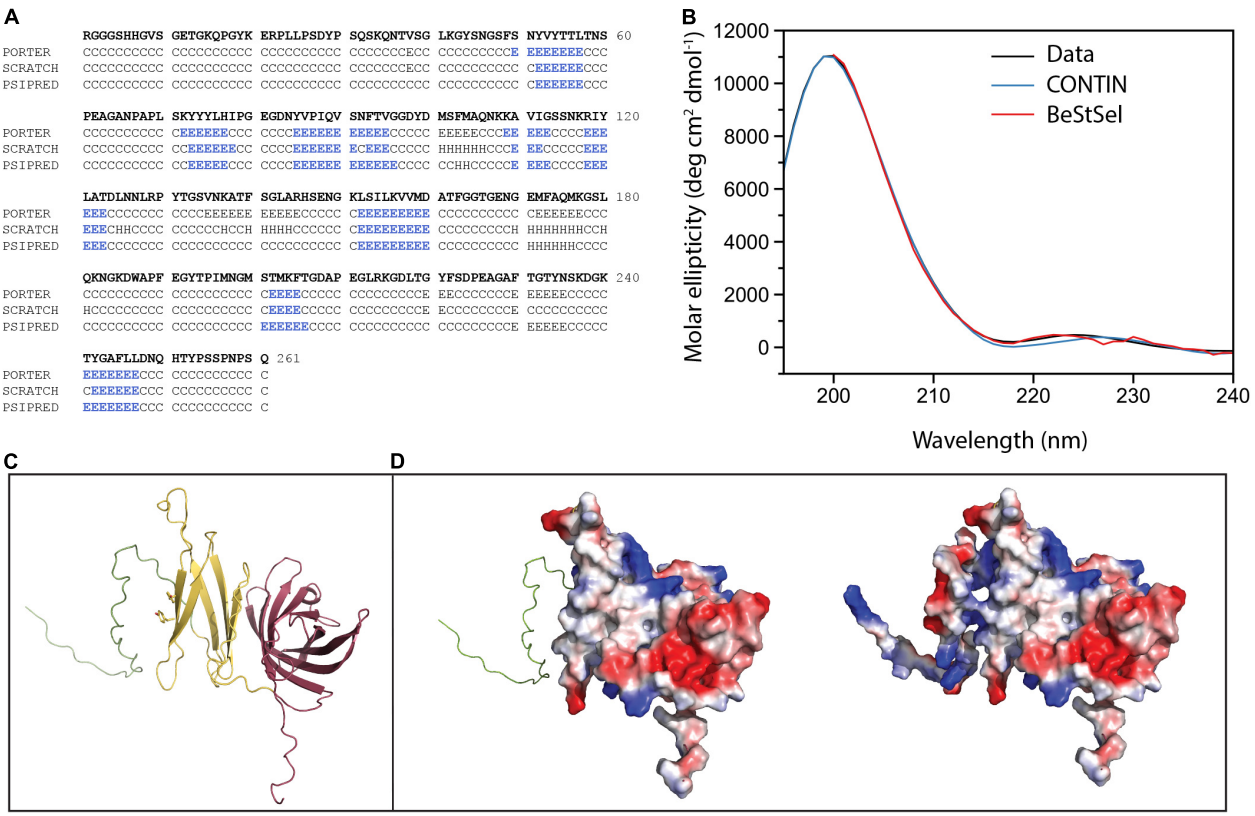

FIGURE 2 | NilC secondary structure and structural models. **(A)** Secondary structure prediction for NilC$_{22-282}$ was performed using Porter, Scratch, and Psipred algorithms (E β-strand, H α-helix, C random coil) with blue highlighting indicating the β-strand elements predicted by each. **(B)** A NilC$_{22-282}$ CD spectrum was collected at 25°C in an AVIV model 420 CD spectrometer. Deconvolution of the spectra using two algorithms leads to excellent agreement with experimental measurement. **(C)** The NilC structural model showing disordered N-term (green), a relatively flexible N-terminal effector domain (yellow), and an 8-stranded barrel TXISS-targeting domain (purple). The two tyrosines conserved among *Xenorhabdus* NilC homologs are shown. **(D)** On the left, the electrostatic surface of effector and barrel domains (red, negative; blue, positive; and white, neutral charge densities) is shown, and, on the right, the electrostatic surface of entire protein, suggesting the charged N-terminal extension may help solubilize the protein despite the hydrophobic patch.

domains of NilC are structurally distinct, the first more open and flexible, the second stably folded (**Figure 2C**).

Taken together, these data present a consistent picture of non-acylated NilC as a highly soluble and folded two-domain protein formed of sections of β-structure and a large fraction of random coil. The C-terminal domain is an 8-stranded barrel, adding support to the hypothesis that this structural motif is the common feature of TXISS cargo proteins. On the other hand, all of our experimental results indicate the N-terminal domain does not adopt a very well-defined structure, and that, under the conditions tested and in the absence of any potential ligands, NilC includes flexible regions and protease-accessible sites.

NilC Is Surface Exposed in *Xenorhabdus nematophila* Cells When Expressed at High Levels

Given the evidence that NilC can be surface exposed in *E. coli* and that its C-terminal domain is predicted to form an 8-stranded barrel TXISS-targeting domain, we revisited the question of whether NilC is also surface exposed in the native context of an *X. nematophila* cell. Previous whole-cell protease-digestion data demonstrated periplasmic orientation of the lipoprotein NilC, based on the observation of protease resistance of NilC in the whole cell but not lysate samples of wild type *X. nematophila* (Cowles and Goodrich-Blair, 2004). Later, another protease digestion experiment to detect surface NilC was performed on an *X. nematophila*Δ*nilR* mutant, in which the absence of the transcription factor NilR causes *nilB* and *nilC* expression to be de-repressed (Cowles and Goodrich-Blair, 2006; Bhasin et al., 2012). In this analysis, slight shaving of NilC was detected in whole cells, indicating some surface exposure (Bhasin et al., 2012). To further examine *X. nematophila* NilC cellular localization, we used the same immuno-dot-blotting approach we had used for *E. coli* (**Figures 3A,B**). We assessed NilC levels in *X. nematophila* wild type compared to an isogenic Δ*nilR* mutant. In addition, we included an isogenic pair of Δ*nilR* strains in which the SR1 locus has been deleted from its native locus, and reintroduced, either as a wild type sequence, or including a *nilCM1Z* start-to-stop codon mutation, at the *att*Tn*7* site downstream of the conserved gene *glmS*, which is involved in peptidoglycan biosynthesis (Craig, 1991; Peters and Craig, 2001; Choi et al.,

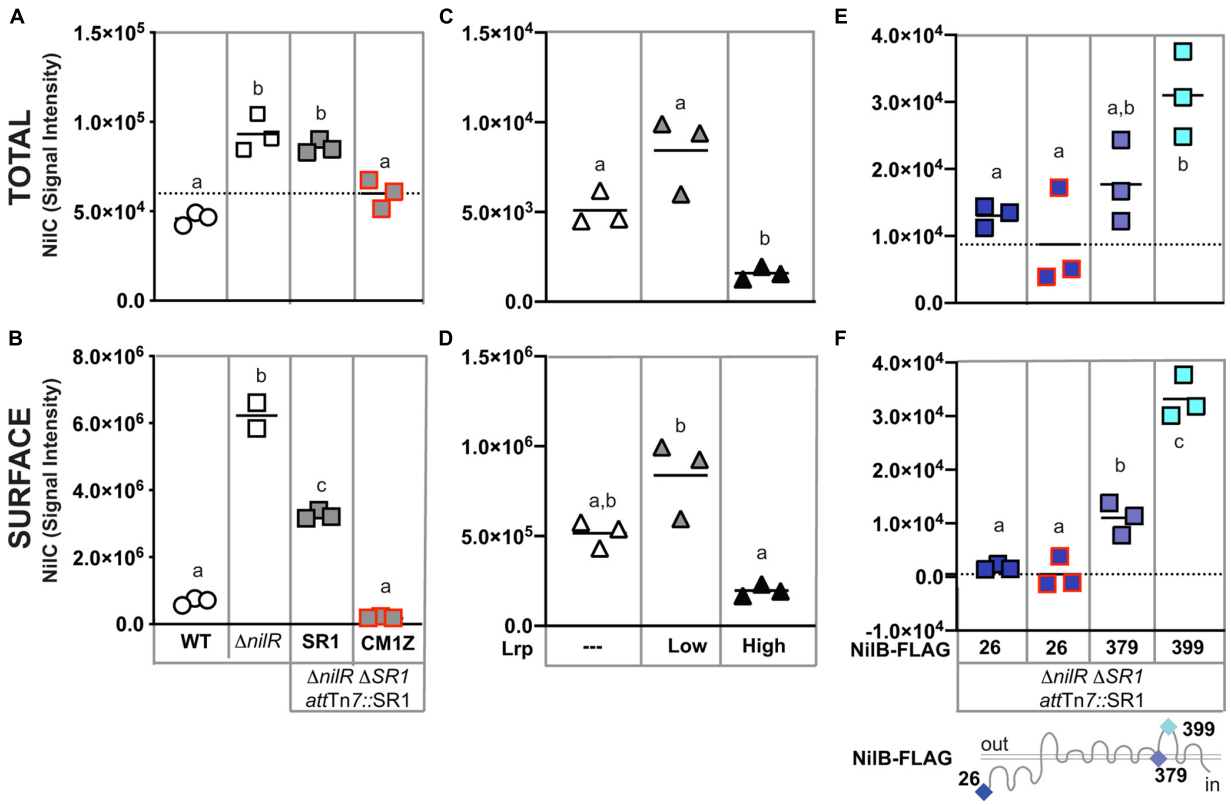

FIGURE 3 | *Xenorhabdus nematophila* NilC is surface exposed by NilB when its expression is de-repressed. Cell lysate **(A,C,E)** or whole cell **(B,D,F)** preparations of LB-grown *X. nematophila* wild type (WT, circles), Δ*nilR* (squares), or Δ*lrp* (triangles) strains. At the *att*Tn*7* site of Δ*nilR*Δ*SR1* strains, wild-type SR1 (gray squares with a black outline) or SR1 with a *nilCM1Z* mutation (a red outline) and/or *nilB*-FLAG insertions (blue-shaded squares, sites of insertion noted beneath and on the NilB schematic bottom) were introduced **(A,B,E,F)**. Δ*lrp* strains were transformed with a vector-only control (white triangles) or plasmids expressing low or high levels of Lrp (gray and black triangles, respectively) **(C,D)**. Treatments were spotted onto nitrocellulose membranes. NilC was detected by immunoblotting with anti-NilC antibodies. Significantly different groups within each panel are indicated with different letters (tested using one-way ANOVA with Tukey's *post hoc* multiple comparisons analysis). Dashed axis lines indicate the mean of the *nilCM1Z* datapoints **(A,E,F)**.

2005). The latter strain served as a negative control for NilC detection by an antibody.

In cell lysates (indicative of overall expression), we detected antibody reactivity in all strains tested, including the *nilCM1Z* negative control, indicating some cross-reactivity by the polyclonal antibody (**Figure 3A**). However, NilC-expressing strains had significantly higher antibody reactivity for whole cells than the *nilCM1Z* control, demonstrating the effective detection of NilC surface exposure using this method. When assessing levels of surface NilC in whole cell preparations of *X. nematophila,* we observed that wild type (*nilR*+) cells had little detectable NilC, while the Δ*nilR* strain had significantly higher signal intensity, indicative of surface NilC being present when *nilC* is de-repressed by deletion of *nilR*. Curiously, in strains in which SR1 had been introduced into the *att*Tn*7* site downstream of *glmS*, we observed a significant reduction in the amount of surface-exposed NilC detected relative to the isogenic parent Δ*nilR* strain, although total NilC levels were not significantly different (**Figure 3B**).

NilR synergistically represses *nilB* and *nilC* with another transcription factor, Lrp (Cowles and Goodrich-Blair, 2004, 2006). *X. nematophila* Lrp controls both mutualistic (with nematodes) and pathogenic (with insects) phenotypes. *X. nematophila* cells with fixed high levels of Lrp display higher levels of biofilm formation, nematode reproduction, and intestinal colonization, while *X. nematophila* cells with fixed low levels of Lrp display greater virulence in insects, compared to each other (Cowles and Goodrich-Blair, 2006; Hussa et al., 2015; Cao et al., 2017; Cao and Goodrich-Blair, 2020). We tested the impact of fixed high or low Lrp expression on NilC surface exposure and found that, as expected, NilC levels and surface exposure were inversely correlated with Lrp levels (**Figures 3C,D**); *X. nematophila* cells expressing high levels of Lrp had significantly lower levels of total and surface-exposed NilC relative to cells lacking or expressing low levels of Lrp.

Having demonstrated above that NilB facilitates NilC surface exposure during heterologous expression in *E. coli*, we endeavored to determine if this is also the case in the native *X. nematophila* context. We used immuno-dot blotting to examine NilC surface exposure in cells expressing select NilB FLAG-tag variants encoded by the SR1 locus integrated at the

*att*Tn*7* site in a Δ*nilR*Δ*SR1* strain background (**Figures 3E,F** and **Supplementary Figure 7**). Our previous work using these and other FLAG-tag insertions across the length of the $TXISS_{OMP}$ NilB revealed a topology consisting of a ∼138-amino acid N-terminal domain and 7 surface loops (Bhasin et al., 2012; **Figure 3**). A variant with a FLAG-tag insertion at the mature, periplasmically oriented N-terminus of NilB (FLAG-26), expresses detectable levels of NilB and functions as well as wild type in colonization. Another variant, with an insertion in a transmembrane helix (FLAG-379), does not express detectable levels of NilB and is insufficient for colonization (Bhasin et al., 2012). These two variants were used to compare surface levels of NilC surface exposure in the relative presence (FLAG-26) or absence (FLAG-379) of detectable NilB. Again, as was noted in other experiments, the total levels of NilC detected within cells correlated with the amount of NilC on the cell surface (compare **Figures 3E,F**). Surprisingly, significantly less surface NilC was detected in the FLAG-26 strain (that expresses detectable levels of NilB) relative to the FLAG-379 strain (which does not express detectable levels of NilB) during growth in LB. This indicates that a basal level of NilC can be surface exposed in the absence of NilB (**Figure 3F**), and that NilB can limit surface exposure of NilC. We next assessed the impact on NilC surface exposure of a FLAG-399 insertion in surface loop 6 of NilB. This variant expressed detectable NilB but is not functional in colonization. The FLAG-399 variant had significantly more surface NilC than either of the other two FLAG variants, suggesting that mutating the sixth extracellular NilB loop results in increased secretion of NilC cargo protein. A similar trend was noted when these same strains were grown in a minimal medium supplemented with casamino acids (**Supplementary Figures 8A,B**), although, in this case, the FLAG-26 expressing strain displayed relatively higher and more variable surface levels of NilC. As an alternate method of detecting surface NilC, *X. nematophila* whole cells grown in defined media supplemented with casamino acids and incubated with anti-NilC antibody (Cowles and Goodrich-Blair, 2004) and a fluorescent secondary antibody was observed using flow cytometry (**Supplementary Figure 8C**). Overall, these data using different growth conditions and immunodetection methods support the conclusion that, in *X. nematophila,* $TXISS_{OMP}$ NilB can either inhibit or promote NilC surface presentation, relative to cells without NilB, which may suggest that $TXISS_{OMP}$ activity is modulated depending on environmental conditions.

Taken together, the data described above are consistent with the model that NilB facilitates surface exposure of NilC, and that, when *nilB* and *nilC* expression is de-repressed by deletion of the transcription factors NilR or Lrp, NilC is surface exposed in *X. nematophila*. Our biophysical data indicate that, like other TXISS cargo proteins, NilC is a two-domain protein, with a C-terminal barrel domain proposed to be the TXISS targeting motif, and an N-terminal domain proposed to be a host-interaction effector. To further explore the possible effector role of *X. nematophila* NilC, we took a two-pronged approach. In the first approach, we used histochemistry to examine the molecules that are specifically presented on the host nematode intestinal surface, where *X. nematophila* adheres in a manner positively influenced by NilB and NilC (Chaston et al., 2013). In the second, we compared the proteomes and metabolomes of *X. nematophila* strains with and without SR1 to identify metabolic pathways and activities that may be impacted by the presence or absence of NilB and NilC.

The *Steinernema carpocapsae* Anterior Intestinal Cecum Expresses a Wheat-Germ Agglutinin-Reactive Material That Contributes to SR1-Mediated *Xenorhabdus nematophila* Colonization

Xenorhabdus bacteria colonize the anterior intestinal cecum (AIC) of their *Steinernema* nematode hosts during the reproductive juvenile and adult stages (**Figures 4A,D**). The AIC is immediately posterior to the basal bulb, a pumping organ that drives ingestion from the mouth, through the esophagus, and into the intestine (**Figure 4A**). To begin investigating the surface chemistry of the AIC bacterial colonization site, we selected three nematodes: *S. carpocapsae*, *S. scapterisci,* and *S. feltiae*. The symbionts of the first two nematodes, *X. nematophila* and *X. innexi*, respectively, both encode NilB and NilC homologs (**Supplementary Figure 4**). The symbiont of *S. feltiae, X. bovienii*, does not. Adult nematodes that had been raised in the presence or absence of their bacterial symbiont were treated with lectin fluorescent conjugates and observed by fluorescence microscopy for lectin binding to host tissues, monitoring frequency of binding to the mouth, the esophagus, the basal bulb, the AIC, and the intestine (**Figure 4B**). We found that all lectins tested had some binding to various tissues in all three nematodes tested. Binding varied according to the media type (lipid agar or liver kidney agar) as well as the presence/absence of bacterial symbiont (**Supplementary Data File 1** and **Supplementary Figure 9**).

We focused our attention on fluorescent conjugate wheat germ agglutinin (F-WGA, which reacts with *N*-acetyl glucosamine or *N*-acetyl neuraminic acid), because this lectin had consistent reactivity with *S. carpocapsae* nematode tissues, and because it previously had been observed to react with material extruded from the intestinal receptacle colonization site of the infective juvenile stage *S. carpocapsae* nematode (Martens et al., 2005). As a control, we included fluorescent conjugate Ulex Europaeus Agglutinin (F-UEA), which reacts with alpha-linked fucose. Observed individuals from all three nematode species from all three cultivation conditions displayed both F-WGA and F-UEA localization to the intestine (**Figure 4C**). In contrast, F-WGA but not F-UEA localized to the AIC. F-WGA localization to the AIC occurred in *S. carpocapsae* and *S. scapterisci,* but not *S. feltiae* consistently at high frequency (88–95%, 66–84%, and 3–59%, respectively), indicating that the two nematode hosts of SR1-encoding symbionts consistently express F-WGA-reactive material at the symbiont colonization site, while the host of the non-SR1-encoding symbiont does not (**Figure 4C**).

Given that both F-WGA and the respective *Xenorhabdus* bacterial symbionts are able to bind to the AIC of both

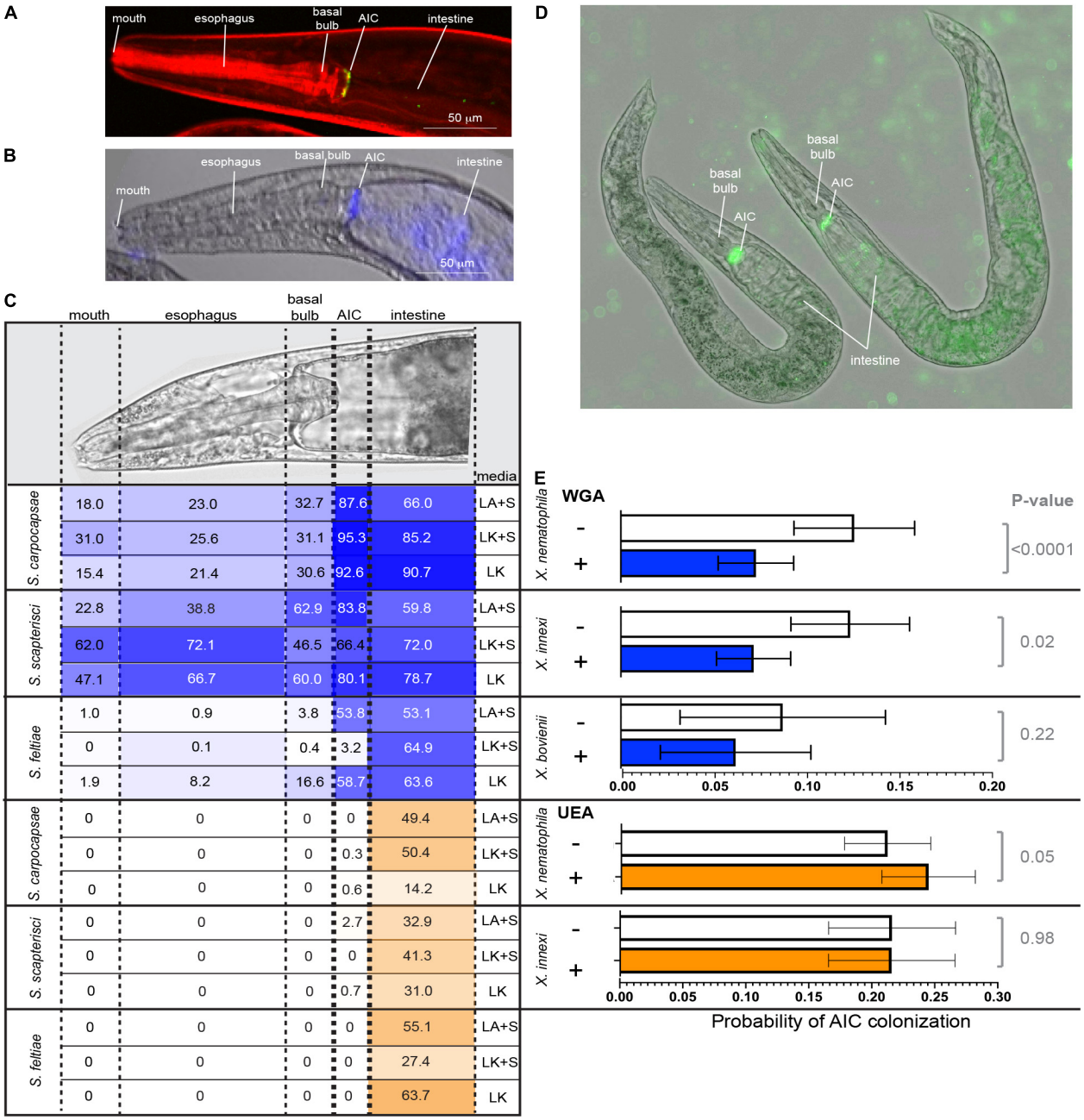

FIGURE 4 | (A) *S. carpocapsae* nematode colonized at the anterior intestinal cecum (AIC) by *X. nematophila* expressing green fluorescent protein. Nematode tissue is stained with rhodamine phalloidin. **(B)** False color overlay (a bright field and fluorescence) of uncolonized *S. carpocapsae* grown on liver kidney agar without symbiont, and then incubated with F-WGA (a blue color) for 24 h before imaging. **(C)** At the top is shown a DIC image of *S. carpocapsae* with assayed body parts (mouth, esophagus, basal bulb, AIC, and intestine), roughly defined by dashed lines. *S. carpocapsae, S. scaptersici,* and *S. feltiae* were grown on lipid agar or liver kidney agar (LA or LK) with their respective symbionts (+S) or on liver kidney agar without their symbionts. Nematodes were incubated for 24 h with either F-WGA (blue, top section) or F-UEA (orange, bottom section) before observation for lectin binding to individual body parts. The percentage of all observed nematodes that had lectin binding at that body part is indicated within each cell, and is also represented by the intensity of shading (darker shading = higher percentage). WGA, but not UEA, reproducibly binds to the AIC, with the highest frequencies observed in *S. carpocapsae* and *S. scapterisci* grown on lipid agar with their respective symbionts. **(D,E)** Competition experiments were conducted in which nematodes cultivated on liver kidney agar without their symbionts were exposed to WGA, UEA, or a PBS control and with their green fluorescent protein-expressing *Xenorhabdus* symbiont. After 24 h, individual nematodes were imaged and assessed for colonization at the AIC. **(D)** Shows *X. nematophila* AIC colonization within two *S. carpocapsae* nematodes incubated without lectin (PBS control). **(E)** Probability of AIC colonization by the symbiont of each nematode (*X. nematophila* colonizing *S. carpocapsae, X. innexi* colonizing *S. scapterisci,* and *X. bovienii* colonizing *S. feltiae*) after incubation without (–; white bars) or with (+) WGA (blue bars) or UEA (orange bars). The probability of AIC colonization in *S. carpocapsae* and *S. scapterisci*, but not *S. feltiae*, was significantly affected by treatment with WGA (*S. carpocapsae*: $F_{3,59} = 3.91$, $p = 0.01$; *S. scapterisci*: $F_{1,72} = 5.37$, $p = 0.02$; *S. feltiae*: $F_{1,32} = 1.5$, $p = 0.23$), but not UEA (*S. carpocapsae*: $F_{1,2684} = 3.70$, $p = 0.05$; *S. scapterisci*: $F_{1,2696} = 0$, $p = 0.9833$).

S. carpocapsae and *S. scapterisci* in the majority of the nematode population, we hypothesized that the WGA-reactive material might be important for colonization of their bacterial symbionts as a binding ligand, a nutrient source, or both. We reasoned that if the WGA-reactive material is involved in colonization, that the addition of soluble WGA to adult nematodes would block bacterial interaction with the WGA-reactive material on the AIC surface. To test this idea, we exposed adult nematodes simultaneously to unconjugated WGA and GFP-expressing bacterial symbionts for 24 h before monitoring by fluorescence microscopy the presence of bacterial colonization at the AIC (**Figure 4D**). The presence of WGA significantly reduced the presence at the AIC of GFP-expressing *Xenorhabdus* symbionts in both *S. carpocapsae* ($p < 0.0001$; note that composite data including both wild type and Δ*SR1* treatments were included in this analysis) and *S. scapterisci* ($p = 0.02$) but not in *S. feltiae* ($p = 0.23$) when compared to a control that was exposed only to the GFP-expressing bacterial symbionts (**Figure 4E**). In contrast, the presence of UEA did not decrease the probability for either *X. nematophila* or *X. innexi* to colonize their nematode hosts (*S. feltiae* was not examined) (**Figure 4E**).

We next considered the possibility that the Nil proteins are responsible for interaction with the AIC WGA-reactive material. If so, then we predict that any Nil-independent adherence to the AIC would not be inhibited by WGA. To test this idea, we analyzed the data to discern the influence of the presence or absence of the SR1 locus on *X. nematophila* colonization of *S. carpocapsae* nematodes exposed or not to WGA. The probability of *X. nematophila* colonization of the *S. carpocapsae* AIC was significantly higher ($p < 0.05$) for SR1 + treatments (0.114 ± 0.022 and 0.146 ± 0.027 with and without WGA, respectively), relative to Δ*SR1* treatments (0.095 ± 0.019 and 0.083 ± 0.017, with and without WGA, respectively). Also, consistent with the role for SR1 in mediating interactions with the WGA-reactive material, the probability of AIC colonization by Δ*SR1 X. nematophila* was not significantly altered by the presence of WGA ($p = 0.36$).

We hypothesized that *X. nematophila* surface-exposed NilC interacts with molecules on the AIC surface. If so, then we predicted that, as with WGA, the addition of free, soluble NilC would inhibit bacterial interaction with the AIC. We exposed nematodes (cultivated in the absence of their symbiont) to purified NilC protein and GFP-expressing *X. nematophila* cells with or without the SR1 locus. In this experiment, the isogenic Δ*SR1 X. nematophila* strains with and without the SR1 locus at the *att*Tn*7* site colonized to similar levels, indicating that the conditions of the experiment were insufficient to distinguish the two strains. However, for both strains, we observed that nematodes exposed to NilC exhibited significantly (*S. carpocapsae* WT $p = 0.0042$, Δ*SR1* $p = 0.0088$) higher rates of colonization compared to nematodes exposed to just the GFP-expressing symbionts (**Figure 5**). This finding was contrary to our prediction and may indicate that free NilC can facilitate colonization, perhaps by signaling for, or directly catalyzing, release of a nutrient from the host-cell surface. To pursue this hypothesis, we created an *X. nematophila* strain, expressing a non-lipidated version of NilC (generated by the introduction of two lipobox mutations: V17A and C20S). This strain was unable to colonize the infective juvenile stage of *S. carpocapsae* nematodes (**Supplementary Figure 3**). Indeed, unlike wild type NilC, the V17A-C20S NilC protein was not detected on the *X. nematophila* cell surface, and was only detected in the supernatant in 2/6 replicate samples (**Supplementary Figure 10**). These data suggest that non-lipidated NilC is predominantly retained within the periplasm.

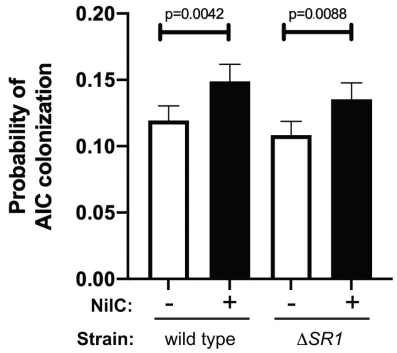

FIGURE 5 | Addition of soluble, purified NilC increases colonization of the anterior intestinal cecum. Mean with standard error of the probability of AIC colonization is shown. Green-fluorescent protein expressing *X. nematophila* wild type or Δ*SR1* mutant was exposed for ~24 h to *S. carpocapsae* nematodes in a buffer with (+) or without (–) purified, soluble NilC protein. Nematodes were observed by microscopy for the presence or absence of *X. nematophila* at the anterior intestinal cecum (AIC). A total of 8,384 observations were made and analyzed using PROC GLIMMIX of SAS to determine if treatment combination (NilC and strain) differed in probability for colonization. There were differences in probability for colonization ($p = 0.0004$), and there was significantly higher AIC colonization in the presence of NilC for both wild type and Δ*SR1*.

Deletion of *nilB* and *nilC* Causes Global Metabolome and Proteome Changes Including Impacts on a Peptidoglycan Precursor and Exopolysaccharide Biosynthesis

Based on the data described above, our working model is that NilB is a $TXISS_{OMP}$ that conditionally facilitates surface exposure of the lipoprotein NilC, which is a host-interaction effector. Since external treatment with WGA inhibits *X. nematophila* interaction at the nematode AIC surface, while soluble NilC enhances this interaction, we infer that NilC either interferes with a host defense pathway, as for the TXISS cargo factor H-binding protein, or helps to acquire a host-derived nutrient, similar to the function of TXISS lipoprotein effectors transferrin and lactoferrin-binding proteins. To gain insights into downstream physiological effects of NilC action, we compared the proteomes and metabolomes of *X. nematophila*Δ*nilR*Δ*SR1* emptyTn*7* relative to the Δ*nilR*Δ*SR1* Tn*7*:*SR1* (for this comparison, referred to as Δ*SR1* and WT, respectively) (**Supplementary Table 1**). We grew the

X. nematophila cells in a minimal medium with glucose as a carbon source (**Supplementary Figure 11**) and harvested cells and supernatant at OD_{600} ∼0.6 for processing and analysis. Whole cell and supernatant samples were analyzed by liquid chromatography tandem mass spectrometry (LC-MS/MS) for proteomic analysis and ultra-high-performance liquid chromatography high-resolution mass spectrometry (UPLC-HRMS) for metabolomic analysis.

In the proteomics comparison of WT and Δ*SR1*, 3,336 proteins were detected in total: 1,742 proteins in whole cell samples and 1,594 proteins in the supernatant samples. Of the 3,336 proteins detected, 61 were considered to be significantly different in abundance between Δ*SR1* and WT based on a Student's *T*-test filter ($p < 0.05$) and a fold change filter ($|FC| > 1$) (**Supplementary Tables 2, 3** and **Figures 6A,B**). In the metabolomics dataset, 85 metabolites were identified in total, and comparisons were made between the metabolomes using partial least square discriminant analysis (PLS-DA) to determine the separation of the strain metabolic profiles (**Supplementary Figure 12**). For both the supernatant and whole cell fractions, there is clear separation of the metabolic profiles between Δ*SR1* and WT. Student's *t*-tests were applied to determine significant metabolites between strains. For the whole cell fraction, 18 metabolites were significant ($p < 0.1$) and 10 metabolites were significant ($p < 0.1$) for the supernatant fraction (**Supplementary Data File 2** and **Supplementary Figure 12C**).

Among the metabolites with elevated abundance in the WT strain were the amino sugars *N*-acetylglucosamine 1/6-phosphate, glucosamine phosphate, and the nucleotide sugar UDP-glucuronate, and, from the PLS-DA analysis (VIP > 1), the nucleotide amino sugar UDP-*N*-acetylglucosamine, the precursor to the exopolysaccharide poly-β - 1,6-*N*-acetylglucosamine (PNAG) (**Figure 7** and **Supplementary Figure 12**). UDP-glucuronate is a central intermediate in the synthesis of precursors for exopolysaccharide and cell wall polysaccharide biosynthesis. The proteome revealed that a putative UDP-glucuronate epimerase (XNC1_2486) (Borg et al., 2021) has lower abundance in WT relative to Δ*SR1* (**Supplementary Table 2**), consistent with the elevated UDP-glucuronate abundances detected in the former. Amino sugars are involved in peptidoglycan and exopolysaccharide biosynthesis and can be used by bacteria as sources of carbon and nitrogen by catabolism through glycolysis (Dobrogosz, 1968). Consistent with this metabolic connection, according to the PLS-DA analysis, relative to Δ*SR1*, whole cell samples of WT had higher abundances of the glycolytic intermediates 3-phosphoglycerate and fructose 1,6-bisphosphate, as well as UDP-glucuronate and UDP-glucose, lipopolysaccharide precursors. The proteomic data also indicated differences between the WT and Δ*SR1* strains in polysaccharide and glycolytic processes.

The differentially abundant proteome included XNC1_2986, predicted to encode a sugar-phosphate-binding transcriptional regulator of the RpiR family, which was more abundant in the Δ*SR1* mutant relative to WT. In addition, LptG (XNC1_4255), a component of the ABC transporter that exports lipopolysaccharide across the inner membrane (Ruiz et al., 2008), was at higher abundance in wild type relative to Δ*SR1*. DacA, a predicted D-alanyl-D-alanine carboxypeptidase that removes the C-terminal D-alanyl from sugar-peptide cell wall precursors during peptidoglycan biosynthesis, was at higher abundance in the WT relative to Δ*SR1*. FtsB, a cell division protein that regulates peptidoglycan biosynthesis, was lower in WT relative to Δ*SR1* (Boes et al., 2019). WT had higher abundance of a PgaA (a.k.a. HmsH) homolog, the secretin for the exopolysaccharide PNAG (Drace and Darby, 2008; Low and Howell, 2018). The mutant had elevated abundance of CsrA, which regulates PNAG biofilm formation negatively and positively in *E. coli* and *Yersinia pestis*, respectively (Parker et al., 2017; Berndt et al., 2019; Silva-Rohwer et al., 2021), and XNC1_4381, predicted to encode a lipoprotein with poly-β-1,6-*N*-acetylglucosamine de-*N*-acetylase activity, similar to PgaB/HmsF (Calder et al., 2020). The *pga* locus is necessary for *X. nematophila* (and *Yersinia pestis*) biofilm formation on the external surfaces of *Caenorhabditis elegans* nematodes, but is not necessary for colonization of *S. carpocapsae* infective juvenile nematode receptacles (Couillault and Ewbank, 2002; Drace and Darby, 2008). Overall, the combined proteomics data indicate that the flux of amino sugar intermediates toward peptidoglycan, exopolysaccharide, and lipopolysaccharide structures is altered in the Δ*SR1* mutant relative to wild type (**Figure 7**).

Biofilm formation can be regulated by c-di-GMP, levels of which are affected by the pool of purine nucleotides (Kim et al., 2014). Among the metabolites that were differentially abundant between the WT and Δ*SR1* were those involved in purine metabolism. Xanthosine, AICAR, guanine, and guanosine were detected at significantly higher abundances in the WT background whole cell fraction than in the corresponding Δ*SR1* fraction (**Supplementary Figure 12**). Metal binding proteins involved in regulating DNA repair, transcription, and translation are differentially abundant between strains, coinciding with the significant purine and pyrimidine metabolites found in the metabolomics analysis. Tag (XNC1_4499), MutM (XNC1_0165), and RecJ (XNC1_1136) are proteins involved in the base-excision repair (BER) pathway. RecJ binds Mg, Mn, and Co and has a significantly higher abundance in the Δ*SR1* mutant in the supernatant fraction. The BER pathway repairs DNA damage caused by oxidation, alkylation, and deamination, and their differential abundance may indicate differences in DNA damage occurring in these strains (Krokan and Bjoras, 2013).

The metabolomics and proteomics analysis described above suggests that the presence of NilB and NilC influences polysaccharide homeostasis. This, combined with the ability of NilC to increase *X. nematophila* colonization at a glycan-rich tissue and our observations of slight structural similarity between NilC and CBM domains (**Supplementary Figure 4**), led us to hypothesize that NilC might have binding and/or cleavage activity for polysaccharides. We tested this in preliminary assays by assessing the ability of purified NilC to bind to chitin-coated beads or to cleave various disaccharide substrates or polysaccharides using fluorogenic substrates with negative results

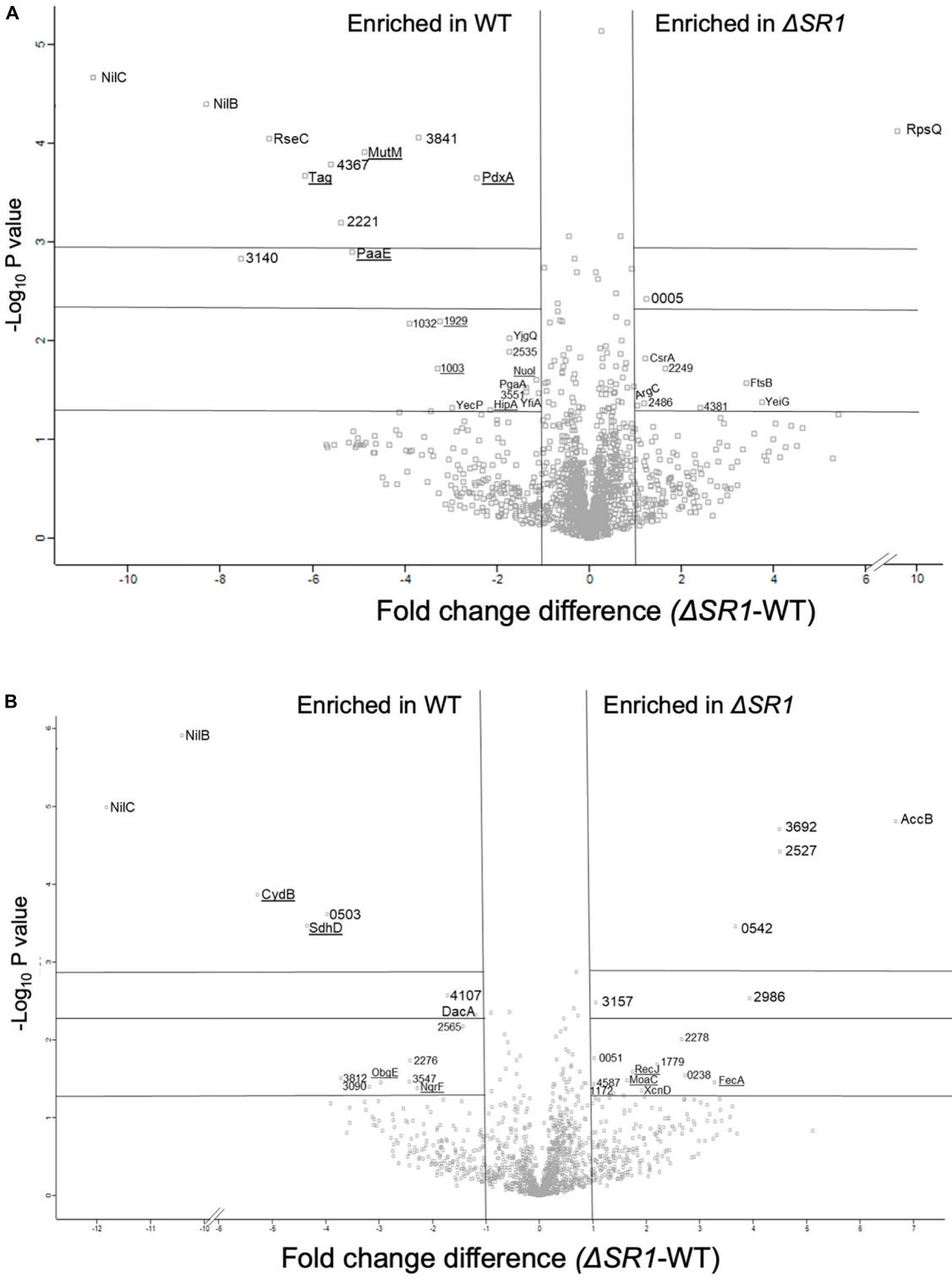

FIGURE 6 | Differentially translated proteins between Δ*SR1* and WT show significant differences in metal-related activities (binding, homeostasis, and metabolic pathways). Volcano plot representations of proteins that are differentially present in *X. nematophila* wild type and Δ*SR1* strains for **(A)** whole cell fraction and **(B)** supernatant fraction. Proteins indicated on the left of the vertical lines were detected at significantly higher levels (| FC| > 1) in wild type, while those listed to the right were detected at significantly higher levels (| FC| > 1) in the Δ*SR1* mutant. Underlined proteins represent proteins with expected metal-binding activity. Significance values (from bottom to top) are indicated by the horizontal lines at $p < 0.05$, 0.005, and 0.001.

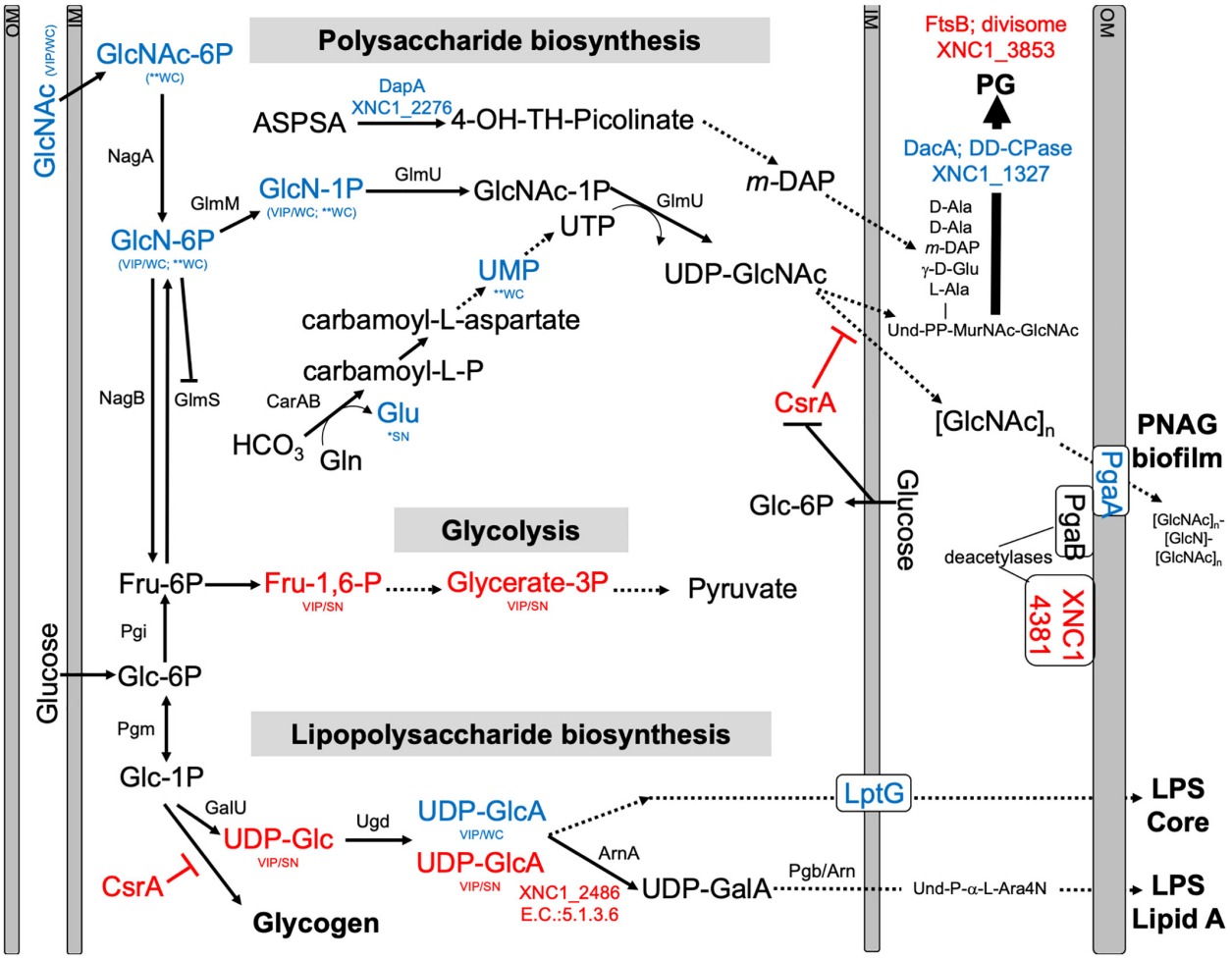

FIGURE 7 | Predicted pathways for amino sugar metabolism leading to peptidoglycan (PG), exopolysaccharide [poly-*N*-acetylglucosamine (PNAG)], lipopolysaccharide LipidA biosynthesis, and glycolysis pathways. Blue and red font texts indicate higher and lower abundance of the indicated metabolites and proteins in WT relative to Δ*SR1*. Asterisks (*) indicate significant differences based on Student's *T*-test, while VIP indicates VIP > 1 in PLS-DA plots, with WC and SN indicating whether the observed difference was in a whole cell or supernatant, respectively. XNC1_4381 shows similarity to PgaB deacetylase, and XNC1_2486 is predicted to convert UDP-glucuronate (UDP-GlcA) to UDP-galacturonate (UDP-GalA), similar to the enzyme ArnA. GlcNAc-6P, *N*-Acetyl-Glucosamine; GlcN-6P, Glucosamine-6-phosphate; GlcN-1P, Glucosamine-1-phosphate; GlcNAc-1P, *N*-Acetyl-Glucosamine-1-phosphate; UDP-GlcNAc, Uridine diphosphate *N*-acetyl glucosamine; Und, Undecaprenyl; MurNac, *N*-Acetyl-Muramic Acid; Fru-6P, Fructose-6-phosphate; Fru-1,6-P, Fructose 1,6 bisphosphate; Glycerate-3P, 3-Phosphoglycerate; Glc-6-P, Glucose-6-phosphate; Glc-1P, Glucose-1-phosphate; UDP-Glc, Uridine diphosphate glucose; UDP-GlcA, Uridine diphosphate glucuronate; UDP-GalA, Uridine diphosphate galacturonate; L-Ara4N, L-4-aminoarabinose. Dashed lines indicate multiple steps in the indicated pathway.

in both cases. We next tested if NilC can bind peptidoglycan (PG), which it would encounter when periplasmically oriented. We chose to use commercially available PG purified from the Gram-positive bacterium *Bacillus subtilis* to avoid potential complications of contaminating lipopolysaccharide from Gram-negative bacterial sources. BSA or NilC was incubated with PG or chitin as a negative control, and the levels of protein that pelleted with these insoluble substrates were quantified (**Figure 8**). We found that, at the highest concentration of polysaccharide tested (500 mg/ml), NilC associated with PG significantly more than with chitin ($p = 0.0454$). Furthermore, NilC associated with PG significantly more than did BSA ($p < 0.0001$). These data suggest that, when in the periplasm, NilC may bind to peptidoglycan.

DISCUSSION

Recent discoveries have revealed that members of the DUF560 family of OMPs are Type XI secretion systems (TXISS) that can move proteins across the outer membrane (Hooda et al., 2016, 2017; Fantappie et al., 2017; da Silva et al., 2019; Bateman et al., 2021; Grossman et al., 2021). TXISS-dependent effectors include binding proteins for transferrin, lactoferrin, factor H, and heme. However, the full range, characteristics, and functions of TXISS cargo remain to be explored. Here, we demonstrate that the lipoprotein NilC, a mutualism species-specificity factor, is a cargo protein for the $TXISS_{OMP}$, NilB (Heungens et al., 2002; Cowles and Goodrich-Blair, 2004, 2008; Bhasin et al., 2012; Chaston et al., 2013; Grossman et al., 2021). Our biophysical data confirm the

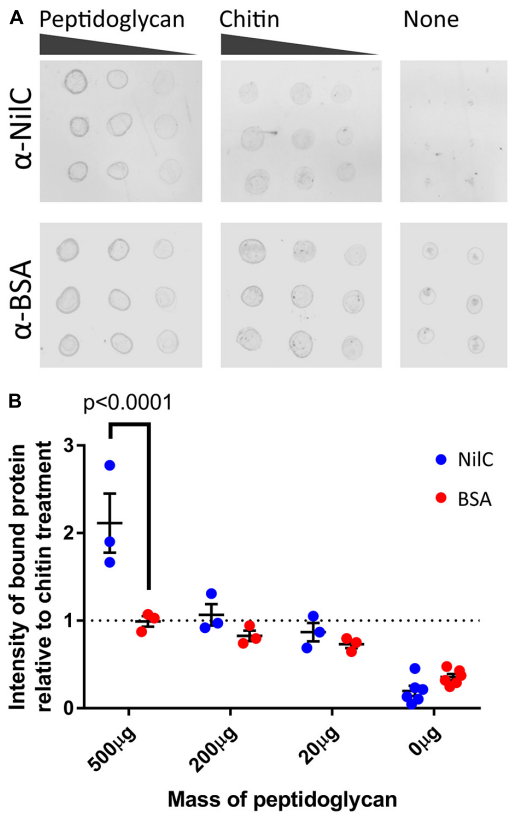

FIGURE 8 | NilC binds peptidoglycan. **(A)** Immuno-dot blots depicting the amount of NilC or bovine serum albumin (BSA) bound to *B. subtilis* peptidoglycan or chitin after an hour of incubation. Three different concentrations of peptidoglycan and chitin were used to provide a gradient (horizontal dots), and 2 μl of each reaction were spotted in triplicate (vertical dots). Immunoblots were probed with the indicated primary antibodies and then labeled with an α-rabbit IgG antibody conjugated to a 680-nm fluorophore for imaging. **(B)** To visualize peptidoglycan binding, protein intensity values were normalized to the average intensity of protein in the chitin samples and plotted. Error bars depict the standard error of each mean. A Tukey's honest significance test was used to compare NilC and BSA intensities; a Dunnett's test was used to compare peptidoglycan-associated protein intensities to chitin-associated protein intensities.

emerging concept that the TXISS cargo is characterized by an N-terminal functional domain that mediates host interactions and a C-terminal domain that targets cargo proteins for secretion by TXISS. Hooda et al. (2017) noted divergent functional N-terminal domains, and a common C-terminal barrel domain of the known TXISS cargo proteins TbpB, HpuA, and fHbp for which structural data were available at that time (Hooda et al., 2017). We now add experimental and bioinformatics data that show this structural framework extends to a TXISS cargo protein with a distinctive N-terminal domain and is thus more generalizable than previously realized. We found that the N-terminal 40 amino acids of NilC are disordered, supporting the emerging concept that many lipoproteins destined for the outer membrane have a long, disordered linker at their N-terminus (El Rayes et al., 2021). In *E. coli*, this linker is important for trafficking by the Lol (localization of lipoproteins) system and for appropriate surface localization of the four extracellular lipoproteins tested, including RcsF (El Rayes et al., 2021). Recent structural data have indicated that RcsF associates with BamA before being transferred to a nascent OMP that is folded by the Bam complex. In this model, the RcsF lipid anchor is embedded in the inner leaflet of the outer membrane, with the long, disordered region threading through the OMP to the surface exposed remainder of the protein (Rodriguez-Alonso et al., 2020). A similar assembly process and resulting topography may also occur for NilC and TXISS (**Figure 9**).

According to the emerging two-domain model for the TXISS cargo, the NilC N-terminal protein sequence between the disordered linker and the C-terminal β-barrel likely comprises the functional effector domain. The molecular function of this effector presumably facilitates mutualistic colonization of the nematode host intestine, for which NilC is required. Some TXISS cargo proteins (e.g., TbpB) are co-receptors for nutrient uptake systems (Eisenbeis et al., 2008; Konopka, 2012; Pogoutse and Moraes, 2017), while another (fHbp) protects from host immunity (Schneider et al., 2006). Our data do not yet distinguish between these two possible functions for NilC. Indeed, our data raise a third possibility that the TXISS cargo can have both periplasmic and extracellular functions. Our demonstration that NilC can bind purified bacterial peptidoglycan suggests that periplasmic NilC binds to the cell wall (**Figure 9**), and is the first experimental indication that NilC may be a carbohydrate binding protein. In this context, we noted an intriguing abundance of tyrosine residues in the N-terminal effector domain. Carbohydrate-aromatic amino acid contacts are a defining characteristic of non-covalent protein carbohydrate-binding pockets due in particular to the favorable CH-π interactions, with tyrosine being the second most frequently carbohydrate-contacting aromatic amino acid (Quiocho, 1986; Weis and Drickamer, 1996; Hudson et al., 2015). A 62-residue stretch of NilC aligns (albeit with low confidence) with the carbohydrate-binding module (CBM) 4/9 domain d1guia (29% identity over 62 residues) (**Supplementary Figure 4D**). While different CBM4 domains recognize diverse glycans using tryptophan or tyrosine residues, in at least one example, the CH-π - binding pocket interactions are donated entirely by tyrosines (Boraston et al., 2002). Conserved tyrosine residues are involved in peptidoglycan peptide recognition in both bacterial lysostaphin (Mitkowski et al., 2019), and eukaryotic peptidoglycan recognition protein-Iα (Guan et al., 2004).

What role, if any, periplasmic NilC plays in nematode host colonization remains to be investigated. *X. nematophila* expressing a V17A-C20S NilC mutant variant is colonization deficient and was not detected consistently in the supernatant, suggesting that, without its covalently attached lipid, this variant NilC is retained in the periplasm. This may be due to sequestration by binding to peptidoglycan, or due to lower efficiency of secretion through TXISS. Regardless, these data argue against a function for periplasmic NilC in facilitating nematode colonization, but do not preclude the possibility that it plays some other cellular role. Periplasmic NilC may modulate peptidoglycan remodeling or stability, activities that could explain the influence of SR1 on polysaccharide and glycolytic

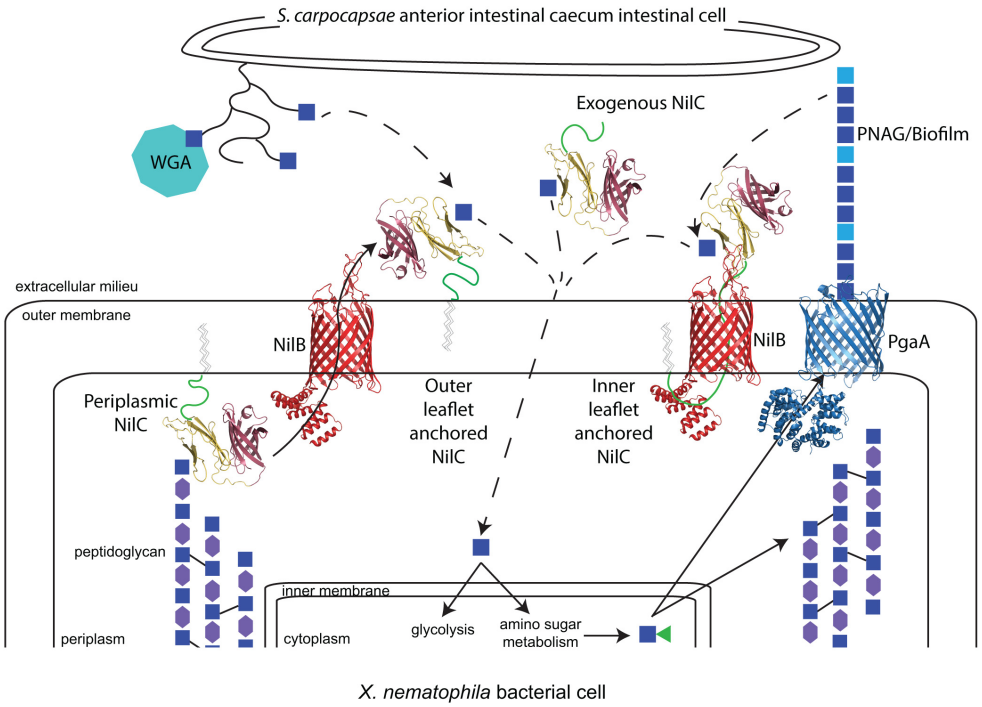

FIGURE 9 | The model of potential molecular interactions occurring during *X. nematophila* colonization of *S. carpocapsae* anterior intestinal cecum epithelial cell surfaces. *N*-acetyl-glucosamine (GlcNAc; blue squares) is present on the *S. carpocapsae* epithelial cell surface, possibly as part of mucin proteins (curved lines), as demonstrated by the binding of wheat germ agglutinin (WGA; teal octagon) to this tissue. GlcNAc is also a component of bacterial peptidoglycan, alternating in β-1,4 linkage with *N*-acetylmuramic acid (MurNAc; purple hexagons) and crosslinked to other polysaccharide chains through peptide linkages (black solid lines). *X. nematophila* encodes homologs of the Pga synthase-dependent exopolysaccharide secretion system for the production of poly-β-1,6-*N*-acetyl-glucosamine (PNAG), composed of GlcNAc and de-acetylated GlcN (light blue squares). A working model based on evidence presented in this study is that periplasm-oriented NilC binds through its N-terminal effector domain (yellow) to GlcNAc residues within peptidoglycan, possibly modulating turnover. NilC can be extracellular, and its transport across the outer membrane by NilB (red) is directed by virtue of its C-terminal β-barrel TXISS-targeting domain (purple). The lipid anchor of NilC may be embedded either in the inner or outer leaflet of the outer membrane. In the former possibility, the long, disordered N-terminal region of NilC (a green cartoon line) may thread through the barrel of NilB, analogous to the structural interactions between the lipoprotein RcsF and associated OMPs (Rodriguez-Alonso et al., 2020). Extracellular NilC may bind to nematode or bacterial glycan-derived GlcNAc and facilitate its uptake (dashed arrows). NilB (red) and NilC models are predictions from Phyre2.0 and AlphaFold, with the N-terminal random coil of NilC represented as a green cartoon line. The structure of PgaA (blue) is PDB 4Y25 (Wang et al., 2016).

metabolism revealed by this study. Similar effects have been observed for the major outer membrane lipoprotein, Lpp, which is predominantly located in the bacterial periplasm where it binds peptidoglycan, and is situationally surface exposed. (Narita and Tokuda, 2011). The predominant function of periplasmic Lpp is in cell envelope structure maintenance. The route by which Lpp is surface exposed and its function, if any, at that location are poorly understood, but are postulated to occur as part of a stress response (Konovalova and Silhavy, 2015; Bahadur et al., 2021; Winkle et al., 2021). Regardless, our findings here suggest that periplasm-surface duality of lipoproteins may be more common than currently appreciated.

The possibility that extracellular NilC serves as the nematode-host interaction effector is supported by our finding that the exogenous addition of soluble, purified NilC can increase *X. nematophila* colonization of the nematode anterior intestinal cecum. If extracellular NilC binds carbohydrates, as suggested above, its substrate may be derived from this surface, which we show here is coated in glycans, including either GlcNAc (a component of peptidoglycan) or *N*-acetylneuraminic acid (Guerardel et al., 2001). Although the glycomes of *Steinernema* nematodes have yet to be elucidated, other nematodes lack *N*-acetylneuraminic (sialic) acid (Bacic et al., 1990), and the intestinal mucus layer is composed, in part, of O-linked serine/threonine glycosylated proteins (mucins) with terminal GlcNAc residues. This mucus layer is part of the nematode host-pathogen interface, and is considered part of the immune defense system. In *C. elegans*, mucins are upregulated in response to *Pseudomonas aeruginosa* infection and elicit downregulation of *P. aeruginosa* metal-binding siderophores and biofilm formation (Troemel et al., 2006; Head et al., 2017). In turn, *P. aeruginosa* can counteract these effects and exploit mucins on *C. elegans*' intestinal surfaces to increase virulence (Wheeler et al., 2019; Hoffman et al., 2020). Specifically, *P. aeruginosa* colonization and biofilm formation are increased by the presence of *N*-acetyl-galactosamine monosaccharides derived from the Mul-1 mucin (Hoffman et al., 2020). Similarly, *X. nematophila* NilC may be involved in sensing host-derived monosaccharides to promote colonization and biofilm formation, although, in this case, to facilitate a mutualistic association.

The interface between a host and bacterium is not exclusively composed of host-derived glycans, and extracellular NilC may promote host interactions through binding of a bacterial-derived carbohydrate, such as an exopolysaccharide component of a surface-adherent biofilm. We identified several links between NilB and NilC and biofilm exopolysaccharides. Our analysis of the global transcription factor Lrp, the regulon of which includes *nilC*, revealed an inverse relationship between NilC surface levels and glass surface biofilm formation, for which the exopolysaccharide is as yet unknown (compare **Figure 4** in this study to Figure 2 of Cao et al., 2017). Furthermore, the abundance of the PgaA secretin of PNAG biofilm exopolysaccharide is reduced in *X. nematophila* cells-lacking *nilB* and *nilC*, suggesting that the Δ*SR1* strain may be defective in PNAG exopolysaccharide biofilm formation. This change in PgaA abundance could be achieved through the RNA-binding protein CsrA (a carbon storage regulator), which is more abundant in Δ*SR1* relative to the SR1+ strain. In *E. coli,* CsrA is a global post-transcriptional regulator that coordinates diverse physiological processes, including iron storage and biofilm formation (Willias et al., 2015; Parker et al., 2017; Berndt et al., 2019; Pourciau et al., 2019) based on its negative regulation of PgaA translation (Wang et al., 2005; Figueroa-Bossi et al., 2014). In *Y. pestis*, biofilm formation is positively regulated by CsrA during growth on alternative carbon sources (Silva-Rohwer et al., 2021). Furthermore, in *Aggregatibacter actinomycetemcomitans*, CsrA-mediated carbon (glycogen) storage and peptidoglycan recycling are both modulated by the presence or absence of PgaA, indicating a complex system of feedback-signaling controlling flux of carbon through energy-deriving, storage, cell wall, and biofilm exopolysaccharide pathways (Shanmugam et al., 2015). Taken together, our data indicate that, as part of their function in nematode colonization, NilB and NilC are integrated with a complex system that balances growth, biofilm formation, carbon uptake and storage, and stress resistance pathways. Future work to identify the *X. nematophila* biofilm exopolysaccharides expressed at the nematode intestinal surface and the role, if any, of NilC in modulating their abundance should shed light on these questions.

A dual function for NilC in both the periplasm and extracellular space raises a further intriguing possibility that the $TXISS_{OMP}$ NilB can control the abundance of NilC that exists in either orientation, perhaps modulated in response to different environmental conditions. Consistent with this idea, we found that, in *X. nematophila*, detectable surface exposure of NilC was observed only for strains in which *nilC* and *nilB* transcription is de-repressed by deletion of either of two transcription factors, NilR and Lrp. While the presence of NilB facilitates surface exposure of NilC during heterologous expression in *E. coli,* we noted a strong and direct correlation between total NilC levels and surface exposure. This phenomenon is similar to that observed for the *N. meningitidis* TXISS cargo protein fHbp. Low-level expression of some fHbp variants is tolerated, but overexpression induces surface exposure (da Silva et al., 2019). In these strains, the presence of the $TXISS_{OMP}$ (Slam 1) is not necessary for, but does enhance the surface localization of fHbp (Fantappie et al., 2017). da Silva et al. (2019) found that the majority of *N. meningitidis* isolates express variant fHbp that is not secreted, suggesting that limiting surface exposure of fHbp likely confers a fitness benefit to the bacterium in a clinical setting (da Silva et al., 2019). Similarly, our finding that wild type *X. nematophila* has little detectable surface exposure of NilC indicates that there is selective pressure to limit surface exposure except under certain environmental conditions. Our finding that *X. nematophila*-expressing NilB variants with FLAG-tag insertions at the periplasmic N-terminus and in a surface-exposed loop display lower and higher NilC surface levels, respectively, relative to a cell-lacking detectable NilB (FLAG-379) indicates that this $TXISS_{OMP}$ may regulate NilC surface exposure in response to periplasmic and extracellular signals.

Our overall working model (**Figure 9**) is that NilC secretion is triggered by the presence of extracellular glycan residues, potentially sensed by the $TXISS_{OMP}$ NilB through one of its surface loop motifs (Bhasin et al., 2012). In the absence of such a glycan (which presumably indicates a non-nematode-host environment), NilC remains periplasmic and bound to peptidoglycan. In the presence of the activating extracellular glycan, TXISS-mediated secretion of NilC, either lipid-anchored in the outer leaflet, or threaded through $TXISS_{OMP}$ NilB and lipid anchored in the inner membrane, facilitates binding or import of amino sugar molecules derived from the host cell surface. This model provides a framework for future studies, elucidating the identities and species specificity of nematode glycans and mucins, testing the ability of the $TXISS_{OMP}$ NilB to recognize and respond to these host molecules by modulating secretion activity, establishing the structural orientation of NilC within the outer membrane, identifying the ligands of NilC N-terminal effector domains and determining the role, if any, of *Xenorhabdus*-derived PNAG or other exopolysaccharides on colonization of the *Steinernema* nematode anterior intestinal cecum.

MATERIALS AND METHODS

Bacterial Strains and Media

Bacterial strains and plasmids used in this study are listed in **Supplementary Table 1** and are described in more detail in the following sections. Bacteria were grown in lysogeny broth (LB) culture media (Miller, 1972) or minimal glucose media (Bhasin et al., 2012), supplemented with 1% LB at either 30°C (for *Xenorhabdus* strains) or 37°C (for *Escherichia coli* strains). For growth of *Xenorhabdus* strains, the LB medium was either stored in the dark (dark LB) or supplemented with 0.1% sodium pyruvate (Xu and Hurlbert, 1990). Strains of *X. nematophila* include those in which the SR1 region has been inserted into the *att*Tn*7* site, downstream of *glmS*. The Tn*7* transposon insertion introduces a new transcriptional terminator that results in 127-bp increase in total *glmS* transcript length (Gay et al., 1986). Previous studies in the closely related *E. coli* and *P. mirabilis* have not detected any detrimental effects from *att*Tn*7* insertion (Craig, 1996; Choi and Schweizer, 2006). Antibiotics were used as indicated at the following concentrations: ampicillin (Amp), 150 μg/ml; chloramphenicol (Cm), 15 μg/ml (*X. nematophila*) and 30 μg/ml

(*E. coli)*; kanamycin (Kan), 50 μg/ml; erythromycin (Erm), 200 μg/ml; and streptomycin (7.5 μg/ml). All transformations were performed *via* electroporation at 2.5 kV for 6 milliseconds, followed by an hour of outgrowth at 37°C in SOC media.

Generation of pETDuet-1 Expression Vectors

pETDuet-1 (Novagen®) served as the plasmid backbone for cloning and expression. A 6xHis tag was added to the C-terminus of NilC *via* site-directed mutagenesis (using forward primer 5′-AGTCCATGGTAAATACAAAATCTAAAATCTATTTAGCTC-3′ and reverse primer 5′-GCTGCGGCCGCTTAGTGGTGGTGATGATGATG-3′) prior to restriction cloning into MCS1 using the *Nco*I and *Not*I restriction sites to create pETDuet/MCS1:NilC Cterm6xHis. NilB-Flag26 was amplified from HGB1200 (Bhasin et al., 2012) and cloned into MCS2 *via* Gibson assembly (using two pairs of primers: NilB forward 5′-ATTAGTTAAGTATAAGAAGGAGATATACATATGAAAAAAATCAAATCCATCGTTATAAC-3′ and NilB reverse 5′-GCTCTCGAGTTAAAAATTACGCTTGAAGTCCAG-3′ plus pETDuet forward 5′-GACTTCAAGCGTAATTTTTAACTCGAGAGCTAATTAACCTAGGCTGCTGCCAC-3′ and pETDuet reverse 5′-ATGTATATCTCCTTCTTATACTTAACTAATATACTAAGATGG-3′) to create the plasmid pETDuet/MCS2:NilB-FLAG-26/MCS1:NilC_Cterm6xHis. Plasmids were transformed into *E. coli* DE3 C43 (Lucigen®) *via* electroporation prior to expression. *nilB* and *nilC* sequences were confirmed by Sanger sequencing at the University of Tennessee (UT) Genomics Core. Expression of NilB and NilC was confirmed *via* immunoblotting of induced lysates using α-FLAG and α-NilC antibodies, respectively.

Measuring NilC Surface Exposure in *Escherichia coli* Co-expression Strains by Immuno-Dot Blotting

Escherichia coli BL21 DE3 C43 strains containing pETDuet-1/MCS2:NilB_26aaflag/MCS1:NilC_Cterm6xHis, pETDuet-1/MCS1:NilC_Cterm6xHis, and no plasmid (HGB 2534, 2535, and 2536, respectively) were raised on defined glucose medium (Orchard and Goodrich-Blair, 2004) plates at 37°C for ∼16 h. HGB 2534 and 2535 plates were supplemented with ampicillin at 150 μg/ml. Biological replicates (10 each) of HGB 2534 and 2535 were cultured into 5 ml of a defined glucose medium supplemented with 1% LB (Amp 150 μg/ml) and incubated at 37°C for ∼16 h. HGB 2536 was cultured in biological triplicate into 5 ml of a defined glucose medium supplemented with 1% LB. Overnight cultures were rinsed 2 x in sterile-defined media, and then half was aliquoted into 5-ml fresh defined glucose media supplemented with 1% LB, and half was aliquoted into 5-ml fresh dark LB. These cultures were incubated at 37°C for 3 h prior to induction with 0.5-mM IPTG. Cultures were induced at 37°C for 2 h. Cultures were equalized to an OD_{600} of 0.6 and rinsed 3 x in Phosphate Buffered Saline (PBS). Note that, even for those cultures that did not grow, sufficient cells were present to allow spotting of the normalized OD amount. For each whole cell sample, 2 μl was spotted onto a nitrocellulose membrane and allowed to dry. Cells were lysed by sonication (30 s at ∼500-rms volts), and 2 μl of each lysate sample was spotted onto a nitrocellulose membrane and allowed to dry. Membranes were immunoblotted and enumerated as described under "Measuring *X. nematophila* NilC surface exposure" below.

Construction of *Xenorhabdus nematophila* Mutants-Expressing Modified NilC

Site-directed mutagenesis of pTn7/SR1 (Cowles and Goodrich-Blair, 2004) was used to generate *nilC*57-V17A-C20S wherein the lipobox was removed by adding a signal peptidase I site and by removing the conserved lipobox cysteine residue (using forward primer 5′-GCCTCTTCTAGAGGAGGGGGTTCT-3′ and reverse primer 5′-TGTAGCAGAAAGTACCAGTGCGAG-3′). Site-directed mutagenesis of pAB001 (Bhasin, Chaston, Goodrich-Blair) and pTn7/SR1-*nilC*57-V17A-C20S was used to generate *nilC*58-6xHis and *nilC*59-V17A-C20S-6xHis wherein 6 histidine residues were encoded onto the C-terminal end of *nilC* (using forward primer 5′-AGTCCATGGTAAATACAAAATCTAAAATCTATTTAGCTC-3′ and reverse primer 5′-GCTGCGGCCGCTTAGTGGTGGTGATGATGATG-3′). The three resulting plasmids were transformed into *E. coli* BW29427, a DAP-dependent, conjugation proficient strain, resulting in HGB2308, HGB2309, and HGB2321. Triparental conjugation was performed using an *X. nematophila* background (either HGB0777 or HGB1251), the appropriate pTn*7* plasmid, and the helper plasmid pUX-BF13 (HGB0283) at a ratio of 3:1:1. Exconjugants were selected for using kanamycin resistance, and insertion into the *att*Tn7 site was confirmed *via* Sanger sequencing (using forward primer 5′-TGTTGGTTTCACATCC-3′ and reverse primer 5′-TACTTATGAGCAAGTATTGTC-3′), resulting in HGB2330, HGB2331, HGB2332, HGB2371, HGB2372, and HGB2373. GFP-expressing strains possessing the modified *nilC* alleles were constructed by conjugating *X. nematophila* stains HGB2330, HGB2331, and HGB2332 and *E. coli* S17-1 λpir-containing pJMC001 (HGB1783) at a ratio of 3:2. Exconjugants were selected for using chloramphenicol resistance and screened for GFP expression using fluorescence microscopy, resulting in HGB2368, HGB2369, and HGB 2370.

Infective Juvenile Colonization Assays

To prepare nematodes for colonization assays, nematode eggs were collected from gravid adult females, developing from infective juvenile nematodes inoculated onto wild type lawns of symbiont and surface sterilized as previously described (Murfin et al., 2012). They were then applied in biological triplicate to LA plates with lawns of treatment bacteria (HGB800, HGB2330, HGB2331, HGB2332, HGB2106, HGB2368, HGB2369, and HGB2370; see **Supplementary Table 1**). Lawns were incubated at 27°C for 9 days and then transferred to white traps to collect emerging infective juveniles. Nematodes were collected and stored in sterile water at 27°C in tissue culture flasks. Frequency of colonization was determined *via* fluorescence microscopy on a

Keyence BZX-700. Briefly, nematodes, which had been raised on the GFP-expressing bacterial strains, were observed for intestinal GFP presence at 4 and 20 days post emergence. Both time points gave similar results, suggesting that no mutant suffered from a persistence defect. Direct counts of average CFU/nematode were determined *via* a grinding assay wherein nematodes that had been raised on non-fluorescent bacterial strains were collected 6 days post emergence, equalized by density, homogenized *via* an electric mortar and pestle, serially diluted, and plated on LB plates to determine CFU. Dilutions of homogenate equivalent to 4 and 0.4 nematodes were used for quantification.

Expression, Purification, and Biophysical Characterization of the NilC Soluble Domain

Expression and Purification of the NilC Soluble Domain

NilC lacking its predicted signal peptide (NilC amino acids 22-282) was cloned by GenScript into the vector pET-28a(+)-TEV using restriction enzymes Nde1 and Not1. The resulting ORF includes an N-terminal hexahistidine tag, followed by a Tobacco Etch Virus protease (TEV) cleavage site. Three amino acids from the cloning (GHM) remain prepended to the NilC sequence. $NilC_{22-282}$ was expressed in *E. coli* BL21(DE3) cells. The $NilC_{62-282}$ construct was prepared using pET-28a(+)-TEV-NilC22-282 as a template where the sequence for residues 22–61 was deleted by inverse PCR with the following primers: forward: 5′-CTTAAGGGATATTCCAACG-3′, reverse: 5′-CATATGGCCCTGAAAATAAAG-3′. The PCR product was treated with a Dpn1 restriction enzyme for 3 h at 37°C, and then phosphorylated with T4 DNA kinase, followed by ligation with T4 DNA ligase at 16°C overnight. Since this construct is based on pET-28A(+) TEV NilC22-282 construct, it has no signal peptide, so it is expressed in the cytoplasm.

For expression, cells were grown at 37°C in LB media until OD_{600} reached ∼0.7, at which point expression was induced by adding IPTG to a final concentration of 1 mm. Protein expression was performed at 25°C overnight. For isotopically labeled protein for NMR experiments, cells were again grown in LB but then transferred to M9 minimal media, supplemented with ^{15}N ammonium chloride (Cambridge Isotope Laboratories) (1g/L of culture). Protein induction and expression were performed as above.

For purification, the cell pellet was resuspended in Buffer A (50 mM Tris-HCl pH 8.0, containing 300-mM NaCl). Cell lysis was preceded by French press. Cell lysate was clarified by centrifugation at 25,000 × g for 30 min at 8°C before being loaded into a 5-ml Ni-NTA column (Qiagen, Germantown, MD, United States). After washing with 100-ml of Buffer A containing 50-mM imidazole, protein was eluted using Buffer A with 500-mM Imidazole. Fractions with target protein were pooled and mixed with TEV protease (final concentration of 1 mg/ml), removing the hexahistidine tag. The sample was dialyzed against Buffer A overnight before removal of the TEV protease using a 1-ml Ni-NTA column. Fractions containing NilC were concentrated before loading into a Sephacryl S-100 HiPrep 16/60 column (Cytiva) for size exclusion chromatography. This step was performed in 50-mM Tris-HCl pH 8.0, containing 150-mM NaCl.

Solution NMR

2D ^{1}H-^{15}N HSQC was performed in a 750-MHz NMR spectrometer equipped with a cryoprobe at the National Magnetic Resonance Facility at Madison. A NilC sample was prepared in 25-mM sodium phosphate buffer pH 6.5, containing 25-mM NaCl, 0.01% sodium azide, 50-μM 2,2-dimethyl-2-silapentane-5-sulfonate (DSS), and 8% D_2O. Experiments were performed at 27°C using a 180-μM NilC concentration. Spectra were processed using Bruker Topspin and referenced to a DSS standard.

Circular Dichroism Spectroscopy

Circular dichroism spectra were collected in an AVIV model 420 CD spectrometer. NilC was prepared at 0.092 mg/ml in a 25-mM sodium phosphate buffer, pH 6.5. Data acquisition was performed at 25°C in a 1-mm path length cuvette using a 5-s averaging time. The CD spectrum of a buffer was measured and subtracted from the NilC spectrum. Secondary structure calculation was performed using the programs Bestsel (Micsonai et al., 2015) and CONTIN/LL (Provencher and Glockner, 1981; van Stokkum et al., 1990).

Limited Proteolysis

Purified NilC at 1 mg/ml (35 mm) was mixed with proteinase K (PK) in a 100:1 molar ratio in 100 ml. The reaction was treated after 1 or 5 min using the following methods: (1) no treatment (2) heating at 95°C for 10 min (3) addition of PMSF to 1-mM final concentration (4) addition of a protease inhibitor cocktail (Roche) to 1 X final concentration. Each sample was then diluted with an SDS-PAGE sample buffer and heated at 95°C for 10 min. All samples were left at 4°C for ∼1 week before running SDS-PAGE. The mass of the major breakdown product was determined by an Electrospray Ionization Mass Spectrometry run in the positive mode. To determine which structural element of NilC this corresponded to, we used both PeptideCutter and MassPeptide (which consider ion charges) to predict all of the possible Proteinase K digestion peptides and their masses, and a simple spread sheet to sum the masses of all possible contiguous peptides to identify those which could be the observed stable fragment.

HGB1211 (*X. nematophila* with *nilR* and SR1 deleted and the SR1 locus carrying a *nilB*-FLAG26 insertion and a *nilC* (M1Z) start-to-stop codon mutation introduced at the *att*Tn*7* locus) were created as described previously (Cowles and Goodrich-Blair, 2004; Bhasin et al., 2012). Briefly, the plasmid pAB001 (Bhasin et al., 2012) (pTn*7*-SR1 *nilB*-FLAG26) was used as a template for site-directed mutagenesis with primers NilCMtoZfor 5′-CAAATTGGAATCATTATTAGAATACAAAATCTAAAATC-3′ and NilCMtoZrev 5′-TTTAGATTTTGTATTCTAATAATGATT CCAATTTGTTT-3′ (Cowles and Goodrich-Blair, 2004). The resulting plasmid, pEVS107:SR1/*nilB*-FLAG26; *nilC* (M1Z), was conjugated into *X. nematophila*Δ*nilR16:Str*Δ*SR1-7:kan*.

Measuring *Xenorhabdus nematophila* NilC Surface Exposure by Immuno-Dot Blotting and Flow Cytometry

NilC surface exposure in *X. nematophila* cells was monitored by immuno-dot blotting of whole bacterial cells. For **Figures 3A,B**, these were HGB800, HGB1102, HGB778, and HGB779; for **Figures 3C,D**, these were HGB1966, 1967, and 1968; for **Figures 3E,F**, these were HGB1200, HGB1211, HGB1207, and HGB1808 (see **Supplementary Table 1**). For **Supplementary Figure 10**, strains tested were HGB800, 1103, 2330, 2371 (see **Supplementary Table 1**). Test strains were struck on LB pyruvate plates with appropriate antibiotics and incubated at 30°C overnight. For each strain, 5 ml of LB that was kept in the dark to prevent generation of reactive oxygen species (dark LB) was inoculated and grown shaking overnight at 30°C. Strains were then sub-cultured 1:1,000 in dark LB and grown overnight (∼16 h) at 30°C with shaking. After growth, cells were spun down from the media and rinsed two times in 1xPBS. Where appropriate, the supernatants were collected and sterilized using a 0.22-mm filter to generate cell-free supernatants. Cell concentrations were normalized to an OD_{600} of 6 and serially diluted 1:3 two times, giving OD_{600} values of 6, 2, and 0.67. Each dilution of whole cells was then spotted in technical triplicate onto a PVDF or a nitrocellulose membrane in 2-μl aliquots and allowed to dry. Lysates were obtained by adding glass beads and shaking vigorously using a Fastprep homogenizer in three cycles of 20 s, shaking, 5 min waiting at 4°C. Lysed cells were centrifuged at 15,871 × *g* for 5 min to remove cellular debris. Lysates and cell-free supernatants were spotted onto nitrocellulose as above allowed to dry. Membranes were blocked with a 50:50 mixture of a Li-cor Intercept Protein-Free Blocking Buffer (P/N: 927-80001) and Tris buffered saline (TBS: 50-mM Tris-Cl, pH 7.6; 150-mM NaCl) for 1 h. Membranes were incubated in a 50:50 Li-cor blocking buffer: TBS supplemented with 0.1% Tween 20 and a 1:1,500 Rabbit Anti-NilC antibody (Pocono labs, received July 23, 2019) for 1 h. Membranes were rinsed 4 times in TBS supplemented with 0.1% Tween 20 prior to incubation with a 1:5,000 Goat anti-rabbit secondary antibody bound to an IRDye 680RD fluorophore. Emission intensity at 700 nm was quantified using an Odyssey Infrared Imaging System and statistically analyzed *via* one-way ANOVA with Tukey's *post hoc* multiple comparisons analysis.

For flow cytometry, test strains were struck on LB pyruvate plates with appropriate antibiotics and grown 30°C for 1–2 days. Cultures of 5 ml of a minimal medium (MM) (Bhasin et al., 2012), supplemented with 0.1% casamino acids with no antibiotics, were inoculated with three biological replicates for each test strain and grown 30°C overnight shaking to a stationary phase. Cells were pelleted by centrifugation at 3,220 × *g* for 5 min and resuspended in 1 ml of phosphate buffered saline (1X PBS:0.137-M NaCl, 0.0027-M KCl, 0.01-M Na_2HPO_4, 0.0018-M KH_2PO_4). Each biological replicate was divided into two treatment groups, one with permeabilization (0.1% TritonX100 in 1X PBS final concentration), and one without permeabilization (PBS) and incubated at 25°C shaking for 10 min. All remaining centrifugation was performed at 6,010 × *g* for 1 min. Samples were washed in 500-μl 1X PBS, and the primary α-NilC IgG antibody (Cowles and Goodrich-Blair, 2004) was added at 1:200 concentration, and incubated at 25°C shaking for 1 h. The samples were washed again in PBS and the secondary goat α-rabbit IgG antibody was added at 1:200 and incubated at 25°C shaking for 1 h. The samples were washed a final time in PBS, and then measured for fluorescence at 488 nm using a BD Biosciences LSR flow cytometer. HGB2018 expressing GFP was used as a 488nm positive control. The gate for positive signal at 488nm was set at 97% of the HGB2018 cells.

Lectin Localization and Bacterial Colonization Competition Assays

Nematode Strains and Preparation

Steinernema carpocapsae ALL strain was obtained from Dr. Harry Kaya (UC-Davis). *S. feltiae* was obtained from the laboratories of Dr. S. Patricia Stock (U Arizona) and was originally isolated in FL, United States. Each of these nematodes is propagated approximately every 3 months through *Galleria mellonella* insects (Vivas and Goodrich-Blair, 2001). *S. scapterisci* was obtained from Becker Underwood Inc. and is maintained by propagation approximately every 3 months through *Acheta domesticus* crickets obtained from local pet stores (Kim et al., 2017). Infective juvenile stage nematodes are stored in water in 50-ml tissue culture flasks in between insect infections.

Lectin Binding Assays

To prepare nematodes for lectin binding and colonization assays, nematode eggs were collected from gravid adult females, developing from infective juvenile nematodes inoculated onto wild type lawns of symbiont and surface sterilized as previously described (Murfin et al., 2012). They were then applied to treatment plates (e.g., bacterial symbiont or liver kidney agar, which enables nematode development without a bacterial symbiont; Martens et al., 2005) as detailed for each experiment. If nematode eggs were not immediately seeded onto treatment plates, they were stored in a sealed dish in dark LB for up to 4 days. After the eggs had been placed on the plates, they were stored at 27°C in the dark for 9 days. Every 3 days, a fresh plate was selected from each treatment and the nematodes collected off the plates by washing and pipetting with 1x PBS. Collected nematodes were placed in a 1.5-ml centrifuge tube and rinsed three additional times with 1x PBS. After rinsing, as much liquid was removed from the tube and 200 μL of 1x PBS added back to equalize the volume within each tube. For treatment with lectin, a final concentration of 27 mM (∼2 μL) of a green fluorescein conjugate lectin was added to the nematode preparation. Tubes were wrapped in foil to inhibit light bleaching and shaken gently overnight on an end-over-end mixer. Nematodes were then rinsed three times with 1X PBS to remove excess lectin before observation *via* fluorescence microscopy on a Keyence BZX-700 microscope. For all data shown in **Figures 4**, **5**, experimental observations of lectin or bacterial localization were blinded, such that the observer was not aware of the treatment. For **Figure 4A**, *S. carpocapsae* nematodes were stained with 6.6-mM rhodamine phalloidin

(Sigma) as described in Chaston et al. (2013) and visualized on a Zeiss LSM 510 confocal microscope (Zeiss, Thornwood, NY, United States) (Sugar et al., 2012). Images for **Figures 4B,D** were taken on a Nikon Eclipse TE300 epifluorescence-inverted microscope. Brightfield and FITC filter images were overlaid and false colored using Image-J.

NilC Protein and Unconjugated Ulex Europaeus Agglutinin and Wheat Germ Agglutinin Lectin Colonization Competition Assays

Xenorhabdus nematophila HGB2018, *X. innexi* HGB2171, and *X. bovienii* HGB1865 bacteria expressing the green fluorescent protein from the *att*Tn*7* locus were used to visualize bacteria at the anterior intestinal cecum colonization site of *S. carpocapsae, S. scapterisci,* and *S. feltiae* FL nematodes, respectively, in the presence or absence of lectin or NilC protein. In addition, to determine the effects of WGA on the colonization of *X. nematophila* with and without SR1, isogenic Δ*SR1* strains with either empty Tn*7* or the Tn*7*-SR1 locus were compared. The green-fluorescent protein was introduced into these strains by integrating the plasmid pJMC001 at the *kefA* site (Bhasin et al., 2012). Nematodes isolated as described above were exposed to GFP-expressing bacterial symbionts alone or with unconjugated WGA, unconjugated UEA, or purified NilC (see above) at 27-mM final concentration, and processed as described above before observing by fluorescence microscopy for the presence or absence of bacteria at the AIC. As above, these experiments were blinded.

Statistical Analysis

Separate one-way analyses of variance were performed in GraphPad Prism to test if treatments differed with respect to mean fluorescence intensity. Tukey's *post hoc* multiple comparisons analysis was used to compare between all levels of treatment. A simple linear regression was used to test if total NilC expression predicted surface exposure of NilC.

For WGA, UEA, and soluble NilC protein experiments related to individual nematode colonization, the binary outcome of colonization was analyzed within generalized linear mixed models using the GLIMMIX procedure (SAS v 9.4, Cary, NC, United States) (Schabenberger, 2005) with a binary distribution and a logit link. The fixed effect of treatment, as well as other confounding variables, such as days observed (6 days total) or the life stage of the nematode (male, female, juvenile), were included in the model. Additionally, random effects to account for biological replicate were included. The *inverse link* option was used within the LS Means statement to obtain model-adjusted probability for colonization by bacterial symbionts. Additional variables, including addition of unconjugated WGA and bacteria, or bacteria alone, the life stage of the nematode, and the day observed that can contribute to colonization status in the assay, were included in models as appropriate. Statistical significance was set at $\alpha = 0.05$.

Proteomics and Metabolomics

Sample Preparation

HGB 1495 (*X. nematophila* ATCC19061 Δ*SR1*Δ*nilR* GFP with integrated empty Tn*7*) and HGB1496 (*X. nematophila* ATCC19061 Δ*SR1*Δ*nilR*GFP with integrated Tn*7* containing SR1) were struck from frozen stocks onto LB pyruvate plates and incubated at 30°C overnight. Three biological replicates for each strain were inoculated in 50 ml of a minimal medium (Bhasin et al., 2012) in a sterile 500-ml flask, and incubated at 30°C, 200 rpm to OD_{600} of 0.6. Based on the findings of Bhasin et al. (2012), growth in this medium to OD_{600} of 0.6 for ∼55 h was expected to maximize *nilB* expression in the HGB1496 strain. Cell lysis was monitored at 260–280 Abs. The 50-ml culture was divided for the metabolomics and proteomics analyses. For proteomic analysis, cell pellets were suspended in an SDS lysis buffer (2% in 100 mM of NH4HCO3, 10-mM DTT). Samples were physically disrupted by bead beating (0.15 mm) at 8,000 rpm for 5 min. Crude lysates were boiled for 5 min at 90°C. Cysteines were blocked by adjusting each sample to 30-mM iodoacetamide and incubating the reaction in the dark for 15 min at room temperature. Proteins were precipitated using a chloroform/methanol/water extraction. Dried protein pellets were resuspended in 2% sodium deoxycholate (SDC) (100-mM NH_4HCO_3), and protein amounts were estimated by performing a bicinchoninic acid (BCA) assay. For each sample, an aliquot of ∼500 μg of protein was digested *via* two aliquots of sequencing-grade trypsin [Promega, 1:75 (w:w)] at two different sample dilutions, (overnight) and subsequent incubation for 3 h at 37°C. The peptide mixture was adjusted to 0.5% formic acid to precipitate SDC. Hydrated ethyl acetate was added to each sample at a 1:1 [v:v] ratio three times to effectively remove SDC. The samples were then placed in a SpeedVac Concentrator (Thermo Fisher Scientific, Waltham, MA, United States) to remove ethyl acetate and further concentrate the sample. The peptide-enriched flowthrough was quantified by a BCA assay, desalted on RPC18 stage tips (Pierce Biotechnology, Waltham, MA, United States) and then stored at −80°C. For metabolomic analysis, frozen samples were thawed at 4°C prior to extraction. Extractions were performed using 1.5 ml of 0.1-M formic acid in 4:4:2 acetonitrile:water:methanol according to the procedure described previously (Dearth et al., 2018).

LC-MS/MS and UPLC-HRMS Analysis

For proteomics analyses, all samples were analyzed on a Q Exactive Plus mass spectrometer (Thermo Fisher Scientific, Waltham, MA, United States), coupled with a Proxeon EASY-nLC 1200 liquid chromatography (LC) pump (Thermo Fisher Scientific, Waltham, MA, United States). Peptides were separated on a 75-μm inner diameter microcapillary column packed with 25 cm of Kinetex C18 resin (1.7 μm, 100 Å, Phenomenex). For each sample, a 2 μg aliquot was loaded in Buffer A (0.1% formic acid, 2% acetonitrile) and eluted with a linear 150-min gradient of 2–20% of Buffer B (0.1% formic acid, 80% acetonitrile), followed by an increase in Buffer B to 30% for 10 min, another increase to a 50% buffer for 10 min and concluding with a 10-min wash at 98% Buffer A. The flow rate was kept at 200 nl/min. MS data were acquired with the Thermo Xcalibur software version 4.27.19, a topN method where N could be up to 15. Target values for the full scan MS spectra were 1 × 106 charges in the 300–1,500 m/z range with a maximum injection time of 25 ms. Transient times corresponding to a resolution of 70,000 at *m/z* 200 were chosen. A 1.6 *m/z* isolation window and fragmentation of precursor ions were performed by higher-energy C-trap dissociation (HCD)

with a normalized collision energy of 30 eV. MS/MS scans were performed at a resolution of 17,500 at m/z 200 with an ion target value of 1 × 106 and a maximum injection time of 50 ms. Dynamic exclusion was set to 45 s to avoid repeated sequencing of peptides.

An established untargeted metabolomics method utilizing ultra-high-performance liquid chromatography, coupled to high-resolution mass spectrometry (UHPLC-HRMS) (Thermo Scientific, San Jose, CA, United States), was used to analyze water-soluble metabolites (Metabolomic Analysis *via* Reversed-Phase Ion-Pairing Liquid Chromatography Coupled to a Stand-alone Orbitrap Mass Spectrometer). Synergi 2.6-μm Hydro RP column 100 Å, 100 mm × 2.1 mm (Phenomenex, Torrance, CA, United States) and an UltiMate 3000 pump (Thermo Fisher Scientific, Waltham, MA, United States) were used to carry out the chromatographic separations prior to full scan mass analysis by an Exactive Plus Orbitrap MS (Thermo Fisher Scientific, Waltham, MA, United States). HPLC grade solvents (Thermo Fisher Scientific, Waltham, MA, United States) were used. Chromatographic peak areas for each detected metabolite were integrated using an open-source software package, Metabolomic Analysis and Visualization Engine (MAVEN). Area under the curve (AUC) was used for further analyses. The raw metabolomics data have been submitted to the MetaboLights data repository under study ID MTBLS3857.

Proteome Database Search Analysis

MS raw data files were searched against the predicted proteins of the *X. nematophila* ATCC 19061 genome (accession FN667742; downloaded 12/20/2017) (Chaston et al., 2013) to which common contaminant proteins had been added. A decoy database, consisting of the reversed sequences of the target database, was appended in order to discern the false-discovery rate (FDR) at the spectral level. For standard database searching, the peptide fragmentation spectra (MS/MS) were analyzed by the Crux pipeline v3.0. The MS/MS was searched using the Tide algorithm and was configured to derive fully tryptic peptides using default settings, except for the following parameters: allowed clip nterm-methionine, precursor mass tolerance of 10 parts per million (ppm), a static modification on cysteines (iodoacetamide; + 57.0214 Da), and dynamic modifications on methionine (oxidation; 15.9949). The results were processed by Percolator to estimate q values. Peptide spectrum matches (PSMs) and peptides were considered to be identified at a q value < 0.01. Across the entire experimental dataset, proteins were required to have at least 2 distinct peptide sequences and 2 minimum spectra per protein. For label-free quantification, MS1-level precursor intensities were derived from MOFF using the following parameters: 10 ppm mass tolerance, a retention time window for extracted ion chromatogram was 3 min, a time window to get the apex for the MS/MS precursor was 30 s. Protein intensity-based values, which were calculated by summing together quantified peptides, normalized by dividing by protein length and then LOESS and median central tendency procedures, were performed on $\log_2$-transformed. Using the freely available software Perseus[1], missing values were replaced by random numbers drawn from a normal distribution (width = 0.3 and downshift = 2.8). This platform was also used to generate the volcano plots.

Peptidoglycan-Binding Assays

NilC was purified as described above in "Expression and purification of the NilC soluble domain." Bovine serum albumin (BSA) was purchased from Fisher Scientific (BP9700100) and used as a negative control for peptidoglycan binding. Peptidoglycan (PG) from *Bacillus subtills* (SMB00288) and chitin (C7170-100G) were purchased from Sigma Aldrich. All reactions were performed in a protein storage buffer (50-mM Tris HCL, 500-mM NaCl pH8). In 50-μl binding reactions, 1 μg of either pure NilC or BSA was combined with 500, 200, 20, or 0 μg of PG or chitin. All reactions were incubated, rotating for 1 h at 37°C. After incubation, reactions were centrifuged at 21,000 G for 3 min to pellet the insoluble fraction and collect the supernatant. This process was repeated two times to ensure complete removal of insoluble components. The remaining pellet was rinsed three times with a protein storage buffer. About 2 μl of each supernatant sample and a pellet sample was dot blotted in technical triplicate onto nitrocellulose membranes. Membranes were heat fixed at 50°C for 10 min to adhere the PG. Membranes were blocked with a 50:50 mixture of Li-cor Intercept Protein-Free Blocking Buffer (P/N: 927-80001) and Tris buffered saline (TBS: 50-mM Tris-Cl, pH 7.6; 150-mM NaCl) for 1 h. NilC membranes were immunoblotted and enumerated as described under "Measuring *X. nematophila* NilC surface exposure" above. BSA membranes were incubated in a 50:50 Li-cor blocking buffer, TBS supplemented with 0.1% Tween 20 and 1:5,000 rabbit anti-BSA IgG [Thermo Fisher Scientific (Waltham, MA, United States), A11133] for 1 h. The membranes were rinsed four times in TBS supplemented with 0.1% Tween 20 prior to incubation with 1:5,000 a Goat anti-rabbit secondary antibody bound to an IRDye 680RD fluorophore. For all membranes, emission intensity at 700 nm was quantified using an Odyssey Infrared Imaging System. A Tukey's honest significance test was used to assess differences between NilC and BSA intensities; a Dunnett's test was used to assess differences between PG binding and chitin binding for each concentration.

DATA AVAILABILITY STATEMENT

The datasets presented in this study can be found in online repositories. The names of the repository/repositories and accession number(s) can be found below: MetaboLights data repository under study ID MTBLS3857.

AUTHOR CONTRIBUTIONS

HG-B and KF contributed to conception and design of the study, contributed to data analysis, and wrote the first draft of the manuscript. AG, CE, EM, NM, and TM designed and performed experiments, analyzed results, and wrote sections of the

[1]https://maxquant.net/perseus/

manuscript. CM and KJ performed experiments and analyzed results. LS performed statistical analyses. PA, RH, and SC contributed to experimental design and analysis. All authors contributed to manuscript revision, read, and approved the submitted version.

FUNDING

This work was supported by grants from the National Science Foundation (IOS- 1353674) to HG-B and KF and the University of Tennessee, Knoxville to HG-B. TM was supported by NIH National Research Service Award T32-GM07215. Funding (or partial funding) for open access to this research was provided by the University of Tennessee's Open Publishing Support Fund.

ACKNOWLEDGMENTS

The authors thank Mengyi Cao, John Chaston, Archna Bhasin, and Xiaojun Lu for generating strains used in this study, Joseph Jackson for advice on flow cytometry analyses, and Madeleine Roberts and Brian Weaver for assistance with ligand-binding assays.

SUPPLEMENTARY MATERIAL

The Supplementary Material for this article can be found online at: https://www.frontiersin.org/articles/10.3389/fmicb.2022.800366/full#supplementary-material

REFERENCES

Bacic, A., Kahane, I., and Zuckerman, B. M. (1990). *Panagrellus redivivus* and *Caenorhabditis elegans*: evidence for the absence of sialic acids. *Exp. Parasitol.* 71, 483–488. doi: 10.1016/0014-4894(90)90074-m

Baek, M., Dimaio, F., Anishchenko, I., Dauparas, J., Ovchinnikov, S., Lee, G. R., et al. (2021). Accurate prediction of protein structures and interactions using a three-track neural network. *Science* 373, 871–876. doi: 10.1126/science.abj8754

Bahadur, R., Chodisetti, P. K., and Reddy, M. (2021). Cleavage of Braun's lipoprotein Lpp from the bacterial peptidoglycan by a paralog of l,d-transpeptidases, LdtF. *Proc. Natl. Acad. Sci. U.S.A.* 118:e2101989118. doi: 10.1073/pnas.2101989118

Banno, M., Komiyama, Y., Cao, W., Oku, Y., Ueki, K., Sumikoshi, K., et al. (2017). Development of a sugar-binding residue prediction system from protein sequences using support vector machine. *Comput. Biol. Chem.* 66, 36–43. doi: 10.1016/j.compbiolchem.2016.10.009

Bateman, T. J., Shah, M., Ho, T. P., Shin, H. E., Pan, C., Harris, G., et al. (2021). A Slam-dependent hemophore contributes to heme acquisition in the bacterial pathogen *Acinetobacter baumannii*. *Nat. Commun.* 12:6270. doi: 10.1038/s41467-021-26545-9

Berndt, V., Beckstette, M., Volk, M., Dersch, P., and Bronstrup, M. (2019). Metabolome and transcriptome-wide effects of the carbon storage regulator A in enteropathogenic *Escherichia coli*. *Sci. Rep.* 9:138. doi: 10.1038/s41598-018-36932-w

Bhasin, A., Chaston, J. M., and Goodrich-Blair, H. (2012). Mutational analyses reveal overall topology and functional regions of NilB, a bacterial outer membrane protein required for host association in a model of animal-microbe mutualism. *J. Bacteriol.* 194, 1763–1776. doi: 10.1128/JB.06711-11

Boes, A., Olatunji, S., Breukink, E., and Terrak, M. (2019). Regulation of the peptidoglycan polymerase activity of PBP1b by antagonist actions of the core divisome proteins FtsBLQ and FtsN. *mBio* 10:e01912-18. doi: 10.1128/mBio.01912-18

Boraston, A. B., Nurizzo, D., Notenboom, V., Ducros, V., Rose, D. R., Kilburn, D. G., et al. (2002). Differential oligosaccharide recognition by evolutionarily-related beta-1,4 and beta-1,3 glucan-binding modules. *J. Mol. Biol.* 319, 1143–1156. doi: 10.1016/S0022-2836(02)00374-1

Borg, A. J. E., Dennig, A., Weber, H., and Nidetzky, B. (2021). Mechanistic characterization of UDP-glucuronic acid 4-epimerase. *FEBS J.* 288, 1163–1178. doi: 10.1111/febs.15478

Calder, J. T., Christman, N. D., Hawkins, J. M., and Erickson, D. L. (2020). A trimeric autotransporter enhances biofilm cohesiveness in *Yersinia pseudotuberculosis* but not in *Yersinia pestis*. *J. Bacteriol.* 202:e00176-20. doi: 10.1128/JB.00176-20

Cao, M., and Goodrich-Blair, H. (2020). *Xenorhabdus nematophila* bacteria shift from mutualistic to virulent Lrp-dependent phenotypes within the receptacles of *Steinernema carpocapsae* insect-infective stage nematodes. *Environ. Microbiol.* 22, 5433–5449. doi: 10.1111/1462-2920.15286

Cao, M., Patel, T., Rickman, T., Goodrich-Blair, H., and Hussa, E. A. (2017). High levels of the *Xenorhabdus nematophila* transcription factor Lrp promote mutualism with the *Steinernema carpocapsae* nematode host. *Appl. Environ. Microbiol.* 83:e00276-17. doi: 10.1128/AEM.00276-17

Chaston, J. M., Murfin, K. E., Heath-Heckman, E. A., and Goodrich-Blair, H. (2013). Previously unrecognized stages of species-specific colonization in the mutualism between *Xenorhabdus bacteria* and *Steinernema nematodes*. *Cell. Microbiol.* 15, 1545–1559. doi: 10.1111/cmi.12134

Chaston, J. M., Suen, G., Tucker, S. L., Andersen, A. W., Bhasin, A., Bode, E., et al. (2011). The entomopathogenic bacterial endosymbionts *Xenorhabdus* and *Photorhabdus*: convergent lifestyles from divergent genomes. *PLoS One* 6:e27909. doi: 10.1371/journal.pone.0027909

Choi, K. H., and Schweizer, H. P. (2006). mini-Tn7 insertion in bacteria with secondary, non-glmS-linked attTn7 sites: example *Proteus mirabilis* HI4320. *Nat. Protoc.* 1, 170–178. doi: 10.1038/nprot.2006.26

Choi, K. H., Gaynor, J. B., White, K. G., Lopez, C., Bosio, C. M., Karkhoff-Schweizer, R. R., et al. (2005). A Tn7-based broad-range bacterial cloning and expression system. *Nat. Methods* 2, 443–448. doi: 10.1038/nmeth765

Couillault, C., and Ewbank, J. J. (2002). Diverse bacteria are pathogens of *Caenorhabditis elegans*. *Infect. Immun.* 70, 4705–4707. doi: 10.1128/IAI.70.8.4705-4707.2002

Cowles, C. E., and Goodrich-Blair, H. (2004). Characterization of a lipoprotein, NilC, required by *Xenorhabdus nematophila* for mutualism with its nematode host. *Mol. Microbiol.* 54, 464–477. doi: 10.1111/j.1365-2958.2004.04271.x

Cowles, C. E., and Goodrich-Blair, H. (2006). nilR is necessary for co-ordinate repression of *Xenorhabdus nematophila* mutualism genes. *Mol. Microbiol.* 62, 760–771. doi: 10.1111/j.1365-2958.2006.05400.x

Cowles, C. E., and Goodrich-Blair, H. (2008). The *Xenorhabdus nematophila* nilABC genes confer the ability of *Xenorhabdus* spp. to colonize *Steinernema carpocapsae* nematodes. *J. Bacteriol.* 190, 4121–4128. doi: 10.1128/JB.00123-08

Craig, N. L. (1991). Tn7: a target site-specific transposon. *Mol. Microbiol.* 5, 2569–2573. doi: 10.1111/j.1365-2958.1991.tb01964.x

Craig, N. L. (1996). Transposon Tn7. *Curr. Top. Microbiol. Immunol.* 204, 27–48. doi: 10.1007/978-3-642-79795-8_2

da Silva, R. A. G., Karlyshev, A. V., Oldfield, N. J., Wooldridge, K. G., Bayliss, C. D., Ryan, A., et al. (2019). Variant signal peptides of vaccine antigen, FHbp, impair processing affecting surface localization and antibody-mediated killing in most meningococcal isolates. *Front. Microbiol.* 10:2847. doi: 10.3389/fmicb.2019.02847

Dearth, S. P., Castro, H. F., Venice, F., Tague, E. D., Novero, M., Bonfante, P., et al. (2018). Metabolome changes are induced in the Arbuscular mycorrhizal fungus *Gigaspora margarita* by germination and by its bacterial endosymbiont. *Mycorrhiza* 28, 421–433. doi: 10.1007/s00572-018-0838-8

Dobrogosz, W. J. (1968). Effect of amino sugars on catabolite repression in *Escherichia coli*. *J. Bacteriol.* 95, 578–584. doi: 10.1128/jb.95.2.578-584.1968

Drace, K., and Darby, C. (2008). The hmsHFRS operon of *Xenorhabdus nematophila* is required for biofilm attachment to *Caenorhabditis elegans*. *Appl. Environ. Microbiol.* 74, 4509–4515. doi: 10.1128/AEM.00336-08

Eisenbeis, S., Lohmiller, S., Valdebenito, M., Leicht, S., and Braun, V. (2008). NagA-dependent uptake of N-acetyl-glucosamine and N-acetyl-chitin oligosaccharides across the outer membrane of *Caulobacter crescentus*. *J. Bacteriol.* 190, 5230–5238. doi: 10.1128/JB.00194-08

El Rayes, J., Szewczyk, J., Deghelt, M., Csoma, N., Matagne, A., Iorga, B. I., et al. (2021). Disorder is a critical component of lipoprotein sorting in Gram-negative bacteria. *Nat. Chem. Biol.* 17, 1093–1100. doi: 10.1038/s41589-021-00845-z

Fantappie, L., Irene, C., De Santis, M., Armini, A., Gagliardi, A., Tomasi, M., et al. (2017). Some Gram-negative lipoproteins keep their surface topology when transplanted from one species to another and deliver foreign polypeptides to the bacterial surface. *Mol. Cell. Proteomics* 16, 1348–1364. doi: 10.1074/mcp.M116.065094

Felli, I. C., and Pierattelli, R. (2015). *Intrinsically Disordered Proteins Studied by NMR Spectroscopy. Advances in Experimental Medicine and Biology*, 1st Edn. Cham: Springer International Publishing.

Figueroa-Bossi, N., Schwartz, A., Guillemardet, B., D'heygere, F., Bossi, L., and Boudvillain, M. (2014). RNA remodeling by bacterial global regulator CsrA promotes Rho-dependent transcription termination. *Genes Dev.* 28, 1239–1251. doi: 10.1101/gad.240192.114

Gay, N. J., Tybulewicz, V. L., and Walker, J. E. (1986). Insertion of transposon Tn7 into the *Escherichia coli* glmS transcriptional terminator. *Biochem. J.* 234, 111–117. doi: 10.1042/bj2340111

Grossman, A. S., Mauer, T. J., Forest, K. T., and Goodrich-Blair, H. (2021). A widespread bacterial secretion system with diverse substrates. *mBio* 12:e0195621. doi: 10.1128/mBio.01956-21

Guan, R., Roychowdhury, A., Ember, B., Kumar, S., Boons, G. J., and Mariuzza, R. A. (2004). Structural basis for peptidoglycan binding by peptidoglycan recognition proteins. *Proc. Natl. Acad. Sci. U.S.A.* 101, 17168–17173. doi: 10.1073/pnas.0407856101

Guerardel, Y., Balanzino, L., Maes, E., Leroy, Y., Coddeville, B., Oriol, R., et al. (2001). The nematode *Caenorhabditis elegans* synthesizes unusual O-linked glycans: identification of glucose-substituted mucin-type O-glycans and short chondroitin-like oligosaccharides. *Biochem. J.* 357, 167–182. doi: 10.1042/0264-6021:3570167

Head, B. P., Olaitan, A. O., and Aballay, A. (2017). Role of GATA transcription factor ELT-2 and p38 MAPK PMK-1 in recovery from acute P. *aeruginosa* infection in C. *elegans*. *Virulence* 8, 261–274. doi: 10.1080/21505594.2016.1222334

Heungens, K., Cowles, C. E., and Goodrich-Blair, H. (2002). Identification of *Xenorhabdus nematophila* genes required for mutualistic colonization of *Steinernema carpocapsae* nematodes. *Mol. Microbiol.* 45, 1337–1353. doi: 10.1046/j.1365-2958.2002.03100.x

Hoffman, C. L., Lalsiamthara, J., and Aballay, A. (2020). Host mucin is exploited by *Pseudomonas aeruginosa* to provide monosaccharides required for a successful infection. *mBio* 11:e00060-20. doi: 10.1128/mBio.00060-20

Hooda, Y., Lai, C. C. L., and Moraes, T. F. (2017). Identification of a large family of Slam-dependent surface lipoproteins in Gram-negative bacteria. *Front. Cell. Infect. Microbiol.* 7:207. doi: 10.3389/fcimb.2017.00207

Hooda, Y., Lai, C. C., Judd, A., Buckwalter, C. M., Shin, H. E., Gray-Owen, S. D., et al. (2016). Slam is an outer membrane protein that is required for the surface display of lipidated virulence factors in Neisseria. *Nat. Microbiol.* 1:16009. doi: 10.1038/nmicrobiol.2016.9

Hudson, K. L., Bartlett, G. J., Diehl, R. C., Agirre, J., Gallagher, T., Kiessling, L. L., et al. (2015). Carbohydrate-aromatic interactions in proteins. *J. Am. Chem. Soc.* 137, 15152–15160. doi: 10.1021/jacs.5b08424

Hussa, E. A., Casanova-Torres, A. M., and Goodrich-Blair, H. (2015). The global transcription factor Lrp controls virulence modulation in *Xenorhabdus nematophila*. *J. Bacteriol.* 197, 3015–3025. doi: 10.1128/JB.00272-15

Jumper, J., Evans, R., Pritzel, A., Green, T., Figurnov, M., Ronneberger, O., et al. (2021). Highly accurate protein structure prediction with AlphaFold. *Nature* 596, 583–589. doi: 10.1038/s41586-021-03819-2

Kelley, L. A., Mezulis, S., Yates, C. M., Wass, M. N., and Sternberg, M. J. (2015). The Phyre2 web portal for protein modeling, prediction and analysis. *Nat. Protoc.* 10, 845–858. doi: 10.1038/nprot.2015.053

Kim, I. H., Aryal, S. K., Aghai, D. T., Casanova-Torres, A. M., Hillman, K., Kozuch, M. P., et al. (2017). The insect pathogenic bacterium *Xenorhabdus innexi* has attenuated virulence in multiple insect model hosts yet encodes a potent mosquitocidal toxin. *BMC Genomics* 18:927. doi: 10.1186/s12864-017-4311-4

Kim, J. K., Kwon, J. Y., Kim, S. K., Han, S. H., Won, Y. J., Lee, J. H., et al. (2014). Purine biosynthesis, biofilm formation, and persistence of an insect-microbe gut symbiosis. *Appl. Environ. Microbiol.* 80, 4374–4382. doi: 10.1128/AEM.00739-14

Kinkead, L. C., Whitmore, L. C., Mccracken, J. M., Fletcher, J. R., Ketelsen, B. B., Kaufman, J. W., et al. (2018). Bacterial lipoproteins and other factors released by *Francisella tularensis* modulate human neutrophil lifespan: effects of a TLR1 SNP on apoptosis inhibition. *Cell. Microbiol.* 20:e12795. doi: 10.1111/cmi.12795

Konopka, J. B. (2012). N-acetylglucosamine (GlcNAc) functions in cell signaling. *Scientifica (Cairo)* 2012:489208. doi: 10.6064/2012/489208

Konovalova, A., and Silhavy, T. J. (2015). Outer membrane lipoprotein biogenesis: Lol is not the end. *Philos. Trans. R Soc. Lond. B Biol. Sci.* 370:20150030. doi: 10.1098/rstb.2015.0030

Krokan, H. E., and Bjoras, M. (2013). Base excision repair. *Cold Spring Harb. Perspect. Biol.* 5:a012583.

Latham, R. D., Torrado, M., Atto, B., Walshe, J. L., Wilson, R., Guss, J. M., et al. (2020). A heme-binding protein produced by *Haemophilus haemolyticus* inhibits non-typeable *Haemophilus influenzae*. *Mol. Microbiol.* 113, 381–398. doi: 10.1111/mmi.14426

Low, K. E., and Howell, P. L. (2018). Gram-negative synthase-dependent exopolysaccharide biosynthetic machines. *Curr. Opin. Struct. Biol.* 53, 32–44. doi: 10.1016/j.sbi.2018.05.001

Martens, E. C., Russell, F. M., and Goodrich-Blair, H. (2005). Analysis of *Xenorhabdus nematophila* metabolic mutants yields insight into stages of *Steinernema carpocapsae* nematode intestinal colonization. *Mol. Microbiol.* 51, 28–45. doi: 10.1111/j.1365-2958.2005.04742.x

Micsonai, A., Wien, F., Kernya, L., Lee, Y. H., Goto, Y., Refregiers, M., et al. (2015). Accurate secondary structure prediction and fold recognition for circular dichroism spectroscopy. *Proc. Natl. Acad. Sci. U.S.A.* 112, E3095–E3103. doi: 10.1073/pnas.1500851112

Miller, J. H. (1972). *Experiments in Molecular Genetics*. Cold Spring Harbor, NY: Cold Spring Harbor Laboratory Press.

Mirdita, M., Ovchinnikov, S., and Steinegger, M. (2021). ColabFold – Making protein folding accessible to all. *bioRxiv* [preprint]. doi: 10.1101/2021.08.15.456425

Mitkowski, P., Jagielska, E., Nowak, E., Bujnicki, J. M., Stefaniak, F., Niedzialek, D., et al. (2019). Structural bases of peptidoglycan recognition by lysostaphin SH3b domain. *Sci. Rep.* 9:5965. doi: 10.1038/s41598-019-42435-z

Murfin, K. E., Chaston, J., and Goodrich-Blair, H. (2012). Visualizing bacteria in nematodes using fluorescence microscopy. *J. Vis. Exp.* 68:e4298.

Narita, S., and Tokuda, H. (2011). Overexpression of LolCDE allows deletion of the *Escherichia coli* gene encoding apolipoprotein N-acyltransferase. *J. Bacteriol.* 193, 4832–4840. doi: 10.1128/JB.05013-11

Orchard, S. S., and Goodrich-Blair, H. (2004). Identification and functional characterization of a *Xenorhabdus nematophila* oligopeptide permease. *Appl. Environ. Microbiol.* 70, 5621–5627. doi: 10.1128/AEM.70.9.5621-5627.2004

Parker, A., Cureoglu, S., De Lay, N., Majdalani, N., and Gottesman, S. (2017). Alternative pathways for *Escherichia coli* biofilm formation revealed by sRNA overproduction. *Mol. Microbiol.* 105, 309–325. doi: 10.1111/mmi.13702

Peters, J. E., and Craig, N. L. (2001). Tn7: smarter than we thought. *Nat. Rev. Mol. Cell. Biol.* 2, 806–814. doi: 10.1038/35099006

Pogoutse, A. K., and Moraes, T. F. (2017). Iron acquisition through the bacterial transferrin receptor. *Crit. Rev. Biochem. Mol. Biol.* 52, 314–326. doi: 10.1080/10409238.2017.1293606

Pourciau, C., Pannuri, A., Potts, A., Yakhnin, H., Babitzke, P., and Romeo, T. (2019). Regulation of iron storage by CsrA supports exponential growth of *Escherichia coli*. *mBio* 10:e01034-19. doi: 10.1128/mBio.01034-19

Provencher, S. W., and Glockner, J. (1981). Estimation of globular protein secondary structure from circular dichroism. *Biochemistry* 20, 33–37. doi: 10.1021/bi00504a006

Quiocho, F. A. (1986). Carbohydrate-binding proteins: tertiary structures and protein-sugar interactions. *Annu. Rev. Biochem.* 55, 287–315. doi: 10.1146/annurev.bi.55.070186.001443

Rodriguez-Alonso, R., Letoquart, J., Nguyen, V. S., Louis, G., Calabrese, A. N., Iorga, B. I., et al. (2020). Structural insight into the formation of lipoprotein-beta-barrel complexes. *Nat. Chem. Biol.* 16, 1019–1025. doi: 10.1038/s41589-020-0575-0

Ruiz, N., Gronenberg, L. S., Kahne, D., and Silhavy, T. J. (2008). Identification of two inner-membrane proteins required for the transport of lipopolysaccharide to the outer membrane of *Escherichia coli*. *Proc. Natl. Acad. Sci. U.S.A.* 105, 5537–5542. doi: 10.1073/pnas.0801196105

Schabenberger, O. (2005). Introducing the GLIMMIX procedure for generalized linear mixed models. *NESUG* 18:1.

Schneider, M. C., Exley, R. M., Chan, H., Feavers, I., Kang, Y. H., Sim, R. B., et al. (2006). Functional significance of factor H binding to *Neisseria meningitidis*. *J. Immunol.* 176, 7566–7575. doi: 10.4049/jimmunol.176.12.7566

Shanmugam, M., El Abbar, F., and Ramasubbu, N. (2015). Transcriptome profiling of wild-type and *pga*-knockout mutant strains reveal the role of exopolysaccharide in *Aggregatibacter actinomycetemcomitans*. *PLoS One* 10:e0134285. doi: 10.1371/journal.pone.0134285

Silva-Rohwer, A. R., Held, K., Sagawa, J., Fernandez, N. L., Waters, C. M., and Vadyvaloo, V. (2021). CsrA enhances cyclic-di-GMP biosynthesis and *Yersinia pestis* biofilm blockage of the flea foregut by alleviating Hfq-dependent repression of the hmsT mRNA. *mBio* 12:e0135821. doi: 10.1128/mBio.01358-21

Sugar, D. R., Murfin, K. E., Chaston, J. M., Andersen, A. W., Richards, G. R., Deleon, L., et al. (2012). Phenotypic variation and host interactions of *Xenorhabdus bovienii* SS-2004, the entomopathogenic symbiont of *Steinernema jollieti* nematodes. *Environ. Microbiol.* 14, 924–939. doi: 10.1111/j.1462-2920.2011.02663.x

Troemel, E. R., Chu, S. W., Reinke, V., Lee, S. S., Ausubel, F. M., and Kim, D. H. (2006). p38 MAPK regulates expression of immune response genes and contributes to longevity in C. *elegans*. *PLoS Genet.* 2:e183. doi: 10.1371/journal.pgen.0020183

van Stokkum, I. H., Spoelder, H. J., Bloemendal, M., Van Grondelle, R., and Groen, F. C. (1990). Estimation of protein secondary structure and error analysis from circular dichroism spectra. *Anal. Biochem.* 191, 110–118. doi: 10.1016/0003-2697(90)90396-q

Vivas, E. I., and Goodrich-Blair, H. (2001). *Xenorhabdus nematophilus* as a model for host-bacterium interactions: rpoS is necessary for mutualism with nematodes. *J. Bacteriol.* 183, 4687–4693. doi: 10.1128/JB.183.16.4687-4693.2001

Wang, X., Dubey, A. K., Suzuki, K., Baker, C. S., Babitzke, P., and Romeo, T. (2005). CsrA post-transcriptionally represses pgaABCD, responsible for synthesis of a biofilm polysaccharide Adhesin of *Escherichia coli*. *Mol. Microbiol.* 56, 1648–1663. doi: 10.1111/j.1365-2958.2005.04648.x

Wang, Y., Andole Pannuri, A., Ni, D., Zhou, H., Cao, X., Lu, X., et al. (2016). Structural basis for translocation of a biofilm-supporting exopolysaccharide across the bacterial outer membrane. *J. Biol. Chem.* 291, 10046–10057. doi: 10.1074/jbc.M115.711762

Weis, W. I., and Drickamer, K. (1996). Structural basis of lectin-carbohydrate recognition. *Annu. Rev. Biochem.* 65, 441–473. doi: 10.1146/annurev.bi.65.070196.002301

Wheeler, K. M., Carcamo-Oyarce, G., Turner, B. S., Dellos-Nolan, S., Co, J. Y., Lehoux, S., et al. (2019). Mucin glycans attenuate the virulence of *Pseudomonas aeruginosa* in infection. *Nat. Microbiol.* 4, 2146–2154. doi: 10.1038/s41564-019-0581-8

Willias, S. P., Chauhan, S., Lo, C. C., Chain, P. S., and Motin, V. L. (2015). CRP-mediated carbon catabolite regulation of *Yersinia pestis* biofilm formation is enhanced by the carbon storage regulator protein, CsrA. *PLoS One* 10:e0135481. doi: 10.1371/journal.pone.0135481

Wilson, M. M., and Bernstein, H. D. (2016). Surface-exposed lipoproteins: an emerging secretion phenomenon in Gram-negative bacteria. *Trends Microbiol.* 24, 198–208. doi: 10.1016/j.tim.2015.11.006

Winkle, M., Hernandez-Rocamora, V. M., Pullela, K., Goodall, E. C. A., Martorana, A. M., Gray, J., et al. (2021). DpaA detaches Braun's lipoprotein from peptidoglycan. *mBio* 12:e00836-21. doi: 10.1128/mBio.00836-21

Xu, J., and Hurlbert, R. E. (1990). Toxicity of irradiated media for *Xenorhabdus* spp. *Appl. Environ. Microbiol.* 56, 815–818. doi: 10.1128/aem.56.3.815-818.1990

Conflict of Interest: The authors declare that the research was conducted in the absence of any commercial or financial relationships that could be construed as a potential conflict of interest.

Publisher's Note: All claims expressed in this article are solely those of the authors and do not necessarily represent those of their affiliated organizations, or those of the publisher, the editors and the reviewers. Any product that may be evaluated in this article, or claim that may be made by its manufacturer, is not guaranteed or endorsed by the publisher.

Advantages of publishing in Frontiers

OPEN ACCESS
Articles are free to read for greatest visibility and readership

FAST PUBLICATION
Around 90 days from submission to decision

HIGH QUALITY PEER-REVIEW
Rigorous, collaborative, and constructive peer-review

TRANSPARENT PEER-REVIEW
Editors and reviewers acknowledged by name on published articles

Frontiers
Avenue du Tribunal-Fédéral 34
1005 Lausanne | Switzerland

Visit us: www.frontiersin.org
Contact us: frontiersin.org/about/contact

REPRODUCIBILITY OF RESEARCH
Support open data and methods to enhance research reproducibility

DIGITAL PUBLISHING
Articles designed for optimal readership across devices

FOLLOW US
@frontiersin

IMPACT METRICS
Advanced article metrics track visibility across digital media

EXTENSIVE PROMOTION
Marketing and promotion of impactful research

LOOP RESEARCH NETWORK
Our network increases your article's readership